

This book forms the proceedings of the International Conference on Liquid Crystals held in December 1973, to mark the 25th anniversary of the founding of the Raman Research Institute, Bangalore. It presents original research papers and state-of-the-art reports by many leading liquid crystal scientists on a wide range of topics of current interest from the physics and chemistry of liquid crystals to their device applications.

This authoritative volume will interest solid state theorists, biophysicists, surface chemists, synthetic organic chemists and graduate students.

© COPYRIGHT INDIAN ACADEMY OF SCIENCES, BANGALORE - 560006

EDITED BY S. CHANDRASEKHAR AND PRINTED FOR THE INDIAN ACADEMY OF SCIENCES
BY BANGALORE BOOK PRINTERS, M. S. R. INDUSTRIAL ESTATE, BANGALORE - 560054.

• .

PRAMANA SUPPLEMENT

LIQUID CRYSTALS

**Proceedings of the International Conference held at the
Raman Research Institute, Bangalore, 3-8 December 1973.**

Edited by : S. CHANDRASEKHAR

PREFACE

This volume forms the proceedings of the International Liquid Crystals Conference held at Bangalore from December 3-8, 1973 to commemorate the 25th Anniversary of the founding of the Raman Research Institute. The Conference was preceded by a week's Winter School on Liquid Crystals organized jointly by the Raman Research Institute, the Indian Institute of Science, Bangalore, and the Tata Institute of Fundamental Research, Bombay. The principal guest speakers at the Winter School were G. W. Gray, G. H. Brown, A. Saupe and P. G. De Gennes, to all of whom we owe a special debt of gratitude for their enthusiasm which contributed in no small measure to the success of the entire two-week programme.

Neither the Conference nor the publication of its proceedings would have been possible without generous grants from the following organizations: Department of Science and Technology, University Grants Commission, Electronics Commission, Council of Scientific and Industrial Research, Department of Atomic Energy, Defence Research and Development Organization, Indian Institute of Science, National Aeronautical Laboratory, Bharat Electronics Limited and Hindustan Lever Limited. It is a pleasure to record our indebtedness to all of them.

My thanks are due to the Directors and Administrative staff of the Raman Research Institute, Indian Institute of Science and National Aeronautical Laboratory for their whole-hearted encouragement and support without which none of this would have taken place. To the Editor of Pramana for agreeing to bring out the Proceedings as a Special Supplement. And finally to my young friends at the Institute for their heroic effort in accomplishing so much in such a short space of time and for looking after the arrangements so well during the Winter School and the Conference.

S. CHANDRASEKHAR

CONTENTS

F. BROCHARD and P. G. DE GENNES : Hydrodynamic properties of fluid lamellar phases of lipid / water	1
G. DURAND : Rayleigh scattering of light in smectic A liquid crystals	23
FRITZ JÄHNIG : The temperature dependence of the viscosities of a nematic	31
F. M. LESLIE : Distorted twisted orientation patterns in nematic liquid crystals	41
N. V. MADHUSUDANA and S. CHANDRASEKHAR : The role of permanent dipoles in nematic order	57
B. R. RATNA, M. S. VIJAYA, R. SHASHIDHAR and B. K. SADASHIVA : Experimental studies of short range order in nematogens of strong positive dielectric anisotropy	69
KALYANI VIJAYAN and G. V. VANI : Crystal structure of <i>n-p</i> -methoxybenzylidene- <i>p</i> -phenylazoaniline	75
B. K. VAINSHTEIN and I. G. CHISTYAKOV : The structure of liquid crystals	79
ADRIAAN DE VRIES : X-ray studies of liquid crystals : V. Classification of thermotropic liquid crystals and discussion of intermolecular distances	93

A. TARDIEU, J. L. RANCK, L. MATEU, D. M. SADLER, T. GULIK-KRZYWICKI and V. LUZZATI : Lipid-water systems : Structure and structural transitions	115
S. CHANDRASEKHAR, S. RAMASESHAN, A. S. RESHAMWALA, B. K. SADASHIVA, R. SHASHIDHAR and V. SURENDRANATH : Pressure induced mesomorphism	117
M. DOMON and J. BILLARD : Prediction of phase diagrams for certain liquid crystalline mixtures	131
BERNARD J. BULKIN, DOLORES GRUNBAUM, TERRY KENNELLY and WAI BONG LOK : Vibrational spectra of liquid crystals. X. Recent progress in the study of infrared and Raman spectra of nematics and nematogenic crystals	155
S. VENUGOPALAN : Far-infrared absorption spectrum of <i>p</i> -azoxyanisole	167
J. M. SCHNUR, J. P. SHERIDAN and M. FONTANA : Raman spectral and thermodynamic studies on the liquid crystal terephthal-bis-(4- <i>n</i> -butylaniline)	175
D. MARZOTKO and D. DEMUS : Calorimetric investigation of liquid crystals	182
H. GASPAROUX, F. HARDOUIN and M. F. ACHARD : Magnetic properties of smectic mesophases	215
N. V. MADHUSUDANA, P. P. KARAT and S. CHANDRASEKHAR : Experimental determination of the twist elastic constant of nematic liquid crystals	225
CLIVE A. CROXTON and S. CHANDRASEKHAR : Statistical thermodynamics of the nematic liquid crystal free surface	237

S. KRISHNASWAMY and R. SHASHIDHAR : Experimental determination of the surface tension of nematic liquid crystals	247
J. A. JANIK, J. M. JANIK, K. OTNES, K. ROSCISZEWSKI and S. WROBEL : Estimation of rotational correlation times for PAA and MBBA by the dielectric relaxation and the neutron quasi-elastic scattering methods	253
E. F. CARR : Some electrical properties and ordering in the <i>p-n</i> -alkoxybenzoic acids	263
R. BLINC, S. LUGOMER and B. ZEKS : Soft mode dynamics in nematic liquid crystals	277
P. P. KARAT and N. V. MADHUSUDANA : Some new types of electrohydrodynamic flow patterns in nematic liquid crystals	285
M. N. AVADHANLU and C. R. K. MURTY : Anomalous alignment and domain formation in nematic liquid crystal: ethoxyphenylazo-phenyl hexanoate	289
S. PAN and C. H. WANG : Relaxation study of the electric field induced hydrodynamic turbulence in nematic liquid crystals by Raman scattering	299
VARAGUR S. V. RAJAN and JULES J. C. PICOT : Thermal instability in a nematic layer	305
RAJARAM NITYANANDA and U. D. KINI : The theory of reflexion and transmission by plane parallel cholesteric films	311
RAJARAM NITYANANDA, U. D. KINI, S. CHANDRASEKHAR and K. A. SURESH : Anomalous transmission (Borrmann effect) in absorbing cholesteric liquid crystals	325

S. CHANDRASEKHAR, G. S. RANGANATH and K. A. SURESH : Dynamical theory of reflexion from cholesteric liquid crystals	341
G. S. RANGANATH, K. A. SURESH, S. R. RAJAGOPALAN and U. D. KINI : Circular dichroism in absorbing mixtures of right and left-handed cholesterics	353
D. DEMUS and G. WARTENBERG : Selective reflection of light in cholesteryl esters	363
G. W. GRAY, K. J. HARRISON and J. A. NASH : Recent developments concerning biphenyl mesogens and structurally related compounds	381
J. CANCEILL, C. GROS, J. BILLARD and J. JACQUES : New series of thermotropic liquid crystals with low temperature smectic A phase	397
J. S. DAVE and K. L. VASANTH : Influence of molecular structure on mixed mesomorphism in some binary systems	415
J. S. DAVE and GEORGE KURIAN : Mesomorphic behaviour of cholesteryl esters : V. cholesteryl 6-alkoxy-2-naphthoates	427
J. S. DAVE and A. P. PRAJAPATI : Mesomorphic behaviour of schiff base compounds : IV. N, N'-Di (4- <i>n</i> -alkoxy- 1-naphthylidene) <i>p</i> -azoanilines and N (4- <i>n</i> -alkoxy-1-naphthylidene) 4'-aminoazobenzenes	435
J. S. DAVE and R. A. VORA : Mesomorphic behaviour of substituted phenylbenzoates : II. <i>p</i> (<i>p'</i> - <i>n</i> -alkoxybenzoyloxy) toluenes	447
WILLIAM E. BACON : Influence of liquid crystalline solvents in chemical reactions	455

C. L. KHETRAPAL, A. C. KUNWAR and A. V. PATANKAR : NMR spectra of molecules oriented in a lyotropic mesophase. Part I : The spectra of pyridazine, pyrimidine and pyrazine	471
C. L. KHETRAPAL, A. C. KUNWAR and K. R. K. EASWARAN : PMR studies on N-methyl formamide oriented in a liquid crystalline nematic phase	483
C. L. KHETRAPAL, A. C. KUNWAR and A. SAUPE : NMR spectra of bicyclic compounds oriented in the nematic phase. Part III : The spectrum of benzo (b) thiophene.	495
MICHIO SORAI, TERUO NAKAMURA and SYŪZŌ SEKI : Thermal studies of benzylideneaniline liquid crystals	503
E. J. AMBROSE : The role of liquid crystals in the organization of living systems	523
H. SAITO and S. FRIBERG : Lyotropic liquid crystals and foam stability	537
SHUNSUKE KOBAYASHI and TERUO SHIMOMURA : Further study on multi-colour display devices with twisted nematic liquid crystals	545
S. L. ARORA and J. L. FERGASON : Twisted nematic liquid crystals and their applications in the field effect displays	553
AUTHOR INDEX	561
SUBJECT INDEX	563

Hydrodynamic properties of fluid lamellar phases of lipid/water

F BROCHARD* and P G DE GENNES**

* Laboratoire de Physique des Solides, Université de Paris-Sud,
91405 Orsay, France

** College de France, 11, Place Marcelin-Berthelot,
75231 Paris Cedex 05, France.

(Translated by G. Clairon)

Abstract. We investigate here the hydrodynamic equations and the low frequency collective modes of a fluid lamellar phase (lipid+water) of the L_α type. We find (1) the modes expected for smectics A, and in particular a second sound propagating with low velocities, (2) a mode of *slip* for the lipid layers. The latter should be observable by Rayleigh scattering, and might give information on the elasticity of the lipid layer. We also make an attempt to correlate the macroscopic parameters governing the modes to the microscopic interactions, and especially to the long range interactions between layers.

1. Introduction

A lipid molecule is composed of a hydrophilic group and one or several long chains of paraffinic hydrophobes. In the presence of water, such molecules display a variety of phases¹. In all cases, the aliphatic chains are gathered in regions where water is excluded. We are concerned here with the 'lamellar' phases and specifically with the phase L_α (according to the classification of ref. 2). In this phase, shown in figure 1, the paraffin chains are approximately liquid and there is no positional order within each lipid layer. Besides, we are assuming that there is no privileged direction in the plane of the layers (no cooperative tilt of the chains). Under these conditions, the symmetry of the phase L_α is that of a *smectic A*³.

From a physicochemical point of view the (water/lipid) L_α phases can be classified into three groups, with slightly different properties⁴.

(a) *Un-charged lipids* : Esters (monoglycerids) or molecules with compensated charge ('zwitter ionic') (lecithins). In this type of materials, the thickness h_E of the water layer is always small (from 5 to 25 Å).

(b) *Charged lipids with only one aliphatic chain (Common soaps)* : Here on account of the electrostatic repulsions (mainly proportional to

$1/h_E^3$) between loaded layers, one could have greater thickness of water h_E . However, in practice, L_α phases with a large h_E are not observable in this group because they are in competition with other arrangements (rod phases, etc.) which are energetically preferable when the percentage of water is high.

(c) *Lipids charged with several chains: (Mitochondrial lipids and chloroplast lipids)*: Here, it appears that (by steric hindrance) the rod phases (etc.) are not favoured. Consequently, the phases L_α remain observable even for strong percentages of water (h_E reaches up to 250 Å).

For a theoretical understanding, the case of a thick water layer is more attractive, since the forces and movements can be described by quasi-microscopic arguments. Unfortunately, the materials of group (c) are often poorly defined, heterogenous; and not accessible to quantitative experimentation. Besides, when the water thickness is large the forces between the layers are very small and the ideal lamellar distribution of figure 1 is almost always disturbed by numerous structural defects. One is thus forced towards group (a) and (b) for which the microscopic analysis is more uncertain. This leads us to study the collective modes of the lamellar phase, based mainly on a *phenomenological analysis* independent of the detailed nature of the forces - (sections 2 and 3). However, when the thickness h_E is large, it is possible to express the phenomenological parameters in terms of simple microscopic parameters, such as the viscosity of the water. This will be analysed in section 4.

The elasticity and large wavelength oscillations of a classical smectic A have been investigated from a microscopic point of view in ref.^{6,7}. Let us recall here the fundamental aspects of this analysis.

(i) The *static* elasticity of a smectic A can be reduced to a Landau-Peierls description where only the unidimensional displacement u of layers (perpendicular to their plane) comes into play. The elastic

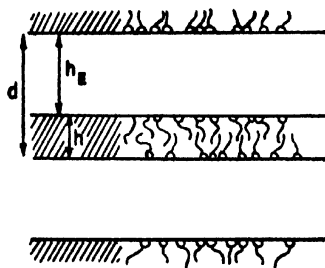


Figure 1 Relative distribution of molecules of lipid and water in the L_α phase. (The polar head of each lipid molecule is shown as a circle) (According to V. Luzzati ref.¹).

energy has a 'mixed' structure where both the derivatives of order 1 and 2 appear

$$F = \frac{1}{2} \bar{B} \left(-\frac{\partial u}{\partial z} \right)^2 + \frac{1}{2} K \left(-\frac{\partial^2 u}{\partial x^2} + \frac{\partial^2 u}{\partial y^2} \right)^2 \quad (1)$$

(in which z is the normal to the layers).

This mixed elasticity has remarkable consequences: long range effects of distortion on the surface⁸; abnormal structure of defects⁹; instability under mechanical tension¹⁰, etc. It will remain valid for the lamellar lipids.

(ii) The *dynamics*, takes into consideration not only the displacement u (with a dilatation of layers $\gamma = \partial u / \partial z$) but also the total change of the density (total dilatation θ). The variables γ and θ are coupled: they give rise to two distinct modes of acoustical propagation. One (first sound) is mainly a longitudinal density wave. The other (second sound) is an oscillation of layers with an almost fixed density. (The name 'second sound' is justified by a close analogy with superfluid helium¹¹). The second sound has been recently observed in Brillouin scattering experiments¹², and also by sound transmission¹³.

In the lamellar lipid phases, one also expects a second sound. A very rough estimation of the parameters (section 3) leads us to anticipate velocities S_2 on the order 10 m/sec. But the most original aspect of the system L_α is different: it is a system with two chemically independent components. To use the language of ref. 7 the number of 'conserved quantities' is increased by one. Comparing with ref. 6, one can state that the variables γ and θ are no longer sufficient to describe the local state of the system: it is necessary to know also the *local concentration of lipid* c or its shift from the value at equilibrium c_0 . We shall write

$$\epsilon_3 = \frac{c_0 - c}{c_0} \quad (2)$$

In order to build up the formal hydrodynamics of the phase L_α , it is the variable ϵ_3 which is the most convenient. On the other hand, in order to connect the hydrodynamical parameters to the concrete properties of the layer, it is often much easier to introduce, instead of ϵ_3 , the relative variation of the surface per polar head A , that is

$$\delta = \frac{A - A_{eq}}{A_{eq}} \quad (3)$$

The quantities ϵ_3 are δ are linked by the relation

$$\epsilon_3 = \gamma + \delta \quad (4)$$

We now analyze the coupled hydrodynamic modes of ϵ_3 , θ and γ : we see that including ϵ_3 (or δ) leads to a new collective mode with low frequency in which the lipid layers are sliding with respect to the water (figure 2).

2. Principles of the dynamics

2.1. Equations without friction

Let us start by writing the form of the elastic energy E in a lamellar system with 2 chemical components, described by the variables θ (total dilatation), u (unidimensional displacement of layers) and δ (surface dilatation per polar head). The energy E (defined here by cm^3) comprises at first the quadratic terms with respect to 3 deformations

$$\begin{aligned}\theta &= \epsilon_1 \\ \gamma &= \frac{\partial u}{\partial z} = \epsilon_2 \\ \gamma + \delta &= \epsilon_3\end{aligned}\tag{5}$$

This contribution can be expressed by

$$E' = \frac{1}{2} \sum_{ij} C_{ij}^{(0)} \epsilon_i \epsilon_j\tag{6}$$

(As in ref. 6 we are utilizing the symbol $C^{(0)}$ for the adiabatic coefficients, and the symbol C for the isothermal coefficients). To the energy E' , as in any smectic A, further terms associated with the curvature of the layers, should be added⁶:

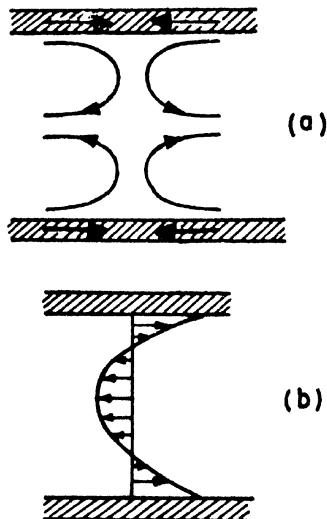


Figure 2 The mode of pure slip in the L_α phase (lipid regions hatched) (a) lines of flow (b) profile of the horizontal velocities.

$$E'' = \frac{1}{2} K \left(\frac{\partial^2 u}{\partial x^2} + \frac{\partial^2 u}{\partial y^2} \right)^2 \quad (7)$$

(Let us stress that for the coefficients K there is no difference between adiabatic and isothermal.) From the energy E one can define the main mechanical agents :

(a) the pressure

$$p = - \frac{\partial E}{\partial \theta} = - \sum_j C_{1j}^{(0)} \epsilon_j \quad (8)$$

(b) the 'vertical' force (parallel to Oz) on the layers, defined as in a classical smectic A'

$$g = - \frac{\delta E}{\delta u} = \frac{\partial}{\partial z} \sum_j C_{2j}^{(0)} \epsilon_j \quad (9)$$

(where the $\delta / \delta u$ is a functional derivative).

(c) the force on the lipid fraction, f

$$f = \nabla \left[\frac{\partial E}{\partial E_3} \right] = \nabla \sum_j C_{3j}^{(0)} \epsilon_j \quad (10)$$

We can then write the equation of acceleration of the fluid under the form

$$\rho \dot{\mathbf{v}} = - \nabla p + f + g + \text{viscous terms} \quad (11)$$

where ρ represents the overall density, $\rho \dot{\mathbf{v}}$ is the mechanical momentum per 1 cm³ of material and $\dot{\mathbf{v}} = \frac{\partial \mathbf{v}}{\partial t}$. (We are limiting ourselves to an approximation of small motions and we are neglecting therefore the difference between $\frac{\partial}{\partial t}$ and $\frac{d}{dt}$). To this equation of acceleration, one must add the equations of conservation for the total mass :

$$\dot{\theta} = \text{div } \mathbf{v} \quad (12)$$

and for the lipid mass :

$$\dot{\epsilon}_3 = \dot{\gamma} + \dot{\delta} = \text{div } \mathbf{v}_L \quad (13)$$

where \mathbf{v}_L is the velocity of the lipid fraction. For the case which is of interest to us here, \mathbf{v}_L will differ from \mathbf{v} mainly in the slip mode of figure 2.

2.2. Scattering effects

The structure of the viscous terms of equation 11 as well as the dissipation associated with *relative* flows ($\dot{\mathbf{u}} - \mathbf{v}_z$ or $\mathbf{v}_L - \mathbf{v}$), remain to be defined.

In the first place, it is convenient to rewrite the terms of friction in eq. 11 by introducing a system of viscous tensions:

$$\begin{aligned} \sigma'_{\alpha\beta} \quad (\alpha, \beta = x, y, z) \\ \rho \dot{\mathbf{v}}|_{\text{viscous}} = \partial_\beta \sigma'_{\beta\alpha} \end{aligned} \quad (14)$$

To analyze the scattering effects, one then calculates the entropy source $T\dot{S}$ by writing the evolution of the total energy from the acceleration equation. It is found that

$$T\dot{S} = \sigma' : \nabla \mathbf{v} + g(\dot{u} - v_z) + \mathbf{f} \cdot (\mathbf{v}_L - \mathbf{v}) + \mathbf{E} \cdot \mathbf{J} \quad (15)$$

In the form (15) we have included all possible type of currents \mathbf{J} and the conjugate fields \mathbf{E} . For instance if \mathbf{J} is a heat current, $\mathbf{E} = -\nabla T/T$. However, in the major part of this work, we shall ignore thermal phenomena for simplicity.

Writing that the total dissipation remains unchanged, if one superposes to the flow studied a simple rotation (modifying in the same manner the three velocities \mathbf{v} , u and \mathbf{v}_L) one can show that the tensor σ' is *symmetrical*. Therefore eq. (15) involves only the symmetrical part of the velocity gradient tensor

$$\sigma' : \nabla \mathbf{v} \rightarrow \sigma'_{\alpha\beta} A_{\alpha\beta} \quad (16)$$

$$\text{with} \quad A_{\alpha\beta} = \frac{1}{2} (\partial_\alpha v_\beta + \partial_\beta v_\alpha) \quad (17)$$

$$\partial_\alpha = \frac{\partial}{\partial x_\alpha}$$

Finally, from the entropy source (15), we can define fluxes ($A_{\alpha\beta}$, $\dot{u} - v_z$, $\mathbf{v}_L - \mathbf{v}$, \mathbf{J}) and forces ($\sigma_{\alpha\beta}$, g , \mathbf{f} , \mathbf{E}) in the thermodynamics of irreversible processes. In the domain of small fluxes, one can assume linear relations between fluxes and forces, with the following properties:

(a) The symmetry of the smectic phase A imposes that the pair (A , σ') is not coupled to the other variables. The relation between σ' and A is of the form*

$$\sigma'_{\alpha\beta} = A_{\gamma\delta} \eta_{\alpha\beta\gamma\delta} \quad (18)$$

where $\eta_{\alpha\beta\gamma\delta}$ is a viscosity matrix, explicitly stated in ref. 7 and which involves five independent parameters. Later on we will write this in a simplified form.

(b) The forces and fluxes normal to the plane of the layers are themselves coupled. We shall write these couplings without including the pair (\mathbf{E} , \mathbf{J}). Then one has

*Summation over repeated indices is assumed throughout this paper.

$$g = L_{22} (\dot{u} - v_z) + L_{23} (v_{Lz} - v_z) \quad (19)$$

$$f_z = L_{32} (\dot{u} - v_z) + L_{33} (v_{Lz} - v_z) \quad (20)$$

with $L_{23} = L_{32}$.

The coefficient L_{22} describes an effect of *permeation*, present even in a system with only one chemical component, and considered first by Helfrich¹⁴. The coefficient L_{33} would describe an effect of diffusion of the lipid molecules from one layer to the other. The coefficient L_{23} connects these two mechanisms. But, in fact, for the lipids which interest us, all these processes are extremely weak, on account of the small solubility of water in the fat regions and vice versa. For this reason, in the rest of this work, we will completely neglect the permeation and diffusion normal to the layers. This amounts to making the coefficients L tend to infinity and therefore taking

$$\begin{aligned} \dot{u} &= v_z \\ v_{Lz} &= v_z \end{aligned} \quad (21)$$

(c) For the component f_{\perp} of force \mathbf{f} , projected on the plane of the layers, we have another simple phenomenological relation : *

$$\mu f_{\perp} = v_{L\perp} - v_{\perp} \quad (22)$$

The relative migration of the lipid with respect to water can be done by slipping, without overcoming any potential barrier : v_L can easily be different from v_{\perp} . We shall call the coefficient of slippage μ .

2.3. The incompressible limit

In the thermotropic smectics A, (with only one chemical component) it is known by direct measurements¹² that the second sound is *very slow* compared to the first one : these two modes are then nearly uncoupled, and it becomes possible to calculate the properties of the second sound by imposing from the beginning $\theta = 0$, i.e., by considering the substance as incompressible¹⁵. The lipid-water systems have interactions between layers which are looser than the thermotropic smectics A : therefore this approximation is surely excellent. It also simplifies the calculation of the modes. The consequences are the following :

(a) the elastic energy (2) is reduced to a form with two variables. Here we find it more convenient to select as independent variables γ and δ (rather than γ and ϵ_3) and we write :

$$E' \rightarrow \frac{1}{2} D_{22}^0 \gamma^2 + D_{23}^0 \gamma \delta + \frac{1}{2} D_{33}^0 \delta^2 \quad (23)$$

The corresponding free energy F' is obtained by replacing the coefficient D^0 by a similar set D . The coefficient \bar{B} which comes in the static

*For any vector, \mathbf{v} , the symbol v_{\perp} represents the component in the plane of the layers.

description (eq. 1) is obtained by minimising F' as regard to δ (for γ fixed). It is equal to

$$\bar{B} = D_{22} - (D_{23}^2/D_{33}) \quad (24)$$

The stability of the system imposes the inequalities :

$$\bar{B} > 0, \quad D_{22} > 0, \quad D_{33} > 0 \quad (25)$$

(b) From a dynamic point of view the incompressibility imposes :

$$\text{div } \mathbf{v} = 0 \quad (26)$$

The pressure p is no longer defined by (8), but becomes an unknown function, to be determined in the process of calculating, by condition (26). In the limit (21) of no permeation, the equation of conservation of the lipid system can be rewritten in the form :

$$\text{div } \mathbf{v}_{L\perp} = \dot{\delta} \quad (27)$$

In the incompressible regime, the viscous tensions σ' are simplified : eq. (18) takes the explicit form

$$\left. \begin{aligned} \sigma'_{zz} &= 2\eta_v \frac{\partial v_z}{\partial z} \\ \sigma'_{\alpha z} &= \eta_M (\partial_\alpha v_z + \partial_z v_\alpha) \\ \sigma'_{\alpha\beta} &= \eta_T (\partial_\alpha v_\beta + \partial_\beta v_\alpha) \end{aligned} \right\} \begin{array}{l} (\alpha, \beta \text{ restricted} \\ \text{to } x \text{ or } y) \end{array} \quad (28)$$

A priori there is still the possibility of adding to $\sigma'_{\alpha\beta}$ a diagonal term

$$\sigma'_{xx} = \sigma'_{yy} = \sigma'_{zz} = \text{const} \frac{\partial v_z}{\partial z} \quad (29)$$

But such a diagonal term can always be incorporated into the pressure p , and must therefore be omitted.

Let us finish this section by a remark on the change of variables carried out in the equation (23): *i.e.*, in passing from the *volume* dilatation ϵ_3 of the lipid fraction to the *bidimensional* dilatation (in a layer) δ .

This change of variable modifies the definition of forces. With ϵ_3 and γ one had the forces

$$\begin{aligned} \mathbf{f} &= \nabla \left(-\frac{\partial E}{\partial \epsilon_3} \right)_{\gamma} \\ g &= \frac{\partial}{\partial \gamma} \left(-\frac{\partial E}{\partial \gamma} \right)_{\epsilon_3} \end{aligned} \quad (30)$$

with δ and γ as variables, one has new forces \mathbf{f}' , g'

$$\begin{aligned}
 f'_z &= 0 \\
 f'_\perp &= \nabla_\perp \left(\frac{\partial E}{\partial \delta} \right) \gamma \\
 g' &= \frac{\partial}{\partial z} \left(\frac{\partial E}{\partial \gamma} \right) \delta
 \end{aligned} \tag{31}$$

Writing $\epsilon_3 = \gamma + \delta$, one can show from (31) that

$$\begin{aligned}
 f'_\perp &= f_\perp \\
 g' &= g + f_z
 \end{aligned} \tag{32}$$

That is to say that all the physical observables are unchanged, as they must be: the two descriptions are indeed equivalent.

3. Collective modes of low frequency

3.1. Simplified calculation of oblique modes

In order to simplify further the discussion of the modes, we are going to make an additional approximation: we will completely neglect the effect of viscous tensions σ' . However, we will still consider the slip coefficient μ . This procedure may seem unorthodox since we are thus isolating a friction mechanism among others. It is in fact justified for the following reasons:

(a) The *second sound* modes are but weakly attenuated in the limit of very small vectors q : our approximation bears only on these small attenuation effects.

(b) As for the mode of *slip* shown in figure 2 the shearing stress described by the parameter μ takes place within *one* layer, and is much more important than the shearing stresses on the scale of the wavelength $2\pi/q$ which are described by the viscous tensions σ' .

This being admitted, let us find the modes for which the amplitudes vary like $\exp(i\mathbf{q} \cdot \mathbf{r} + i\omega t)$ and let us assume that $q_x \neq 0$, $q_z \neq 0$ but $q_y = 0$. Let us first study the following modes

$$v_x \neq 0 \quad v_z \neq 0 \quad v_y = 0$$

which are more interesting to us. The equation of acceleration (11), (free from the viscous tensions) taken in the form of equation (31) gives now the following:

$$\left. \begin{aligned}
 i\omega \rho v_x &= -iq_z p + g' \\
 i\omega \rho v_z &= -iq_x p + f_x
 \end{aligned} \right\} \tag{33}$$

with

$$\left. \begin{aligned}
 g' &= iq_z [D_{22}^0 \gamma + D_{23}^0 \delta] \\
 f_x &= iq_x [D_{23}^0 \gamma + D_{33}^0 \delta]
 \end{aligned} \right\} \tag{34}$$

(Let us stress that the curvature terms obtained from equation (7) are negligible in g' except for a particular case with which we shall deal later on).

While writing

$$\operatorname{div} \mathbf{v} = i(q_x v_x + q_z v_z) = 0$$

we obtain

$$\nabla^2 p = -q^2 p = i(q_x g' + q_z f_x) \quad (35)$$

We can eliminate p from the equation (33) and get

$$i\omega \frac{\partial v_x}{\partial z} = -\omega^2 \gamma = -\frac{q_x^2 q_z^2}{q^2 \rho} [\gamma (D_{22}^0 - D_{23}^0) + \delta (D_{23}^0 - D_{33}^0)] \quad (36)$$

Now using the slip equation (22) and the conservation laws (27) and (26), we are led to

$$\begin{aligned} \dot{\delta} &= \frac{\partial v_{Lx}}{\partial x} = \frac{\partial v_x}{\partial x} + \mu \frac{\partial f_x}{\partial x} \\ &= -\frac{\partial v_z}{\partial z} + \mu \frac{\partial f_x}{\partial x} \\ &= -\dot{\gamma} + \mu \frac{\partial f_x}{\partial x} \end{aligned} \quad (37)$$

or

$$(i\omega + \mu D_{33}^0 q_x^2) \delta + (i\omega + \mu D_{23}^0 q_x^2) \gamma = 0 \quad (38)$$

Equations (36) and (38) form a linear homogenous system for δ and γ . The solution is non-vanishing when the determinant Δ is equal to 0:

$$\Delta = (\omega^2 - \omega_0^2)(i\omega + \mu D_{33}^0 q_x^2) - \omega_1^2(i\omega + \mu D_{23}^0 q_x^2) = 0 \quad (39)$$

We have defined the following auxiliary frequencies

$$\left. \begin{aligned} \omega_0 &= \frac{q_x q_z}{q} \left[\frac{D_{22}^0 - D_{23}^0}{\rho} \right]^{\frac{1}{2}} \\ \omega_1 &= \frac{q_x q_z}{q} \left[\frac{D_{33}^0 - D_{23}^0}{\rho} \right]^{\frac{1}{2}} \end{aligned} \right\} \quad (40)$$

We assume for the moment that q_x and q_z are both not equal to 0 and are comparable (oblique modes) so that $\omega_0 \neq 0$ and $\omega_1 \neq 0$. The roots of equation (39) are separated into two well defined groups:

(a) *Modes of second sound* (ω relatively large)

$$\omega_2^2 \simeq \omega_0^2 + \omega_1^2 = \frac{q_x^2 q_z^2}{q^2} \frac{D_{22}^0 + D_{33}^0 - 2D_{23}^0}{\rho} \quad (41)$$

The form of the dispersion relation (41) is exactly the same as for a classical smectic A. (We will discuss the orders of magnitude for the velocities in section 4). In the mode (41) one has practically $\delta = -\gamma$, that is to say $\epsilon_3 = 0$ (the lipid concentration remains unchanged).

(b) *Modes of slip* (ω small)

$$-i\omega_{\mathbf{x}1} = \mu q_{\mathbf{x}}^2 \frac{D_{22}^0 D_{23}^0 - D_{23}^0{}^2}{D_{22}^0 + D_{33}^0 - 2 D_{23}^0} \quad (42)$$

This new mode is completely damped (ω is purely imaginary). In this mode the two velocities v_{\perp} and $v_{\mathbf{x}}$ are different. The pressure p balances the horizontal tensions

$$p = -\frac{\partial E}{\partial \delta}$$

The pressure p balances also the vertical tensions

$$p = -\frac{\partial E}{\partial \gamma}$$

The tensions are totally balanced and the terms of acceleration $\rho \dot{\mathbf{v}}$ in the equation of motion are negligible. The equality

$$\frac{\partial E}{\partial \delta} = \frac{\partial E}{\partial \gamma}$$

gives the ratio of the amplitudes :

$$\frac{\gamma}{\delta} = \frac{D_{33}^0 - D_{23}^0}{D_{22}^0 - D_{23}^0} \quad (43)$$

It is interesting to note that $\gamma / \delta \neq 0$ even if the coefficient of coupling D_{23}^0 is equal to 0. A slip (associated with δ) and a swelling (associated with γ) are always coupled by means of the pressure p . Let us point out finally that the mode of slip is probably isothermal : therefore the coefficient D^0 in (42) and (43) should be replaced by the coefficients D .

Besides these modes in which $v_{\mathbf{x}}$ and $v_{\mathbf{s}}$ are not zero which we have just classified, we *must* mention another mode of different polarisation

$$\begin{aligned} v_{\mathbf{y}} &\neq 0 \\ v_{\mathbf{x}} &= v_{\mathbf{s}} = 0 \end{aligned}$$

With our approximation of zero viscous tensions these modes appear static ($\omega = 0$). A more detailed calculation including viscous tensions leads to a hydrodynamic transversal mode which is expected in all the smectics A and which has the following dispersion relation :

$$-i\omega = \frac{\eta_{\mathbf{M}} q_{\mathbf{z}}^2 + \eta_{\mathbf{T}} q_{\mathbf{x}}^2}{\rho} \quad (44)$$

This mode gives practically no contribution to the scattering of light and is therefore of small interest.

3.2. Inclusion of damping effects

Let us come back now to the slip modes with v_x and $v_z \neq 0$ and let us include the viscous tensions $\sigma_{\alpha\beta}$ which had been omitted in the previous paragraph. They are defined in the equation (28). Writing once more the complete equation of acceleration (11) and eliminating the pressure by $\text{div } \mathbf{v} = 0$, one is led to the following simple relation

$$[i\omega (i\omega + \tilde{\nu}q^2) + \omega_0^2] \gamma - \omega_1^2 \delta = 0 \quad (45)$$

in which ω_0 and ω_1 remain defined by equation (39). The quantity $\tilde{\nu}$ is an effective kinematic viscosity depending on the orientation of the vector \mathbf{q} , and defined explicitly by :

$$\rho \tilde{\nu} = q^{-4} [\eta_M (q_z^4 + q_x^4) + 2(\eta_V - \eta_M + \eta_T) q_x^2 q_z^2] \quad (46)$$

(Naturally if by chance the three viscosities η_V , η_M and η_T become equal, $\rho \tilde{\nu}$ coincides with their common value).

The equation of slip (38) remains unchanged : the determinant obtained from (38) and (45) is of the following type

$$\begin{aligned} \Delta' &= [\omega_0^2 - \omega^2 + i\omega \tilde{\nu} q^2] [i\omega + \mu D_{33}^0 q_x^2] \\ &+ \omega_1^2 (i\omega + \mu D_{23}^0 q_x^2) = 0 \end{aligned} \quad (47)$$

The discussion of the roots of Δ' is not significantly modified when \mathbf{q} is *small* and *oblique*

(a) For the *second sound* one has now a slightly damped frequency

$$\begin{aligned} \omega &= \omega_2 + \frac{1}{2}i [\tilde{\nu}q^2 + \frac{\omega_1^2}{\omega_2^2} (D_{33}^0 - D_{23}^0) \mu q_x^2] \\ \omega &= \omega_2 + \frac{1}{2} [\tilde{\nu}q^2 + \frac{(D_{33}^0 - D_{23}^0)^2}{D_{33}^0 + D_{22}^0 - 2D_{23}^0} \mu q_x^2] \end{aligned} \quad (48)$$

The damping contains two contributions. One is due to the macroscopic shearing stress of the material and is described by $\tilde{\nu}$. The other results from the slip and depends only on q_x^2 . Detailed studies of the damping as a function of the orientation of \mathbf{q} should in principle give all the coefficients of friction which we have introduced (η_V , η_M , η_T and μ).

(b) For the mode of *slip* which takes place at a lower frequency one easily verifies that the damping caused by the viscosities η does *not* modify the law of relaxation (42) as one considers only the lowest order in ω

3.3. Case where the wavefronts are perpendicular to the layers

Let us examine now the particular case $q_x = 0$. Then the frequencies ω_0 and ω_1 defined by equation (40) vanish, and (in the approximation without viscous tensions) one is led to equation (39) with a double root $\omega = 0$ plus a simple root $\omega \neq 0$. We are going to discuss separately the meaning of these three roots:

(a) One of the roots $\omega \simeq 0$ corresponds to a mode of *pure undulation*^{6, 7} as shown in figure 3. In order to determine a more accurate value of ω we must include the terms of curvature occurring in the elastic energy (eq. 6) and also the viscous tensions. We obtain then

$$-i\omega_{\text{und}} = \frac{Kq_x^2}{\eta_M} \quad (49)$$

In this mode $\epsilon_3 \simeq 0$ (the lipid concentration is not modulated). The mode of undulation must make an important contribution to the scattering of light⁶. In practice it is often masked by *static* undulations existing in the material and mainly due to the irregularities of their limiting surface^{8, 23}.

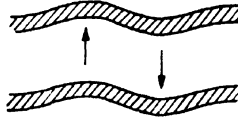


Figure 3 Pure undulation mode: the distance between layers and concentration in lipid are not modulated.

(b) The second root $\omega \simeq 0$ is associated with *simple shearing* (v_x varying with x) analogous to the transversal mode of isotropic fluids. Here also to calculate correctly the relation of dispersion we must take into consideration the viscous tensions: the result being the following:

$$-i\omega_{\text{shear}} = \frac{\eta_M q_x^2}{\rho} \quad (50)$$

This mode occurs at a higher frequency than the previous one and is probably difficult to observe in *light scattering*.

(c) The third root which appears directly while making $\omega_0 = \omega_1 = 0$ in equation (39) describes the pure mode of *slip* in figure 2. Here the total velocity \mathbf{v} vanishes, but the relative velocity of the lipid \mathbf{v}_L is not equal to zero. The dispersion relation is

$$-i\omega_{\text{slip}} = \mu D_{33}^0 q_x^2 \quad (51)$$

Let us note that (51) differs from (42): this special behaviour of the modes $q_x = 0$ is a constant property of lamellar structures. The frequencies of slip and of undulation are probably comparable.

From an experimental point of view the mode (51) ought to have an intensity comparable to that of Brillouin doublet in oil — that is to say, much weaker than the intensity due to a mode of a pure undulation. It is in principle possible to eliminate the latter by a suitable selection of polarisation⁶⁻⁸ but it is not certain that this precaution will be sufficient. It is, therefore, preferable to study the mode of slip by utilizing *oblique* wave vectors \mathbf{q} : the slip must then give a Rayleigh scattering well separated in frequency from the second sound (figure 4).

After the case $q_x = 0$ we ought to discuss the other special case $q_x = 0$. But the behaviour for $q_x = 0$ is controlled by the *permeation* process⁷. This seems difficult to control in a phase L_a : the migration of molecules through the layers will always be facilitated by defects in the structure (dislocations, focal conics,). For this reason the modes $q_x = 0$ do not deserve special attention at the moment.

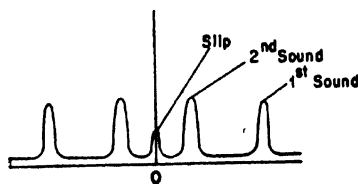


Figure 4 Spectrum of inelastic scattering of light from the L_a phase with the scattering wave vector \mathbf{q} oblique with respect to the layers. The central Rayleigh component would be caused mainly by slip.

4. The water-rich phases

As explained in the introduction, the case of lamellar systems L_a with a large water thickness h_B is difficult to study experimentally, but interesting theoretically:

- (a) the lipid layers are only weakly coupled, hence the elastic parameters will be much smaller than those obtained for thermotropic smectics.
- (b) the dominant interactions are more or less independent of the details of the molecular structure.
- (c) the mechanical behaviour of water is (probably) well described by the viscosity η_B of bulk water.

Therefore, we are going now to concentrate on the limit of large h_B , and try to connect the macroscopic coefficients introduced in section 2 to some microscopic parameters.

4.1. Energies of interaction and static elasticity

We are going to limit ourselves to the case of charged lipids to which *pure* water has been added (no salt dissolved). Let us first consider

where h_E is large. The energy of the electrostatic repulsion between layers has been analysed long ago⁵: for large h_E it takes a form totally independent from the charge density (due to the polar heads on one interface). For two opposite lipid layers one gets (per polar head)

$$F_{e1} = \frac{QA}{h_E} \sim \frac{QA}{d} \quad (52)$$

$$Q = \frac{\pi D}{4} \left(\frac{k_B T}{e} \right)^2 \quad (53)$$

where A is the surface per polar head, D the dielectric constant of pure water and e the charge of the counter-ions. Instead of the thickness d of a layer ($d = h_E + h_L \sim h_E$) it is sometimes convenient to take into consideration the total concentration in lipid c (molecules/cm³). Since each lipid layer has two surfaces one can write

$$c A d = 2 \quad (54)$$

and for the electrostatic energy

$$F_{e1} = \frac{1}{2} Q c A^2 \quad (55)$$

The Van der Waals attractions between layers give a contribution (per head) of the following form¹⁶:

$$F_{vw} = \frac{-MA}{12\pi d^2} = -\frac{M}{48\pi} \frac{n^2}{A} \quad (56)$$

The quantity M has the dimensions of energy. When d is very small compared to the ultraviolet wavelengths of absorption of the material, M is independent of d . For greater values of d , M decreases according to a complex law described in ref.¹⁶. A typical value of M is 10^{-14} ergs for $d = 100$ Å.

- Finally, as Parsegian⁵ has noted very early, one must include the interfacial energy lipid-water. In order to discuss it let us first define a surface A_0 per polar head which is the equilibrium surface for a double lipid layer immersed in a very great thickness of water ($d \rightarrow \infty$). This surface is realized in a Mueller membrane¹⁷. For the values of d which are of interest to us the surface A will be slightly different from A_0 . It is then correct to write the *interfacial* energy under the simplified form (per polar head)

$$F_{int} = \text{constant} + \frac{1}{2} \chi (A - A_0)^2 \quad (57)$$

Here χ is a coefficient of compressibility (of the order of 10^{16} CGS). The form (57) ensures that $A \rightarrow A_0$ in equilibrium whereas the other energies (F_{e1} and F_{vw}) are negligible ($d \rightarrow \infty$).

While minimising $F_{e1} + F_{vw} + F_{int}$ for a concentration c well defined and fixed, one can calculate the surface of the equilibrium $A_{eq}(b)$. The

resulting law is usually complicated, but it is simplified within the limit for small c (d large) because when d increases the Van der Waals interactions are decreasing much quicker, than the electrostatic interactions. Therefore, one gets

$$A_{eq} = \frac{A_0}{1 + QC/\chi} \quad (58)$$

This simple law gives a reasonable fit to the classical measurements by Skoulios¹ on soaps (for which however the thickness h_E is not very great.)

We are now going to study the fluctuations around the equilibrium value (58) and around the average thickness d , to calculate the *isothermal* rigidities D_{22} , D_{23} , D_{33} defined in analogy with the equation (23). For that, we have to relate the variables A and d to the microscopic dilatations δ and γ

$$\left. \begin{aligned} \delta &= \frac{A - A_{eq}}{A_{eq}} \\ \gamma &= \frac{d - d_{eq}}{d_{eq}} \end{aligned} \right\} \quad (59)$$

After two differentiations of the form $F_{el} + F_{vw} + F_{int}$, we obtain the following equations :

(a) For the coefficient of 'vertical rigidity' of the layers

$$D_{22} = -\frac{12Q}{d^2} - \frac{4Q}{d^2} \frac{A_{eq} - A_0}{A_{eq}} - \frac{M}{\pi d^3} \quad (60)$$

$$D_{22} \cong -\frac{12Q}{d^2} \quad (d \text{ large}) \quad (61)$$

This corresponds to values $D_{22} \sim 10^5$ CGS for $d = 100 \text{ \AA}$.

(b) For the coefficient of 'horizontal elasticity'

$$D_{33} = \chi c A_0^2 \quad (62)$$

Typically $D_{33} \sim 10^7$ CGS.

(c) For the cross coefficient

$$D_{23} = \frac{2Q}{d^2} \left(1 + \frac{A_0}{A_{eq}} \right) \sim \frac{4Q}{d^2} \quad (63)$$

$$D_{23} \sim \frac{1}{2} D_{22} \quad (64)$$

Finally, we have to estimate the coefficient of the *energy of curvature* defined by (7). This term is due mainly to the lipid regions.

One can therefore, write

$$K = k \frac{1}{d}$$

in which k is a characteristic coefficient for the energy of distortion in an isolated double layer. This coefficient has been discussed recently by Helfrich¹⁸ in connection with the elastic properties of vesicles. He estimates $k \sim 5 \cdot 10^{-13}$ ergs.

Finally, from these order of values we can try to draw a few conclusions regarding parameter B (defined by eq. 24) and the characteristic length $\lambda = (B/K)^{\frac{1}{2}}$. These two parameters are those which control the whole static elasticity (refer equation 1). They could be measured by experiments of the type described in reference⁸. Our estimate (very approximate), for $d = 100 \text{ \AA}$, is $\bar{B} \sim 10^5$ CGS and $\lambda \sim 100 \text{ \AA}$. If we ignore the difference between adiabatic coefficients and isothermal coefficients this leads us to second sound velocities (eq. 41) on the order of 10 m/sec.

4.2. Coefficients of friction

The most interesting factor here is the coefficient of *slip* μ . One can obtain it simply by examining a case of uniform slip where water flows parallel to the lipid layers (figure 2b). It is important to note that there can be no velocity within the lipid region: 'tails' cannot have a velocity different from the 'heads' and the 'heads' on the two sides of a lipid layer have the same velocity for the mode under consideration.

Let us use a reference frame where the lipid layers are at rest ($v_L = 0$). The profile of the velocity in the aqueous region has the Poiseuille form:

$$v(z) = -a(z^2 - \frac{1}{4} h_E^2) \quad (65)$$

for which we have taken the origin of all the z 's at the middle plane of the aqueous region. The constant in equation (65) ensures that $v = v_L = 0$ at the lipid-water interface ($z = \pm h_E/2$). The average water velocity associated with the profile (65) is

$$v_E = \frac{1}{h_E} \int_{-h_E/2}^{h_E/2} dz v(z) = \frac{a h_E^2}{6} \quad (66)$$

The hydrodynamic velocity v is the weighted average

$$v = \frac{h_E \rho_E v_E + h_L \rho_L v_L}{h_E \rho_E + h_L \rho_L} \quad (67)$$

where ρ_E and ρ_L are the density in the two phases. Here, since $v_L = 0$, we have

$$v = \frac{a \rho_E h_E^3}{\rho_E h_E + \rho_L h_L} \quad (68)$$

and the equation which defines a as a function of v . Besides the force per cm^2 on an lipid-water interface is

$$\eta_E \left. \frac{\partial v}{\partial z} \right|_{z=h_E/2} = -\eta_E a h_E \quad (69)$$

The force on a lipid layer is twice as large (because there are two sides) and the force per cm^3 is :

$$f = \frac{-2a \eta_E h_E}{d} \quad (70)$$

We introduce in equation (70) the value of a , which has been inferred from (68) and we compare the result with the definition of μ (eq. 22) :

$$\mu f = v_L - v = -v \quad (71)$$

The result is

$$\mu = \frac{1}{12} \frac{\rho_E h_E}{\rho_E h_E + \rho_L h_L} \frac{h_E d}{\eta_E} \quad (72)$$

In the limit $h_E \gg h_L$ this reduces to $\mu = \frac{d^2}{12 \eta_E}$

In view of the difficulty of the problem we have not attempted a systematic study of the macroscopic viscosities η_v , η_T , η_M as functions of the microscopic parameters. However, one can think that the coefficient η_T must contain an important contribution due to the lipid fraction : η_T is associated to distortions for which v_x , for instance, varies along y ; these distortions are also involved in the surface viscosities of a monomolecular film¹⁹. One expects, therefore, a coefficient η_T of the following type

$$\eta_T = \frac{h_L \eta_L + h_E \eta_E}{d} \quad (73)$$

in which η_L is a high viscosity. As for the coefficient η_M , which is related to a relative slip of successive layers, one is tempted to infer it from an equation of the following form :

$$\frac{d}{\eta_M} = \eta_E \frac{h_E}{\eta_E} + \frac{h_L}{\tilde{\eta}_L} \quad (74)$$

in which $\tilde{\eta}_L$ is another viscosity of the lipid medium associated to a relative slip of the two halves of the hydrophobic layer and is probably, rather large. One would get then

$$\eta_M = \eta_E \frac{d}{h_E} \simeq \eta_E \quad (75)$$

Finally the viscosity η_v probably involves complex processes (connected perhaps to the change of thickness of the lipid double layer when its surface per polar head changes) and we are not able to make predictions on η_v .

It is important to note finally that the components of the viscosities which are associated with the lipid (for instance $\tilde{\eta}_L$ and η_L in the above discussion probably show a *strong dependence on frequencies*: the lipid has long relaxation times. Some of these relaxation times (going up to 10^{-5} sec) are already known through nuclear relaxation²⁰: it would be very interesting to compare this information with mechanical measurements (second sound and first sound) determining $\eta(\omega)$.

5. Conclusions

The observations of the collective modes in a lamellar phase L_α could give us some information regarding the interactions between layers and also on specific dissipative processes of the lipid region.

The second sound may be difficult to observe because of the viscosities which are introduced by the lipidic component: In order to have narrow lines, one should, in principle, utilise very small values of q , that is to say, develop a special technique of Brillouin scattering with small angles and low frequencies. However it is also possible that the classical Brillouin measurements (high $\omega \sim 10^{10} \text{ sec}^{-1}$) may give an acceptable spectrum if, for these high frequencies, the lipid behaves just like an elastic solid (the viscosity $\eta_L(\omega)$ becoming purely imaginary).

The mode of slip could be detected in Rayleigh scattering with oblique wave vectors. (This is advantageous since one does not need a very well oriented specimen). Incidentally this mode must exist not only in a lamellar phase, but also in hexagonal phases.

One should insist on the fact that our discussion of the orders of magnitude in Section 4 is very brief. For instance, we have estimated only the isothermal elastic coefficients and not the adiabatic coefficients which are taken into consideration for the second sound. We have poor knowledge of the friction coefficients except (fortunately) for the parameter μ . We have also ignored all the phenomena which appear outside the macroscopic limit $q \rightarrow 0$, $\omega \rightarrow 0$. In fact, at least for large water thickness, it is possible to extend the analysis to $q \sim 1/d$. If one assumes that the predominant friction is due to the water (rather than to the lipid) one finds²¹ the so-called 'peristaltic' modes already discussed by several authors in connection with thick soap films²².

References

- 1 SKOULIOS A *Adv. Coll. Int. Sci.* **1** 79 (1967); LUZZATI V, MUSTACCHI M, SKOULIOS A and HUSSON F *Acta Cryst.* **13** 660 (1960)
For a general review including biological lipids, see, LUZZATI V, Biological Membranes, E. and D. Chapman, Acad. Press (1968)
- 2 TARDIEU A *These d'Orsay* (1972); TARDIEU A *J. Mol. Biol.* **75** 711-733 (1973)
- 3 SACKMANN H and DEMUS D *Mol. Cryst.* **2** 81 (1966)
- 4 GULIK-KRZYWICKI T, TARDIEU A and LUZZATI V *Mol. Cryst. Liquid Cryst.* **8** 285 (1969)
- 5 PARSEGAN V A *Sci.* **156** 939 (1969); PARSEGAN V A *Trans. Far. Soc.* **62** 848 (1966); LANGMUIR I J. *Chem. Phys.* **6** 873 (1938); VERWEY E J J. *Theor. Overbook* The stability of lyophobic colloids (Elsevier, Amsterdam 1948); LANDAU L Collected papers, Pergamon Press)
- 6 DE GENNES P G *J. Phys. (Paris)* **30** C4 65 (1969)
- 7 MARTIN P C, PARODI O and PERSHAN P S *Phys. Rev. A* **6** 2401 (1972)
- 8 DURAND G *C.R.A.S.* **275B** 629 (1972); RIBOTTA R, DURAND G and LITSTER J D *Solid State Commun.* **12** 27 (1973); CLARK N A, PERSHAN P S *Phys. Rev. Lett.* **30** 3 (1973)
- 9 DE GENNES P G *C.R.A.S.* **275B** 939 (1972); BIDAUX R, BOCCARA N and SARMA G *J. de Phys. (Paris)* **34** 661 (1973)
- 10 DELAYE M, RIBOTTA R and DURAND G *Phys. Lett.* **44A** 139 (1973)
- 11 DE GENNES P G *Solid State Commun.* **10** 753 (1972)
- 12 LIAO Y, CLARK N and PERSHAN P S *Phys. Rev. Lett.* **30** 639 (1973)
- 13 CANDAU S *Private Commun.*
- 14 HELFRICH W *Phys. Rev. Lett.* **23** 372 (1969)
- 15 DE GENNES P G (Liquid Crystals), *Oxford* (to be published)
- 16 NINHAM B W and PARSEGAN V A *J. Chem. Phys.* **53** 9 (1970)
- 17 MUELLER P J. *Theor. Biol.* **4** 268 (1963); *Nature, Lond.* **194** 979 (1962a)
- 18 HELFRICH W *Z. Naturforsch* **28c** 693 (1973)
- 19 GAINES G L *Interscience, New York* (1966); JOLY M J. *Chem. Phys.* **44** (1947)
- 20 CHARVOLIN J and RIGNY P J. *Chem. Phys.* **58** 3999 (1973)
- 21 BROCHARD F *These d'Orsay* (1974)
- 22 VRIJ A *J. Col. Sci.* **19** 1 (1964)
- 23 A temporal analysis of the scattered light has enabled recently to separate the thermal fluctuations from the strong static signal, and to study the dynamic mode of undulation (G. Durand - Proceedings of this Conference).

DISCUSSION

(The oral presentation by Dr de Gennes included a more general coverage of the smectic state, to which the following discussion refers).

Janik: Don't you think that the Apollonius effect could be studied by the positron annihilation method?

de Gennes: I know very little about positron annihilation in insulators. For smectics A or for nematics, an interesting situation would occur if the annihilation took place preferentially on *defects* of the structure (disclinations, dislocations, focal conics).

Schnur: Could precise specific heat or volume measurements be an appropriate technique to determine the reality of the model of the texture in smectic A you have described?

de Gennes : I fear that the volume fraction which is strongly distorted is too small to give an observable effect.

Schnur : Is ΔV always a scalar when doing dilatometric experiments on smectic phases ?

de Gennes : ΔV probably scales like the energy in most transitions ; the dilation coefficient and the specific heat should have similar singularities.

Rustichelli : I think that x-ray diffraction, although it is not able to confirm the Apollonius solution, could be used to exclude the grain boundary solution. Indeed this solution should produce two peaks differing by $\pi/2$ angle when the sample is rocked in a monochromatic beam.

de Gennes : We do not know the density of grain boundaries. Scattering of x-rays by dislocations in smectics seems to be a much more complicated problem than scattering of x-rays by dislocations in solids. We must first have the optical analogue of x-ray topography. By light beams one should be able, if you have a few dislocations, to see them as curved wedges. It comes close in spirit to your Borrmann effect.*

I am worried about all small angle scattering studies. There are too many effects to be considered.

* Nityananda R, Kini U D, Chandrasekhar S and Suresh K A, this conference.

Rayleigh scattering of light in smectic A liquid crystals*

G DURAND

Laboratoire de Physique des Solides†, Université Paris-Sud,
Centre d'Orsay 91405 - Orsay (France)

* Work supported by "Délégation Générale à la Recherche Scientifique
et Technique" under contract 68/01/194 and 73/7/1729

† Associated with C.N.R.S.

Abstract. Recent light scattering experiments in smectic A in the homeotropic geometry are reviewed. As predicted by de Gennes, the dominating scattering process is the layer undulation. This undulation can be static and reveals the defects of the plates which sandwich the sample. It can be dynamical, from thermal excitation of the mode predicted by de Gennes; it is then quenched by the plates for low wave vector. These experiments give an accurate way to measure the penetration length of de Gennes and the diffusivity of orientation in smectic A materials.

Introduction

Nematic liquid crystals give rise to an intense Rayleigh scattering. Observed long ago by Chatelain¹, it has been explained by de Gennes² in terms of thermally excited angular fluctuations of the "director" \mathbf{n} , the local mean molecular orientation. The Orsay group has predicted³ and observed⁴ the dynamics of these fluctuations. Since then, many Rayleigh scattering experiments have allowed interesting measurements in nematics, from for instance the stabilizing effects of external fields⁵, to the critical divergence of the twist elastic constant close to a quasi second order smectic A to nematic phase transition⁶. Smectic materials are also expected to give rise to a strong Rayleigh scattering, at least because they are made of anisotropic molecules; their angular fluctuations are as strongly coupled to light waves as in nematics. De Gennes has shown⁷, however, that the existence of spatial correlation in smectics (the "layered" structure) forbids the thermally excited angular fluctuations of the director to have a large amplitude, except for the "layer undulation" mode, of wave vector \mathbf{q} parallel to the layers. In fact, for usual samples contained between glass plates, light scattering has first been observed from static wall induced layers, undulations^{8,9} observable because of the anomalously large¹⁰ penetration length of these distortions; the thermally excited dynamical undulation mode has only been observed¹¹ very recently. In this paper, we review the Rayleigh scattering experiments on smectic A

performed at Orsay; we explain the quenching effect of the walls; we show how the spatio-temporal analysis of the scattering allows the measurement of the penetration length of de Gennes and of the angular diffusivity of the director in a smectic A.

1. The wall quenching effect

The glass plates boundaries limiting an unusual smectic A sample of homeotropic orientation can have two different effects on the structure of the material. First, when they are not exactly planar, they force a layer static undulation to adjust to their irregularities, at least for small enough amplitude and wave vector (the layer normal displacement u should be smaller than a layer thickness a , with $qu < 1$). Let us call \bar{B} the elastic constant associated with layer compression at constant temperature, as defined in ref. 7, and K the Frank splay elastic constant of the smectic material. A small amplitude plate undulation will be damped¹⁰ normally to the layer on a length L defined by $q^2 \lambda L = 1$, where λ is the penetration length of de Gennes $\lambda = (K/B)^{1/2}$, of the order of a . λ is much larger than in nematics, where it is defined as: $q \lambda \sim 1$. The large multiplying factor $(q \lambda)^{-1}$ comes from the fact that, to relax the splay distortion imposed by the undulating plate (weak curvature elasticity), one has to allow a layer compression or dilation (strong normal elasticity); as the associated distortion energies must be comparable, the undulation damping takes an unusually long distance to settle. Of course, for sample of finite thickness d , one can immediately classify the plate undulations by their wave vector, introducing the critical value q_c defined as $q_c^2 \lambda d/\pi = 1$. When q is smaller than q_c , static undulations enter all the material; on the other hand, they remain localized close to the plates when q is larger than q_c .

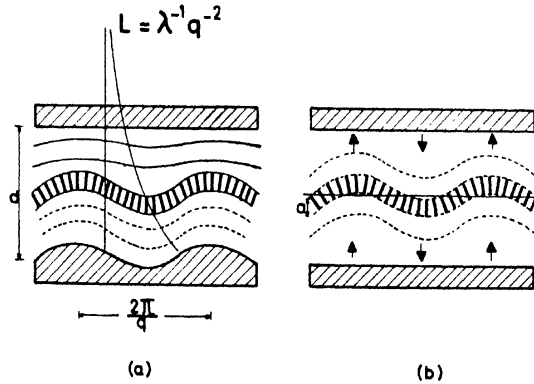


Figure 1 A homeotropic smectic A sample, between two glass plates. In (a) an imperfect plate imposes a static undulation of the smectic layers ($L > d$). In (b) a thermal undulation of the layers implies a compression (or dilation) of the boundaries layers and is quenched by the plates for low q_{\perp} .

Perfectly planar plates have a more subtle effect on the structure. They play more or less the same role as a stabilizing (magnetic) field, by quenching the angular fluctuations of the director of wave vector q smaller than q_c . To understand this effect, we write, as in ref. 7, the free energy density F associated with a layer displacement $u(z)$, where z is the normal to the layers,

$$\begin{aligned} F &= \frac{1}{2} \left[\bar{B} \left(\frac{\partial u}{\partial z} \right)^2 + K \left(\frac{\partial^2 u}{\partial x^2} \right)^2 \right] \\ &= \frac{1}{2} K \left[\lambda^{-2} \left(\frac{\partial u}{\partial z} \right)^2 + \left(\frac{\partial^2 u}{\partial x^2} \right)^2 \right] \end{aligned}$$

here $\partial^2 u / \partial x^2$ stands for the divergence $\partial / \partial x (\theta)$, with $\theta = \partial u / \partial x$, the tilt angle of the layer, supposed to be in the x, z plane. The undulation modes can be defined by their wave vector q , (q_z, q_\perp) with the boundary condition $q_z = \pm l(\pi/d)$ (l is an integer from 1 to ∞). Expressed in terms of u , F presents a minimum at $q_\perp = 0$, as would a nematic. However, light scattering intensity I is proportional to the mean square of the angular fluctuation $\theta = q_\perp u$. F can be written now as

$$\begin{aligned} F &= \frac{1}{2} K \left[l^2 \left(\frac{\pi}{d\lambda} \right)^2 \frac{1}{q_\perp^2} + q_\perp^2 \right] \theta^2 \\ &= \frac{1}{2} K \left(l^2 q_c^4 / q_\perp^2 + q_\perp^2 \right) \theta^2 \end{aligned}$$

the thermal average of θ^2 is now

$$\langle \theta^2 \rangle = \frac{k_B T}{K (q_\perp^2 + l^2 q_c^4 / q_\perp^2)} \sim I$$

(k_B is the Boltzman constant and T the absolute temperature).

- The light scattering intensity I is maximum for $q_\perp = l^{1/2} q_c$. For the fundamental mode ($l = 1$), the maximum appears at $q_\perp = q_c$. Physically, this maximum is easy to understand; for large q_\perp , θ^2 decreases as q_\perp^{-2} as it would in a nematic material; the undulation wave vector is almost parallel to the layers and does not imply layer compression (L is much smaller than d). For small q , the nematic-like contribution vanishes, but a given θ implies a large layer compression (L is now much larger than d), diverging at $q_\perp = 0$.

We can make an estimate of the damping time τ of the layer undulation in a perfect material. As long as the angular fluctuations of the director remain purely damped (see ref. 7 and 12), by analogy with the splay mode of nematics³, one can write: $\frac{1}{\tau} = \frac{K}{\eta} (q_\perp^2 + l^2 q_c^4 / q_\perp^2)$ where η is an effective splay viscosity for the smectic. Of course, in the presence of boundaries, η should be q dependent to take into account the different friction between the shear flow in the bulk and the backflow

close to the boundaries, and also the permeation. We assume that these effects are negligible close to (and of course above) q_c . Another effect could be observable, in principle, in the presence of boundaries. q_z is fixed to π/d and the undulation mode could merge, for low q_\perp , into a propagative "second sound" mode (see ref. 7). To estimate this effect, we compare the transit time t of second sound across the sample, to τ . The second sound velocity⁷ is of the order $v \sim \theta (\bar{B}/\rho)^{1/2}$ where ρ is the specific mass of the liquid crystal and $\theta \sim q_z/q = \frac{l\pi}{dq}$; writing $t > \tau$ gives

the condition $(\lambda/d)^2 < \frac{K\rho}{\eta^2}$ —independent of l , for the purely damped regime;

$\frac{K\rho}{\eta^2} \equiv \frac{K}{\eta} / \frac{\eta}{\rho}$ is the usual ratio of the diffusivity of orientation K/η to the diffusivity of vorticity η/ρ , of the order of 10^{-4} . One sees that for all samples of reasonable thickness ($d > 2000 \text{ \AA}$), the pure damping condition is always fulfilled. In this naive approximation (no permeation, η independent of q), one immediately sees that the damping rate $1/\tau$ should be maximum for the same value of q_\perp ($q_\perp = l^{1/2} q_c$) which maximizes I .

These properties of the smectic texture of finite thickness d , around $q_\perp = q_c$, have of course a wider application than light scattering. For instance, q_c is known to be the wave vector of the lowest threshold buckling instability of smectic A under dilation, or under a destabilizing field. This is easy to understand. In these phenomena the anisotropy of the smectic material is involved though the coupling energy of interaction with the applied field (say H) of the form $\frac{1}{2} \chi_a H^2 \theta^2$, where χ_a is the anisotropy of susceptibility, and θ the angle between \mathbf{n} and \mathbf{H} . To find the threshold for a structure distortion, one has to express F in term of θ^2 ; as explained previously, $q = q_c$ minimizes F , and corresponds to the lowest threshold.

2. Experimental results

We consider always a smectic A in an homeotropic geometry. The eigenmodes of propagation in such a strong uniaxial material, are the ordinary and extraordinary waves, of wave vector \mathbf{k}_o and \mathbf{k}_e . As explained in ref. 8, the scattered light (\mathbf{k}') is concentrated on cones of axis \mathbf{n} , when one considers only momentum transfer $\mathbf{q} = \mathbf{k}_L - \mathbf{k}'$ parallel to the layers (figure 2). (Here \mathbf{k}_L is the laser illuminating wave vector ordinary or extraordinary polarized). These cones correspond to $|\mathbf{k}_o'| = \text{const.}$ or $|\mathbf{k}_e'| = \text{const.}$ In fact, as q_z can be $l \frac{\pi}{d}$, one should find some scattering on adjacent coaxial cones, but its intensity is expected to decrease rapidly.

The first observation⁸ of Rayleigh scattering on smectic A showed the existence of an intense conical scattering which, analysed through a light

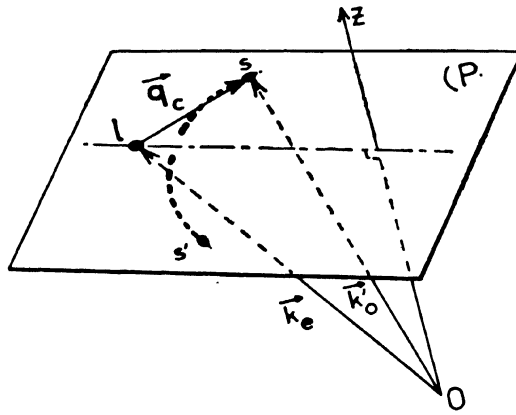


Figure 2 The conical geometry for Rayleigh scattering in a smectic A, when the momentum transfer \mathbf{q} is parallel to the layers. The cones correspond to $|\mathbf{k}'_0| = \text{const.}$, where \mathbf{k}'_0 is the (ordinary) scattered light wave vector. P is a plane parallel to the layers. The sample is placed at point O. l is the trace of the (extraordinary) incoming laser light. s and s' are the points which illuminate under dilation (ls is proportional to q_c). They are located close to the maximum q extension of the static signal from glass plate defects.

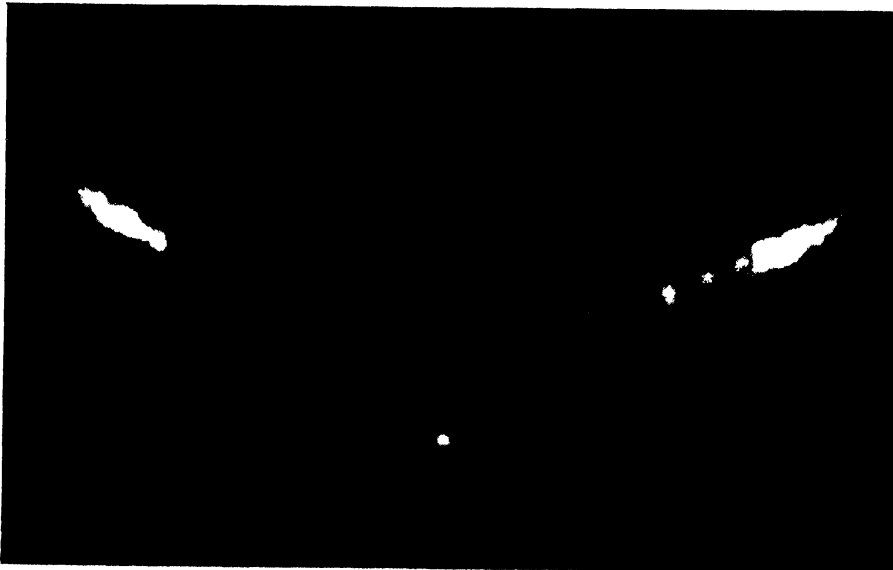


Figure 3 A picture of the screen P showing the 2 bright spots on the scattering cone of figure 2. This indicates a transient layer undulation at $q = q_c$, when the sample is under dilation (by courtesy of R. Ribotta).

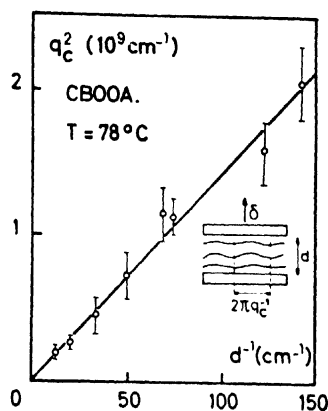


Figure 4 Linear dependence of q_c^2 versus the inverse thickness d^{-1} of a sample of CBOOA. The slope of the line gives $\lambda = 22 \pm 3 \text{ \AA}$.

beating spectrometer, was found to be static diffraction of light. From the aperture of the cone, one deduces immediately the ratio of the indices n_e and n_o . The angular dependence of the scattered intensity on the cone, apart from a trivial extinction in the plane of symmetry (figure 2), showed a decrease for large q_{\perp} . Samples of smaller thickness d ($100 \mu < d < 800 \mu$) showed a larger q_{\perp} extension of the static signal. This observation was consistent with a scattering from layer undulation, induced by irregular plates. For $q_{\perp} < q_c$, the perturbation of the layers extends in all the bulk ($L > d$) and gives a large scattered intensity.

* These observations became quantitative when a mechanical dilation was applied on the sample¹³ (the first one was in fact an uncontrolled disturbance of the sample; the dilation was later controlled by piezoelectric ceramics). In that case, at about the maximum extension of the static signal, one sees the transient appearance of two bright spots (figure 3). These spots are evidence of a regular undulation of the texture, visible under a microscope, of definite wave vector length q_c but of random orientation. In fact, a plot of q_c^2 versus d^{-1} gave a linear dependence (figure 4) as expected, ($q_c^2 \lambda d = \pi$) with the first accurate determination of λ ($\lambda = 22 \pm 3 \text{ \AA}$ in CBOOA at 78°C). The threshold of this instability (z dilation expected to be $2\pi\lambda$) and its dynamical behavior are now under extensive study.

The last point was to observe the thermally excited undulation of layers, as predicted by de Gennes. This required glass plates of very good surface quality. Static undulations are not too serious *optically*: one can always observe a fluctuating signal with a light beat spectrometer, using the static scattered light as a local oscillator ("heterodyne" regime);

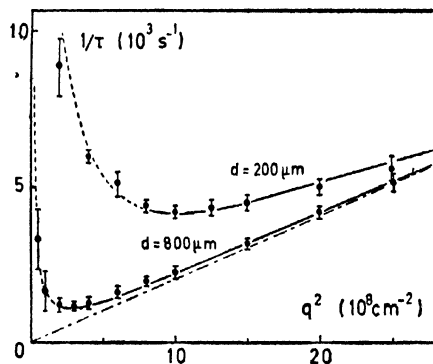


Figure 5 Damping rate of the thermally excited undulation mode of the smectic layers. For large wave vectors ($q_{\perp} > q_c$), the behaviour is the one of an unbounded sample, very similar to the one of a nematic. For short wave vectors ($q < q_c$), the compression energy of smectic layers gives rise to strong restoring forces and the damping rate increases strongly. The damping is minimum for $q_{\perp} = q_c$. The solid curves are the predicted hyperbolas (see text).

but static undulations can *mechanically* quench the thermal undulation; roughly speaking, they are equivalent to a tilt of \mathbf{q} , no more parallel to the layers; the increase of F results in a smaller amplitude for the thermal fluctuations (of constant energy $\frac{1}{2} k_B T$). Using $\lambda/40$ plates, the static conical scattering was found to be weak; the time dependence analysis of the scattered light on the cone with the right polarization showed an exponential decaying correlation function characteristic of a dynamical undulation. The signal was almost purely "heterodyne" like, which gave an unambiguous determination of τ . An angular dependence of τ , normal to the scattering cone, showed the expected maximum corresponding to the fundamental mode $l = 1$.

It was now possible to measure τ (max) for different q_{\perp} , following the cone. The damping rate τ^{-1} showed the expected hyperbolic behaviour versus q_{\perp}^2 (see figure 5), with a minimum at $q_{\perp} = q_c$. This point was checked by comparing $\tau^{-1}(q_c)$ for different thickness samples. λ can be derived from this experiment and was found to agree reasonably with previous determination ($\lambda = 14 \text{ \AA} \pm 1$ at $T = 75^\circ \text{C}$ in CBOOA). It was not possible to check an eventual q dependence of η or the onset of permeation on the damping, the results up to now remaining too inaccurate for small q_{\perp} , where the intensity of the fluctuating signal vanishes. To avoid this difficulty, one should measure I directly. Unfortunately, this is very difficult to do accurately in the strong "heterodyne" regime.

In the limit of large q_{\perp} , the observed damping time τ^{-1} becomes a linear function of $(q_{\perp})^2$. From the slope of this straight line, one derives the diffusivity of orientation K/η , which has a nematic-like value ($K/\eta = 2.0 \pm 0.2 \cdot 10^{-6}$ cgs for CBOOA at $T = 75^\circ \text{C}$).

The good agreement between the model and the experimental results may be surprising, in view of the simplifying assumptions made. In particular, it seems that defects in the sample are not too important in the damping of undulations. This is likely due to the small mobility of the defects (dislocations), limited by permeation. It could be more important with very thick samples.

3. Conclusion

Light scattering from homeotropic glass plate sandwiched smectic A has been observed. For low surface quality boundaries, the scattering is static. It can be explained by the unusual attenuation length of undulations induced by the plates across the layers. With high surface quality plates, the dynamic thermally excited undulations of the layers predicted by de Gennes are observed. For large wave vectors, these undulations have a free space behavior, with a nematic like diffusivity of orientation. Decreasing their wave vector, their damping time presents a maximum for the wave vector q_c which minimizes the distortion free energy (expressed in terms of angular deflection of the director). q_c is also observed directly as being the buckling instability wave vector of the layers under dilation. All these independent measurements of q_c , currently under way on different smectic A samples, give a coherent value for λ ($\lambda \sim 20\text{\AA}$), the penetration length of de Gennes. All the observed boundaries effects are just a consequence of the highly anisotropic elasticity of smectic A materials, crystal like across the layers and liquid crystal-like in the layers. We are now beginning analogous experiments on unbounded thin films of smectic A.

Acknowledgements

The author would like to thank all the members of the Orsay Group for stimulating discussions and partial disclosure of their experimental results.

References

- 1 CHATELAIN P *Acta Crystallogr.* **4** 453 (1951)
- 2 DE GENNES P G *C.R. Acad. Sci. Paris* **266B** 15 (1968)
- 3 Orsay Group on Liquid Crystals *J. Chem. Phys.* **51** 876 (1969)
- 4 Orsay Liquid Crystal Group *Phys. Rev. Lett.* **22** 1361 (1969)
- 5 MARTINAND J L and DURAND G *Solid State Commun.* **10** 815 (1972)
- 6 DELAYE M, RIBOTTA R and DURAND G *Phys. Rev. Lett.* **31** 443 (1973)
- 7 DE GENNES P G *J. Physique colloq.* **30** C4 65 (1969)
- 8 RIBOTTA R, DURAND G and LITSTER J D *Solid State Commun.* **12** 27 (1973)
- 9 CLARK N and PERSHAN P S *Phys. Rev. Lett.* **30** (1973)
- 10 DURAND G *C.R. Acad. Sci. Paris* **275B** 629 (1972)
- 11 RIBOTTA R, SALIN D and DURAND G *Phys. Rev. Lett.* **32** 6 (1974)
- 12 MARTIN P C, PARODI O and PERSHAN P S *Phys. Rev. A* **6** 2401 (1972)
- 13 DELAYE M, RIBOTTA R and DURAND G *Phys. Lett.* **44A** 139 (1973)

DISCUSSION

Janik: If I remember correctly, there is also a component in Rayleigh scattering for which reorientations are responsible. How is this component separated from what you measure?

Durand: The 'Rayleigh wing' scattering intensity is weaker by a factor $(qa)^2$ where q is the momentum transfer and ' a ' a molecular length. Here $(qa)^2 \sim 10^{-6}$. The spectrum is larger by the same factor — the spectral density is then typically 10^{-12} smaller.

Bulkin: In your curve of $\frac{1}{\tau}$ vs. q^2 , what are the values of τ , and the approximate difference between the two curves shown?

Durand: The orientational diffusivity D is nematic like, with $D \sim 10^{-6}$ cgs.

Rustichelli: Did you perform the light scattering experiments under negative pressure also in some smectics B?

Durand: We are now doing Rayleigh scattering on smectic B, and trying to see if it is within our experimental capacity. We are not sure. It may be that smectic B is a solid-like material and the intensity is so low that we cannot see anything. It may be that in some smectics B you may have the de Gennes-Sarma structure.

The temperature dependence of the viscosities of a nematic*

FRITZ JÄHNIG†

Physique de la Matière condensée – Collège de France
11, place Marcelin-Berthelot 75231 Paris Cedex 05

* This work was supported by the Deutsche Forschungsgemeinschaft.

† On leave from the Physik-Department der Technischen Universität München, Germany.

Abstract. The temperature dependence of the viscosities of a nematic without a second order transition at lower temperatures is discussed in the first part. For the rotational viscosity γ_1 the experimental results yield an Arrhenius behaviour. The compressional viscosities are caused by an intramolecular relaxation process. For MBBA this process is proposed to originate in the flexibility of the hydrocarbon chain thereby fixing its temperature dependence. In the vicinity of the nematic-isotropic transition the relaxation of the nematic order parameter represents another slow relaxation process. Mean field theory seems to be sufficient to describe its contribution to the attenuation of sound. If, at lower temperatures, a second order transition to a smectic A phase exists the fluctuations of the smectic order parameter relax also slowly. Treating this transition in analogy to the λ -transition in He a divergence of certain viscosities is found proportional to $(T - T_{AN})^{-0.33}$.

Introduction

To discuss the temperature dependence of the viscosities of a nematic phase we separate the problem in two parts. In the first part, we treat a nematic which shows a first order transition at lower temperatures to a smectic or solid phase thus excluding an influence of the low temperature phase. As an example we always take MBBA. In the second part, we treat a nematic with a second order transition to a smectic A phase at lower temperatures. In this case pretransitional effects show up.

1. Nematic with a first order transition at lower temperatures

1.1 The incompressible system

Let us start recalling briefly the definition of the viscosities for an incompressible nematic. We use the Leslie¹ viscosities α_i defined by the relation between the dissipative stress tensor π'_{ij} and the forces $A_{ij} = \frac{1}{2} (\nabla_i v_j + \nabla_j v_i)$ and $N = (\partial n / \partial t) - \frac{1}{2} \text{rot } \mathbf{v} \times \mathbf{n}$, where \mathbf{v} is the velocity and \mathbf{n} the director,

$$\begin{aligned} \pi'_{ij} = & -\alpha_1 n_k n_l A_{kl} n_i n_j - \alpha_2 n_i N_j - \alpha_3 n_j N_i - \alpha_4 A_{ij} \\ & - \alpha_5 n_i n_k A_{kj} - \alpha_6 n_j n_k A_{ki}. \end{aligned} \quad (1.)$$

The Onsager - Parodi² relation

$$\alpha_2 + \alpha_3 = \alpha_6 - \alpha_5 \quad (2)$$

reduces the number of viscosities to 5. Usually two "rotational" viscosities are introduced

$$\left. \begin{aligned} \alpha_1 &= \alpha_3 - \alpha_2 \\ \gamma_2 &= \alpha_3 + \alpha_2. \end{aligned} \right\} \quad (3)$$

For simple shear flow experiments three different geometries are possible depending on the relative orientation of \mathbf{n}_0 (the preferred axis), \mathbf{v} , and the velocity gradient (figure 1). The corresponding viscosities are usually referred to as Miesowicz³ viscosities η_i^M .

The temperature dependence of the α_i 's was investigated theoretically by Imura and Okano⁴. They started by writing down the stress tensor π'_{ij} not in terms of the director n_i as in (1) but in terms of the nematic order parameter $Q_{ij} = S (n_i n_j - \frac{1}{3} \delta_{ij})$ and deduced the following relations, in lowest order of the temperature dependent magnitude S of the order parameter,

$$\begin{aligned} \alpha_1 (T) &\sim S^2 (T), \\ \alpha_{2,3,5,6}(T) &\sim S (T), \quad \gamma_{1,2}(T) \sim S (T), \\ \alpha_4 (T) &\sim \exp (U_{\eta_3^M}/kT). \end{aligned} \quad (4)$$

As α_4 is the viscosity of the isotropic phase it is independent of S in lowest order and has the well known Arrhenius behaviour with an activation energy $U_{\eta_3^M}$. These expressions explain qualitatively the experimental results^{5,6} for MBBA (figure 2). The viscosity η_1^M shows a

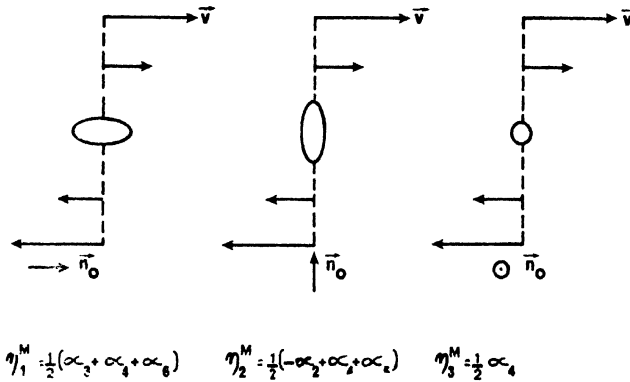


Figure 1 The definition of the Miesowicz viscosities.

marked contribution of the S dependent viscosities α_3 and α_6 . But if one plots this contribution, $\eta_3^M - \eta_1^M = -\frac{1}{2}(\alpha_3 - \alpha_6)$, divided by the experimental NMR values⁷ for $S(T)$, against temperature one finds no constant but rather an exponential behaviour indicating an Arrhenius factor also for other viscosities in (4).

This can more easily be seen from experiments⁸⁻¹⁰ which measure directly for example $\nu_1(T)$ (figure 3). Evaluating the results of Prost and Gasparoux⁸ obtained by the method of a slowly rotating magnetic field one gets for

$$\nu_1(T) \sim S(T) \exp(U_{\tau_1}/kT) \quad (5)$$

an activation energy $U_{\tau_1} = 11.5$ kcal/mole. For other nematics U_{τ_1} is approximately the same indicating a common relaxation process.

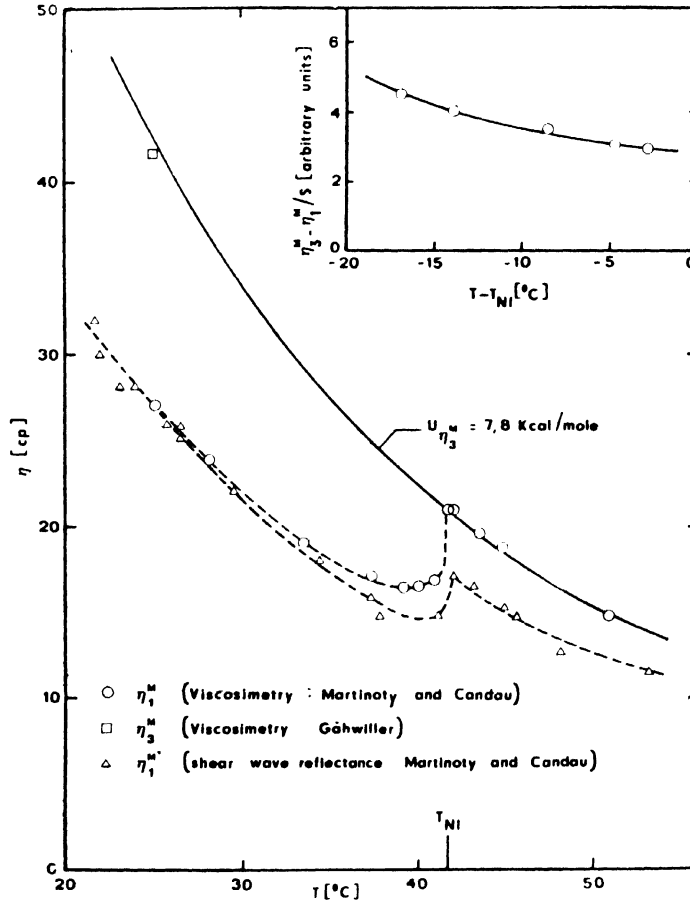


Figure 2 The temperature dependence of two Miesowicz viscosities for MBBA.*

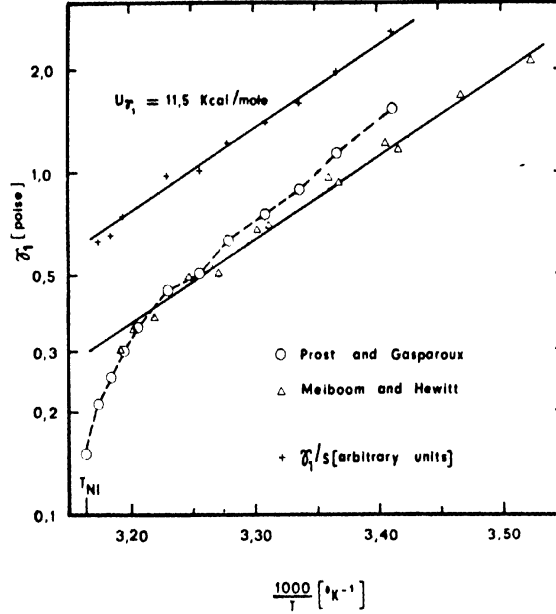


Figure 3 The temperature dependence of the rotational viscosity for MBBA.

For higher frequencies equations (4) and (5) have to be generalized in a way which will be discussed below for the compressible system. Another effect which will be treated in more detail below is the relaxation of the nematic order parameter in the vicinity of the nematic - isotropic phase transition¹¹. Its influence on the shear flow viscosities can be seen by comparing the low frequency viscosities measured by flow experiments with the high frequency viscosities measured with a shear wave reflectance method at 15 - 85 MHz (figure 2).

1.B The compressible system

The compressible nematic is described by two more viscosities¹². We are especially interested in the anisotropy of the compressional viscosities $\Delta\eta = \eta_{||} - \eta_{\perp}$, where parallel and perpendicular refer to the preferred axis n_0 . This quantity determines the anisotropy of the attenuation of sound

$$\Delta\alpha = \alpha_{||} - \alpha_{\perp} \sim \Delta\eta. \quad (6)$$

(These α 's should not be confused with Leslie's α_i).

Arguments like the ones of Imura and Okano⁴ yield

$$\Delta \eta (T) \sim S(T). \quad (7)$$

But the experimental results^{13, 14} for $\Delta \eta$ yield a strong frequency dependence of $\Delta \eta$ in the MHz region at room temperature indicating again an additional temperature dependence, of the type

$$\Delta \eta_i (\omega, T) \sim S(T) \frac{\tau_i (T)}{1 + (\omega \tau_i (T))^2} \quad (8)$$

$\omega = 2\pi f$ being the sound frequency and τ_i the relaxation time for an internal relaxation process,

$$\tau_i (T) = \tau_m \exp (U_\eta / kT) \quad (9)$$

where τ_m is a microscopic time. A fit of the frequency dependence of $\Delta \eta$ yields $\tau_i = 2.0 \cdot 10^{-8}$ sec. at room temperature¹⁵.

To predict the temperature dependence of $\Delta \eta$ we need U_η , i.e., a microscopic interpretation of the relaxation process. I proposed this process to originate in a common property of most nematics, the flexibility of the hydrocarbon chain¹⁶. The relaxation takes place between *trans* and *gauche* states. The chain of MBBA corresponds to the case of pentane, for which the activation energy was determined by ultrasonic measurements¹⁷ to be $U_\eta = 4.2$ kcal/mole and $\tau_m \approx 10^{-11}$ sec. These values yield at room temperature $\tau_i = 1.0 \cdot 10^{-8}$ sec, in good agreement with the above cited experimental value for MBBA.

Experiments on $\Delta \alpha$ do not show the temperature dependence of $\Delta \eta_i$ directly (figure 4) because of the influence of the order parameter relaxation mentioned above. Therefore we have two contributions

$$\Delta \eta = \Delta \eta_i + \Delta \eta_q \quad (10)$$

with

$$\Delta \eta_q (T) \sim C_q (T) \frac{\tau_q (T)}{1 + (\omega \tau_q (T))^2} \quad (11)$$

$C_q (T)$ being a coupling parameter. Subtraction of the theoretical values for $\Delta \eta_i (T)$ from the measured¹⁸ values of $\Delta \eta (T)$ yields the temperature dependence of the critical part. The best fit is

$$\Delta \eta_q (T) \sim |T - T_{NI}|^{-4/3} \quad (12)$$

This has to be compared with (11), under the experimental condition $\omega \tau_q \ll 1$,

$$\Delta \eta_q (T) \sim C_q (T) \tau_q (T) \quad (13)$$

The critical temperature dependence of τ_q was determined from light scattering¹⁹ as $\tau_q (T) \sim |T - T_{NI}|^{-4/3}$, which leads us to the conclusion that C_q has no critical temperature behaviour. The deviation of the critical exponent τ_q from of the mean field value 1 can be

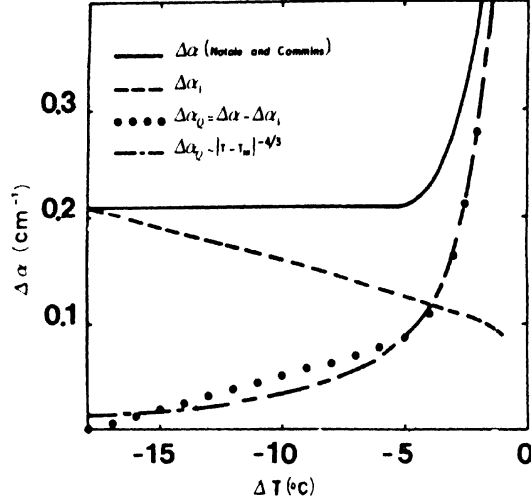


Figure The temperature dependence of the anisotropy of the ultrasonic attenuation, for $f = 3.5$ MHz.

accounted for by the noncritical temperature dependence of the average viscosity.

2. Nematic above the transition to a smectic A of second order

Above a smectic A – nematic phase transition of second order the fluctuations of the smectic order parameter give rise to pretransitional effects. The critical contribution to the Frank elastic constants has been calculated by de Gennes²⁰. The critical viscosities were treated recently by myself together with F. Brochard²¹. Using the framework of linear response theory and the fluctuation – dissipation theorem we found for the critical part of the viscosities for an incompressible nematic, in the low frequency limit,

$$\tilde{\alpha}_1 \sim \frac{q_s^2 T \tau_\Psi}{16 \pi \xi} \quad (14)$$

and

$$\tilde{\alpha}_1 \sim \tilde{\alpha}_3 \sim \tilde{\gamma}_2 = \tilde{\gamma}_1 \quad (15)$$

where τ_Ψ is the relaxation time of the smectic order parameter Ψ , ξ the coherence length, and q_s is defined in terms of the smectic layer distance d as $q_s = 2\pi/d$.

A qualitative understanding of the result for $\tilde{\gamma}_1$ may be gained from considerations which are partially contained also in a preprint by

McMillan²². We apply a magnetic field rotating at a low frequency ω to a nematic just above the transition temperature T_{AN} . The director follows the field, with a constant delay. The torque which the director opposes to this rotation is

$$\Gamma = \gamma_1 \omega \quad (16)$$

(and has to be supplied by the rotation of the magnetic field). Now in the cybotactic groups the layers give rise to a particular contribution $\tilde{\Gamma}$ to this restoring torque. The layers follow the director with an angle

$$\delta = \omega \tau_{\Psi} \quad (17)$$

between the director and the normal to the layers. The torque $\tilde{\Gamma}$ can be derived from the elastic energy of a smectic A

$$F_{el} = \frac{q_s^2 \langle \Psi^2 \rangle}{2M} \delta^2 \quad (18)$$

(M^{-1} is an elastic constant) as

$$\tilde{\Gamma} = \frac{\partial F_{el}}{\partial \delta} = \frac{q_s^2 \langle \Psi^2 \rangle \tau_{\Psi}}{M} \omega. \quad (19)$$

To take account of the fact that we are treating the fluctuations of the smectic order parameter we substitute $\langle \Psi^2 \rangle$ by the fluctuations over a region ξ

$$\langle \Psi^*(\xi) \Psi(0) \rangle = \frac{MT}{4\pi\xi}. \quad (20)$$

Comparing the result for $\tilde{\Gamma}$ with (16) yields the above result for $\tilde{\gamma}_1$ (except for a factor $\frac{1}{4}$).

The critical temperature dependence of $\tilde{\gamma}_1$ is determined by τ_{Ψ} and ξ . In mean field theory ($\epsilon = T - T_{AN}$)

$$\xi \sim \epsilon^{-1/2}, \quad \tau_{\Psi} \sim \epsilon^{-1} \sim \xi^2 \quad (21)$$

therefore

$$\tilde{\gamma}_1 \sim \xi \sim \epsilon^{-0.5}. \quad (22)$$

But the AN-transition is probably similar to the λ -transition in He, for which mean field theory does not hold. Instead of (21) we use according to static and dynamic scaling theory²³

$$\xi \sim \epsilon^{-0.66}, \quad \tau_{\Psi} \sim \xi^{3/2} \quad (23)$$

and get the result

$$\tilde{\gamma}_1 \sim \xi^{\frac{1}{2}} \sim \epsilon^{-0.33}. \quad (24)$$

McMillan's result agrees with (14) under the same assumptions for the type of the phase transition. The result (14) holds in general (as long as the Ornstein-Zernike relation is valid), even for the more complicated case of an influence of two-dimensional quasi-order²⁴.

A numerical estimate for the temperature region over which a $\tilde{\gamma}_1 > 0.1 \rho$ should be observable, yields $T - T_{AN} < 1^\circ\text{C}$.

For compressible system also the bulk viscosity and the anisotropy $\Delta\eta$ diverge like $\tilde{\gamma}_1$.

In conclusion, I wish to say that this work was done in the pleasant and stimulating atmosphere of P G de Gennes' group at the College de France.

References

- 1 LESLIE F M *Quart. J. Mech. Appl. Math.* **19** 357 (1966); see also Orsay Liquid Crystal Group *J. Chem. Phys.* **51** 816 (1969)
- 2 PARODI O *J. Phys. (Paris)* **31** 581 (1970)
- 3 MIESOWICZ M *Nature (London)* **158** 27 (1946)
- 4 IMURA H and OKANO K *Jap. J. Appl. Phys.* **11** 1440 (1972)
- 5 MARTINOTY P and CANDAU S *Mol. Cryst. Liquid Cryst.* **14** 243 (1971)
- 6 GAHWILLER Ch *Phys. Lett.* **36A** 311 (1971)
- 7 LI PLSANT J P and PAPON P preprint
- 8 PROST J and GASPAROUX H *Phys. Lett.* **36A** 245 (1971)
- 9 HIPPEL G and SCHNIEDER F *Z. Naturforsch.* **27a** 976 (1972)
- 10 MEIBOOM S and HEWITT R C *Phys. Rev. Lett.* **30** 261 (1973)
- 11 de GENNES P G *Mol. Cryst. Liquid Cryst.* **12** 193 (1971)
- 12 JÜHNIG F and SCHMIDT H *Ann. Phys. (New York)* **71** 129 (1972)
- 13 LORD JR A E and LABELS M M *Phys. Rev. Lett.* **25** 570 (1970)
- 14 WUTSEL JR G C SPEER R S LOWRY B A and WOODARD M R *J. Appl. Phys.* **43** 1495 (1972)
- 15 JÜHNIG F *Z. Phys.* **258** 199 (1973)
- 16 JÜHNIG F *Chem. Phys. Lett.* **23** 199 (1973)
- 17 PIERCY J E and RAO M G S *J. Chem. Phys.* **46** 3951 (1967)
- 18 NATALE G G and COMMINS D E *Phys. Rev. Lett.* **28** 1439 (1972)
- 19 STINSON T W LITSTER J D *Phys. Rev. Lett.* **25** 503 (1970)
- 20 de GENNES P G *Solid State Commun.* **10** 753 (1972)
- 21 JÜHNIG F and BROCHARD F J *Phys. (Paris)* **35** 301 (1974)
- 22 McMILLAN W L *Phys. Rev.* **A9** 4 (1974)
- 23 BROCHARD F J *Phys. (Paris)* **34** 411 (1973)
- 24 KOSTERLITZ J M *J. Phys.* **C7** 1046 (1974)

DISCUSSION

Janik: From what you said I understand that the ratio of the viscosity coefficients for MBBA and PAA is about 10, whereas that of the self diffusion coefficients for PAA and MBBA is about 3. Could you comment on that?

Jühnig: The relation between the self diffusion coefficients and the viscosities in a nematic is in a simple approximation assumed to be given by

the Stokes formula for isotropic liquids. But this assumption is a very crude one as for a nematic (i) the ellipsoidal shape of the molecules should be taken into account (the problem of the motion of an ellipsoid in an isotropic liquid has been solved long ago). (ii) a combination of viscosities should enter in the analogue of the Stokes formula, and (iii) the boundary condition at the surface of the moving molecule should also be important. With respect to this boundary condition PAA seems to be an extraordinary substance different from most other nematics including MBBA.

As far as I know the Stokes formula for nematics has not been derived, but may be Leslie can comment on this question.

Leslie: Commenting on the possibility of a solution similar to the approximate Stokes solution for an isotropic liquid, this does not seem possible. The chief obstacle is that the orientation must presumably vary over a large range of values in order to satisfy a suitable boundary condition.

Darbari: You mentioned that the observed sound attenuation is mainly due to viscous processes. Further, you showed the temperature dependence of the viscosity to be non-arrhenius. It has been well established in the literature for several systems that at such temperatures cooperative effects dominate the transport behaviour which should give a rise to a distribution of relaxation times instead of a discrete relaxation time. In the light of the above, how do you justify the discrete relaxation time used in your explanation for MBBA data?

Jähnig: My starting point was the experimental result of a single relaxation time behaviour at room temperature, for MBBA. With increasing temperature a second relaxation process becomes important, the relaxation of the order parameter. I think your question refers to the experimental results of Eden, Garland and Williamson* on the attenuation of sound in unoriented MBBA. They indeed claimed that in the vicinity of the nematic-isotropic phase transition more than one relaxation process has to be taken into account. I have two of them.

* Eden D, Garland C W and Williamson R C J. *Chem. Phys.* **58** 1861 (1973).

Distorted twisted orientation patterns in nematic liquid crystals

F M LESLIE

University of Strathclyde, Glasgow, Scotland.

Abstract. Twisted orientation patterns apparently occur in some nematic liquid crystals between parallel plates if the preparation of the solid surfaces induces different tangential alignments of the anisotropic axis at the two plates. In such an orientation pattern, the anisotropic axis is everywhere parallel to the plates, but varies uniformly across the gap, being the same in any plane parallel to the plates. Ericksen has shown that this form of orientation pattern is a solution of the continuum theory equations for all admissible energy functions. However, given the practical interest in such arrangements, it is natural to seek to determine if other solutions are possible with lower energies, and therefore the more likely to occur in practice. Employing the Frank-Oseen energy function, one finds that there can be other solutions in which the orientation of the anisotropic axis is no longer always parallel to the plates. Consequently, it is of interest to determine when such solutions occur, and equally whether they have lower energies than the twisted solution. Not surprisingly, these questions depend upon the relative magnitude of the coefficients in the energy function. While the analysis is somewhat complex, an indication of the likely behaviour follows from an examination of some limiting cases. However, should a certain pair of the coefficients be equal, a fuller discussion is possible. Available estimates for the coefficients for some materials suggest that such distorted twisted orientation patterns may be rather uncommon.

1. Introduction

By suitable prior treatment of the solid surfaces, it is possible to produce twisted orientation patterns in a static sample of nematic liquid crystal between parallel glass plates. In early papers, Mauguin^{1, 2} describes how he obtained such orientation patterns by first aligning the sample uniformly parallel to the surfaces, and then rotating one plate in its own plane relative to the other. Later, Chatelain³ achieved the same result by rubbing the two glass surfaces in given directions and arranging the plates so that these were not coincident. By either method, one obtains an orientation pattern in which the direction of the optic axis is everywhere parallel to the glass plates, and changes uniformly with distance from one limiting direction to another as one traverses the gap between them.

In recent years, there has been increased interest in such orientation patterns, and their response to external magnetic or electric fields, partly

on account of their use in electro-optic display devices, as for example Schadt and Helfrich⁴ discuss, but also because they provide a useful opportunity to test the degree of consistency between existing continuum theory and experimental observations in the presence of various orienting influences, as for instance Leslie⁵ describes. Within the context of continuum theory, twisted orientation patterns are solutions of the relevant equations in the absence of magnetic or electric fields for all possible free energy functions, as Ericksen⁶ demonstrates. On the other hand, if one employs a quadratic energy of the type proposed by Oseen⁷ and Frank⁸, Leslie⁵ notes that other solutions can exist in which the orientation of the optic axis is no longer parallel to the plates, and the aim of the present paper is to determine when such solutions are likely to occur. The answer to this question depends of course upon the relative magnitudes of the material constants in the Oseen-Frank free energy. However, available estimates of these coefficients for some nematic liquid crystals suggest that non-parallel twisted orientation patterns may be rather uncommon.

As is generally done for nematic liquid crystals, the calculations described below employ the notion that the elongated molecules at the liquid crystal-solid interface adhere to the solid surface. Consequently, as one rotates the plates relative to each other, the total amount of twist introduced into the sample can increase indefinitely. At this point, it is important to appreciate that this is at variance with some observations by Mauguin¹. In his experiments, if the relative rotation of the plates exceeded a right angle, he found that the liquid crystal somehow relaxed so that the total twist remained less than this amount. One explanation of his observations is that the plates dictate a particular direction to the molecules in contact, but that the total twist may relax by an integral multiple of π if this leads to a smaller free energy in the sample. As a result, it may be that one should restrict one's discussion of solutions so that the total twist in the liquid crystal is always less than a right angle. Nonetheless, it is felt desirable not to impose this restriction initially, since it may turn out that other methods of inducing parallel alignment lead to different behaviour. However, at the end of the paper we do consider an alternative boundary condition which effectively achieves conformity with Mauguin's experiences.

2. Continuum theory

To describe static, isothermal configurations in nematic liquid crystals, the equations employed are essentially those derived from different standpoints by Oseen⁷, Frank⁸, Ericksen⁹ and Leslie¹⁰, of which a brief summary follows. If so desired, further details are readily available in the papers quoted, or in a number of the other references. In this section, it is convenient to use Cartesian tensor notation.

As is generally the case in theories for these anisotropic liquids, one describes the orientation of the optic axis by a unit vector field \mathbf{d} , and assumes that \mathbf{d} and $-\mathbf{d}$ are physically indistinguishable. In the absence of

external body forces influencing the optic axis, the components of the vector \mathbf{d} satisfy the partial differential equations

$$\left(\frac{\partial W}{\partial d_{i,j}} \right)_{,i} - \frac{\partial W}{\partial d_i} + \gamma d_i = 0, \quad (2.1)$$

in which γ is a scalar to be determined, and W the free energy per unit volume, which is an isotropic function of the vector \mathbf{d} and its gradients for nematic liquid crystals, and further is unchanged by the replacement of \mathbf{d} by $-\mathbf{d}$. Depending upon one's viewpoint, the above represent either the Euler-Lagrange equations for a minimum of the free energy, or a conservation law for the orientation of the optic axis. Given the assumption of incompressibility, Ericksen⁹ shows that the equations of conservation of linear momentum integrate to yield

$$p + W + \chi = p_0, \quad (2.2)$$

where p is the unknown hydrostatic pressure, χ the scalar potential of any conventional body forces present, and p_0 an arbitrary constant. Moreover, he finds that conservation of angular momentum is satisfied identically, on account of the form of free energy considered. Should one wish to evaluate them, the stress and couple stress vectors on a surface with unit normal \mathbf{n} , \mathbf{t} and \mathbf{l} respectively, are given by

$$\left. \begin{aligned} t_i &= -pn_i - \frac{\partial W}{\partial d_{k,j}} d_{k,i} n_j, \\ l_i &= e_{ijk} d_j \frac{\partial W}{\partial d_{k,p}} n_p, \end{aligned} \right\} \quad (2.3)$$

e_{ijk} denoting the alternating tensor.

For the present investigation, the free energy function selected is that put forward independently by Oseen⁷ and Frank⁸, so that

$$2W = \left\{ \begin{aligned} &(\alpha_1 - \alpha_2 - \alpha_4) (d_{i,i})^2 + \alpha_2 d_{i,j} d_{i,j} \\ &+ \alpha_4 d_{i,j} d_{j,i} + (\alpha_3 - \alpha_2) d_i d_j d_{k,i} d_{k,j}, \end{aligned} \right\} \quad (2.4)$$

the coefficients being constants. Subsequently, Ericksen¹¹ has proposed that these coefficients satisfy certain inequalities on the grounds that a stable uniform alignment represents a state of minimum energy. Here, we accept these, but assume further that

$$\alpha_1 > 0, \quad \alpha_2 > 0, \quad \alpha_3 > 0, \quad (2.5)$$

thereby excluding the possibility that any of the above three coefficients be zero.

Finally, consistent with Ericksen's stability hypothesis, Dafermos¹² discriminates between various solutions by choosing that with least free energy as the stable solution. Below, given more than one solution, we adopt this approach and regard that with lowest energy as the most likely to occur in practice.

3. Solutions

We consider a layer of nematic liquid crystal confined between parallel plates a distance $2h$ apart. To examine appropriate solutions of the above equations, it is convenient to choose a set of right-handed Cartesian axes with the z -axis perpendicular to the plates, and such that the origin of co-ordinates is equidistant from the solid boundaries. If the thickness of the sample is small compared with the dimensions of the plates, variations in the orientation parallel to the solid surfaces seem unlikely, and therefore one examines solutions of equations (2.1) and (2.4) in which the unit vector \mathbf{d} takes the form

$$\begin{aligned} d_x &= \cos \theta(z) \cos \phi(z), & d_y &= \cos \theta(z) \sin \phi(z), \\ d_z &= \sin \theta(z). \end{aligned} \quad (3.1)$$

After manipulation to eliminate the scalar γ , equations (2.1) reduce to (see Leslie⁵)

$$\begin{aligned} 2f(\theta)\theta'' + \frac{d}{d\theta}f(\theta)\theta'^2 - \frac{d}{d\theta}g(\theta)\phi'^2 &= 0, \\ g(\theta)\phi'' + \frac{d}{d\theta}g(\theta)\theta'\phi' &= 0, \end{aligned} \quad (3.2)$$

where

$$\begin{aligned} f(\theta) &= \alpha_1 \cos^2 \theta + \alpha_3 \sin^2 \theta, \\ g(\theta) &= (\alpha_2 \cos^2 \theta + \alpha_3 \sin^2 \theta) \cos^2 \theta, \end{aligned} \quad (3.3)$$

and the prime denotes differentiation with respect to the z co-ordinate.

At the solid surfaces, we assume that the orientation of the anisotropic axis is fixed, and therefore consider boundary conditions of the type

$$\theta(h) = \theta(-h) = 0, \quad \phi(h) = -\phi(-h) = \phi_0, \quad (3.4)$$

in which one may regard the constant angle ϕ_0 as positive without loss of generality. While Mauguin's observations, and also the remarks of Leger¹³, prompt one to restrict the range of this angle so that

$$0 \leq \phi_0 \leq \pi/4, \quad (3.5)$$

it seems desirable not to do so initially. However, later we discuss briefly an alternative boundary condition which appears to achieve this limitation.

As mentioned previously, the equations (3.2) have a simple solution, subject to the boundary conditions (3.4),

$$\theta = 0, \quad \phi = \phi_0 z/h. \quad (3.6)$$

This of course corresponds to the observed twisted orientation pattern.

Somewhat less obviously, the equations (3.2) can also have a solution in which the angle θ varies, and, in this event, the equations integrate to yield

$$g(\theta) \phi' = a, \quad f(\theta) \theta'^2 + g(\theta) \phi'^2 = b, \quad (3.7)$$

a and b being constants of integration. We consider a continuously differentiable solution with the properties

$$\theta(z) = \theta(-z), \quad \phi(z) = -\phi(-z), \quad (3.8)$$

and thus

$$\theta'(0) = 0, \quad \phi(0) = 0. \quad (3.9)$$

Also it is convenient to employ the notation

$$\theta(0) = \theta_0. \quad (3.10)$$

Hence, if one combines equations (3.7), it follows that

$$f(\theta) \theta'^2 = a^2 \{ 1/g(\theta_0) - 1/g(\theta) \}. \quad (3.11)$$

In view of the assumptions (2.5), a necessary condition for a solution of this type is that the right-hand-side of equation (3.11) remains positive.

The function $g(\theta)$, defined by equation (3.3)₂, is clearly even in θ , and further examination shows that either it decreases monotonically to zero as θ increases from zero to $\frac{1}{2}\pi$, or it initially increases to a maximum and then decreases monotonically to zero for that range of values of its argument. In the former case, one obtains solutions in which θ increases (or decreases) monotonically from zero at the plates to a maximum (or minimum) at the centre of the gap, for all values of θ_0 between zero and $\frac{1}{2}\pi$. On the other hand, in the latter case, while the orientation also changes monotonically, such solutions exist only for a restricted range of the parameter θ_0 . Consequently, it is necessary to note two distinct types of solution, in which either

$$0 < |\theta_0| < \frac{1}{2}\pi, \quad \text{if } \alpha_3 \leq 2\alpha_2, \quad (3.12)$$

or

$$0 < \theta_m \leq |\theta_0| < \frac{1}{2}\pi, \quad \text{if } \alpha_3 > 2\alpha_2, \quad (3.13)$$

where the angle θ_m is given by

$$\sin^2 \theta_m = (\alpha_3 - 2\alpha_2) / (\alpha_3 - \alpha_2), \quad (3.14)$$

this expression being less than unity since α_2 is positive.

With the above restrictions upon the parameter θ_0 , equations (3.7)₁ and (3.11) yield solutions in which the angle θ changes monotonically from zero at the solid surfaces to the value θ_0 in the centre of the gap, and they take the form

$$\left. \begin{aligned} az &= g(\theta_0)^{\frac{1}{2}} \operatorname{sgn} \theta_0 \int_{\theta}^{\theta_0} \left\{ \frac{f(u)g(u)}{g(u) - g(\theta_0)} \right\}^{\frac{1}{2}} du, \quad 0 \leq z \leq h, \\ \phi &= g(\theta_0)^{\frac{1}{2}} \operatorname{sgn} \theta_0 \int_{\theta}^{\theta_0} \left\{ \frac{f(u)}{g(u)\{g(u) - g(\theta_0)\}} \right\}^{\frac{1}{2}} du, \quad 0 \leq \phi \leq \phi_0, \end{aligned} \right\} \quad (3.15)$$

provided of course that

$$ah = g(\theta_0)^{\frac{1}{2}} \operatorname{sgn} \theta_0 \int_{\theta_0}^{\theta_0} \left\{ \frac{f(\theta)g(\theta)}{g(\theta) - g(\theta_0)} \right\}^{\frac{1}{2}} d\theta, \quad (3.16)$$

and

$$\phi_0 = g(\theta_0)^{\frac{1}{2}} \operatorname{sgn} \theta_0 \int_{\theta_0}^{\theta_0} \left\{ \frac{f(\theta)}{g(\theta)\{g(\theta) - g(\theta_0)\}} \right\}^{\frac{1}{2}} d\theta. \quad (3.17)$$

While the equation (3.16) simply serves to evaluate the constant a , equation (3.17) more importantly determines θ_0 as a function of the given parameter ϕ_0 , or conversely gives ϕ_0 as a function of θ_0 .

To discriminate between the solutions (3.6) and (3.15), when the latter exists, we compare their energies. Employing equations (2.4), (3.1) and (3.3), one finds that the total energy per unit area of the plates, W , is given by

$$W = \frac{1}{2} \int_{-h}^h \left\{ f(\theta) \theta'^2 + g(\theta) \phi'^2 \right\} dz. \quad (3.18)$$

Hence, if one denotes the value of this expression for the parallel, twisted solution by W_p , it follows from equations (3.6) that

$$W_p = \alpha_2 \phi_0^2/h, \quad (3.19)$$

and, if the value corresponding to the non-parallel, twisted solution is W_{n-p} , equations (3.7)₁ and (3.11) at once yield

$$W_{n-p} = a^2 h/g(\theta_0). \quad (3.20)$$

Therefore, the latter solution is the more likely to occur if

$$a^2 h^2/g(\theta_0) < \alpha_2 \phi_0^2. \quad (3.21)$$

From the above, one sees that the question of the existence of the non-parallel, twisted solution requires an investigation of the relationship (3.17), and further the prediction of its possible occurrence involves

both expressions (3.16) and (3.17). In the general case, some progress is possible by examining the limiting behaviour when θ_0 is small or close to $\frac{1}{2}\pi$. However, when two of the coefficients in the free energy are equal, a full discussion proves straightforward, and we turn to this special case in the next section.

4. A special case

To gain some information regarding the behaviour of the non-parallel, twisted solution, it is helpful initially to restrict one's attention to the particular case in which the Frank-Oseen coefficients α_2 and α_3 are equal in magnitude, since this leads to considerable simplification in the analysis. In this event, the relations (3.16) and (3.17) reduce to

$$ah = \alpha_2^{\frac{1}{2}} \cos \theta_0 \operatorname{sgn} \theta_0 \int_0^{\theta_0} \left\{ \frac{f(\theta)}{\sin^2 \theta_0 - \sin^2 \theta} \right\}^{\frac{1}{2}} \cos \theta d\theta, \quad (4.1)$$

and

$$\phi_0 = \alpha_2^{-\frac{1}{2}} \cos \theta_0 \operatorname{sgn} \theta_0 \int_0^{\theta_0} \left\{ \frac{f(\theta)}{\sin^2 \theta_0 - \sin^2 \theta} \right\}^{\frac{1}{2}} \frac{d\theta}{\cos \theta}; \quad (4.2)$$

here, θ_0 can be any positive or negative acute angle, on account of the condition (3.12). Also, the criterion (3.21) for the occurrence of this type of solution becomes

$$ah < \alpha_2 \phi_0 \cos \theta_0. \quad (4.3)$$

With the aid of substitution

$$\sin \theta = \sin \theta_0 \sin \lambda, \quad (4.4)$$

the expressions (4.1) and (4.2) take the somewhat more manageable forms

$$ah = \alpha_2^{\frac{1}{2}} \cos \theta_0 \int_0^{\pi/2} f(\theta)^{\frac{1}{2}} d\lambda, \quad (4.5)$$

and

$$\phi_0 = \alpha_2^{-\frac{1}{2}} \cos \theta_0 \int_0^{\pi/2} f(\theta)^{\frac{1}{2}} \frac{d\lambda}{\cos^2 \theta}. \quad (4.6)$$

The further change of variable

$$t = \tan \lambda \quad (4.7)$$

in the first of the above integrals leads to

$$ah = (\alpha_1 \alpha_2)^{\frac{1}{2}} \cos \theta_0 \int_0^{\infty} \left(1 + \frac{kt^2 \sin^2 \theta_0}{1+t^2} \right)^{\frac{1}{2}} \frac{dt}{1+t^2}, \quad (4.8)$$

where

$$k = (\alpha_2 - \alpha_1) / \alpha_1, \quad (4.9)$$

and a similar change of variable

$$t = \cos \theta_0 \tan \lambda \quad (4.10)$$

in the second yields

$$\phi_0 = (\alpha_1 / \alpha_2)^{\frac{1}{2}} \int_0^{\infty} \left(1 + \frac{kt^2 \sin^2 \theta_0}{\cos^2 \theta_0 + t^2} \right)^{\frac{1}{2}} \frac{dt}{1+t^2}. \quad (4.11)$$

From the results (4.8) and (4.11), one can draw certain conclusions. However, it is convenient to treat separately three distinct cases.

$$(1) \quad \underline{\alpha_2 > \alpha_1 \quad (k > 0)}$$

In this case, a comparison of the expression (4.8) with the appropriate multiple of (4.11) immediately shows that the condition (4.3) holds. Moreover, from equation (4.11), one can conclude that ϕ_0 is a monotonic increasing function of θ_0 , and that

$$\lim_{\theta_0 \rightarrow 0} \phi_0 = (\alpha_1 / \alpha_2)^{\frac{1}{2}} \pi/2, \quad \lim_{\theta_0 \rightarrow \pm \pi/2} \phi_0 = \pi/2. \quad (4.12)$$

Therefore, in this case, the non-parallel, twisted solution becomes a possibility once the overall twist exceeds a critical value, which is less than the angle π . In this solution, the distortion of the parallel, twisted orientation pattern grows monotonically with increasing twist until the anisotropic axis becomes perpendicular to the plates at the centre of the gap, at which point the total twist in the sample is equal to π . If it proves feasible to produce larger static twist in a layer of nematic liquid crystal, corresponding solutions appear to take the form of a combination of solutions of this type. On the other hand, if the largest static twist possible is a right angle, so that the restriction (3.5) applies, this non-parallel, twisted solution remains a possibility only if

$$\alpha_2 > 4\alpha_1. \quad (4.13)$$

As noted initially, should such a second solution be available, it seems the more likely to occur, since it has a lower energy than the corresponding parallel, twisted solution.

$$(ii) \quad \underline{\alpha_1 > \alpha_2} \quad (k < 0)$$

Here, a similar comparison of the expressions (4.8) and (4.11) shows that the condition (4.3) is not satisfied. As a result, one anticipates that the parallel, twisted solution persists as the twist in the sample increases in this particular case.

$$(iii) \quad \underline{\alpha_1 = \alpha_2} \quad (k = 0)$$

In the event that all three coefficients are equal, the expressions (4.8) and (4.11) reduce to

$$ah = \alpha_2 \cos \theta_0 \cdot \frac{1}{2}\pi, \quad \phi_0 = \frac{1}{2}\pi. \quad (4.14)$$

Consequently, in this very special case, should the overall twist be equal to π , solutions of the type (3.15) exist for all values of θ_0 . Even more surprisingly, they all have the same energy as the corresponding parallel, twisted solution (3.6).

5. The general case

Returning to the general case, it proves possible to obtain some insight into conditions necessary for the occurrence of this second type of solution by evaluating the integrals in equations (3.16) and (3.17) in certain extreme cases. For this purpose, it is again helpful to employ the substitution (4.4) to give the alternative forms

$$ah = g(\theta_0)^{\frac{1}{2}} \int_0^{\pi/2} \left\{ \frac{f(\theta)h(\theta)}{F(\theta, \theta_0)} \right\}^{\frac{1}{2}} d\lambda, \quad (5.1)$$

and

$$\phi_0 = g(\theta_0)^{\frac{1}{2}} \int_0^{\pi/2} \left\{ \frac{f(\theta)}{h(\theta) F(\theta, \theta_0)} \right\}^{\frac{1}{2}} \frac{d\lambda}{\cos^2 \theta}, \quad (5.2)$$

in which

$$h(\theta) = g(\theta) / \cos^2 \theta = \alpha_2 \cos^2 \theta + \alpha_3 \sin^2 \theta, \quad (5.3)$$

and

$$\begin{aligned} F(\theta, \theta_0) &= \{g(\theta) - g(\theta_0)\} / (\sin^2 \theta_0 - \sin^2 \theta) \\ &= 2\alpha_2 - \alpha_3 + (\alpha_3 - \alpha_2)(\sin^2 \theta_0 + \sin^2 \theta). \end{aligned} \quad (5.4)$$

Below, we find it convenient to discuss separately two different cases.

$$(i) \quad \underline{2\alpha_2 > \alpha_3}$$

When this condition holds, it follows from (3.12) that there is no lower limit upon the magnitude of the parameter θ_0 , and further an

examination of the function $F(\theta, \theta_0)$ defined above shows that it is never zero. Therefore, one can expand the integrand in the expression (5.2) in powers of $\sin^2 \theta_0$ to eventually obtain

$$\begin{aligned} \phi_0 = & \left\{ \alpha_1 / (2\alpha_2 - \alpha_3) \right\}^{\frac{1}{2}} \frac{\pi}{2} \left[1 + \right. \\ & + \left\{ \alpha_3 / \alpha_1 - (\alpha_3^2 - \alpha_3 \alpha_2 + \alpha_2^2) / \alpha_2 (2\alpha_2 - \alpha_3) \right\} \frac{\sin^2 \theta_0}{4} \\ & \left. + O(\sin^4 \theta_0) \right]. \end{aligned} \quad (5.5)$$

In the same manner, the equations (5.1) and (5.2) finally yield

$$\begin{aligned} & \alpha_2 \phi_0^2 - a^2 h^2 / g(\theta_0) \\ = & \alpha_1 \left\{ \alpha_3 / \alpha_1 - (\alpha_3^2 - \alpha_3 \alpha_2 + \alpha_2^2) / \alpha_2 (2\alpha_2 - \alpha_3) \right\} \frac{\pi^2 \sin^4 \theta_0}{32} \\ & + O(\sin^6 \theta_0). \end{aligned} \quad (5.6)$$

Hence, if the coefficients satisfy

$$(2\alpha_2 - \alpha_3) / \alpha_1 > 1 + (\alpha_3 - \alpha_2)^2 / \alpha_3 \alpha_2, \quad (5.7)$$

it follows from the above and the conditions (2.5) and (3.21) that the non-parallel twisted solution has a lower energy than the parallel twisted solution for a range of values of the total twist exceeding a critical value given by

$$\phi_0^c = \frac{\pi}{2} \left\{ \alpha_1 / (2\alpha_2 - \alpha_3) \right\}^{\frac{1}{2}}. \quad (5.8)$$

Clearly, the inequality (5.7) implies that this critical angle is less than $\pi/2$, in view of the assumptions (2.5).

At the other extreme, it is possible to show with the aid of the substitution (4.10) that

$$\lim_{\theta_0 \rightarrow \pm \pi/2} \phi_0 = \pi/2, \quad \lim_{\theta_0 \rightarrow \pm \pi/2} \left\{ ah / g(\theta_0)^{\frac{1}{2}} \right\} = \int_0^{\pi/2} f(\lambda)^{\frac{1}{2}} d\lambda. \quad (5.9)$$

Therefore, as in the special case just discussed, complete distortion of the parallel orientation pattern takes place when the total twist is equal to the angle π . Also, in this limit, the criterion (3.21) that the second solution has a lower energy than the parallel, twisted solution reduces to

$$\left. \begin{aligned} E(1 - \alpha_1 / \alpha_3) &< (\alpha_2 / \alpha_3)^{\frac{1}{2}}, & \alpha_3 > \alpha_1, \\ E(1 - \alpha_3 / \alpha_1) &< (\alpha_2 / \alpha_1)^{\frac{1}{2}}, & \alpha_1 > \alpha_3, \end{aligned} \right\} \quad (5.10)$$

where $E(k)$ denotes a complete elliptic integral of the second kind, defined, by

$$E(k) = 2/\pi \int_0^{\pi/2} (1 - k \sin^2 \lambda)^{1/2} d\lambda. \quad (5.11)$$

At this point, it is helpful to introduce the notation

$$\xi = \alpha_3 / \alpha_2, \quad \eta = \alpha_1 / \alpha_2, \quad (5.12)$$

which allows one to express the inequality (5.7) in the form

$$\eta < \xi(2 - \xi) / \{\xi + (\xi - 1)^2\}, \quad (5.13)$$

and the condition (5.10) as

$$\begin{aligned} E(1 - \eta/\xi) &< \xi^{-1/2}, \quad \xi > \eta, \\ E(1 - \xi/\eta) &< \eta^{-1/2}, \quad \eta > \xi. \end{aligned} \quad (5.14)$$

From these, it follows that the inequalities (5.7) and (5.10) define domains in the first quadrant of the (ξ, η) plane, which we outline in the accompanying sketch (figure 1). In this way, one sees that the condition (5.7) is the stronger of the two, since, if the coefficients satisfy it, they also satisfy (5.10).

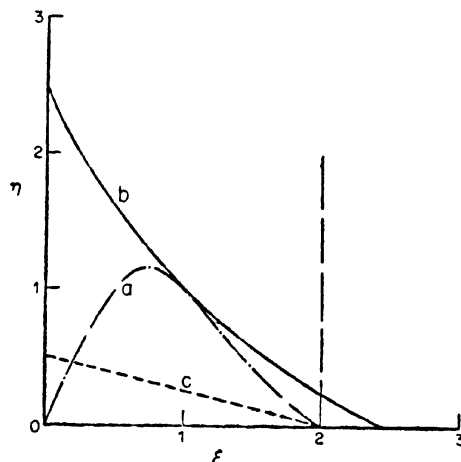


Figure 1 The domain defined by the inequality (5.7) lies below the curve *a*, that by (5.10) is to the left of curve *b*, and that by (5.15) is to the left of line *c*. The broken vertical line divides the plane into the two cases discussed in section 5.

Unfortunately, one cannot readily determine the nature of the dependence of ϕ_0 upon θ_0 for intermediate values of this parameter. In particular, it does not seem possible in general to establish the monotonicity of the relationship. Equally, no information is available concerning the relative

energies in this range, except of course for the special case discussed earlier.

However, if the coefficients satisfy the inequality (5.7), one can state that our analysis does allow a smooth transition from the parallel twisted solution to a non-parallel solution when the total twist exceeds the value given by equation (5.8). Also, when this condition holds, this second solution is the more likely to occur for overall twists close to the angle π . On the other hand, should the non-parallel solution be available at intermediate values of θ_0 , with the twist angle ϕ_0 less than the value given by equation (5.8), and with a lower energy than the corresponding parallel, twisted solution, the possibility does exist of an abrupt transition to a distorted solution at a total twist smaller than $2\phi_0^c$. In the same way, if the coefficients satisfy the inequality (5.10), but not (5.7), a similar abrupt transition can presumably occur at some point.

Finally, for a smooth distortion before the total twist attains the value $\pi/2$, it is necessary that

$$2\alpha_2 > \alpha_3 + 4\alpha_1, \quad (5.15)$$

or, with the notation (5.12),

$$\xi + 4\eta < 2. \quad (5.16)$$

The sketch also shows the relevant portion of the (ξ, η) plane which satisfies this inequality. From this, one obtains an impression of the restrictive nature of this last inequality.

$$(ii) \quad \alpha_3 \geq 2\alpha_2$$

When the equality holds, the situation is similar to that just discussed in that the parameter θ_0 takes the same range of values, but, when the inequality occurs, there can no longer be a smooth transition from one solution to the other, since θ_0 must take values satisfying the condition (3.13). In either event, an inspection of the integral (5.2) shows that it becomes singular when θ_0 approaches the limits zero or $\pm \theta_m$, as the case may be. Consequently, here, one extreme of the range of values of θ_0 requires exceedingly large twists in the layer. In addition, a relatively straightforward calculation shows that the non-parallel solution always has a higher energy than the parallel, twisted solution in this limit.

At the other extreme, one can repeat the analysis carried out earlier for values of θ_0 close to $\pm \frac{1}{2}\pi$. Consequently, the results (5.9) remain valid, and the second solution has a lower energy than the parallel, twisted solution in this limit if the inequality (5.10) holds.

Here, therefore, there can be no smooth transition from one orientation pattern to the other, and, from the sketch of the various domains in the (ξ, η) plane, it is clear that an abrupt transition seems possible only

for a very limited range of values of the coefficients. Moreover, should one impose the additional requirement that the total twist be at most a right angle, there appears to be little likelihood of this latter possibility.

6. Discussion

Estimates are available for the Frank-Oseen coefficients for two nematic liquid crystals. For p-azoxyanisole, Saupe¹⁴ obtained

$$\xi = 3.8, \quad \eta = 1.6, \quad (6.1)$$

in the notation (5.12). Also, there are a number of recent measurements for the material MBBA (see for example Haller¹⁵ and Leger¹⁶), and typically one finds that

$$\xi = 2.0, \quad \eta = 1.6, \quad (6.2)$$

with slight variations. In view of these estimates, the foregoing analysis apparently excludes any possibility of the parallel, twisted orientation pattern in these particular materials distorting in the manner discussed above. Nevertheless, the situation may differ for other nematic liquid crystals. However, for the two materials quoted, our predictions disagree with observations in one important respect. On account of the boundary condition employed above, one can have parallel, twisted solutions with total twist greater than a right angle, and, as mentioned earlier, this is contrary to observations by Mauguin¹. Consequently, we briefly examine an alternative boundary condition which removes this conflict.

Rather than prescribe the orientation of the optic axis at the solid surface, Papoular and Rapini¹⁷ introduce a surface energy, which essentially gives rise to a couple stress condition at the interface. In particular, they consider a form of interfacial energy which is a minimum for perpendicular orientation of the optic axis at the solid surface, but a similar treatment with parallel orientation minimising the surface energy presents no problems. Here, we introduce such a surface energy with the property that it is a minimum when the alignment is parallel and in a given direction. One relatively simple form of surface energy per unit area meeting this requirement, and also with necessary invariance and symmetry properties, is

$$2w = \delta_1 (d_i n_i)^2 - \delta_2 (d_i c_i)^2, \quad (6.3)$$

in which δ_1 and δ_2 are positive constants, \mathbf{n} is the unit normal to the surface, and \mathbf{c} a given unit vector, which represents the prescribed direction on the surface. Jenkins and Barratt^{18, 19} consider the related problem of a liquid crystal - isotropic liquid interface, and by parallel reasoning a possible boundary condition for the present problem is

$$l_i = c_{ijk} d_k \frac{\partial w}{\partial d_j}, \quad (6.4)$$

1 being the couple stress defined in equation (2.3)₂. This is consistent with the approach of Papoular and Rapini.

As earlier, we discuss the situation where the two surfaces have been treated to induce parallel alignment in non-coincident directions. Without loss of generality, therefore, one can write

$$c_x = \cos \phi_0, \quad c_y = \epsilon \sin \phi_0, \quad c_z = 0, \quad \text{on } z = \epsilon h, \quad (6.5)$$

where ϵ is either plus or minus one, and, moreover, the constant, positive angle ϕ_0 satisfies the condition (3.5). As before, the equations (3.2) have a parallel, twisted solution

$$\theta = 0, \quad \phi = \bar{\phi} z/h, \quad (6.6)$$

where $\bar{\phi}$ is the unknown orientation at the upper plate. Here, however, the boundary condition (6.4) leads to the equation

$$2\alpha_2 \bar{\phi} = h\delta_2 \sin 2(\phi_0 - \bar{\phi}), \quad (6.7)$$

which of course determines the parameter $\bar{\phi}$. Whatever the values of the coefficients α_2 and δ_2 and the gapwidth h , the above equation always has one root between zero and ϕ_0 . However, there can be others with greater magnitude. To discriminate between a multiplicity of solutions, one again examines the energy per unit area, which here takes the form

$$E = \alpha_2 \bar{\phi}^2 / h - \delta_2 \cos^2(\phi_0 - \bar{\phi}), \quad (6.8)$$

to determine that with least energy.

The roots of equation (6.7) depend upon the magnitude of the dimensionless number ζ defined by

$$\zeta = \alpha_2 / h\delta_2. \quad (6.9)$$

In the event that this is small compared with unity, the root with least magnitude is

$$\bar{\phi} = \phi_0 (1 - \zeta) + O(\zeta^2), \quad (6.10)$$

and the related energy takes the form

$$E = \alpha_2 \phi_0^2 / h - \delta_2 + O(\zeta). \quad (6.11)$$

Clearly, this is the smallest energy possible, and hence, in this limit, the solution with total twist approximately equal to $2\phi_0$ appears that most likely to occur. Therefore, using this alternative boundary condition, our prediction in the limit of small ζ corresponds to the experimental conclusion of Mauguin.

While the type of boundary condition employed above removes the conflict between theory and experiment in this instance, it naturally needs

more detailed examination. Equally, there is the possibility that other approaches may also eliminate the discrepancy. Finally, we remark that in these, as in the above, it seems likely that one may be able under certain circumstances to approximate the boundary condition by regarding the optic axis as fixed at the solid surface.

Acknowledgements

I am indebted to Dr A J Hyde for drawing my attention to some aspects of Mauguin's work, and to Dr P J Barratt for helpful discussions.

References

- 1 MAUGUIN C *Bull. Soc. Fr. Mineral* **34** 71-117 (1911)
- 2 MAUGUIN C *Phys. Z.* **12** 1011-1015 (1911)
- 3 CHATFLAIN P *Bull. Soc. Fr. Mineral* **66** 105-130 (1943)
- 4 SCHAT M and HELFRICH W *Appl. Phys. Lett.* **18** 127-128 (1971)
- 5 LESLIE F M *Mol. Cryst. Liquid Cryst.* **12** 57-72 (1970)
- 6 ERICKSEN J L *J. Fluid Mech.* **27** 59-64 (1967)
- 7 OSEEN C W *Ark. Mat. Astron. Fys.* **19A** (9) 1-19 (1925)
- 8 FRANK F C *Discuss. Faraday Soc.* **25** 19-28 (1958)
- 9 ERICKSEN J L *Arch. Ration. Mech. Anal.* **9** 371-378 (1962)
- 10 LLSLIT F M *Arch. Ration. Mech. Anal.* **28** 265-283 (1968)
- 11 ERICKSEN J L *Phys. Fluids* **9** 1205-1207 (1966)
- 12 DAFERMOS C M J. *Soc. Ind. Appl. Math.* **16** 1305-1318 (1968)
- 13 LEGER L *Solid State Commun.* **10** 697-700 (1972)
- 14 SAUPE A *Z. Naturforsch* **15A** 815-822 (1960)
- 15 HALLER I J. *Chem. Phys.* **57** 1400-1405 (1972)
- 16 LEGER L *Solid State Commun.* **11** 1499-1501 (1972)
- 17 RAPINI A and PAPOULAR M *J. Phys. (Paris)* **30** C4 54-56 (1969)
- 18 JENKINS J T and BARRATT P J *Quart. J. Mech. Appl. Math.* (in press)
- 19 BARRATT P J and JENKINS J T *J. Phys.* **A6** 756-769 (1973)

DISCUSSION

de Gennes: There is something very natural in your diagram where the twist constant is large compared to the other two. In usual materials, as you pointed out, this is not the case — in fact, the twist constant is lower. But we have this nice case of the smectic pre-transitional effect in which the bend and twist constants become very large compared to splay. I would expect your condition to be fulfilled in twisted nematics near the smectic transition.

The role of permanent dipoles in nematic order

N V MADHUSUDANA and S CHANDRASEKHAR

Raman Research Institute, Bangalore 560006, India.

Abstract. We propose a new model for the statistical description of short range order in nematic liquid crystals of positive dielectric anisotropy. We consider the molecules to be cylindrically symmetric and assume the pair potential to be of the form $A^*P_1(\cos \theta_{ij}) - B^*P_2(\cos \theta_{ij})$ which favours an antiparallel arrangement of the permanent dipoles. From physical considerations, antiferroelectric long range ordering is not expected to be present in nematics. Applying the Krieger-James approximation, solutions are obtained with an *apolar* or $P_2(\cos \theta)$ type of *long range order*, but allowing for *antiferroelectric short range order*. Two important consequences of the theory are (i) the mean dielectric constant should *increase* slightly on passing from the nematic to the isotropic phase, (ii) the magnetic and electric birefringence in the isotropic phase should both vary approximately as $(T-T^*)^{-1}$, where T^* is the hypothetical second order transition point, except when the dipolar interactions are very strong, in which case the electric birefringence should exhibit a *slower* variation at temperatures well above T^* . Choosing values of A^*/B^* , illustrative calculations are given of the long range and short range order parameters, dielectric properties, electric and magnetic birefringence. The results are in general agreement with the experimental data for such compounds.

Introduction

The part played by permanent dipoles in determining nematic liquid crystalline properties has been the subject of considerable discussion. Indeed the first theory of the nematic phase, proposed by Max Born¹ in 1916, was based on purely dipolar interactions. Early experiments² to detect free charges on the surface of the liquid crystal, carried out with a view to testing Born's theory yielded negative results; more significantly compounds were found, *e.g.*, quinquephenyl³ and the alkylazobenzenes⁴, that do not possess permanent dipole moments but do nevertheless exhibit the nematic phase. The dipole theory was therefore abandoned. However, the vast majority of nematogens are in fact polar molecules, yet it is generally assumed that the dipolar contribution to nematic stability is negligible. In this paper, we put forward a new point of view regarding the influence of permanent dipoles on orientational order in nematics. We shall confine our attention for the present to materials of positive dielectric anisotropy in which the dipole moment is assumed to be along the major molecular axis.

It has been shown recently⁵ that the Krieger-James approximation is an improvement over the mean field treatment in describing pretransition phenomena in the isotropic phase of a nematic liquid crystal. The theory was developed assuming a $P_2(\cos \theta_{ij})$ type of interaction between neighbouring molecules i and j , where $P_2(\cos \theta)$ is the Legendre polynomial of the second order. The temperature dependence of the magnetic and electric birefringence in the isotropic phase of p -azoxyanisole calculated on the basis of this model was similar to that expected from the phenomenological theory^{6,7} and was in qualitative agreement with the observed behaviour. We now extend this treatment to include permanent dipole interactions also.

The Model

Let us suppose for simplicity that the molecules are cylindrically symmetric rods so that the dipole moment is along the major molecular axis. Evidently, nearest neighbours will tend to be antiparallel. However, the absence of long range translational order in the nematic liquid precludes the possibility of antiferroelectric long range order. We postulate, therefore, that the system has an antiferroelectric type of short range order, but no antiferroelectric long range order. The near neighbour correlations giving rise to antiparallel short range order will extend over a certain correlation length. But as far as a distant molecule is concerned, its interaction with this antiferroelectric cluster will clearly be *apolar* in nature, *i.e.*, it will be fully equivalent whether the molecule is pointing 'up' or 'down'. To express this in a mathematically tractable form we shall resort to the Krieger-James approximation⁸.

We choose a space-fixed cartesian coordinate system XYZ, with the Z axis parallel to the uniaxial direction of the nematic medium. Let us assume that every molecule is surrounded by z nearest neighbours, no two of the z neighbours being nearest neighbours of each other. The pair potential between the central molecule i and one of its neighbours j is taken to be

$$E(\theta_{ij}) = A^*P_1(\cos \theta_{ij}) - B^*P_2(\cos \theta_{ij}) \quad (1)$$

and the interaction between j and the *rest of the medium* to be

$$V(\theta_j) = -BP_2(\cos \theta_j) \quad (2)$$

Here P_1 and P_2 are the Legendre polynomials of the first and second order, θ_{ij} is a function of the usual spherical coordinates θ_i , φ_i , θ_j and φ_j , A^* , B^* and B are interaction parameters. (We ignore the volume dependence of the potential functions as it does not play an important part except in certain calculations, *e.g.*, the determination of the absolute value of T_c for a specific compound).

The relative weight for a given configuration of the cluster of $(z+1)$ molecules is

$$\prod_{j=1}^z f(\theta_{ij}) g(\theta_j) \quad (3)$$

where

$$f(\theta_{ij}) = \exp[-E(\theta_{ij})/kT]$$

$$g(\theta_j) = \exp[-V(\theta_j)/kT]$$

The relative probability that the central molecule i and one of its nearest neighbours, say one, are oriented along θ_i, φ_i and θ_1, φ_1 is then

$$\psi(\theta_i, \varphi_i; \theta_1, \varphi_1) = f(\theta_{i1}) g(\theta_1) \prod_{j=2}^z \int \int f(\theta_{ij}) g(\theta_j) d(\cos \theta_j) d\varphi_j$$

Since this probability should be the same irrespective of which molecule is regarded as the central one,

$$\psi(\theta_i, \varphi_i; \theta_1, \varphi_1) = \psi(\theta_1, \varphi_1; \theta_i, \varphi_i) \quad (4)$$

which represents the *consistency* relation.

In view of the assumed form of the potential, (4) can be re-expressed in the form⁵

$$\frac{\exp[BP_2(\cos \theta_i)/kT]}{[\int \int \exp\{-(A^*/kT)P_1(\cos \theta_{ij}) + (B^*/kT)P_2(\cos \theta_{ij}) + (B/kT)P_2(\cos \theta_j)\} d(\cos \theta_j) d\varphi_j]^{z-1}} = \text{constant}$$

This relation has to be satisfied for all values of $P_2(\cos \theta_i)$. Thus, if A^*/B^* is known, the parameter B influencing long range order can be deduced in terms of B^* at every temperature. In principle B^* can be determined for a specific compound from the transition temperature, provided, of course, proper allowance is made for the volume dependence of the potential function.

The short range order parameters are given by

$$P_1(\cos \theta_{ij}) = \frac{\int \int P_1(\cos \theta_{ij}) \psi(\theta_i, \varphi_i; \theta_j, \varphi_j) d(\cos \theta_i) d\varphi_i d(\cos \theta_j) d\varphi_j}{\int \int \psi(\theta_i, \varphi_i; \theta_j, \varphi_j) d(\cos \theta_i) d\varphi_i d(\cos \theta_j) d\varphi_j}$$

$$P_2(\cos \theta_{ij}) = \frac{\int \int P_2(\cos \theta_{ij}) \psi(\theta_i, \varphi_i; \theta_j, \varphi_j) d(\cos \theta_i) d\varphi_i d(\cos \theta_j) d\varphi_j}{\int \int \psi(\theta_i, \varphi_i; \theta_j, \varphi_j) d(\cos \theta_i) d\varphi_i d(\cos \theta_j) d\varphi_j}$$

and the long range order parameter

$$Q = \frac{\int \int P_2(\cos \theta_i) \psi(\theta_i, \varphi_i; \theta_j, \varphi_j) d(\cos \theta_i) d\varphi_i d(\cos \theta_j) d\varphi_j}{\int \int \psi(\theta_i, \varphi_i; \theta_j, \varphi_j) d(\cos \theta_i) d\varphi_i d(\cos \theta_j) d\varphi_j}$$

The internal energy of the system

$$U = \frac{1}{2} Nz [A^* P_1(\cos \theta_{ij}) - B^* P_2(\cos \theta_{ij})].$$

Using the above equations we have calculated the internal energy and the order parameters for three representative values of A^*/B^* , viz., 0.2, 0.5 and 3.2. The integrals were evaluated numerically using Simpson's rules on an IBM 360 computer. Illustrative curves are shown in figures 1 and 2.

The internal energy plotted as a function of $1/T$ (figure 1) shows the characteristic sigmoid shape. The curves for the ordered and disordered phases meet at the second order transition point T^* . [As we shall see later, T^* is also the temperature at which the short range order parameter $P_2(\cos \theta_{ij})$ in the isotropic phase $= 1/(z-1)$]. The first order transition point T_c is the temperature at which the shaded areas are equal, i.e., when the Helmholtz free energies of anisotropic and isotropic phases are equal. The present calculation gives $T^*/T_c = 0.951, 0.953$ and 0.967 , for $A^*/B^* = 0.2, 0.5$ and 3.2 respectively as compared with 0.95 obtained when the permanent dipolar interaction is neglected⁵. The mean field theory gives $T^*/T_c \simeq 0.90$.

The curves for the short range and long range order parameters as functions of temperature are shown in figure 2. $P_1(\cos \theta_{ij})$ is negative signifying antiparallel ordering. All these curves show discontinuous changes at T_c ; the long range order drops to zero at the transition, but the short range order persists even in the isotropic phase.

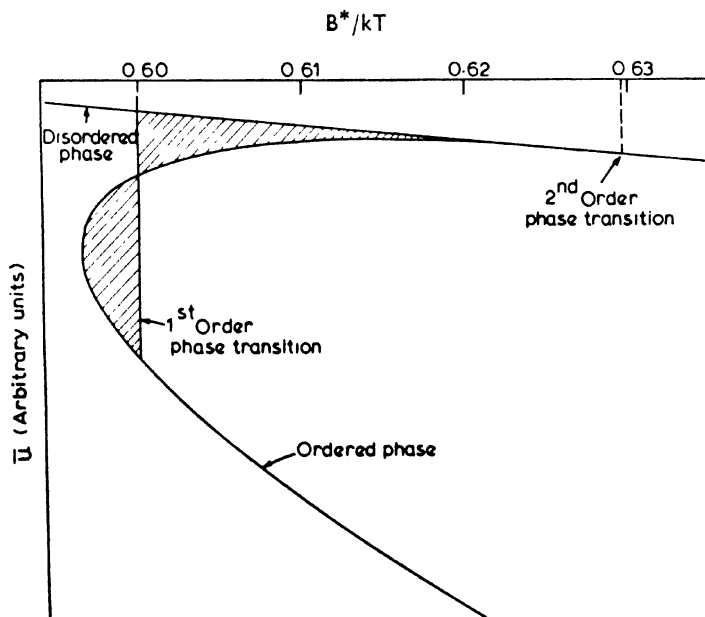


Figure 1 Plot of the internal energy vs reciprocal of temperature for $A^*/B^* = 0.5$. At the first order transition point the shaded areas are equal and at the second order transition point $c_2 = 1/7$.

For comparison, we present in figure 3 the universal curves for the order parameters when the permanent dipole interaction is neglected⁵. As is to be expected putting $A^* = 0$ reduces the value of Q considerably. It is also of interest to note that this curve lies much below the universal curve of the mean field theory according to which $Q \simeq 0.44$ at T_c .

Dielectric constants of the ordered phase

We shall now investigate the dielectric properties of the ordered phase to test whether the model leads to the correct magnitude of the anisotropy. The compounds with nitrile end groups studied by Schadt⁹ show a very strong static dielectric anisotropy. Before developing a theory of the dielectric properties, it must be noted that a low voltage (~ 2 V) was used in these measurements to avoid any disturbing influence on the alignment of the sample, so that the orientational energy due to the external field is small compared to the intermolecular interactions. The field dependent orientational energy arises from two factors (i) the anisotropy of the low frequency molecular polarizability, $\Delta\alpha$, and (ii) the net permanent dipole moment of the molecule. We shall follow closely the treatment of Maier and Meier¹⁰ who have applied the Onsager theory to take into account the effect of the cavity field produced in the medium.

The effective induced dipole moments per molecule along and perpendicular to the unique axis of the medium are respectively

$$\bar{m}_1 = \left[\alpha + \frac{2}{3} \Delta\alpha Q \right] FhE_1$$

$$\bar{m}_2 = \left[\alpha - \frac{1}{3} \Delta\alpha Q \right] FhE_2$$

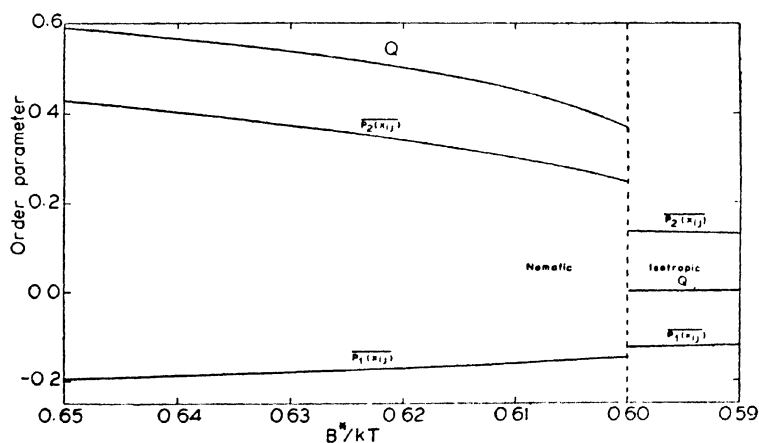


Figure 2 Plot of the short-range order parameter $\bar{P}_1(x_{1j})$ and $\bar{P}_2(x_{1j})$ and the long-range order parameter Q , vs. B^*/kT ; $A^*/B^* = 0.5$.

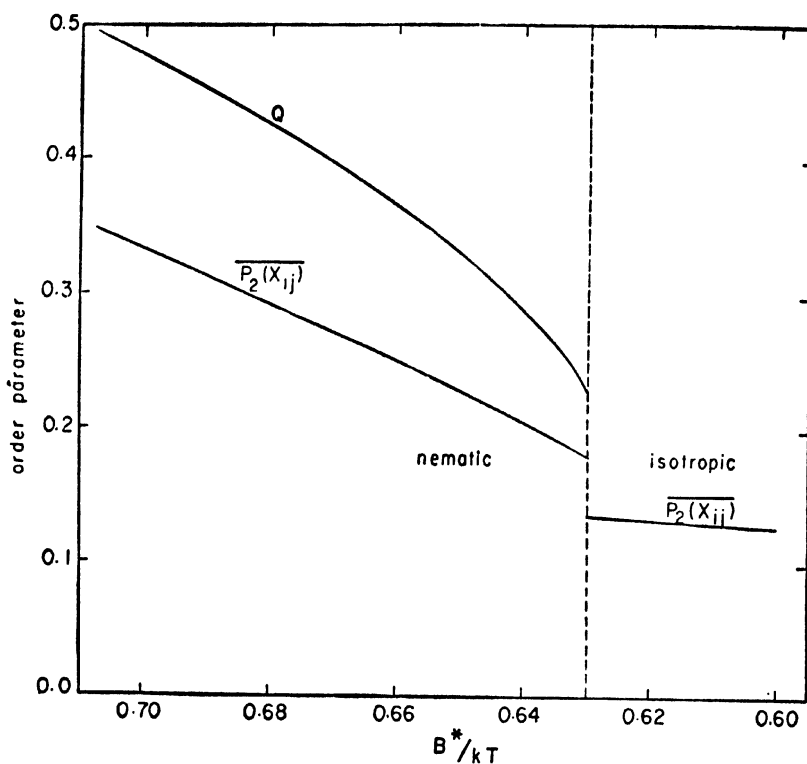


Figure 3 Plot of the short-range order parameter $\overline{P_2(x_{ij})}$ and the long-range order parameter Q vs. B^*/kT ; $A^* = 0$.

where $h = 3\epsilon/(2\epsilon + 1)$ is the cavity field factor, ϵ is the average dielectric constant, $F = 1/(1 - \alpha f)$ is the reaction field factor, α the average polarizability, $f = 4\pi N\rho(2\epsilon - 2)/3M(2\epsilon + 1)$, ρ the density, M the molecular weight and E the applied electric field. (Strictly speaking, these factors require some corrections to allow for the anisotropic dielectric constant, but as we are interested in the order of magnitude of the dielectric anisotropy we shall neglect these corrections.) $Q = \frac{1}{2}(3\cos^2\theta - 1)$ where θ is the angle which the long molecular axis, assumed to be the direction of maximum polarizability, makes with the uniaxial direction.

To calculate the effective permanent dipole moment, we choose XYZ as the space fixed coordinate system, Z being parallel to the unique axis of the medium, and $\xi\eta\zeta$ as the molecule fixed coordinate system, ζ coinciding with the long axis of the molecule. Let ν be the Eulerian angle between the ξ -axis and the line of intersection of the XY and $\xi\eta$ planes, and ν' the angle between this line and the X-axis. We assume as

before that the molecules are cylindrically symmetric so that the permanent dipole moment μ is parallel to the long molecular axis. Since the potential energy of the dipoles due to the external field is small, we can write the effective dipole moment along the field direction as

$$\bar{\mu}_2 = \frac{\int \dots \int [1 + (\mu_{x1} + \mu_{xj}) hE_2/kT] \mu_{x1} \phi(\theta_1, \varphi_1; \theta_j, \varphi_j) \sin\theta_1 d\theta_1 d\varphi_1 \sin\theta_j d\theta_j d\varphi_j}{\int \dots \int [1 + (\mu_{x1} + \mu_{xj}) hE_2/kT] \phi(\theta_1, \varphi_1; \theta_j, \varphi_j) \sin\theta_1 d\theta_1 d\varphi_1 \sin\theta_j d\theta_j d\varphi_j}$$

$$\bar{\mu}_1 = \frac{\int \dots \int [1 + (\mu_{x1} + \mu_{xj}) hE_1/kT] \mu_{x1} \phi(\theta_1, \varphi_1; \theta_j, \varphi_j) \sin\theta_1 d\theta_1 d\varphi_1 \sin\theta_j d\theta_j d\varphi_j}{\int \dots \int [1 + (\mu_{x1} + \mu_{xj}) hE_1/kT] \phi(\theta_1, \varphi_1; \theta_j, \varphi_j) \sin\theta_1 d\theta_1 d\varphi_1 \sin\theta_j d\theta_j d\varphi_j}$$

where $\mu_{x1} = \mu F \cos \theta_1$

and $\mu_{xj} = \mu F \sin \nu'_1 \sin \theta_j$.

(The integration over ν' is essentially the same as integration over φ and hence need not be shown separately). The above integrals then reduce to the form :

$$\bar{\mu}_1 = \frac{hF^2\mu^2}{kT} [\cos^2\theta_1 + \overline{\cos\theta_1 \cos\theta_j}] E_1$$

$$\text{and } \bar{\mu}_2 = \frac{hF^2\mu^2}{kT} [\frac{1}{2} \sin^2\theta_1 + \overline{\sin\nu'_1 \sin\nu'_j \sin\theta_1 \sin\theta_j}] E_2$$

$$\text{Since } \frac{\epsilon_{||} - 1}{4\pi} E_1 = N \frac{\rho}{M} [\bar{m}_1 + \bar{\mu}_1],$$

$$\epsilon_{||} = 1 + 4\pi \frac{N\rho hF}{M} [\alpha + \frac{2}{3} \Delta\alpha Q + \frac{F\mu^2}{3kT} (2Q+1) + \frac{F\mu^2}{kT} \overline{\cos\theta_1 \cos\theta_j}]$$

and similarly

$$\epsilon_{\perp} = 1 + 4\pi \frac{N\rho hF}{M} [\alpha - \frac{1}{3} \Delta\alpha Q + \frac{F\mu^2}{3kT} (1-Q) + \frac{F\mu^2}{kT} \overline{\sin\nu'_1 \sin\nu'_j \sin\theta_1 \sin\theta_j}]$$

In the case of the nitrile compounds we assume $\rho \simeq 1.2$, the average polarizability $\alpha = 28 \times 10^{-24} \text{ cm}^3$, $\Delta\alpha = 15 \times 10^{-24} \text{ cm}^3$ (evaluated by assuming additivity of the bond polarizabilities extrapolated to low frequency and a reasonable structure of the molecule), $\mu = 5 \text{ D}$ along the long axis of molecule. Substituting the theoretically derived Q (figure 2), the calculated variation of $\epsilon_{||}$, ϵ_{\perp} as well as $\epsilon = \frac{1}{2}(\epsilon_{||} + 2\epsilon_{\perp})$ are shown in figure 4. It should be emphasized that if the volume variation is also taken into account, we should get a much more rapid temperature variation of the dielectric constants especially near T_c , but it does not affect the orders of magnitude that we are interested in at present. A comparison with the experimental data of Schadt shows that the theory does indeed lead to the right magnitude of the dielectric anisotropy of these strongly

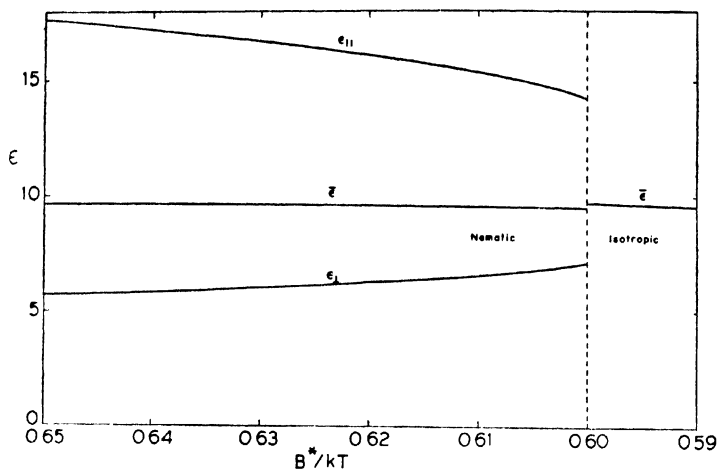


Figure 4 Variation of the dielectric constants $\epsilon_{||}$, ϵ_{\perp} and $\bar{\epsilon} = \frac{1}{2}(\epsilon_{||} + 2\epsilon_{\perp})$ in the nematic and isotropic phases $A^*/B^* = 0.5$.

positive materials. It may be pointed out that if there was antiparallel long range order the dielectric anisotropy would be negative (in analogy with antiferromagnetism).

An interesting result that emerges from Schadt's measurements⁹ on the nitrile compounds is that the mean dielectric constant increases by a few per cent at the nematic-isotropic transition, the value being *higher* in the isotropic phase. The suggestion has been made that this may possibly be attributed to a second order flexoelectric effect¹¹, but in fact a more straightforward explanation can be given in terms of the present model: the increase in the average polarizability (or dielectric constant) of the isotropic phase arises from the decrease in the antiferroelectric short range order $\overline{P_1(\cos \theta_{1j})}$ at T_c (figure 2). The theoretical variation of the mean dielectric constant in the nematic and isotropic phases is shown in figure 4.

Electric and magnetic birefringence in the isotropic phase

We shall first consider the effect of an electric field on the isotropic phase. Unlike the dielectric measurements discussed in the previous section which employ low fields, electric birefringence measurements in the isotropic phase usually require strong fields, ~ 4 kV/cm. When the field is very strong, there is actually a slight shift in the transition temperature in materials of strong positive anisotropy¹², as is to be expected. However, in the present discussion, we shall ignore this small change in

T_c (about 5×10^{-3} K for 4 kV/cm). The theoretical treatment in this case is somewhat more complex because the electric field induces a long range order parameter $\overline{P_1(\cos \theta)}$ in addition to the usual long range parameter Q .

The relative weight for a given configuration of the cluster of $(z+1)$ molecules is now

$$\prod_{j=1}^z f(\theta_{1j}) g(\theta_j) \chi(\theta_i) \chi(\theta_j)$$

where $f(\theta_{1j})$ is the same as defined in (3),

$$g(\theta_j) = \exp \{ [AP_1(\cos \theta_j) + BP_2(\cos \theta_j)] / kT \}$$

$$\chi(\theta_i) = \exp \{ [Fh\mu EP_1(\cos \theta_i) + \frac{1}{2} \Delta \alpha Fh^2 E^2 P_2(\cos \theta_i)] / kT \}$$

$$\chi(\theta_j) = \exp \{ [Fh\mu EP_1(\cos \theta_j) + \frac{1}{2} \Delta \alpha Fh^2 E^2 P_2(\cos \theta_j)] / kT \},$$

and A is another interaction parameter to be determined.

Therefore

$$\begin{aligned} \phi(\theta_1, \varphi_1; \theta_1, \varphi_1) &= f(\theta_{11}) g(\theta_1) \chi(\theta_i) \chi(\theta_j) \\ &\times \prod_{j=2}^z \int \int f(\theta_{1j}) g(\theta_j) \chi(\theta_j) d(\cos \theta_j) d\varphi_j \end{aligned} \quad (5)$$

Since the induced long range order is very small (10^{-4} or less) we may use the infinitesimal approximation. We expand $f(\theta_{1j})$ as

$$f(\theta_{1j}) = \frac{1}{2} D \sum_{k=0}^{\infty} (2k+1) c_k P_k(\cos \theta_{1j})$$

where

$$c_k = \frac{\int P_k(\cos \theta_{1j}) f(\theta_{1j}) d(\cos \theta_{1j})}{\int f(\theta_{1j}) d(\cos \theta_{1j})} \quad (6)$$

is a measure of the short range order in the absence of an external field, and D is the denominator of (6).

Similarly,

$$g(\theta_j) \chi(\theta_j) = \sum_{k=0}^{\infty} a_k P_k(\cos \theta_j) \quad (7)$$

As before, the consistency relation reads

$$\phi(\theta_1, \varphi_1; \theta_1, \varphi_1) = \phi(\theta_1, \varphi_1; \theta_1, \varphi_1).$$

Using (5), (6) and (7), the consistency relation takes the form

$$\frac{1 + a_1 P_1(\cos \theta) + a_2 P_2(\cos \theta)}{\chi(\theta) [1 + a_1 c_1 P_1(\cos \theta) + a_2 c_2 P_2(\cos \theta)]^{z-1}} = \rho \text{ (constant)}$$

We rewrite this as

$$1 + a_1 P_1(\cos \theta) + a_2 P_2(\cos \theta) = \rho [C_0 + C_1 P_1(\cos \theta) + C_2 P_2(\cos \theta)]$$

where

$$C_m = (m + \frac{1}{2}) \int P_m(\cos \theta) \chi(\theta) \left[\sum_{l=0}^{\infty} a_l c_l P_l(\cos \theta) \right]^{z-1} d(\cos \theta).$$

Therefore, for the weakly ordered system,

$$a_1 = C_1/C_0 = (z-1) c_1 a_1 + Fh \mu E / kT$$

$$a_2 = (z-1) c_2 a_2 + \frac{\Delta \alpha Fh^2 E^2}{3 kT} + \frac{(Fh \mu E)^2}{3 k^2 T^2} + \frac{1}{3} (z-1) a_1 c_1 \frac{Fh \mu E}{kT} + \frac{(z-1)(z-2)}{3} a_1^2 c_1^2$$

Hence, the electrically induced long range order

$$\begin{aligned} Q_{el} &= \frac{\int \dots \int P_2(\cos \theta_1) \phi(\theta_1, \varphi_1; \theta_2, \varphi_2) d(\cos \theta_1) d\varphi_1 d(\cos \theta_2) d\varphi_2}{\int \dots \int \phi(\theta_1, \varphi_1; \theta_2, \varphi_2) d(\cos \theta_1) d\varphi_1 d(\cos \theta_2) d\varphi_2} \\ &= \frac{1}{3} (a_2 + c_2 a_2 + \frac{1}{3} c_1 a_1^2) \\ &= \left[\frac{\Delta \alpha Fh^2 E^2}{3 kT} + \frac{(Fh \mu E)^2}{3 k^2 T^2} \frac{1 - (z-1) c_1^2}{\{1 - (z-1) c_1\}^2} \right] \frac{1 + c_2}{5 \{1 - (z-1) c_2\}} \\ &\quad + \frac{1}{15} \frac{c_1 (Fh \mu E)^2}{k^2 T^2 \{1 - (z-1) c_1\}^2} \end{aligned} \quad (8)$$

The short range order parameters c_1 and c_2 depend only on the two particle interaction constants A^* and B^* . If the applied field is magnetic, we put $F = h = 1$, $\mu = 0$ and replace $\Delta \alpha$ by $\Delta \eta$ in (8) to obtain⁵

$$Q_{mag} = \frac{\Delta \eta H^2}{15 kT} \frac{1 + c_2}{1 - (z-1) c_2} \quad (9)$$

Since there is no spontaneous $\overline{P_1(\cos \theta)}$ type of long range order in the nematic phase, the second order transition point is determined by the temperature T^* at which $c_2 = 1/(z-1)$. Thus as has been shown previously⁵, Q_{mag} given by (9) varies as $(T - T^*)^{-1}$ to a very good approximation. On the other hand, if the dipolar interactions are very large, Q_{el} given by (8) may exhibit a slower variation. For example, it is found that for $A^*/B^* = 0.2$ and 0.5 , the exponent $\gamma \sim 1.0$ as in the case

of magnetic birefringence. However for $A^*/B^* = 3.2$, $\gamma \sim 0.7$. The Kerr constant measurements of Schadt and Helfrich¹³ on some strongly positive nematogenic materials indicate that the γ may indeed be less than 1 at temperatures well above T_c . Further studies on the magnetic and electric birefringence of such materials would be of much interest.

In principle the arguments put forward here should, with suitable modifications, be applicable to negatively anisotropic materials also. Further, this model has a bearing on the flexoelectric effect¹⁴. Qualitatively, it can be seen that the magnitude of the effect will be diminished because of the tendency of the neighbouring dipoles to be antiparallel.

References

- 1 BORN M *Sitz. d. Phys.-Math.* **25** 614 (1916)
- 2 SZIVESSY G *Z. Phys.* **31** 159 (1926)
- 3 VORLANDER D *Z. Phys. Chem.* **A126** 449 (1927)
- 4 VAN DER VEEN J, DE JEU W H, GROBBEN A H and BOVEN J *Mol. Cryst. Liquid Cryst.* **17** 291 (1972)
- 5 MADHUSUDANA N V and CHANDRASEKHAR S *Solid State Commun.* **13** 377 (1973); *Pramāṇa* **1** 12 (1973)
- 6 DE GENNES P G *Mol. Cryst. Liquid Cryst.* **12** 193 (1971)
- 7 MADHUSUDANA N V and CHANDRASEKHAR S *Liquid Crystal and Ordered Fluids* Vol. 2 ed JOHNSON J F and PORTER R S (Plenum, New York) p. 657 (1973)
- 8 KRIEGER T G and JAMES H M *J. Chem. Phys.* **22** 496 (1954)
- 9 SCHADT M *J. Chem. Phys.* **56** 1494 (1972)
- 10 MAIER W and MEIER G *Z. Naturforsch.* **A16** 262 (1961)
- 11 DERZHANSKI A and PETROV A G *Phys. Lett.* **34A** 427 (1971)
- 12 HELFRICH W *Phys. Rev. Lett.* **24** 201 (1970)
- 13 SCHADT M and HELFRICH W *Mol. Cryst. Liquid Cryst.* **17** 355 (1972)
- 14 MEYER R B *Phys. Rev. Lett.* **22** 918 (1969)

DISCUSSION

de Vries: Your model has z nearest neighbours around the reference molecule. You stated that of these z molecules no two are nearest neighbours of each other. How do you physically picture this?

Chandrasekhar: It merely implies that in writing down the pairwise interaction of the central molecule with its z nearest neighbours, the interaction between any two of the z neighbours is neglected. It is an approximation that is often used in such problems.

Blinic: You are in fact using the Bethe approximation.

Chandrasekhar: Yes, that is correct. It is Bethe's method as modified by Krieger and James for treating orientational transitions in crystals.

Blinic: Why not also include the P_1 type of long range order in the theory?

Chandrasekhar: We have made the physically realistic assumption that long range antiferroelectric order is not present in the nematic liquid. Indeed even ferromagnetism in the liquid state is considered to be improbable*.

Nityanaha: Was the exponent of the magnetic birefringence 0.7 from the analytical form of the expressions or from fitting the numerical results? As a question of principle I felt it should be one near T_c for a Bethe type of calculation.

Chandrasekhar: The exponent $\gamma \sim 1$ for magnetic birefringence and < 1 for electric birefringence when dipolar interactions are large result from the analytical form of the expressions at temperatures *not too close* to the second order transition point T^* . The particular value of 0.7 for the electric case was, of course, got for a specific ratio of the P_1 to P_2 types of interaction. Very close to T^* , the exponent does in fact tend to approach unity.

* See e.g., Honda K and Kato Y *Phys. Lett.* 44 497 (1973)

Experimental studies of short range order in nematogens of strong positive dielectric anisotropy

**B R RATNA, M S VIJAYA, R SHASHIDHAR and
B K SADASHIVA**

Raman Research Institute, Bangalore 560006, India.

Abstract. The magnetic and electric birefringence in the isotropic phase of 4'-*n*-hexyl-4-cyanobiphenyl, a nematogen of high positive dielectric anisotropy, have been measured as functions of temperature. Both show a $(T-T^*)^{-1}$ dependence in the range of temperatures studied. We also report the dielectric constants of 4'-*n*-octyloxy-4-cyanobiphenyl measured in the nematic and isotropic phases. The mean dielectric constant shows a slight increase on passing from the nematic to the isotropic phase. These results are in conformity with the model of antiferroelectric short range order proposed by Madhusudana and Chandrasekhar.

Introduction

It has been experimentally established that the magnetic birefringence^{1,2,3} in the isotropic phase of a nematogen can be described in terms of de Gennes' model according to which the temperature dependence is given by $(T-T^*)^{-1}$ where T^* is the hypothetical second order transition point. On the other hand, the electric birefringence of the few compounds that have been studied^{2,4} does not follow this type of behaviour. For example, in *p*-azoxyanisole (PAA) there is a reversal of sign of electric birefringence a few degrees above the nematic-isotropic transition point T_* ². Madhusudana and Chandrasekhar⁵ have shown that this reversal in PAA can be explained on the basis of the phenomenological model when proper allowance is made for the contributions of the polarizability and the permanent dipole moment. From their theory it follows that compounds with dipole moments parallel to the long molecular axis should show a temperature dependence similar to that of magnetic birefringence, viz., as $(T-T^*)^{-1}$. Schadt and Helfrich⁴ have measured the Kerr constant (in the isotropic phase) of some compounds with strong positive dielectric anisotropy and have reported that the temperature dependence of the electric birefringence is expressible as $(T-T_*)^{-\tau}$ where τ ranges between 0.5-0.7. They have remarked that it would be of interest to see if the magnetic birefringence of such compounds also exhibit a slower temperature variation.

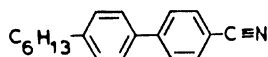
Madhusudana and Chandrasekhar⁶ have recently proposed a model of antiferroelectric short range order in materials which have strong positive dielectric anisotropy. Two important consequences of their theory are

(i) the mean dielectric constant should increase slightly on going over from the nematic to the isotropic phase, (ii) the electric and magnetic birefringence should show essentially the same type of behaviour, viz., $(T - T^*)^{-1}$. However, if the dipolar or $P_1 \cos \theta_{11}$ interactions are extremely strong, much greater than $P_2 \cos \theta_{11}$ interactions, then the electric birefringence may exhibit a slower variation at temperatures well above T_* , whereas the magnetic birefringence should still vary as $(T - T^*)^{-1}$. The present experimental study was undertaken to verify these predictions.

So far no extensive studies of both magnetic (Δn_M) and electric birefringence (Δn_E) of a strongly positive material have been reported. We have carried out precise measurements of Δn_M and Δn_E , using highly purified 4'-*n*-hexyl-4-cyanobiphenyl (HCB), over a wide range of temperatures. It is established that the temperature variation of both Δn_M and Δn_E is well represented by $(T - T^*)^{-1}$ throughout the range, in agreement with the prediction of Madhusudana and Chandrasekhar. We have also measured the principal dielectric constants in the nematic and isotropic phases of 4'-*n*-octyloxy-4-cyanobiphenyl (OOCB). The value of ϵ obtained by extrapolating the isotropic dielectric constant ϵ_{is} into the nematic phase is found to be significantly higher than the mean dielectric constant $\bar{\epsilon}$ in the nematic phase confirming an earlier observation by Schadt⁷. This result is again in agreement with the theory of antiparallel correlation.

Experimental

(1) *Electric and magnetic birefringence*: HCB⁸ used in the experiments



was synthesized in the laboratory. The nematic-isotropic transition temperature was 29.1° C. The conductivity of the sample was of the order of 10^{-10} ohm⁻¹ cm⁻¹.

The schematic diagram of the experimental set up used for the magnetic and electric birefringence measurements is shown in figure 1. Light from He-Ne gas laser was linearly polarized at an angle of 45° to the field direction. The emergent light from the sample was allowed to fall on a $\lambda/4$ plate whose principal axes were inclined at 45° to the field (electric or magnetic) direction, so that the phase retardation could be measured as a rotation of the plane of polarization. The angle of rotation was measured by means of a graduated analyzer (Winkel-Zeiss No. 103071) reading to an accuracy of 0.02°. The position of the minimum intensity was located using a photomultiplier tube (Philips PW 4111) in conjunction with a

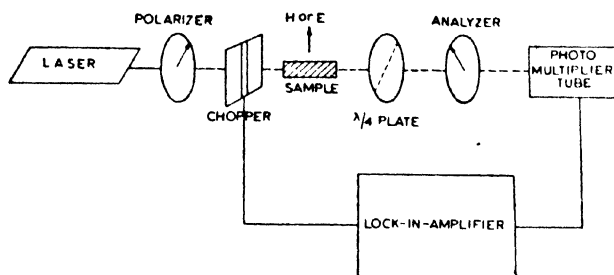


Figure 1 Schematic diagram showing the experimental set up used for the electric and magnetic birefringence measurements.

lock-in-amplifier (Unipan-Selective Nanovoltmeter, type 227, Homodyne Rectifier Voltmeter, type 202B). For magnetic birefringence measurements the incident light was modulated using an electronic chopper (American Time Products, type TNC-1.8C) of frequency 400 Hz. For electric birefringence measurements the AC field itself served as the modulation.

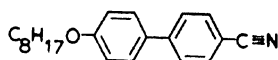
An optical cell of 1 cm path length was used for the electric birefringence measurements. Electrodes made of non-magnetic stainless steel were inserted in the cell with teflon spacers. The separation between the electrodes was 0.32 cm. A 500 Hz AC field of 3.12 kV/cm was used. As the sample had very low conductivity, there was no electrohydrodynamic instability at this field. The glass cell was enclosed in a copper chamber with suitably provided optically flat glass windows. This chamber was electrically heated. The temperature of the sample was measured by Chromel-Alumel thermocouple to an accuracy of 0.025° C.

HCB being a strongly positive compound its electric birefringence is expected to be an order of magnitude greater than the magnetic birefringence with the fields normally available in the laboratory. In order that the Δn_M could be measured to the same accuracy as Δn_E it was necessary to increase the path length, and a separate cell was designed for this purpose. The sample was contained in a narrow teflon tube of length 10 cm sealed at both ends using optical windows. The sample tube was inserted in a copper jacket to ensure good thermal capacity and the entire assembly was placed inside a heater whose temperature could be controlled accurately. By keeping temperature probes at different positions of the sample tube it was ascertained that there were no temperature gradients within the sample. A magnetic field of 6.9 kgauss was used.

The chambers containing the sample cells were filled with nitrogen to prevent oxidation of the sample. The cell constants were evaluated by measuring the Kerr constant and Cotton-Mouton constant of nitrobenzene.

The absolute accuracy of the measurement for electric birefringence was found to be about 1% and that for magnetic birefringence 1.5%.

(2) *Dielectric constants*: The substance studied was OOCB⁸ which has



a nematic range of 67–80.5°C. Below 67°C it exhibits a smectic phase which however has not been identified.

The dielectric constants were measured at 1 kHz using a General Radio impedance bridge (Type 1656) with a digital readout and capable of measuring the capacitance to an accuracy of 0.1 pf. The dielectric cells consisted of two tin-oxide coated glass plates. The separation between the electrodes was fixed by 25–50 μ thick mylar spacers. The cell was kept inside an electrically heated copper chamber provided with glass windows for checking the alignment of the sample visually during the measurements. This chamber was evacuated and filled with nitrogen. Homeotropic alignment was obtained by treating the glass plates with a surface agent. A 17 kgauss magnetic field was used to align the sample homogeneously. The dielectric constant was determined by measuring the capacitance of the cell without and with the sample. The bridge voltage across the capacitor plates was very low (300 mV) and did not have any disturbing influence on the alignment of the sample. The values of ϵ_{\parallel} obtained from the independent measurements in the two geometries matched to within $\pm 0.2\%$. Thus the relative values of ϵ_{\parallel} and ϵ_{\perp} are reckoned to be accurate to within these limits, but absolute values are estimated to be accurate to only $\pm 3\%$.

Results

The plot of the reciprocal of the electric and magnetic birefringence versus temperature is shown in figure 2. The magnetic birefringence measured upto 12°C above the transition temperature (T_*), shows $(T - T^*)^{-1}$ behaviour throughout. Measurement above this temperature was not possible owing to the fact that the variation of Δn_M became comparable to the accuracy of the instrument. However, the electric birefringence could be measured upto 25°C above T_* and it also shows a similar temperature dependence throughout the range. Both measurements give the same value of T^* ($T^* = 28^\circ\text{C}$, $T_* - T^* = 1.1^\circ\text{C}$).

Figure 3 shows the variation of the principal dielectric constants of OOCB with temperature. It exhibits large anisotropy ($\epsilon_{\parallel} > 2\epsilon_{\perp}$) evidently

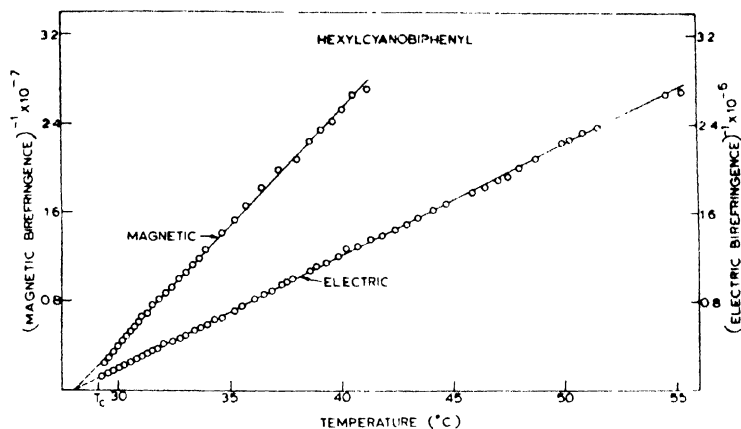


Figure 2 Plot of the reciprocal of the magnetic and electric birefringence versus temperature in HCB. (Both give the same T^* , $T^* = 28^\circ\text{C}$, $T_o - T^* = 1.1^\circ\text{C}$).

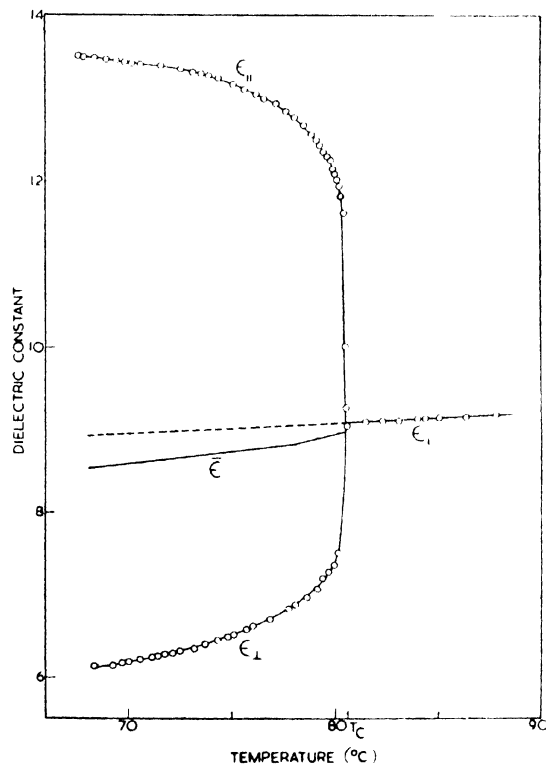


Figure 3 Principal dielectric constants of OOCB. ($\bar{\epsilon}$ is the mean dielectric constant evaluated from the experimental values of ϵ_{\parallel} and ϵ_{\perp} . The broken line denotes the extrapolated value of ϵ_{\perp}).

because of the strong dipole moment along the molecular axis. The mean dielectric constant, $\bar{\epsilon} = \frac{1}{3}(\epsilon_{\parallel} + 2\epsilon_{\perp})$ is also shown in the figure. It can be seen that it is 2-3% lower than the extrapolated value of ϵ_{is} denoted by the dashed line. This is in accordance with the theory of antiferroelectric short range order in nematic liquid crystals of positive dielectric anisotropy.

Acknowledgements

We wish to thank Professor S Chandrasekhar for his continued interest and advice and Dr N V Madhusudana for valuable suggestions and help in setting up the apparatus.

References

- 1 ZADOC-KAHN J *Ann. Phys. (Paris)* **11** 455 (1936)
- 2 TAVITKOV V N and RYUMTSEV E I *Sov. Phys. Crystallogr.* **13** 225 (1968)
- 3 STINSON T W and LITSTER J D *Phys. Rev. Lett.* **25** 503 (1970)
- 4 SCHADT M and HELFRICH W *Mol. Cryst. Liquid Cryst.* **17** 355 (1972)
- 5 MADHUSUDANA N V and CHANDRASEKHAR S *Liquid Crystals and Ordered Fluids* Vol. 2, ed JOHNSON J F and PORTER R S (Plenum, New York) p. 657 (1973)
- 6 MADHUSUDANA N V and CHANDRASEKHAR S, This conference (1973)
- 7 SCHADT M J. *Chem. Phys.* **56** 1494 (1972)
- 8 GRAY G W, HARRISON K J and NASH J A *Ele. Lett.* **9**(6) 130 (1973)

Crystal structure of *n*-*p*-methoxybenzylidene-*p*-phenylazoaniline

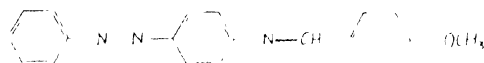
KALYANI VIJAYAN* and G V VANI**

* Materials Science Division, National Aeronautical Laboratory
Bangalore 560017, India

** Raman Research Institute, Bangalore 560006, India.

Abstract. The crystal structure of *n*-*p*-methoxybenzylidene-*p*-phenylazoaniline, a nematogenic compound of positive dielectric anisotropy has been determined by x-ray diffraction methods using single crystals. It is established that the nearest neighbours are oriented antiparallel with respect to each other.

As part of a programme of x-ray investigations on mesogenic compounds the crystal structure analysis of *n*-*p*-methoxybenzylidene-*p*-phenylazoaniline



in its crystalline phase was undertaken. The compound forms a nematic mesophase at 149° C and becomes isotropic at 184° C.

Orange coloured needles of the compound were obtained by slow evaporation from a solution in toluene. The space group and unit cell dimensions were determined from oscillation and Weissenberg pictures and are given in table 1 along with other relevant crystal data. Three-dimensional intensity data were collected from reciprocal levels h ko, h kl, $h=0, 1, 2, 3, 4$ and 5 using nickel filtered copper radiation. It must

Table 1

Molecular formula	$C_{20}H_{17}ON_3$
Space group	$P2_1/c$
$a = 9.79 \pm 0.04 \text{ \AA}$	
$b = 23.75 \pm 0.04 \text{ \AA}$	
$c = 15.67 \pm 0.03 \text{ \AA}$	
$\beta = 112^\circ 26'$	
$Z = 8$	
$\mu = 6.356 \text{ cm}^{-1}$	
$\rho_{\text{calc}} = 1.26 \text{ gm cm}^{-3}$	
$\rho_{\text{obs}} = 1.25 \text{ gm cm}^{-3}$	

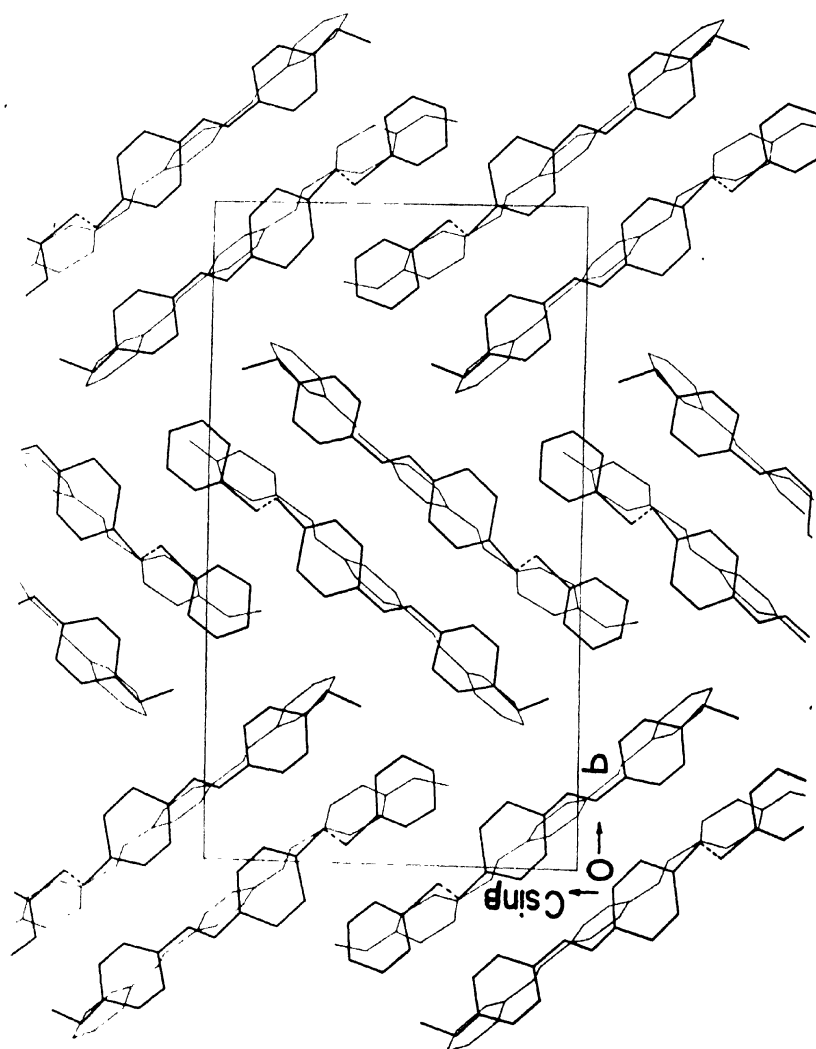


Figure 1 (i)

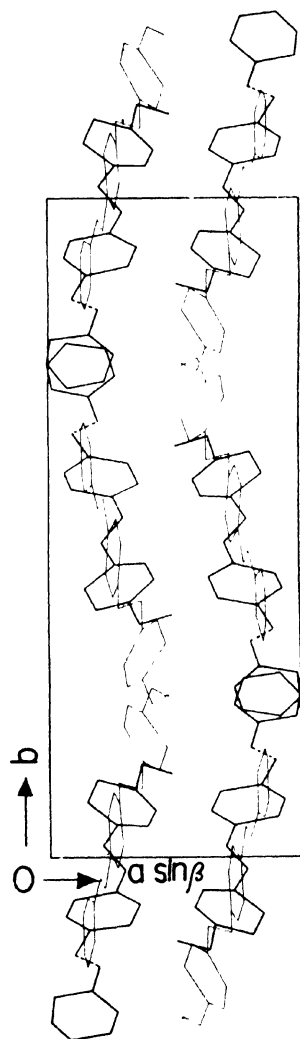


Figure 1 (ii)

Figure 1 View of the structure as seen perpendicular to the (i) *a*-axis and (ii) *c*-axis. The thick and the thin lines denote the crystallographically independent molecules in the unit cell. The broken lines denote the $-N \equiv N-$ bond.

be mentioned that even with optically clear single crystals the diffraction pattern was not of high quality and moreover they did not extend to the high angle region. The photographically recorded intensities were estimated visually and were corrected for Lorentz-polarisation factors, absorption and spot shape effects.

The solution of the structure was initiated by computing a three-dimensional Patterson map. The continuous distribution of vector density in the Patterson map indicated only the possible orientations of the molecules in the unit cell. Trial calculations were, however, carried out on the basis of molecular models fixed by examining a few intense low angle reflections. The solution of the structure was simultaneously attempted by the direct methods¹ also. The MULTAN computer programme of Germain *et al.*², as modified by Ramakumar and Murthy for the IBM 360/44 computer, was used for generating the signs of reflections. From the E-map corresponding to the best solution of the MULTAN, a few atoms of one of the molecules in the asymmetric part could be identified; but, there was no indication of the atomic positions of the other crystallographically independent molecule in this map. Using the set of atomic positions obtained from the E-map as the starting point and employing packing considerations and trial calculations the complete structure was derived in several stages. The initial R-factor for the correct model was 51.9% for 1074 observed reflections. The positional and thermal parameters of the atoms have been refined to $R = 17.3\%$ by leastsquares method. Further refinement of the structure is in progress.

Figures 1(i) and 1(ii) show the arrangement of molecules in the planes perpendicular to the *a*- and the *c*-axes respectively. The two crystallographically independent molecules in the unit cell are oriented antiparallel to each other and are nearly one above the other, separated by a distance of about 5 Å along the *a*-direction. The planes of the benzene rings in the two molecules are not parallel, the maximum tilt between them being about 90° near the molecular centres. Also, in each molecule, the benzene ring to which the methoxy group is attached is tilted with respect to the plane of the other two rings. Detailed description of the molecular geometry and other structural features will be discussed elsewhere.

The authors wish to thank Prof S Chandrasekhar and Dr S Ramaseshan for their keen interest in the problem; Dr M Vijayan for many useful discussions; Dr B Swaminatha Reddy, Mr T P Singh and Mr T N Bhat for help in computations; Mr S Ramakumar and Mr M R N Murthy for making modified version of the MULTAN programme available to them.

References

- 1 KARLE I L and KARLE J *Acta Cryst.* **21** 849 (1966)
- 2 GERMAIN G, MAIN P and WOOLFSON M M *Acta Cryst.* **A27** 368 (1971)

The structure of liquid crystals

B K VAINSHTEIN and I G CHISTYAKOV

Institute of Crystallography, Academy of Sciences of the USSR,
Leninsky pr. 59, Moscow B-333, USSR.

Abstract. The investigation of the structure of liquid crystals was carried out with the help of x-ray analysis and calculations of statistical distribution functions. The latter are the functions of inter-atomic distances, and their one-dimensional sections are: (i) the linear distribution function of atoms in the axis of texture, and (ii) the cylindrical distribution function of atoms in the basic plane.

The angular distribution of the long molecular axes and the degree of orientation in the liquid crystal was also used.

Besides the calculation method, the method of optical synthesis of functions was also applied.

For the study of the structure of liquid crystals one can also use the idea of the paracrystalline state and investigate the influence of various disturbances on the diffraction pattern.

In the present work we shall attempt to analyse some problems connected with x-ray studies of liquid crystals which have been carried out during the last decade. Information on earlier work can be found in the detailed review by Brown¹ and in Gray's monograph².

•

1. On the classification of liquid crystals

It is known that the classification of liquid crystals accepted shortly after their discovery is of a rather general character. The necessity of taking into account the polymorphism of liquid crystal structures, the presence of the molecular order intermediate between a solid and liquid makes it necessary to combine the ideas of symmetry with those of statistics. In a liquid crystal of an ordinary classical type the elongated molecules are oriented in one direction which leads to macroscopic anisotropy of properties. At the same time, the substance possesses the rheological properties of a liquid. In a solid crystal the molecules are arranged regularly in three dimensions. One can describe the liquid crystalline state by proceeding from a solid crystal and introducing in it the various distortions of ordering which can be characterized by statistical distribution functions. To these can be referred:

1. shifts of the molecules along the z -axis (the direction of preferred orientation of the long molecular axes is taken as the z -axis). These distortions can be characterized by the displacement function $\tau(z)$.

2. azimuthal rotations around the z -axis described by the rotation function $f(\psi)$.

3. inclinations of the molecules to the z -axis defined by the angular distribution function of the molecular axes $D(\alpha)$.

4. deviations in two-dimensional periodicity in the plane XY which are described by the $W(xy)$ function of distortions of the ideal network. This function can be used both for characterizing the molecular arrangement within the smectic layers and for characterizing the arrangement of the projection of the molecular centers of gravity in the basal plane. These functions themselves possess a definite symmetry, and therefore their use in one or other combinations characterize the symmetry and structure of the liquid crystal. Apparently, such statistical symmetry elements as $W(xy)$, $D(\alpha)$ are peculiar to all structures; on these grounds, we can denote them by one symbol:

$$B_i = [W(xy), D(\alpha), f(\psi)]$$

The index $i = 1 \dots 5$ denotes the two-dimensional translation group: 1-square group, 2-hexagonal group, 3-rectangular group, 4-rhombic group, 5-monoclinic group. Thus the symbol of the structure of the classical nematic mesophase can be written as

$$\tau_\infty(z)(B_1)$$

where $\tau_\infty(z)$ is the symbol of operation of the infinitely small translations. Peculiar to some nematic liquid crystals is the pseudo layer structure (5). In this case, the displacement function should be ascribed to the molecular group $\tau_\infty^*(z)$. For the oblique cybotactic nematic mesophases one has to take into account the angle of inclination of the molecules to the pseudo layers $\varphi(\hat{eN})$: $\tau_\infty^*(z) B_i \varphi(\hat{eN})$.

Peculiar to cholesteric liquid crystals is the helical symmetry $\mathcal{C}_\bullet(z)A$: here C is the period of the cholesteric helical structure (pitch of the helix).

In order to describe the smectic liquid crystals, it is necessary to introduce additional characteristics, namely: to indicate the period C of the layer, the symmetry elements (if necessary) characterizing the layer itself, the angle $\varphi(\hat{eN})$ between the direction of the long molecular elements S_i describing the mutual disposition of the layers ($m, 2, \bar{1}$) and so on.

Thus the symbol of symmetry of smectic liquid crystals is written as

$$CBS_i, \varphi, S_2$$

Determination of the various combinations of statistical symmetry elements and additional characteristics allows one to separate 60 types of smectic structures.

In an extension of such a systematization one can take into account the block structure of liquid crystals. To characterize the block liquid crystal aggregate we can use the following notation:

$$[\mathbf{x}] \times [\mathbf{y}]$$

where $[\mathbf{x}]$ is the symbol of the block structure, \mathbf{x} – the symbol of the mutual ordering of the blocks and $[\mathbf{y}]$ – the symbol of the structure of the intermediate zones.

It goes without saying that the above scheme is only tentative and, to some extent, hypothetical. Only a few types of liquid crystal structures have been investigated. We can apply to them with certainty some of the symbolic notations.

2. The matrix of distortions and optical modeling of the structure

Some parameters of disordering of the liquid crystal structures can be estimated by using the theory of a "paracrystal"³⁻⁵. The matrix of root-mean-square mutual shifts of the centres of neighbouring molecules is, in the general case, of the form

$$\begin{vmatrix} \Delta_{xx} & \Delta_{xy} & \Delta_{xz} \\ \Delta_{yx} & \Delta_{yy} & \Delta_{yz} \\ \Delta_{zx} & \Delta_{zy} & \Delta_{zz} \end{vmatrix}$$

In accordance with these representations we can analyze the influence of various distortions on the diffraction patterns. To do this we must construct two-dimensional models of the structure and obtain diffraction patterns in a laser beam from their reduced images (masks)⁶⁸.

It should be noted that, using two-dimensional models, we cannot describe directly the distortions in three dimensions. If the model is built up in the x, z -coordinates, then the deviations along y are omitted. However, indirectly this can be taken into account by, let us say, imaging the inclined molecules of a different length. The rotation of the molecules in the x, y plane can be carried out by using images of the molecules of different thickness etc.

Figure 1 shows a model of the ideal two-dimensional crystal, and its diffraction pattern.

Let us trace the influence of various distortions on the character of the diffraction pattern. Figure 2a shows a model in which the periodicity between the centers of the molecules is disrupted in the x -direction (the

same, naturally, refers to the y -direction). The matrix components are Δ_{xy} and Δ_{xz} (radial statistics). This leads to the appearance of diffuse equatorial reflections (figure 2b). Figure 3 illustrates the influence of the shifts. If the latter are insignificant and continuous, then this corresponds to the correlated inclination of the layers. Here Δ_{xz} and $\Delta_{xy} \neq 0$. In reciprocal space we have a system of two-dimensional rods the diameter of which increases with the z -coordinate. Intersection of these rods with the system of the layer planes perpendicular to them leads to the formation of point assemblies in zero plane ($l = 0$). With increasing l -order these assemblies smear out into circles which merge thereafter (figure 3b).

Figure 4a, b shows a model of a smectic liquid crystal with distortions of periodicity along the x - and z -axes, and the corresponding diffraction pattern.

Of special interest is the consideration of the inclination of the molecules relative to the z -axis, since this distortion is, apparently, peculiar to all liquid crystals. A model of the liquid crystal with inclination in the layers is shown in figure 5. The angle of inclination for different molecules is different, but it changes within the limits of 30° with respect to the z -axis. In this case $\Delta_{xz} = \Delta_{xy} \neq 0$. On the diffraction pattern of figure 5b, in addition to sharp layer reflections along the meridian ($h = k = 1$), we can observe diffuse equatorial reflections. Such diffraction patterns bear a strong resemblance to the x-ray patterns of smectic liquid crystals (type A).

Now let us trace the influence of the correlated inclinations of the molecules relative to the z -axis. Figure 6a shows a model of the smectic liquid crystal with the correlated inclination at an angle φ to the z -axis. The diffraction pattern of figure 6b has two equatorial reflections located along the diagonal inclined to the equator at angle φ . The function $D(\alpha)$ characterizing the deviation of the molecular axes with respect to the texture axis Z is shown up in figure 6b. The intensity maximum lies on the beam corresponding to the φ angle.

The alternating inclinations of the molecules in the layers (figure 7a) lead to the appearance of four equatorial reflections (figure 7b).

The models shown in figures 6 and 7 elucidate the structure of smectic liquid crystal of C-type. Figure 8a shows a model of the smectic structure with variation of the angle of inclination of the molecules from one layer to another. The diffraction pattern exhibits six equatorial reflections (figure 8a). The function $D(\alpha)$ is shown up in figure 8b. An x-ray pattern of the smectic phase E of dipropyl-*p*-terphenyl-4,4' carboxylate, possessing such six equatorial reflections, is given in Ref. (55). It may well be that the molecular arrangement analogous to that shown in the model (figure 8) elucidates the origin of these reflections.

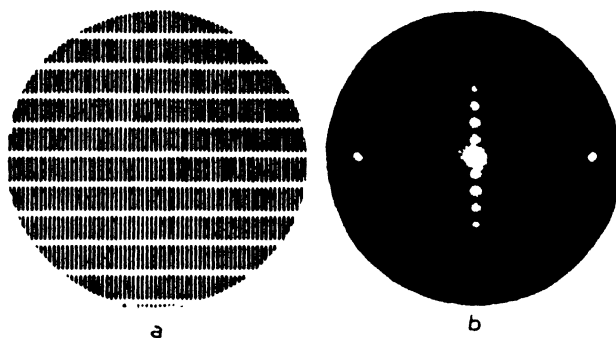


Figure 1 Model of the ideal "smectogenic" crystal (a) and optical diffraction pattern (b).

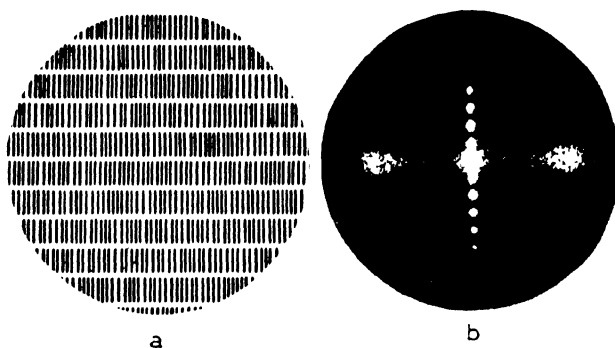


Figure 2 Distortion periodicity in the direction OX (a) and its influence on the diffraction pattern (b).

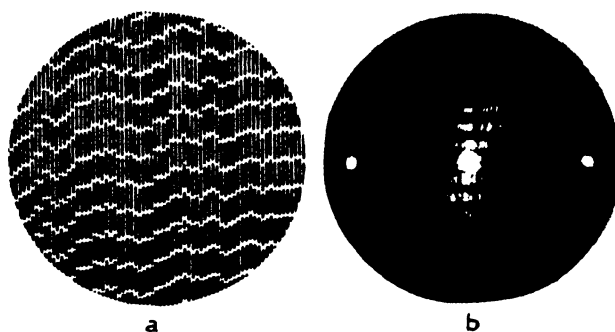


Figure 3 Shifts (a) and their influences on the diffraction pattern (b).

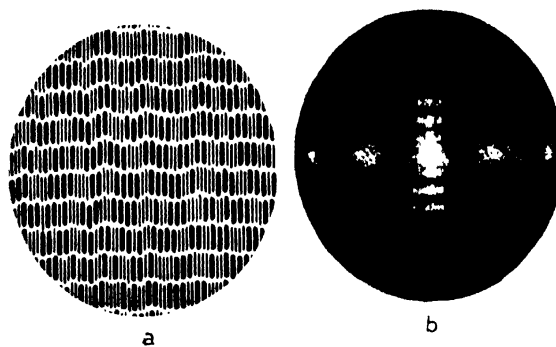


Figure 4 Distortions of periodicity in the directions OX and OZ (a) and their influences on the diffraction pattern (b)

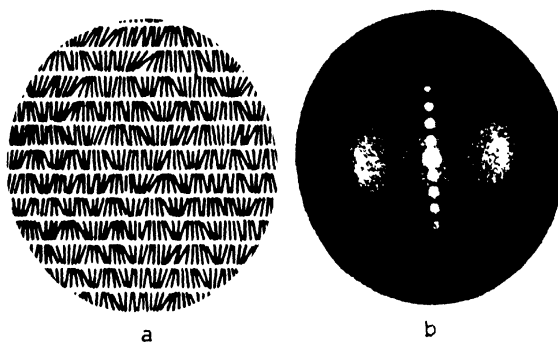


Figure 5 Model of the smectic liquid crystal with inclinations of the molecules in the layers (a) and the corresponding optical diffraction pattern (b)

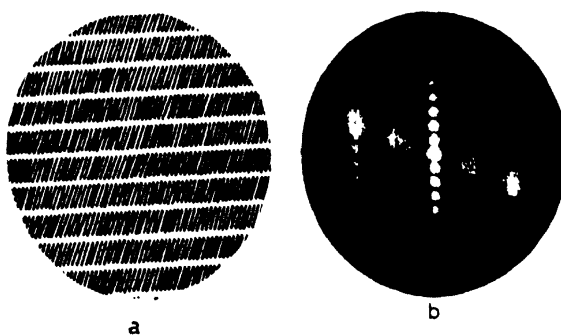


Figure 6 Model of the smectic liquid crystal with the correlated inclination of the molecules in layers (a) and the optical diffraction pattern (b).

The nematic crystals possess shifts in addition to other distortions. In this case $\Delta_{xz}u \Delta_{yz} \neq 0$.

A model of the "nematogenic" crystal and its optical diffraction picture are shown in figure 9. The continuous shift at $\Delta_{xy} = \Delta_{yx} = 0$ without distortions along the x -axis (figure 10a) leads to the appearance of the layer lines along the meridian (figure 10b). Due to distortions along the x -axis (figure 11a), the regions of one-dimensional diffraction on layer lines decrease, while at the equator the reflections of intermolecular interference smear out in the meridional direction (figure 11b). Such a picture resembles, in general outlines, the x-ray patterns from real nematic mesophases.

3. X-ray analysis of liquid-crystal structures

The investigation of nonoriented liquid crystal samples is usually carried out by means of an analysis of the change in the interplanar distances with the change of temperature⁷⁻⁹, or by measurements of the intensity of the main reflections¹⁰⁻¹³. The most effective method is the calculation of the radial distribution function¹⁴⁻¹⁶.

More detailed information on the structure can be obtained from x-ray patterns of oriented samples. In this case, in order to analyze the structure, we can use the cylindrical distribution function (cylindrical Patterson function)²⁶⁻⁴⁴:

$$Q(rz) = 2 \iint |F(RZ)|^2 J_0(2\pi rR) \cos(2\pi zZ) 2\pi R dR dZ \quad (1)$$

This function gives the most exhaustive description of the structure since when calculating it we use the intensity distribution throughout the full volume of reciprocal space.

However, in a number of cases, we can use the one-dimensional sections of the function $Q(rz)$. The Fourier transform of the intensity distribution along the meridian yields the linear distribution function of the atoms:

$$\rho(r) = \rho_0 + \frac{1}{\pi} \int i(S) \cos(Sr) dS \quad (2)$$

This function reveals the intramolecular interatomic distances. The Fourier-Bessel transform of the intensity along the equator gives the cylindrical distribution function of the projections of the atoms on the basal plane:

$$2\pi r Z_m(r) = 2\pi r Z_0 + 4\pi^2 r \int i(R) J_0(2\pi rR) R dR \quad (3)$$

Integral (3) can also be used for computing the cylindrical distribution function of the projections of the molecular axes on the basal plane $2\pi r Z_m(r)$. In this case

$$I(R) = \frac{I_s - |\bar{F}_s|^2}{|\bar{F}_s|^2}$$

Here $|\bar{F}_s|^2$ and $|\bar{F}_s|^2$ are the square of the averaged structure amplitude of the molecule and its mean-square, respectively. Their values are defined by the expressions:

$$|\bar{F}_s|^2 = [\sum_{j=1}^n f_j(R) J_0(2\pi r_{jk} R)]^2$$

$$|\bar{F}_s|^2 = \sum_k \sum_j f_k f_j J_0(2\pi r_{jk} R)$$

The value $2\pi r_{jk}$ is the number of the molecular centers of gravity falling on 1\AA^2 .

The intensity distribution $I(\theta)$ along the arc of the main equatorial reflection allows calculations of the degree of orientation of the molecules in a liquid crystal:

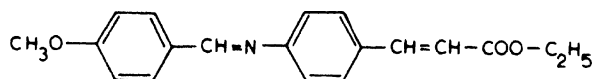
$$S = 1 - \frac{3}{2} \sin^2 \alpha$$

where

$$\sin^2 \alpha = \frac{\int_0^{\pi/2} I(\theta) \sin^3 \theta d\theta}{\int_0^{\pi/2} I(\theta) \sin \theta d\theta}$$

Let us consider the problem of polymorphism of liquid crystal phases. As already mentioned, we may assume that there exists a large variety in smectic structures. Some of them can already be differentiated from the investigations of textures and the miscibility criterion which allows us to distinguish between modifications A, B, C, D, E, F, G⁶⁸. Here we shall restrict ourselves to consideration of the structures which were characterized by the x-ray method.

Phase A. As an example, let us take ethyl ether *p*-anisalamino cinnamic acid (EEAC):



This compound forms, in addition to a nematic phase, smectic phase A and a low-temperature monotropic mesophase B. In phase A the molecules are grouped into layers in such a way that the long molecular axes turn out to be perpendicular to the layers and packed in an antiparallel fashion¹⁷. There is a certain statistical angular distribution which is characterized by the function $D(\alpha)$. The structure appears to be optically uniaxial and positive. Stratification of the structure is clearly revealed when plotting the function of the cylindrical distribution of the atoms $Q(rz)$ (figure 12). This function was found both by calculation and by optical methods. Comparison of these functions is shown in figure 12. According to the above considered classification, the symmetry symbol of phase A for EEAC will be $C : B_2 : 2$.

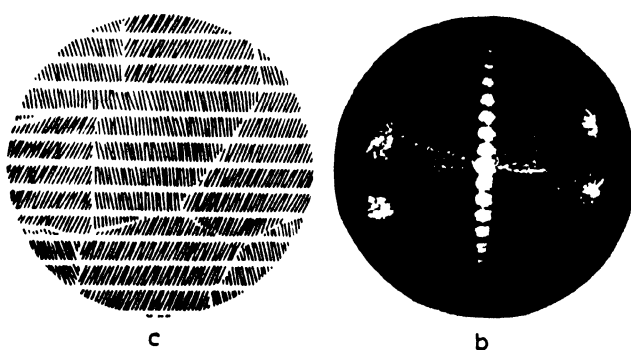
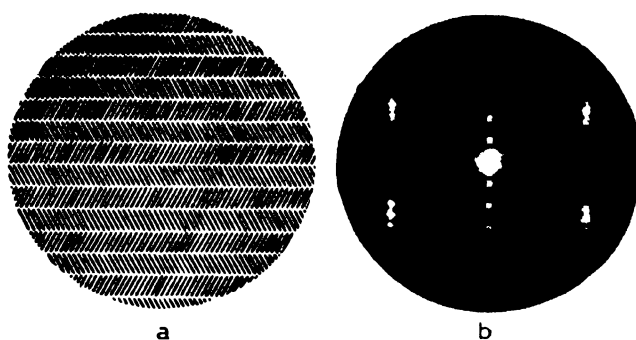


Figure 7 Model of the smectic liquid crystal with the alternating inclinations of the molecules in the layers (a), and the corresponding diffraction pattern (b). Figure c illustrates another case of the molecular ordering which also leads to the splitting of the equatorial reflexions in the diffraction pattern.

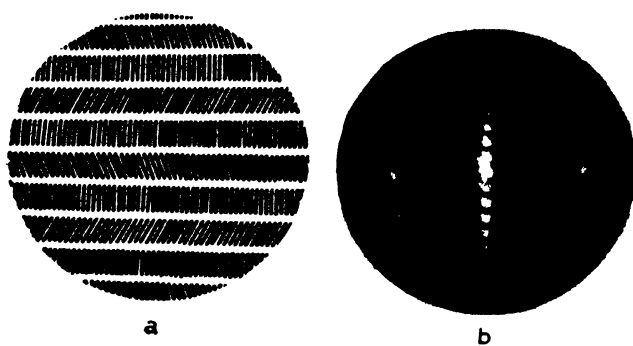


Figure 8 Model with different correlated inclinations of the molecules in the layers (a) and the corresponding diffraction pattern (b).

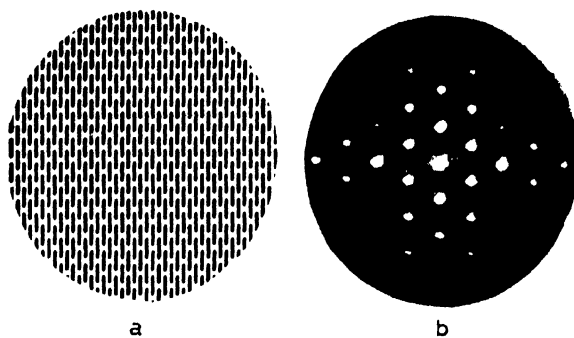


Figure 9 Model of the nematogenic crystal (a), and its diffraction pattern (b).

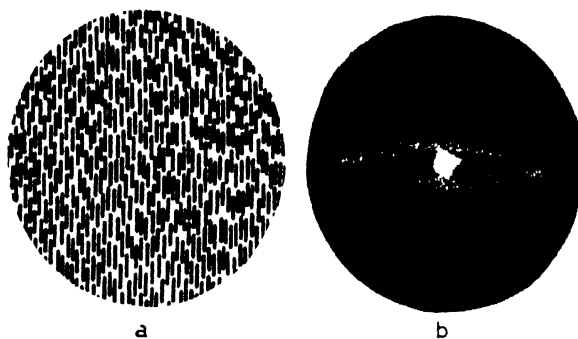


Figure 10 Shifts and distortions of periodicity in the OX direction (a) and the corresponding diffraction pattern (b).

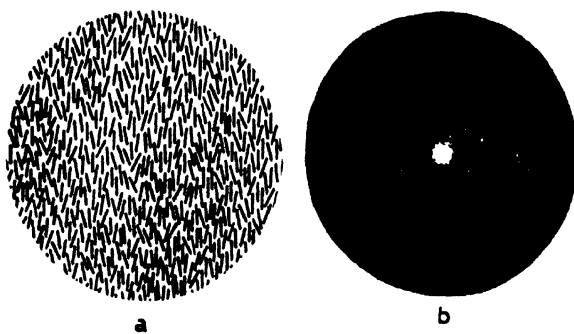
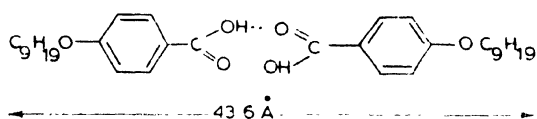


Figure 11 Model of the nematic liquid crystal (a) and its diffraction pattern (b).

Phase B. The low-temperature monotropic modification of FEAC may serve as an example. As it has recently been shown, the fact that the layers can glide relative to one another, while within the layer there may be preserved the ordered two-dimensional structure^{70, 71}, can be considered as the difference between phase B and phase A. As is shown in Ref. (17), the x-ray patterns of EEAC in phase B possess the system of diffuse but still clearly expressed hexagonal reflections. In our opinion, this may serve as evidence that the molecular arrangement in smectic layers is characterized by the distribution function W_1 (m 6 : m) of the first kind, so that the symmetry symbol will be $C \cdot A_2 : 2$. The structure of phase B for EEAC is optically uniaxial and positive.

It is known that in phase B there may exist a correlated inclination of the molecules in layers^{18, 19}. *p*-Benzylidene-di-*p*-butylaniline (BB \tilde{A}) may serve as an example of such a compound. In contrast to EFAC, the molecules in the layers have a correlated inclination in this compound, thereby making an angle of 32° with the smectic planes (figure 13). Thus, in this case, the symmetry symbol will be $C \cdot B_2 : 2 \cdot \varphi$.

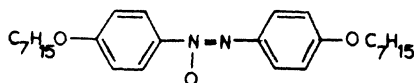
Phase C. As an example of C-type mesophase, we take *p*-nonyloxybenzoic acid (NOBC) the molecules of which form dimers:



The molecules in smectic layers have a correlated inclination $\varphi = 54^\circ$. This is clearly revealed by the characteristic arrangement of the intermolecular reflections. They split into four maxima¹⁷; this is expressed in the form of the function $Q(1z)$ shown in figure 14. This function is calculated for a sample oriented by an electric field. The model data indicate that the 54° maxima comprise the interatomic vectors directed along the long molecular axes, and owe their origin only to intramolecular interference. These maxima will coincide with those of the self-convolution function $\tilde{\rho}^2(r)$ plotted for the point distribution of the atoms in a NOBC molecule. A possible variant of the smectic phase packing is shown in figure 13; the corresponding optical modelling is illustrated in figure 7. The symmetry symbol must include the mirror plane parallel to smectic layers and the defining change in the inclination of the molecules from one layer to another.

$$C \cdot B \cdot m \cdot \varphi.$$

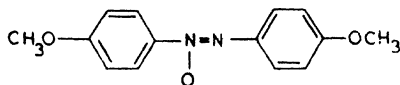
The homologues of *p*-alkoxyazoxybenzene, for instance, *p*-heptyloxyazoxybenzene (HOAOB) may serve as another example of C-phase-forming



substances. The angle of inclination, φ , of the molecules in the layer is equal to 30° ^{22,23}. The x-ray patterns do not reveal any change in the direction of the molecular tilting. Therefore, in this case the symmetry symbol will be $C \cdot B \cdot \varphi$.

Phases D, E. The investigation of these phases has been carried out in Refs. (12, 13). It is known that phase D is optically isotropic, and its "outer ring" is very weak. Thus the cubic packing of the particles representing the spherical agglomerates of molecules with the packing period $\alpha = 61 \text{ \AA}$ ¹³ may be suggested. The x-ray patterns of modification E possess three closely located maxima instead of one reflection in the region of the "outer ring". We believe that this may be the consequence of the change in the inclination of the molecules in layers which is illustrated by the optical modelling of the structure (figure 8).

As for the structure of nematic liquid crystals, it is known that in the classical case, for example, for *p*-azoxyanisole the substance was thought



to be a complex of independent molecular swarms containing the 10^5 – 10^7 molecules. Later on, the medium of the liquid crystal was assumed to be continuous. In this case the symmetry of the classical nematic mesophase can be written as

$$\tau(z) \cdot B$$

When the nematic mesophase is formed from the smectic one, and especially at temperatures not too remote from the point of phase transformation, there may exist the "fragments" of smectic layers, *i.e.*, small agglomerates of molecules. The nematic phases of NOBC and NOAB which are formed on melting the smectic phase C may be used as an example. In this case the x-ray patterns show a "two-points" or "dumb-bells" appearance in the region of small angles corresponding to the molecular length. This is conditioned by reflection of pseudo stratified groupings from planes (figure 16)⁷⁻¹⁴.

The bifurcated small-angle x-ray reflections owe their origin to the pseudo stratified structure and tilted arrangement of the molecules in pseudo layers. To estimate the sizes of these groupings one can use the

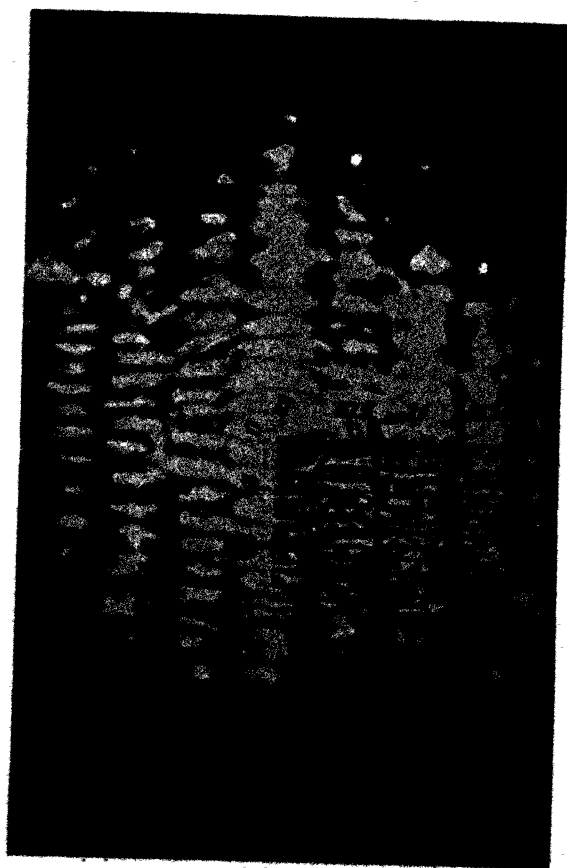


Figure 12 Cylindrical distribution function of the interatomic distances $Q(r, z)$ for the smectic A phase of EAAC oriented by magnetic field.

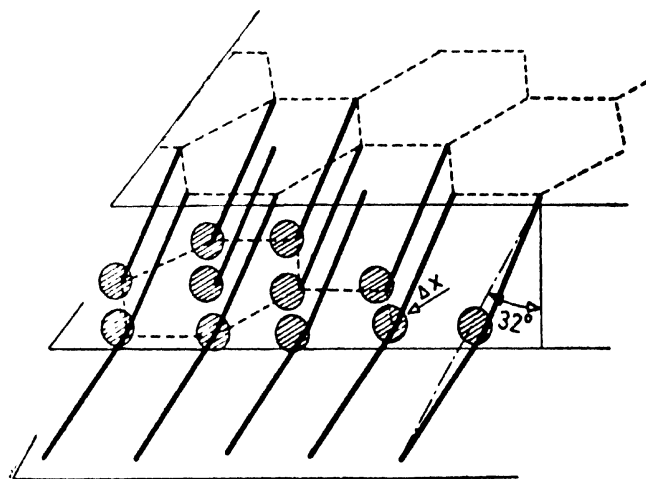


Figure 13 Scheme for the molecular arrangement in smectic planes of the liquid crystal of *p*-benzylidene-di-*p*-butylaniline.

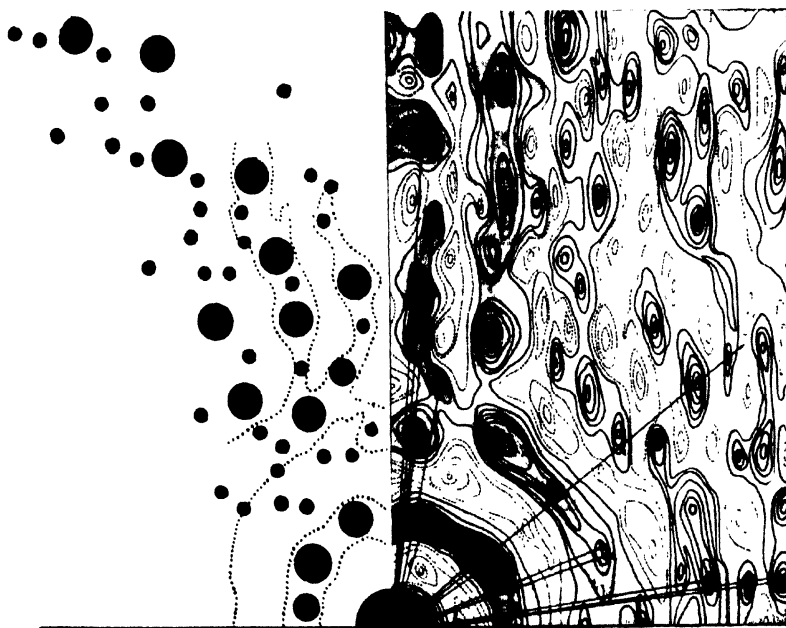


Figure 14 Function $Q(r, Z)$ for the smectic C phase of NOBC and the function $\tilde{p}(r)$.

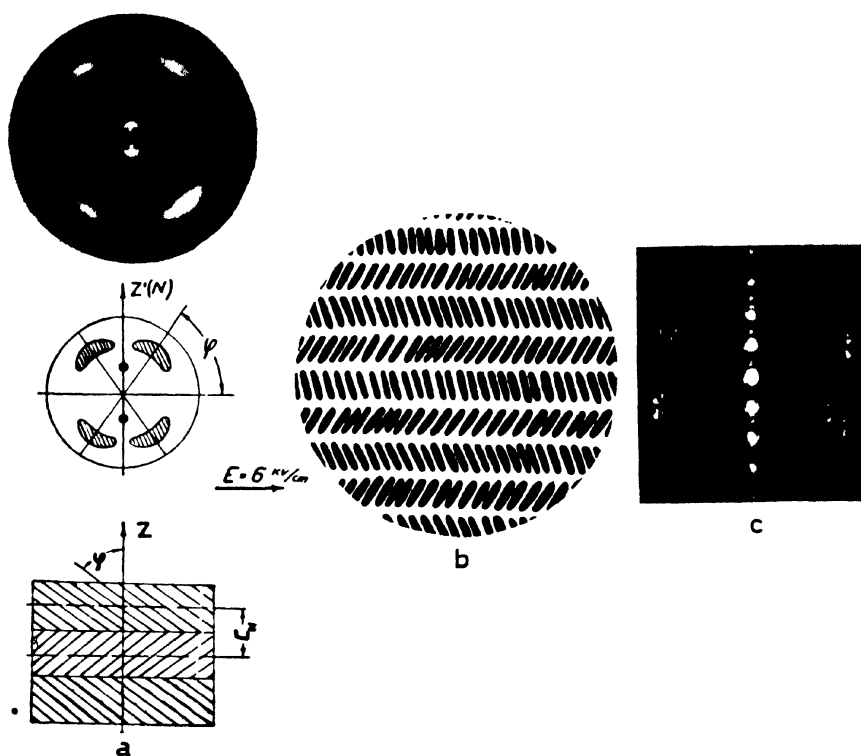


Figure 15 (a) X-ray pattern from smectic phase of NOBC oriented by an electric field and scheme for the molecular packing:
 (b) structure model,
 (c) optical diffraction pattern from the model.

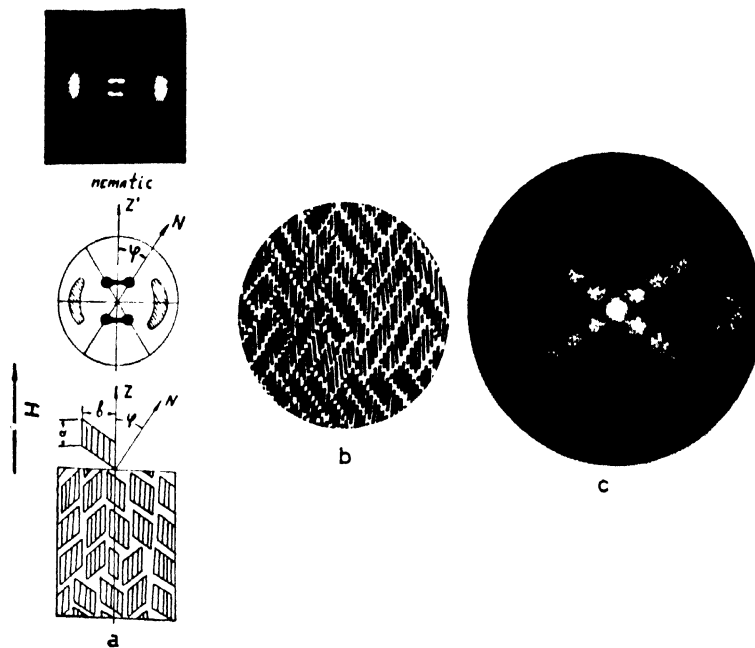


Figure 16 (a) X-ray pattern of the nematic phase of *p*-heptyloxyazoxybenzene, and scheme for the molecular orientation :
 (b) structure model,
 (c) optical diffraction pattern from the model.

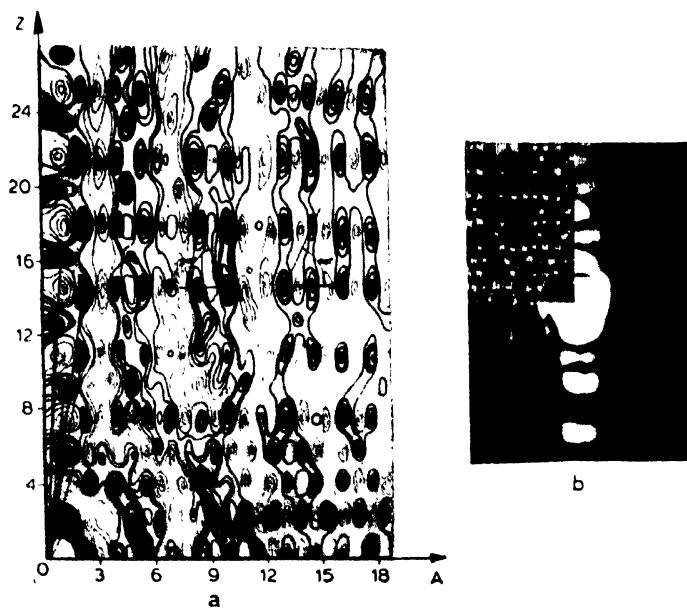


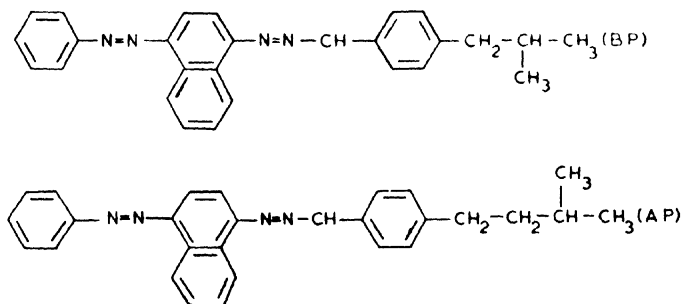
Figure 17 (a) function $Q(r, Z)$ of the nematic phase of NORC (b) comparison

work²⁵ where structural factors for oblique crystallites were calculated. If we assume that to an oblique crystallite there corresponds a pseudo layer and that the form of the dumb-bell-like reflection is defined by the parameter $\frac{b \sin \varphi}{a} = 0.8$, then, taking, for instance, $\varphi = 34^\circ$ (at $t = 90^\circ\text{C}$) and $a = 28 \text{ \AA}$, NOAB we find $b = 33 \text{ \AA}$. Thus pseudo stratification extends to the groups which consist of 30 to 40 molecules. The symbol of such a cybotactic "oblique" mesophase is $\tau_{\infty}^g(z) \text{ B } \varphi$.

4. Investigation of the structure with the help of the distribution function

The examples of the distribution function $Q(rz)$ used for characterizing the mesophase structure have been given above²⁶⁻³⁹.

In order to analyze the influence of the external factors — temperature, flow, electric and magnetic fields etc., on the structure of a liquid crystals it is quite sufficient to use only one-dimensional functions $\rho(r)$ and $2\pi rZ(r)$. As an example, let us present curves $\rho(r)$ for the system p-isobutylbenzaminonaphthylazobenzene (AP)³⁶. Both substances belong to one homologue series. The AP molecule differs from the BP molecules in the presence of an extra CH_2 group:



The curves $\rho(r)$ for mixtures of different composition are shown in figure 18. It can be seen that all the curves possess the 2.1 \AA peak. If we project all the atoms of the molecule on to the z -axis and find the average most-frequently occurring distance, then this latter will be equal to 2.4 \AA . Taking account of statistical tiltings of the molecules near Z ($\cos \theta = 0.88$) leads to the decrease in this distance down to 2.1 \AA which explains the origin of this peak on the $\rho(r)$ curves. The averaged distance for BP molecules is 4.4 \AA , for AP molecules it is equal to 4.2 \AA , and with consideration of the inclination these distances decrease to 3.96 \AA and 3.7 \AA , respectively. These values elucidate the origin of the corresponding peaks on the $\rho(r)$ curves. The peaks of the cylindrical distribution function $2\pi rZ(r)$ owe their origin to both intramolecular and intermolecular interference. The contribution which arises from intra-

molecular interference prevails. The dependence of the function $2\pi r Z_a(r)$ on the magnitude of a magnetic field for *p*-heptyloxazoxybenzene at 94°C (figure 19) can be used as an example. The peaks become sharpened and

Figure 18 Linear distribution functions of the atoms for the mixtures AP and BP.

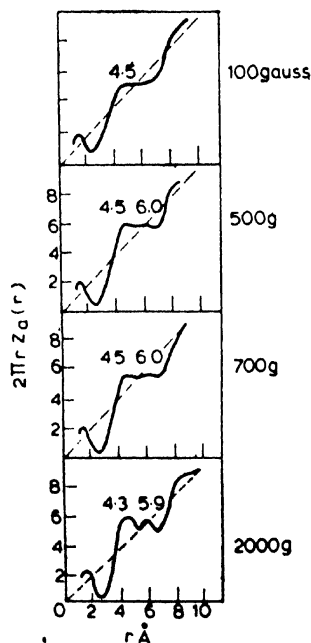
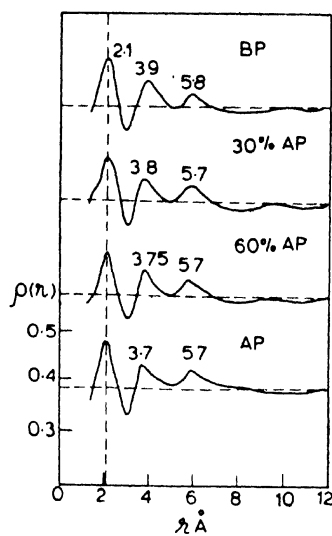


Figure 19 Functions $2\pi r Z_a(r)$ for *p*-heptyloxazoxybenzene oriented in different magnetic fields at $t = 94^\circ\text{C}$.

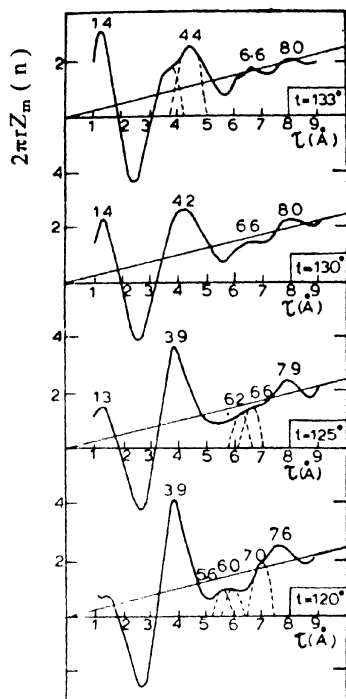


Figure 20 Functions $2\pi rZ_m(r)$ for *p*-azoxyanizole oriented by an electric field at different temperatures.

are displaced to smaller distances when the field increases. This indicates an increase in the molecular ordering.

• An example of the cylindrical function of the projections of the molecular axes on the basal plane $2\pi rZ_m(r)$ is shown in figure 20 for PAA oriented by a constant electric field at different temperatures. With increasing temperature the peaks on the curves smooth out.

The function $D(\alpha)$ characterizing the structure of a liquid crystal is important, too. It defines the distribution of the molecular axes relative to the z -axis, and determines the number of the molecules dN , the long axes of which make angles from α to $\alpha + d\alpha$.

The measurement of the intensity distribution along the arc of the main equatorial reflection enables us to calculate the degree of orientation S . Let it be noted that the degree of orientation S is the microscopic value, it approaches the degree of ordering S — the thermodynamic parameter of the mesophase⁴⁵⁻⁵⁰ at a sufficiently homogeneous orientation of a sample as a whole.

In particular, the temperature dependence of the degree of orientation depends on the value of the orientational factor⁵²⁻⁵⁵. As an example, we

take the dependence of S for PAA on magnetic field strength (figure 21). The value is first seen to increase rapidly with the change of the field up to 1000–2000 G, then the increase of $\Delta S/\Delta B$ considerably slows down but up to 18000–19000 G a slight increase can still be observed. The analogous dependence can also be traced for the change in the birefringence value $\Delta n = \Delta n(H)^{36}$.

The function $D(\alpha)$ for PAA at $t = 118^\circ\text{C}$ oriented by a magnetic field of 8000 G is shown in figure 22a. In the expression for $\sin^2 \alpha$ the α -angle is the average angle of inclination of the molecules relative to z . In fact as it has been determined, the function $D(\alpha)$ represents the density of the long molecular axes on a sphere of molecular orientation. Hence, the number of the molecules of the aggregate $dN(\alpha)$ which lie in the interval from α to $\alpha + d\alpha$ will be:

$$dN(\alpha) = D(\alpha) \sin \alpha d\alpha$$

The change dN for $\Delta\alpha = 3^\circ$ found from the values $D(\alpha)$ for PAA is characterized by the Gaussian distribution about the average value $\alpha = 30^\circ$ (figure 22b).

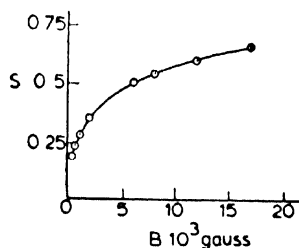


Figure 21 Dependence of the degree of orientation S for p -azoxyanizole vs. magnetic field.

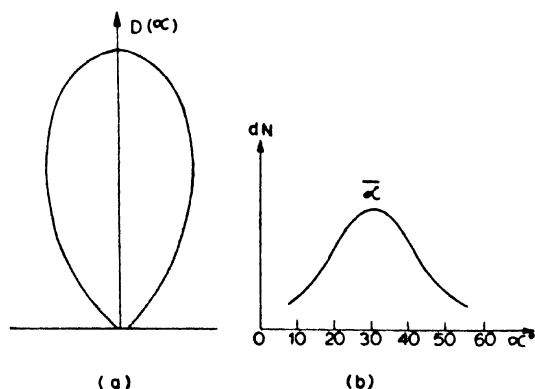


Figure 22 (a) function $D(\alpha)$ for p -azoxyanizole, (b) dependence of the number of dN molecules on the angle of inclination relative to the z -axis.

References

- 1 BROWN G H and SHAW W G *Chem. Rev.* **57** 1049 (1957)
- 2 GRAY G W *Molecular Structure and the Properties of Liquid Crystals* (Academic Press, London and New York) 1962
- 3 VAINSHTEIN B K *Diffraction of X-rays by Chain Molecules* (Elsevier, Amsterdam) 1966
- 4 SCHUBNIKOV A W and KOPZIK W A *Symmetry in Science and Art* (Nauka, Moscow) 1972
- 5 HOSEMAN R and BAGCHI S N *Direct Analysis of Diffraction by Matter* (Amsterdam) 1962
- 6 KRIGBAUM W R, POIRIER I C and COSTELLO M J *Mol. Cryst. Liquid Cryst.* **20** 133 (1973)
- 7 DE VRIES A *Mol. Cryst. Liquid Cryst.* **10** 219 (1970)
- 8 DE VRIES A *Mol. Cryst. Liquid Cryst.* **11** 361 (1970)
- 9 DE VRIES A *Mol. Cryst. Liquid Cryst.* **20** 119 (1973)
- 10 TERAUCHI H, TAKEUCHI T and KUSABAYASHI S *Japan J. Appl. Phys.* **11** 1862 (1972); **11** 763 (1972)
- 11 McMILLAN W L *Phys. Rev.* **A6** 936 (1972)
- 12 SACKMANN H and DEMUS D *Fortschr. Chem. Forsch.* **12** 349 (1969)
- 13 SACKMANN H and DEMUS D *Mol. Cryst.* **2** 81 (1966)
- 14 CHISTYAKOV I G *Dissertations*, 1963, 1972
- 15 KRIGBAUM W R, CHATANI Y and BARBLER P G *Acta Crystallogr.* **B26** 97 (1970)
- 16 GULRICH L W and BROWN G H *Mol. Cryst.* **3** 493 (1968)
- 17 CHISTYAKOV I G, SCHABISHEV L S, JARENOV R I and GUSAKOVA L A *Mol. Cryst. Liquid Cryst.* **7** 279 (1969)
- 18 LEVELUT A M and LAMBERT M C.R. *Acad. Sci. (Paris)* **272B** 1018 (1971)
- 19 DOUCET J, LAMBERT M and LEVELUT A M *J. Phys. (Paris)* **32** C5a 247 (1971)
- 20 DE VRIES A and FISHEL D L *Mol. Cryst. Liquid Cryst.* **16** 311 (1972)
- 21 LANDAU L D and LIFSHITZ E M *Statistical Physics* (Pergamon Press) 1968
- 22 CHISTYAKOV I G and CHAIKOVSKI W M *Mol. Cryst. Liquid Cryst.* **7** 269 (1969)
- 23 GELERINTER E *Appl. Phys. Lett.* **18** 84 (1971)
- 24 TAYLOR T R, FERGASON J L and ARORA S L *Phys. Rev. Lett.* **24** 359 (1970)
- 25 GERASIMOV W I and ZWANKIN D I *Wisokomol. Soed (USSR)* **AXI** 2652 (1969)
- 26 CHISTYAKOV I G and VAINSHTEIN B K *Kristallografia* **8** 570 (1963) [*Soviet Phys. Crystallogr.* **8** 458 (1963)]
- 27 VAINSHTEIN B K and CHISTYAKOV I G *Sov. Phys.-Dokl.* **8** 1044 (1964)
- 28 CHISTYAKOV I G *J. Struct. Chem. (USSR)* **5** 507 (1964)
- 29 VAINSHTEIN B K and CHISTYAKOV I G *Growth Cryst. (USSR)* **5A** 133 (1968)
- 30 CHISTYAKOV I G *Liquid Crystals* (Nauka, Moscow) 1966
- 31 CHISTYAKOV I G *Sov. Phys.-Usp.* **9** 551 (1967)
- 32 CHISTYAKOV I G and CHAIKOVSKI W M *Kristallografia* **12** N5 883 (1967) [*Sov. Phys. Crystallogr.* **12** 770 (1968)]
- 33 VAINSHTEIN B K, CHISTYAKOV I G, KOSTERIN E A and CHAIKOVSKI W M [*Sov. Phys.-Dokl.* **12** 405 (1967)]
- 34 VAINSHTEIN B K, KOSTERIN E A and CHISTYAKOV I G *Dokl. I Conference on Liquid Crystals (USSR)*, Ivanovo, p. 5 (1972)
- 35 KOSTERIN E A and CHISTYAKOV I G *Kristallografia* **13** N2 295 (1968) [*Sov. Phys. Crystallogr.* **12** 770 (1968)]
- 36 GUSAKOVA L A and CHISTYAKOV I G *Kristallografia* **13** 543 (1968) [*Sov. Phys. Crystallogr.* **13** 452 (1968)]
- 37 KOSTERIN E A and CHISTYAKOV I G *Kristallografia* **14** 321 (1969) [*Sov. Phys. Crystallogr.* **14** 252 (1969)]
- 38 VAINSHTEIN B K, CHISTYAKOV I G, KOSTERIN E A and CHAIKOVSKI W M *Mol. Cryst. Liquid Cryst.* **8** 457 (1969)

- 39 VAINSHTEIN B K, KOSTERIN E A and CHISTYAKOV I G *Dokl. Akad. Nauk (USSR)* **199** 75 (1971)
- 40 VAINSHTEIN B K, CHISTYAKOV I G, KOSTERIN E A and INOZEMTZEVA A D *Kristallografia* **16** 717 (1971)
- 41 VAINSHTEIN B K, CHISTYAKOV I G and INOZEMTZEVA A D *Kristallografia* **17** 484 (1972)
- 42 CHISTYAKOV I G and SCHABISCHEV L S *Dokl. I Conference on Liquid Crystals (USSR)*, Ivanovo, p. 50 (1970)
- 43 DELORD P and FALGUEIRETTES J *C.R. Acad. Sci. (Paris)* **267** 1177 (1968).
- 44 DELORD P *These. Montpellier* (1970)
- 45 MAIER W and SAUPE A *Z. Naturforsch.* **12a** 668 (1958)
- 46 MAIER W and SAUPE A *Z. Naturforsch.* **14a** 882 (1959)
- 47 MAIER W and SAUPE A *Z. Naturforsch.* **15a** 287 (1960)
- 48 CHANDRASEKHAR S and MADHUSUDANA N V *Mol. Cryst. Liquid Cryst.* **10** 151 (1970)
- 49 CHANDRASEKHAR S and MADHUSUDANA N V *Acta Crystallogr.* **27A** 303 (1971)
- 50 CHANDRASEKHAR S and MADHUSUDANA N V *Mol. Cryst. Liquid Cryst.* **17** 37 (1972)
- 51 WATKINS CH L, JOHNSON JR. CH S J. *Phys. Chem.* **75** 16 2452 (1971)
- 52 CHISTYAKOV I G *Dokl. I Conference on Liquid Crystals (USSR)* Ivanovo, p. 19 (1972)
- 53 SAUPE A *Angew. Chem.* **7** 97 (1968)
- 54 DIELE S, BRAND P and SACKMANN H *Mol. Cryst. Liquid Cryst.* **16** 105 (1972)
- 55 DIELE S, BRAND P and SACKMANN H *Mol. Cryst. Liquid Cryst.* **17** 163 (1972)
- 56 FREDERIKS W K and ZOLINA W J. *Rusck. Fiziko-Chim. Obtschestwa (USSR), Parth Phys.* **62** 457 (1930)
- 57 ZWILTKOV W N *Colloid. J. (USSR)* **33** 154 (1971)
- 58 MARININ W and ZWETKOV W *JETP* **9** 1388 (1939)
- 59 DELORD P and MALET J *C.R. Acad. Sci. (Paris)* **270B** 1107 (1970)
- 60 VAINSHTEIN B K *Dokl. Akad. Nauk (USSR)* **112** 737 (1957)
- 61 VAINSHTEIN B K *Kristallografia* **2** 29 (1957)
- 62 JABOK J, MALET J and DELORD P *C.R. Acad. Sci. (Paris)* **273B** 190 (1971)
- 63 MACGILLAVRY C H and BRUINS E M *Acta Crystallogr.* **1** 156 (1948)
- 64 CARLISLE C H and SMITH C H *Acta Crystallogr.* **B27** 1068 (1968)
- 65 DL VRIJS A J. *Chem. Phys.* **56** 4489 (1972)
- 66 DEAS H D *Acta Crystallogr.* **5** 542 (1952)
- 67 KRIGBAUM W R, PIORIER J C and COSTELLO M J *Mol. Cryst. Liquid Cryst.* **20** 133 (1973)
- 68 INOZEMTZEVA A D *Dissertation* (1973)
- 69 SACKMANN H and DEMUS D *Mol. Cryst. Liquid Cryst.* **21** 239 (1973)
- 70 DE GENNES P G and SARMA G *Phys. Lett.* **38A** 219 (1972)
- 71 DE GENNES P G *Mol. Cryst. Liquid Cryst.* **21** 49 (1973)

X-ray studies of liquid crystals* : V. Classification of thermotropic liquid crystals and discussion of intermolecular distances†

ADRIAAN DE VRIES

Liquid Crystal Institute, Kent State University, Kent, Ohio 44242, USA

Abstract. Several modifications in the current system of classification of liquid crystals are proposed. Nematics are divided into ordinary, intermediate, normal cybotactic and skewed cybotactic; cholesterics are defined as comprising two types, nematic cholesteric (spontaneously twisted nematic) and smectic cholesteric (spontaneously twisted smectic C); smectic E is separated into normal E and tilted E; smectic G is indicated as a possible variant of smectic E; and smectic H is set apart from smectic B. The diffraction patterns of the various phase types (both random and aligned) are discussed, in particular with reference to their use as a classification tool, and many examples of diffraction patterns are given.

A comprehensive study is made of the average intermolecular distance D which is obtained from the diameter of the outer diffraction ring(s). D ranges reported are (in Å): 4.97 (S_{II}), 4.85-4.98 (S_A), 4.88-4.97 (S_K), 4.85-5.15 (N_{se}), 4.93-5.13 (N_a), 4.96-5.46 (I). All data are combined in one graph, and the discussion centers around an analysis of this graph. Some comments are made about the packing in the most dense (lowest D) phases.

PART I

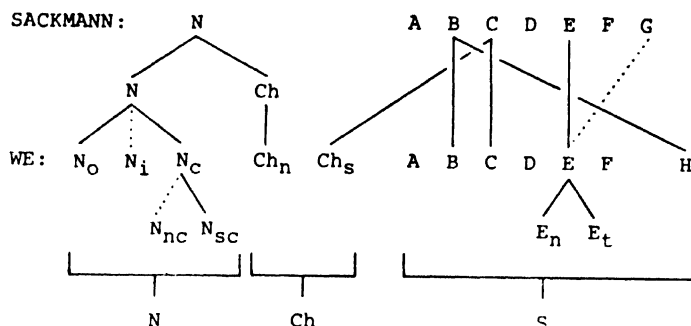
Nomenclature and classification

Relationship between our classification and that of Sackmann

Present classification of liquid crystals rests heavily on the work of Sackmann and his co-workers, Arnold, Demus and others. Sackmann's classification is based mainly on the "miscibility rule", developed by him and his colleagues. This rule says that if two liquid crystals are miscible in all proportions, they belong to the same type. With this rule, Sackmann and co-workers have been able to assign all liquid crystal phases investigated by them to the types listed on the first line of table 1: one nematic phase, N, and seven smectic phases, A through G¹. The miscibility criterion does not recognize the cholesteric phase as different from the nematic phase, but Sackmann and Demus¹ make an exception to

* This is a continuation of the series formerly entitled "X-ray Photographic Studies of Liquid Crystals". The previous paper in this series is Ref. 21.

† Research supported in part by the National Science Foundation under Grant No. GH34164X.

Table 1 Classification of liquid crystals

their own rule by allowing a different symbol, Ch, for the cholesteric phase "because of the well-known differences in their structures and their properties" between N and Ch phases. This is indicated on the second line in table 1, where the one N phase is subdivided into the regular nematic phase, N, and the cholesteric phase, Ch.

It is important to note that this distinction between N and Ch is based not on the miscibility criterion, but on differences in structure and properties. Using the same argument, *i.e.*, differences in structure and properties (with particular reference to the structure as indicated by the x-ray diffraction pattern, and to the optical properties), we would like to propose some modifications in the classification scheme presented in the first two lines of table 1. These modifications are indicated on the third and fourth line of table 1 (identified by "we"). The relationships between our symbols and Sackmann's symbols are indicated by lines: full lines for proven relationships, dotted lines for suggested relationships. So as not to overcrowd the picture, no lines have been drawn if the symbols are the same and if there is a one to one relationship (*e.g.*, our A and Sackmann's A are identical). Below we will discuss the various relationships in some more detail.

In the last line of table 1 we have indicated how we group the phase types into the three main categories of nematic (N), cholesteric (Ch) and smectic (S).

Use of the diffraction pattern for identification

The x-ray diffraction pattern of a liquid crystal (randomly oriented) consists of one or more "inner rings" (diffraction rings close to the center of the diffraction pattern; the corresponding diffraction angles are of the order of a few degrees) and one or more "outer rings" (diffraction rings with diffraction angles of the order of 20°).

Random N phases have one inner ring and one outer ring, and both are diffuse (figure 1). Isotropic (I) phases have similar diffraction patterns,

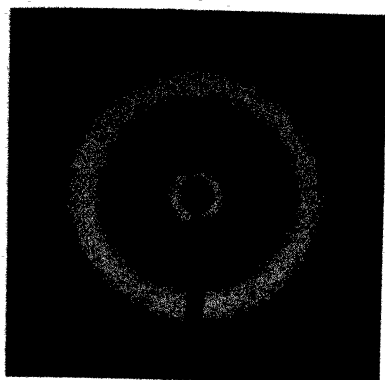
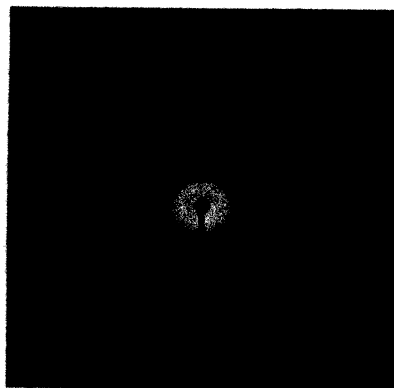
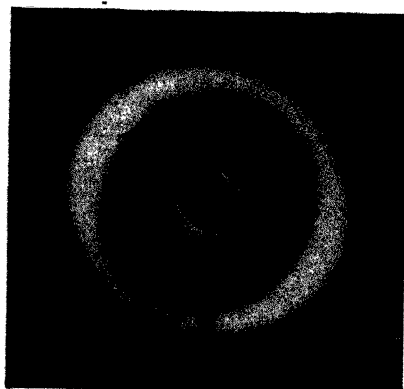


Figure 1 Diffraction pattern of a quite randomly oriented sample of a non-cybotactic nematic.



ORDINARY

SKEWED CYBOTACTIC

Figure 2 Diffraction patterns of N_o (left) and N_{sk} (right). Top photographs are from fairly randomly oriented samples, bottom ones are from well aligned samples.

but the inner ring is generally more diffuse than that of the corresponding nematic phase. The best way to distinguish, by x-rays, between N and I is by using "aligned" samples: for aligned N phases the rings split up into crescents or spots, whereas I phases usually cannot be aligned and will always show rings.

Differentiation between the various types of N and Ch phases cannot be commented upon without getting ahead of our discussion, and hence will be deferred till below.

The distinguishing characteristic of random S phases, as compared to N or I, is that the inner ring is sharp, and that there may be more than one (the various inner rings correspond to the different orders of diffraction against the smectic planes). To differentiate between the many types of S phases one considers the appearance and the number of the outer ring(s) and the way in which inner and outer rings split up on alignment, as will be discussed in some detail below.

The diffraction patterns of the most highly ordered S phases are rather similar to those of some crystalline (K)² phases. A discussion of the differences between these S and K patterns would become too involved, and falls outside the scope of this paper.

Nematic phases

As indicated in table 1, we have divided the nematic phases (N) into "cybotactic nematic" (N_c),^{3,4} "ordinary nematic" (N_o),* and "intermediate nematic" (N_i); the cybotactic nematic phases can be further subdivided³ into "normal cybotactic nematic" (N_{nc}) and "skewed cybotactic nematic" (N_{sc}).

Difference between skewed cybotactic and ordinary nematics: N_{sc} and N_o phases can be distinguished by their very distinctly different x-ray diffraction patterns (figure 2). For randomly oriented samples the most obvious difference is the relative intensity of the two diffraction rings (top two photographs in figure 2): for N_o , the intensity of the inner ring is less than, or at the most equal to, the intensity of the outer ring; for N_{sc} , the intensity of the inner ring is far greater than that of the outer ring. For aligned samples the most striking difference is the appearance of the maxima in the inner ring (bottom two photographs in figure 2): for N_o we find two crescents, for N_{sc} four discrete spots. It was the location of these four spots that led us to the formulation of the structure of the N_{sc} phase:⁴ whereas in the N_o phase the molecules are free to move—with respect to their neighbors—in the direction of their long axis, in the N_{sc} phase the molecules are regularly arranged in groups (cybotactic groups,

* Earlier,³ we used for this kind of nematic phase the name "classical nematic", but this name yields the same abbreviation N_o as does "cybotactic nematic". For this reason we now prefer the name "ordinary nematic".

see figure 3), and within these groups the molecules are no longer free to move in the direction of their long axis but are locked in place much like in a smectic layer.

Cybotactic groups as pretransition effect: In their recent papers, Sackmann and Demus¹ and de Gennes²⁹ appear to regard cybotactic groups as a pretransition effect. While this may be so, we have to point out that the cybotactic nematic phase of bis- (4'-*n*-octyloxybenzal)-2-chloro-1,4-phenylenediamine⁴ presents a behaviour which is rather unusual for a pretransition effect. The structure of this cybotactic phase, although changing continuously for the first 100° C below the N-I point, remained virtually unchanged from about 20°C above the K-N point all the way down to the K-N point: the overall appearance of the diffraction pattern stayed the same, the intermolecular distance between the molecules and the interplanar spacing of the cybotactic groups were constant, and the variation in the angle of tilt was within the error of the measurement (for numerical data see table 2 in Ref. 4).

Normal and skewed cybotactics: As indicated in figure 3, in the N_{sc} phase the angle (ϕ) between the long molecular axis and the boundary planes of the cybotactic group is significantly different from 90°; for this reason we have called this phase *skewed* cybotactic. From general considerations³ one would expect that there would also exist *normal* cybotactic nematics (N_{nc}) with $\phi = 90^\circ$, but the existence of these phases has not been verified so far (hence the *dotted* line in table 1 between N_c and N_{nc}).

Intermediate nematics: In table 1 we have inserted, between N_c and N_{sc} , the intermediate nematic phases, N_i . In this group we classify those phases that are not distinctly cybotactic but neither completely ordinary. We think here, in particular, of some of the 4, 4'-di-*n*-alkoxyazoxybenzenes. The ethyl, butyl, and higher members of this series have (in their nematic phase) x-ray diffraction patterns⁵ that definitely identify them as N_{sc} phases⁴. The diffraction patterns of the methyl and propyl members look

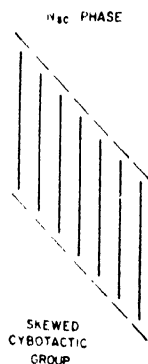


Figure 3 Schematic representation of a skewed cybotactic group. The heavy full lines indicate the molecules, the broken lines give the positions of the boundary planes which are perpendicular to the plane of the paper.

much like those of N_o phases, but because of the strong cybotactic character of the other homologues we consider it probable that the nematic phase of the methyl and propyl compounds has remnants of cybotactic structure, and hence we would like to classify it as N_l . For this reason we also consider these compounds a rather poor choice for the measurement of properties of the *ordinary* nematic phase. This conclusion is not without importance, since the methyl homologue, *p*-azoxyanisole, is probably the most extensively studied of all liquid crystals.

Cholesteric phases

Nematic cholesterics and smectic cholesterics: The cholesteric phase (Ch) has also been called "twisted nematic" or, probably better, "spontaneously twisted nematic". We propose the name "nematic cholesteric" and the symbol Ch_n for these phases, to emphasize at the same time their cholesteric character and their relationship with nematic phases, and to distinguish them from a new kind of cholesteric phase which we want to introduce into the Ch category. It is well established now^{6-8, 30} that just as there are spontaneously twisted nematic phases there are also spontaneously twisted smectic C phases, and for these phases we propose the name "smectic cholesteric" and the symbol Ch_{sm} , to indicate that they behave optically as cholesterics¹ (they were originally even classified⁶ as cholesterics), but that structurally they are related to the smectics.*

This classification of twisted S_C phases as cholesteric phases would remove an inconsistency in Ref. 1 with regard to the optical properties of S_C . In table 2 of Ref. 1, S_C is described as optically biaxial, but on p. 259 of Ref. 1 it is noted that twisted S_C phases can have pseudoisotropic textures, which implies that twisted S_C is uniaxial (as one would predict on the basis of its structure). Our designation Ch_n separates these uniaxial phases from the biaxial S_C phases and puts them with Ch_{sm} in the uniaxial Ch category, and thus removes any conflict with respect to the optical properties.

X-ray diffraction patterns: The x-ray diffraction patterns of Ch_n phases are quite similar to those of N phases, and those of Ch_{sm} phases are similar to those of S_C phases. One difference is that because of the twisted structure it is not possible to have a preferred direction for the molecular axis, and thus photographs like those for aligned nematics (figure 2) or aligned smectic C's (see figure 6 below) are impossible. We have no data on Ch_n phases, but for Ch_{sm} phases we have always obtained diffraction rings without maxima and minima (just like in the isotropic phase). This is quite a contrast with the behavior of N phases, for which we have found it extremely difficult to obtain uniform diffraction rings.

* Our symbols Ch_n and Ch_{sm} can also be taken to stand for the "chiral nematic" and "chiral smectic", names which have been used for these phase by other authors.

Cholesterol related compounds also distinguish themselves from most other liquid crystalline materials by the much smaller radius ($2\theta \approx 16^\circ$) of the outer ring in the x-ray diffraction pattern (usually the outer ring has $2\theta \approx 20^\circ$)⁴. To stress that this is a property of the cholesterol molecule and not of the cholesteric phase we have shown this difference in figure 4 for the isotropic phases of two representative compounds.

Smectic phases

Division into classes: For the classification of smectic phases we have already proposed elsewhere⁹ a scheme in which the phase types are grouped into three main classes (called α , β , and γ) on the basis of the structure of the phase as evidenced in the appearance of the outer diffraction ring(s). This new classification is summarized in table 2. It has the advantage of grouping together phases of similar structure, and thus it forms a more convenient basis for the discussion of the various phase types. Examples of diffraction patterns in the three main classes are given in figure 5.

Class α

Our smectic A, D and F classifications are identical to those of Sackmann (table 1). Our smectic C phases are those of Sackmann minus the "twisted smectic C phases" which we have classified as cholesterics (table 1, and above under "Cholesteric Phases").

Smectic A and C. Examples of well aligned smectic A and smectic C phases are given in figure 6. The line one can draw between the centers of the maxima in the outer ring stands perpendicular to the preferred direction of the long axis of the molecules⁴, and the line one can draw through the inner ring maxima stands perpendicular to the preferred direction of the smectic planes. From this it follows that in the A phase of figure 6 the molecules stand perpendicular to the smectic planes and in the C phase at an angle* (our measurements of this angle on x-ray photographs gave a value of 41° for the angle between molecules and planes).

Table 2 Classification of smectic phases

<i>Outer ring</i>	<i>Phase type</i>	<i>Class</i>
Diffuse	A, C, F, (D)	α
Sharp, one	B	β
Sharp, several	E, G, H	γ

* There are indications that the distinction between S_A and S_C is not always as clear-cut as in this case. We hope to discuss this in more detail elsewhere.

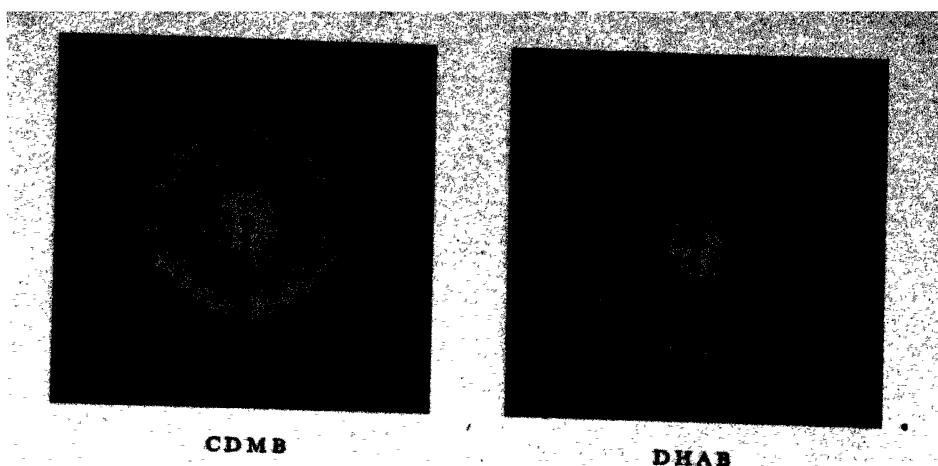


Figure 4 Diffraction patterns of the isotropic phases of cholesterol 2,4-dimethylbenzoate (CDMB, left) and 4,4'-di-*n*-heptyloxyazoxybenzene (DHAB, right). CDMB has a Ch_n phase at lower temperatures, DHAB a N_n phase. The photographs are on the same scale.

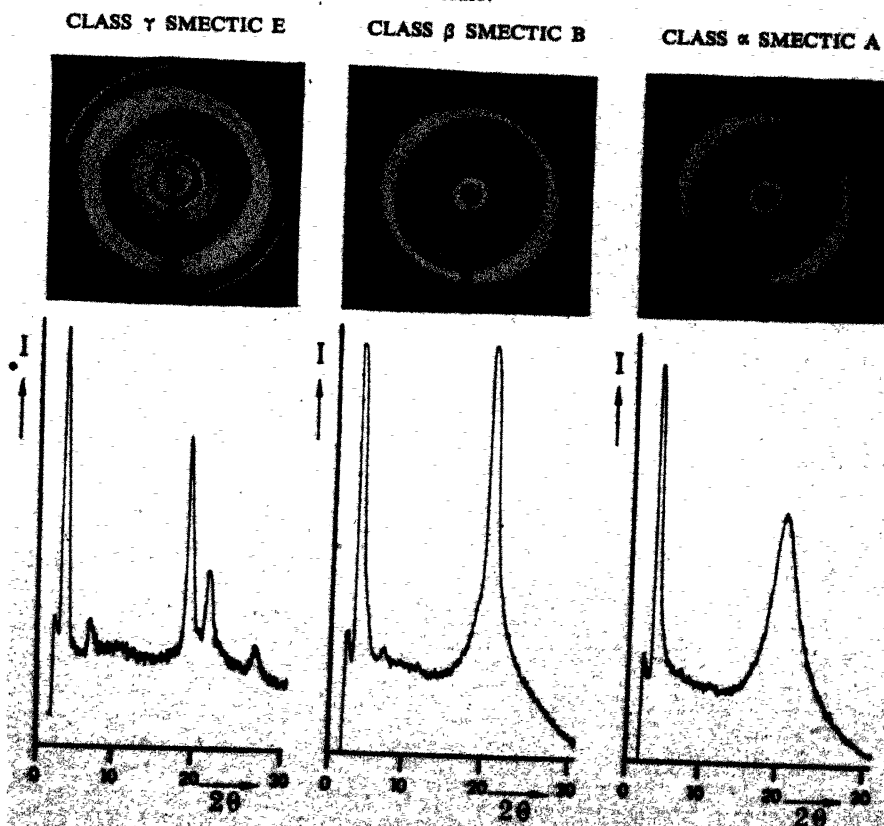


Figure 5 Diffraction patterns and densitometer traces of Sm_n , Sm_n , and Sm_n (left to right; for the Sm_n phase the trace is from a photograph of shorter exposure than the one reproduced here, so as to give a better indication of the relative intensities of the diffraction rings). The photographs are on the same scale.

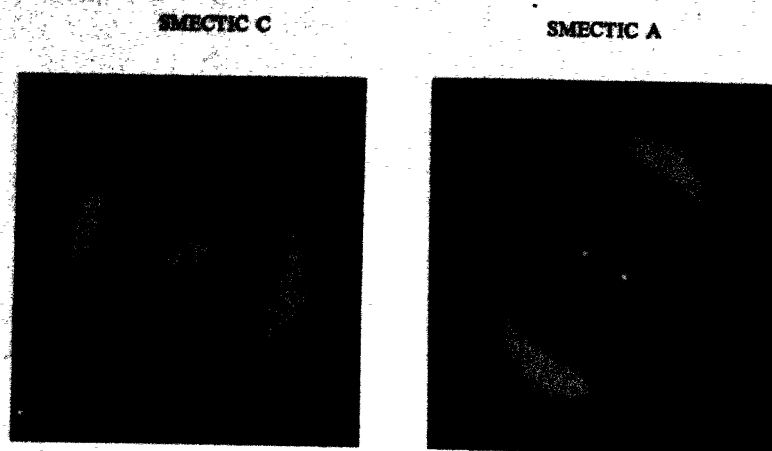


Figure 6 Diffraction patterns of well aligned samples of S_C (left) and S_A (right).

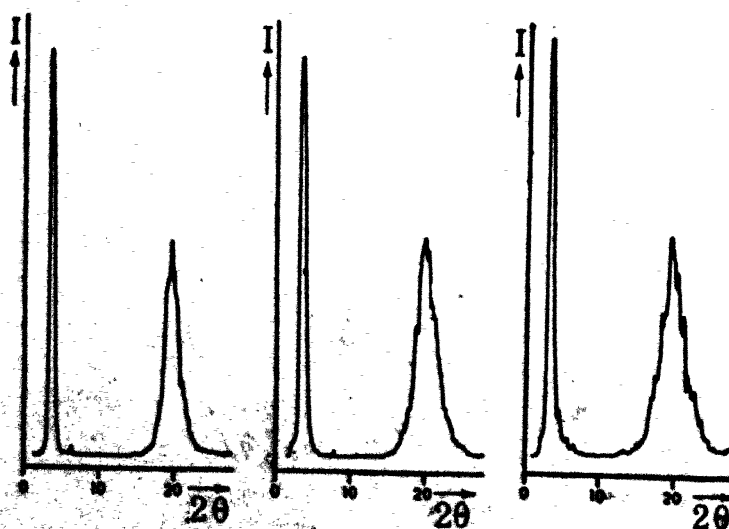
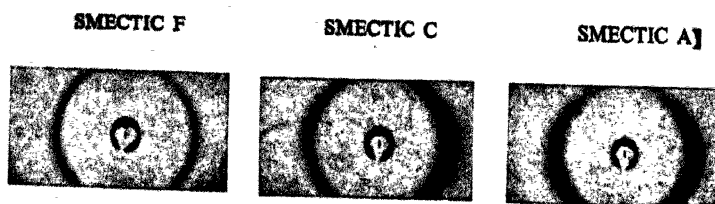


Figure 7 Diffraction patterns and denitometer traces of the S_F , S_C and S_A phases of one compound.

Smectic F. We have no x-ray photographs of aligned S_F phases, and to our knowledge none have been published, but since F appears to be similar to C^{1,10} we expect the diffraction patterns to be similar too. Diffraction patterns of a randomly oriented sample of a compound which exhibits F as well as C and A are shown in figure 7. The diameter of the inner ring is seen to decrease in the order $F \rightarrow C \rightarrow A$, indicating an increase in layer thickness, presumably due to a decrease in tilt†. The outer ring increases in width (in the same sequence), signifying a decrease in order with temperature (as one would expect).

Smectic D. Smectic D is characterized by the appearance of its inner diffraction ring in aligned samples¹³: the ring splits up into six spots in an approximately hexagonal arrangement (figure 8). The structure proposed for S_D on the basis of this hexagonal arrangement¹³ is quite different from the structure of all other smectic phases, and thus there is some doubt as to whether S_D should be called "smectic". For this reason we have put S_D in brackets in table 2.

Class β

The only phase type in this class is S_B , and in our B category we do not include the H phases, although the miscibility criterion would equate H with B¹⁴. We differentiate between B and H because in our opinion there are significant structural differences between the two types: whereas S_H has a well defined three-dimensional lattice¹⁵, we submit that S_B has not more than a two-dimensional lattice, confined to the individual smectic layers⁹‡. This difference in structure is reflected in differences in the x-ray diffraction photographs. In figure 9 we have diffraction patterns from two very well aligned samples of H and B, both with the preferred direction of the molecular axis approximately parallel to the incident x-ray beam. The main differences are: (a) H has many sharp reflections originating from well defined lattice planes, B has no sharp reflections other than the six maxima on the outer ring*. (b) The six sharp outer maxima of B are of approximately equal intensity; because of the three-dimensional lattice of H this would never be possible for this phase.

† Decrease of tilt with increasing temperature is a quite general phenomenon in liquid crystals: we have noticed that the smectic layer thickness is always greater than (or at least equal to) the layer thickness in the corresponding crystalline phase, S_C always precedes S_A (if both are present)¹ and TBBA shows a continuous decrease of tilt with temperature^{11,12}.

‡ During the writing of this paper another manuscript¹⁶ came to our attention which also differentiates between B and H, describing B as "a translationally ordered phase with no orientational order" and H as "a phase with translational and orientational order".

* The maxima look diffuse because of over-exposure; shorter exposures show the maxima to be sharp. We reproduced here the over-exposed photo so as to allow better judgment of the presence of weak additional maxima. (We could not find any).

Class γ

Smectic E. For this phase we propose (see table 1) a subdivision into E_n (normal E) and E_t (tilted E). X-ray data for some E phases suggest the molecules to be oriented normal to the smectic planes,^{9, 13} and this has been confirmed by studies¹ which indicate an optically uniaxial structure. These phases we would like to classify as E_n . Other E phases appear to be optically biaxial,¹⁷ which suggests that the molecules here are tilted with respect to the planes. These phases we would like to classify as E_t . This distinction between E_n and E_t would avoid (just like the distinction between Ch_n and C, made above) having uniaxial and biaxial phases with the same classification.

- *Smectic G.* As indicated by the dotted line in table 1 between Sackmann's G and our E, we would like to suggest the possibility that G and E basically have the same structure†. The distinction between G and E has been made¹ solely on the basis of their diffraction pattern (especially the outer rings), and in our opinion the two diffraction patterns are actually quite similar (figure 10). E has two strong outer rings, relatively close together, and a weaker one, somewhat farther out. G has two strong outer rings, quite close together, and a much weaker one, a little farther out. Thus the diffraction patterns suggest that the difference between E and G might be a difference in detail rather than a difference in kind‡. Further studies, especially of aligned samples, of a larger variety of E and G phases will be necessary to settle this point.

Smectic H. Our reasons for distinguishing between B and H have been discussed above under "Class β ". We would like to add here some comments concerning the possibility of finding both normal and tilted structures in H and B (as under "Smectic E" where we distinguished between E_n and E_t). It is clear that in Sackmann's B category there are normal (uniaxial) as well as tilted (biaxial) phases^{1, 18}; thus, if H would not be recognized as a different category, we would advocate a distinction between B_n and B_t . Within our classification scheme (table 1), however, so far only normal B phases^{19, 20} and tilted H phases (BBEA¹⁵ * and TBBA¹⁹) have been found. The fact that the tilted phases appear to

† The layer thickness for the G phase reported in Ref. 10 suggests a tilted structure (from the data in Ref. 10 we calculated an angle of 48° between molecules and planes). Thus, G might be really E_t , and it would be interesting to compare its diffraction pattern with that of the E_t phase of Ref. 17.

‡ Pursuing the direction of change from E to G (i.e., narrowing of the separation between the two strong outer rings and decrease of the intensity of the weaker outer ring) to the limit, one arrives at the diffraction pattern of B (only one strong outer ring). This suggests the possibility of a close similarity between the structures (within the smectic layers) of B, E and G.

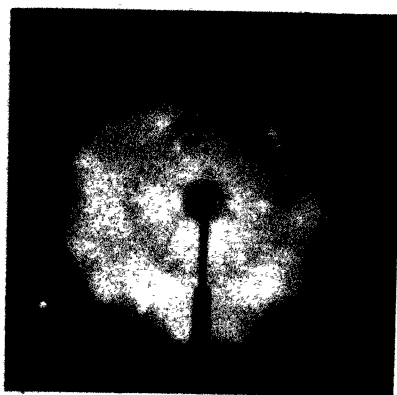
* We now prefer the abbreviation BBEA over BEA (used in Ref. 15), so as to be consistent with the abbreviations used for other members of the same homologous series²¹.



SMECTIC D

Figure 8 Photograph of the inner diffraction ring region of a well aligned sample of S_D .¹²

SMECTIC H



SMECTIC B



Figure 9 Diffraction patterns of very well aligned samples of S_H (left) and S_B (right). For S_H the molecules are close to being parallel with the incident x-ray beam, for S_B they are almost exactly parallel.

SMECTIC E



SMECTIC G

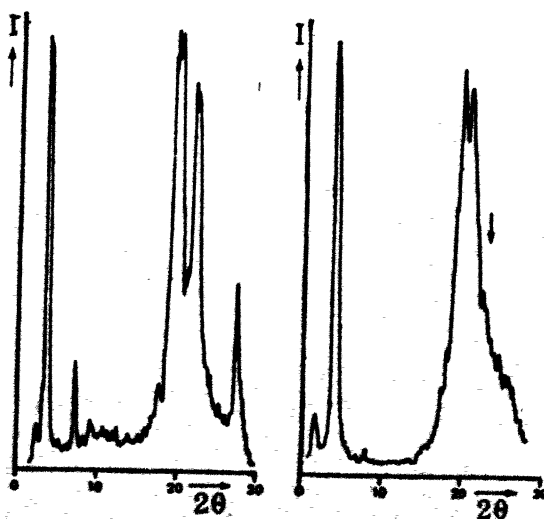


Figure 10 Diffraction patterns and densitometer traces of S_D^{12} (left) and S_D^{10} (right). The arrow in the S_D trace indicates the position of the weak third outer ring.

be the more ordered ones agrees with the general trend in this respect found in liquid crystals (note, *e.g.*, that, if a compound has both A and C phases, C always precedes A in order of increasing temperature^{1,3}; see also footnote † on page 99).

Three dimensional lattice. The x-ray diffraction patterns of E¹³ and H¹⁵ indicate that both structures have a three-dimensional lattice^{9,15}. Thus the difference between these phases and crystalline solids might be merely the *extent* over which the three-dimensional lattice persists. This dependence of phase type on the extent of local order appears to be a general principle in liquid crystallinity, as indicated in table 3.

Table 3 Phase types differing by the extent of local order

<i>Type of order</i>	<i>Short range</i>	<i>Long range</i>
Three-dimensional lattice	S _H	K ^(a)
Pseudo-hexagonal packing	(S _F , S _C , S _A) ^(b)	S _H (S _B)
Parallel arrangement, layered	N _{sc}	S _C
Parallel arrangement, random	1	N _o

(a) K = crystalline solid

(b) Phase types between brackets are merely suggested as possibly belonging in the categories indicated

Difference between γ and β phases. In table 2 we have used the character of the outer ring(s) to distinguish between β and γ phases. As stressed elsewhere,⁹ this is only a preliminary classification. We expect that the fundamental difference between β and γ phases will turn out to be the presence of a three-dimensional lattice in γ phases and its absence in β phases.

PART II

Intermolecular distances

Introduction

The structural parameters that can be obtained from the positions of the x-ray diffraction maxima²² (*i.e.*, from the corresponding diffraction angles) are indicated in figure 11 and listed in table 4. We will confine our discussions here to the average intermolecular distance (D) between neighboring parallel molecules (a limited discussion of l and d values may be found in Ref. 21) of all liquid crystalline and isotropic phases for which we have been able to find reasonably accurate values. This

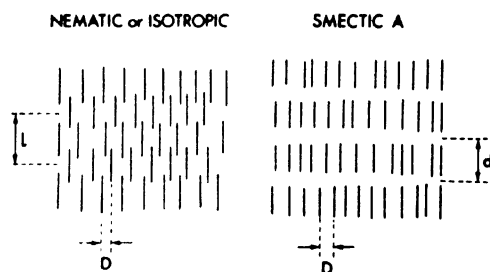


Figure 11 Schematic representations of the molecular arrangement in N_o or I (left) and S_A (right). The lines are the molecules. The molecular length is indicated by l , the intermolecular distance by D , and the layer thickness by d .

Table 4 Structural parameters in various phases that can (+) or cannot (–) be determined

Parameter		S	N	I
Inter-molecular distance	D	+	+	+
Molecular length	l	–	\pm	+
Layer thickness	d	+	\pm	–

parameter D is calculated from the diffraction angle(s) of the outer diffraction maxima. It is of particular interest because it gives a good indication of the packing density of the material concerned.

Presentation of data

D has always, in all phases, been found to increase with temperature^{21,23,11}. An example of this temperature dependence has been given in figure 12²⁴. The most exhaustive way to analyze possible trends and relationships between the available D data would be to plot the data for each compound as in figure 12 and to combine the plots from all compounds. We found, however, that such a combined plot becomes extremely difficult to survey. For this reason we have plotted the data as follows. We have first classified all data according to phase type, and arranged the phase types in sequence of decreasing order. Within each phase type we have arranged the compounds in sequence of increasing magnitude of the lowest temperature of measurement for each compound. The data are listed in table 5 and the resulting graph is shown in figure 13.

Smectic phases

TBBA data: The D values for the H and A phases of TBBA (the two squares in figure 13 connected by straight lines to the single square in the

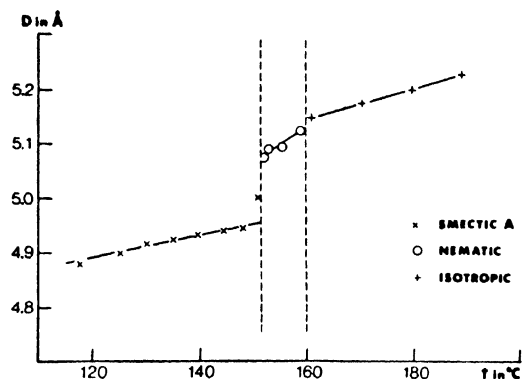


Figure 12 The intermolecular distance D as a function of temperature, in the S_A , N_o , and I phases of EABAC²⁴ (see table 5). The last value in the S_A range, near the S - N point, probably represents a pretransition effect.

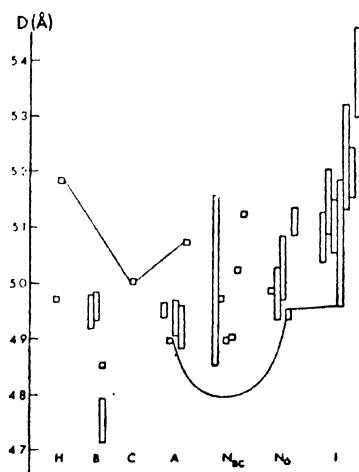


Figure 13 Plot of D according to phase type and compound. Squares generally represent single measurements (squares were used instead of lines, for better visibility), rectangles represent the ranges of D for the temperature ranges investigated (usually the full stability range).

C region) appear to be exceptionally high when compared with the other H, B*, and A values. This is also apparent from the calculated density²² of the H phase of TBBA, which is 0.99 gr/cm³, as compared to the lowest

* Since the packing within the smectic layer may be expected to be similar for B and H, the D values may be expected to be similar too.

Table 5 Data used in figure 13(a)

Phase	Compound	Abbreviation	D(Å)	<i>t</i> (°C)	Reference
H	4- <i>n</i> -butyloxybenzal-4'-ethylaniiline terephthal-bis- (4- <i>n</i> -butylaniline)	BBEA (b)	4.97	44.6	15
		TBBA	5.18	125	11
B	<i>p</i> - <i>n</i> -hexyloxybenzylidene-5-amino-2-butoxypyridine <i>n</i> -amyl-4 (4- <i>n</i> -dodecyloxybenzylideneamino) -cinnamate ethyl-4 (4-ethoxybenzylideneamino) -cinnamate	HABP	4.92-4.98	52.5-86	20
		ADBC	4.93-4.98	77-93	23
		EBAC	4.71-4.79	79.5-115	23
			4.85	85	19
C	terephthal-bis- (4- <i>n</i> -butylaniline)	TBBA	5.00	150	11
A	4- <i>n</i> -heptyloxybenzal-4'-ethylaniiline ethyl- <i>p</i> -ethoxybenzal- <i>p</i> -aminobenzoate <i>p</i> - <i>n</i> -hexyloxybenzylidene-5-amino-2-butoxypyridine ethyl- <i>p</i> -acetoxybenzol- <i>p</i> -azocinnamate terephthal-bis- (4- <i>n</i> -butylaniline)	HpBEA	4.94-4.96	57.5-63.5	21
		EEB	4.89-4.90	71.5-80.4	21
		HABP	4.90-4.97	86-100	21
		EABAC	4.88-4.96	115-151.5	24
		TBBA	5.07	175	11
N..	bis- (4'- <i>n</i> -octyloxybenzal)-2-chloro-1,4-phenylenediamine bis- (4'- <i>n</i> -nonyloxybenzal)-2-chloro-1,4-phenylenediamine bis- (4'- <i>n</i> -pentyloxybenzal)-2-chloro-1,4-phenylenediamine bis- (4'- <i>n</i> -hexyloxybenzal)-2-chloro-1,4-phenylenediamine bis- (4'- <i>n</i> -decyloxybenzal)-2-chloro-1,4-phenylenediamine bis- (4'- <i>n</i> -dodecyloxybenzal)-2-chloro-1,4-phenylenediamine	BOCP	4.85-5.15	60-179	4
		BNCP	4.97	98	4
		BPCP	4.89	100	4
		BHxCP	4.90	100	4
		BDcCP	5.02	115	4
		BDoCP	5.12	134	4

Phase	Compound	Abbreviation	D(Å)	<i>t</i> (°C)	Reference
N _o	4- <i>n</i> -pentyloxybenzal-4'-ethylaniiline	PBEA	4.98	55.7	21
	4- <i>n</i> -hexyloxybenzal-4'-ethylaniiline	HxBEA	4.93-5.02	58-69	21
	4- <i>n</i> -heptyloxybenzal-4'-ethylaniiline	HpBEA	4.97-5.08	63.5-67.5	21
	ethyl- <i>p</i> -ethoxybenzal- <i>p</i> -aminobenzoate	EEB	4.93-4.95	80.4-87.6	22
	ethyl- <i>p</i> -acetoxybenzol- <i>p</i> -azocinnamate	EABAC	5.08-5.13	151.5-160	24
I	4- <i>n</i> -pentyloxybenzal-4'-ethylaniiline	PBEA	5.03-5.13	59-84	21
	4- <i>n</i> -heptyloxybenzal-4'-ethylaniiline	HpBEA	5.08-5.20	67.5-108	21
	4- <i>n</i> -hexyloxybenzal-4'-ethylaniiline	HxBEA	5.05-5.15	69-108	21
	ethyl- <i>p</i> -ethoxybenzal- <i>p</i> -aminobenzoate	EEB	4.96-5.18	87.6-190	21, 22
	<i>p</i> - <i>n</i> -hexyloxybenzylidene-5-amino-2-butoxypyridine	HABP	5.13-5.32	100-185	20
	ethyl- <i>p</i> -acetoxybenzol- <i>p</i> -azocinnamate	EABAC	5.15-5.24	160-190	24
	bis- (4'- <i>n</i> -octyloxybenzal)-2-chloro-1,4-phenylenediamine	BOCP	5.30-5.46	179-238	20

(a) Compounds are listed in the order in which they are plotted in figure 13 from left to right
 (b) BEA in Ref. 15

calculated density for the other B and H phases, which is 1.05 gr/cm^3 . We do not know whether or not these high D values are caused by errors³², but we shall drop them anyway because we are concerned here with finding general trends and relationships, and for this purpose it is better to leave out all clearly exceptional data. We cannot judge the D value for the C phase of TBBA, since it is the only C phase measured, but, to be on the safe side, we shall omit this data point in our subsequent discussions, too.

EBAC data: For the B phase of EBAC (the third compound in the B region in figure 13) we have data from two sources: one single value from Ref. 19 and data for the full stability range from Ref. 23 (table 5). Since the single value falls outside the full range, at least one of the sources must be in error. The D values from Ref. 23 are much lower than any of the other D values in figure 13; the lowest D yields a calculated density of 1.31 gr/cm^3 which seems extremely high for a smectic phase²⁵. For this reason the EBAC data from Ref. 23 appear questionable and will be left out in our subsequent discussions.

Remaining smectic data: Leaving out the exceptional data from TBBA and EBAC, we find that the remaining smectic data (figure 14) fall within a very short range, varying only from 4.85 \AA to 4.98 \AA (table 5).

This lack of difference, between S_A on the one hand and S_B and S_H on the other hand, is somewhat disturbing. B and H phases are low temperature phases with respect to A phases, and B and H phases have a more regular packing of the molecules within the smectic layer than A phases. Thus one would expect D to be lower for B and H than for A, but figure 14 indicates D to be about the same for B as for A and possibly even somewhat higher for H. This disturbing general trend is confirmed

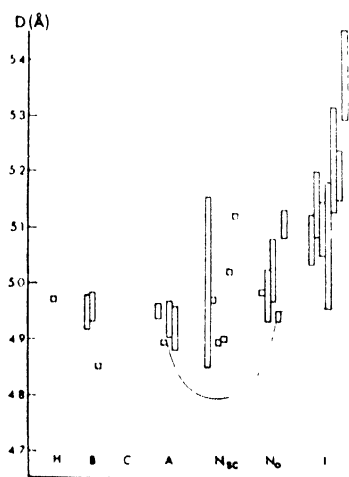


Figure 14 As Figure 13, but with some exceptional data left out.

by two specific cases: in TBBA (with the sequence $H \rightarrow C \rightarrow A$) the D for S_H is considerably higher than for S_C and S_A (figure 13, table 5), and in HABP (with the sequence $B \rightarrow A$) the D at the end* of the B phase (4.98\AA) is higher than the D at the beginning* of the A phases (4.90\AA ; table 5).

The reason for this is not clear. It seems unlikely that the actual density would go up on going from H or B to C or A (measurements on other compounds²⁵ indeed indicate, as expected, the opposite). Thus the most likely explanations for a decrease in D when going from H or B to C or A appear to be:

(a) The number of nearest neighbors decreases when going from H or B to C or A. This would allow a density drop at the transition to the higher temperature phase, even with a decrease in D .

(b) The decrease is only apparent, not real, and is caused by the use of incorrect formulas. For S_B , the parameter calculated directly from the diameter of the outer ring is not D , but the distance d_o between the lattice planes which cause the outer diffraction maximum. D is subsequently calculated from d_o under the assumption of a regular hexagonal packing of the molecules (figure 15). If this assumption would be incorrect, the D value would be in error, too. For S_A and S_C , D has been calculated with the formula⁴ $2D \sin \theta = 1.117\lambda$, where θ is one half of the diffraction angle and λ is the wavelength of the radiation. This formula is based upon a number of assumptions and approximations, and if any one of these would not be allowed, this would cause an error in the calculated value of D .

A comparison between measured and calculated densities for a number of A, B, C, and H phases would seem to be an appropriate first step in an attempt to solve this problem. Meanwhile, for lack of a better solution, we shall keep using the current methods for calculating D .

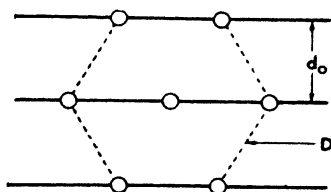


Figure 15 The relationship between D and d_o (the interplanar spacing calculated from the position of the outer diffraction ring) for S_A , assuming hexagonal arrangement of the molecular axes. The circles give the positions of the molecular axes (which are perpendicular to the plane of the paper), the full lines represent the planes containing the molecular axes (within the smectic layers), and the broken lines indicate the hexagonal arrangement.

* Going in the direction of increasing temperature.

Nematic and isotropic phases

N_o and I phases: If we disregard for a moment the N_{sc} data, there is a very clear trend in figure 14: going from the left to the right, *D* increases fairly steadily when going from the smectics through the N_o phases and the I phases to the highest temperature I phase*. This increase is just what one would expect for going to higher temperatures and to decreasing alignment of neighboring molecules.

N_{sc} phases: N_{sc} phases are nematic phases with smectic-like local order⁴. This dual nature appears to be confirmed by figure 14: the *D* values of the N_{sc} phases encompass the complete range of *D* values of S and N_o phases combined.

**Conclusions from low D values*

Comparison with molecular dimensions: The lowest *D* values in figure 14 are 4.85 Å, both for the B phase of EBAC and for the N_{sc} phase of BOCP (table 5)†. It is instructive to compare this *D* value with some molecular dimensions. The most bulky part of the molecules in most liquid crystals (apart from cholesterol related compounds) is the benzene ring. Figure 16 shows the projections of two benzene rings standing with

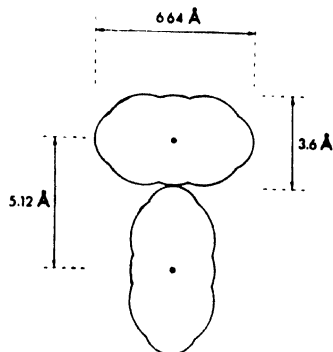


Figure 16 Projection of two benzene rings, perpendicular to each other and in close contact, each standing with one of its C-H bonds perpendicular to the plane of the paper.

* The EEB data (S_A, N_o, I), connected in figure 14 by thin lines, form an exception. Since the *D* values for this compound are consistently low²¹, the EEB data probably should also be considered "exceptional" and thus be excluded from consideration when establishing general trends.

† It is interesting to note that in a recent paper²¹ on the structure of hydrocarbon chains of lipids it is reported that in structures in which the hydrocarbon chains are stiff and parallel, these chains, packed in a hexagonal lattice, also have an intermolecular distance of 4.85 Å. This suggests that in liquid crystals the 4.85 Å might represent the smallest intermolecular distance allowed by the hydrocarbon chains at the ends of the molecules.

one of their C-H bonds perpendicular to the plane of the paper (in this orientation the molecules require the least amount of space in the plane of the paper). It is clear from figure 16 that the minimum distance between the centers of two molecules that would allow rotation of one molecule without displacement of the other molecule is 5.12 \AA . This is much more than the experimentally determined average intermolecular distance $D = 4.85 \text{ \AA}$ quoted above. This leads us to important conclusions with regard to the packing mode and the possibility of rotation of the molecule around its long axis.

Suggested packing mode: An average intermolecular D value of 4.85 \AA requires a much closer packing than represented in figure 16. The only satisfactory model appears to be the pseudo-hexagonal herringbone packing^{15, 26} shown in figure 17. For ordered phases like S_B and S_H we expect the order indicated in figure 17 to be well maintained. For disordered phases like S_A and N_c we expect a much more disordered packing, but still with basically the same molecular arrangement.

Restriction on rotation in smectic B: As pointed out above, a D of 4.85 \AA implies that rotation of a molecule requires considerable ($\approx 0.3 \text{ \AA}$) displacements of the neighboring molecules. From figure 17 it is clear that in the herringbone packing not only full rotation but even appreciable oscillation around the long axis necessitates considerable displacement of neighbors. Such displacements cannot be ruled out in disordered phases like S_A and N_{cs} ,* but we submit that they *can* be ruled out for S_B . The sharp profile of the outer diffraction ring of S_B (figure 5) is evidence of the existence of well defined lattice planes. Displacements of the magnitude necessary for large oscillations in the herringbone packing would destroy these lattice planes, and hence are not allowed. A "disorder" in

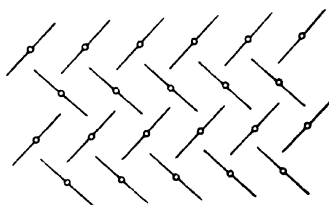


Figure 17 Schematic representation of the pseudo-hexagonal herringbone packing, as seen along the long axes of the molecules. The lines indicate the orientation of the molecular planes and the circles mark the positions of the molecular axes; the circles form a hexagonal array.

* For tilted or skewed phases, like S_H , S_{E1} , S_C and N_{cs} , we have argued elsewhere²⁷ that appreciable oscillations are not likely to occur. Others also have recently argued against rotation in S_H and S_C ^{16, 28}. So for these phases the question of displacement is not relevant.

S_B , in terms of part of the molecules (up to 50%) being rotated a full 180° is quite possible,[†] however, and in our opinion even quite likely.

Acknowledgements

I want to acknowledge here the contributions of Mr Andrew Olah and Mr Lawrence Rubens to the preparation of the figures. I am very grateful to Dr H Sackmann for sending the x-ray photographs reproduced in figures 7, 8, and 10, and I thank Dr G H Brown for permission to use his drawings as a model for figure 11.

I also want to acknowledge the fact that it was Dr J Doucet who stimulated my interest in the comparison of D values of different compounds by his work on this subject in his thesis,¹¹ and I want to express my appreciation to Dr M Lambert who provided me with a copy of this thesis.

References

- 1 SACKMANN H and DEMUS D *Mol. Cryst. Liquid Cryst.* **21** 239 (1973)
- 2 VERBIT L *Mol. Cryst. Liquid Cryst.* **15** 89 (1971); *Liquid Crystals* 3 (Gordon and Breach, London) 1089 (1972)
- 3 DE VRIES A *Mol. Cryst. Liquid Cryst.* **10** 31 (1970)
- 4 DE VRIES A *Mol. Cryst. Liquid Cryst.* **10** 219 (1970)
- 5 CHISTYAKOV I G and CHAIKOWSKY W M *Mol. Cryst. Liquid Cryst.* **7** 269 (1969); *Liquid Crystals* 2, Part II (Gordon and Breach, London) 803 (1969)
- 6 LECLERCQ M, BILLARD J and JACQUES J C.R. *Acad. Sci. (Paris)* **C266** 654 (1968); *Mol. Cryst. Liquid Cryst.* **8** 367 (1969); *Liquid Cryst.* 2 Part II (Gordon and Breach, London) 579 (1969)
- 7 URBACH W Z and BILLARD J C.R. *Acad. Sci. (Paris)* **B274** 1287 (1972)
- 8 BILLARD J *Bull. Soc. franc. Miner. Cryst.* **95** 206 (1972)
- 9 DE VRIES A *Mol. Cryst. Liquid Cryst.* **24** 337 (1973)
- 10 DEMUS D, DIELE S, KLAPPERSTÜCK M, LINK V and ZASCHKE H *Mol. Cryst. Liquid Cryst.* **15** 161 (1971); *Liquid Crystals* 3 (Gordon and Breach, London) 493 (1972)
- 11 DOUCET J Thèse pour Docteur de 3ème cycle, Université de Paris-Sud, Centre d'Orsay (1972)
- 12 TAYLOR T R, ARORA S L and FERGASON J L *Phys. Rev. Lett.* **25** 722 (1970)
- 13 DIELE S, BRAND P and SACKMANN H *Mol. Cryst. Liquid Cryst.* **17** 163 (1972)
- 14 URBACH W Z and BILLARD J "Polymorphism of smectic phases" Paper #34 at the Fourth International Liquid Crystal Conference, Kent, August 1972
- 15 DE VRIES A and FISHEL D L *Mol. Cryst. Liquid Cryst.* **16** 311 (1972)
- 16 MEYER R J and McMILLAN W L *Phys. Rev.* **A9** 899 (1974)
- 17 COATES D, HARRISON K J and GRAY G W *Mol. Cryst. Liquid Cryst.* **22** 99 (1973)
- 18 DEMUS D *Wiss Z Univ. Halle* **21** 41 (1972)
- 19 LEVELUT A M and LAMBERT M C.R. *Acad. Sci. (Paris)* **B272** 1018 (1971)
- 20 DE VRIES A unpublished work
- 21 DE VRIES A *Mol. Cryst. Liquid Cryst.* **20** 119 (1973)
- 22 DE VRIES A *Mol. Cryst. Liquid Cryst.* **11** 361 (1970); *Liquid Crystals* 3 (Gordon and Breach, London) 457 (1972)

[†] Such a disorder is forbidden in S_B and in other tilted phases^{27,28}.

- 23 DIELE S, BRAND P and SACKMANN H *Mol. Cryst. Liquid Cryst.* **16** 105 (1972) ;
Liquid Crystals 3 (Gordon and Breach, London) 481 (1972)
- 24 DE VRIES A and CARPENTER R E to published
- 25 DEMUS D and RURAISKI R Z. *Phys. Chem. (Leipzig)* **253** 53 (1973)
- 26 GULRICH L W and BROWN G H *Mol. Cryst.* **3** 493 (1968)
- 27 DE VRIES A to be published
- 28 McMILLAN W L *Liquid Crystals and Ordered Fluids* **2** (Plenum Press, New York)
141 (1974)
- 29 DE GENNES P G *Mol. Cryst. Liquid Cryst.* **21** 49 (1973)
- 30 HELFRICH W and OH C S *Mol. Cryst. Liquid Cryst.* **14** 289 (1971)
- 31 TARDIEU A, LUZZATI V and REMAN F C *J. Mol. Biol.* **75** 711 (1973)
- 32 DE VRIES A *J. Chem. Phys.* **61** 2367 (1974)

DISCUSSION

Janik : Neutron diffraction studies with deuterated PAA performed by Riste *et al* in Norway show two diffuse peaks in the nematic phase, similar to what you observe as two rings. They also give evidence of pre-transition effects below melting. The authors claim that there is a soft solid in a region of a few degrees below melting.

de Vries : I have never observed pre-transition effects in the solid phase myself, but this might well be due to the fact that I have never paid any particular attention to the solid phase. As far as I remember from a presentation recently given by Dr. Pynn at a Liquid Crystal Institute Seminar about his neutron work (in collaboration with Dr. Riste), there appeared to be no conflicts between his results and mine.

Gray : Have you ever observed both a cybotactic nematic and an ordinary or classical nematic phase in the same compound?

de Vries : No, but it would be very interesting if this were to be found.

Kaul : With the high degree of order in the smectic H phase that is shown by x-ray, what other studies were made to show that it is not just another crystalline phase rather than a liquid crystal phase?

de Vries : There are several points to indicate that. My colleagues in Kent who work with the Mossbauer effect, have investigated exactly the same smectic H phase that I have been studying. The spectra are very typical of the smectic phase and not at all like what they found in a solid phase. Secondly, microscopic textures are typical of smectic phases and not of solids. Thirdly, the transition temperatures involving a smectic H with the higher liquid crystal phase always lie on nice smooth continuous curves whereas transition temperatures from solids to liquid crystal do not. Fourthly, these transitions show no supercooling, whereas most transitions involving solid phases show considerable supercooling.

Billard: Just a remark about the classification problem, which we can compare with classical crystallography. In crystallography we can have different structures with the same symmetry class. If we have similar structures we have similar symmetry groups. I think that the isomorphism proves the similarity of structures and is a test of strong connection between two phases. Do you think that we can have two operational classifications:

1. the miscibility system, and
2. the structural system?

de Vries: I definitely think there is room for these two classification systems, and possibly even more different systems (*e.g.*, one based on the 'optical properties'), each in its own right and with its own specific advantages and disadvantages. In addition to these independent classifications one should also consider, in my opinion, an overall classification system containing the information of all methods that are useful for identifying difference between phases. This 'overall classification' system, in my view, should incorporate the maximum differentiation between phases that is practically useful, *e.g.*, if we had, say, four different methods for distinguishing phase types, and if for a phase X and a phase Y three of the methods would show no difference, but the fourth method would show a significant difference between X and Y, then, in my view, these two phases X and Y should be assigned different phase types. In order to avoid this system of fine differentiation becoming so complex that it would be of no practical use, it should also incorporate some 'broader' classification symbols, like, N, Ch, and S from table 1 and $S(\alpha)$, $S(\beta)$ and $S(\gamma)$ from table 2.

Chandrasekhar: Did you find evidence for a strong temperature dependence of tilt angle in smectic C from your x-ray pictures?

de Vries: You have smectic C phases which apparently have little or no variation of tilt angle with temperature. One type of smectic C phase has a constant tilt angle. On the other hand, the smectic C phase of TBBA has a continuously varying tilt angle which even goes completely to zero. I would like to look at it from the point of what determines the way the molecules are packed. I think two different kinds of forces are acting in these two types of C phases, and I would like to distinguish between them on that basis.

Bulkin: The hexagonal spot array in smectic B and smectic D looked alike, yet you did not comment on the similarity here. Please explain.

de Vries: The hexagonal array of diffraction maxima in S_B is in the outer ring, and suggests the presence of a hexagonal (two-dimensional) lattice *within the smectic layer*. The (pseudo-) hexagonal array of diffraction maxima in S_D is in the *inner* ring (the outer ring falls outside the

area reproduced in the figure), and suggests, according to Diele *et al**, a cubic arrangement of spherical micelles, which would appear to effectively eliminate layered structure in the sense one conventionally associates with smectic phases.

Jahnig: I do not understand your so-called 'cybotactic' and 'intermediate' nematic phases. As regards the 'cybotactic' nematic you conclude from the absence of a strong temperature variation of your additional scattering pattern that this scattering pattern is not a pre-transitional effect. But this I think is not convincing. There are examples in nature where pre-transitional effects do not show a strong temperature variation. As regards the 'intermediate' nematic I want to ask you whether this phase has anything to do with the intermediate state of a nematic-smectic A phase transition introduced by de Gennes on a well-defined basis.

de Vries: Regarding your question on the pre-transition effect, I do not know about the experimental data you talked about. As far as x-ray experiments are concerned there is a very strong direct link between what you see in the x-ray pattern and the molecular orientation that exists in the material. If the formation of cybotactic groups was a pre-transition effect, you would have at some temperature above the transition no cybotactic groups at all, but just the ordinary nematic phase. And then you will get small groups forming slowly. Then they start to expand, and expand so much that they become smectic-like in behaviour. Thus, in a way the nematic-isotropic pre-transition effects are related to the cybotactic groups. If you look at this transition, you have a slow diminishing of the cybotactic nature. But over 20°, which is quite considerable, the x-ray pattern shows that the groups do not increase in size, the number of groups does not increase, the groups do not increase in their rigidity, they remain exactly the same. But then all of a sudden at the N-S transition point they go over from cybotactic to smectic.

* Diele S, Brand P and Sackmann H *Mol. Cryst. Liquid Cryst.* 17 163 (1972)

Lipid-water systems : Structure and structural transitions

A TARDIEU, J L RANCK, L MATEU, D M SADLER,
T GULIK-KRZYWICKI and V LUZZATI

Centre de Génétique Moléculaire, C.N.R.S., 91190 - Gif-sur-Yvette
(France)

A remarkable property of lipids is to unite in one phase a well ordered long range organization and different types of disordered short range conformation ¹.

Several phases, belonging to the lamellar class, have been studied by x-ray diffraction techniques ^{2,3}. They have been shown to differ mainly by the conformation and the organization of the hydrocarbon chains, which may undergo order-disorder transitions as a function of temperature and/or water concentration. Some aspects of these order-disorder transition phenomena have been considered, in correlation with the chemical composition of the lipids ⁴.

Most of these phases present characteristic features when studied by freeze-etching techniques.

References

- 1 LUZZATI V (1968) *Biological Membranes*, ed. D. Chapman 1 71-123. Academic Press, London and New York
- 2 LUZZATI V *et al.* (1972) *Proceedings of the 8th FEBS Meeting*, North Holland, Amsterdam, 173-183
- 3 TARDIEU A, LUZZATI V, REMAN F C (1973) *J. Mol. Biol.* 75 711-733
- 4 RANCK J L *et al.* (1974) *J. Mol. Biol.* 85 249-277

DISCUSSION

Nityananda : Is there any evidence from the x-ray patterns for the type of wavy lamellae you showed us ?

Tardieu : At low angles, the x-ray data are a series of reflections which can all be indexed in a two dimensional oblique lattice. The model proposed is in excellent agreement with the intensities of the reflections, the chemical and the electron microscopy data.

Ambrose : I admired your electron micrographs. Could you tell me what method of fixation was used and whether the method can be used to study preparation of natural lipids from various cell components after removal of protein ?

Tardieu : Freeze etching technique does not require any fixation procedure. It has been shown, by a comparative study of some lipid water systems by x-ray and electron microscopy, that this technique was able to preserve the structures observed at a high temperature in lipid water systems.

Gray : Have you done any experiments on the effects of incorporating known concentrations of specific hydrocarbons (*e.g.*, *n*-decane) in the various lamellar phases you have described, to see whether this throws any further light on the organisation of the lipid alkyl chains?

Also, is there any evidence whether high concentrations of added hydrocarbon can convert lamellar phases into, say, reversed hexagonal phases?

Tardieu : Up to approximately 10%, hydrocarbons are easily incorporated in phospholipids. In lamellar phases, they are mainly localized in the middle of the hydrocarbon leaflet. In phases with liquid hydrocarbon chains, the properties of the phases are to a large extent insensitive to the addition of further hydrocarbon.

But addition of decane to synthetic lecithins which normally form a L_β' phase (with tilted chains) induces the formation of a L_β phase (chains perpendicular to the lamellae).

Bulkin : Have you studied mixtures containing two pure phospholipids, *e.g.*, lecithin and phosphatidylserine?

Tardieu : No.

Schnur : Have you studied the dynamic properties of the intraconversion of the various alkyl conformations?

Tardieu : The data presented here were obtained with systems in equilibrium. Systematic studies of the kinetic aspects of these transitions are just beginning, and for the moment we have just some preliminary results.

Pressure induced mesomorphism

S CHANDRASEKHAR *, S RAMASESHAN †
A S RESHAMWALA †, B K SADASHIVA *
R SHASHIDHAR * and V SURENDRANATH *

* Raman Research Institute, Bangalore 560006

† Materials Science Division, National Aeronautical Laboratory,
Bangalore 560017.

Abstract. The paper reports the discovery of mesomorphism induced by pressure in materials that do not exhibit the liquid crystalline phase at atmospheric pressure. This observation verifies a prediction of the theory of melting of molecular crystals.

Experiments were conducted on the first two members of the *p n*-alkoxybenzoic acid series. These two compounds, the methoxy- and ethoxybenzoic acids, do not form liquid crystals at atmospheric pressure whereas the third and higher homologues do. However, as the pressure is raised both compounds exhibit mesophases, initially a nematic phase and then, at higher pressures, a smectic phase as well. Experimental phase diagrams are presented which establish for the first time the existence of the solid-nematic-isotropic and solid-smectic-nematic *triple points* in single component systems.

Introduction

Under what circumstances can the solid-liquid crystal-isotropic liquid triple point be observed experimentally? A study of the phase diagrams given by the theory of melting of molecular crystals discussed by Chandrasekhar *et al.*¹ provides an answer to this question. Two representative *P-T* diagrams evaluated from the theory are shown in figure 1. In figure 1(a) the orientational barrier of the molecule is large enough for the nematic phase to occur at zero pressure. As the pressure increases, both the solid-nematic and the nematic-isotropic transition temperatures increase, the slope dT/dP for the latter being greater in accordance with the experimental data available for *p*-azoxyanisole (PAA)²⁻⁶ and *p*-azoxyphenetole (PAP)². Figure 1(b) represents a more interesting case. Here the barrier is just below the critical value for the nematic phase to occur at zero pressure, As the pressure increases there is initially only a single transition, namely, the solid-liquid melting transition, but at higher pressures branching takes place and there are two transitions, the solid-nematic and the nematic-isotropic. Thus the theory makes the important prediction that the liquid crystalline phase can be induced by pressure in materials that are non-mesomorphic at atmospheric pressure, and also that at a certain pressure

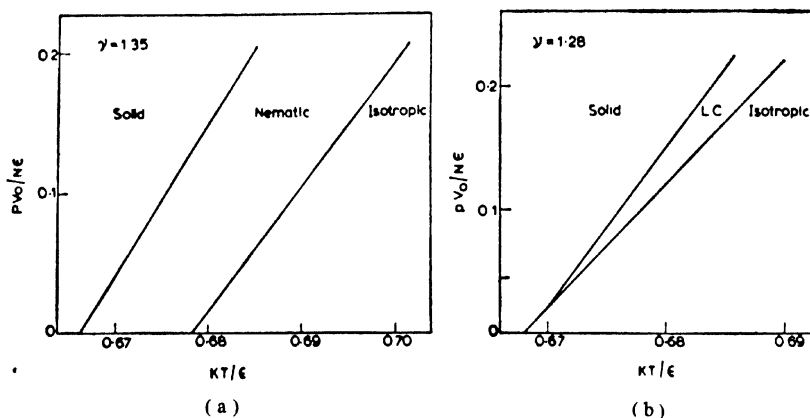


Figure 1 Theoretical phase diagrams evaluated for two values of ν , where ν is a measure of the relative barriers for the rotation of a molecule and for its diffusion to an interstitial site, (a) $\nu = 1.35$ (b) $\nu = 1.28$.

and temperature there should exist a solid-liquid crystal-isotropic liquid triple point. Experiments were undertaken to verify these conclusions.

After surveying various possible materials, it was decided to choose for these studies the first two members of the *p-n*-alkoxybenzoic acid series. These two members, methoxy- and ethoxybenzoic acids, do not show any mesomorphism whereas propoxybenzoic acid and the higher homologues exhibit at least one liquid crystalline phase⁷. Moreover, a mixture of the first two members shows a nematic phase, indicating that mesomorphism may be latent in each of them. It therefore appeared that the chances of observing liquid crystallinity in either of these two compounds at pressures easily attainable in the laboratory might be quite favourable.

Experimental

A 100-ton single acting hydraulic press (figure 2) was employed for the experiments. A schematic diagram of the press is shown in figure 3. The press has a 4" diameter movable ram which can be worked upwards by a hydraulic pump. The high pressure cell, containing the encapsulated sample, the pressure transmitting medium and the heater, is held inside a binding ring (B) to prevent extrusion. A cooling jacket (J) used in series with a heat exchanger serves to prevent the pistons from getting overheated. A stainless-steel piston (SP) presses the cell from above. This piston has a central bore for taking out the thermocouple leads. As the movable ram is raised, the entire assembly moves up and presses against a stationary plate fixed to the body of the press. The amount of fluid that is pumped was accurately controlled by a manual pump so that the pressure could be built up very gradually.

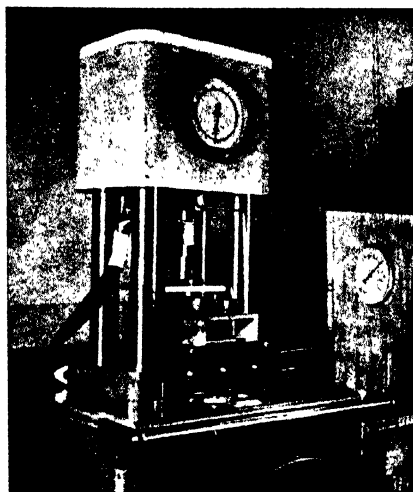


Figure 2 Photograph of the 100 ton press used for the experiments.

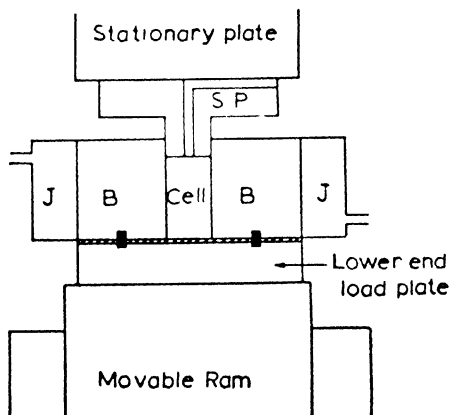


Figure 3 Schematic diagram of the press.

Since the nematic-isotropic transition is usually weakly first order, it was necessary to select a probe of high sensitivity. The obvious choice was DTA in which the difference between the reference and sample temperatures is plotted versus the sample temperature. Ideally the curve should be a horizontal line except when a transition occurs. However, in the present experiments, because of limitations of space – the pressure cell was only 1" in diameter and contained the encapsulated sample, the heating element and the pressure transmitting medium – and also because of the

poor thermal conductivity of the sample holder and the natural temperature gradient set up by the graphite heater, a major problem that was encountered initially was the 'drift', which resulted in a base line that was very steeply inclined. To offset this the recorder pen had to be brought back to zero whenever it reached full scale, which was not a satisfactory procedure as there was every possibility of missing a sharp transition. The problem was overcome finally by experimentation with the design of the cell which required precise machining of its components and critical positioning of the sample and reference junctions of the thermocouple. A suitable geometry of the cell was arrived at which minimised this drift.

The sample was contained in a capsule made of glass filled teflon (supplied by Fluoro Carbon Industries, USA) which was sealed using a teflon plug. The advantages of using teflon are that it does not react with any of the compounds and that it flows under pressure thereby providing an airtight seal. The pressure transmitting medium was talc which surrounded the sample capsule on all sides. A thin graphite sleeve was used as the heater. A high current, low voltage source supplied power to the heater. By varying the current at a controlled rate any desired rate of heating could be achieved. Chromel-alumel thermocouples were used for temperature measurements. The correction due to pressure for these thermocouples is extremely small in the pressure range studied and was neglected. The temperature difference (ΔT) was fed to a Keithley nanovolt amplifier and the output of the amplifier to the Y-axis of a Moseley X-Y recorder. The sample temperature was fed to the X-axis. An amplification of 1000 was used for ΔT for all experiments. This amplification was enough to drive a 10 μ V signal to full scale of the recorder. The linearity of the amplifier under experimental conditions was checked beforehand. In series with the differential (ΔT) was a zero-suppression unit which could suppress upto 40 mV of the thermocouple signal with a resolution of 1 μ V. The line pressures were measured by a calibrated transducer (Type G 1-366 of Groseby Instruments, Surrey, England) reading to an accuracy of 1%. In order to evaluate the true pressure as seen by the sample, a small correction has to be applied. By measuring the resistance variation with pressure of a standard manganin gauge⁸ immersed in silicone oil in the sample capsule, the true pressures were calibrated against the line pressures. The correction was found to be less than 2% over the entire range of pressures investigated.

Results and discussion

p-Azoxyanisole (PAA): To test the experimental set up, we first conducted experiments on PAA for which some data are available³⁻⁷. For each pressure, DTA runs were recorded for at least two heating rates and the average of the transition temperatures taken. All the transition temperatures were recorded during heating as there was always some supercooling

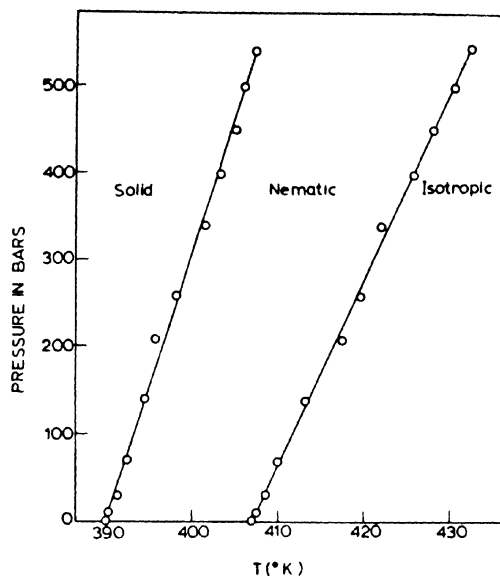


Figure 4 Experimental variation of the transition temperatures with pressure for *p*-azoxyanisole

Table 1. dT/dP for PAA in $^{\circ}/\text{kbar}$

	Solid-nematic	Nematic-isotropic
Hulett ²	32.0 up to 300 bars	48.6 up to 300 bars
Pushin and Grebenschtschikow ³	25.6 up to 2 kbars	39.4 up to 1 kbar
Robberecht ⁴	32 up to 850 bars	48 up to 935 bars
Deloche, Cabane and Jerome ⁵	23.7 up to 3 kbars	25.7 up to 3 kbars
McColl and Shih ⁶	—	46 up to 640 bars
Present work	32 up to 540 bars	47 up to 540 bars

during the cooling part of the cycle. The results obtained for different pressures for PAA are plotted in figure 4. The slopes dT/dP evaluated for the solid-nematic and nematic-isotropic transitions are $32^{\circ}/\text{kbar}$ and $47^{\circ}/\text{kbar}$ respectively. Table 1 gives a comparison of these values with the other experimental data available for PAA. We see that our slopes agree very well with those of Hulett², Robberecht⁴ and McColl and Shih⁶.

The values of Deloche *et al.*⁵ are rather different, probably because, as the authors themselves point out, helium gas which served as the pressure transmitting medium contaminated the sample.

p-Azoxyphenetole (PAP): Experiments were done for PAP up to a pressure of ~ 590 bars. Figure 5 shows the phase diagram. The slopes of the solid-nematic and nematic-isotropic transitions are $36^\circ/\text{kbar}$ and $46^\circ/\text{kbar}$. They agree well with the only other available set of data on PAP, *viz.*, $37^\circ/\text{kbar}$ and $47.6^\circ/\text{kbar}$ obtained by Hulett². Thus having tested the reliability of the experimental set up, studies on methoxy- and ethoxybenzoic acids were undertaken.

p-Methoxybenzoic acid: Figure 6 shows the DTA runs taken for methoxybenzoic acid at four different pressures (only the portions of the DTA records near the peaks are shown). The first record was taken at a pressure of 1 bar, *i.e.*, at atmospheric pressure. There is a single transition, the peak giving the solid-liquid transition temperature. In the next record, taken at 12 bars we see another small kink just separated from the main peak. This in fact shows that there are now *two* first order transitions separated on the temperature axis by about 1° . This new pressure induced phase has been identified (as will be described later) as the nematic phase. In the third record obtained at 24 bars, the separation between the two transitions has increased to $\sim 2.2^\circ$. At 61 bars, they are nearly 5° apart. When the pressure is increased even further, an interesting

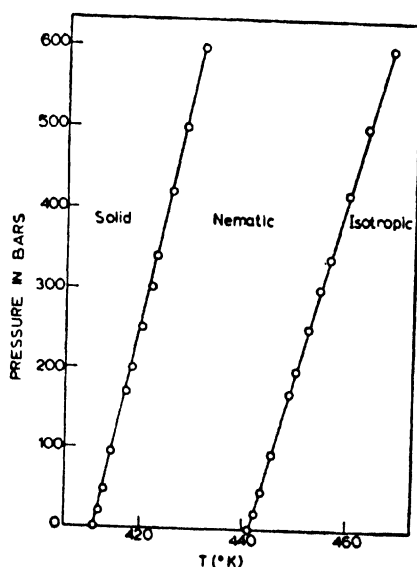


Figure 5 Experimental variation of the transition temperatures with pressure for *p*-azoxyphenetole.

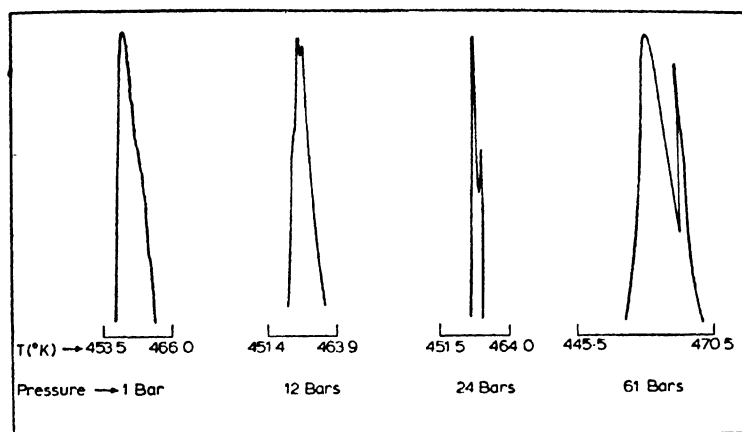


Figure 6 DTA records taken for methoxybenzoic acid at different pressures.

situation develops as can be seen in figure 7, which gives the DTA run at 145 bars. Here the nematic-isotropic transition is nearly 12° away from the first transition, but in addition, there is evidence that the first transition itself has started to split. There are now two distinct peaks separated by about 1.5° . As we shall see later, this new phase has been identified as the smectic phase. The complete data obtained for methoxybenzoic acid are plotted in figure 8. Measurements were made up to a pressure of 252 bars at which the nematic-isotropic transition is 21° away from the solid-smectic transition. The limitation of the experiment was set primarily by the temperature rather than by pressure. Teflon which was used to encapsulate the sample starts softening around 260°C and it was not safe to go to much higher temperatures. It shows clearly the solid-nematic-isotropic triple point at ~ 6 bars and 457.4 K and the solid-smectic-nematic triple point at ~ 96 bars and 458.4 K .

It should be emphasized that

- (i) Each experimental point marked in the diagrams is the average of at least 2 runs taken at 2 different heating rates (the rates were between 0.5 to $2.5^\circ/\text{min.}$)
- (ii) After completing the set of measurements with increasing pressure, the pressure was brought back to atmospheric pressure when a *single transition* was again observed. This transition temperature was the same as that obtained at the beginning of the experiment proving that the sample was completely free from any contamination.

p-Ethoxybenzoic acid: The phase diagram for ethoxybenzoic acid is given in figure 9. The behaviour is similar to that of methoxybenzoic acid. There is a single transition till 3 bars. At 8 bars the nematic phase has just appeared. At 96 bars the smectic phase also starts appearing. The maximum pressure that we could go to was 233 bars because of the temperature limitation mentioned earlier. Here again we have the two triple points at ~ 5 bars and 467.2 K and ~ 87 bars 468.5 K respectively. As before, it was verified that the sample was completely free from contamination by noting the reproducibility of the temperature of the single transition at atmospheric pressure before and after the experiment.

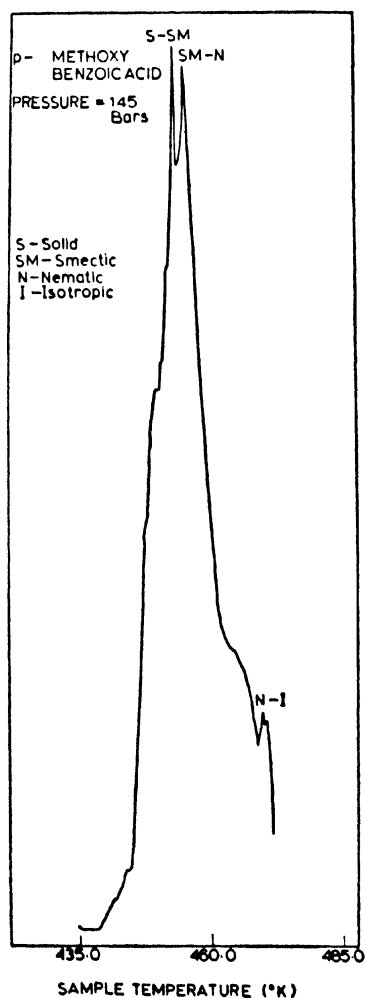


Figure 7 DTA run taken for methoxybenzoic acid at a pressure of 145 bars.

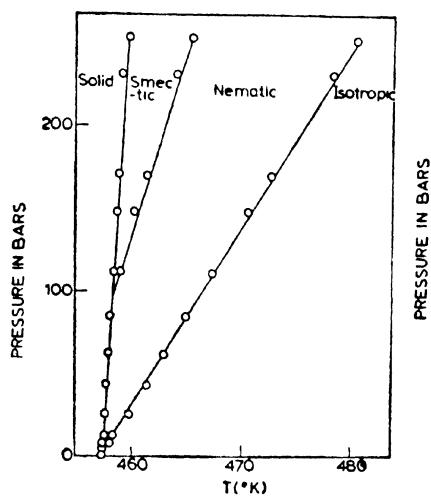


Figure 8 Experimental phase diagram for methoxybenzoic acid showing the solid-nematic-isotropic and solid-smectic-nematic triple points at ~ 6 bars and 457.4 K and ~ 94 bars and 458.4 K respectively.

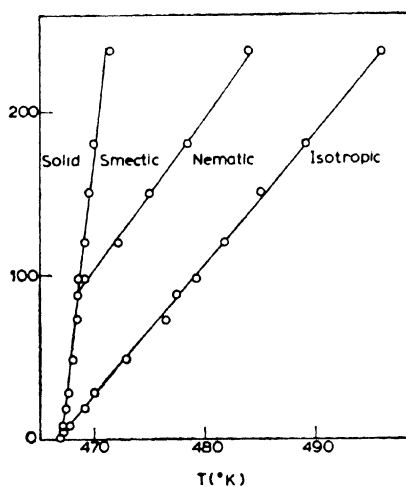


Figure 9 Experimental phase diagram for ethoxybenzoic acid showing the solid-nematic-isotropic and solid-smectic-nematic triple points at ~ 5 bars and 467.2 K and ~ 87 bars and 468.5 K respectively.

Identification of the phases

To identify the pressure induced phases an optical cell was constructed. A schematic diagram of the cell is given in figure 10.

The apparatus consists of a stainless steel stationary base plate (SP) in which is fitted a fused silica anvil (A). A thin stainless steel ring (R) is shrunk fitted to this anvil by heating both of them to 400°C. The inner diameter of this ring is slightly greater at the top to enable the other anvil, also made of fused silica and fixed to a top plate (TP), to just rotate inside the ring. The two anvils can be pressed against each other by screwing the top plate. The sample ($\sim 100 \mu$ thick) is contained between the anvils in a hole in a teflon spacer as shown in figure 10. The teflon spacer requires very accurate machining on both sides so as to match the anvils perfectly. Only then was it possible to contain the sample without leaks. The top and bottom plates are provided with windows for optical observations. The entire assembly is inside a heater and the temperature of the sample is probed by a chromel-alumel thermocouple. All observations were made in transmitted light using a Leitz polarizing microscope equipped with a camera. The pressure developed was very roughly estimated using the known values of dT/dP for PAA.

At lower pressures ethoxybenzoic acid shows a single intermediate phase which exhibits the typical schlieren texture of a nematic liquid crystal

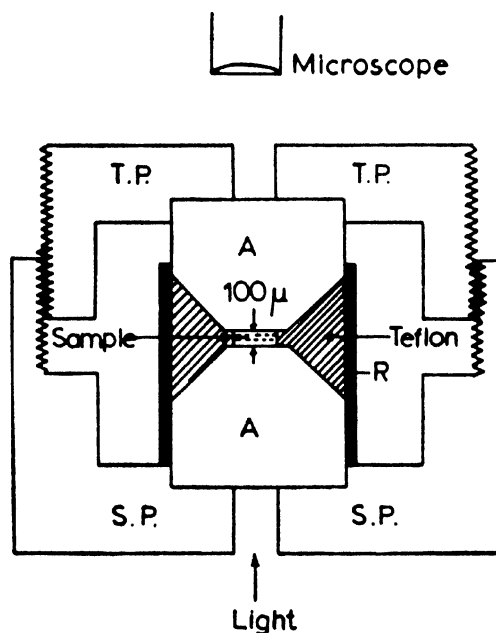


Figure 10 Schematic diagram of the optical cell.

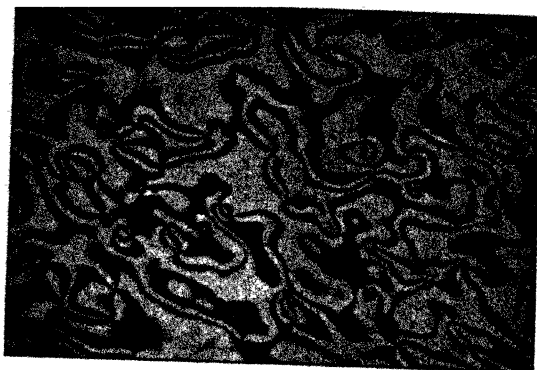


Figure 11 Schlieren texture exhibited by ethoxybenzoic acid (crossed polars, x 90).



Figure 12 Focal conics and batonnets formed by ethoxybenzoic acid (crossed polars, x 90).



Figure 13 Batonnets shown by methoxybenzoic acid (crossed polars, x 90).

(figure 11). At higher pressures, it was found that on cooling the isotropic liquid a nematic phase (with a schlieren texture) appeared first, which then transformed at a lower temperature to another phase showing the focal conic texture and batonnets (figure 12) characteristic of a smectic. On further cooling it went over to the solid phase making the field of view completely opaque. The pressure induced phases of methoxybenzoic acid also exhibit similar textures. Figure 13 shows batonnets formed by the smectic phase of this compound. Thus the pressure induced phases in both methoxy- and ethoxybenzoic acids have been identified as the nematic and smectic phases.

Conclusions

Methoxy- and ethoxybenzoic acids, which are non-mesomorphic at atmospheric pressure, have been found to exhibit nematic and smectic phases at higher pressures. The transitions were detected by DTA and the phases were identified by optical microscopy. The phenomenon of pressure induced mesomorphism and the occurrence of solid-nematic-isotropic and solid-smectic-nematic triple points in single component systems have been established experimentally for the first time.

Acknowledgements

We are extremely thankful to Mr M T Srivatsa for his assistance in making the zero suppression unit and to Mr K Jagannath Rao and Mr V Venu for precise machining of the components of the cell.

References

- 1 CHANDRASEKHAR S, SHASHIDHAR R and TARA N, *Mol. Cryst. Liquid Cryst.* **10** 337 (1970); **12** 245 (1971); CHANDRASEKHAR S and SHASHIDHAR R *Mol. Cryst. Liquid Cryst.* **16** 21 (1972)
- 2 HULETT G A *Z. Phys. Chem.* **28** 629 (1899)
- 3 PUSHIN and GREBENSCHTSCHIKOW W *Z. Phys. Chem. (Leipzig)* **124** 270 (1926)
- 4 ROBBERECHT J *Bull. Soc. Chim. Belge* **37** 597 (1936)
- 5 DELOCHE B, CABANE B and JEROME D *Mol. Cryst. Liquid Cryst.* **15** 197 (1971)
- 6 MCCOLL J R and SHIH C S *Phys. Rev. Lett.* **29** 85 (1972)
- 7 BENNET G M and JONES B *J. Chem. Soc.* 420 (1939)
- 8 BRIDGMAN P W *Proc. Am. Acad. Arts Sci.* **74** 1 (1940); JAYARAMAN A, HUTSON A R, McFEE J H, CORIELL A S and MAINES R G *Rev. Sci. Instrum.* **38** 44 (1967)

DISCUSSION

Schnur: Have you checked for PAA, for which all the numbers are known, whether the P - T diagram is in accordance with the Clausius-Clapeyron equation?

Shashidhar: Several measurements of ΔH are available, but the most detailed and systematic studies appear to be those of Arnold*. Using his values of ΔH , and the $\Delta V/V$ values of Maier and Saupe†, we get dT/dP for the solid–nematic and nematic–isotropic transitions to be 32.1 and 47.8°/kbar respectively. The experimental values are 32 and 47°/kbar, confirming that the Clausius–Clapeyron equation is obeyed.

Schnur: Have you checked if the smectic–nematic transition also fits the Clausius–Clapeyron equation?

Shashidhar: As we have no idea of the volume change and heat of transition for the smectic–nematic transition, it is not possible to check this.

Bulkin: Are you sure that you have ruled out solid–solid phase transitions?

Shashidhar: We are quite sure that what we have observed is not a solid–solid transition. Usually a solid–solid transition has a lower heat of transition than the melting transition, but we see from our DTA runs that the opposite is the case—the second transition is much weaker than the first one, a feature which is characteristic of mesophase transitions in general. But a more direct proof comes from an examination of these phases in a high pressure optical cell. The intermediate phases exhibit textures characteristic of liquid crystals. I have shown photographs of some of these textures.

Boccara: 1. Do you know the value of the discontinuities of the specific volume near the triple points?

2. What are the values of the slopes of the various transition lines at the triple points?

Shashidhar: 1. No, we have not carried out any measurements of the specific volume.

2. The values of the slopes (dT/dP) at the triple points are as follows:

	Methoxybenzoic acid	Ethoxybenzoic acid
Solid–smectic	10°/kbar	17°/kbar
Smectic–nematic	45°/kbar	109°/kbar
Nematic–isotropic	94°/kbar	126°/kbar

* Arnold H Z. *Phys. Chem. (DDR)* **226** 146 (1964)

† Maier W and Saupe A Z. *Naturforsch.* **15a** 287 (1960)

Dave : Have any calculations been made by extrapolation as to where the nematic phase should appear for pure methoxy- and ethoxy-benzoic acids at atmospheric pressure ?

Shashidhar : We have not made any such calculations.

Schnur : Have you observed the monotropic solid II phase in PAA on cooling in your pressure experiment ?

Shashidhar : No, we have not. In fact all the DTA runs were taken on heating only as cooling invariably resulted in supercooling of the nematic phase.

Rustichelli : You said you changed the pressure. Did the value of the temperature also change ?

Shashidhar : The experiment was done in the following way : The pressure was kept constant and the DTA run was taken by changing only the temperature. This gave the transition temperatures for that pressure. The procedure was repeated for different pressures.

Rustichelli : Is it possible to fix the temperature and increase the pressure ? It will be nice to see if the effect can be observed this way.

Shashidhar : It is possible, but there are some experimental difficulties which have to be overcome to do this.

Prediction of phase diagrams for certain liquid crystalline mixtures*

M DOMON and J BILLARD

Laboratoire de Physique de la Matière condensée

Collège de France, Paris and

Université des Sciences et des Techniques de Lille, France.

Abstract. With simplifying hypotheses, sufficient for many practical cases, it is possible to calculate the phase diagrams of mixtures of thermotropic liquid crystals. The determination, for each pure component, of the nature of each one of its phases, of the temperatures and of the enthalpy changes of its transitions allows the calculation of phase diagrams for mixtures of compounds with the same liquid crystalline phases.

If two components do not exhibit the same liquid crystalline phases, virtual transitions for these compounds are considered. (A virtual transition regards two unstable phases of one compound.) If the two phases can be stable in other conditions, the temperature and the enthalpy change of the virtual transition are calculated from the characteristics of real transitions.

The temperatures of equilibrium of three phases in binary systems can be determined by the intersection of two curves, each one of these depending only on the characteristics of the transitions (real or virtual) of one of pure component. Conversely with the temperatures of the three-phase points and the characteristics of real transitions of one pure compound we can calculate the temperature and the enthalpy change of a virtual transition even if one of the two phases is never stable in the pure compound.

Miscellaneous types of binary phase diagrams of two components with different stable liquid crystalline phases are treated. Practical rules are given. Some virtual transitions of p-alkyl-p'-alkoxytolans are determined. If we can observe a monotropic transition in a pure compound, its coinciding with the virtual transition with or without liquid crystallinity is verified by some experiments.

1. Introduction

Mixtures of mesomorphous compounds are utilized in a number of practical applications. Particularly, stable mesophases at low temperatures can be obtained by eutectic depression²⁻⁴. Therefore, it is useful to be able to foresee the range of temperature for the existence of the mesophases versus their composition, that is to say, to be able to calculate the isobaric phase diagram of mixtures from the characteristics of the pure components.

* Most of these results are given in greater detail in M. Domon's dissertation¹.

diagrams can be used to identify the mesophases, and their calculation guide experimental study³.

For non-mesomorphogenic compounds virtual existence ranges can be used⁶. They allow the comparison of all members of a homologous series, even of those which have no mesophase. Mixtures of non-mesomorphogenic compounds present stable mesophases⁶⁻¹². Mixtures exhibit mesophases which do not exist in pure components (*e.g.*, mixtures of p,p' propyl azoxydibenzoate and azoxyphenetol¹³). Knowledge of the virtual transitions is often sufficient to determine such mixtures.

Hypotheses and general relations

Under simplifying hypotheses, isobaric phase diagrams of the mixtures of a number of components which all have the same mesophase (or the same mesophases) can be calculated from the thermodynamic data of the pure components. The hypotheses are⁴

1. No chemical reaction between the components ;
2. Immiscible or totally miscible solid phases ;
3. The solid, liquid and mesomorphous solutions are perfect ;
4. The differences of specific heats at constant pressure of two phases in equilibrium are negligible.

With these hypotheses the molar fraction x_k of a pure component k in the solid state in a solution is given by a relation due to Chatelier¹⁴, Schröder¹⁵ and van Laar¹⁶.

$$x_k = \exp(\lambda_k)$$

$$\lambda_k = -\frac{\Delta H_k^*}{R} \left(\frac{1}{T_k^*} - \frac{1}{T} \right) \quad (1)$$

where R is the gas constant. This solubility x_k only depends on the temperature T , the molar enthalpy ΔH_k^* and on the temperature T_k^* of melting of the pure component k . So the solubility curve of a component k only depends on the characteristics of the pure component k . If a component presents crystalline polymorphism its solubility also depends on the characteristics $T_k^1, \Delta H_k^1; T_k^2, \Delta H_k^2; \dots T_k^p, \Delta H_k^p; \dots T_k^n, \Delta H_k^n$ of its solid-crystal transitions. At a temperature T situated between T_k^{p-1} and T_k^p its solubility x_k is such that

$$x_k = \exp(\lambda_k)$$

$$\lambda_k = -\sum_{i=1}^p \frac{\Delta H_k^i}{R} \left(\frac{1}{T_k^i} - \frac{1}{T} \right) \quad (2)$$

Thus, x_k is a continuous monotonically growing function of $T > 0$ situated between $\exp(\Delta H_k^* / RT_k^*)$ and $\exp(\Delta H_k^* / RT_k^*) > 1$. It presents an inflexion point for $T = \Delta H_k^* / 2R$.

From this solubility curve we can deduce the temperature and the enthalpy of decomposition of an intermediary compound, the melting of which is not congruent.

The nomograms give the solubility at a given temperature (figure 1) or the temperature where the solubility has a given value (figure 2) versus the enthalpy and the temperature of melting. These nomograms can be used for the components having a crystalline polymorphism with,

for $T_k^{p-1} < T < T_k^p$,

$$\Delta H_k^* = \sum_{i=p}^n \Delta H_k^i$$

and
$$T_k^* = \frac{\sum_{i=p}^n \Delta H_k^i}{\sum_{i=p}^n \frac{-\Delta H_k^i}{T_k^i}}$$

With the same simplifying hypothesis, the molar fractions of the components k in two binary solutions α and β in equilibrium are given by relations of van Laar¹⁷:

$$x_k^\alpha = \frac{1 - \exp(\lambda_1^{\alpha\beta})}{\exp \lambda_k^{\alpha\beta} - \exp \lambda_1^{\alpha\beta}} \quad \text{and} \quad x_k^\beta = x_k^\alpha \exp(\lambda_k^{\alpha\beta})$$

with
$$\lambda_i^{\alpha\beta} = -\frac{\Delta H_i^{\alpha\beta}}{R} \left(\frac{1}{T_i^{\alpha\beta}} - \frac{1}{T} \right).$$

These relations contain the enthalpies and the temperatures for the transitions from the state α to the state β of the pure components k and 1.

3. Isobaric phase diagrams of binary mixtures of components which have the same mesophases

The enthalpic analysis of the pure components give then sufficient data to calculate the isobaric diagrams of the binary mixtures of components which have the same mesophases. The values obtained this way are sufficiently near the observed values for many practical cases^{4,18,19}. Depending on the values of the enthalpies and of the temperatures of transition, the spindle of the equilibrium curves of two perfect solutions (which is always entirely situated between the two transition temperatures) can present different forms (figure 3)^{17,20}. The two curves can have the same concavity, (a) and (c), or different concavities, (b), or one of the two curves can have an inflexion point, (d), (e) and (f). If the two components have the same temperatures of transition the spindle is just a horizontal straight line. This is the case, particularly, for the enantiomeric compounds^{21,22}.

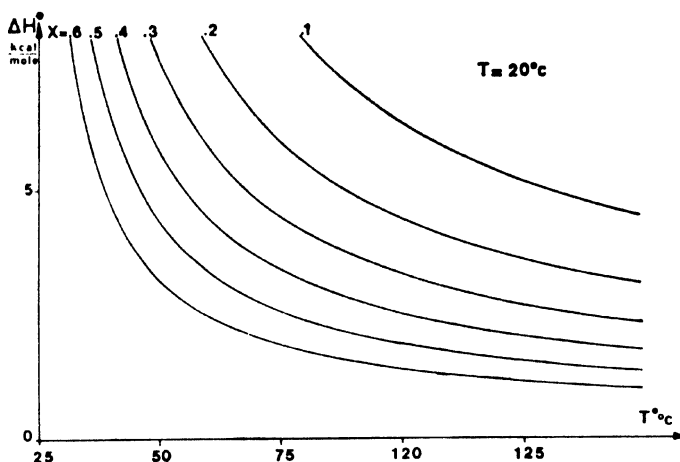


Figure 1 Nomogram representing, at a given temperature T , the solubility X of a pure compound in a perfect solution *versus* its melting enthalpy ΔH^* and its melting temperature T^* .

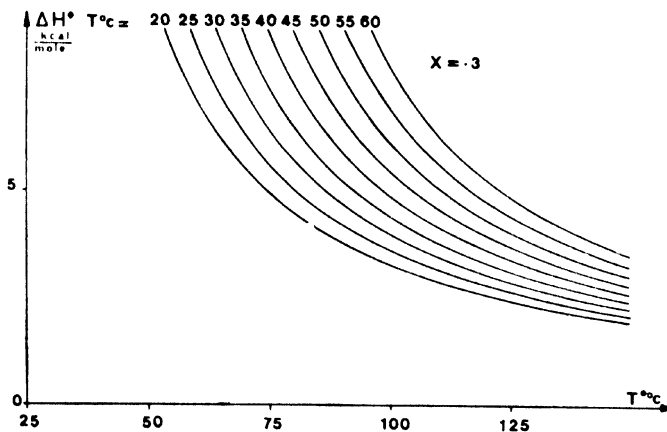


Figure 2 Nomogram representing the temperature T for which a pure compound has a given solubility X in a perfect solution *versus* the melting enthalpy ΔH^* and the melting temperature T^* .

4. Isobaric phase diagrams for binary mixtures of components which do not form continuous mesomorphic solutions

(a) Virtual transitions

Often the two components of a mixture do not have the same mesophases (an example is to be found in Ref. 23). The extrapolation of the equilibrium spindle of the two solutions gives a transition temperature for the

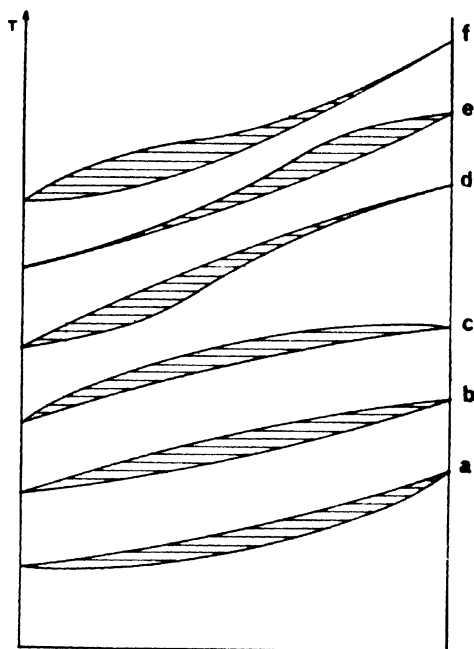


Figure 3 The six possible forms of the spindles of equilibrium of two perfect solutions from J. J. van Laar.¹¹

component without mesophase which is situated below its melting points. This transition is then a virtual transition⁶. For the mixtures of a mesomorphogenic component and a non-mesomorphogenic component several cases are possible (figure 4). In the first case (figure 4, on the top) the phase diagram is *hypomesomorphogenic* and in the second case (figure 4, on the bottom) it is *hypermesomorphogenic*. Another possible aspect of hypermesomorphogenic phase diagram is given by figure 5.

The hypermesomorphogenic phase diagrams have a curve of solubility of the non-mesomorphogenic component in the mesomorphous solution M: the arc he' . The extrapolation of this curve gives a temperature T_B^{CM} for the crystal-mesophase transition of the non-mesomorphogenic component. This temperature is higher than the melting point of the B component. This crystal-mesophase transition is then also virtual.

In the hypomesomorphogenic phase diagrams (figure 4, on the top) there is solubility curve fg of the mesomorphogenic component A in the liquid solution L. For the component A, the extrapolation of this curve gives a crystal-liquid transition temperature situated in the range of

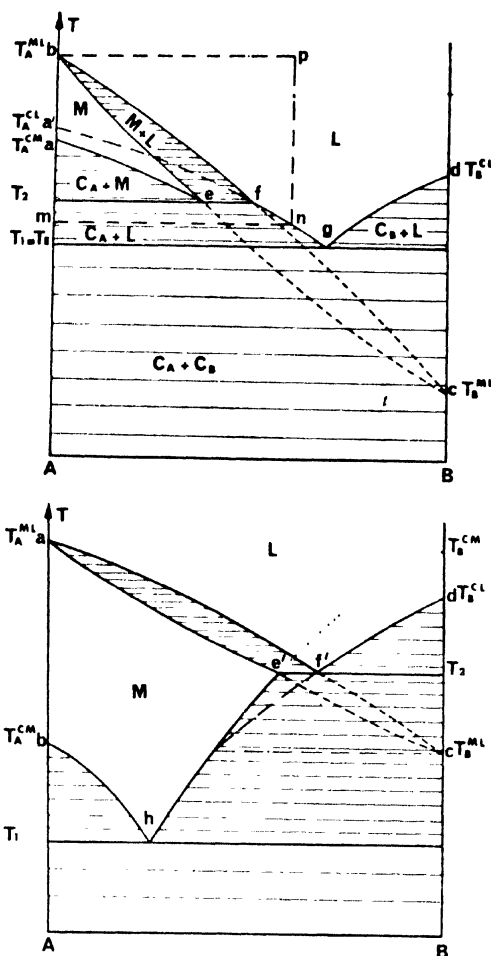


Figure 4 Isobaric phase diagrams of the mixtures of a mesomorphogenic component with a non-mesomorphogenic component.

Top: hypomesomorphogenic phase diagram;

Bottom: hypermesomorphogenic phase diagram.

stability of its mesomorphic phase M. Then this transition of A is also virtual.

To sum up, a component without a stable mesophase has a real melting point T^{OL} (figure 6) and two virtual transition temperatures: (T^{OM}) for the virtual crystal-mesophase transition and (T^{ML}) for the virtual mesophase-liquid transition. A component which has a stable mesophase has, first, two real transitions: crystal-mesophase at the temperature T^{OM} and mesophase-liquid at the temperature, T^{ML} and secondly, a virtual crystal-liquid transition at temperature (T^{OL}).

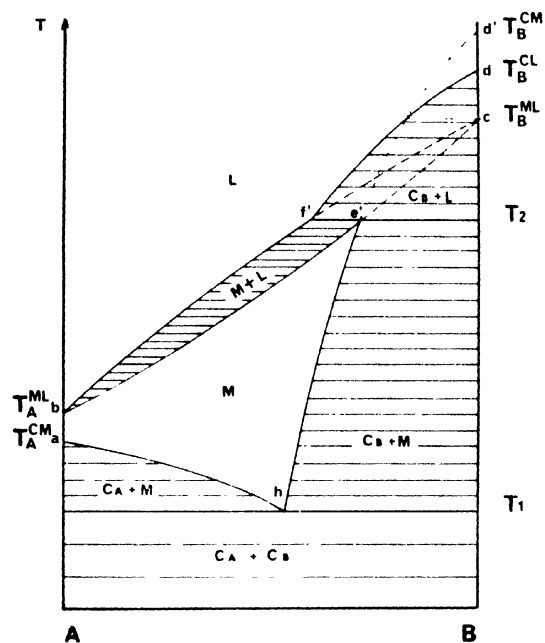


Figure 5 Other isobaric hypermesomorphogenic phase diagram of the mixtures of a mesomorphogenic component with a non-mesomorphogenic compound.

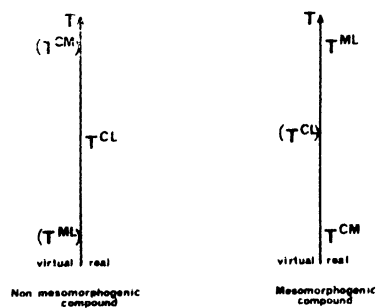


Figure 6 Orders of succession of the transition temperatures.

The order of succession of these temperatures can be understood in another way. The variations of the free molar enthalpy G versus the temperature T can be schematically written as it is indicated in figure 7. For a component which has a stable mesophase M (figure 7a) the extrapolations of the curves, which are relative to the crystalline (C) and liquid (L) phases, cross at the virtual transition temperature (T^{OL}) which is situated between the real transition temperatures T^{OM} and T^{ML} . For non-mesomorphogenic component (figure 7b) the free enthalpy of a mesomorphic phase (M) would be greater than those of the stable phases (C) and (L). And (T^{ML}) is really less than T^{OL} and (T^{OM}), and (T^{OM}) really greater than T^{OL} . This interpretation of the virtual transitions explains that they coincide with the monotropic transitions when these ones can be observed (see section 5).

With still the same hypothesis (section 2) we see for the enthalpies of these transitions:

$$\Delta H^{OL} = \Delta H^{OM} + \Delta H^{ML}$$

The calculation of the entropy along the cycle $m b p n$ (figure 4a) gives:

$$\Delta S^{OL} = \Delta S^{OM} + \Delta S^{MO}$$

hence

$$\begin{aligned} T^{OL} &= T^{OM} \left[1 + \frac{\Delta H^{ML} (T^{ML} - T^{OM})}{\Delta H^{OM} T^{ML} + \Delta H^{ML} T^{OM}} \right] \\ &= T^{ML} \left[1 - \frac{\Delta H^{OM} (T^{ML} - T^{OM})}{\Delta H^{OM} T^{ML} + \Delta H^{ML} T^{OM}} \right] \end{aligned}$$

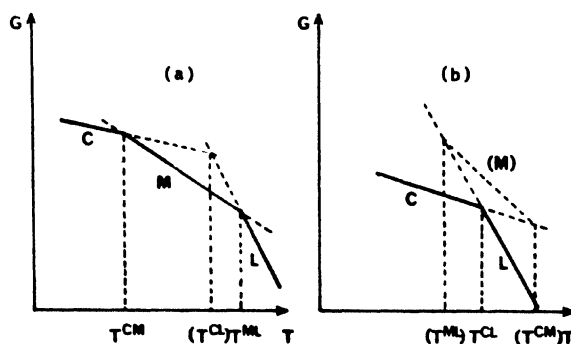


Figure 7 Schematic variations of the free molar enthalpy G versus the temperature T for a compound having a stable mesophase M (a) and for a compound without stable mesophase (b).

In the case of a mesomorphogenic component

$$\Delta H^{cm} > 0 \quad \text{and} \quad \Delta H^{ml} > 0$$

it gives

$$(\Delta H^{cl}) > 0$$

but $T^{cm} < T^{ml}$

so that $T^{cm} < (T^{cl}) < T^{ml}$.

In the case of a component without stable mesophase the values ΔH^{cl} and T^{cl} only are directly measurable. On the experimental phase diagrams the solubility curves in the liquid and mesomorphic solutions are practically confused²⁴. A straight line can often take the place of these two curves, particularly if $(\Delta H^{ml}) \ll \Delta H^{cl}$, it gives also

$$(\Delta H^{cm}) \simeq \Delta H^{cl} > 0.$$

For a phase diagram of the mixtures of this component with another component which has a stable mesophase M, the hypothesis $(\Delta H^{ml}) < 0$ involves the impossibility for the equilibrium spindle of the M and the liquid solutions to be found between the clarification points of the two components. This is topologically impossible; also

$$(\Delta H^{ml}) > 0.$$

From the relation which exists between the transition temperatures and the inequality

$$(T^{ml}) < (T^{cm})$$

it can be affirmed

$$(T^{ml}) < T^{cl} < (T^{cm})$$

for a non-mesomorphogenic compound. In this case, there are two independent relations between the six characteristics of the three transitions. Supplementary data are then necessary to completely determine the four quantities which characterize the two virtual transitions.

(b) Calculation of the phase diagrams

If the temperatures and the enthalpies of all the transitions are known the curves which constitute a binary phase diagram can be calculated and thus their points of intersection determine the three-phase points. A remark simplifies these calculations. We shall first consider the particular case of figure 4b. At the point e' the solubility of the component B in solid state in the mesophase M is

$$x_B^M = \exp(\lambda_B^{CM})$$

It is equal to the concentration of B in M in equilibrium with the liquid phase L :

$$x_B^M = \frac{1 - \exp \lambda_A^{ML}}{\exp \lambda_B^{ML} - \exp \lambda_A^{ML}}$$

Following

$$\exp \lambda_A^{ML} = \frac{1 - \exp (\lambda_B^{CM} + \lambda_B^{ML})}{1 - \exp \lambda_B^{CM}} = \frac{1 - \exp \lambda_B^{CL}}{1 - \exp \lambda_B^{CM}}$$

The second member of this last equation only depends on the characteristics of the pure component B. We call it the *relative solubility* $\psi_B^{CML}(T)$ of B. The coordinates of the point e' are then given by the intersection of the solubility curve of A (which only depends on pure A) with the relative solubility curve of B in the M and L solutions (which only depends on pure B).

Most generally $\psi_I^{\alpha\beta\gamma}(T)$ is the ratio of the complements to one of the solubilities of component I in the pure state α in the perfect solutions γ and β . It is also the ratio of the solubilities of other compounds than I in the perfect solutions γ and β in equilibrium with pure I in the state α . We have

$$\Psi_I^{\alpha\beta\gamma} = \frac{\bar{\Delta}C}{\Delta B} \quad (\text{figure 8}).$$

This function of the temperature is zero for $T = T_I^{\alpha\gamma}$. For $T = 0$ $\psi = 1$ and when $T \rightarrow \infty$ it has a limiting value situated between 1 and

$$\frac{\Delta H_I^{\alpha\gamma}}{\Delta H_I^{\alpha\beta}} \frac{T_I^{\alpha\beta}}{T_I^{\alpha\gamma}}. \quad \text{It has a discontinuity for } T = T_I^{\alpha\beta}.$$

If $T_J^{\beta\gamma} < T_I^{\alpha\beta} < T_I^{\beta\gamma}$, and if the roots of $\Psi_I^{\alpha\beta\gamma} = \exp \lambda_J^{\beta\gamma}$ exist, they are two in number and are situated between $T_J^{\beta\gamma}$ and $T_I^{\alpha\beta}$. If $T_I^{\beta\gamma}$ is smaller than $T_I^{\alpha\beta}$ and than $T_J^{\beta\gamma}$ there is always one solution and only one situated between $T_J^{\beta\gamma}$ and $T_I^{\alpha\beta}$. If $T_I^{\beta\gamma}$ is smaller than $T_I^{\alpha\beta}$ and $T_J^{\beta\gamma}$ there are one or three solutions situated between $T_J^{\beta\gamma}$ and $T_I^{\beta\gamma}$.

The intersection of two spindles can be determined just as easily. Let us take the example of two components I and J which have a continuous solution M_1 either solid or mesomorphic and which have the same mesophase M_2 (figure 9). The spindles constituted by the curves of equilibrium of the perfect solutions M_1-M_2 and M_2-M_3 cross for certain values of the pure components transitions characteristics. The perfect solution M_2 is not continuous in this case; there is no full miscibility for the components I and J in the state M_2 . At an intersection point of two spindles

$$x_I^2 = \exp \lambda_I^{12} \frac{1 - \exp \lambda_I^{12}}{\exp \lambda_I^{12} - \exp \lambda_J^{12}} \text{ for the spindle } M_1 - M_2$$

$$\text{and } x_I^2 = \frac{1 - \exp \lambda_I^{23}}{\exp \lambda_I^{23} - \exp \lambda_J^{23}} \text{ for the spindle } M_2 - M_3.$$

The equality of these two molar fractions can be simply written :

$$\Psi_I^{123} = \Psi_J^{123}.$$

The results are analogous for every three-phase points which are constituted by the equilibrium of three perfect solutions particularly if there is an intermediate mesomorphic solution which none of the components has (for example figure 3 of Ref. 25).

There are two physically significant roots of $\Psi_I^{\alpha\beta\gamma} - \Psi_J^{\alpha\beta\gamma}$ and are situated between $T_I^{\beta\gamma}$ and $T_J^{\alpha\beta}$ if $T_I^{\alpha\beta} < T_I^{\alpha\gamma} < T_I^{\beta\gamma}$ and $T_J^{\alpha\beta} < T_J^{\alpha\gamma} < T_J^{\beta\gamma}$.

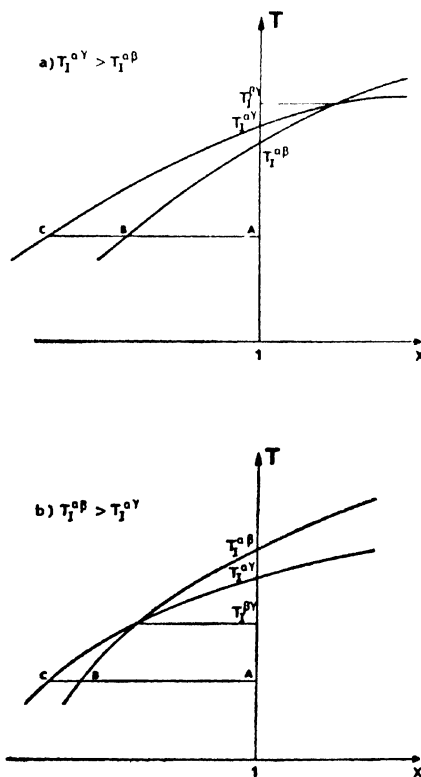


Figure 8 Solubility curves of a pure compound I being in α modification, in perfect solutions the modifications of which are β and γ .

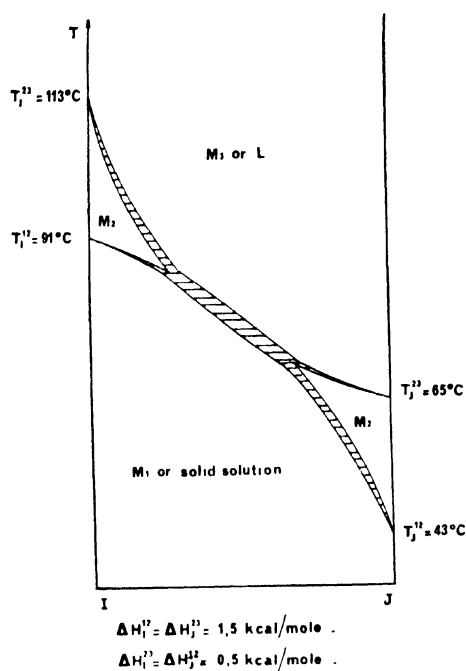


Figure 9 Isobaric phase diagrams of the mixtures of two compounds which have the same mesophase M_2 but not as a continuous solution.

If $T_I^{\alpha\beta} > T_I^{\alpha\gamma} > T_I^{\beta\gamma}$, $T_J^{\alpha\beta} > T_J^{\alpha\gamma} > T_J^{\beta\gamma}$ and $T_J^{\beta\gamma} < T_I^{\alpha\beta}$, the equation has solutions only if

$\frac{\Delta H_I^{\alpha\gamma}}{\Delta H_I^{\beta\gamma}} < \frac{\Delta H_J^{\alpha\gamma}}{\Delta H_J^{\beta\gamma}}$. When there are any solutions, they are two in number and are situated between $T_J^{\beta\gamma}$ and $T_I^{\alpha\beta}$. If $T_I^{\alpha\beta} < T_I^{\alpha\gamma} < T_I^{\beta\gamma}$ and $T_J^{\alpha\beta} > T_J^{\alpha\gamma} > T_J^{\beta\gamma}$ there is at least one solution.

A binary eutectic point is such that²⁶:

$$x_1^I + x_2^I = 1 \quad \text{or} \quad \exp \lambda_1 + \exp \lambda_2 = 1.$$

To sum up, all the three phases points of the binary phase diagrams can be determined by the intersections of solubility curves and of relative solubility curves (they only depend on pure components).

(c) *Determination of the virtual transitions from the isobaric binary phase diagrams*

For a pure compound without the M_2 phase but which has the M_1 and M_3 phases, the temperatures and the enthalpies of the virtual transitions

(M₁ M₂) and (M₂ M₃) can be determined from three-phase points of a binary diagram for mixtures of this compound, where there are first the M₁ and M₂ phases and, secondly, M₂ and M₃ phases [for example the temperatures T₄ and T₅ of figure 10 permit one to determine the transitions (CN) and (NL) of B]. In fact at the eutectic temperatures T₄,

$$\exp \lambda_A^{CM} (T_4) + \exp \lambda_B^{CM} (T_4) = 1$$

But [section 4(a)]

$$\exp \lambda_B^{CL} (T) = \exp \lambda_B^{CM} (T) \exp \lambda_B^{ML} (T)$$

Then, first, $\exp \lambda_B^{ML} (T_4)$; and secondly :

$$\exp \lambda_B^{ML} (T_4) = \frac{\exp \lambda_B^{CL} (T_4)}{1 - \exp \lambda_A^{CM} (T_4)}$$

At the temperature T₅ [section 4(b)]

$$\exp \lambda_A^{ML} (T_5) = \phi_B^{CML} (T_5);$$

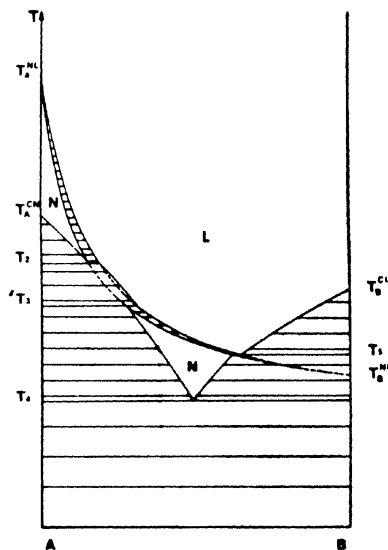


Figure 10 Hypomesomorphogenic phase diagram with two disjoint nematic domains calculated for :

- $T_A^{CN} = 91^\circ \text{C}$, $\Delta H_A^{CN} = 5.40 \text{ kcal mole}^{-1}$;
- $T_A^{NL} = 113^\circ \text{C}$, $\Delta H_A^{NL} = 0.40 \text{ kcal mole}^{-1}$
- $T_B^{CL} = 79^\circ \text{C}$, $\Delta H_B^{CL} = 9.9 \text{ kcal mole}^{-1}$;
- $(T_B^{NL}) = 65^\circ \text{C}$ and $(\Delta H_B^{NL}) = 2.4 \text{ kcal mole}^{-1}$

then

$$\exp \lambda_B^{ML}(T_5) = \frac{\exp \lambda_A^{ML}(T_5) \exp \lambda_B^{CL}(T_5)}{\exp \lambda_A^{ML}(T_5) + \exp \lambda_B^{CL}(T_5) - 1}$$

The knowledge of two values of $\exp \lambda_B^{ML}$ allows one to calculate (ΔH_B^{ML}) and (T_B^{ML}) , and hence (ΔH_B^{CM}) and (T_B^{CM}) . The characteristics so obtained can be used to predict other phase diagrams.

(d) *Miscellaneous types of phase diagrams*

The discussion of miscellaneous possible cases allows one to understand some already known types of phase diagrams; it also permits to foresee some types of phase diagrams which do not seem to have been so far observed. The case of the last figure (figure 10) is an example. Figure 11 gives another example. To calculate the phase diagrams for the mixtures of components, which do not have the same mesophases it is necessary to know first, the real transitions characteristics and secondly the useful virtual transitions characteristics. For example in the case of figure 12 it is necessary to know the virtual tsansitions (C-L) for A and B, (C-M₁) and (M₁-L) for B and (M₂-L) for A. In certain cases the mixture of two non-mesomorphogenic components can give a mesophase. This effect

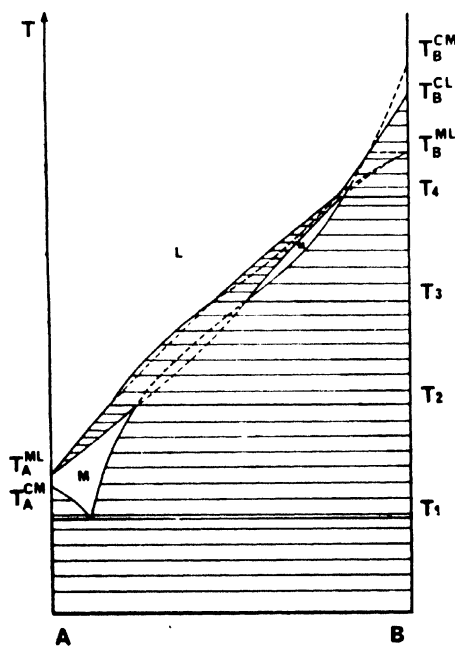


Figure 11 Hypermesomorphogenic phase diagram with two disjoined mesomorphic domains *M*.

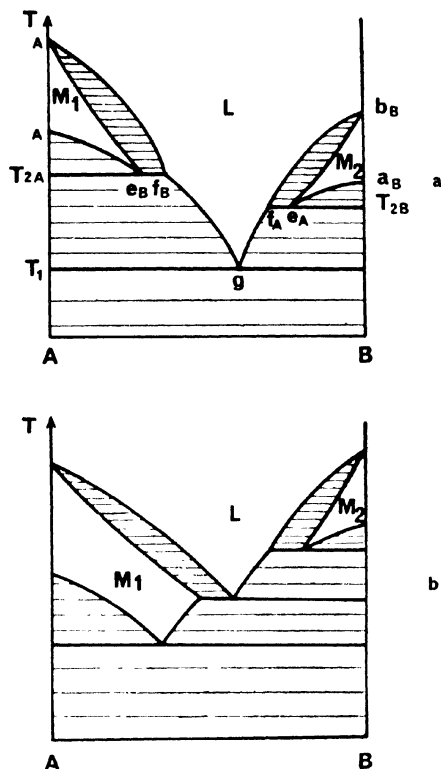


Figure 12 Isobaric phase diagrams of two mesomorphogenic components with different mesophases where there is no equilibrium between these mesophases. (a) The phase diagram is twice hypomesomorphogenic. (b) The phase diagram is once hypermesomorphogenic and once hypomesomorphogenic.

can be calculated. Indeed if the pure components have virtual temperatures for the crystal-mesophase M transitions not too different of their melting points, the equilibrium spindle between M and the liquid phase can be situated above the eutectic point.

The binary phase diagrams must satisfy certain topological rules. For example, if M_1 is a phase which has its temperature range always under that of the M_2 phase in pure compounds, M_1 is always under the curves which separate it from M_2 in the binary phase diagrams. Another example: for the mixtures of a component having a stable mesophase M and a non-mesomorphogenic component their phase diagrams are hypermesomorphogenic if these two components are not miscible in the solid state and if the temperature of the virtual M -liquid transition is higher than that of the real M -liquid transition.

5. Experimental tests

(a) Coincidences between virtual and monotropic transitions

A first test can be deduced from the available data. Cholesteryl myristate has a smectic phase and a cholesteric phase; the characteristics of its real transitions are known²⁷. Cholesteryl stearate is not mesomorphogenic but has, by cooling, two monotropic mesophases: a cholesteric and a smectic. The characteristics of its melting and of its monotropic transitions have been measured²⁷. The calculated phase diagram (figure 13) is hypermesomorphogenic both for the smectic solution and the cholesteric solution. The cholesteric and liquid phases must appear at 75.4°C and 78.2°C. The experimental values are 75°C and 78°C²⁸. Then there is no discrepancy between the measured and calculated values if we suppose the coincidence of the virtual and monotropic transitions.

This coincidence is once more tested by the study of the following mixtures: di-*n*. octyloxy-4,4' - dimethyl-2,2' - tolan and di-*n*. decyloxy-4, 4' - dimethyl-2,2' - tolan²⁹. These two components have monotropic nematic-liquid transitions, the first at 63.5°C and the second at 63°C. A stable nematic phase appears in their mixtures at 45°C which transforms quickly into the liquid phase at 63°C.

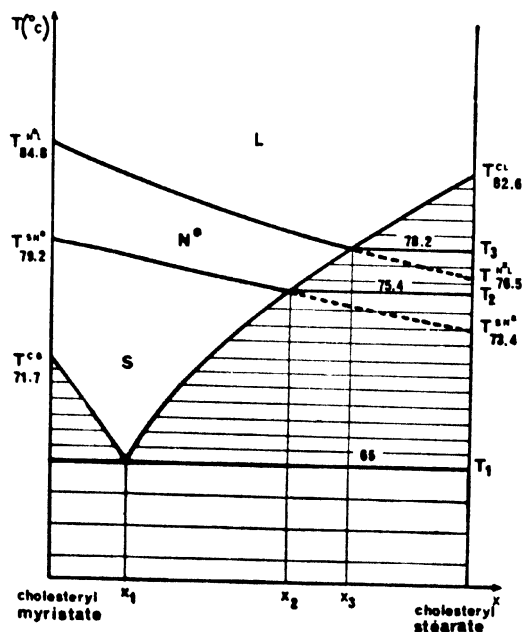


Figure 13 Isobaric phase diagram calculated for the mixtures of cholesteryl myristate and cholesteryl stearate.

(b) *The virtual transitions are characteristic of a pure compound*

Other experimental tests have been done with some p,n-alkyl p',n-alkoxytolans^{30,4}. These compounds are listed in table 1. For two non-nematogenic homologs the characteristics of the virtual transitions have been deduced from the three phase point temperatures of hypernematogenic mixtures of these components with other nematogenic homologs. The three phase points used are the ones situated at the temperatures T_1 and T_2 (figures 14 and 15). To vary the conditions, the nematogenic components have been chosen with nematic ranges situated at the most widely different possible temperatures.

The three phase point temperatures (first T_1 for the nematic eutectic and secondly T_2 for the liquid eutectic point (figure 14) or liquid peritectic point (figure 15) are obtained by observation of contact samples^{31,5} in a polarizing microscope (Leitz, Panphot) with a heating and cooling stage (Mettler, FP5). The results obtained for the compounds No. 1 and 7 (table 1) are listed in table 2. Within the experimental uncertainty, the virtual transitions characteristics obtained do not depend on the second component of the mixtures. It generalizes for the tolans the results obtained for the Schiff's bases^{32,24}. The magnitudes are the same as for the real transitions of the other homologs. The transition characteristics for some methoxy alkyl tolans are so known (table 3). Their changes *versus* the carbon number p of their alkyl chain are written on figure 16. The data for the virtual transitions of the butylmethoxytolan and for the monotropic transition of the propylmethoxytolan do not break the regularity.

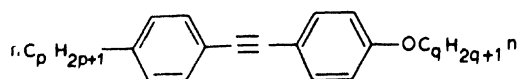
(c) *Isobaric binary phase diagrams forecast*

With the knowledge of the transitions for the non-nematogenic compounds No. 1 and 7 (table 2) it is possible, first, to calculate the isobaric phase diagrams of their mixtures with other homologs (nematogenic) and secondly, the isobaric phase diagram for the mixtures composed with these two non-nematogenic components.

The phase diagrams for the mixtures of a nematogenic component with a non-nematogenic component are hypernematogenic. In table 4 the eutectic temperatures T_1 for the nematic eutectic points and the temperatures T_2 for the eutectic or peritectic points of the liquid phase are listed. Some of these mixtures are nematic at room temperature. The equimolar mixture of compounds No. 7 and 14 are nematic between 16 and 56° C.

The calculated isobaric phase diagram (figure 17) for the mixtures of the two non-nematogenic tolans No. 1 and 7 has an intermediary nematic phase. This phase is really observed. Its temperature ranges calculated and measured are listed in table 5. Their coincidences show that this nematic phase can be considered as perfect. Its existence does not result

Table 1. Characteristics of the transitions (C denote crystalline, N nematic and L liquid phase) of p,n-alkyl p',n-alkoxytolans with formula



If there are differences between data from first melting and second melting then just the data from second melting are given. The values between parentheses are obtained with differential scanning calorimetry for monotropic transitions.

Compound No.	<i>p</i>	<i>q</i>	T^{CN} (°C)	ΔH^{CN} ($\frac{\text{k cal}}{\text{mole}}$)	T^{CL} (°C)	ΔH^{CL} ($\frac{\text{k cal}}{\text{mole}}$)	T^{NL} (°C)	ΔH^{NL} ($\frac{\text{k cal}}{\text{mole}}$)
1	1	9	—	—	72.5	11.2	—	—
2	2	8	—	—	76	9.9	(65)	(0.16)
3	3	1	—	—	66	5.0	(61)	(0.15)
4	3	2	90	4.9	—	—	98.5	0.21
5	3	6	59.5	5.6	—	—	75.5	0.25
6	3	7	48	5.6	—	—	70.5	0.22
7	4	1	—	—	47.5	4.1	—	—
8	5	1	43	4.2	—	—	55	0.14
9	5	5	48.5	3.8	—	—	68.5	0.19
10	6	1	39	6.2	—	—	42	0.11
11	6	4	46.5	3.7	—	—	69.5	0.18
12	7	1	39	5.1	—	—	54	0.12
13	7	3	41	5.4	—	—	63	0.22
14	8	2	47.5	4.1	—	—	73.5	0.22
15	9	1	41	7.45	—	—	53.5	0.21

from the new compound formation but depend only on the depression of the solidification temperature.

6. Conclusion

For mixtures of chemically similar components, particularly for the derivatives of a same series, the simplifying hypotheses used here, allow the prediction, with calculations, of isobaric binary phase diagrams with sufficient accuracy for numerous applications to the nematic phases. In this manner it is possible to advance the purely descriptive state in this field. Numerous experimental phase diagrams, even apparently sophisticated ones

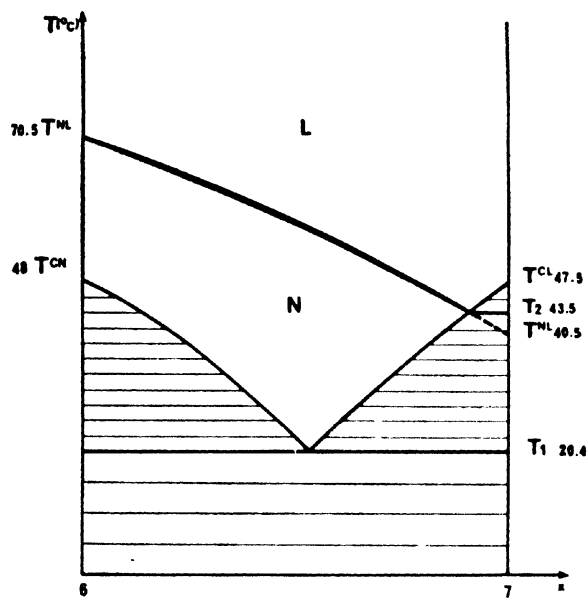


Figure 14 Isobaric phase diagram of mixtures of propylheptyloxytolan (6) and butylmethoxytolan (7).

Table 2. Temperatures of three phase points T_1 and T_2 (see figures 14 and 15) of the isobaric phase diagrams of the mixtures of non-nematogenic and nematogenic tolans and characteristics of the virtual nematic-liquid (N-L) and crystal-nematic (C-N) transitions of the non-nematogenic compounds. The numbers of the compounds are the same as in table 1.

compound without stable nematic phase No.	other compound of the mixtures No.	T_1 (°C)	T_2 (°C)	(T^{NL}) (°C)	(ΔH^{NL}) ($\frac{\text{k cal}}{\text{mole}}$)	(T^{CN}) (°C)	(ΔH^{CN}) ($\frac{\text{k cal}}{\text{mole}}$)
1	12	33.7	57.9	59.5	0.31	72.9	10.89
	14	38.3	64	60.9	0.34	72.9	10.86
7	15	20.5	42.2	40.7	0.17	47.8	3.93
	6	20.4	43.5	40.0	0.16	47.8	3.94

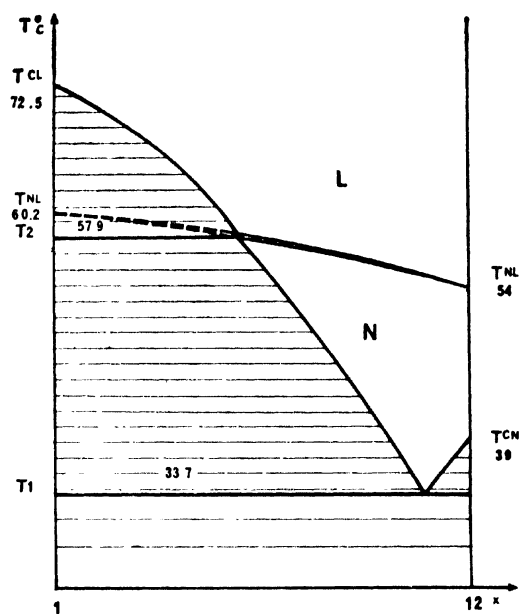


Figure 15 Isobaric phase diagram of mixtures of methylnonyloxytolan (1) and heptyl-methoxytolan (12).

Table 3. Characteristics of the transitions of some *p,n*-alkyl *p'*-methoxytolans (for notations see table 1).

<i>p</i>	T^{on} (°C)	$\left(\frac{\Delta H^{\text{on}}}{\text{kcal}}\right)$ mole	T^{CL} (°C)	$\left(\frac{\Delta H^{\text{CL}}}{\text{kcal}}\right)$ mole	T^{NL} (°C)	$\left(\frac{\Delta H^{\text{NL}}}{\text{kcal}}\right)$ mole
3	66.16	4.85	66	5.0	61	0.15
4	47.8	3.94	47.5	4.10	40.3	0.16
5	43	4.2	43.4	4.3	55	0.14
6	39	6.2	39.05	6.3	42	0.11
7	39	5.1	39.3	5.2	54	0.12
9	41	7.45	41.3	7.7	53.5	0.21

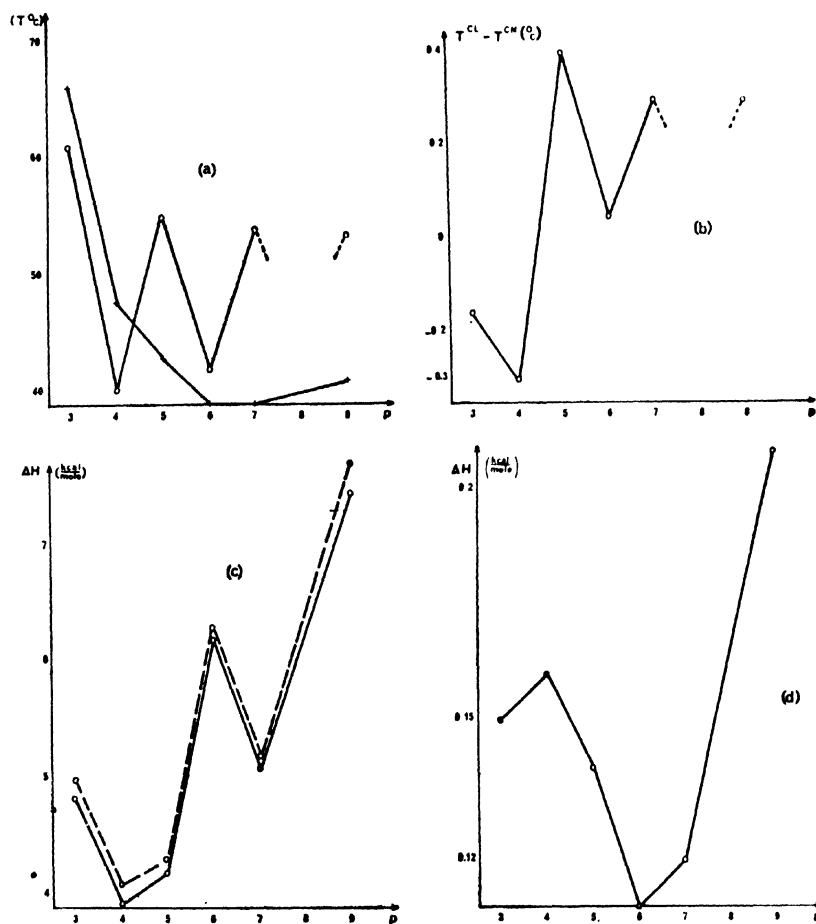


Figure 16 Temperatures and enthalpies of the transitions of p-n-alkyl-p'-methoxytolans (see table I): (a) T^{CN} + and T^{NL} 0; (c) ΔH^{CN} continuous line and ΔH^{CL} non-continuous line (d) ΔH^{NL} .

(for example the phase diagrams No. C VIII and C XI in ref. 33) can be understood. New types of phase diagrams are predicted. This forecast can aid their experimental discovery. Virtual transitions are included in the characteristics of a pure compound. They coincide with the monotropic transitions when these last can be observed. Their knowledge allows the study of the evolution of the stability of the mesophases in a chemical series, also when certain of its homologs have neither a stable nor a monotropic mesophase.

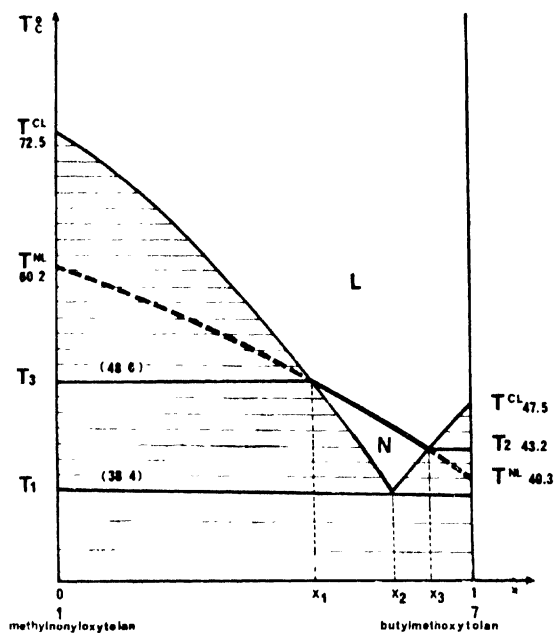


Figure 17 Isobaric phase diagram calculated for the mixtures of methynonyloxytolan (1) and butylmethoxytolan (7).

Table 4. Temperatures T_1 of eutectic point of the nematic phase and T_2 of eutectic or peritectic point of the liquid phase of the mixtures of nematogenic and non-nematogenic tolans (their numbers are the same as in table 1).

non nemato- genic tolan	nemato- genic tolan	T_1 (°C)		T_2 (°C)	
		calc.	measured	calc.	measured
7	8	14.3	22.0	41.6	41.9
1	15	34.7	35.5	57.6	54.3
7	14	16.0	16.8	43.0	43.2
1	6	40.3	37.8	65.6	64.3
1	13	33.5	33.0	61.5	62.2
7	13	12.6	16 ± 5	43.4	42.7

Table 5. Limits of existence of the nematic phase in the mixtures of butylmethoxytolan and methylnonyloxytolan (see phase diagram figure 17).

i (of T_i in figure 17)	molar fraction (calc.)	T (°C)	
		calc.	measured
1	0.17	38.4	38.3
2	0.09	43.2	43.0
3	0.31	48.6	45.3

We have only considered¹ cases of phase diagrams for systems having more than two components, where intermediate solids appear, or for the systems where imperfect solutions exist. A preliminary examination of the isothermal phase diagrams (involving the parameters pressure and molar fractions) indicates that it is more diverse than the isobaric phase diagrams.

Acknowledgements

We thank Dr J Jacques and the members of his laboratory for their positive cooperation. We also thank Mr B Soulestin for his help in numerical calculations and for drawing the pictures. This work is supported by the Centre national de la Recherche scientifique.

References

- 1 DOMON M, Thèse de Doctorat de spécialité, Lille (1973)
- 2 DEMUS D *Z. Naturforsch.* **22A** 285 (1967)
- 3 STEINSTRÄSSER R and POHL L *Z. Naturforsch.* **26B** 87 (1971)
- 4 MALTHÈTE J, LECLERCQ M, DVOŁAŹKY M, GABARD J, BILLARD J, PONTIKIS V and JACQUES J, *Mol. Cryst. and Liquid Cryst.* **23** 233 (1973)
- 5 BILLARD J *Bull. Soc. Fr. Mineral Crystallogr.* **95** 206 (1972)
- 6 BOGOJAWLEVSKY A and WINOGRADOW N *Z. Phys. Chem.* **60** 433 (1907) and **64** 229 (1908)
- 7 VORLÄNDER D and GAHREN A *Ber. Deut. Chem. Ges.* **40** 1966 (1907)
- 8 PRINS A *Z. Phys. Chem.* **67** 689 (1909)
- 9 MŁODZIEJOWSKI A *Z. Phys. Chem.* **20** 317 (1923)
- 10 WALTER R *Ber. Deut. Chem. Ges.* **59** 962 (1926)
- 11 VORLÄNDER D and OST K *Ber. Deut. Chem. Ges.* **71B** 1688 (1938)
- 12 BENNETT G M and JONES B J. *Chem. Soc.* 420 (1939)
- 13 SACKMANN H and DEMUS D *Z. Phys. Chem.* **230** 285 (1965)
- 14 LE CHATÉLIER H *C.R. Acad. Sci.* **100** 50 (1885)
- 15 SCHRÖDER I *Z. Phys. Chem.* **11** 449 (1893)
- 16 VAN LAAR J J *Arch. Neerl. Sci. Exactes. Natur.* **II** 8 264 (1903)
- 17 VAN LAAR J J *Z. Phys. Chem.* **63** 216 (1908) and **64** 257 (1908); *Thermodynamik einheitlicher Stoffe und binäre Gemische*. Groningen (1936)
- 18 HSU E C H and JOHNSON J F *Mol. Cryst. and Liquid Cryst.* **20** 177 (1973)
- 19 DEMUS D, FIETKAU CH, SCHUBERT R and KEHLER H *Mol. Cryst. and Liquid Cryst.* **25** 215 (1974)

- 20 REISMAN A *Phase equilibria* Academic Press, London (1970)
- 21 LECLERCQ M, BILLARD J and JACQUES J *Mol. Cryst.* **8** 367 (1969)
- 22 DOLPHIN D, MULJANI Z, CHENG J and MEYER R B *J. Chem. Phys.* **58** 413 (1973)
- 23 de KOCK A C *Z. Phys. Chem.* **48** 129 (1904)
- 24 DEWAR M J S and GOLDBERG R S *J. Org. Chem.* **35** 2711 (1970)
- 25 DEMUS D, KÖLTZ K H and SACKMANN H *Z. Phys. Chem.* **249** 217 (1972)
- 26 JOHNSTON J J *Phys. Chem.* **29** 882 (1925)
- 27 BARRALL E M II, PORTER R S and JOHNSON J F *J. Phys. Chem.* **71** 1224 (1967)
- 28 GALANTI A V and PORTER R S *J. Phys. Chem.* **76** 3089 (1972)
- 29 JACQUES J, BILLARD J, MALTHÈTE J and GABARD J *Fr. Pat.* **73** 22 841 (1973)
- 30 MALTHÈTE J, LECLERCQ M, GABARD J, BILLARD J and JACQUES J *C.R. Acad. Sci.* **273C** 265 (1971)
- 31 KOFLER L and KOFLER A *Thermomikromethoden zur Kennzeichnung organischer Stoffe und Stoffgemische.* Verlag Chemie, Weinheim (1954)
- 32 DAVE J S and LOHAR J M *Indian J. Chem.* **4** 386 (1966)
- 33 DEMUS D, SACKMANN H, KUNICKE G, PELZL G and SALFFNER R *Z. Naturforsch.* **23a** 76 (1968)

DISCUSSION

Schnur: Are all the curves you have shown based on equilibrium values? What was done to take into account monotropic and super-cooled phases?

Billard: These results are valid for equilibrium states. In certain cases only monotropic transitions coincide with virtual transitions. We cannot foresee the supercooling phenomena with these calculations.

Vasanth: (1) For a particular composition of a binary mixture, is the transition from the mesomorphic state to the isotropic liquid sharp?

(2) Could you throw some light on the nature of the spindles and the significance of the shaded region?

Billard: (1) If we have two binary solutions in equilibrium, the clarification phenomenon is at one temperature just as pure components.

(2) The spindles are formed by two curves limiting the domain of existence of the phases. In the shaded region of the phase diagram we have two phases in equilibrium. The vertical width gives the temperature range of the transformation of a phase into the other for a system having a given composition. The horizontal width represents the difference between the molar fractions of the two solutions in equilibrium at a given temperature.

Gray: Dr. Vasanth asked an earlier question about the spindle in the phase diagram and I am not sure that Dr. Billard's answer was clear to him. I would ask Dr. Billard to confirm that the thickness of the spindle reflects the spread nature of a particular transition, *i.e.*, the temperature range over which say the nematic-isotropic liquid occurs for a given composition. The real point is that transitions such as that for nematic-isotropic liquid are usually not as precise as those for pure single compounds.

Billard: Thank you for your help.

Vibrational spectra of liquid crystals. X. Recent progress in the study of infrared and Raman spectra of nematics and nematogenic crystals

BERNARD J BULKIN, DOLORES GRUNBAUM,
TERRY KENNELLY and WAI BONG LOK

Hunter College of the City University of New York,
695 Park Avenue, New York, N.Y. 10021, USA

Abstract. Progress in three areas of vibrational spectra of nematic phases is described. These include the interpretation of lattice vibrations of nematogenic crystals, changes in the C-H stretches in the infrared spectrum near the nematic-isotropic transition, and the observation of infrared optical activity in twisted nematic phases.

1. Introduction

For many years there has been interest in whether or not infrared and Raman spectroscopy could really yield information about phase transitions in complex molecular systems. While there is little dispute over the fact that the spectra show numerous changes at phase transitions, it has been a matter of some speculation as to whether these changes can be interpreted satisfactorily. For complex organic molecules these doubts arise in the following way: With the current state of intermolecular and intramolecular potential theory, one generally has to rely on a particular interaction dominating any change which one wishes to interpret. In addition there should be relatively few forces which are different in form or parametrization in a particular problem. Finally, one would hope for a separation of intra- and intermolecular effects, or at least, an observation which is completely dominated by one or the other.

For organic crystals, and in particular for nematogenic materials, one has every reason to believe that this would not be the case. Because of the complexity of the organic molecules involved, there is a wide variety of intermolecular interactions involved. Even the simplest liquid crystals contain at least three different elements (C, H, O, or C, H, N) and many contain both oxygen and nitrogen. Non-equivalent C-H bonds are often present, as well as different types of oxygen. Thus one can expect that the intermolecular forces responsible for the crystal lattice will be complex if viewed from the perspective of atom-atom interactions.

A second problem comes in the relative flexibility of the molecules themselves. Many of the liquid crystals contain substituents which have

low frequency torsional vibrations. *e.g.*, methyl and alkoxy groups. The barriers are sufficiently high so that one may expect a number of conformations to be present in these molecules, and the possibility of intramolecular conformational changes certainly exists. A further complication exists in that the molecules have low symmetry (generally C_1). If the torsional frequencies fall between 150 and 300 cm^{-1} , we may expect them to interact with the lattice modes, which are found between 10 and 140 cm^{-1} .

Despite all these apparent difficulties, our group undertook a study of nematic, smectic and cholesteric mesophases *via* infrared and Raman spectroscopy several years ago. Several other groups have also been carrying out related studies. In this paper we wish to report recent results we have obtained from the vibrational spectra. We will discuss only nematic spectra in this paper. Three aspects will be presented. First, some recent work on the interpretation of the lattice vibration spectra of 4, 4'-azoxydianisole (PAA) will be presented. Second, we will discuss some changes we have observed in the intramolecular vibrations of 4-ethoxybenzylidene, 4'*n*-butyl aniline (EBBA). Finally, we will present some work on infrared optical activity induced by a twisted nematic phase.

2. Lattice vibrations of nematogenic crystals

The lattice vibrations of PAA have been reported in the Raman spectrum by us¹ and others², as well as in the far infrared region³. While our Raman work is done on single crystals, allowing assignment of modes to symmetry species, the infrared studies we carried out were only done on polycrystalline samples. PAA crystallizes in the C_{2h}^5 unit cell symmetry, with four molecules/unit cell. There are thus 24 possible lattice vibrations, dividing equally among A_g , A_u , B_g , and B_u representations. Since the unit cell has a center of symmetry, there are no predicted coincidences between infrared and Raman spectra. Three of the twelve infrared active modes are acoustical vibrations, and are expected to be at zero frequency in the approximation to which we will treat the crystal here.

Figure 1 shows the Raman spectrum of two views of the single crystal in the lattice vibration region. First, we note the high quality of these spectra. It is clearly possible to obtain relatively high resolution spectra in this region with a modern Raman instrument. Note that modes less than 20 cm^{-1} from the exciting line are readily observed. Figure 2 shows the far infrared spectrum in the same region. This is a polycrystalline sample, as noted above. It is more difficult to discern the low frequency modes here. As we shall see, this may be due to the fact that, none exist, however, the energy of the instrument is extremely limited in this region.

On comparing the two spectra, one notes that some bands are observed at approximately the same frequencies in the two sets of spectra, while

some striking differences also exist. The most interesting difference is that the highest frequency bands in the Raman spectrum are at about 90 cm^{-1} , while in the infrared a band at 135 cm^{-1} is definitely due to a lattice vibration, and the band at 150 cm^{-1} probably involves the combination of a lattice mode and an internal torsion. Bulkin and Lok³ have also reported the infrared spectrum of MBBA (the methyl analog of EBBA) in this region and find the same phenomenon (higher frequency far infrared than Raman lattice vibrations) when compared to the Raman spectra of MBBA obtained by Mitra *et al*⁴. Bulkin and Eng⁵ have found the same separation of highest frequency lattice vibrations in the octyloxy benzoic acid crystal. This phenomenon clearly needs to be explained. It is discussed further below for the PAA case.

Let us consider the other extreme of comparison between the infrared and Raman spectra. What does it mean when the infrared and Raman

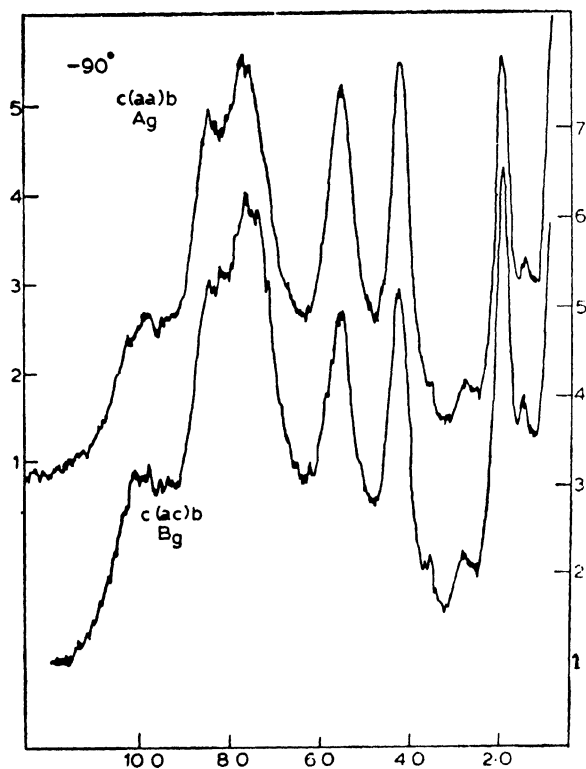


Figure 1 Raman spectrum of PAA, $0\text{--}100\text{ cm}^{-1}$. Spectrum is that of a single crystal in two views of the polarization analyzer, isolating A_g and B_g active Raman bands (from Ref. 1).

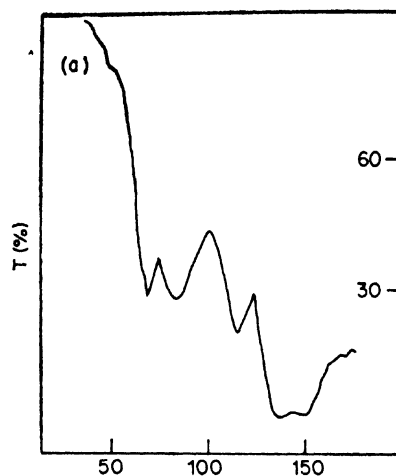


Figure 2 Far infrared spectrum of PAA, polycrystalline sample between crystal quartz plates, vs. reference of crystal quartz (from Ref. 3).

spectra both show modes at exactly the same frequency? In the limit of no intermolecular coupling between molecules in the unit cell, all translations along a particular co-ordinate, or hindered rotations about a particular axis, will appear at the same frequency. As the coupling increases, these co-ordinates should split into four distinct modes. In setting out to interpret the spectra, we have been interested in the question of whether coincidences in the spectra reflect weak intermolecular coupling or accidental degeneracy.

Bulkin and Prochaska¹ have reported that the Raman spectrum of PAA shows the presence of a "soft mode". Such a feature was also remarked upon in the far infrared spectra³. The existence of a soft mode was predicted from statistical mechanical calculations⁶. Pre-transition effects in the Raman spectra of MBBA were also noted by Billard *et al.*⁷

Several years ago, we began to attempt a calculation of the lattice vibrations of PAA in the $\mathbf{k} = 0$ approximation. The details of this calculation are published separately⁸. However, in reviewing recent progress in this field, we wish to summarize how these calculations explain some of the experimental observations just described.

The principle of the calculation is straightforward, although there are aspects of the methodology, not discussed herein, which are rather complex. A potential function was constructed which consisted of two parts. First a static dipolar term was included, using the three dipoles of each molecule. There are thus a total of 12 oriented dipoles in each

Table 1. Observed¹ and calculated lattice vibration frequencies

Symmetry Species	Translatory ²			Rotatory ²		
Ag						
observed	30	52	70	16	74	91
calculated	28	55	62	20	69	94
Bg						
observed	30, 37	52	70	16	74, 90	95
calculated	37	60	69	25	82	101
Au						
observed	50	70	—	135, 150	84	50 ?
calculated	51	69	0 ³	130	89	55
Bu						
observed	—	—	70?	115	84 ?	50 ?
calculated	0 ³	0 ³	67	119	78	52

Notes: 1. Raman data (Ag, Bg) from ref. 2, single crystal frequencies at -90° .
Far infrared (Au, Bu) data from ref. 7, polycrystalline sample at 25° .

2. Modes are primarily rotatory or translatory in nature, however, the translation-rotation interaction force constants are not negligible.

3. Acoustical modes.

unit cell. Second, atom-atom interaction parameters were obtained from other works. These were not refined in any way. We simply chose the atom-atom interactions which seemed most appropriate and transferred them to our system. The potential so obtained yielded an energy minimum at the equilibrium geometry of the crystal with respect to translational and rotational motion about all the co-ordinates. It was differentiated twice and evaluated about the equilibrium position to obtain the force constants. From these force constants frequencies were calculated using a harmonic approximation.

These frequencies, together with the experimentally observed frequencies, are shown in table 1. In this table the observed frequencies are assigned to the calculated ones on the basis of closest fit. In some cases an arbitrary choice was made. For Raman active modes, where single crystal data were available, the A_g and B_g modes can be separated experimentally; this was done in making assignments. In the far infrared the data are far less complete. We have assumed, in several cases in the far infrared, that more than one mode is giving rise to absorption at a particular frequency.

Note first the rather good agreement between calculation and experiment which is observed here. It is important to point out again that the calculated frequencies do not use the experimental data at all.

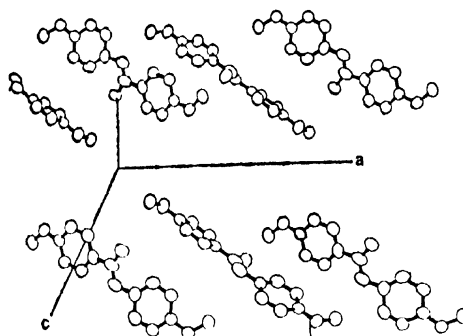


Figure 3 Packing of PAA molecules in the crystal, based on x-ray work of Krigbaum⁹.

In table 1, the modes have been labelled as translatory or rotatory in nature. This is an approximate designation only, as the intermode coupling force constants are often large. The packing of PAA molecules in the crystal is shown in figure 3, reproduced from x-ray work by Krigbaum *et al*⁹. Table 1 is arranged in columns, with respect to this figure, in which modes are translatory along *a*, *b*, and *c* respectively, and rotatory about these same axes. Again, these are approximate designations. As one goes down a column, through the various symmetry species, the different couplings between these modes are seen. These are very similar, then, to the coupling of internal co-ordinates into symmetry co-ordinates which is used in intramolecular force constant calculations.

The calculations show that the infrared spectrum is indeed predicted to have higher frequency lattice vibrations than anything found in the Raman spectrum. It is interesting to see how these high frequency modes arise. They are not due to a mass effect, that is they are not coming from the *G* matrix terms in the calculation. Rather they arise from a very strong intermolecular coupling along certain rotatory co-ordinates. One can see that the highest frequency infrared band and the lowest frequency Raman band are due to the same type of rotatory motion, according to this calculation. There is a very strong intermolecular coupling between some of the molecules. This gives rise to a situation in which the infrared bands in the two species are approximately coincident, as are the Raman bands, but the two pairs of bands are widely separated. It is this sort of specific anisotropic coupling which one expects to see in nematogenic materials. This co-ordinate, which couples so strongly, can be seen by reference to figure 3. It is a rotation about an axis which is 24° from the *a* axis of the crystal. This is primarily a rotation normal to the long axis of the molecules. The most strongly coupled translations are along the *b* axis of the crystal. This is also the motion perpendicular to the long axis.

By contrast, we note that the translations along the long axis of the crystal (*c*) are very weakly coupled. The calculation predicts that all three will occur at nearly the same frequency. It is of interest that this mode is predicted to occur in the 70 cm^{-1} region of the spectrum, which is where the observed soft mode was found.

These calculations are useful in both interpretation of the spectra and in helping us to make our qualitative ideas of nematic liquid crystal formation more quantitative. It is often said, for example, that when a crystal forms a liquid crystal certain intermolecular interactions are maintained while others are lost. It is known that there is great motional freedom in a liquid crystal of the nematic type along the long axis, but little perpendicular to the long axis. The calculations show that this will be the case when viewed from the hindered motions of a unit cell.

A final aspect of these calculations should also be noted. Some texts stress the importance of dipolar interactions in formation of the liquid crystals. We can almost reproduce the observed frequencies by omitting the static dipole contribution to the energy. This is only about 2% of the total lattice energy, and affects the frequencies only slightly. While the individual dipole terms are large, the number of van der Waals' type terms overwhelms the dipolar contribution, and these terms are primarily responsible for the lattice energy.

3. The C-H stretching region in the nematic phase

In the course of doing a complete study of the infrared spectrum of oriented MBBA and EBBA, we have had occasion to examine the spectra of homogeneous and homeotropically aligned samples as a function of temperature through the complete infrared spectrum. The far infrared work has been referred to in passing above³. In this section, we wish to show another type of spectral change which can be seen in the C-H stretching region. Results which are similar in all respects have been observed for both MBBA and EBBA. The EBBA results will be shown here.

Figure 4 shows the infrared spectrum of solid EBBA and the nematic material just above the C-N phase transition. In figure 5 the approximate assignments of the C-H stretching region bands are shown. Most of the intensity comes from the *n*-butyl group, but some comes from the ethyl group as well. The aromatic C-H stretches are not shown in these spectra.

Figures 6 and 7 show what happens in this region when homogeneous and homeotropically aligned samples are heated through the nematic phase and into the isotropic liquid. As can be seen from the spectra, although the two alignments give slightly different spectra the observation is the same: At a temperature below the N-I transition the bands in the C-H region broaden considerably. Before the transition occurs they sharpen, with some shifts in frequency maxima being observed.

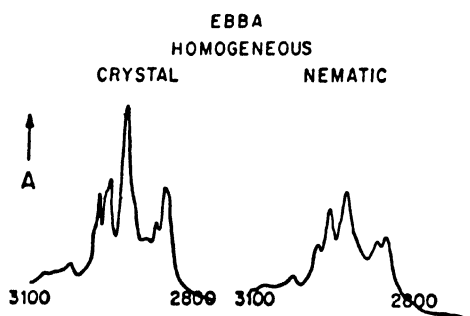


Figure 4 Infrared spectrum of solid and nematic EBBA in the aliphatic C-H stretching region.

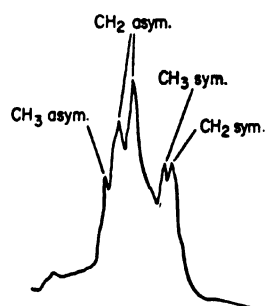


Figure 5 Approximate assignments of aliphatic C-H stretches of EBBA.

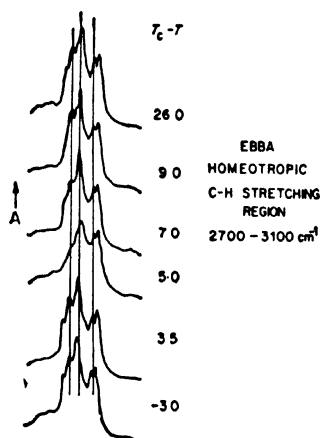


Figure 6 Infrared spectrum of homeotropically aligned EBBA in the nematic phase and slightly above the nematic-isotropic transition temperature (T_c). Vertical lines represent constant frequency.

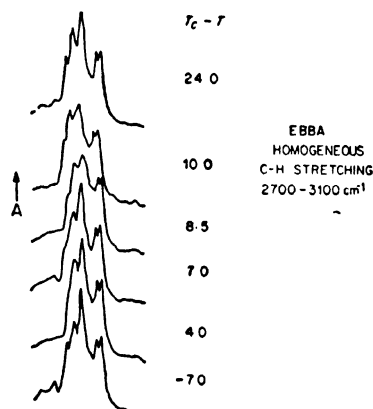


Figure 7 Analogous spectra to those shown in figure 5 for homogeneously aligned EBBA. The constant frequency lines are omitted for clarity.

How do we interpret these figures? First, it is interesting to note the similarity between the spectra in crystal and nematic phases. While there are some differences in band width, there are no drastic changes taking place. This means that the conformation or distribution of conformations occurring in the crystal probably also occurs in the low temperature region of the nematic phase.

As the temperature is raised the bands broaden. This means that changes in conformation are occurring on the time scale of a C-H vibration. As the redistribution of conformations takes place, the band widths are

expected to increase. Once a new distribution is established, or the interconversions are occurring much faster than the time scale of a molecular vibration, the bands sharpen again. The slight shift in some frequencies reflects the new mean field environment of the C-H groups.

We do not know how significant is the difference in temperature between the observation for homogeneous and homeotropic spectral broadening. The transition temperatures for the two alignments were assumed to be the same. If this is true, then the broadening occurs at slightly different temperatures below the phase transition. Other measurements made by us¹⁰ indicate that the S value (order parameter) measured from the infrared spectrum of the homogeneous alignment alone is different from that obtained using both the homogeneous and homeotropic alignment. If this is the case at a particular temperature, then one might predict that the transition temperatures should be different. This would be based on the assumption of a particular S value for the nematic to isotropic transition.

Martire and others^{14, 15}, from thermodynamic work, have speculated on the role of the conformations of the hydrocarbon end chains in the entropy change associated with the N-I transition. Schnur¹⁶ has obtained evidence from the Raman spectra of long alkyl chain alkoxy azoxy benzenes that there are changes in the accordion mode region as the phase transitions are traversed. We believe that this work on the C-H stretching region spectra represents further evidence along these lines. Studies on deuterated samples of EBBA are in progress to more clearly elucidate the transition. These will serve two purposes. First, in partially deuterated, e.g. deuterated *n*-butyl chain only, samples, the C-D stretching region of the hydrocarbon chain will be separated from that of the methoxy or ethoxy groups. Second, the mass effect of the deuterium will change the vibrational frequency and hence the temperature at which the observation of the broadening should take place. Thus these studies are needed to provide more definitive confirmation of this explanation of the observed phenomenon.

4. Induced infrared optical activity in twisted nematics

Recently, there have been a number of reports of the presence of infrared optical activity in the spectra of liquid crystals. Chabay noted this in the case of cholesterics¹¹, as did Shrader and Korte¹². The theory of the effect has also been discussed¹³.

In the course of other studies on the measurement of the order parameter *via* the infrared spectrum of nematics (see above) we have also noted this infrared optical activity. If two infrared windows are treated so as to give homogeneous alignment, and then the windows are set so that the directors are perpendicular to one another, the nematic phase should execute a quarter of a helical turn between the two plates.

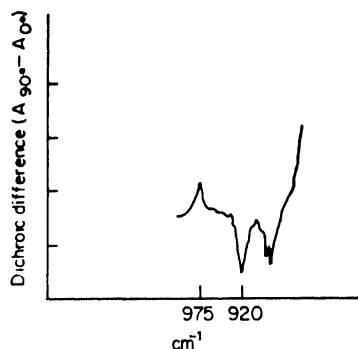


Figure 8 Dichroic difference spectra ($A_{90^\circ} - A_{0^\circ}$) for EBBA aligned in the twisted nematic arrangement.

This is a method of making a pseudo-cholesteric phase from a nematic without resorting to the technique of adding an optically active material.

When the infrared spectrum of such a phase is examined using polarized infrared radiation, we would ordinarily expect to see no effect at all on the spectrum in the two positions of the polarizer. This is because we should have an even distribution of molecules along all directions. Figure 8 shows that this is not the case. In the 1000 cm^{-1} region of EBBA we see that the dichroic difference, recorded on a Perkin-Elmer Model 180 spectrometer, shows both a positive and a negative deflection for the bands in that region. What this means is that the two components are being absorbed differently as they pass through the medium. This is another way of stating that there is infrared optical activity.

The magnitude of the dichroic difference induced in the infrared by twisted nematics will be, we believe, a sensitive probe of the ordering of solutes by nematic mesophases. We are currently studying the infrared optical activity induced in a series of aromatic nitriles of the general formula Phenyl_xCN where $x = 1, 2$, and 4 .

Acknowledgements

The generous support of this work by the US Army Research Office-Durham is gratefully acknowledged. Portions of the work were also supported by a grant from the American Cancer Society. The infrared optical activity measurements were made at Perkin-Elmer Corp. through the co-operation of Dr Robert Hannah.

References

- 1 BULKIN B J and PROCHASKA F T *J. Chem. Phys.* **54** 635 (1971)
- 2 AMER N, SHEN Y R and ROSEN H *Phys. Rev. Lett.* **24** 718 (1970)
- 3 BULKIN B J and LOK W B *J. Phys. Chem.* **77** 326 (1973)
- 4 BORER W J MITRA S and BROWN C *Phys. Rev. Lett.* **27** 379 (1971)
- 5 BULKIN B J and ENG J unpublished work
- 6 KOBAYASHI K K *Mol. Cryst. Liquid Cryst.* **13** 137 (1971)

- 7 BILLARD J, DELHAYE M, MERLIN J C and VERGOTEN G *Compt. Rend.* **273B** 1105 (1971)
- 8 GRUNBAUM D and BULKIN B J J. *Am. Chem. Soc.* (to be published)
- 9 KRIGBAUM W, BARBER P G and CHATANI Y *Acta Cryst.* **B26** 97 (1970)
- 10 BULKIN B J, LOK W B and KENNELLY T, in J. Johnson and R. Porter, eds., *Ordered Fluids and Liquid Crystals*, Vol. 2, Plenum Press, New York, 1974
- 11 CHABAY I *Chem. Phys. Lett.* **17** 283 (1972)
- 12 SCHRADER B and KORTE E H *Angew. Chem. Int. Ed.* **11** 226 (1972)
- 13 HOLZWORTH G and HOLZWORTH N A W *J. Opt. Soc. Am.* **63** 324 (1973)
- 14 MARTIRE D G and CHOW L C *J. Phys. Chem.* **75** 2005 (1971)
- 15 WILLEY D G and BROWN G H *J. Phys. Chem.* **76** 99 (1972)
- 16 SCHNUR J M *Mol. Cryst. Liquid Cryst.* **23** 155 (1973)

DISCUSSION

Janik: I have several comments and questions :

(1) I understand that your calculations and results correspond to the most stable phase of solid PAA.

(2) We made a far-infrared study of MBBA and also obtained the 135 cm⁻¹ peak. As it survives melting we rather think that it is connected with OCH₃ vibration (torsion about long molecular axis).

(3) Neutron diffraction work with deuterated PAA performed by Riste *et al.* in Norway leads to the conclusion that in the soft solid region a few degrees below melting there exists a soft mode corresponding to large angle torsions of the molecule.

Bulkin: In response to your first question, yes, we are calculating only the stable solid. In response to the second point, we have already published the far-infrared spectrum of MBBA*. In that paper, we show that the band at 135 cm⁻¹ does indeed persist to the liquid phase. However, it disappears in solutions in CCl₄ (at correspondingly greater pathlengths, pathlength concentration being kept constant). This implies that the mode is of intermolecular origin. Finally, with regard to your third point, I am very pleased to hear of the neutron diffraction data. We have previously reported the existence of a soft-mode for PAA in the soft solid region**. Amer and Shen have disputed this observation. However, it has been predicted by Kobayashi from statistical mechanical considerations. In addition, the observations of our laboratory and of Billard *et al.* on MBBA confirm this effect.

* Bulkin B J and Lok W B *J. Phys. Chem.* **77** 326 (1973)

** Bulkin B J and Prochaska F T *J. Chem. Phys.* **54** 635 (1971)

Far-infrared absorption spectrum of *p*-azoxyanisole

S VENUGOPALAN

Raman Research Institute, Bangalore 560006 India.

Abstract. The far-infrared absorption of *p*-azoxyanisole has been studied in the range 20-200 cm^{-1} , as a function of temperature. The distinct bands in the room temperature spectrum persist even at temperatures very close to the crystal-nematic transition and no marked pre-transition effects are present. A broad absorption band is seen in the spectra of the isotropic, nematic and supercooled nematic phases. The position of this band shifts down by $\sim 10 \text{ cm}^{-1}$ on going from the nematic to the isotropic phase.

1. Introduction

The study of the vibrational spectra of liquid crystals has been of considerable interest in recent years¹. Infrared absorption and Raman spectra of several liquid crystals have been investigated and have provided useful information regarding the characteristics of the different mesophases. The low frequency modes in these spectra are of particular interest as these are related to the intermolecular forces in liquid crystals. So far, very few studies have been reported on the far-infrared spectra of liquid crystals²⁻⁵. In this paper, we present some preliminary results of our study of the absorption of *p*-azoxyanisole (PAA) in the region of 20-200 cm^{-1} . The far-infrared spectrum of PAA in the crystalline, nematic and isotropic phases has been reported earlier by Bulkin *et al.*^{3,4}. The present study shows some differences as compared to their work.

2. Experimental procedure

The spectra were obtained using the Polytec FIR 30 interferometer* with an on-line Nova 1200 computer†. The interferograms were Fourier transformed in real time and no apodization was used. To eliminate atmospheric water vapour, the interferometer was kept evacuated during all the measurements. The spectral range of 20-200 cm^{-1} was covered using two different beam splitters. One had a usable transmission range of 20-160 cm^{-1} and the other had a range of 50-450 cm^{-1} . The spectra in the two ranges were obtained with resolutions of 4 and 5 cm^{-1} respectively. In the region of

* Polytec GmbH & Co., 7501, Reichenbach, Karlsruhe, West Germany

† Data General Corporation, Southboro, Mass. 01772, USA.

overlap of the two ranges, the observed transmission through the sample agreed to within $\pm 2\%$ except near the minima in the efficiency of transmission for either beamsplitter. As is known, the noise in the ratioed spectrum can become rather high in such regions.

The PAA samples were contained between two quartz windows of diameter 25 mm and thickness 1.2 mm at the centre. They were cut parallel to the c -axis and their surfaces polished. The windows were wedged at an angle of 1° to eliminate interference fringes. As a result of the reflection from the beamsplitter, the radiation is partially polarized with the vertical component of the electric vector being more intense. α -quartz has a doubly degenerate infrared and Raman active zone-centre optical phonon⁶ at 128 cm^{-1} , its polarization lying in the plane normal to the c -axis. Hence, in order to minimize the absorption of the windows at $\sim 128\text{ cm}^{-1}$, the c -axis was kept vertical.

The windows were pressed together in intimate contact and the reference spectrum was obtained at several temperatures, so as to take into account its temperature dependence. Thus, for a given pair of reference and sample spectra, the difference in temperature between the two was certainly within 10°C . The reference spectra were quite free from effects of interference fringes arising from either the windows or the extremely small spacing between them. The effective aperture was 15 mm and the sample thickness was usually $\sim 100\text{ }\mu$.

PAA supplied by Eastman Kodak Co. was used in this study. The crystal-nematic and nematic-isotropic transition temperatures of the material were 118 and 135°C respectively. Polycrystalline samples were prepared by two different methods. In the first, PAA was finely ground and sieved to eliminate particles larger than $40\text{ }\mu$. The sieved powder was then spread into a fairly uniform layer between the quartz windows. Though no effort was made to precisely control the thickness of the layer, it is estimated to be $\sim 100\text{ }\mu$. Sieving the powder ensured that the particle size in the sample was smaller than the shortest wavelength in the spectral region of the present measurements. It was experimentally found that this procedure diminished radiation losses due to scattering, especially at the shorter wavelengths.

In the second method, a bubble-free film of the isotropic liquid was formed between the windows and the thickness of the film was kept at $\sim 100\text{ }\mu$ using a teflon spacer. The isotropic liquid was then slowly cooled. This again resulted in a polycrystalline sample in which the crystallite size was much larger than the average wavelength in the spectral region of interest. Thus, this method of sample preparation was also effective in diminishing the loss of radiation due to scattering.

The measurements in the nematic and isotropic phases were carried out on films of thickness $\sim 100\text{ }\mu$. It was possible to maintain the liquid sample between the windows, without any leakage into the surrounding

vacuum. No attempt was made to orient the nematic sample. Though the cell windows were wedged, the parallelism of the liquid film can, in principle, create interference fringes that can distort the ratioed spectrum. However, from the available data on the refractive indices of α -quartz⁷ in the far-infrared region and on the dielectric constants of liquid crystalline PAA in the microwave region⁸, it is to be expected that such fringes will be of a very small amplitude. Indeed, experimentally no observable effects were seen.

The windows together with the sample were held in a copper block which was heated with a variable temperature cell*. Measurement and control of temperature were accomplished using a cu-constantan thermocouple in conjunction with a TC/30 temperature controller†. Temperature measurements were accurate to $\pm 1^\circ\text{C}$ and fluctuations were within 0.5°C . After the controller indicated the desired temperature, about 15 min. were allowed for the sample to reach thermal equilibrium before carrying out any measurements.

3. Experimental results and discussion

3.1. Crystalline phase

Figure 1 shows the absorption spectrum of polycrystalline PAA at room temperature. Trace A shows the spectrum obtained using sieved powder. It is seen that clear absorption bands are present at 45, 68, 94, 140 and 156 cm^{-1} . The shoulder at $\sim 86\text{ cm}^{-1}$ is noteworthy as it was repeatedly observed in different measurements. Weak absorption features have also been observed at 31, 39 and 56 cm^{-1} . The mode at 31 cm^{-1} is in a region of poor signal-to-noise ratio and the other two appear as shoulders riding a slope. For these reasons it was not always easy to discern these features. However, the other features shown here were always clearly observable. Trace B shows a typical spectrum obtained when the sample was prepared by slow cooling from the isotropic phase. Comparison with trace A shows that the main features are common to both. The mode which appears as a shoulder at $\sim 86\text{ cm}^{-1}$ in Trace A, is now more clearly seen. On the basis of this and other similar spectra obtained by us, it appears that there are actually two modes here, situated at ~ 86 and 94 cm^{-1} . The two modes could not be resolved more distinctly even with a spectral resolution of 2 cm^{-1} ; presumably this is due to the close proximity of the modes and the fact that the line-width of each at room temperature is greater than 4 cm^{-1} . The weak absorption line observed at $124 \pm 1\text{ cm}^{-1}$ is also manifested as a perceptible shoulder in trace A, as is shown in the inset. However, it was not readily reproducible each time a new sample was prepared. Also, as α -quartz exhibits a strong

* Spectroscopic Accessory Co., 241, Main Road, Sidcup, Kent DA 146 QS, UK.

† Polytec GmbH & Co.

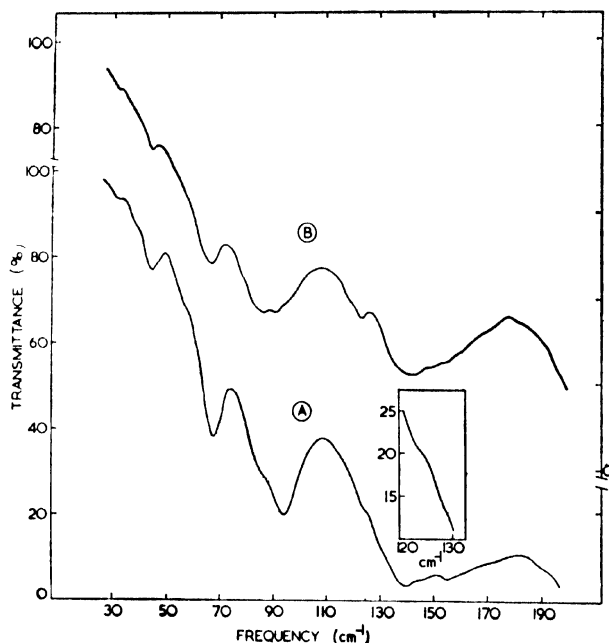


Figure 1 Far-infrared absorption spectrum of polycrystalline PAA at 25°C. (A) Sample prepared with sieved powder. The region 120–130 cm^{-1} is shown enlarged in the inset. (B) Sample prepared by slow cooling from the isotropic phase.

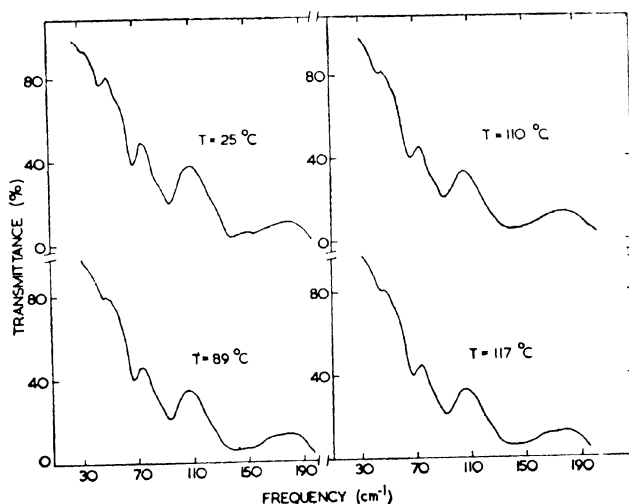
absorption around 128 cm^{-1} , slight distortions may occur in the ratioed spectrum in the vicinity of this line. For these reasons, the identification of this line as an absorption mode of PAA must be regarded as tentative at present. Further experiments to ascertain this are in progress.

With either method of sample preparation, we have not observed the modes at 115 cm^{-1} and 180 cm^{-1} , reported earlier³. Table I lists the absorption frequencies observed in polycrystalline PAA at 25°C in the range 30–200 cm^{-1} . The accuracy of the line positions is $\pm 1 \text{ cm}^{-1}$, except for the weaker features denoted by an asterisk. In these cases as well as for the broader lines, the frequencies are accurate to $\pm 2 \text{ cm}^{-1}$. The frequencies reported earlier³ are also listed for comparison.

The temperature dependence of the absorption spectrum in the crystalline phase is shown in figure 2. As PAA is heated, there is a gradual reduction in the intensity of all the absorption bands. The modes observed at 140 cm^{-1} and 156 cm^{-1} at room temperature become broadened and less distinct. No marked frequency shifts are seen except for the mode at 94 cm^{-1} which shifts down by $\sim 2.5 \text{ cm}^{-1}$ at 117°C as compared

Table 1 Far-infrared absorption frequencies of polycrystalline PAA (in cm^{-1}) at 25°C , in the range $30\text{--}200\text{ cm}^{-1}$. The weaker lines are denoted by an asterisk.

Present work	31*	39*	45	56*	68	86	94	—	124*	140	156
Reference 3	—	—	50	—	70	84	—	115	—	135	150

**Figure 2** Absorption spectrum of polycrystalline PAA at different temperatures.

to 25°C . It can be seen that the distinct absorption lines seen at room temperature persist even at temperatures close to the crystal-nematic transition and that no marked pretransition effects are manifested. In this respect as also regarding the features observed in the spectra as a function of temperature, the present results differ from those reported earlier³.

3.2. Liquid crystalline and isotropic phases

Figure 3 shows the spectra in the isotropic and liquid crystalline phases. Trace A shows the spectrum of the isotropic phase at 140°C , while traces B, C and D show the spectra in the nematic phase at 131.5 , 120 and 103.5°C , respectively. It should be noted that at 103.5°C , the nematic phase is supercooled. All four traces are characterized by one broad absorption band and a shoulder at $\sim 50\text{ cm}^{-1}$. It is of interest to note here that in case of *p*-azoxyphenetole also, a broad absorption band was

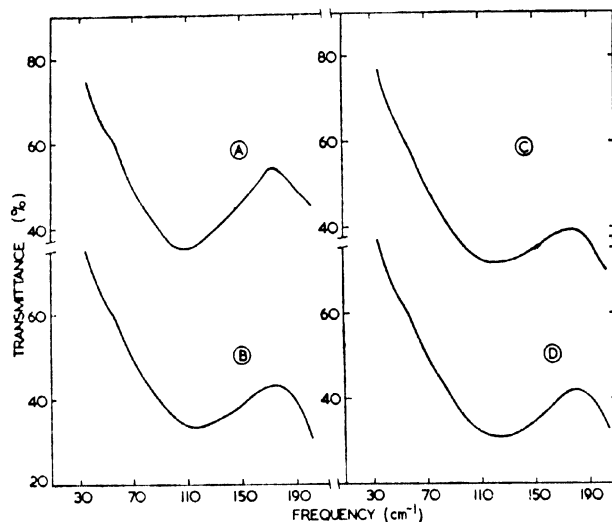


Figure 3 Absorption spectrum of PAA in the isotropic and nematic phases. (A) Isotropic phase at 140°C. (B) Nematic phase at 131.5°C. (C) Nematic phase at 120°C. (D) Supercooled Nematic phase at 103.5°C.

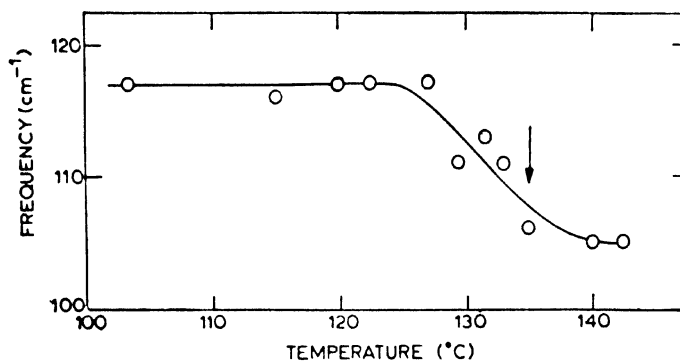


Figure 4 The frequency at maximum absorption for the band shown in figure 3, as a function of temperature. The solid line is a smooth curve drawn through the experimental points. The arrow denotes the nematic-isotropic transition point.

observed and it was attributed to the orientational vibrations of the molecule about its long axis². The position of the band in figure 3 was seen to exhibit a temperature dependence which is shown in figure 4. The data points correspond to the frequency at maximum absorption for each temperature and the solid line is a smooth curve drawn through the

experimental points. In the isotropic phase, owing to the more symmetric shape of the band, the position of maximum absorption could be estimated with better accuracy and was found to be $105 \pm 2 \text{ cm}^{-1}$. However, in the nematic phase the band is shallower and less symmetric, rendering the estimation somewhat more difficult. Hence, the frequencies indicated in figure 4 for the nematic phase are accurate to within $\pm 5 \text{ cm}^{-1}$. Nonetheless, the trend of the temperature dependence shown here was reproducible with different samples. Thus, it is of interest to consider the origin of this absorption band^{2,9} and inquire if the higher frequency of the band in the nematic phase is related to the orientational order obtaining in that phase.

In this context, it is desirable to extend the study of the liquid crystalline phase with aligned samples and polarized radiation. It is also of interest to determine the symmetries of the modes observed in the crystalline phase, through polarization studies on single crystals. Such information should prove useful in understanding the external modes and intermolecular forces in PAA. We plan to pursue further studies related to these aspects in the near future.

Acknowledgements

The author expresses his thanks to Professor S. Chandrasekhar for many valuable discussions and for his keen interest and encouragement during this work.

References

- 1 See for example, the review article by CHANDRASEKHAR S and MADHUSUDANA N V *Appl. Spectrosc. Rev.* 6 (2) 189 (1972)
- 2 L'VOVA A S, SABIROV L M, AREFEV I M and SUSHCHINSKII M M *Opt. Spectrosc.* 24 322 (1968)
- 3 BULKIN B J and LOK W B *J. Phys. Chem.* 77 326 (1973)
- 4 BULKIN B J, GRUNBAUM D, KENNELLY T and LOK W B Paper presented at this Conference
- 5 SCIESINSKA E, SCIESINSKA J, TWARDOWSKI J and JANIK J A (to be published)
- 6 SCOTT J F and PORTO S P S *Phys. Rev.* 161 903 (1967)
- 7 RUSSELL E E and BELL E E *J. Opt. Soc. Amer.* 57 341 (1967)
- 8 CARR E F and SPENCE R D *J. Chem. Phys.* 22 1481 (1954)
- 9 KROON S G and VAR DER ELSKEN J *Chem. Phys. Lett.* 1 285 (1967)

DISCUSSION

Khetrapal: You pointed out that Bukin *et al.* have carried out a theoretical calculation of frequencies that predicts a band near 119 cm^{-1} and this is identified with the mode they observe at 115 cm^{-1} . However, this mode is absent in your spectrum. Does this imply that you disagree with their calculation also?

Venugopalan : It should be noted that other prominent bands of the room temperature spectrum observed previously *, agree fairly well with the present study. In view of this and the observed strength of absorption for the mode at 115 cm^{-1} in the earlier work, we would have expected to observe that band also. In order to eliminate possible effects arising from the technique of sample preparation, we have used sieved powder, powder pressed into a thin disc as well as samples obtained by slow cooling from the isotropic phase. In all the cases, we have failed to observe the band at 115 cm^{-1} . Regarding the empirical calculation of the frequencies by Bulkin *et al.* †, I am not familiar with the complete details of that work at present.

* Bulkin B J and Lok W B J. *Phys. Chem.* 77 326 (1973).

† Bulkin B J, Grunbaum D, Kennelly T and Lok W B Paper presented at this Conference.

Raman spectral and thermodynamic studies on the liquid crystal terephthal-bis- (4-*n*-butylaniline)

J M SCHNUR and J P SHERIDAN*

Naval Research Laboratory, Washington, D. C. 20375

M FONTANA

Istituto di Fisica, Università degli Studi, Parma, Italy

Abstract. Terephthal-bis-(4-*n*-butylaniline) possesses one solid and five fluid phases, viz., smectic B, smectic C, smectic A, nematic and isotropic, upon heating. Raman spectral and differential scanning calorimetric data are presented for all observed phases. The thermal evidence clearly indicates that the smectic C-smectic A transition is of simple second order. The spectroscopic data suggests that the smectic B phase is much more solid-like in nature than that observed in other liquid crystalline phases.

1. Introduction

Previous investigations of liquid crystals have emphasized the importance of obtaining definitive data on the degrees of freedom available to the molecules in the various mesophases and their importance in determining the stability of a given phase^{1,2}. Furthermore, phase transitions in smectic liquid crystals are not well understood. A mean field model for smectic A has been proposed by Kobayashi³ and, independently, by McMillan⁴ in which they predict the possibility of a second-order phase change for the smectic A-nematic transition. de Gennes⁵ has pointed out an analogy between smectic A liquid crystals and superconductors and, on this basis, predicts behavior similar to that observed at the superconductor-normal metal phase transition. However, Cheung *et al.*⁶ indicate that the critical exponents involved are those for the λ transition in He⁴, rather than for the superconductor. Again, in relation to the smectic C-smectic A transition, de Gennes⁷ has suggested that the transition is in many ways analogous to the superfluid-normal transition in liquid helium. It is possible that this transition could be of second order, and optical measurements by Taylor *et al.*⁸ and electron paramagnetic resonance data obtained by Gelerinter and Fryburg⁹ suggest that it may indeed be so in certain cases.

The liquid crystal terephthal-bis- (4-*n*-butylaniline) (TBBA) is of special interest because it possesses five fluid phases: smectic B, smectic C,

* Georgetown University. N.R.L. Research Associate

smectic A, nematic and isotropic. It thus provides an ideal system on which to carry out a comprehensive investigation of the structures of various mesophases. The information gained from such a study will, hopefully, lead to a better understanding of the role of various degrees of molecular freedom in liquid crystal phase transformations.

Published work on TBBA, one by Taylor *et al.*⁸ reported that the tilt angle in the smectic C phase changes continuously with temperature until it vanishes at the smectic C-smectic A phase transition, thus suggesting that the transition is of second-order type. Current work on this material is part of an informal collaborative effort between Lambert and Doucet¹⁰ who have performed x-ray spectroscopic analysis of the material, Charvolin, who has recently completed an NMR study on it, and the present authors, who are studying the material by means of Raman spectroscopy and differential scanning calorimetry (dsc). Preliminary dsc work has been reported by Urbach and Billard¹¹ and Luz and Meiboom¹².

Figure 1 is a pictorial representation of this molecule. One can see the large number of possibilities for intramolecular degrees of freedom, including both rotation of alkyl tails about the central core and rotation of the outer two benzene rings with respect to the center.

The authors have initiated an attempt to use both microcalorimetry and Raman spectroscopy as probes to aid in determining the molecular environment existent in each observed phase. Preliminary results are reported in this work, along with some resultant self-consistent speculations.

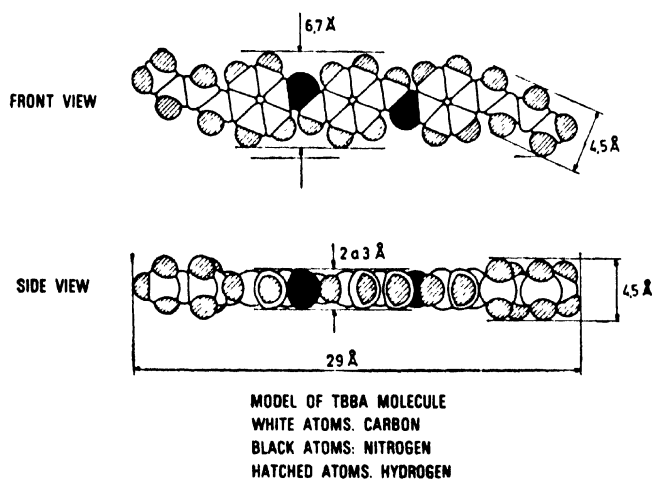


Figure 1 Pictorial representation of TBBA.

2. Experimental

Differential scanning microcalorimetry (dsc)

Both partially deuterated and non-deuterated samples of TBBA were studied using the technique of dsc. The samples (obtained from Jean Charvolin) were outgassed and then stored in an argon chamber. The argon was continually cycled over hot copper and through a molecular sieve to remove oxygen, water, and particulate matter. Sample pans were first weighed and placed into the chamber. Samples were then hermetically sealed in the aluminium sample pans and subsequently removed from the chamber. The experiment was performed in a Perkin-Elmer dsc II, capable of a resolution of 10^{-6} calories per second.

Figure 2 shows the results for the calorimetric experiment. A large enthalpic (ΔH) change is observed in TBBA between the solid phase

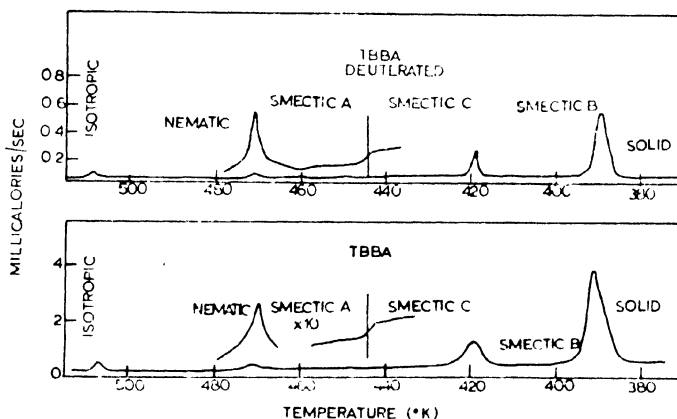


Figure 2 Dsc tracings of TBBA and deuterated TBBA (TBBA-D) with vertical axis proportional to C_p . (The nematic-Sm A and Sm A-Sm C transitions are shown enlarged by 20 in the top figure; the values marked on the y-axis in the bottom figure are after multiplication by 10).

Table 1. Transition temperatures and enthalpies of TBBA

Compound	T_1	ΔH_1^*	T_2	ΔH_2	T_3	ΔH_3	T_4	ΔH_4	T_5	ΔH_5	ΣH
TBBA	113°C	4.34	140°C	0.90	173°C	—	195°C	0.07	232°C	0.18	5.58
TBBA ¹	113°C	—	142°C	—	169°C	—	197°C	—	233°C	—	—
TBBA ²	113°C	—	144°C	—	173°C	—	200°C	—	236°C	—	—
TBBA-D	112°C	3.89	146°C	1.07	174°C	—	201°C	0.13	238°C	0.32	5.42

* Enthalpies given in kilocalories-mole⁻¹.

¹ These: Etude aux rayons X des phases cristallines et mesomorphes du TBBA, Jean Doucet, Université Paris-Sud, Centre d'Orsay (1972).

² T. Taylor, S. Arora and J. Ferguson *Phys. Rev. Lett.* **25** 722 (1970).

(S) and the smectic B phase (B); a smaller, but still quite large ΔH appears between smectic B and smectic C (C), and a finite jump in the heat capacity (C_p) but zero ΔH is observed between smectic C and smectic A (A), clearly indicative of a simple second order phase transition¹³. Such a simple type of higher-order phase transition has rarely been observed in nature, the superconductor-normal metal phase transition being the only other known example. The smectic A to nematic (N) phase transition is definitely not of second order in the Ehrenfest²¹ sense. However, since it exhibits extremely large pre-transition effects (not related to the purity of the sample), this transition may be similar to a λ transition such as that seen from He II to He I¹³. While the nature of this transition is not entirely clear, it looks very similar to typical anomalous or diffusive first order transitions¹³. The nematic to isotropic phase (I) transition is clearly first order, having a ΔH observed between the values for the smectic B and smectic C transitions. The partially deuterated TBBA (TBBA-D) (alkyl tails completely deuterated) scan exhibits significant differences from that of its isotropic partner TBBA. The first phase transition, solid to the first smectic phase occurs approximately at the same temperature as TBBA. Similarly, the B-C and C-A transition temperatures are nearly the same for TBBA and TBBA-D, whereas the A-N and N-I enthalpies are substantially different. This could be due to the importance of the tails in determining the stability of phases or due to differences in purity of the samples.

Raman spectra

Experimentally, the scattered light was viewed at 90°, dispersed with a Spex double monochromator and detected with an ITT FW 130 cooled photomultiplier and photon counting electronics. The exciting 5145Å line of an argon ion laser was depolarized to minimize extraneous polarization effects. Our samples (obtained from the Laboratoire de Physique des Solides, Orsay, France) showed purity of better than 99.9% by dsc and were slightly yellow. The samples were contained in 0.8 mm capillary tubes situated in an inert atmosphere oven. Temperature was continuously monitored and was accurate to about 0.1° C. Fluctuations were less than 0.05° C.

Observations of the bands studied in this experiment were severely handicapped by the presence of fluorescence which appeared to increase with irradiation. This was especially severe at the higher temperatures. It was found that by first outgassing the samples under vacuum and then backfilling with dry N₂ prior to the sealing of capillaries, this laser-induced degradation of TBBA was significantly decreased (but not eliminated). At higher temperatures, spectra were obtained by running several samples in different, but overlapping, spectral regions.

As a result of the decomposition and fluorescence problems, a krypton laser was also employed. A different photomultiplier tube was also

used (RCA C31034) to obtain sensitivity to 900 nm. The 7552, 6764, 6471 and 5309 Å laser lines were used in the experiment with most of the work done with the 6471 Å line.

Spectra for TBBA in the 50–200 cm^{-1} regions are shown in figure 3 for all observed phases in TBBA. The solid phase contains a large number of bands in the lower frequency region.

The moderately low frequency spectra in figure 3 show only small changes between the solid phase and smectic B phase. The most notable changes are the deformation of the peak at 150 cm^{-1} and the possible appearance of a peak at 180 cm^{-1} . In smectic C, the 150 cm^{-1} band almost disappears as does the peak at 180 cm^{-1} . However, the structure at 100 cm^{-1} is retained and quasi-elastic scattering has increased.

Smectic A shows another increase in quasi-elastic scattering coupled with the loss of all features except for one shoulder that remains at 80 cm^{-1} . The nematic phase has still stronger elastic scattering with the 80 cm^{-1} shoulder retained. The isotropic phase exhibits a much lower quasi-elastic scattering and the shoulder at 80 cm^{-1} has discontinuously disappeared at the phase transition.

Figure 4 depicts low frequency spectra obtained near the solid-smectic B phase transition and also in smectic C. A third monochromator was used to ensure the elimination of the spurious instrumental effects so common in this low frequency region. The solid phase exhibits a pronounced peak at 22 cm^{-1} . This peak is also present, although somewhat broadened, in the smectic B phase. At the smectic B–smectic C transition point, this peak disappears.

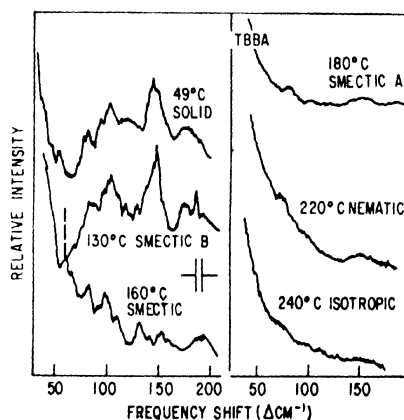


Figure 3 Raman spectra of TBBA (all phases), 50–200 cm^{-1} region. Spectral resolution is 1 cm^{-1} (5145 Å).

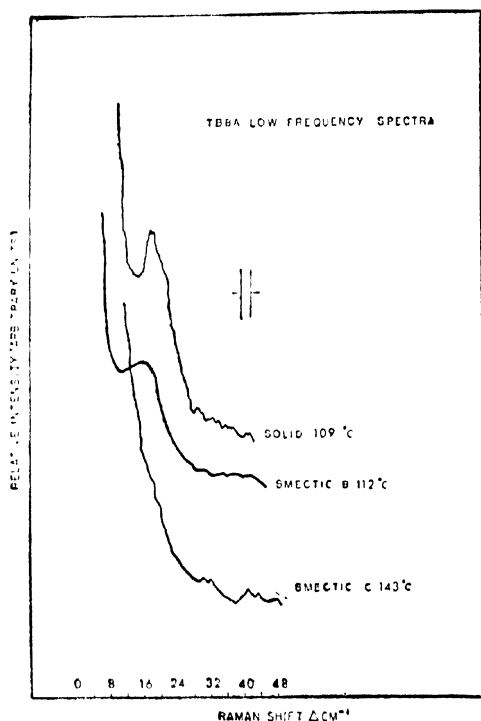


Figure 4 Raman spectra of TBBA : S, B and C phases, 10–50 cm^{-1} region. Spectral resolution is 0.5 cm^{-1} (5145 \AA).

The crystalline and smectic B spectra are similar below 200 cm^{-1} . Of particular interest is their similarity in the low frequency region (figures 3 and 4). This result is important since the modes in this frequency region are generally "lattice" modes and, as such, are very sensitive to the local ordering and dynamics of the molecules. Thus, we may conclude from the spectra that the vibrational structure and dynamics of TBBA in the smectic B and crystalline phases are remarkably similar. This result becomes even more clear when we compare it with what takes place at what should be a rather less abrupt smectic B–smectic C transition. Now there are distinctive and marked differences between the two spectra. At very low frequencies, the 19 cm^{-1} peak totally disappears in the smectic C phase. There are also drastic changes in the 50 to 200 cm^{-1} region. The resulting smectic C spectrum is much more similar to those obtained in other smectic systems¹² in the same low frequency region. Indeed, we find it very similar to the spectra of the smectic A and nematic mesophases in TBBA. In the isotropic phase, all low frequency resonances disappear as expected and observed in other liquid crystal systems.

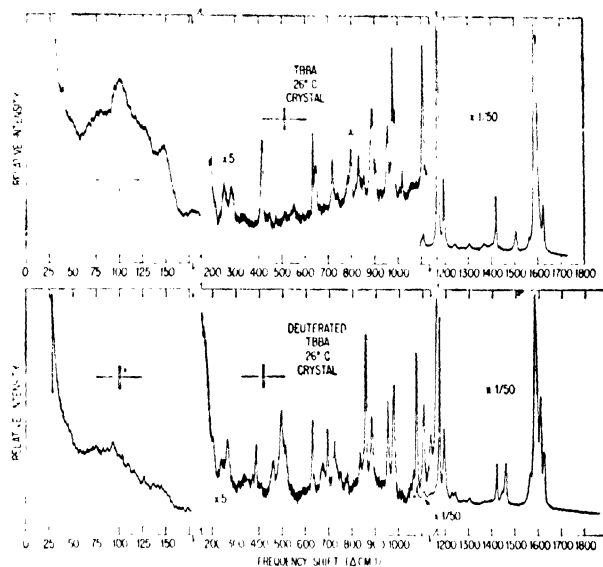


Figure 5 Raman spectra of TBBA and TBBA-D solid, 35–1700 cm^{-1} region. Spectral resolution is 5 cm^{-1} (6471 Å).

- Figure 5 shows the Raman spectra of both TBBA and TBBA-D using the 6471 Å laser line. The peak at 150 cm^{-1} for TBBA is now substantially smaller and was apparently enhanced by resonance effects in the 5145 Å experiment. Spectral studies at 5309 Å, 6764 Å, and 7552 Å substantiate this thesis. The spectra for the TBBA-D below 200 cm^{-1} exhibit a substantial shift toward lower frequencies with much less defined peaks. This might be expected due to the slightly heavier weight of each molecule.
- However, the amount of change between the two spectra is certainly substantial. The spectra between 200 and 900 cm^{-1} show many changes between the deuterated and non-deuterated samples (figure 6), indicating as expected¹⁴ that this frequency region can provide much information on the nature of the chain skeletal and C-H motions in the molecule. Of particular interest is the doublet observed in TBBA between 250 and 300 cm^{-1} . This band may be associated with the accordion band discussed in previous Raman work¹. The theoretical considerations discussed in this work would predict (figure 7) a band for TBBA between 250 and 300 cm^{-1} . The added mass of deuterates would cause the shift observed in these bands for TBBA-D (figure 6).

Preliminary studies of the smectic B and smectic C phases in this region show dramatic changes of the bands in the 200 to 800 cm^{-1} region. However, decomposition still remains a serious problem even for the 7552 Å laser line.

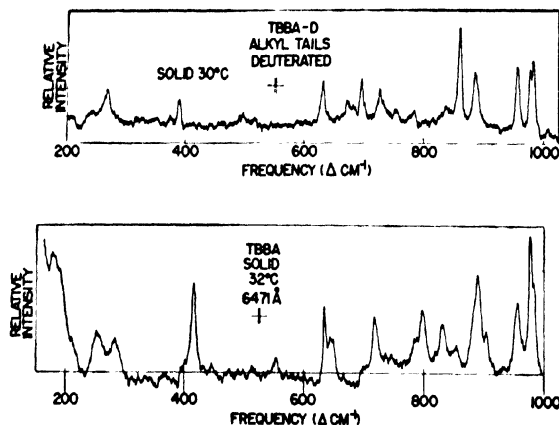


Figure 6 Raman spectra of TBBA and TBBA-D solid, 200–1000 cm^{-1} region. Spectral resolution is 2 cm^{-1} .

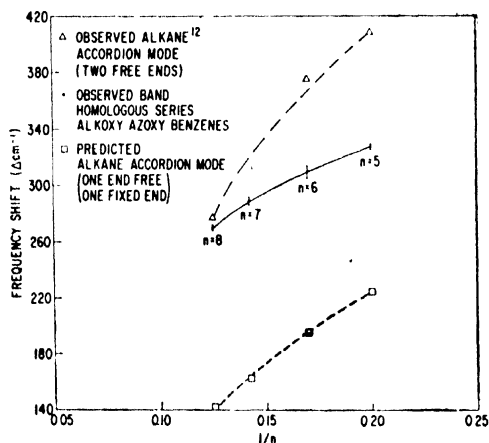


Figure 7 Curves of expected frequencies for accordion mode having two free ends, one fixed end, and the probable observed frequencies for this band in the alkoxy azoxy benzene series.

The spectra in the 1550–1650 cm^{-1} region were quite interesting (figure 8). The solid phase exhibits a strong peak at 1589 cm^{-1} , with a small band at about 1625 cm^{-1} . In the smectic B phase and in all higher temperature phases, the 1589 cm^{-1} band substantially decreases while a new band appears at 1562 cm^{-1} and the 1625 cm^{-1} band strengthens as if two side bands had appeared. This region has been thought to be associated with the C–N¹³ stretch and Schiff bases, and quite possibly the new bands are the result of a symmetry restriction being lifted in the fluid phases.

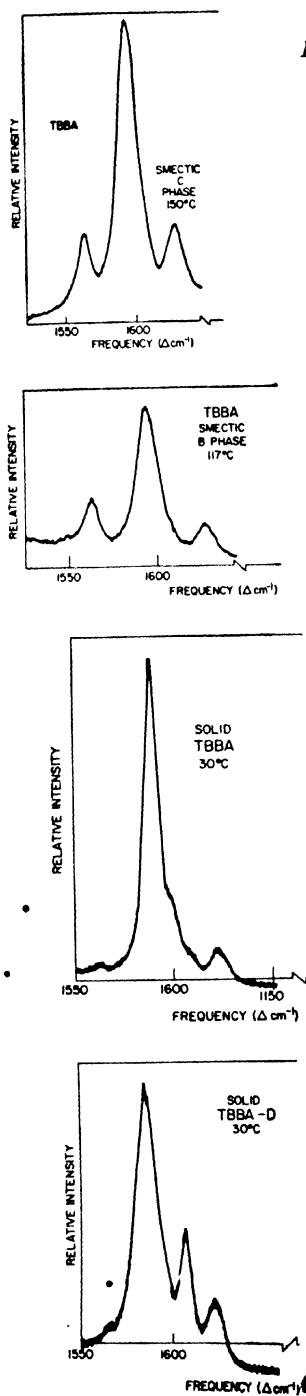


Figure 8 Raman spectra of TBBA, S, B, C phases, 1550–1650 cm⁻¹ region, TBBA-D S phase. Spectral resolution is 2 cm⁻¹

3. Discussion

The Raman spectrum exhibited by smectic B with its well-defined peaks implies not only that the system can still sustain cooperative intermolecular vibrations, but indeed that such modes are at least partially propagating in an ordered structure. Thus, in the smectic B phase, we may have a stacking of quasi-crystalline planes which retain to a large extent the ordering and rigidity of the crystalline phase.

This conclusion is in very good agreement with recent x-ray work on TBBA¹⁰ in which Bragg spots, characteristic of hexagonal coordination in the smectic planes, were observed. Such ordering is found to be of intermediate range, typically extending over 50 "unit cells". This range is sufficient to yield the essentially ordered Raman scattering we observe in the smectic B phase. In order to analyze more quantitatively the model for the behavior of TBBA, Raman data on monodomain samples are needed so that mode symmetries can be obtained from polarization analysis. In this respect, TBBA in its smectic B phase provides a most interesting system since it behaves — vibrationally — as a crystal even though it can be poured. In fact such systems can sustain shear modes only in determined directions. Thus, in a monodomain sample, it should be possible to observe drastic changes in a low frequency spectrum simply by varying the scattering geometry. An investigation of this type involving elastic constants¹⁶ has been recently reported in a smectic A system, and we are presently pursuing this aspect of the problem involving optical modes. We are also currently studying monodomain samples of TBBA via Raman spectroscopy.

The data presently available, however, when coupled with the aforementioned x-ray work and with NMR results^{17, 18} allow us to make some reasonable speculations on the structural and dynamic behavior of TBBA. For instance, the NMR evidence suggests that molecular rotation without diffusion occurs in the smectic B phase. However, a free, liquid-like rotation seems to be highly improbable since the average molecular separation is about equal to the molecular diameter. This, plus the fact that we observe "phonon" modes indicative of mechanical coupling in the smectic B phase, imply that the rotation should be collective, for instance like that of cogwheels in a gear mechanism. This "cogwheel-like" mode might possibly give rise to the broad peak at 19 cm^{-1} in the Raman spectrum, and thus the mode would correspond to a relative rotation of the molecules about their axes in the crystalline phase. At the B to C transition, the molecules become truly free to diffuse and rotate, although some degree of coupling must remain as indicated by the presence of some residual structure in the low frequency scattering. The 19 cm^{-1} peak has, however, disappeared and only the tail of strong quasi-elastic scattering is observed. This would be expected if the "cogwheel" mode is now diffusive.

The dsc results show at least two and perhaps three kinds of transitions. The solid-B, B-C, and the N-I transition are definitely first order. The smectic C to smectic A is apparently a normal transition of the second kind, with only a ΔC_p to show the transition point. It is possible that the smectic A to nematic is a transition somewhere between the classical first and classical second phase transitions. However, the lack of any change in C_p before or after the transition would strongly suggest that it is first order. The temperature changes observed for the deuterated samples, the increase in ΔH for the intermediate phase transitions in the deuterated samples, coupled with the Raman and other optical investigations³, enable us to make some speculations on the nature of the structure of the various phases.

At the solid to smectic B phase transition, planes might be allowed to move with respect to one another but substantial coupling between molecules probably still persists, thus permitting x-ray data to show residual ordering in the third dimension. Some rotation may be allowed of the entire molecule or its parts in this phase, but if so, it is probably of the collective nature previously discussed. Alternatively a random dislocation on a millisecond time scale may occur. At the smectic B to smectic C phase transition, the coupling between the molecules might break, destroying any residual third-dimension order. This could explain the relatively large ΔH observed at this transition. If the tails of the TBBA molecule are fixed with respect to the central core and the molecules are coupled in phase in a plane, the molecule will exhibit an apparent tilt with respect to the axis of the plane to x-ray and optical microscopy. This would be the case if the central cores were lined up at right angles to the planes. If, in the smectic C phase, some rotation becomes permitted, either for the entire molecule with respect to other molecules about the long axis, or perhaps rotation of the alkyl tails about the central core, then the apparent observed angle will be seen to decrease as a function of temperature following the increase in free volume. At some point there would be free rotation and a zero tilt angle would be observed. This could be the molecular basis for the transition of simple second kind observed by dsc for the C-A transition. It would also explain the optical microscopy⁴, EPR⁹ and x-ray¹⁰ results. A variation of this speculation has been made on an a priori basis by McMillan¹⁹ about smectic C.

In the smectic A phase, more conformational freedom could be allowed as well as the break-up of the planes at the smectic A to nematic phase transition. This transition has been discussed by several authors^{3-5, 20} and a second order transition has been predicted. However, this is not in agreement with our current experimental findings, that is, neither a λ second order phase transition nor a simple second order transition occur between the smectic A to nematic phase transition as was previously observed between the smectic C to smectic A phase.

This model, although speculative, does allow a basis for future experimental work and is consistent with previous experimental observations. Future work is planned to ascertain the validity of the previous model. More definitive calorimetric work is being carried out on TBBA with selectively deuterated samples. In particular, only the tails will be deuterated in order to determine the effect of simply changing the weight of the tails. If the model is correct, substantial changes should still be observed in the smectic C to smectic A transition and they may also affect the smectic A to nematic and nematic to isotropic while having much less effect on the lower two phase transitions. The use of isotopic carbon-13 in the tails would also be advantageous to this work. Specific volume measurements will also be made. The accordion band of the alkyl tails will be more thoroughly investigated, using both selectively deuterated samples and members of the homologous series and its temperature dependence ascertained. Oriented monodomain low frequency Raman spectra will be obtained for the smectic B and solid phases. Temperature dependence of various bands will be obtained. NMR of TBBA substituted with various isotopes should be carried out in order to definitively determine the onset of rotation of the complete molecule and various parts of it. The effect of pressure on the transition points should be determined to help discover the nature of the various transitions. It may be that the C-A transition will be one of the few "real" transitions to obey the thermodynamic rules of a classical²¹ simple second order transition since C_p is a regular variable, *i.e.*, does not approach a high or infinite value in the vicinity of the phase transition.

References

- 1 SCHNUR J *Phys. Rev. Lett.* **29** 1172 (1971)
- 2 MAIER W and SAUPE A *Z. Naturforsch.* **14a** 882 (1959); **15a** 287 (1960); **16a** 8 16 (1961)
- 3 KOBAYASHI K *Mol. Cryst. Liquid Cryst.* **13** 137 (1971)
- 4 McMILLAN W *Phys. Rev. A.* **4** 1238 (1971)
- 5 DE GENNES P G *Solid State Commun.* **10** 753 (1972)
- 6 CHEUNG L, MEYER R and GRULER H *Phys. Rev. Lett.* **31** 349 (1973)
- 7 DE GENNES P G *C. R. Acad. Sci. Paris B.* **274** 278 (1972)
- 8 TAYLOR T, ARORA S and FERGASON J *Phys. Rev. Lett.* **25** 733 (1970)
- 9 GELERINTER E and FRYBURG G *Appl. Phys. Lett.* **18** 84 (1971)
- 10 DOUCET J, LEVELUT A M and LAMBERT M *Mol. Cryst. Liquid Cryst.* in press
- 11 URBACH F and BILLARD C. *R. Acad. Sci. Paris* **274** 1287 (1972)
- 12 LUZ F and MEIBOOM S *J. Chem. Phys.* **59** 275 (1973)
- 13 MAYER J and STREETER S F *J. Chem. Phys.* **7** 1019 (1939)
- 14 SCHNUR J *Mol. Cryst. Liquid Cryst.* in press
- 15 VERGOTEN G, These, Laboratoire de Physique, U.E.R. de Pharmacie, Lille, Paris (1973)
- 16 DELAYE M, RIBOTTA R and DURAND G *Phys. Rev. Lett.* **31** 443 (1973)
- 17 DOANE J W, PARKER R S, CUIKLY B, JOHNSON D L and FISHEL D L *Phys. Rev. Lett.* **28** 1694 (1973)
- 18 CHARVOLIN J Université Paris-Sud, Orsay, France, personal communication
- 19 McMILLAN W *Phys. Rev. A.* **8** 1921 (1973)
- 20 LEE F, TAN H, SHIH Y and WOO C *Phys. Rev. Lett.* **31** 1117 (1973)
- 21 EHRENFEST P *Leiden Comm.un. Suppl.* **75b** (1933)

DISCUSSION

Janik : The rotations could be studied by measuring Raman line profiles and applying the VV and VH method.

Schnur : Such work is currently being carried out on monodomain samples in Parma at the Instituto di Fisica by Marco Fontana in collaboration with Dr. Sheridan and myself at N.R.L.

de Vries : You explained that the gradual decrease in the smectic C phase of TBBA is due to a gradually increasing rotation around the long axis. This appears to be in conflict with a recent paper by McMillan and Meyer, who state that in smectic C the dipoles do not rotate but are aligned, and a paper I have recently submitted which claims to prove that in a tilted phase the molecule cannot rotate.

Schnur : There are two points in answer to your comment -

1. The model that I suggested involved collective rotation in B-C phases and also another type, hindered - perhaps intramolecular - rotation in the C phase with increased torsional freedom as a function of temperature, the important one being the hindered rotation.

2. Despite your theoretical considerations I must depend more heavily on experimental observations in order to make models hoping to approximate real systems. Thus the comprehensive NMR work by Luz and Meiboom*, unequivocally shows rotation in B phase. This also agrees with the work of Charvolin and the microwave experiment by Carr. All call for some type of rotation.

Carr : Are any of the rotations that exist in the nematic phase restricted in the smectic C?

Schnur : I believe so. These may however involve intramolecular rotations. Such as the alkyl tail freely rotating about the central core - or perhaps free rotation can occur in parts of the alkyl tail causing conformational changes. Another possibility is free rotation of the two outer rings with respect to the centre ring. I do not know if microwave spectroscopy would detect differences between these varied types of rotation.

Carr : The relaxation times that are associated with the dipole moments do not appear to change at transition temperatures between nematic and smectic phases. This indicates that the dipoles are not greatly affected.

Demus : Which kind of calorimeter did you use?

Schnur: Perkin Elmer DSC-2.

Demus: In the case of transition entropies of ~ 10 cal/mole deviations may be 100%. And I think it is very difficult to say whether a transition is of first order or second order.

Schnur: We were able to reproduce our results on ten separate samples. We never had more than 10% fluctuations in specific heat.

Demus: An adiabatic calorimeter may be better.

Schnur: I agree with you.

Calorimetric investigation of liquid crystals

D MARZOTKO and D DEMUS

Sektion Chemie der Martin-Luther-Universität Halle-Wittenberg
402 Halle, German Democratic Republic.

Abstract. The homologous series, di-*n*-alkyl 4, 4'-azoxycinnamates, di-*n*-alkyl 4, 4'-azoxy- α -methylcinnamates, 2, 5 bis-[4-*n*-alkylphenyl]-pyrazines, 2, 5-bis-[4-*n*-alkoxyphenyl]-pyrazines, di-*n*-alkyl 4, 4'-terphenyldicarboxylates, 4-*n*-alkoxybiphenylcarboxylic acids, have been investigated by means of a Perkin-Elmer DSC 1B Calorimeter. Some unexpected results have been found: a decreasing trend of the enthalpies of the smectic-isotropic transition within one series; enthalpies of the smectic C-isotropic transition with higher values than the enthalpies of melting in another series.

The relations of the transition enthalpies with some specialities of molecular structure are shown.

A review of the so far known values of the transition enthalpies in connection with the types of modification which participate in the transitions-is given.

1. Introduction

Calorimetry is a valuable method for the detection of phase transitions. It yields quantitative results, therefore, conclusions may be drawn concerning the nature of the phases which participate in the transitions.

Till now only few homologous series of liquid crystalline substances have been investigated by calorimetry. We present the results of the investigation of 6 homologous series which are of special interest since they possess not only nematic phases, but also smectic modifications of different types.

2. Experimental

The transition enthalpies have been determined with a Perkin-Elmer Differential Scanning calorimeter DSC 1-B. Calibration of the apparatus was performed using the tabulated heats of very pure indium, bismuth and tin.

The errors of the enthalpy values consist mainly of the error in the reproducibility of the base line and the peaks and of the error in the determination of the area of the peaks by planimetry. Table 1 shows that the maximal error increases with decreasing enthalpy value. In some cases of smectic C-smectic A transitions with enthalpies about 10 to 50 calories

Table 1. Maximal errors of transition enthalpies

kcal/mole			relative error
	4		$\pm 1 \%$
2	...	4	$\pm 2 \%$
1	.	2	$\pm 3 \%$
0.5	1	$\pm 5 \%$
0.2	...	0.5	$\pm 10 \%$
0.1	...	0.2	$\pm 25 \%$
0.05	0.1	$\pm 50 \%$
0.01	.	0.05	$\pm 100 \%$

the error may increase to 100%. Then the transition is observed only qualitatively with a possible upper limit of the enthalpy value. By repeated measurement on the same sample we could show that in most cases the deviations of the enthalpy were less than the maximal error. Only in the case of substances with very high transition temperatures greater deviations caused by decomposition of the substances have been observed.

For comparison some compounds which had been investigated previously by precision calorimetry¹⁴⁻¹⁸ have been included in our work. The deviations in no case exceeded the values listed in table 1.

The substances had already been used for other investigations and have been described elsewhere.

We use the following units of measure and abbreviations:

transition enthalpy	ΔH [kcal / mole]
transition entropy	ΔS [cal / mole. deg.]
temperature	t [°C]
isotropic liquid	I
nematic liquid	N
cholesteric liquid crystal	CH
smectic liquid crystal	
of the type A, B, C etc.	S_A, S_B, S_C etc.

3. Results

Di-n-alkyl 4, 4'-azoxycinnamates

We have investigated the members 2 to 12 and 16 of the series of the di-*n*-alkyl-4, 4'-azoxycinnamates. The results are listed in table 2 and graphically shown in figure 1.

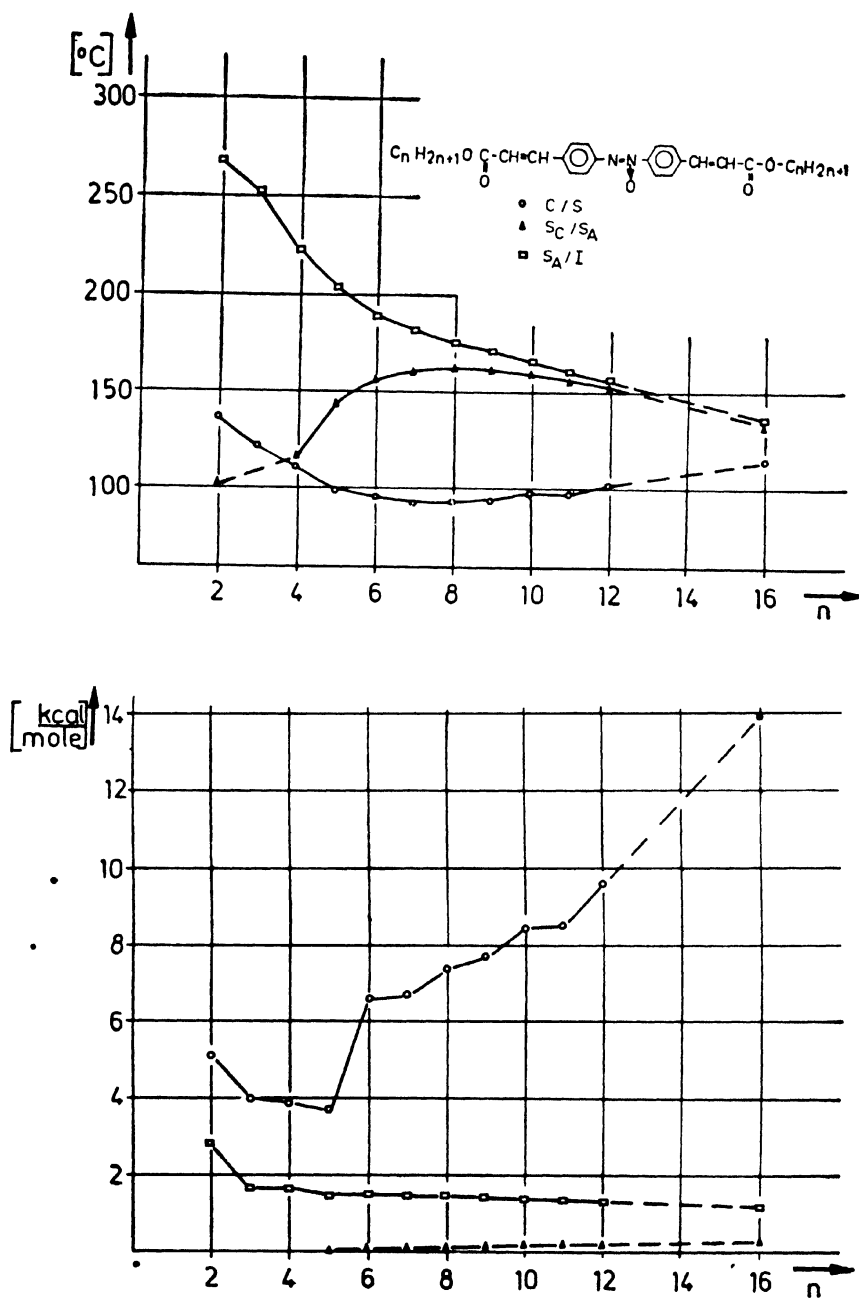


Figure 1 Di-*n*-alkyl azoxycinnamates
top: transition temperatures; bottom: transition enthalpies.

Table 2. Di-*n*-alkyl 4, 4'-azoxycinnamates^{19,20,21}

$$\text{C}_n\text{H}_{2n+1}\text{OOC}-\text{CH}=\text{CH}-\text{C}_6\text{H}_4-\text{N}-\text{N}-\text{C}_6\text{H}_4-\text{CH}=\text{CH}-\text{COOC}_n\text{H}_{2n+1}$$

\downarrow
 O

<i>n</i>	transition				transition				transition				isotropic
	<i>t</i>	ΔH	ΔS	<i>S_c</i>	<i>t</i>	ΔH	ΔS	<i>S_A</i>	<i>t</i>	ΔH	ΔS	ΔS	
2	135.7	5.21	12.7		100.4 ^b	^c	^c		267	2.77		5.13	
3	120.7	3.96	10.1		—	—	—		252	1.66		3.16	
4	111.2	3.93	10.2		115.3	^d	^d		222	1.64		3.30	
5	99.4	3.70	9.3		142.9	<0.01	<0.01		203.0	1.47		3.08	
6	95.1	6.66	18.1		156.1	0.05	0.12		188.7	1.53		3.32	
7	80 ^a	3.31 ^a	9.4 ^a										
	92.0	3.39	9.3		160.0	0.09	0.20		182.5	1.46		3.21	
8	92.4	7.40	20.2		162.3	0.14	0.33		175.3	1.47		3.27	
9	94.3	7.67	20.9		161.6	0.16	0.38		170.7	1.44		3.24	
10	97.6	8.47	22.8		159.0	0.19	0.44		165.2	1.41		3.21	
11	97.3	8.51	23.0		156.1	0.21	0.48		160.2	1.37		3.16	
12	101.6	9.59	25.6		152.8	0.21	0.51		156.2	1.33		3.09	
16	81-88 ^a	0.58 ^a	1.6 ^a										
	107.1	13.91	36.6		133.0	0.29	0.71		135.0	1.14		2.79	

(a) Transition solid II/solid I

(b) Transition in the supercooled region (monotropic)

(c) Transition not observed because of insufficient supercooling

(d) Transition not observed because of too small a value of transition enthalpy

As known from other homologous series the melting enthalpies increase with increasing chain length. Only the ethyl ester shows a deviation typical for initial members of homologous series¹¹. By addition of the enthalpy of the transition solid II/solid I the member 7 fits well in the trend of the series.

The enthalpies of the transition S_C/S_A have very low values and also show an increasing trend within the series. The smectic C-modification of the butyl ester has been reported earlier by texture observation²⁰. Obviously the enthalpy of the transition to smectic A for this substance is too little to be detected by the DSC method.

The enthalpies of the transition smectic A/isotropic lie in the expected limit between 1 and 3 kcal/mole. But the trend in the homologous series is completely unexpected: never before has been observed a decrease of clearing enthalpies with increasing chain length.

A possible explanation for this behaviour is given in the summarizing discussion of this paper.

Di-n-alkyl azoxy- α -methylnamates

The di-*n*-alkyl azoxy- α -methylnamates have already been investigated earlier by DTA¹¹ and two members by precision calorimetry¹⁶. The DTA did not allow the observation of the transitions S_C/S_A , and the enthalpies of the transitions S_A/N and N/I could be evaluated only as a sum of their values. Because of the overlapping of the transition peaks separate values were not obtainable. Most of the melting enthalpies (see figure 2, table 3) are in good accordance with the literature values. Only in some members of the series there are deviations. They can be explained by the fact that we have observed additional transitions in the solid state. In these cases the accordance with the literature values is better if we add the enthalpies of solid state transition and melting. The melting enthalpies show no regular trend within this series.

The enthalpies of all other types of transition increase with increasing chain length. The transitions S_C/S_A possess very small values. For instance, the enthalpies of the transition N/I even for the lowest members are about ten times greater.

2,5-bis-[4-n-alkylphenyl]-pyrazines

We have investigated the first 10 members of the series of the 2,5-bis-[4-*n*-alkylphenyl]-pyrazines (table 4, figure 3). The substances have been prepared by Schubert *et al*²⁵. The polymorphism of this series has been reported previously by texture and miscibility investigation²³.

The first 2 members show anomalously high melting enthalpies compared with the higher members. A regular trend of the melting enthalpies is not observable.

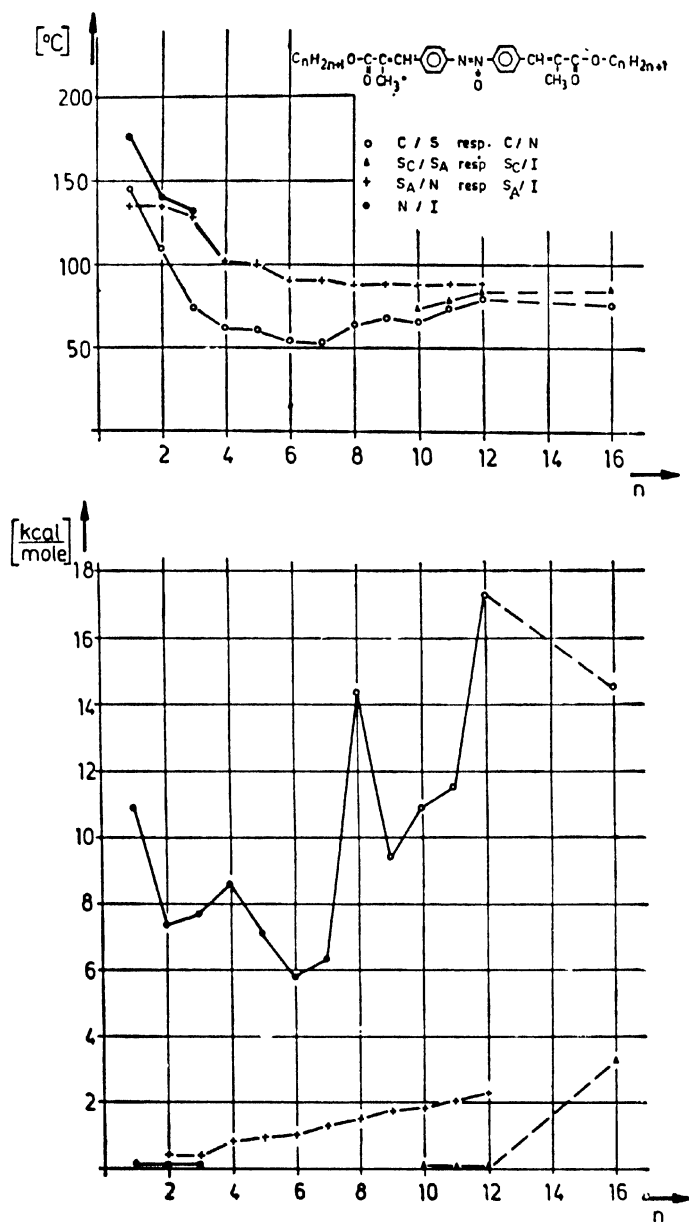
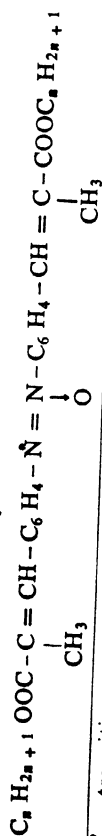


Figure 2 Di-*n*-alkyl azoxy- α -methylcinnamates
top: transition temperatures; bottom: transition enthalpies

Table 3. Di-*n*-alkyl azoxy- α -methylcinnamates 11, 16, 19, 22



n	CH ₃			O			CH ₃			isotropic					
	solid	transition	transition	transition	transition	transition	transition	transition							
	t	ΔH	ΔS	Sc	t	ΔH	ΔS	S _A	t	ΔH	ΔS	N	t	ΔH	ΔS
1	145.4	10.90	26.0	-	-	-	-	-	135.6 ^b	-	-	-	176.5	0.09	0.20
2	~ 75 ^a	1.90 ^a	5.5 ^a	-	-	-	-	-	-	-	-	-	-	-	-
	108.9	7.37	19.2	-	-	-	-	-	-	-	-	-	-	-	-
3	74.2	7.72	22.2	-	-	-	-	-	135.1	0.41	1.01	140.7	0.09	0.21	0.21
4	62.0	8.64	25.8	-	-	-	-	-	129.0	0.43	1.08	131.3	0.10	0.25	0.25
5	~ 55 ^a	2.37 ^a	7.2 ^a	-	-	-	-	-	102.3	0.77	2.04	-	-	-	-
	60.8	7.10	21.3	-	-	-	-	-	-	-	-	-	-	-	-
6	-	0.25 ^a	0.78 ^a	-	-	-	-	-	100.1	0.91	2.44	-	-	-	-
	54.0	5.80	17.7	-	-	-	-	-	-	-	-	-	-	-	-
7	53.1	6.29	19.3	-	-	-	-	-	90.7	1.03	2.83	-	-	-	-
8	63.0	14.41	42.8	-	-	-	-	-	90.6	1.28	3.51	-	-	-	-
9	~ 57 ^a	0.58 ^a	1.7 ^a	-	-	-	-	-	88.4	1.48	4.10	-	-	-	-
	68.4	9.39	27.6	-	-	-	-	-	-	-	-	-	-	-	-
10	~ 54 ^a	0.65 ^a	2.0 ^a	-	-	-	-	-	88.8	1.75	4.82	-	-	-	-
	65.0	10.88	32.2	74.2	<0.01	<0.03	-	-	-	-	-	-	-	-	-
11	73.0	11.54	33.3	78.3	<0.01	<0.03	-	-	88.0	1.83	5.06	-	-	-	-
12	79.0	17.32	49.2	83.7	0.03	0.08	-	-	88.7	2.05	5.65	-	-	-	-
16	~ 70 ^a	5.71 ^a	16.6 ^a	-	-	-	-	-	87.9	2.23	6.16	-	-	-	-
	75.6	14.53	41.6	84.4	3.24	9.06	-	-	-	-	-	-	-	-	-
(a)	Transition solid II / solid I														
(b)	Transition in the supercooled region														
(c)	Transition not observed because of not sufficient supercooling														

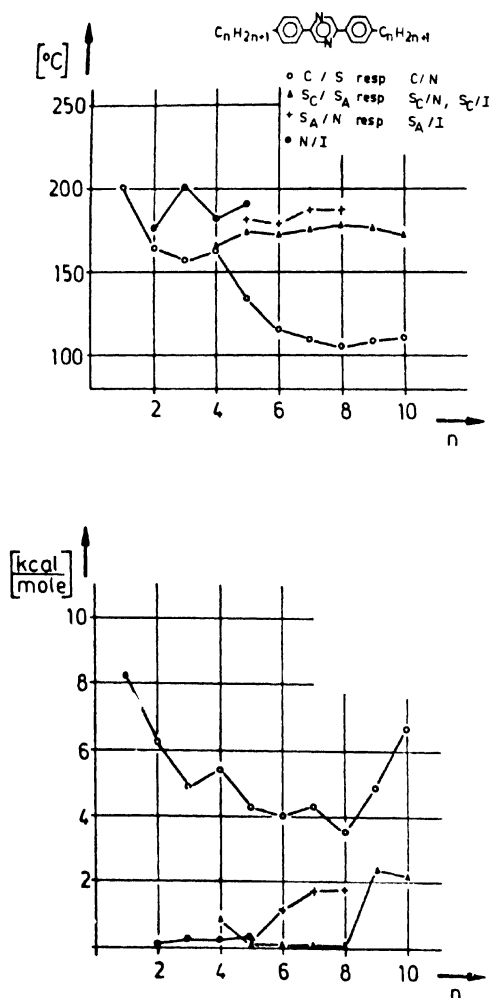
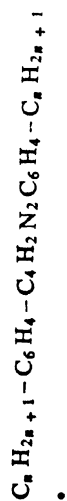


Figure 3 Di- n -alkylphenylpyrazines
top: transition temperatures; bottom: transition enthalpies

All transition enthalpies lie in the expected limits. As usual, the enthalpies of the transition S_A/N and N/I increase within the series. Possibly the enthalpies of the transition S_C/S_A show a slight decreasing trend, but the maximal error (see table 1) in this region does not allow an accurate statement of this fact. It is a little surprising that the clearing enthalpy (S_C/I) of the 9th member exceeds that of the 10th.

Table 4. 2,5-Bis-[4-*n*-alkylphenyl]-pyrazines^{23,25}

<i>n</i>	transition			transition			transition			isotropic		
	<i>t</i>	ΔH	ΔS	<i>t</i>	ΔH	ΔS	<i>t</i>	ΔH	ΔS	<i>t</i>	ΔH	ΔS
1	201.0	8.16	17.2	-	-	-	-	-	-	-	-	-
2	163.8	6.22	14.2	-	-	-	-	-	-	176.2	0.08	0.18
3	157.3	4.88	11.3	-	-	-	-	-	-	200.7	0.26	0.55
4	161.3	5.35	12.3	166.4	0.85	1.94	-	-	-	181.9	0.23	0.50
5	134.3	4.29	10.5	173.6	0.08	0.19	182.2	0.29	0.6	191.3	0.36	0.78
6	116.1	3.97	10.2	172.3	0.09	0.21	179.2	1.17	2.6	-	-	-
7	109.6	4.34	11.3	175.0	0.08	0.18	187.0	1.76	3.8	-	-	-
8	104.6	3.46	9.2	178.0	0.06	0.13	187.0	1.79	3.9	-	-	-
9	108.8	4.85	12.7	177.0	2.38	5.28	-	-	-	-	-	-
10	111.2	6.68	17.4	171.5	2.14	4.81	-	-	-	-	-	-

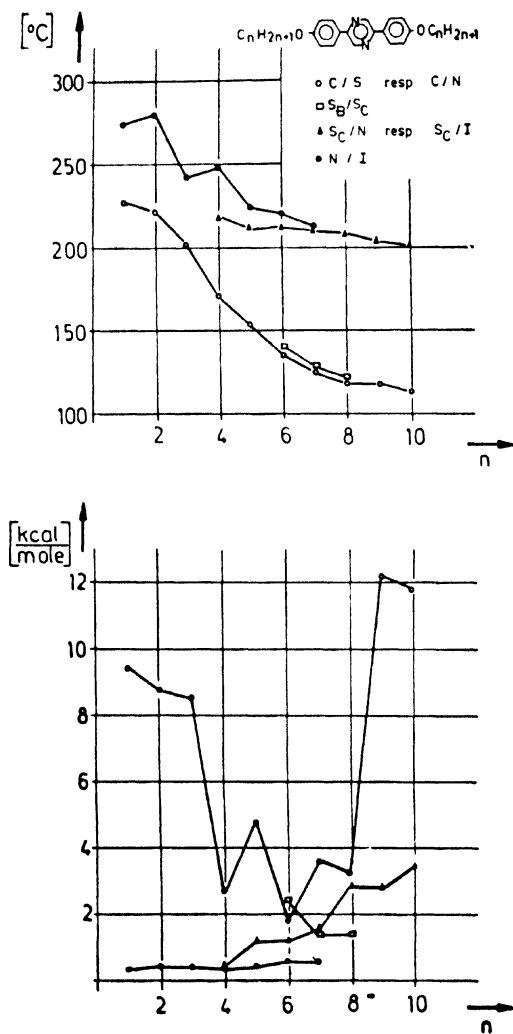
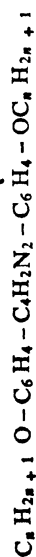


Figure 4 Di- n -alkoxyphenylpyrazines
top: transition temperatures; bottom: transition enthalpies

2,5-Bis-[4- n -alkoxyphenyl]-pyrazines

We have investigated 10 members of the homologous series of the 2,5-bis-[4- n -alkoxyphenyl]-pyrazines (table 5, figure 4). The substances have been prepared by Schubert *et al*²⁵. The polymorphism of this series has been reported by microscopy and miscibility properties²⁴.

Table 5. 2,5-Bis-[4-*n*-alkoxyphenyl]-pyrazines^{24,25}

<i>n</i>	solid	transition			transition			transition			isotropic		
		<i>t</i>	ΔH	ΔS	<i>S_B</i>	<i>t</i>	ΔH	ΔS	<i>S_C</i>	<i>t</i>	ΔH	ΔS	ΔS
1	228	9.40	18.8			-	-	-	-	274	0.32	0.6	
2	221	8.65	17.5			-	-	-	-	280	0.42	0.8	
3	~ 155 ^a	^b				-	-	-	-				
	202	8.49	17.9			-	-	-	-	242	0.45	0.9	
4	~ 155 ^a	1.41 ^a	3.5 ^a			-	-	-	-				
	170.3	2.69	6.0			-	-	-	218	0.46	0.38	0.7	
5	~ 56 ^a	^b				-	-	-	-				
	153.4	4.66	10.9			-	-	-	211	1.18	0.39	0.8	
6	~ 130 ^a	0.75 ^a	1.9 ^a										
	135.7	1.83	4.5			139.6	2.38	5.76	212	1.21	2.5	1.2	
7 ^c	~ 126.0	3.62	9.1			128.5	1.41	3.50	211	1.57	3.3	1.2	
8 ^c	118.8	3.17	8.1			121.1	1.37	3.46	209	2.93	6.1	-	
9	118.7	12.26	31.3			-	-	-	204	2.78	5.8	-	
10	~ 75 ^a	^b											
	113.0	11.81	30.5			-	-	-	201	3.47	7.3	-	

(a) Transition solid II/solid I

(b) Transition by calorimetry not observed

(c) These members also possess transitions in the solid state; their temperatures and enthalpies have not been determined

The melting enthalpies of the first 3 members are relatively high. The members 4 to 8 possess low melting enthalpies, which may be explained by the occurrence of additional transitions in the solid state. A regular trend is not observable.

The enthalpies of the transitions S_C/N and N/I increase regularly with increasing chain length. It is noteworthy that the transition enthalpies S_B/S_C possess uncommonly high values considering that it is as a smectic/smectic transition. This points to great structural differences between these types of phases. These enthalpy values decrease within the series. This unusual behaviour is to be discussed later.

Di-n-alkyl p-terphenyl-4, 4''-dicarboxylates

We have investigated the members 2 to 10 of the series of the di-*n*-alkyl *p*-terphenyl-4, 4''-dicarboxylates (table 6, figure 5). The substances have been prepared by Schubert *et al*²⁷. The polymorphism of the series has been established in former studies by microscopy, miscibility investigations²⁶ and x-ray diffraction²⁸. This series is of special interest because we have found in it for the first time smectic E-modifications.

The melting enthalpies increase with increasing chain length. If we add the enthalpy of the transition solid II/solid I of the member $n=2$ to its melting enthalpy, then the sum exceeds the melting enthalpy of the following member. This may be interpreted as the already mentioned exceptional characteristic of initial members of homologous series. Alternation of the melting enthalpies is not found.

The enthalpies of the transition S_A/I increase slightly within the series. Only the member $n=2$ has relatively too large a value. Also, this behaviour indicates the exceptional properties of the initial member of the series.

The enthalpies of the transition S_C/S_A show, as expected, very low values. For the hexylester the enthalpy is so low that the transition could not be detected by the DSC, but only by texture observation²⁶.

The smectics E are highly ordered states in comparison with smectic A²⁸. For this reason the relatively high transition enthalpy between these 2 types is not unexpected. It is to be noticed that the value from the ethyl to the propyl ester decreases. The butyl ester does not possess an E-modification. We will discuss this behaviour later.

4-n-Alkoxy-3'-subst.-biphenyl carboxylic acids

We have investigated 4 members of the series with the 3'-substituent $R = H$ and additionally, for the purpose of comparison, the hexadecyl derivatives with $R = Cl, Br, NO_2$ (table 7, figure 6). The substances have been prepared by the methods of Gray^{29,30}. The liquid crystalline

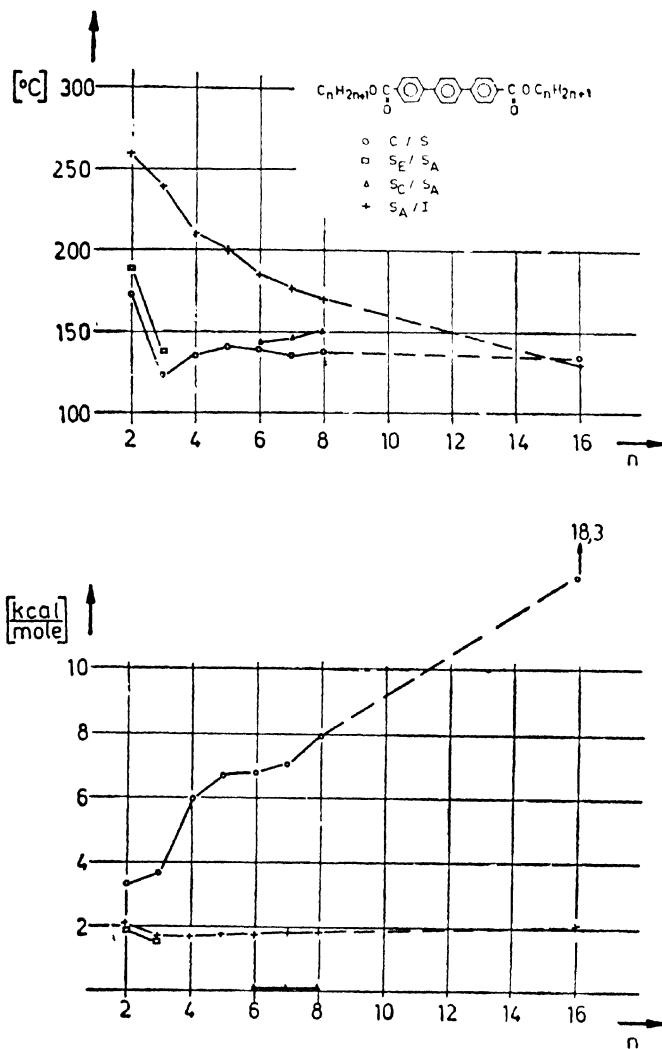
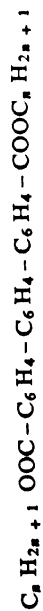


Figure 5 Di-*n*-alkyl terphenyldicarboxylates
top: transition temperatures; bottom: transition enthalpies

modifications of these compounds have already been classified by microscopy and miscibility investigations^{31,32}.

All compounds with $R = H$ possess enantiotropic transitions in the solid state with remarkably large enthalpies. The clearing enthalpies are extraordinarily high, higher than the melting enthalpies, even if we add to

Table 6. Di-*n*-alkyl *p*-terphenyl-4, 4'-dicarboxylates ^{26,27}

<i>n</i>	solid	transition			transition			transition			isotropic	
		<i>t</i>	ΔH	ΔS	<i>S_B</i>	<i>t</i>	ΔH	ΔS	<i>S_C</i>	<i>t</i>		ΔH
2	~	145 ^a	1.76 ^a	4.2 ^a								
		173.0	3.28	7.4		188.5	1.88	4.06				
3		122.0	3.73	9.4		137.1	1.49	3.64				
4		134.5	5.98	14.7								
5		139.4	6.74	16.3								
6		138.5	6.78	16.5								
7		135.3	7.05	17.3								
8		138.1	7.95	19.3								
16		134.1	18.3	44.9								

(a) Transition solid II / solid I

(b) Transition enthalpy very little, it could not be detected by DSC

(c) Transition in the unstable region (monotropic)

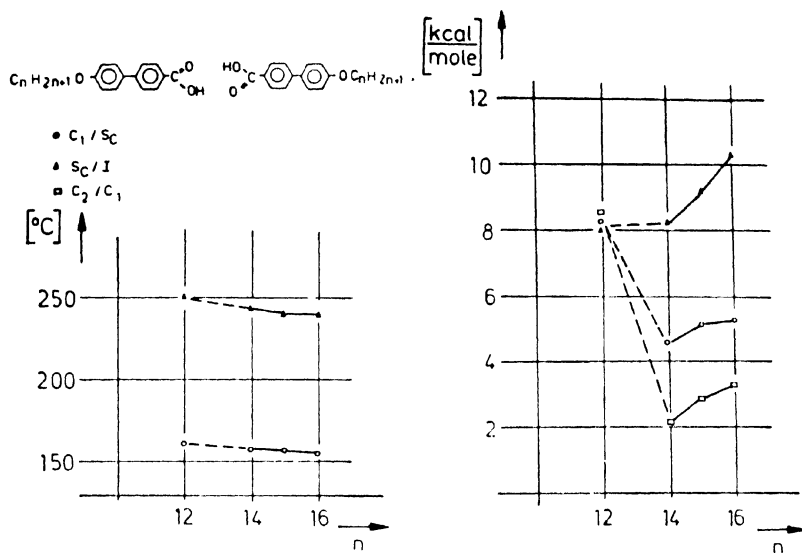
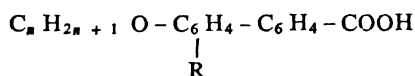


Figure 6 n -Alkoxy biphenyl carboxylic acids
left: transition temperatures; right: transition enthalpies

Table 7. 4- n -Alkoxy-3'-subst.-biphenyl carboxylic acids 29-32



n	• R	solid	transition			S_C	transition			isotropic
			t	ΔH	ΔS		t	ΔH	ΔS	
12	H		84.5 ^a	8.54	23.9	249		8.06	15.4	
			161.4	8.18	18.8					
14	H		153.2 ^a	2.16	5.1	244		8.24	15.9	
			156.9	4.56	10.6					
15	H		138 ^a	2.88	7.0	240		9.16	17.9	
			156.5	5.10	11.9					
16	H		140 ^a	3.28	7.9	241		10.24	19.9	
			154.9	5.32	12.4					
16	Cl		117.5	17.0	43.5	208		3.70	7.7	
16	Br		122 ^b	3.66	9.2	202		3.42	7.2	
			124.5	14.3	36.0					
16	NO ₂		126.8	19.76	49.4	-		1.44 ^c	3.1 ^c	

(a) Transition solid II/solid I

(b) Transition solid II/ S_C

(c) Sum of the values of the transitions S_C/S_D , S_D/S_A , S_A/I

these the enthalpies of the transition in the solid state. They show an increasing trend within the series.

In the compounds with substituents $R = Cl, Br, NO_2$ (see table 7) the melting enthalpies are only slightly influenced. But the clearing temperatures and the clearing enthalpies are dramatically decreased with increasing size of the substituents. It is to be assumed that this effect is due mainly to the steric effect of the substituents.

4. Discussion

4.1. General remark

It should be remarked generally that the discussion of ΔS instead of ΔH makes very little difference. The variation of absolute transition temperature is too small (even in extreme cases a ratio 1 : 2 is not exceeded) compared with the possible variation in transition enthalpies (variations of some orders of magnitude are possible).

4.2. Trends of transition enthalpies in homologous series

Melting enthalpies: The trend of the melting enthalpy in a homologous series commonly does not follow a general rule. But the following peculiarities are often to be observed:

- The melting enthalpies of the initial one or two members of a series show unusually high values. The same kind of irregularity exists for the melting and clearing temperatures. The clearing temperatures of the higher homologues alternate regularly, as is well known. The exceptional behaviour of the initial members is explained by the relatively great variation in the molecule by the addition of the first methyl group in comparison to the variation in the molecule by the addition of methylene groups in the higher homologues³⁹. The irregularity of the melting enthalpy may be caused by the same fact. It is to be expected also that the crystal structures of the initial members are different. This opinion is supported by the fact that these members often do not form mixed crystals, but in their phase diagrams there occur eutectics.
- In some series a regular trend is found only for several neighbouring members but not for the whole series. It is to be expected that, in these cases, only the members with a regular trend possess the same or very similar crystal structures. A regular trend may consist of alternating or increasing values of melting enthalpy.

Sometimes enantiotropic transitions in the solid state are found. Commonly the melting enthalpies in these cases are relatively low and do not correspond to the values of the neighbouring members. Mostly a better correspondence is obtained if the enthalpy of the solid/solid transition is added to the melting enthalpy.

Enthalpies of the transition N/I : Commonly the clearing enthalpies and entropies of the nematic phases show alternating behaviour and an increasing trend with increasing chain length^{1,11,14,15}.

The theory of Maier and Saupe³³ demands constant values for the order parameter at the clearing point and for ΔS and therefore cannot explain the strong alternation. It is known that successive members of a homologous series may exhibit an alternation in the order parameter⁴³. This fact can be explained by the molecular statistical theory of Chandrasekhar *et al.*^{44,45}. According to the few experimentally verified examples the potential energy function of this theory seems to have alternating values in a homologous series⁴⁵. Therefore the alternation of transition enthalpies may also be possibly explained by Chandrasekhar's theory.

The increasing trend of the clearing enthalpies of the higher members cannot be interpreted by the Maier-Saupe theory. This theory would suppose for such a behaviour increasing anisotropies of the polarizability. As is indicated by the decreasing clearing temperatures in most series, this is not the case. We assume that the tendency to form the smectic state, realized by the occurrence of cybotactic "smectic" groups in the nematic state, has a raising trend within a series and causes increasing clearing enthalpies. The nearer the transition S/N to the clearing point, the more pronounced is the elevated value of the clearing enthalpy.

The alternating and the increasing of the clearing enthalpies is shown in figure 7 for two well comparable series. The di-alkylazoxybenzenes¹ have clearing points between 32 and 71°C, the di-alkoxyazoxybenzenes between 122 and 168°C. The comparison of these series yields some interesting results. The enthalpies for the lower clearing alkyl compounds are higher than those of the higher clearing alkoxy compounds, and the increasing trend is more pronounced at the alkyl derivatives. Without doubt the alkoxy compounds possess much higher anisotropies of the polarizability than the alkyl ones. But at the strongly elevated clearing temperatures their alkyl chains are to be assumed much less stretched than in the alkyl derivatives, for it is known that the content of rotation isomers in alkyl chains is temperature dependent⁴⁰. This fact has two consequences: Firstly, because of the higher volume of the compounds with a higher content of rotation isomers, the intermolecular distance is increased with raising alkyl chain and the intermolecular energy is diminished. The observed enhancement of the clearing enthalpies in this series probably is due to smectic short range order. Secondly, in the lower clearing series there is an increase of the anisotropy of the polarizability with growing alkyl chain, and this effect supports the increasing tendency of the clearing enthalpies caused mainly by the quasi smectic short range order. This opinion is strongly supported by the generally raising clearing temperatures in the alkyl series and the decreasing clearing temperatures in the alkoxy series¹.

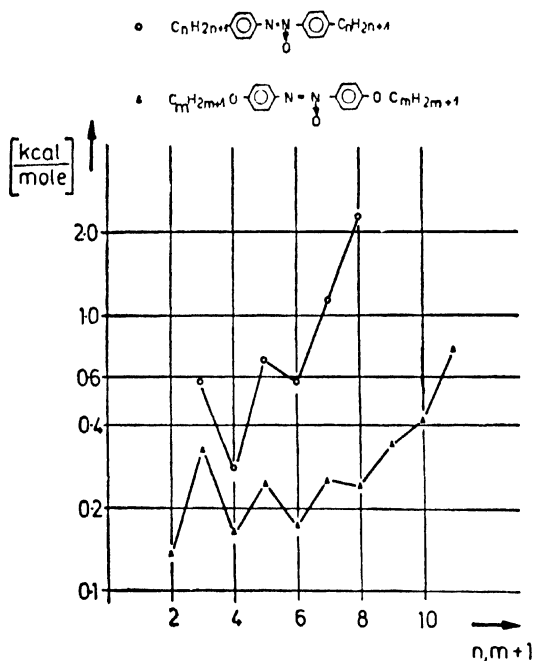


Figure 7 Enthalpies of transition N/I

Enthalpies of the transition S/I: The clearing enthalpies of the smectic modifications in a homologous series generally exhibit an increasing trend. Arnold¹⁸ has tried to calculate increments of the clearing enthalpy for the addition of a methylene group and has found the value $\Delta(\Delta H) = 0.36$ kcal/mole in the di-alkoxyazoxybenzenes. By comparison with other series it becomes clear that this is not a generally valid increment. Indeed, in the di-alkylazoxycinnamates now we have even a series with decreasing clearing enthalpies which could yield only a negative increment. Figure 8 shows the clearing enthalpies of the di-alkylazoxycinnamates and azoxy- α -methylcinnamates, the former having a decreasing trend starting from higher values, the latter an increase. We explain this fact analogous to the behaviour of the nematics. The azoxy- α -methylcinnamates because of the lateral methyl group have less densities than the cinnamates relative to the same temperature³⁵. Therefore in the lower members the intermolecular energy of the α -methylcinnamates is weaker than for azoxycinnamates. Except the relative high clearing points of the lower members, the α -methylcinnamates possess clearing points below 100° C, while the azoxycinnamates up to the highest members show clearing points above 130° C. Therefore for instance the undecyl ester of the azoxy- α -methylcinnamates has higher densities than the corresponding azoxycinnamate and the relation of their clearing enthalpies is explainable. This

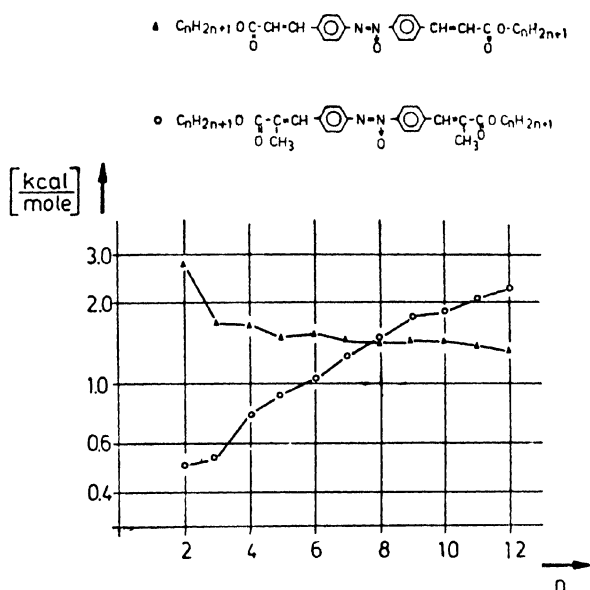


Figure 8 Enthalpies of the transition S_A/I
For $n = 2, 3$: $0 = \text{sum of } S_A/N + S_A/I$

trend in the series may be supported by a faster decrease of the anisotropy of the polarizability in the azoxycinnamates. Although no molecular statistical theory of the smectic state is known it is to be assumed that the anisotropy of the polarizability plays a comparable role as for the nematic state.

A remarkable decrease of the clearing enthalpies with growing lateral substituent is clearly to be seen in the case of the 3'-substituted 4'-alkoxybiphenyl carboxylic acids (table 7). This fact supports the opinion explained above.

Enthalpies of transitions within the liquid crystalline state: Generally the enthalpies of transitions within the liquid crystalline state show an increasing trend with growing alkyl chain^{1,3,7,8,11,15,42}. But in some special cases we have found a decrease (e.g., transition S_B/S_C in table 5, transition S_B/S_A in table 6; for some further examples see Marzotko¹⁴).

We try to give an interpretation for this behaviour. Figure 9 shows the temperature dependence of the free energies F of say, a low temperature modification (curve 1) and high temperature modification (curve 2). The intersection point corresponds to the transition temperature. The slopes of the curves are :

$$\left(\frac{\partial F}{\partial T} \right)_{P(1)} = -S_{(1)} \quad (2)$$

$$\left(\frac{\partial F}{\partial T} \right)_{P(2)} = -S_{(2)} \quad (3)$$

The difference of eqs. (3) and (2) yields :

$$\left(\frac{\partial F}{\partial T} \right)_{P(2)} - \left(\frac{\partial F}{\partial T} \right)_{P(1)} = -S_{(2)} + S_{(1)} = -\Delta S \quad (4)$$

At the transition point we have :

$$\Delta S = \frac{\Delta H}{T}$$

This means that the transition entropy or the transition enthalpy is measured by the difference of the slopes of the F-T curves. Modifications with similar properties and therefore similar temperature dependence of F give low transition enthalpies ("low relative stability", compare curves 2 and 3 in figure 9). In the case of greater differences in the temperature dependence of F also more pronounced transition enthalpies occur ("high relative stability", compare curves 1 and 3 in figure 9).

4.3. Energetic aspects of polymorphism

By investigation of the miscibility properties Sackmann and Demus³⁶ have classified the liquid crystalline modifications of a great number of substances into one nematic or cholesteric and till now 7 smectic groups. The modifications of the different groups follow the rule of the temperature sequence. According to this rule the modifications occur only in the following sequence with rising temperature :

$$S_B \ S_B \ S_C \ S_D \ S_A \ N \ I$$

Till now no substance with all these phases is known. The different variants of polymorphism arise by the lack of one or more of these phases. In reality for instance, the following variants exist :

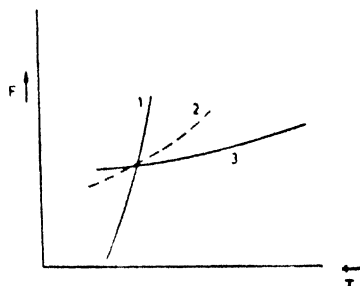


Figure 9 Temperature dependence of free energies of different phases.

(α)	S_B	S_B		S_A		I
(β)		S_B	S_C	S_A	N	I
(γ)			S_C	S_D	S_A	N I

The rule of the temperature sequence of the liquid crystalline modifications may be explained in terms of the fact that there occurs a stepwise decrease of the state of order at each transition³⁶. Therefore it is not to be expected that a less ordered state will change with rising temperature to a more ordered state.

Each transition will be connected with a transition enthalpy. Suppose the magnitude of the steps from one state of order to another are not equal and depend on their place in the above-mentioned sequence, we should expect characteristic values of transition enthalpies for each type of transition. With the aid of figure 10 (table 8) we are able to test this assumption. Figure 10 shows the limits of the enthalpies of the respective transitions, observed in the cited literature.

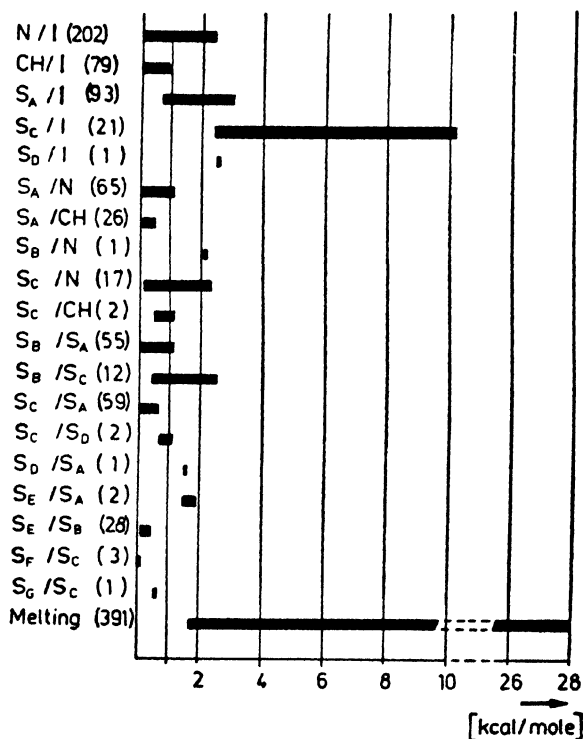


Figure 10 Enthalpies of transitions for different types of liquid crystals.

Table 8.

	Transition	Number of cases	Transition Enthalpy (kcal/mole)
1)	N/I	202	0.02 - 2.30
	CH/I	79	0.02 - 0.9
	S _A /I	93	0.7 - 3.0
	S _C /I	21	2.4 - 10.2
	S _D /I	1	2.5
	S _A /N	65	0.05 - 1.10
	S _A /CH	26	0.1 - 0.46
	S _B /N	1	2.11
	S _C /N	17	0.16 - 2.30
	S _C /CH	2	0.5 - 1.1
	S _B /S _A	55	0.1 - 1.1
	S _B /S _C	12	0.44 - 2.5
	S _C /S _A	59	<0.01 - 0.66
	S _C /S _D	2	0.68 - 1.0
	S _D /S _A	1	1.6
	S _B /S _A	2	1.49 - 1.88
	S _B /S _B	28	0.12 - 0.44
	S _F /S _C	3	0.04 - 0.12
	S _G /S _C	1	0.56
	Melting	391	1.7 - 28
References (1-14)			

We see that the melting enthalpy in most cases exceeds strongly the other transition enthalpies with the exception of only a very small number of S_C/I transitions.

The N/I and CH/I transitions lie in the same region according to the fact that the torsion of a nematic phase to a cholesteric one demands only very small amounts of energy⁴¹.

The clearing enthalpies of S_A, S_C and S_D generally lie in a higher region than nematic clearing enthalpies, while the transitions S/N in several cases are very low. This is in good agreement with the higher order of the smectic state compared to the nematics.

There are some transitions with commonly extreme low enthalpies, namely S_C/S_A and S_F/S_C. For the S_C/S_A transitions the enthalpies in some cases

are too little to be detected by the DSC 1-B. From x-ray investigations we know that the structures of these phases differ only very slightly³⁶.

Also transition enthalpies between the highly ordered smectic phases S_B and S_B have low values. But if high ordered smectic phases change to the relatively low ordered S_C or S_A phases, the corresponding enthalpies lie in a higher region, for instance S_B/S_A , S_B/S_C , S_B/S_A .

As is to be seen clearly, the transition enthalpies of one kind of transition may vary considerably. This variation depends on the molecular structure in general and especially on its position in the homologous series. Some of these connections between molecular structure and transition enthalpies have already been mentioned above.

Considering all these facts we may say that calorimetry is a valuable help to detect polymorphism and can yield some clues to phase classification. But an exact classification on the basis of calorimetry alone is not possible.

4.4. Transition enthalpies and density changes

Till now only for a very limited number of substances have the density changes at the transitions been determined^{35,37} (literature cited in ref. 38). As far as can be judged from these limited number of cases, we can say that transitions with high (or low) enthalpies show also high (or low) density changes.

Acknowledgement

We are indebted to Dr F Fröhlich for the permission to use the calorimeter, to Prof Dr H Schubert for giving a large number of substances and to Prof Dr H Sackmann for stimulating discussions and his interest in this work.

References

- 1 VAN DER VEEN J, DE JEU W H, WANNINKHOF M W M and TIENHOVEN C A M *J. Phys. Chem.* **77** 2153 (1973)
- 2 GRAY G W and HARRISON K J *Symposia of the Faraday Society* No. 5 54 (1971)
- 3 COATES D, HARRISON K J and GRAY G W *Mol. Cryst. Liquid Cryst.* **22** 99 (1973)
- 4 SMITH G W and GARDLUND Z G *J. Chem. Phys.* **59** 3214 (1973)
- 5 BARRALL II E M, BREDFELDT K E and VOGEL M J *Mol. Cryst. Liquid Cryst.* **18** 195 (1972)
- 6 LECLERCQ M, BILLARD J and JACQUES J *Mol. Cryst. Liquid Cryst.* **8** 367 (1969)
- 7 ELSEER W and ENNULAT R D *J. Phys. Chem.* **74** 1545 (1970)
- 8 YOUNG W R, HALLER J and AVIRAM A *IBM J. Res. Develop.* **15** 41 (1971)
- 9 BARRALL II E M *Anal. Calorim.* **2** 121 (1970)
- 10 ENNULAT R D and BROWN A J *Mol. Cryst. Liquid Cryst.* **12** 367 (1971)
- 11 ARNOLD H, DEMUS D, KOCH H J, NELLES A and SACKMANN H Z. *Phys. Chem.* **240** 185 (1969)

- 12 DEMUS D, DIELE S, KLAPPERSTÜCK M, LINK V and ZASCHKE H *Mol. Cryst. Liquid Cryst.* **15** 161 (1971)
- 13 DEMUS D, KLAPPERSTÜCK M, RURAINSKI R and MARZOTKO D *Z. Phys. Chem.* **246** 385 (1971)
- 14 MARZOTKO D *Dissertation (Halle)* 1973
- 15 ARNOLD H *Z. Phys. Chem.* **226** 146 (1964)
- 16 ARNOLD H, EL-JAZAIRI E B and KÖNIG H *Z. Phys. Chem.* **234** 401 (1967)
- 17 ARNOLD H and ROEDIGER P *Z. Phys. Chem.* **239** 283 (1968)
- 18 ARNOLD H, JACOBS J and SONNTAG O *Z. Phys. Chem.* **240** 177 (1969)
- 19 DEMUS D and SACKMANN H *Z. Phys. Chem.* **222** 127 (1963)
- 20 PELZL G, DEMUS D and SACKMANN H *Z. Phys. Chem.* **238** 22 (1968)
- 21 ARNOLD H and SACKMANN H *Z. Elektrochem. Ber. Bunsenges* **63** 1171 (1959)
- 22 PELZL G and SACKMANN H *Symposia of the Faraday Society* No. **5** 68 (1971)
- 23 DEMUS D, KÖLZ K H and SACKMANN H *Z. Phys. Chem.* **249** 217 (1972)
- 24 DEMUS D, SACKMANN H and SALFNER R *Wiss. Z. Univ. Halle* **22** (2) 143 (1973)
- 25 SCHUBERT H, HACKER R and KINDERMANN K *J. Prakt. Chem.* (4) **37** 12 (1968)
- 26 DEMUS D, KÖLZ K H and SACKMANN H *Z. Phys. Chem.* **252** 93 (1973)
- 27 SCHUBERT H, LORENZ H J, HOFFMANN R and FRANKE F *Z. Chem.* **6** 337 (1966)
- 28 DIELE S, SACKMANN H and BRAND P *Mol. Cryst. Liquid Cryst.* **16** 105 (1972)
- 29 GRAY G W, HARTLEY J B and JONES B *J. Chem. Soc.* 1412 (1955)
- 30 GRAY G W, JONES B and MARSON F *J. Chem. Soc.* 393 (1957)
- 31 DEMUS D, KUNICKE G, NEELSEN J and SACKMANN H *Z. Phys. Chem.* **225** 71 (1974)
- 32 DEMUS D, KUNICKE G, NEELSEN J and SACKMANN H *Z. Naturforsch.* **23a** 84 (1968)
- 33 MAIER W and SAUPE A *Z. Naturforsch.* **13a** 564 (1958); **14a** 882 (1959); **15a** 287 (1960)
- 34 CHISTYAKOV I G and CHAIKOVSKY V M *Mol. Cryst. Liquid Cryst.* **7** 269 (1969)
- 35 DEMUS D and RURAINSKI R *Z. Phys. Chem.* **253** 53 (1973)
- 36 SACKMANN H and DEMUS D *Mol. Cryst. Liquid Cryst.* **21** 239 (1973)
- 37 PRICE F P and WENDORFF J H *J. Chem. Phys.* **75** 2839 (1971); **75** 2849 (1971); **76** 276 (1972)
- 38 SACKMANN H and DEMUS D *Fortschr. Chem. Forsch.* **12** 349 (1969)
- 39 GRAY G W *Molecular Structure and the Properties of Liquid Crystals* (Academic Press, London, New York) 1962
- 40 STUART H A *Molekülstruktur* (Springer-Verlag, Berlin, Heidelberg, New York) (1967)
- 41 SAUPE A *Angew. Chem.* **80** 99 (1968)
- 42 DUREK D, BATURIC-RUBCIC J, MARCELJA S and DOANE J W *Phys. Lett.* **A43** 273 (1973)
- 43 CHISTYAKOV I G and CHAIKOVSKY V M *Mol. Cryst. Liquid Cryst.* **7** 269 (1969)
- 44 CHANDRASEKHAR S and MADHUSUDANA N V *Acta Crystallogr.* **A27** 303 (1971)
- 45 CHANDRASEKHAR S, MADHUSUDANA N V and SHUBHA K *Symposia of the Faraday Society* No. **5** 26 (1971)

DISCUSSION

Saupe: Can the high transition enthalpies of 8–9 kcal/mole for the smectic C–isotropic liquid transitions in the 4-*n*-alkoxybiphenyl–carbolic acid series be due to a change in the degree of molecular association by hydrogen bonds? What other reason would you suggest for the unusually large entropies?

Demus: By means of infrared spectroscopy we have investigated alkoxybenzoic acids. There is no remarkable change of dissociation at the

clearing point. We believe that this should be the same for alkoxy-biphenyl carboxylic acids. Of course, there is a temperature dependence of dissociation, also in the mesomorphic state. This is indicated for instance by the anomalous temperature dependence of dielectric anisotropy, as we have found for some members of this homologous series.

The high clearing enthalpy might be due to the large aromatic part of the double molecules which are comparable to quinquephenyl systems. This should not be due to a remarkable extent to dissociation effects, for in the case of 3'-substituted alkoxybiphenyl carboxylic acids we have the usual low values for the clearing enthalpies.

Schnur: You have shown enthalpy of transition values for the smectic A-N transition. Are you positive that this transition is of first order? Could your experiment tell the difference between an anomalous first order transition and a λ type second order phase transition?

Demus: We have used the DSC method. This method yields λ -curves also for melting of ordinary pure solids. Therefore this method does not seem suitable for investigations concerning this kind of transition. But considering other facts, for instance the validity of Gibb's phase rule, we believe that all transitions with liquid crystals so far investigated are of the first order.

Magnetic properties of smectic mesophases

H GASPAROUX, F HARDOUIN and M F ACHARD

Centre de Recherches Paul Pascal. Université de Bordeaux I-Domaine
Universitaire - 33405 Talence (France)

Abstract. After a description of the two experimental methods that we have used to determine the magnetic anisotropy $\Delta\chi$ of some smectic phases, we present and discuss the results obtained on two smectic A samples. First experiments concerning a smectic C material are also reported.

Introduction

In the first part of this paper we describe briefly the two experimental techniques that we have used in order to obtain the magnetic properties of a smectic phase. The first is the Faraday method and the second is an adaptation of Krishnan's flip angle method.

We present and discuss in the second part, the results which characterize two different smectic A materials. In the last part we report a preliminary experiment on a smectic C which shows the possibility of our methods,

1 Experimental techniques

The magnetic properties of these materials have been investigated by two different methods: both of them allow us to determine the diamagnetic anisotropy $\Delta\chi$ of a nematic or a smectic mesophase.

1. Evaluation of the diamagnetic anisotropy ($\Delta\chi$) from a static magnetic susceptibility measurement using the Faraday method

We define χ_{\parallel} or χ_{\perp} as the magnetic susceptibility measured in the direction parallel or perpendicular to the magnetic field.

SOLID AND LIQUID STATES

When the solid state is a microcrystalline powder without any preferred orientation, the χ_{\parallel} value is identical to the mean magnetic susceptibility $\bar{\chi}$ of the material. If the considered solid is magnetically isotropic, the χ_{\parallel} values (that is to say the experimental value in the Faraday method) which characterize the solid and the liquid phases are not only identical but equal to the mean magnetic susceptibility $\bar{\chi}$.

NEMATIC AND SMECTIC PHASES

The macroscopic magnetic anisotropy, *i.e.* $\Delta\chi = \chi_{\parallel} - \chi_{\perp}$, can be easily deduced from the χ_{\parallel} measurement since it is known that

$$\Delta\chi = \frac{3}{2} (\chi_{\parallel} - \bar{\chi}) \quad (\text{if } \Delta\chi > 0)$$

This quantity is proportional to the order parameter of the considered phase. The experimental set-up currently used and the interpretation of the measurements have been previously described for different studies concerning the cholesteric and the nematic mesophases¹⁻³.

2. Direct magnetic anisotropy determination of mesophases

NEMATIC PHASES

The theoretical study of the molecular motion induced in nematic phase by a rotating magnetic field has been developed already⁴. We want only to recall that the analysis of the variation in the moment transmitted to the cup, which depends on the frequency ω of the rotated magnetic field H_0 , can furnish an evaluation of the magnetic anisotropy.

At each rotational frequency ω a stationary state occurs and for a critical frequency ω_c , defined as the maximum value of the transmitted moment, it can be written that

$$\frac{M}{V} = \frac{1}{2} \Delta\chi H_0^2$$

where V is the sample volume and M is the magnetic moment.

We have shown⁴ that the experimental value of $\Delta\chi$ deduced from this method is always about 15 to 20% lower than the real $\Delta\chi$ value; we have explained the reasons for such an under-evaluation. Besides it must be pointed out that it is a good method for the determination of the twist viscosity γ_1 in a nematic phase^{5, 6}.

SMECTIC PHASES

The behaviour of the smectic phases that we have investigated does not resemble that of the nematic phases. We have found for example that the Smectic A phases behave as single crystals in the presence of a strong enough magnetic field. The sample presents a single domain which perfectly follows the magnetic field rotation with an increasing phase difference due to the mechanical torque of the quartz wire suspension.

The crystal orientation in the field is adjusted so that the largest algebraic susceptibility in the plane of rotation lies in the direction of the field. If the magnet is turned through an angle α , the crystal will turn through a smaller angle ϕ . If the magnet rotation is continued, when $\alpha - \phi = \pi/4$ the crystal will suddenly flip around to a new equilibrium position. The usual name of this method is: "Krishnan's flip-angle method".

Following the standard procedure we can obtain the diamagnetic anisotropy $\Delta\chi$ of the sample by the relation :

$$\frac{(\Delta\chi)_T}{(\Delta\chi_{\text{ref}})_T} = \frac{(\alpha - \frac{\pi}{4}) m^{-1}}{(\alpha_{\text{ref}} - \frac{\pi}{4}) m_{\text{ref}}^{-1}}$$

$\Delta\chi_{\text{ref}}$: magnetic anisotropy of the reference

α : critical angle for the sample

α_{ref} : critical angle for the reference

m : weight

This measurement, though not absolute, is very accurate, the relative accuracy being about 0.1%. The experimental set-up that we have used is similar to that described in a previous publication⁴ but the magnetic field strength was increased to 21 kgauss by using an electro-magnet.

II Magnetic properties of the smectic A phases

1. Determination of χ_{\parallel} and $\Delta\chi$ by the faraday method

MAGNETIC PROPERTIES OF P-CYANO BENZILIDENE-P'OCTYL OXYANILINE (CBOOA)

In figure 1 are presented the χ_{\parallel} values for a large temperature range which covers the solid smectic, nematic and liquid phases⁸. Cooling in

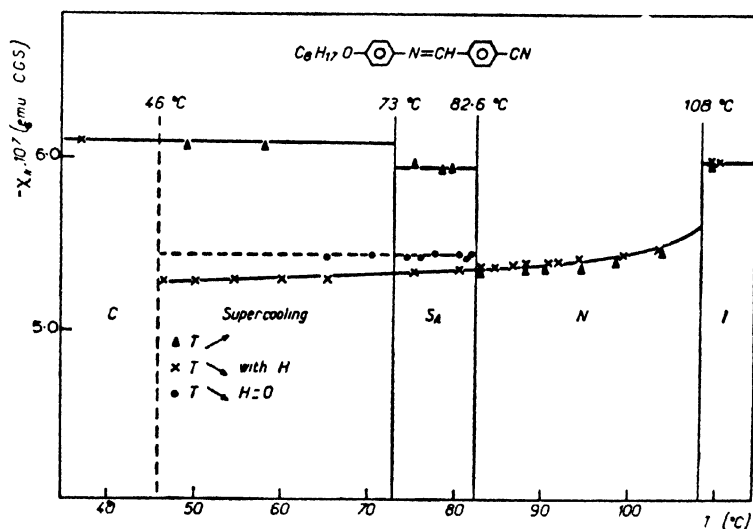


Figure 1 Thermal variation of the magnetic susceptibility of p-cyano-benzilidene-p'-octyl-oxyaniline (CBOOA)

the presence of the magnetic field allows us to get a well ordered smectic phase, completely transparent, which presents a large supercooling temperature range. It might be possible however that the order could be improved by application of a stronger and more homogeneous magnetic field as we will show later. Such a situation is precluded by the Faraday method because a large magnetic field gradient is necessary.

If the cooling down from the isotropic phase is done without the magnetic field several defects appear at the nematic-smectic A transition which are responsible for the slight increase of $\chi_{||}$ at this transition. Finally if after the magnetic susceptibility determination of the solid, the thermal variation of $\chi_{||}$ is observed for an increasing temperature, the determined order of the smectic phase is never good. It is necessary to go up to the S_A -N transition to obtain an orientation induced by the magnetic field.

From the experimental curve (figure 1), obtained when the temperature is going down from the liquid state in the presence of the magnetic field, we have established the thermal variation of the diamagnetic anisotropy $\Delta\chi$ (figure 2).

This result shows that, when the temperature of this material decreases, the order parameter increases continuously in the nematic and smectic states; there is no discontinuity through $N \rightarrow S_A$ transition since this is a second order transition¹.

MAGNETIC PROPERTIES OF P-OCTYLOXYBENZOATE P'-PENTYLBNZENE

The temperature range where the smectic A phase exists is very small (56.2 – 56.5°C) but it can be largely extended by supercooling. In such experimental conditions the liquid crystal is smectic A between 44°C and 56.5°C . The thermal variation of $\chi_{||}$ and $\Delta\chi$ have been investigated (figures 3 and 4). It must be noted that the curve $\chi_{||} = f(T)$ (see figure 3) exhibits a discontinuity at the nematic-smectic A transition even when the magnetic field is applied during the overall cooling process

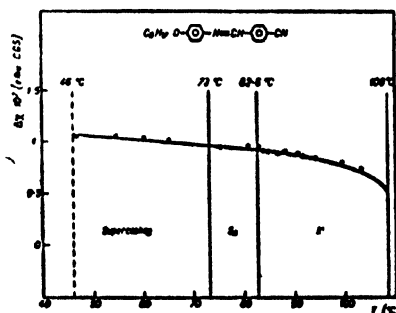


Figure 2 Thermal variation of the diamagnetic anisotropy of CBOOA.

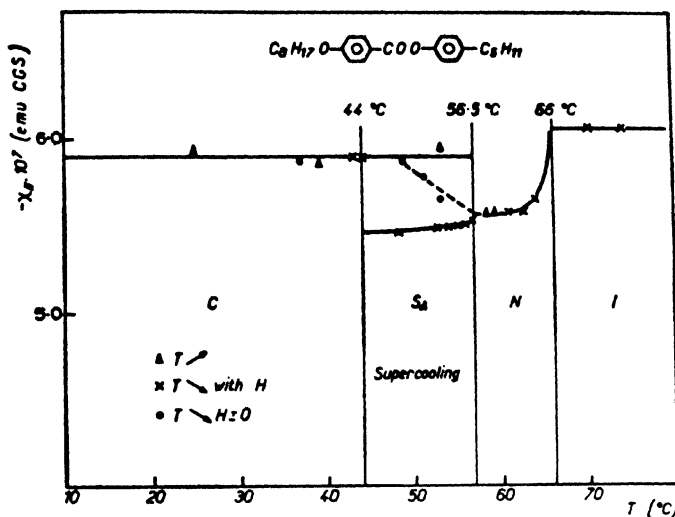


Figure 3 Thermal variation of the magnetic susceptibility of p-octyloxybenzoate-p'-pentylbenzene.

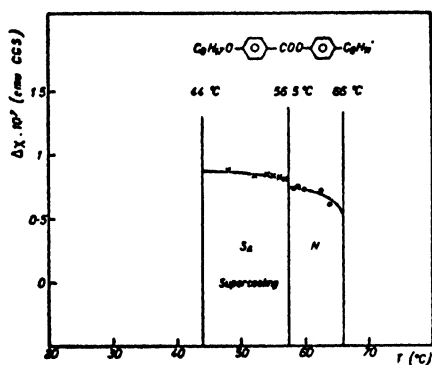


Figure 4 Thermal variation of the diamagnetic anisotropy of p-octyloxybenzoate-p'-pentylbenzene.

This discontinuity is, again, found on the curve $\Delta\chi = f(T)$ (see figure 4) and gives supplementary argument for a transition of the first order type as it has been shown for some other compounds.

2. $\Delta\chi$ direct determination in the smectic phase.

As previously explained¹ the determination of $\Delta\chi$ in the nematic phase furnishes an incorrect evaluation of this quantity; we report therefore

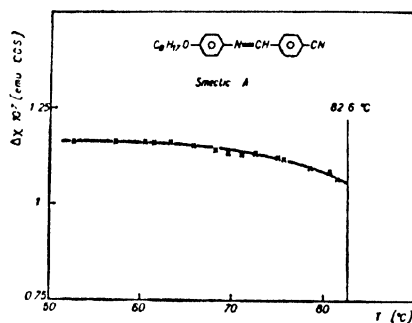


Figure 5 Direct measurement of diamagnetic anisotropy in the Smectic A phase of CBOOA.

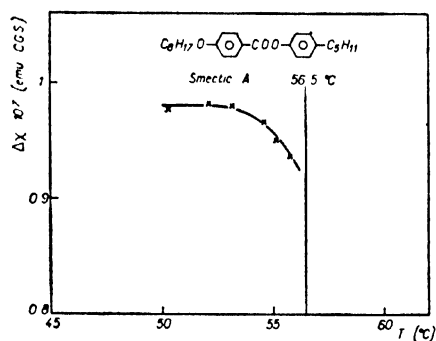


Figure 6 Direct measurement of diamagnetic anisotropy in the Smectic A phase of the p-octyl-oxybenzoate-p'-pentylbenzene.

the results obtained in the smectic phase only. In figure 5 the results obtained in CBOOA sample by using Krishnan's critical angle method are reported. Similar experiments done with the p-octyloxybenzoate-p'-pentylbenzene are summarized in figure 6.

3. Analysis and discussion of the experimental data

COMPARISON BETWEEN THE TWO EXPERIMENTAL METHODS

By comparing on one hand figures 3 and 5 and on the other figures 4 and 6 we ascertain that the thermal variation curves of $\Delta\chi$ are very similar whatever the experimental method used. It is necessary to emphasize however that the experimental values got from Krishnan's method are about 5 to 7% higher than those determined by Faraday's method.

Two reasons might be proposed to explain this discrepancy :

The magnetic field strength used for the direct determination of $\Delta\chi$ ($H = 9.5$ kgauss) is stronger than the one applied in the Faraday method ($H = 5$ to 7 kgauss).

Furthermore, only in Krishnan's method the magnetic field applied to the sample is homogeneous. These two remarks allow us to explain the fact that the measured diamagnetic anisotropy is larger when the second method is used (figures 5 and 6). In such experimental conditions the magnetically induced orientation of the molecules is more effective than in the Faraday's method.

VARIATION OF THE ORDER PARAMETER IN THE NEIGHBOURHOOD OF THE SECOND ORDER TRANSITION $S_A \rightarrow N$

To account for such a transition, a theory has been recently proposed by Kobayashi⁹ and McMillan¹⁰ independently; this is a microscopic model which starts from an interaction potential between the molecules. By this way two order parameters are introduced, the first one indicating the orientational order β and the second one the translational order σ . For a smectic A phase the diamagnetic anisotropy $\Delta\chi$ is proportional to the orientational order parameter β .

Our experimental results obtained in CBOOA sample are in good agreement with McMillan's theory which predicts a continuous variation of β through a transition $S_A \rightarrow N$. It must be noted that with our experimental accuracy we do not detect any slope discontinuity at the transition temperature as it has been shown recently by Cabanne and Clark¹¹ who have investigated the same material by nuclear quadrupole resonance. A further investigation of the curve $\Delta\chi = f(T)$ determined from high magnetic field measurements might allow us to clear up this point.

As proposed by Cabanne and Clark¹¹ for CBOOA a similar discussion can be carried out for the present result. The existence of a quasi second order transition $S_A \rightarrow N$ in CBOOA has already been shown in other materials by several methods^{6, 12-14}; this is a confirmation of de Gennes' prediction¹⁵. Our study shows however that in agreement with other observations, it seems difficult to generalize it to all $S_A \rightarrow N$ transitions.

III Study of smectic C phases

We only report our first results and the difficulties that we have met during these experiments. The material that we have studied is bis-(4'-n decyloxybenzal)-2-chloro-1,4-phenylenediamine (DOBCP).

1. $\Delta\chi$ and $\chi_{||}$ measurements with the Faraday balance

In figure 7 the thermal variation of $\chi_{||}$ is presented. Unlike the smectic A materials cooling in the presence of the magnetic field does not allow us

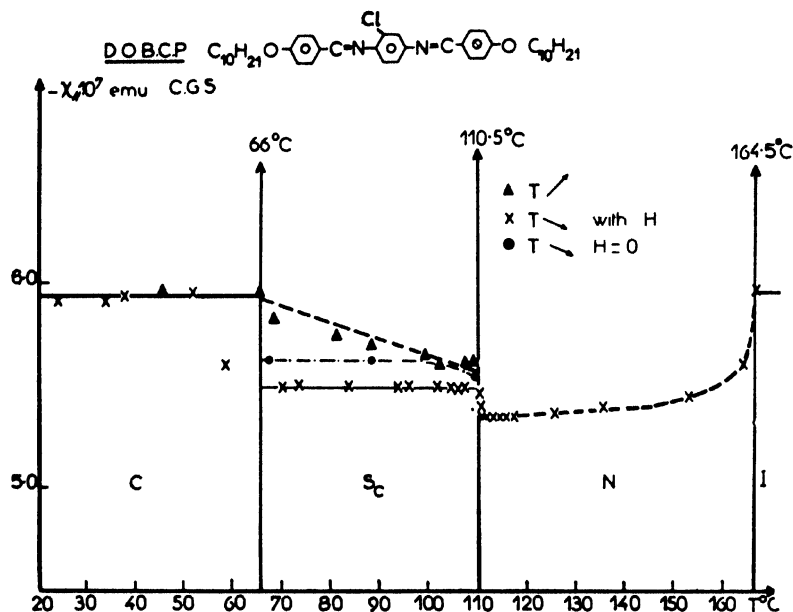


Figure 7 Thermal variation of the magnetic susceptibility of bis- (4'-n decyloxy-benzal) 2 chloro-1,4-phenylenediamine (DOBCP).

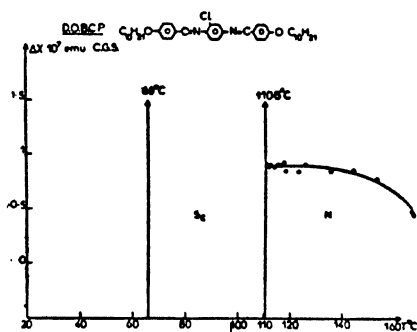


Figure 8 Thermal variation of the diamagnetic anisotropy in the nematic phase of DOBCP.

to get a well ordered smectic C phase. We can however observe that the application of a magnetic field does improve the order.

Whether a magnetic field is applied or not, there appear several defects at the nematic-smectic C transition; it is only possible to give a variation of $\Delta\chi$ in the nematic domain (figure 8), but the same evaluation in the smectic C phase cannot be done.

As already shown by Wise *et al.*¹⁶ it is necessary to have a magnetic field greater than 10 kG to obtain a good orientation in this material.

2. Measurements of $\Delta\chi$ by rotating field method

If the sample is slowly cooled in the presence of a magnetic field greater than 14 kG the molecular director will remain parallel to the field in the smectic C phase as shown by Wise *et al.*¹⁶. But such a preparation does not lead to a single crystal with the smectic layers parallel throughout the sample. As illustrated by these authors "the only constraint on the smectic C layers is that they are formed such that the molecules within them are tilted at the same common angle". The planes can have an infinite number of directions about the magnetic field direction. The interpretation of the rotating field method used for smectic A samples is not adequate: we are attempting to develop a model to explain the behaviour of a smectic C sample in a rotating field. As a first step, we plan to prepare a single monodomain in order to make a $\Delta\chi$ determination by the classical method as we have used for the study of smectic A.

In conclusion we can say that it is possible to make diamagnetic anisotropy measurements on smectic A samples either by Faraday's method or by the rotating magnetic field method. In this last method the smectic A phase behaves like a single crystal. However in the case of smectic C phase the interpretation of magnetic measurements is not so straightforward; our first results do not allow us to make a good $\Delta\chi$ determination for such phases.

References

- 1 REGAYA B and GASPAROUX H *C.R. Acad. Sci.* **232** 724 (1971)
- 2 GASPAROUX H, REGAYA B and PROST J *C.R. Acad. Sci.* **272** 1168 (1971)
- 3 REGAYA B, GASPAROUX H and PROST J *Rev. de Phys. Appl.* **7** 83 (1972)
- 4 GASPAROUX H and PROST J *J. de Phys.* **32** 953 (1971)
- 5 PROST J and GASPAROUX H *Phys. Lett.* **36A** 245 (1971)
- 6 HARDOUIN F, ACHARD M F and GASPAROUX H *Solid State Commun.* (to be published)
- 7 KRISHNAN K S and BANERJEE S *Phil. Trans. Roy. Soc.* **A234** (1935)
- 8 HARDOUIN F, ACHARD M F and GASPAROUX H *C.R. Acad. Sci.* **277** 551-554 (1973)
- 9 KOBAYASHI K K *J. Phys. Soc. Japan* **29** 101 (1970); *Mol. Cryst. Liquid Cryst.* **13** 137 (1971)
- 10 MCMILLAN *Phys. Rev.* **A4** 1238 (1971) *Phys. Rev.* **A6** 936 (1972)
- 11 CABANNE B and CLARK W G *Solid State Commun.* **13** 129 (1973)
- 12 LEGER L *Phys. Lett.* **44A** 535 (1973)
- 13 DELAYE N, RIBOTTA R and DURAND G *Phys. Rev. Lett.* **31** 443 (1973)
- 14 CHEUNG L, MEYER R B and GRULER M *Phys. Rev. Lett.* **31** 349 (1973)
- 15 DE GENNES P G *Solid State Commun.* **10** 753 (1973)
- 16 WISE R A, SMITH D H and DOANE J W *Phys. Rev.* **A7** 1366 (1973)

DISCUSSION

Leslie: When measuring the difference between the susceptibilities of a nematic using a rotating magnetic field, you assume that the angle between the field and the anisotropic axis attains the theoretically predicted maximum of 45° . Would it be possible to confirm this by some means?

Gasparoux: We have not attempted to verify this. I think that it is perhaps possible to find an answer to your question by optical observation.

Birendra Bahadur: What are the relative and absolute accuracies in your measurements?

Gasparoux: In the Faraday method the accuracies are respectively 1% and 3% and in the rotating magnetic field method the accuracies are approximately of the order of 0.1% and 1%.

Experimental determination of the twist elastic constant of nematic liquid crystals

N V MADHUSUDANA, P P KARAT and
S CHANDRASEKHAR

Raman Research Institute, Bangalore 560006.

Abstract. The Freedericksz transition associated with a twist distortion in a nematic liquid crystal cannot be detected optically when viewed along the twist axis. Because of this difficulty, there have not been any direct determinations of the twist elastic constant k_{22} as a function of temperature except for the well-known studies of Freedericksz and Tsvetkov who used a total internal reflexion technique.

Optical theory shows that an important parameter in determining the behaviour of such a medium is the ratio of the retardation ($=\pi \Delta n/\lambda$, where Δn is the birefringence of the untwisted medium) to the twist per unit length. For light propagation along the twist axis, Δn is large and it can be shown that with the usual experimental geometry in which the director is anchored to the walls at either end, the twist does not reveal itself in transmitted light. On the other hand, when Δn is small the optical properties of the medium are very sensitive to distortions. To reduce the effective Δn , observations were made in a direction inclined at a large angle to the twist axis. The Freedericksz transition could then be detected easily.

Experimental values of k_{22} determined by this method are presented for a few compounds. The critical divergence of k_{22} in the vicinity of the smectic A-nematic transition point in *p*-cyanobenzylidene-*p'*-octyloxy-aniline has been studied and is discussed in the light of de Gennes's theory.

Introduction

There has been considerable interest of late in the measurement of the elastic constants of nematic liquid crystals as it is recognised that short range order has a profound influence on the magnitudes of some of these constants. In simple nematics, the elastic constants can be related directly to the long range orientational order parameter by using the mean field approximation^{1, 2, 3}; the ratios of the elastic constants should then be essentially temperature independent. This is in fact found to be nearly so for *p*-azoxyanisole and *p*-azoxyphenetole⁴. But if the short range order is sensitive to temperature, as is the case in a nematic which exhibits a smectic phase at lower temperatures, the ratio of the bend to the splay

constants varies considerably in the nematic range^{4,5}. This effect is particularly pronounced when the smectic A-nematic transition is quasi-second order. The bend and twist constants are then expected to increase rapidly as the temperature approaches the smectic A-nematic point^{6,7}, whereas the splay constant is expected to show normal behaviour throughout. Direct measurements of the bend and splay constants have confirmed these conclusions^{8,9}.

A simple and direct method of determining the elastic constants is to measure the critical field corresponding to the Fredericksz transition^{10,11}:

$$H_c = \frac{\pi}{x_0} \left(\frac{k_{11}}{\Delta\chi} \right)^{\frac{1}{2}}$$

where x_0 is the thickness of the sample, $\Delta\chi$ is the anisotropy of the volume magnetic susceptibility of the medium. By using a suitable optical arrangement for detecting the deformation, the splay and bend constants, k_{11} and k_{33} , have been determined by this technique^{11,12}. However, under normal conditions of observation this method is not suitable for determining the twist constant k_{22} for reasons which will be discussed below.

The usual experimental geometry for producing twist is shown in figure 1*a*. The maximum deformation φ_m takes place in the mid-plane and at a field H slightly above H_c ,

$$\frac{H}{H_c} = 1 + \frac{1}{2} \varphi_m^2 + \frac{11}{196} \varphi_m^4 + \dots$$

If the error in determining H_c is not to exceed about 1%, the maximum value of $\varphi_m \approx 0.2$ radians. Now, consider thin sections of the deformed medium parallel to the glass plates, each section being of thickness 10^{-7} cm. If $x_0 = 20 \times 10^{-4}$ cm, then, as a rough order of magnitude, the average

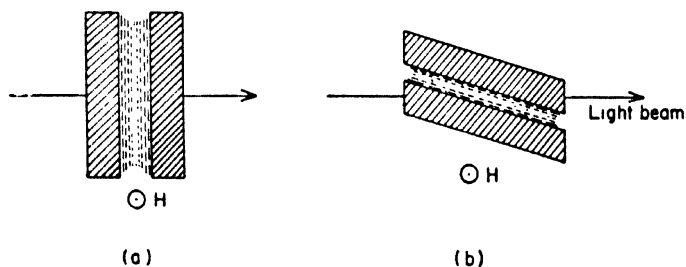


Figure 1 The geometry of the experimental set up for observing twist deformation. (a) the conventional geometry and (b) the present set up. The magnetic field H is perpendicular to the plane of the paper in both cases.

twist per layer $\beta \approx 2 \times 10^{-5}$ rad. If the birefringence of the nematic is 0.2, the phase retardation γ between the ordinary and the extraordinary rays per layer $\approx 2 \times 10^{-3}$, so that $\gamma/\beta \approx 10^2$. Optical theory¹³⁻¹⁵ shows that under these circumstances the normal waves are linearly polarized, and that the directions of polarization rotate with the director. This behaviour can be readily appreciated in terms of the Poincare sphere (figure 2 a).

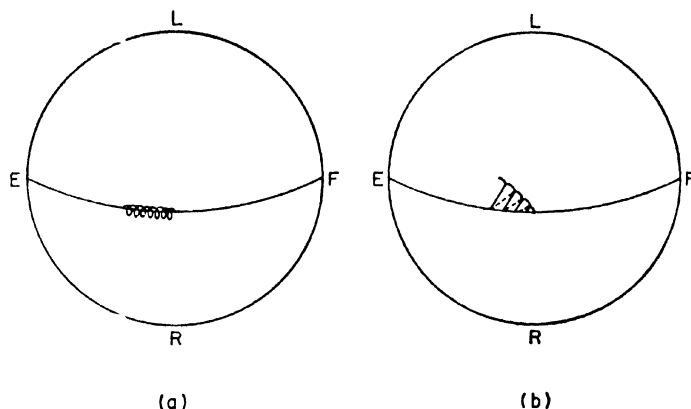


Figure 2 Illustration on the Poincare sphere of the propagation of linearly polarized light through the sample corresponding to (a) the set up in Figure 1 a and (b) that in figure 1 b. Changes in the state of polarization of the light beam are traced as follows: The point on the equator representing linearly polarized incident light is rotated in the proper sense through an angle γ about the equatorial axis corresponding to the azimuth of the first birefringent layer. This operation is repeated for the next layer where longitude is greater by 2β compared to that of the previous layer and so on.

If the incident light beam is linearly polarized along the director axis of the first section, we can see that the polarization state of the beam remains very close to the equator as it traverses the medium, *i.e.*, the light beam remains linearly polarized, and that the director is 'dragging' the polarization state along with it. Thus with the usual experimental geometry in which the director is anchored to the walls at either end, the state of polarization of the emergent beam is exactly the same as for the untwisted medium, and the twist deformation cannot be detected optically.

Because of this difficulty, Fredericksz and Tsvetkov¹⁶ employed a total internal reflection technique using a beam incident at a suitable angle on the specimen contained between a convex lens and a prism. More recently, following a suggestion by de Gennes, Cladis¹⁷ has made use of

the rotation of the conoscopic interference figure when the specimen gets deformed. Other methods which have been investigated are :

by studying the light scattering in an appropriate geometry¹⁸

by producing a cholesteric using a chiralic impurity and then untwisting the sample using an external field¹⁹

by determining the threshold field for a twisted nematic, the field being parallel to the twist axis (in this case, one needs to know the other two elastic constants²⁰; however, it should be pointed out that the γ/β problem discussed earlier will be important in this case also.)

by observing the rotation in the electrohydrodynamic flow pattern under the action of an external magnetic field¹².

However, none of these methods has been widely employed because of various difficulties inherent in each of them. We shall now discuss a simple technique which can be used with the sample taken in the usual configuration.

The Method

In order to be able to detect the twist deformation in transmitted light with the configuration shown in figure 1 a, γ/β has to be small, say about 4 or 5. Obviously, β can never be large near the threshold field, but it can be increased to some extent by applying very high fields. However, even with the highest fields normally attainable (≈ 25 kG) there will not be sufficient sensitivity to measure the deformation. An alternative method is to reduce the effective γ by viewing the index ellipsoid obliquely, say at $\sim 5^\circ$ to the director. In such a case the extraordinary index is given by the well-known equation²¹

$$\frac{1}{n_{\theta}^2} = \frac{\sin^2 \theta}{n_o^2} + \frac{\cos^2 \theta}{n_e^2}$$

where θ is the angle between the director and the direction of observation which should be in the plane containing the director and the normal to the glass plates. Under these circumstances, γ/β is reduced to ~ 4 or 5 even though the effective layer thickness is increased because of the obliquity. The effect of this on the polarization state of the emerging beam is to introduce an additional large phase difference between the ordinary and extraordinary rays as will be clear from figure 2 b. The deformation can therefore be easily detected by optical methods.

Experimental arrangement

The specimen was contained between two flat polished glass plates, the rim of which was cut and polished at an oblique angle to avoid refraction effects at the glass-air interface (figure 1 *b*). Standard mylar spacers, or at higher temperatures, mica spacers were used. The actual thickness of the sample was always measured by means of a channelled spectrum obtained by focussing white light on an air gap left deliberately unfilled for this purpose. The sandwich was mounted in a massive copper block which had a groove at the proper angle. The block in turn was slid inside an electrically heatable oven which itself was evacuated and filled with nitrogen during the experiment. The temperature was controlled by heating the oven with a stabilized DC supply and could be measured to $\pm 0.02^\circ\text{C}$ by means of a copper-constantan thermocouple. The orientation of the sample was ensured by a previous rubbing of the glass plates. For the Freedericksz transition to occur, the director must be truly oriented at 90° to the external field. Even a small deviation of the order of $1-2^\circ$ will give a long tail at lower fields and there is no critical field*. In order to ensure this exact alignment, the whole oven was mounted on a specially constructed platform whose alignment with respect to the field could be adjusted to an accuracy of $1-2'$ of arc. Further, the platform itself rested on levelling screws so that the alignment of the sample could be varied in every possible manner. When the sample is aligned at exactly 90° , there should be no particular preference for the tilt of the director one way or the other in the field. Hence walls are formed in the field of view. The sample orientation was achieved by fixing the field at a value higher than the critical field and adjusting the alignment till the maximum number of threads could be observed.

The magnetic field was measured using a Hall-probe fluxmeter which was calibrated against an NMR unit. The accuracy of the field measurement was $\sim 1-2\%$. The observations were made using sodium light. The specimen was observed through a low power microscope and a well-aligned area was selected for observations. The incident beam was polarized at 45° to the vertical. The emergent beam passed through a $\lambda/4$ plate whose principal axes were at 45° to the vertical and then through an analyser which could be rotated. The deformation was detected visually. The critical field was taken to be the lowest field which when switched off did not produce any change in the field of view.

Results

(a) *p*-Azoxyanisole (PAA):

This is one of the few compounds for which the anisotropy of volume susceptibility $\Delta\chi$ has been measured in the nematic range^{23, 24}. The value

* See, for instance, the calculations by Papoular and Rapini²⁵ which bring out this effect.

of $\Delta\chi$ were taken from the recent measurements of Gasparoux *et al*²⁴. The density data of Maier and Saupe²⁵ were used in the calculations. The results are shown in figure 3. Our values are somewhat lower (by 6–8%) compared to the data of Freedericksz and Tsvetkov¹⁶ as recalculated by Saupe¹¹ mainly because the $\Delta\chi$ values that we have used are lower than those of Foex²³ which were used by Saupe. When one allows for this difference, the agreement between the two sets of data is quite good.

(b) *p*-Azoxyphenetole (PAP):

No susceptibility data are available for this compound. However, since the anisotropy of magnetic susceptibility arises essentially from the aromatic rings, we assumed that the molar susceptibility of PAA and PAP are the same. Using the values of the order parameter²⁶ and density²⁷, we have calculated the twist elastic constant. The results are shown in figure 3. The only other measurement for this compound is that due to

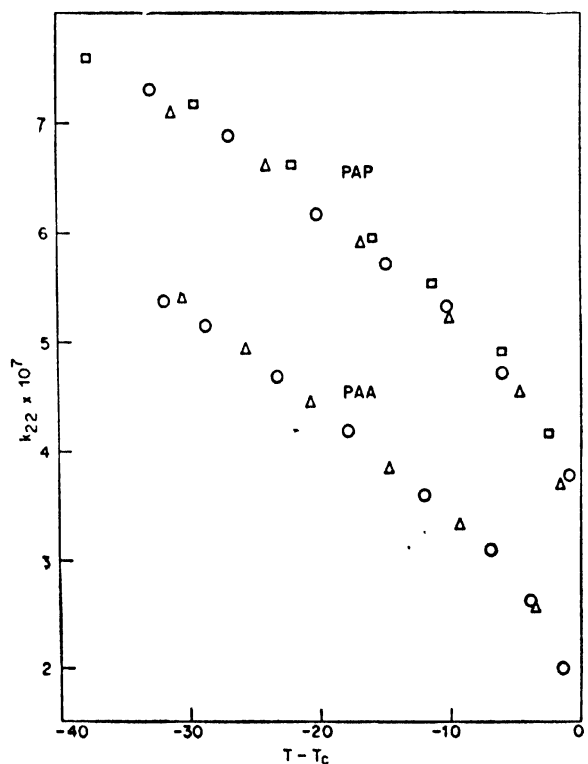


Figure 3 The twist elastic constants of PAA and PAP *versus* the relative temperature. Squares, circles and triangles represent independent measurements on different samples.

the Orsay group²⁸ carried out by dissolving a small quantity of a chiralic impurity and untwisting the mixture by means of a magnetic field. Again our measured value at that temperature is lower, but as we do not know the value of $\Delta\chi$ used in the earlier measurement, we merely point out that the Orsay measurement at one temperature on PAA also yielded a value higher than that reported by Saupe.

The ratio of k_{22} values of PAP and PAA agree approximately with the theoretical ratio given in our earlier paper. However the ratio is not independent of temperature but decreases somewhat at lower temperature (from ~ 1.6 near T_* to ~ 1.4 near T_*-30). Further the ratio is lower than that found in the case of k_{11} ($1.8-2.0$), which exhibits a maximum at a few degrees below T_* .

(c) N-p-Cyanobenzylidene-p-n-octyloxyaniline (CBOOA)

This is an interesting compound as it exhibits both the smectic A and nematic phases. The smectic A-nematic transition has generally been assumed to be second order—no heat of transformation could be detected within experimental limits. However, the recent investigation by Cladis on a highly purified specimen shows that this may not be true¹⁷. Moreover, from theoretical considerations Halperin and Lubensky²⁹ have claimed that this transformation should be at least weakly first order.

de Gennes⁶ has drawn an analogy between this transition and the superconductor—normal transition and has suggested that the pre-translational increase in k_{22} and k_{33} should follow the relation

$$\Delta k \propto \xi \propto \frac{1}{(T - T_{AN}^*)^\gamma}$$

where Δk is the excess value of the elastic coefficient and ξ the coherence length of the smectic-like regions, and T_{AN}^* is the hypothetical second order phase transition point if the transition is weakly first order, or the actual transition point itself if it is truly second order. The mean field value for γ is 0.5, but de Gennes argued that the behaviour might not correspond to the mean field description and in such a case $\gamma = 0.66$. Following this suggestion, there have been several measurements of the bend elastic constant^{8,9} which have been claimed to agree with the latter result. The only determination of the twist elastic constant of CBOOA has been that of Durand *et al.*¹⁸ who studied the light scattering and they too obtained the result $\gamma = 0.65$. However, recently Cladis has measured k_{33} of CBOOA with varying amounts of dissolved impurity and by using a least square analysis of the data. She has shown that $\gamma \approx 0.5$ for CBOOA and increases to 1 as the impurity content increases.

We have determined the bend and twist elastic constants of CBOOA (figures 4 and 5). The smectic-nematic transition point of our sample was

(83° C.) (The purest sample used by Cladis had a transition temperature of 83.4° C). The bend constant k_{33} was studied with a homeotropically aligned sample and the twist k_{22} with a homogeneously aligned sample using the technique described earlier. We may express k_{22} in the form

$$k_{22} = C_1 S^2 + C_2 (T - T_{AN}^*)^{-\gamma} \quad (1)$$

where $C_1 S^2$ is the pure nematic contribution, S is the order parameter and C_1 , C_2 are constants. A similar relation holds good in the case of k_{33} . We took the order parameter from the NMR measurements of Cabane and Clark³⁰. The mass susceptibility of CBOOA have been reported recently³¹ but since the density data are not yet known, they could not be converted to volume susceptibility. Therefore, in actual calculations we used the relation $\Delta \chi \propto S$. A graphical procedure for determining γ has been employed by a number of investigators but since the reliability of this procedure is doubtful, we used a least squares fitting programme which involved scanning the transition temperature and treating the other three constants as free parameters. Ideally, one should have an independent estimate of the pure-nematic contribution, *i. e.*, the value of the coefficient C_1 . However, since there is no method of estimating this, we treated C_1 also as a free parameter. Figure 6 shows the minimum in r.m.s. error as a function of T_{AN}^* . The computations yielded

$$\gamma(k_{33}) = 0.55$$

$$\gamma(k_{22}) = 0.54$$

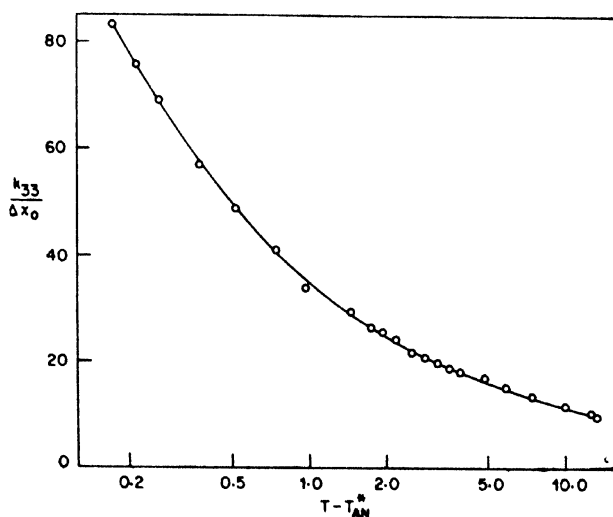


Figure 4 Bend elastic constant of CBOOA versus the relative temperature ($T - T_{AN}^*$)

The experiment on k_{22} was repeated on a commercial sample of CBOOA (Eastman Kodak). The A-N transition point was 82.7°C , and the value of γ for two independent sets of measurements found to be 0.52 and 0.49. However it was observed that C_2 was significantly less for this material

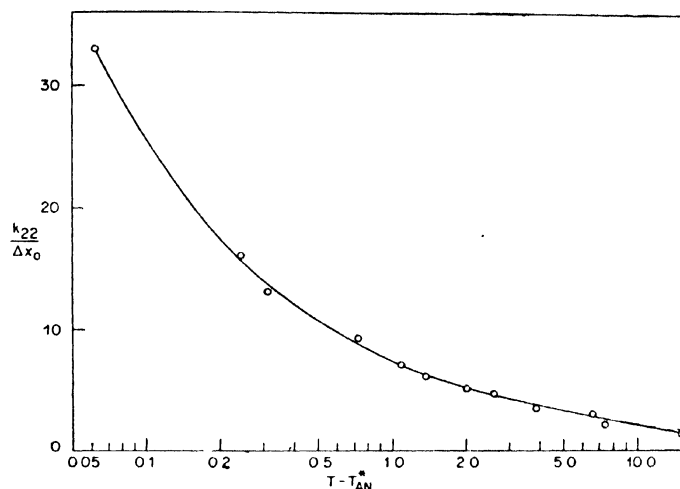


Figure 5 Twist elastic constant of CBOOA versus the relative temperature ($T - T_{AN}^*$)

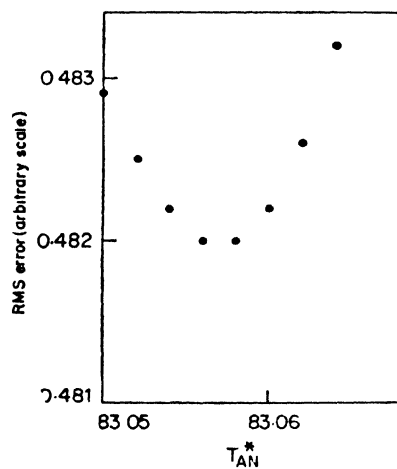


Figure 6 Least squares analysis of data using eq. (1): RMS error versus T_{AN}^* .

suggesting that impurities do influence the short range order effects. Thus our preliminary values of the critical exponents for both elastic constants are closer to the mean field value and in fair agreement with the recent measurements of Cladis¹⁷. It therefore appears reasonable to conclude that the mean field description of this transition is valid in the present case.

Twist viscosity

It is in principle possible to estimate the twist viscosity coefficient γ_1 using the present set-up. If we have a *small* twist deformation and switch off the magnetic field suddenly, the deformation relaxes to zero with a characteristic time constant τ given by

$$\tau = \left(\frac{\gamma_1}{\Delta\chi} \right) \frac{1}{H_c^2}$$

Hence τH_c^2 is a measure of γ_1 . Theoretically, it has been suggested⁷ that the excess viscosity due to fluctuations of the smectic-order parameter should show a divergence as $(T - T_{AN}^*)^{-0.33}$ while $\Delta k_{22} \propto (T - T_{AN}^*)^{-0.66}$.

Hence we should expect

$$\tau \propto (T - T_{AN}^*)^{0.33}$$

i.e., the relaxation time should *decrease* near the nematic-smectic A point. The relaxation time was estimated by switching off a field $H \approx 1.1 H_c$ and then noting the time taken for the sample to return to the undistorted state. It was observed that the relaxation time initially increased as the temperature was lowered, and very near T_{AN} , it *decreased* in value. This is in agreement with the expected trend.

Acknowledgements

We are grateful to Dr Ribotta and to Dr Durand for giving us the sample of CBOOA used in the experiments. Our thanks are also due to Dr Saupe for useful discussions and to Dr Khetrapal for the least squares fitting program.

References

- 1 SAUPE A Z. *Naturforsch.* 15a 810 (1960)
- 2 CHANDRASEKHAR S, MADHUSUDANA N V and SHUBHA K *Acta Crystallogr.* 28A 28 (1972)
- 3 CHANDRASEKHAR S, MADHUSUDANA N V and SHUBHA K *Symposia of the Faraday Society No. 5, Liquid Crystals*, p. 26
- 4 GRULER H, SCHEFFER T J and MEIER G Z. *Naturforsch.* 27a 966 (1972)
- 5 GRULER H Z. *Naturforsch.* 23a 474 (1973)
- 6 DE GENNES P G *Mol. Cryst. Liquid Cryst.* 21 49 (1973)
- 7 JAHNIG F. *This Conference*

- 8 CHEUNG L, MEYER R B and GRULER H *Phys. Rev. Lett.* **31** 349 (1973)
- 9 LEGER L *Phys. Lett.* **44A** 535 (1973)
- 10 FREEDERICKSZ V and ZOLINA V *Trans. Faraday Soc.* **29** 919 (1973)
- 11 SAUPE A *Z. Naturforsch.* **15a** 815 (1960)
- 12 HALLER I *J. Chem. Phys.* **57** 1400 (1972)
- 13 DE VRIES A *Acta Crystallogr.* **4** 219 (1951)
- 14 CHANDRASEKHAR S, RANGANATH G S, KINI U D and SURESH K A *Mol. Cryst. Liquid Cryst.* **24** 201 (1973)
- 15 RANGANATH G S, CHANDRASEKHAR S, KINI U D, SURESH K A and RAMASESHAN S *Chem. Phys. Lett.* **190** 556 (1973)
- 16 FREEDERICKSZ V and TSVETKOV V *Phys. Z. Sowjet Union* **6** 490 (1934)
- 17 CLADIS P E *Phys. Rev. Lett.* **31** 1200 (1973)
- 18 DELAYE M, RIBOTTA R and DURAND G *Phys. Rev. Lett.* **31** 443 (1973)
- 19 DURAND G, LEGER L, RONDELEZ F and VEYSSIE M *Phys. Rev. Lett.* **22** 227 (1969)
- 20 LESLIE F M *Mol. Cryst. Liquid Cryst.* **12** 57 (1970)
- 21 RAMACHANDRAN G N and RAMASESHAN S *Handb. der Phys.* Vol. XXV/1 (Berlin Springer-Verlag.) p. 68
- 22 RAPINI A and PAPOULAR M *J. Phys.* **30** C4-54 (1969)
- 23 FOEX J. *J. Phys.* **10** 960 (1929)
- 24 GASPAROUX H and PROST J *J. Phys.* **32** 953 (1971)
- 25 MAIER W and SAUPE A *Z. Naturforsch.* **15a** 287 (1960)
- 26 CHANDRASEKHAR S and MADHUSUDANA N V *Acta Crystallogr.* **A27** 303 (1971)
- 27 BAUER E and BERNAMONT J *J. Phys.* **7** 19 (1936)
- 28 Orsay Liquid Crystals Group, *Ordered Fluids and Liquid Crystals*, ed. JOHNSON J F and PORTER R S (Plenum Press) p. 447 (1970)
- 29 HALPERIN B I and LUBENSKY T C *Solid State Commun.* **14** 997 (1974)
- 30 CABANE B and CLARK G *Solid State Commun.* **13** 129 (1972)
- 31 GASPAROUX H, HARDOUIN F and ACHARD M F. *This Conference*

DISCUSSION

Rustichelli : What is the minimum twist that you could measure ?

Madhusudana : We estimated that a twist angle of $\sim 1/5$ radian could be detected for a typical sample thickness of $\sim 20\mu$. This is at the middle of the specimen where the deformation is maximum. In other words a twist per unit length of ~ 0.02 radian per micron could be detected.

Mishra : Cladis's value of the critical exponent is 0.5. Can you comment on that ?

Madhusudana : Cladis has made a detailed study of the value of γ as a function of the purity of the sample. She finds that γ is 0.5 for very pure samples and goes up to 1 when impurities are added.

de Gennes : I am very sorry that the theory came first. I think that some of the earlier work, that of the Harvard group and also that of the Orsay group, has been influenced by the theoretical work. You might have smectics which obey the mean field and this would give $\gamma = \frac{1}{2}$ as Cladis says, and you might have smectics which are helium-like which would give $2/3$. There may be further complications like what Lubensky is studying in which the fluctuations of the director may be reduced and can act on the system as radiation pressure would act on superconductors and can change the nature of the transition. The force or pressure required for the formation of the layers of the ordered state is singular and it has not been taken into account by any of the theories.

Statistical thermodynamics of the nematic liquid crystal free surface

CLIVE A CROXTON* and S CHANDRASEKHAR

Raman Research Institute, Bangalore 560006, India

*Permanent address : Cavendish Laboratory, University of Cambridge, Cambridge, UK

Abstract. The possible development of stable density oscillations in the form of a structured liquid-vapour density transition at the surface of simple liquids has been proposed and the thermodynamic consequences for the surface tension discussed. The principal effect on the surface tension-temperature characteristic is that just beyond the triple point certain systems should show a surface tension which *increases* with temperature : moreover, such behaviour has been observed experimentally. We now extend the treatment to include the *orientational* contributions to the surface excess quantities for a nematic liquid crystal. It is found that the possibility exists both for the development of positive slopes and discontinuities in the surface tension-temperature characteristic. We find that the slope $\partial \gamma / \partial T$ is determined as a competition between orientational order and spatial disorder which develops at the liquid surface. Should the situation corresponding to highly ordered orientational states occur, the $\gamma(T)$ characteristic will show a *positive* slope, although with increasing temperature and spatial delocalisation of the liquid surface the usual monotonic decreasing function will be regained. Again, discontinuities in the slope and absolute value of the $\gamma(T)$ characteristic would be expected with the discontinuous variation of the order parameter at the nematic-isotropic transition temperature.

Introduction

The complete specification of the structural features of the liquid-vapour transition zone at the surface of a nematic liquid crystal involves both the spatial and the orientational distributions. In the case of simple liquids, the structural features of the density transition have been calculated, and the one and two particle distributions determined. It has been shown¹ that under certain circumstances stable density oscillations in the transition profile may develop in the vicinity of the liquid surface, and these relatively ordered states have a profound effect on the principal excess thermodynamic functions of the free surface, in particular the surface tension $\gamma(T)$.

It may be quite easily shown that the gradient of the $\gamma(T)$ characteristic is related to the excess entropy per unit area developed at the liquid surface as follows :

$$d\gamma/dT = -s = -(S_{\sigma} - S_{\beta})$$

where the subscripts σ and β refer to surface and bulk states respectively. Thus we see that should the situation $S_\sigma < S_\beta$ arise, corresponding to relatively ordered surface states, then the $\nu(T)$ characteristic may actually show a *positive* slope. Of course, such a situation if it is to occur is only likely to be observed at temperatures just above the triple point: thermal delocalisation of the liquid surface with increasing temperature will inevitably result in a progressive disordering and the usual monotonic decreasing form of $\nu(T)$ will be regained corresponding to $S_\beta < S_\sigma$. Systems exhibiting the stable oscillatory density profile are most likely to be found amongst the liquid metals, and indeed White² has shown that provided care is taken to ensure that a truly *equilibrium* measurement of $\nu(T)$ is made, then such positive slopes are observed and are particularly pronounced in the case of Zn, Cu and Cd. By equilibrium measurement is meant that there should be no net efflux of particles from the liquid surface, or that the chemical potential should be constant across the surface. This is achieved in practice by ensuring that the liquid is in equilibrium with its own vapour. This point is crucial with regard to the observation of positive slopes and as we shall see, the indications are that the $\nu(T)$ characteristics for liquid crystals are likely to show such positive regions over limited temperature ranges. It is clear then that from an experimental standpoint such precautions are essential.

Theory

It would be fair to say that for simple systems the current theoretical position regarding the one and two particle distribution functions is controversial. It is not appropriate to sustain the controversy here, except to say that the controversy centres primarily on the form of the single particle distribution function $g_{(1)}(z)$ which describes the spatial distribution of the centres of gravity of the particles. In consequence the positive slope to the $\nu(T)$ function, depending as it does on the development of low entropy (*i.e.*, oscillatory) surface states, is equally controversial. The current theoretical situation is reviewed elsewhere³ and for present purposes we shall assume an uncontroversial profile of the form shown in figure 1. Stable density oscillations are unlikely to develop in the case of nematic liquid crystal systems although such a situation may arise in the surface states of *smectic* compounds.

We enquire as to what contribution the *orientational* features at the surface of the assembly are likely to make to the $\nu(T)$ characteristic.

We assume a short range anisotropic intermolecular pair interaction of the form⁴

$$\phi_{12}(r_{12}, \cos \theta_{12}) = -\phi_0 \exp(-r_{12}/r_0)^2 \left(\frac{2}{3} \cos^2 \theta_{12} - \frac{1}{3} \right) \quad (1)$$

where r_{12} is the separation of the centres of mass of the molecules, θ_{12} is the relative orientation of their long axes, and r_0 is a constant \sim molecular length. In the bulk liquid we may assume a single particle potential in the mean field approximation

$$\phi_1(\cos \theta_1) = -\phi_0 \left(\frac{3}{2} \cos^2 \theta_1 - \frac{1}{2} \right) \eta \quad (2a)$$

where ϕ_0 is a constant, and θ_1 is the orientation of the representative molecule relative to the mean local orientational order whose measure is

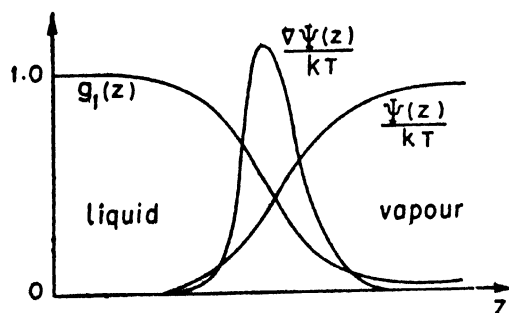


Figure 1 Schematic variation of the single particle distribution of molecular centres $g_1(z)$, the potential of mean force $\Psi(z)$, and its gradient $\nabla \Psi(z)/kT$ in the vicinity of the liquid surface.

given by η . Clearly, the single particle potential at the liquid surface will be modified both by the structural delocalisation across the transition zone, and by the development of a surface field whose effect we assume will be to impress an orienting torque on the surface molecules. The former effect serves to *diminish* the local order, whilst the latter will *enhance* it. Notice that no specification of the orientation of molecules relative to the surface is yet made: we do not, however, generally anticipate that surface tension is likely to be isotropic³. In the case of simple spherical molecules, the first effect is discussed in terms of a spatial decoupling of the interaction¹ between a representative molecule and its neighbours. The single particle potential (2a) is now modified in the vicinity of the surface to read

$$\phi_1(z_1, \cos \theta_1) = -\phi_0 \left(\frac{3}{2} \cos^2 \theta_1 - \frac{1}{2} \right) \eta(z) \quad (2b)$$

The single particle potential of mean force $\Psi(z)$ is related by the Boltzmann relation to the single particle distribution $g_{(1)}(z)$ as

$$g_{(1)}(z) = \exp [-\Psi(z)/kT]$$

so that $\Psi(z)$ serves to 'switch off' or decouple the interaction across the transition zone. A convenient model decoupling potential is then quite simply $[\exp(-\Psi(z)/kT) - 1]$ which we take to describe the spatial modification of the single particle potential as the centre of gravity passes through the collective field in the transition zone. The surface *field* may then be taken as $-\nabla\Psi(z)$ (figure 1) and we propose a local associated *orientational* model potential $[1 - \exp\{-c\nabla\Psi(z)\}/kT]$, where c is a constant governing the strength and range of the orienting torque. We therefore finally arrive at the following single particle potential (see eq. 2b):

$$\begin{aligned} \phi_1(z_1, \cos \theta_1) = & -\phi_0\left(\frac{3}{2} \cos^2 \theta_1 - \frac{1}{2}\right) \left\{ \eta - \epsilon_0 \left[\exp\left(-\frac{\Psi(z)}{kT}\right) - 1 \right] \right. \\ & \left. + \epsilon_1 \left[1 - \exp\left(-\frac{c\nabla\Psi(z)}{kT}\right) \right] \right\} \end{aligned} \quad (3)$$

where ϵ_0 and ϵ_1 are coefficients which are to be determined. In particular we observe that the factor in the brackets $\{\}$ represents an *effective order parameter*, spatially dependent upon z and appropriate to the liquid surface. Now we may write

$$\phi_1(z_1, \cos \theta_1) = \frac{\iint \phi_{12}(r_{12}, \cos \theta_{12}) g_{(1)}(z_2, \cos \theta_2) dz d\hat{z}}{\iint g_{(1)}(z_2, \cos \theta_2) dz d\hat{z}} \quad (4)$$

where the integrals range over all positions z and orientations \hat{z} of molecule 2, and where $g_{(1)}(z_2, \cos \theta_2) = \exp[-\phi_2(z_2, \cos \theta_2)/kT]$. From (4) and (1) it follows that

$$\eta = \left\langle \left(\frac{3}{2} \cos^2 \theta_2 - \frac{1}{2} \right) g_{(1)}(2) \right\rangle \quad (5)$$

$$\epsilon_0 = \left\langle \left[\exp\left(-\frac{\Psi(z_2)}{kT}\right) - 1 \right] \left(\frac{3}{2} \cos^2 \theta_2 - \frac{1}{2} \right) g_{(1)}(2) \right\rangle \quad (6)$$

$$\epsilon_1 = \left\langle \left[1 - \exp\left(-\frac{c\nabla\Psi(z_2)}{kT}\right) \right] \left(\frac{3}{2} \cos^2 \theta_2 - \frac{1}{2} \right) g_{(1)}(2) \right\rangle \quad (7)$$

and these may be determined self-consistently. It may be shown quite easily that $\eta(z) \rightarrow \eta$ as $z \rightarrow -\infty$, i.e., $\eta(z)$ attains its asymptotic bulk value. It is now straightforward, using the standard statistical thermodynamic relations to write down expressions for the surface excess entropy per unit area ($= -d\gamma/dT$) developed at the liquid surface:

$$\begin{aligned}
 -\frac{d\gamma}{dT} = & -\frac{\phi_0\rho}{T} \int_{-\infty}^{\infty} g_{(1)}(z) \left(\eta^2 - \epsilon_0^2 \left[\exp\left(-\frac{\Psi(z)}{kT}\right) - 1 \right]^2 \right. \\
 & + \epsilon_1^2 \left[1 - \exp\left(-\frac{c\nabla\Psi(z)}{kT}\right) \right] dz + \frac{\phi_0\rho}{T} \int_{-\infty}^0 \eta^2 dz \\
 & + \rho k \int_{-\infty}^{\infty} g_{(1)}(z) \ln \Xi(z, \eta, \epsilon_0, \epsilon_1) dz - \rho k \int_{-\infty}^0 \ln \Xi(z, \eta) dz
 \end{aligned}$$

$$\text{where } \Xi(z, \eta) = \int_0^1 \exp \left[\frac{\phi_0\eta}{kT} \left(\frac{3}{2} \cos^2\theta - \frac{1}{2} \right) \right] d(\cos\theta)$$

$$\begin{aligned}
 \Xi(z, \eta, \epsilon_0, \epsilon_1) = & \int_0^1 \exp \left[\left(\frac{\phi_0}{kT} \right) \left\{ \eta - \epsilon_0 \left(\exp\left(-\frac{\Psi(z)}{kT}\right) - 1 \right) \right. \right. \\
 & \left. \left. + \epsilon_1 \left[1 - \exp\left(-\frac{c\nabla\Psi(z)}{kT}\right) \right] \right\} \left(\frac{3}{2} \cos^2\theta - \frac{1}{2} \right) \right] d(\cos\theta) \quad (8)
 \end{aligned}$$

In the absence of an accurate and explicit knowledge of the single particle distribution $g_{(1)}(z)$ we can only examine the formal aspects of equation (8). Analogous expressions for the surface excess free energy per unit area $[-\gamma(T)]$ may be written down quite easily: for present purposes, however, we need only consider the temperature derivative given above.

Discussion

As we observed earlier, the surface tension would not, in general, be expected to be isotropic. That is, we would generally expect the surface tension to depend upon the orientation of the molecules at the surface⁵, and this in itself may show a weak temperature dependence. We assume, however, that in specifying the *effective* order parameter $\eta(z)$ we specify only the *degree* of local order: details of the precise surface orientation will be implicitly contained in the spatial distribution of molecular centres $g_{(1)}(z)$.

In figure 2 we give a schematic indication of how the effective order parameter may vary with temperature. At low temperatures, just beyond the crystal-nematic point, the spatial delocalisation may be sufficiently low and the surface orientational field correspondingly high such that there is a net *enhancement* of the order parameter over its bulk value. Under these circumstances careful consideration of (1) or (7) shows that initially

at least, the $\nu(T)$ characteristic should actually show a positive slope. Of course, with increasing spatial delocalisation of the surface and the corresponding relaxation of the surface field the usual monotonic decreasing function of temperature is regained. With the discontinuous variation of the bulk order parameter η with temperature we see from (7) that we would expect a discontinuity of slope at the transition temperature. Consideration of the expression for the absolute value of $\gamma(T)$, not given here, would lead us to anticipate a discontinuity in γ also. These features are shown in figure 2. It is also possible that with the catastrophic variation

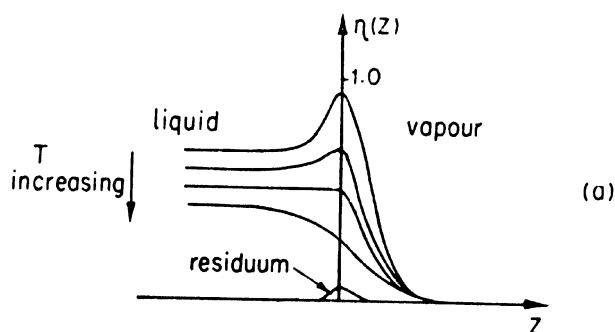


Figure 2(a) Schematic variation of the effective order parameter $\eta(z)$ in the vicinity of the nematic liquid crystal surface. At low temperatures there is a net surface enhancement of the local orientational order attributed to surface field effects overcoming spatial delocalizational disorder. With increasing temperature the balance is reversed, and progressive spatial and surface field relaxation results on a surface depression of the local order parameter. With the catastrophic bulk variation of η at the transition temperature, a weak surface residuum may persist for a short thermal range beyond the transition.

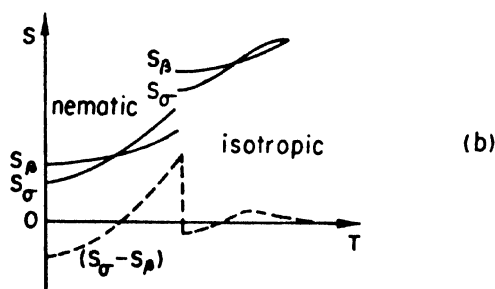


Figure 2(b) Schematic variation of the bulk and surface entropy curves with temperature on the basis of the behaviour of $\eta(z, T)$.

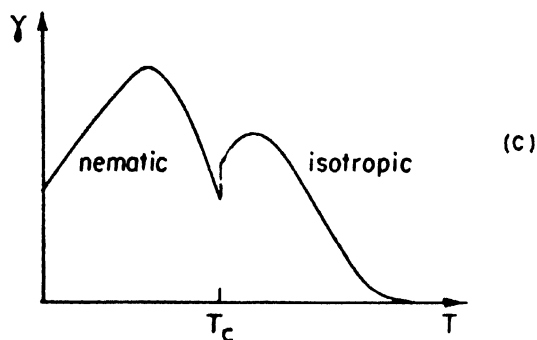


Figure 2(c) Schematic variation of the $\gamma(T)$ characteristic on the basis of equations (1) and (8).

of $\eta \rightarrow 0$ at the transition temperature, the weak surface field may establish a small residuum of orientational order at the *isotropic* liquid surface over a short thermal range. In this case, a second positive region to the $\gamma(T)$ characteristic may be observed. This feature is also indicated in figure 2.

One further possibility is the *thermally retarded* surface enhancement of the order parameter (figure 3). In this case the surface orientational order is sufficient to offset the spatial disorder of the molecular distribution of centers, and $\eta(z)$ is depressed at the surface with respect to the bulk value. A monotonic decreasing $\gamma(T)$ characteristic is of course obtained. In the vicinity of the transition temperature, however, the bulk value of η may have decreased sufficiently just prior to the transition that a surface

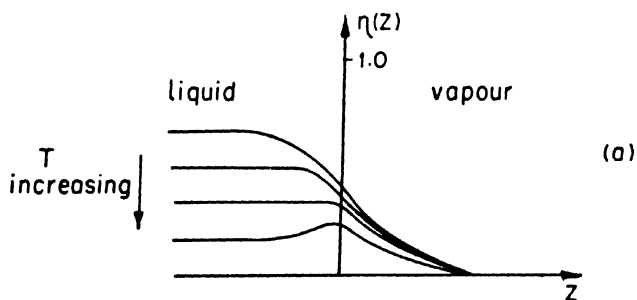


Figure 3(a) Schematic variation of the effective order parameter $\eta(z)$ in the vicinity of the nematic liquid crystal surface. Whilst at low temperatures there is a net depression of the surface value of $\eta(z)$, the bulk value of the order parameter becomes sufficiently low just prior to the transition that an effective surface enhancement develops. Since positive slopes in the $\gamma(T)$ characteristic depend only upon the *relative* values of the bulk and surface entropies per unit area, it is clear that an increase in γ may be anticipated immediately before the nematic-isotropic transition.

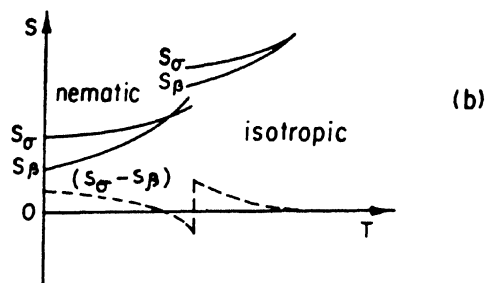


Figure 3(b) Schematic variation of the bulk and surface entropy curves with temperature on the basis of the behaviour of $\eta(z, T)$.

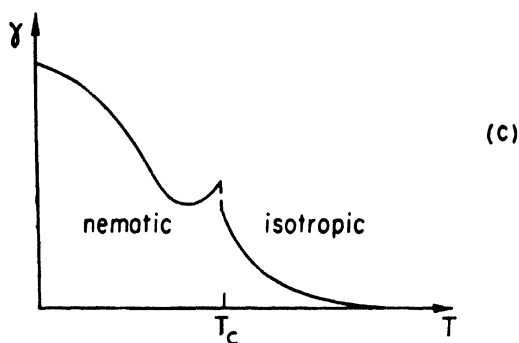


Figure 3(c) Schematic variation of the $\gamma(T)$ characteristic on the basis of equations (1) and (7).

enhancement of $\eta(z)$ is eventually achieved. This requires the rate of surface entropy production to be slower than that of the bulk, where surface entropy production develops with temperature subject to the surface field constraint. Under these circumstances then, we should expect a positive slope to immediately precede the transition to an isotropic system (figure 3). Of course, the discontinuity of slope and absolute value of the $\gamma(T)$ characteristic would occur as before.

It is not being suggested that any one system is likely to develop all these features, but attention is drawn to features of the $\gamma(T)$ characteristics which may develop in principle, and which careful equilibrium experimentation may reveal. Most of the features described above, except for the positive slope immediately after the melting transition, have been observed⁶. The possibility exists of enhancing or suppressing certain features of the $\gamma(T)$ characteristic by means of electric or magnetic fields whose effect would be to enhance or depress the value of the effective order parameter

at the liquid crystal surface. We emphasize once again that the post-melting positive slope in liquid metal systems was not observed experimentally until stringent precautions were taken to ensure liquid-vapour equilibrium across the transition zone, and that similar precautions in the case of liquid crystal measurements are essential bearing in mind the complicated form of the $\gamma(T)$ characteristic.

References

- 1 CROXTON C A and FERRIER R P J. *Phys. C* 4 1909 (1971) ; 4 1921 (1971) ; 4 2433 (1971) ; 4 2447 (1971)
- 2 WHITE D W G *Trans. Metall. Soc. AIME* 236 796 (1966)
- 3 CROXTON C A *Liquid state physics - A statistical mechanical introduction*, Cambridge University Press (1974) Ch. 4 ; CROXTON C A *Adv. Phys.* July (1973)
- 4 McMILLAN W *Phys. Rev.* 4A 1238 (1971)
- 5 CHANDRASEKHAR S *Mol. Cryst.* 2 71 (1966)
- 6 FERGUSON A and KENNEDY S J *Phil. Mag.* 26 41 (1938) ; SCHWARTZ W M and MOSELEY H W J. *Phys. Colloid. Chem.* 51 826 (1947)

DISCUSSION

Nityananda : You emphasized that a net efflux of molecules could destroy surface order. This efflux is of the same order as the unidirectional influx and efflux which occur even for an equilibrium surface. Why is it that they do not destroy surface order?

Croxtton : Quite clearly, for the measurement of an equilibrium thermodynamic parameter the physical conditions appropriate to thermodynamic and mechanical stability must apply. For a free liquid surface continuity of normal (perpendicular) pressure and of chemical potential across the liquid vapour density transition specifies the equilibrium and stability of the surface. Unless the liquid surface is in equilibrium with its vapour, the condition on the chemical potential is not satisfied. The equilibrium structure of the transition zone is then established in a statistical sense, and perhaps the analogy with two travelling waves moving in opposite directions yet specifying a standing wave might give some indication of the mechanism. This effect has, in fact, been observed directly in the course of molecular dynamic machine simulation of a free liquid argon surface*. White† has dramatically demonstrated the effect of non-equilibrium on the form of the $\gamma(T)$ characteristic, and it is quite clear that a net transport of particles from the liquid surface has a disruptive effect on whatever structural features there are in the transition zone.

* Croxtton C A and Ferrier R P J. *Phys. C* 4 1909 (1971) ; 4 1921 (1971) ; 4 2433 (1971) ; 4 2447 (1971).

† White D W G *Trans. Metall. Soc. AIME* 236 796 (1966) ; Croxtton C A *Liquid state physics - A statistical mechanical introduction*, Cambridge University Press (1974) Ch. 4.

Jahnig: If I understood you correctly, you did not take into account the boundary condition for the orientation of the molecules at the surface of the nematic. But this boundary condition should be important and may give an additional temperature dependence.

Croxton: Certainly the surface tension will be sensitively dependent upon the orientation of the molecular axes with respect to the free surface *: we do not propose that γ is isotropic or independent of the molecular orientation. In specifying an effective order parameter $\eta(z)$ we merely specify the net degree of local order, irrespective of the particular orientation. It may be that the orientation does vary with temperature, but this temperature dependence is not incorporated in $\eta(z, T)$ in this development: indeed it is difficult to see how it could be. We assume that the single particle distribution of molecular centres $g_{(1)}(z)$ in fact contains the information relating to the particular molecular orientation. Certainly we would anticipate different forms of transition profile for a system whose molecules are in one case aligned parallel, and in the other aligned perpendicular to the surface. If there is any thermal variation of the orientation of the molecular axes with temperature, and what evidence there is suggests that such temperature dependence is very weak, then this would be incorporated in $g_{(1)}(z, T)$ which, of course, already exhibits a pronounced spatial relaxation with increasing temperature.

de Gennes: The data recorded by White are on the metal zinc. In what sense are we sure that the statistical effects you describe cannot be related to electronic effects which are quite specific with metals?

Croxton: I think the statistical structure of the surface is not specific to metals but more to geometric exclusion effects, simply because these effects can be reproduced with nothing more sophisticated than hard spheres. For example, if we consider ball bearings packed in a gravitational field and shake them down, then along the free surface nothing but the geometry will generate 2 or 3 atomic layers. Again if we consider ball bearings in a rectangular tray filled up to a reasonably high density so that geometric effects can assert themselves then all round the boundary we will get two or three layers. This is obviously because of the constraint of the boundary.

This, in principle, is no different from what we have in liquids. Here the surface molecules are compacted and this is responsible for the structural effects. One need not invoke any electronic effects.

* Chandrasekhar S *Mol. Cryst.* 2 71 (1966).

Experimental determination of the surface tension of nematic liquid crystals

S KRISHNASWAMY and R SHASHIDHAR

Raman Research Institute, Bangalore 560006

Abstract. Equilibrium measurements of surface tension have been carried out on *p*-anisaldazine and *p*-azoxyanisole in the nematic and isotropic phases using the pendant drop method. The drop was completely enclosed in a chamber filled with inert atmosphere and maintained at all times in equilibrium with its saturated vapour. The surface tension-temperature characteristic shows a marked anomaly for both compounds; the slope in the nematic phase is initially negative and then reverses sign as the temperature approaches the nematic-isotropic transition point. For *p*-anisaldazine the slope again becomes negative immediately after the transition whereas for *p*-azoxyanisole the positive slope extends for a few degrees in the isotropic phase before changing sign at higher temperatures. The observed features are in qualitative agreement with the theoretical predictions of Croxton and Chandrasekhar.

Introduction

The experimental data available on the surface tension of nematic liquid crystals are meagre and rather conflicting. Ferguson and Kennedy¹ found for all the three nematic compounds they studied, viz., *p*-azoxyanisole (PAA), *p*-azoxyphenetole and *p*-anisaldazine, that the slope of the surface tension-temperature ($\gamma-T$) characteristic was initially negative but reversed sign as the temperature approached the nematic-isotropic transition point (T_*). Naggiar² obtained for PAA a monotonically decreasing function throughout the nematic range. The values of Schwartz and Moseley³ as well as those of Gorskii and Sakevich⁴ for PAA also showed a decreasing trend except that the γ values obtained by the former had a tendency to be constant very near T_* .

However, none of these measurements were carried out under equilibrium conditions. Recent studies on the surface tension of liquid metals⁵ have demonstrated the importance of having the liquid in equilibrium with its saturated vapour so that there is no net flux of atoms across the liquid-vapour interface. The $\gamma-T$ characteristic determined under these conditions showed an inversion which was completely missed in all previous non-equilibrium measurements. Therefore, it was evident that an equilibrium experiment is essential for obtaining the true form of the $\gamma-T$ characteristic of the liquid crystal.

The surface tension of a nematic liquid crystal is expected to be strongly dependent on the alignment of the molecules at the free surface⁶. Since the molecular orientation is highly influenced by wall effects care had to be taken that measurements are not effected by the orienting influence of the solid surface in contact with the liquid crystal. This was a major factor to be considered in the choice of the experimental technique. After examining various possibilities, it was decided to use the pendant drop method which is known to be suitable for viscous liquids⁷. This method has several advantages:

- (i) Only a very small fraction of the total surface area of drop is in direct contact with the solid surface and the results are *independent* on the angle of contact.
- (ii) It is a static method so that the viscous drag of liquid does not play any part.
- (iii) The approach to hydrodynamic equilibrium is rapid, which is an important point to be borne in mind for viscous liquids.

Andreas *et al.*⁸ have shown that the surface tension γ can be calculated from the pendant drop profile by $\gamma = g \rho d_{\max}^2 / H$ where g is the acceleration due to gravity, ρ the density, d_{\max} is the maximum diameter of the drop and H is a correction factor which depends on the shape of the drop. The shape can be characterized by a ratio $S = d_1 / d_{\max}$, d_1 being the diameter of the drop measured at a height equal to d_{\max} from the vertex. Andreas *et al.* obtained a table of $1/H$ vs. S from measurements on various pendant drops of conductivity water whose surface tension is accurately known. Later more accurate tables have been compiled by numerical solutions of the fundamental differential equation which exactly governs the shape of the pendant drop acted upon by gravitational and surface energy forces. Ryong-Joon Roe *et al.*⁹ made a further improvement whereby the attainment of hydrodynamic equilibrium can be verified. This is done by measuring the diameters of the pendant drop at several heights instead of only two. Tables required for the determination of $1/H$ from the different characteristic ratios of the drop diameters have also been computed by these authors. By ascertaining the constancy of $1/H$ values obtained from the different ratios, the attainment of equilibrium is confirmed and the accuracy of the results improved. We have used for our calculations of γ , this method by Ryong-Joon Roe *et al.*

Experimental

A drop of the liquid crystal was formed at the tip of a thin uniform capillary tube. The tip was ground so that it was free from any irregularities. The upper end of the tube was connected through a rubber tube to a hypodermic syringe. The drop size could be controlled by a fine

adjusting screw attached to the piston of the syringe. The lower portion of the capillary was completely enclosed in an air-tight thermostatic chamber. The top portion of the tube was enclosed in another heater with independent temperature controlling facility. The main chamber had two optically flat glass windows to allow the drop to be photographed. In order to prevent the vapour from condensing on glass, two additional side heaters were provided which could bring the windows to the same temperature as that at the centre of the chamber.

During the experiment the drop was in an atmosphere of nitrogen and was maintained at all times in equilibrium with its saturated vapour. To have a steady drop the entire system had to be at the same temperature, for even a gradient of less than 0.25°C between the top and bottom portions of the capillary tube was enough to push the drop completely into or out of the tube. Before taking the photograph at any temperature, it was visually checked that the drop was stationary for at least 15 min. A parallel beam of light from a mercury lamp was made to fall on the drop and focussed by a suitable lens system onto the focal plane of the camera. It was checked beforehand that the photographic system did not introduce any distortion. A green filter was used to avoid chromatic aberration effects. The temperature of the drop was measured using chromel-alumel thermocouple, the junction being kept close to the drop. As a preliminary check of the experimental set up, measurements were made on pure water and the values obtained at different temperatures agreed to within 1.5% with the reported values.

Results and discussion

p-anisaldazine: Experiments were first done on anisaldazine. The nematic-isotropic transition temperature of the sample was 182.2°C which appears to be the highest reported for this compound. Measurements were repeated using capillary tubes of different sizes and the values were found to be quite consistent. The γ - T characteristic obtained from the photographs of a single drop at different temperatures is shown in figure 1. We see that initially γ decreases with increase of temperature. But as T_* is approached, the slope changes and γ reaches a maximum at 182.1°C , which was the temperature closest to T_* at which measurements could be made. Above T_* , γ starts decreasing again, rapidly at first and then more gradually at higher temperatures.

p-azoxyanisole (PAA): Measurements were also made on PAA ($T_* = 135.2^{\circ}\text{C}$). The γ - T curve is shown in figure 2. Here again γ shows a decreasing trend at lower temperatures, but starts increasing near T_* . A special feature here is that γ continues to increase in the isotropic phase reaching a maximum at 139.3°C after which it decreases again.

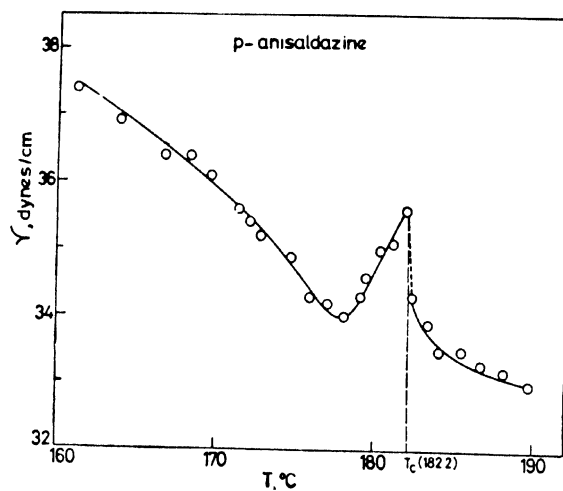


Figure 1 Surface tension of *p*-anisaldazine in the nematic and isotropic phases.

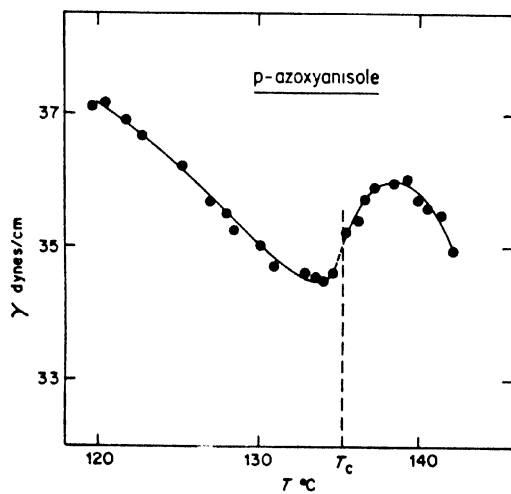


Figure 2 Surface tension of *p*-azoxyanisole in the nematic and isotropic phase.

The observed features of the γ - T characteristic of both compounds are in qualitative agreement with the theory of Croxton and Chandrasekhar¹⁰. There is evidence that in PAA the molecules are almost parallel to the

free surface¹¹ and that the orientation is practically independent of temperature in the nematic range. The surface orientation in anisaldazine is not known. In order to investigate the dependence of γ on molecular alignment at the free surface experiments are underway subjecting the drop to external fields.

Acknowledgement

The surface tension studies were initiated by Professor S Chandrasekhar. We are grateful to him for many useful discussions.

References

- 1 FERGUSON A and KENNEDY S J *Phil. Mag.* **26** 41 (1938)
- 2 NAGGIAR V *Ann. Physique* **18** 5 (1943)
- 3 SCHWARTZ W M and MOSLEY H W J. *Phys. Colloid Chem.* **51** 826 (1947)
- 4 GORSKII F K and SAKEVICH N M *Sov. Phys. Crystallogr.* **12** 586 (1968)
- 5 WHITE D W G *Trans. Metall. Soc. A I.M.E.* **236** 796 (1966) and *Metals, Materials and Metallurgical Reviews* p. 73 (July 1968)
- 6 CHANDRASEKHAR S *Mol. Cryst.* **2** 71 (1966)
- 7 RYONG-JOON ROE J. *Phys. Chem.* **69** 2809 (1965)
- 8 ANDREAS J M, HAUSER E A and TUCKER W B J. *Phys. Chem.* **42** 1001 (1938)
- 9 RYONG-JOON ROE, BACHETTA V L and WANG P M G J. *Phys. Chem.* **71** 4190 (1967)
- 10 CROXTON C A and CHANDRASEKHAR S - this Conference
- 11 LANGEVIN D and BOUCHIAT M A J. *de Physique* **33** C₁-77 (1972)

DISCUSSION

Billard : What method are you using to control the chemical purity of your samples ?

Shashidhar : The compounds were purified by several recrystallisations and the purity checked by measuring the nematic-isotropic transition temperature. However, it appears that the purity of sample does not critically affect the shape of the $\gamma-T$ curve. For instance, with anisaldazine the measurements were first made on a sample having $T_c = 181.5^\circ\text{C}$ and subsequently on a purer sample having $T_c = 182.2^\circ\text{C}$ (which appears to be the highest reported for this compound), but the $\gamma-T$ characteristic had essentially the same features in both cases.

Kaul : The error involved in using a flat capillary should be taken into account because the contact surface area varies with the drop size, in the case of a flat capillary. Would not it be better to use a capillary with the outer walls tapered ?

Shashidhar : It may be better to use a capillary tube with a sharp edge as suggested by you, though I feel it is unlikely to make much difference as far as the surface tension-temperature characteristic is concerned.

Leslie : Do you know the orientation of the anisotropic axis at the surface of the drop? Presumably the surface tension varies with this orientation, and one possible explanation of the shape of the curve near the isotropic transition is that the orientation changes near the transition.

Shashidhar : There is experimental evidence that in PAA the molecules are nearly parallel to the free surface and that their orientation is independent of temperature*. It would appear therefore that the suggestion that the shape of the curve is due to the change in orientation is not right. The surface orientation is not known in the case of anisaldazine.

* Langevin D and Bouchiat M A *J. de Physique* 33 C₄-77 (1972)

Estimation of rotational correlation times for PAA and MBBA by the dielectric relaxation and the neutron quasielastic scattering methods

J A JANIK

Institute of Nuclear Physics, Krakow, Poland

J M JANIK

Institute of Chemistry of the Jagiellonian University, Krakow, Poland

K OTNES

Institutt for Atomenergi, Kjeller, Norway

K ROSCISZEWSKI

Institute of Physics of the Jagiellonian University, Krakow, Poland

S WROBEL

Institute of Physics of the Jagiellonian University, Krakow, Poland

Abstract. Dielectric measurements in the microwave region were made for PAA over a wide temperature interval. The parameters of the Cole-Cole semicircle correspond to the dielectric relaxation time $\tau_d = 2.3 \cdot 10^{-11}$ s, for nematic PAA at 125°C. This relaxation time corresponds, we believe, to a rotation around the long PAA axis of the dipole moment of the molecule. We should stress the fact that the n^2 value is different from the extrapolated ϵ'_∞ value (for all temperatures), indicating the existence of a faster process (ca. $3 \cdot 10^{-12}$ s), possibly connected with a rotation around the long PAA axis of OCH_3 groups.

Additional information about rotational correlation time may be obtained from neutron quasielastic scattering (QNS) data for not too low momentum transfers. With this aim in view we have analysed the QNS data for nematic MBBA. Each QNS run was fitted by a curve composed of two Lorentz contours convoluted with the Gaussian resolution and added together with a certain fittable mixing factor. One of these Lorentzians appeared to be momentum transfer independent, indicating that it is connected with rotational jumps. Its width gave the effective rotational correlation time τ_o for MBBA at ca. 25°C as equal to ca. $3 \cdot 10^{-12}$ sec.

Introduction

In earlier papers, neutron quasielastic scattering (QNS) spectra for nematic PAA were interpreted in terms of translatory diffusion¹⁻⁵. According to

the theories of QNS⁶⁻⁹, such an interpretation is correct only if the neutron wavevector transfer κ is very small, a condition which has so far been fulfilled in experiments⁵. It was argued, on the basis of dielectric relaxation experiments¹⁰, that rotational motions of the PAA molecule about its long axis, being responsible for relaxation times of the order of 10^{-11} s, cannot contribute significantly to a broadening of neutron peaks, thus giving the right to interpret neutron data in terms of translatory diffusion even for larger κ . However, a discrepancy between the diffusion coefficients so estimated for large κ ^{1,3,4} and those for small κ , which amounted to a factor of five, made the above argument suspicious.

In view of this situation, we decided to extend the previously published dielectric relaxation data for PAA¹⁰ to a wider frequency region in order to detect the possible appearance of another relaxation region besides the one at 10^{-11} s. We also decided to interpret the QNS measurements with MBBA¹¹ on the basis of a new Rosciszewski theory⁹ from which times between rotational jumps of protons in the molecule may be estimated, and compared the results with the dielectric relaxation times for PAA.

There is of course some doubt whether we are entitled to compare dielectric measurements for one substance (PAA) and QNS measurements for another (MBBA). In dielectric measurements performed in the GHz region only rotations about long molecular axes may play any role. In QNS measurements proton jumps corresponding to the same rotations should be seen as well as proton jumps of CH₃ end groups about their triple axes. We may expect that the rotational motions involved in both types of measurements are similar for PAA and MBBA. An advantage of MBBA over PAA in neutron measurements lies in the lower temperatures of the nematic region for the former, resulting in smaller inelastic (phonon) backgrounds which must be subtracted in the process of isolation of QNS peaks.

Preliminary results of some of these measurements have already been published in a letter¹².

Dielectric relaxation measurements

Dielectric measurements for PAA were made for frequencies: 300 kHz, 1.70 GHz, 6.69 GHz, 9.76 GHz, 22.68 GHz and 37.31 GHz in the Institute of Physics of the Jagiellonian University in Krakow. The temperature region from ca. 95°C to ca. 160°C was covered. Figure 1 presents ϵ' and ϵ'' vs. temperature. Figure 2 presents for one temperature (125°C) the Cole-Cole diagram. Similar diagrams may be made for other temperatures. From arcs of the circles so obtained, dielectric relaxation times were determined, and from their temperature dependences activation barriers for isotropic and nematic phases were estimated by applying the Bauer formula¹³. Table 1 presents the values.

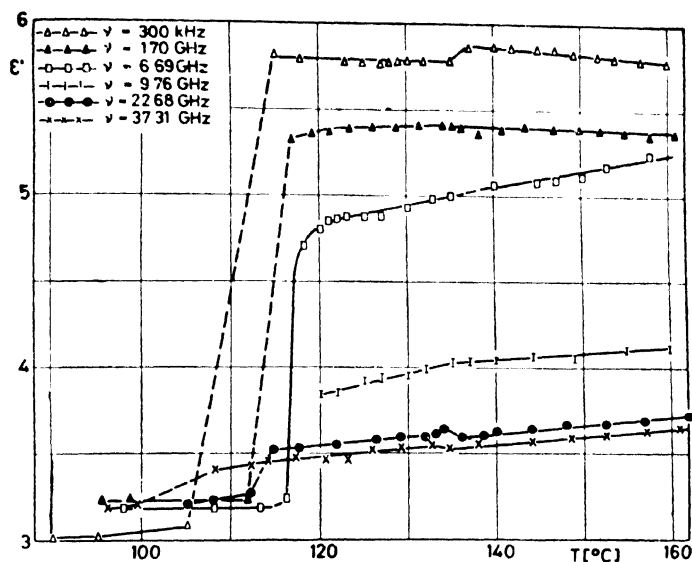


Figure 1 (a) ϵ' vs. temperature for PAA.

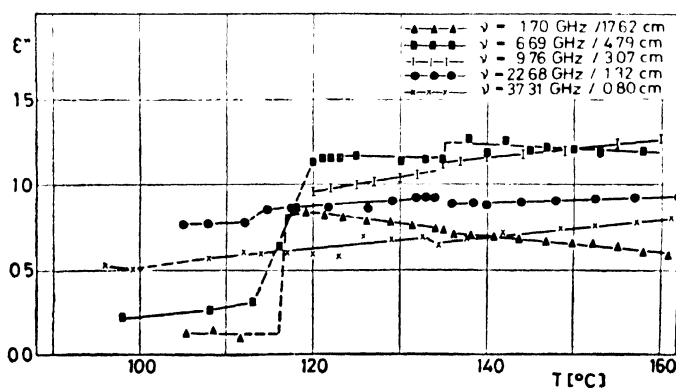


Figure 1 (b) ϵ'' vs. temperature for PAA.

These results, although more accurate, are essentially the same as those published before¹⁰ on the basis of poorer experimental material (three frequencies only). A new phenomenon which was discovered with more frequencies involved in making Cole-Cole diagrams is this: the extrapolated ϵ'_∞ values differ from the corresponding n^2 values, as may be seen in figure 2. There is a possibility that it is an indication of a second relaxation region, and the corresponding relaxation times are ca. $3 \cdot 10^{-12}$ s.

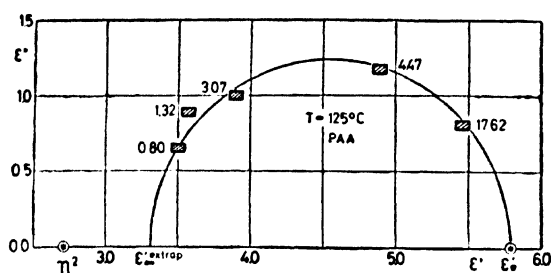


Figure 2 The Cole-Cole diagram for PAA at 125°C.

Table 1. Dielectric relaxation times and activation barriers obtained from Cole-Cole diagrams based upon results of figure 1 for PAA.

Phase	Activation barrier (Kcal/mole)	Temperature (°C)	Relaxation time (10^{-12} s)
Isotropic	2.2	160	17.8
		155	18.8
		150	19.4
		140	20.1
		130	21.7
Nematic	2.7	125	22.8
		120	24.0

We interpret these results as follows: Relaxation times (10^{-11} s) and the barriers collected in table 1 correspond to rotation about the long axis of the main dipole moment, which in the PAA molecule is connected with the N_2O group. It is a possibility that additional dipole moments connected with CH_3 end groups execute a much faster motion about the same axis, giving the second relaxation region (ca. $3 \cdot 10^{-12}$ s).

Neutron quasielastic scattering measurements

Neutron scattering measurements for MBBA were made at the JEEP II reactor in the Institute for Atomenergi at Kjeller. By applying a magnetic field it was possible to orient the sample and to perform measurements in two "geometries" $\mathbf{x} \parallel \mathbf{n}$ and $\mathbf{x} \perp \mathbf{n}$ (\mathbf{n} is the nematic director), as described, for instance, in Ref. 2. Figure 3 presents typical data, after subtraction

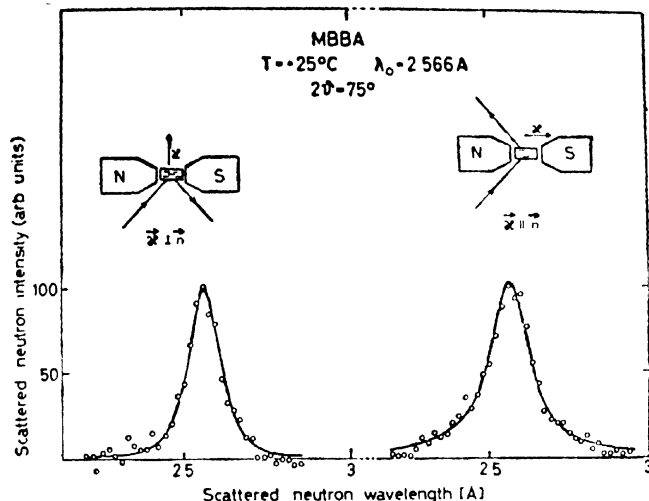


Figure 3 Neutron quasielastic peaks for nematic MBBA. Solid lines correspond to theoretical fits as explained in the text.

of the inelastic (phonon) background. There are altogether 21 such runs distributed among three values of κ , from the 2.4 \AA^{-1} to 3.5 \AA^{-1} interval. Results were fitted to the form of scattering law derived by Rosciszewski⁹.

$$S_s(\kappa, \omega) = \frac{1}{\pi} \left[F^\infty \frac{\Gamma_1}{\Gamma_1^2 + \omega^2} + (1 - F^\infty) \frac{\Gamma_2}{\Gamma_2^2 + \omega^2} \right] F_{(\omega)}^{\text{vib}} F_{(\omega)}^{\text{libr}} + \frac{1}{\pi} \left[1 - F_{(\omega)}^{\text{vib}} \cdot F_{(\omega)}^{\text{libr}} \right] \frac{\Gamma_3}{\Gamma_3^2 + \omega^2} \quad (1)$$

where Γ_1 , Γ_2 and Γ_3 are parameters characterizing the three Lorentzians, $\hbar/2\pi\omega$ is the energy transfer at the scattering, and F^∞ , $F_{(\omega)}^{\text{vib}}$ and $F_{(\omega)}^{\text{libr}}$ are certain formfactors. The physical meaning of the formula is as follows: We assume that a proton in the molecule performs (a) translatory jumps together with the whole molecule; average time between jumps is τ'_0 and the duration of the jump is τ'_1 ; (b) rotatory jumps about a certain axis; average time between jumps is τ_0 and the duration of the jump is τ_1 . Moreover, we assume that $\tau'_0 \gg \tau'_1$ and $\tau_0 \gg \tau_1$. Under these assumptions the first Lorentzian represents a broadening of the neutron line caused by translatory jumps only and $\Gamma_1 = \hbar/\pi\tau'_0$, second Lorentzian represents a broadening caused by translatory and rotatory jumps together and $\Gamma_2 = \hbar/\pi\tau_{00}$, $\frac{1}{\tau_{00}} = \frac{1}{\tau'_0} + \frac{1}{\tau_0}$ and the third term is only for the sake of simplicity assumed as Lorentzian - Γ_3 , having thus no simple physical meaning, representing in a complicated manner inelastic anharmonic effects mixed together with translations and rotations.

In our fitting procedure we made the best choice of four parameters; F^∞ , $F_{(\omega)}^{\text{vib}}$, $F_{(\omega)}^{\text{libr}}$, Γ_2 and $\Gamma_3 \cdot \Gamma_1$ was not treated as a fittable parameter because the τ'_0 value was approximately known from the NMR data¹⁴ as being equal to 10^{-9} s. It has appeared that F^∞ is very small, thus making negligible the contribution of the first term of the formula (1). Γ_2 values obtained in this fitting could be put equal to $\frac{h}{\pi\tau_0}$ in view of the above quoted τ'_0 value. In this way we came to the conclusion that our neutron data for MBBA are explained by rotations (one Lorentzian) and inelastic anharmonic terms (another Lorentzian) only. Figure 4 presents the effective τ_0 vs. κ^2 obtained in this way for both "geometries", and figure 5 the $F_{(\omega)}^{\text{vib}} \cdot F_{(\omega)}^{\text{libr}}$ vs. κ^2 .

We interpret these results as follows: τ_0 , being a molecular property, is not dependent on κ and may be understood as an effective time between rotational proton jumps in the MBBA molecule; it amounts to ca. $3 \cdot 10^{-12}$ s. $F_{(\omega)}^{\text{vib}} \cdot F_{(\omega)}^{\text{libr}}$ is a product of Debye-Waller factors corresponding to translatory vibrations of the whole molecules and librations of the whole molecule about its long axis; its behaviour with κ showing a decreasing tendency with κ increasing is a reasonable one for Debye-Waller factors. The main task is now to interpret the observed anisotropy *i.e.* the different values of τ_0 for $\kappa \parallel \mathbf{n}$ and $\kappa \perp \mathbf{n}$ and the same for $F_{(\omega)}^{\text{vib}} \cdot F_{(\omega)}^{\text{libr}}$. We shall give here a *possible* explanation not claiming that this is a unique one.

The neutron experiment with $\kappa \parallel \mathbf{n}$ has little sensitivity to proton rotational jumps about the long molecular axis; it sees preferentially proton jumps of CH_3 end groups about their triple axes. The experiment with $\kappa \perp \mathbf{n}$, on the other hand, sees both types of proton jumps. As in the first motion only six protons are involved, whereas in the second one all twenty protons take part, we should observe the rotational quasielastic component enhanced in comparison with the inelastic anharmonic one for the $\kappa \perp \mathbf{n}$ case. It is indeed so, because we see from figure 5 that $F_{(\omega)}^{\text{vib}} \cdot F_{(\omega)}^{\text{libr}}$ is much larger for $\kappa \perp \mathbf{n}$ than for $\kappa \parallel \mathbf{n}$. In view of this picture, the difference in τ_0 for $\kappa \parallel \mathbf{n}$ and $\kappa \perp \mathbf{n}$ ($2.5 \cdot 10^{-12}$ and $3.3 \cdot 10^{-12}$ s respectively) may be treated as evidence that CH_3 end groups rotate about their triple axes faster than does the whole molecule about its long axis.

Conclusions

1. Dielectric relaxation measurements performed in the GHz region in nematic PAA led to the relaxation time of ca. $2 \cdot 10^{-11}$ s, which is interpreted as being connected with reorientations of the main dipole moment of the molecule about its long axis.
2. An indication of the second dielectric relaxation region was obtained in these measurements with PAA; the corresponding relaxation time is ca. $3 \cdot 10^{-12}$ s and is perhaps connected with rotations of the CH_3 end groups about the long molecular axis.

3. Neutron incoherent quasielastic scattering measurement performed in nematic MBBA led to an *effective* time between rotational jumps of protons in the molecule of ca. $3 \cdot 10^{-12}$ s. By using two "geometries", $\kappa \parallel n$ and $\kappa \perp n$, it was possible partly to separate the two motions: proton rotational jumps in CH_3 groups about their triple axes and

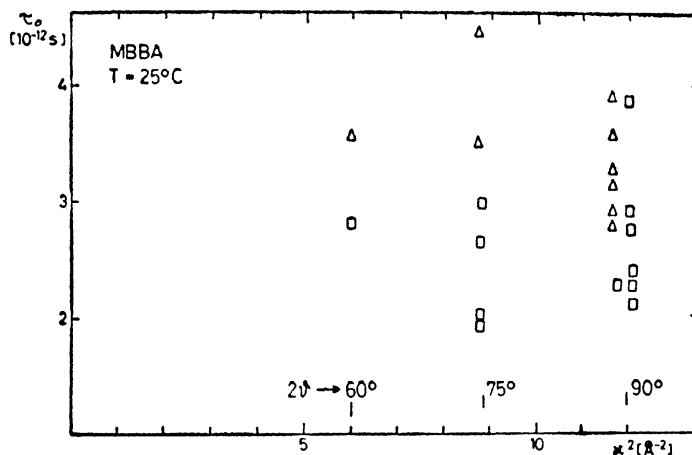


Figure 4 τ_0 vs. κ^2 for MBBA. \square corresponds to $\kappa \parallel n$, Δ corresponds to $\kappa \perp n$.

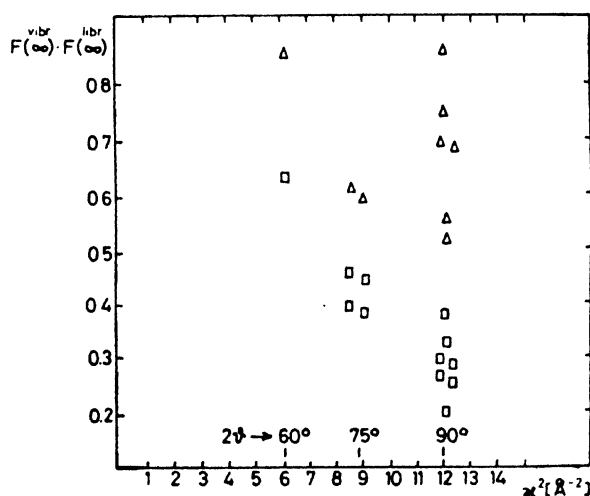


Figure 5 $F_{(\infty)}^{\text{vibr}} / F_{(\infty)}^{\text{libr}}$ vs. κ^2 for MBBA. \square corresponds to $\kappa \parallel n$, Δ corresponds to $\kappa \perp n$.

rotational jumps of all protons in the MBBA molecule about the long molecular axis.

References

- 1 JANIK J A, JANIK J M, OTNES K and RISTE T *Mol. Cryst. Liquid Cryst.* **15** 18 (1971)
- 2 JANIK J A, JANIK J M, OTNES K and PYNN R *IAEA Symposium on Inelastic Neutron Scattering* Grenoble, p. 515 (1972)
- 3 LEADBETTER A J and TEMME F (to be published)
- 4 BLINC R, DIMIC V, PIRIS J, VILFAN M and ZUPANCIC I *Mol. Cryst. Liquid Cryst.* **14** 97 (1971)
- 5 TOPLER J, ALEFELD B and SPRINGER T *Mol. Cryst. Liquid Cryst.* **26** 297 (1974)
- 6 LARSSON K E *Phys. Rev.* **A3** 1006 (1971)
- 7 LARSSON K E *J. Chem. Phys.* **59** 4612 (1973)
- 8 ROSCISZEWSKI K *Acta Phys. Pol.* **A44** 549 (1972)
- 9 ROSCISZEWSKI K (to be published)
- 10 JANIK J A, WROBEL S, JANIK J M, MIGDAL A and URBAN S *Faraday Symposia of the Chemical Society* **6** (1972)
- 11 OTNES K, JANIK J A, JANIK J M and ROSCISZEWSKI K (to be published in *Physica*)
- 12 JANIK J A, JANIK J M, NGUYEN THI TOA, ROSCISZEWSKI and WROBEL S *Phys. Status. Solidi (a)* **18** K143 (1973)
- 13 BAUER E *Cah. Phys.* **144** 20 1
- 14 SAMULSKI E T, DYBOWSKI C R and WADE C G *Phys. Rev. Lett.* **29** 340 (1972)

DISCUSSION

de Vries: On your last slide I noticed a 90° bond angle just to the right of the right-most benzene ring. Is this angle meant to be that way or is this an oversight?

Janik: It is perhaps an improper perspective of the drawing. There is no right angle there of course.

Demus: If the centre of Cole-Cole-plot lies directly on the axis this is interpreted as a single relaxation mechanism. In PAA you suppose a second fast relaxation. I want to ask where the centre of your Cole-Cole-plot lies for PAA?

Janik: It lies not far from the ϵ' axis for 10⁻¹¹s relaxation region. Where it lies for the supposed second region is impossible to say.

Darbari: (1) Will it not be interesting to substitute the methyl group with some larger group and observe if the faster τ_c corresponds to this substitution?

(2) If one studies such a dynamic phenomenon in smectics perhaps the so-called rotation of the overall molecule may further be hindered and one may be able to isolate the two processes as you propose.

Janik: (1) Yes, or one may deuterate certain groups of interest, and compare with results for the non-deuterated sample.

(2) This is perhaps a good idea, although one must be very careful in such comparisons because, no doubt, the rotational situation in liquid crystals is very complicated.

Saupe: A difference between ϵ'_{∞} and the (extrapolated) refractive index n^2 as obtained from measurements in the visible range is quite commonly observed. It is due or partly due to the neglect of the infrared part, that is, the molecular polarizability connected with a distortion of its structure.

Janik: Yes, certainly. Our explanation of $n^2 \neq \epsilon'_{\infty}$, which is consistent with a faster dielectric relaxation region, is a 'possible' explanation.

de Vries: (to Usha Deniz): You mentioned that the comparison of the neutron data of the crystalline phase at 27°C and the supercooled S_B phase showed that in the latter there is a motion of the H atoms which is not present in the former. Would a rotation of the end methyl groups about their C-C bond be sufficient to explain these effects or would the rotation have to involve more carbon atoms? Since I would probably classify this S_B phase as an S_H phase I would expect that there would be little possibility for rotation of anything but the end groups.

Usha Deniz: If we had a reliable model on the basis of which we could work out the dynamics of HBPA in the liquid crystalline phases, we could then use the ratio of the intensities of the translational and rotational contributions to our spectra to find out how many protons take part in the rotational motion of the molecule. This would indeed tell us whether it is only the protons of the end methyl groups which take part in such a rotational motion. Since such a reliable model is not there at present, I will have to repeat my experiments with a sample in which the relevant parts of the molecule are deuterated. The reduction in intensity of the rotational wings as compared to that in the translational peak would then give me the answer to your question.

Some electrical properties and ordering in the *p-n*-alkoxybenzoic acids

E F CARR

Physics Department, University of Maine, Orono, Maine 04473, USA.

Abstract. The work discussed here involves the *p-n*-alkoxybenzoic acids, propyloxy-through nonyloxy-benzoic acid. Much of the discussion is concerned with a review of earlier work on *p-n*-butyloxy and *p-n*-nonyloxybenzoic acid. Some preliminary results are presented on other benzoic acids and results on other materials are discussed in so far as they relate to the benzoic acids. The *p-n*-alkoxybenzoic acids exhibit some unusual changes in dielectric properties at transition temperature, and these are explained by assuming an abrupt change in concentration of the monomer at the transition. The conductivity anisotropy exhibits some unusual behavior in the nematic phase and this is explained by assuming the existence of hydrogen-bonded clusters as well as a cybotactic structure involving dimers.

1. Introduction

The work discussed here involves the *p-n*-alkoxybenzoic acids, propyloxy through nonyloxybenzoic acid. The first four exhibit only a nematic phase, but the last three exhibit both nematic and smectic C phases. Work on other materials will be mentioned only in so far as it relates to these materials. Gray¹ has given a general discussion of this homologous series. The transition temperatures have been reported by Gray and Jones² and by Herbert³ who also measured the transition energies.

The experimental techniques which involve microwave dielectric loss measurements and also the use of these measurements to indicate the degree of molecular alignment in the presence of electric fields have been discussed earlier⁴. The electrical conductivity was measured with an electrometer employing dc voltages that were low enough to avoid appreciable polarization effects. These measurements were simplified since only the ratios of the conductivities parallel and perpendicular to the nematic director were necessary. The resistivities of most of the samples were the order of 10⁹ ohm-cm.

2. Dielectric properties

Microwave dielectric properties

Chou and Carr⁵ have reported the temperature dependence of the dielectric loss at a frequency of 24.5 GHz for *p-n*-nonyloxybenzoic acid (NOBA) as shown in figure 1. In the nematic phase (117-143°C) a 10 kG

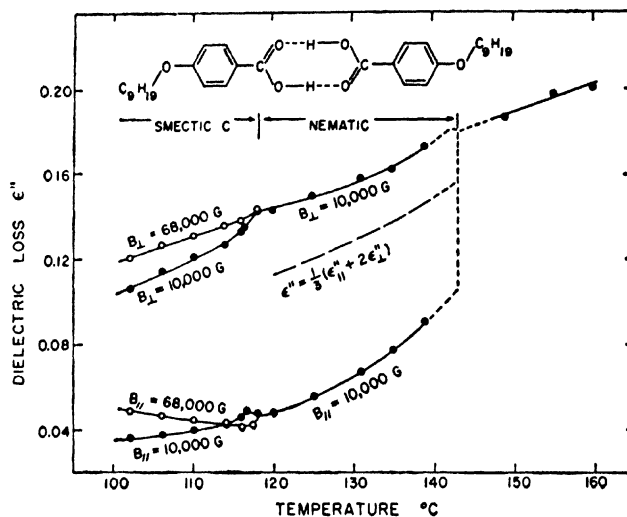


Figure 1 Temperature dependence of the dielectric loss at a frequency of 24.5 GHz in magnetic fields of 10 and 68 kG parallel and perpendicular to the microwave electric field in *p*-*n*-nonyloxybenzoic acid. With permission.

magnetic field was sufficient to align the nematic director perpendicular to the polarized microwave electric field giving maximum absorption and parallel to the microwave field giving minimum loss. The results in the smectic C phase were obtained by cooling from the nematic phase in the presence of a magnetic field. A 68 kG field appears to be more effective in aligning the director than a 10 kG field when aligning the director perpendicular to the microwave field but the parallel case is confusing. Because of uncertainties which may involve alignment due to wall effects, unwanted reflections due to a low power loss, or the structure in the nematic phase before cooling, the parallel case still remains confusing. The most significant information concerning the smectic phase is that if the dielectric loss changes at the nematic-smectic transition, the change is small. This implies that the freedom of rotation of the dipoles about the long molecular axes is not greatly affected in going from the nematic to the smectic C phase.

The changes in the dielectric loss at the nematic-isotropic transition are unusual⁶. If it can be assumed that the average value of the dielectric loss in the nematic phase can be represented by $\frac{1}{3}(\epsilon''_{\parallel} + 2\epsilon''_{\perp})$, figure 1 shows a sizable change in the average value of the loss at the nematic-isotropic transition. A similar change has been reported⁷ for *p*-*n*-butoxybenzoic acid (BOBA), but a change of this magnitude is unusual for liquid crystals. Preliminary measurements on octyloxy and heptyloxybenzoic acid also indicate a sizable change in the average value of the dielectric loss at the transition.

The possibility of this sizable change in the dielectric loss at the nematic-isotropic transition being associated with other liquid crystals that form linear dimers was checked using *p*-methoxycinnamic acid. This material is not very stable so the results shown in figure 2 are not of high quality, but they do show a change in the average value of the dielectric loss at the transition. Schultz and Meier⁸ have observed a similar effect for butylbenzoic acid. These results imply that this change in the loss is common to liquid crystals that form linear dimers.

A possible explanation for the change in dielectric loss at the nematic-isotropic transition may be associated with a small percentage of monomer or open dimer. This idea assumes that because of the breaking and reforming of hydrogen bonds there may be a sufficient concentration of the monomer or open dimer to affect the dielectric properties. The formation and destruction of hydrogen bonds in *p*-heptoxybenzoic acid have recently been investigated by Deloche and Cabane⁹ using NMR techniques. Since Schultz and Meier⁸ were able to observe an appreciable absorption in *p*-*n*-butylbenzoic acid, and the dimer should not exhibit a dipole moment, it seems that an appreciable concentration of the monomer or open dimer would have been present. In order to explain the abrupt change in loss at the transition it is necessary to assume that the concentration of monomer or open dimer must change abruptly at the transition. This would result in an increase in the dipole moment due to the carboxyl group. The relaxation time of the carboxyl group probably does not change much at the transition, but it may be quite

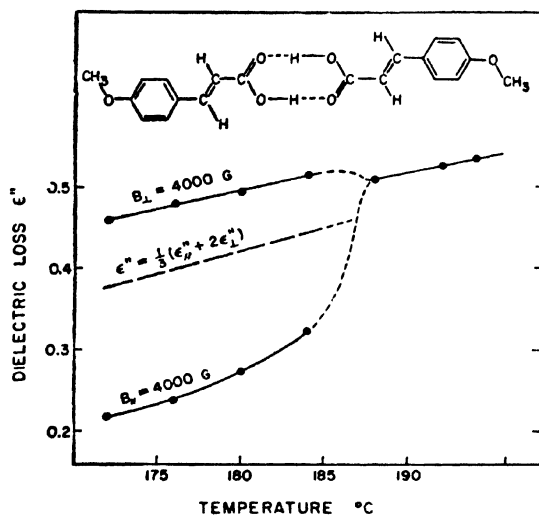


Figure 2 Temperature dependence of the dielectric loss at a frequency of 24.5 GHz in a magnetic field of 4 kG parallel and perpendicular to the microwave electric field in *p*-methoxycinnamic acid.

different from that of the alkoxy groups which could allow for a higher loss at 24.5 GHz. Axmann¹⁰ has measured the characteristic relaxation time in 4,4'-di-*n*-hexyloxyazobenzene and 4,4'-di-*n*-octyloxyazobenzene and reported no appreciable changes in the relaxation times at the transition temperatures. In view of Axmann's results it seems unlikely that a change in the relaxation time, which was associated with the alkoxy group of the benzoic acids, could account for the change in loss at the transition. However, a change in concentration of the monomer or open dimer may affect the relaxation time which is associated with the alkoxy groups of the benzoic acids. Although the transition energies³ in the alkoxybenzoic acids are higher than in many other liquid crystals, they will not permit large changes in concentration of the monomer or open dimer.

Static or low frequency dielectric properties

Some information concerning the static dielectric constant can be obtained by investigating the molecular alignment in audiofrequency electric fields. An ordering is preferred such that the dielectric constant is a maximum in the direction of the field if effects due to ionic conduction are absent. Chou and Carr¹¹ have obtained results which show the preferred direction for the director in the nematic and smectic phases of NOBA due to a 20 kHz electric field. These results are shown in figure 3. The two dashed curves that show the dielectric loss in the presence of a 10 kG magnetic field are merely to indicate the dielectric loss when the director is parallel and perpendicular to the microwave electric field as shown in figure 1. The data for the 20 kHz field were obtained in the absence of any magnetic field. The results in figure 3 show that the preferred direction for the long molecular axes is parallel

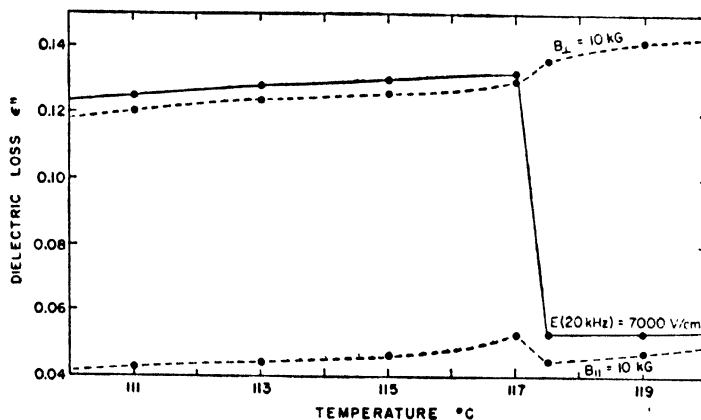


Figure 3 Dielectric loss at 24.5 GHz for NOBA as a function of temperature in the presence of a 20 kHz electric field at 7 kV/cm. Reproduced with permission from *Ordered Fluids and Liquid Crystals*, Plenum Press (to be published).

in the nematic and perpendicular in the smectic phase to a 20 kHz electric field. This implies that the static dielectric anisotropy changes sign at the nematic-smectic transition. A possible explanation for the change in the dielectric anisotropy involves a mechanism reported by Maier and Meier¹² and discussed recently by Martin, Meier and Saupe¹³. This mechanism involves a molecular rotation about an axis perpendicular to the long molecular axis and is associated with the component of the dipole moment parallel to the long axis. Because of symmetry this would not apply to the dimer but could apply to a monomer due to the dipole moment parallel to the long axis. If the concentration of the monomer decreases with a decrease in temperature at the nematic-smectic transition, the dielectric constant in the direction of the director could decrease which might allow for the change in sign of the dielectric anisotropy. The concentration of the monomer involved would probably be quite small because the dielectric anisotropy in the nematic phase near the transition is probably between $\Delta\epsilon' = 0.01$ and $\Delta\epsilon' = 0.02$ for NOBA. Earlier work¹¹ indicated that the dielectric anisotropy decreased in the nematic phase with a decrease of temperature rather than increase as expected. This decrease in the dielectric anisotropy could also be explained by assuming a decrease in the concentration of the monomer with a decrease in temperature. Although the concentration of the monomer required for the explanation given here is probably much larger than that expected by other investigators, Deloche and Cabane⁹ have predicted a decrease in the concentration of the monomer with a decrease in temperature.

The dielectric anisotropy was checked for the heptoxy- and octyloxy-benzoic acids at the nematic-smectic C transition. The results were comparable to those shown in figure 3 in that the dielectric anisotropy changed sign at the nematic-smectic C transition. The sign of the dielectric anisotropy of *p*-heptoxybenzoic acid in the nematic phase has been uncertain⁷. It is so small that it can easily be affected by impurities. A very pure sample showed that it is positive in the upper part of the nematic range and it is still slightly positive a couple of degrees above the nematic-smectic transition, but it is difficult to establish that the change of sign does not take place above the nematic-smectic transition. The dielectric anisotropy for the propoxy- to hexoxy-benzoic acids is positive in the nematic phase.

3. Conductivity anisotropy

Chou and Carr¹¹ have investigated the electrical conductivity anisotropy in NOBA as a function of both time and temperature as shown in figures 4 and 5. Figure 4 shows the ratios of the conductivities parallel and perpendicular to the nematic director as a function of time, where σ_{\parallel} and σ_{\perp} represent the conductivity parallel and perpendicular to the nematic director respectively. The data for the upper curve were obtained after heating from the solid to the nematic at 134° C and the data for

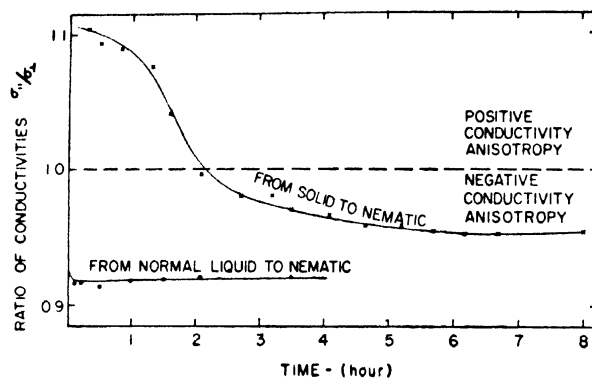


Figure 4 Time dependence of the ratio of the dc conductivities for NOBA at 134°C. Reproduced with permission from *Ordered Fluids and Liquid Crystals*, Plenum Press (to be published).

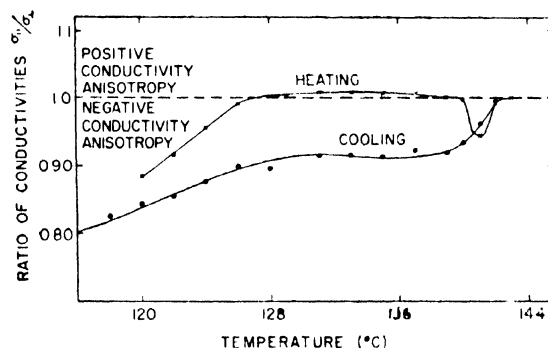


Figure 5 Temperature dependence of the ratio of the dc conductivities for NOBA. Reproduced with permission from *Ordered Fluids and Liquid Crystals*, Plenum Press (to be published).

the lower curve were obtained after cooling from the isotropic liquid to 134°C. The upper curve showed that the direction corresponding to maximum conductivity changed from parallel to perpendicular to the nematic director in a couple of hours.

The data for the heating curve in figure 5 were obtained after the sample had been melted from the solid and kept at 120°C for about 7 hours. The data for the cooling curve were obtained after the sample had remained in the isotropic liquid for about 1 hour. The heating and cooling rates were about 10 min. per degree. Results on other samples of NOBA varied a little but the results were essentially the same. The heating curves always showed a dip in the neighborhood of 141°C, and

the cooling curves would often show a small dip here. The dip in the heating curve in the neighborhood of 141°C is very interesting and may imply that more than one mechanism is necessary to explain the results of figures 4 and 5.

In view of the x-ray¹⁴ and conductivity anisotropy^{15,16} results in *p*-heptoxyazoxybenzene, the possibility of dimers forming cybotactic groups (layered structures) as shown in figure 6a must be considered¹¹. In order to allow for a time dependence as shown in figure 4, a structure illustrated in figure 6b was suggested¹¹. It was suggested that both mechanisms are involved in the entire nematic range, but that one may predominate in any portion of the range. The structure illustrated in figure 6b may bend and become entangled with other hydrogen bonded clusters or cybotactic groups as well as dimers and monomers. This might be the arrangement when heated from the solid to the nematic phase. Equilibrium could be approached by a process of breaking up and reforming clusters. This would involve a rapid formation and destruction of hydrogen bonds. The dimers might prefer a layered structure quickly but the tendency to form hydrogen bonded clusters could prevent this. If a cybotactic structure like that illustrated in figure 6a is formed, then polymerization as illustrated in figure 6b could take place rather quickly. This might aid in explaining the greater degree of ordering in the cooling curve if it could be assumed that the cybotactic mechanism was more effective in the upper portion of the nematic phase than in the lower portion. This might also explain the dip in the heating curve in the neighborhood of 141°C.

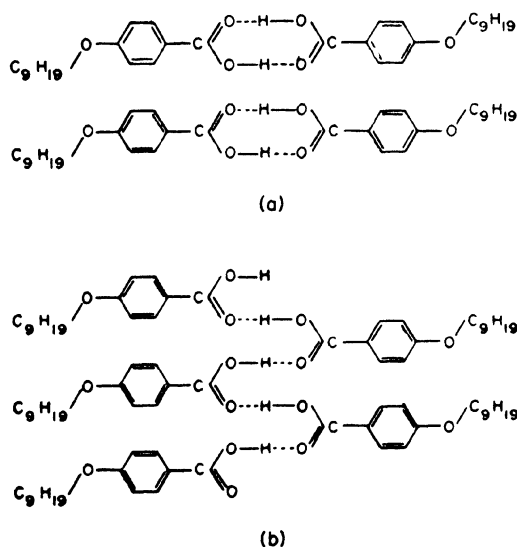


Figure 6 Possible structures for NOBA.

The most stable state should correspond to the minimum value of the ratio of the conductivities but this is probably never reached. If an experiment was carefully carried out with the intention of reaching equilibrium it would require so much time that decomposition of the sample would upset the state of the system. It seems strange that the conductivity anisotropy as shown for the heating curve could change to positive at 128° C, but when one changes the temperature of an entangled structure, the size of the cluster may change and some of the ordered regions may be broken up. Temperature gradients may play an important role. It should be pointed out that not all heating curves showed a positive conductivity anisotropy, although they showed a dip in the neighborhood of 141° C.

It was reported earlier¹¹ that the sign of the conductivity anisotropy normally did not change when the sample was heated quickly from a temperature of 134° C to the isotropic liquid and cooled quickly to 134° C, but if it remained in the normal liquid for at least half an hour, it always returned to 134° C with a negative conductivity anisotropy. This observation is difficult to understand and will be investigated further. It would appear that mechanisms such as those that are discussed here may be involved just above the transition, but this is difficult to accept.

Rondelez¹⁶ investigated the conductivity anisotropy in *p*-octyloxybenzoic acid (OOBA) and reported a positive conductivity anisotropy for the entire nematic range. Preliminary measurements by the author agreed with Rondelez's work in the upper portion of the nematic range, but in the lower nematic range results have been obtained which show both positive and negative conductivity anisotropies. The lower portion of the nematic range of *p*-heptoxybenzoic acid showed a positive conductivity anisotropy but in some cases $\sigma_{||} / \sigma_{\perp}$ was very close to one. For a very pure sample a negative conductivity anisotropy was observed in *p*-heptoxybenzoic acid just below the nematic-isotropic transition. The anisotropy was very small and could not be observed after the sample had decomposed by heating for a few hours. This implies that impurities have some effect on the anisotropy. A comparison of the results on the nonyloxy-, octyloxy- and heptoxy-benzoic acids indicate some consistencies, but the observation of a positive conductivity anisotropy just below the nematic-isotropic transition in OOBA is hard to explain. OOBA was purified by recrystallization while the other two were purified by recrystallization and chromatographic methods. In view of possible impurity effects, studies are now in progress to repeat most of the measurements discussed here with emphasis on purity.

4. Molecular alignment due to electric fields

The effect of a low frequency electric field on the molecular alignment in NOBA has been investigated by Chou and Carr and some of these results are shown in figure 7. These results are similar to those published

earlier⁵ except the cut-off frequency is much higher. The nematic director was initially aligned parallel to the microwave electric field with a 2 kG magnetic field. The increase in absorption with an increase in electric field intensity shows that the preferred direction for the nematic director is perpendicular to low audio frequency fields. The conductivity anisotropy for the results shown in figure 7 was negative ($\sigma_{\perp} > \sigma_{\parallel}$). Figure 3 shows that the preferred direction of the director for frequencies above the cut-off frequency is parallel to the electric field. These results can be explained by the counteraction of the dielectric and conductivity anisotropies which are of opposite sign. The explanation is similar to that presented earlier^{4,17} except for a change in sign of both the dielectric and conductivity anisotropies.

A comparison¹¹ of the relative effectiveness of a magnetic and 100 Hz electric field for producing molecular alignment in NOBA indicates that the torque on the sample is proportional to E^2 . This comparison is only for a small range of fields and is made at a value of the dielectric loss corresponding to a random orientation of the molecules. This behavior is similar to that reported earlier¹⁷ for materials exhibiting positive conductivity and negative dielectric anisotropies.

Figure 7 shows that low audio frequency fields do not rotate the nematic directors of all the clusters by 90 degrees. This was the case for materials exhibiting positive conductivity and negative dielectric anisotropies and was later shown to be consistent with a detailed theoretical treatment by Helfrich¹⁸. Viscosity measurements are not available for a theoretical discussion of the results on NOBA, but the results appear to

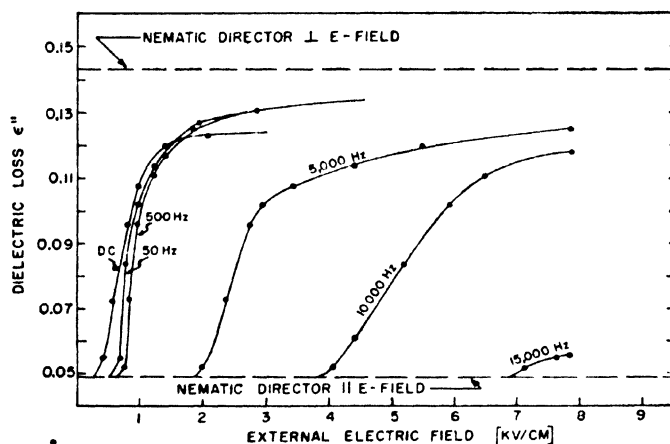


Figure 7 Dielectric loss in *p*-*n*-nonyloxybenzoic acid at a microwave frequency of 24.5 GHz as a function of an externally applied electric field. The individual curves are for various frequencies of the electric field applied parallel to a 2000-G magnetic field. The temperature was 120° C.

indicate that the conductivity is a maximum perpendicular to the nematic director. This implies that the structure in the nematic phase is more like a smectic A than smectic C type structure. This is consistent with the optical observations of Taylor, Fergason and Arora¹⁹ in that they reported that the nematic phase was uniaxial. It should be pointed out that the sign of the conductivity anisotropy in their work was not known, so it is not certain that a comparison with the work discussed here should be made. Chistyakov *et al*²⁰ have investigated the nematic and smectic phase of NOBA employing x-ray techniques, but due to the uncertainties concerning the use of electric fields, it is difficult to relate the work to that discussed here.

An investigation⁷ of the frequency dependence of electric fields for producing molecular alignment in *p-n*-butoxybenzoic acid (BOBA) showed that low audio frequency fields were more effective than fields of much higher frequencies. The nematic phase of this material exhibits positive dielectric and positive conductivity anisotropies. The preferred direction for the directors due to ionic conductivity is consistent with earlier work¹⁷ and the results also suggest that the torque which is associated with the conductivity anisotropy is proportional to E^2 . Preliminary results on the propoxy-, pentoxy- and hexoxy-benzoic acids indicate a behavior similar to that reported for BOBA. These materials also show intensive light scattering in the presence of low audio frequency fields, which may seem a little unusual since they exhibit a positive dielectric anisotropy.

A few measurements have been reported¹¹ on the effect of dc and low audio frequency electric fields in the smectic C phase of NOBA. These results were obtained by cooling from the nematic to the smectic phase in the presence of the fields. The results showed that there is an effect on the alignment due to electric fields which is frequency dependent. Although a detailed study has not been carried out, the results do indicate a behavior that is more consistent with a smectic C than smectic A type of structure.

5. Conclusions

The results on the nematic phase of the *p-n*-alkoxybenzoic acids, which also exhibit a smectic C phase, seem to indicate the presence of monomers, dimers, cybotactic groups and hydrogen bonded clusters. The concentration and sizes of the various groups should be temperature dependent. In general, the various clusters of molecules probably involve both the cybotactic and hydrogen bonding mechanisms. The most stable state in NOBA appears to correspond to the smallest value of the ratio of the conductivities parallel and perpendicular to the nematic director, ($\sigma_{\parallel} / \sigma_{\perp}$). This state of the system is approached by a process of breaking up and reforming of clusters of molecules which also involves the destruction and formation of hydrogen bonds. A small change in the concen-

tration of the monomer at the transition temperatures has been suggested to explain the dielectric behaviour at the transitions.

It is not clear how the model discussed here can explain the structure in the smectic C phase of NOBA. If the planar structure shown in figure 6*b* is permitted to bend, the tilt angle that is associated with the smectic C phase would be difficult to understand. One might assume that the smectic C phase is primarily a stack of planes similar to that illustrated in figure 6*b*, but stacked in such a way as to look like the stack was subjected to shearing forces. This could allow for the tilt angle, but the rotation of the directors with magnetic fields⁵ of 10 kG or less while the tilt angle may remain constant presents a problem. Since this rotation is a very slow process compared to the destruction and formation of hydrogen bonds it might be assumed that equilibrium is being approached where the most stable state corresponds to the new direction preferred by the long molecular axes.

There is evidence¹¹ that the structure in the smectic C phase can vary as it does in the nematic phase, but it does not appear to exhibit the time dependence of the nematic phase. When a sample of NOBA was cooled from the nematic to the smectic phase and returned to the nematic it returned to the nematic phase with the sign of the conductivity anisotropy unchanged regardless of the original sign of the anisotropy. This observation implies that more consideration should be given to the structure in the nematic phase when investigating smectic C phases, and some of the uncertainties concerning structure in smectic C phases may be due to variation in structure.

A structure like that suggested in figure 6*b* might imply an increase in viscosity with time, but it could also be suggested that the best ordered sample could have the lowest values for the viscosity. The absolute values of the resistivity appeared to decrease with time by more than that expected from decomposition. Therefore, a decrease in viscosity may be likely.

Molecular alignment in liquid crystals due to ionic conduction appears to be so common, and the responsible mechanism so well behaved, that it seems a comparable behaviour should be found in other systems.

Acknowledgements

The author would like to thank Dr Louis S Chou and Mr William T Flint for their assistance. He would also like to express his appreciation to the US Army Research Office, Durham, for their financial support.

References

- 1 GRAY G W *Molecular Structure and the Properties of Liquid Crystals*, Academic Press, Inc. (London), Ltd., London (1962)
- 2 GRAY G W and JONES B J. *Chem. Soc.* p. 4179 (1953)

- 3 HERBERT A J *Trans. Faraday Soc.* **63** 555 (1967)
- 4 CARR E F *Adv. Chem. Ser.* **63** 76 (1967)
- 5 CHOU L S and CARR E F *Phys. Rev. A* **7** 1639 (1973)
- 6 AXMANN A *Z. Naturforsch.* **21a** 615 (1966); CARR E F *J. Chem. Phys.* **37** 104 (1962)
- 7 FLINT W T and CARR E F *Mol. Cryst. Liquid Cryst.* **22** 1 (1973)
- 8 SCHULTZ E, MECKE W and MEIER G Private Communication
- 9 DILOCHI B and CABANE B *Mol. Cryst. Liquid Cryst.* **19** 25 (1972)
- 10 AXMANN A *Z. Naturforsch.* **21a** 290 (1966)
- 11 CHOU L S and CARR E F *Proc. ACS Sym. on Ordered Fluids and Liquid Crystals*, Chicago (Aug. 26-31, 1973). To be published by Plenum Press, New York
- 12 MAIER W and MEIER G *Z. Naturforsch.* **A16** 1200 (1961)
- 13 ANNA J MARTIN, MEIER G and SAUPE A *Symposium of the Faraday Society* No. **5** 119 (1971)
- 14 DI VRIIS A *Mol. Cryst. Liquid Cryst.* **10** 219 (1970)
- 15 MC LEMORE D P and CARR E F *J. Chem. Phys.* **57** 3245 (1972)
- 16 RONDELEZ F *Solid State Commun.* **11** 1675 (1972)
- 17 TWITCHELL R P and CARR E F *J. Chem. Phys.* **46** 2765 (1967); CARR E F *Mol. Cryst. Liquid Cryst.* **7** 253 (1969)
- 18 HILFICH W J *J. Chem. Phys.* **51** 4092 (1969)
- 19 TAYLOR T R, FLERGASON J L and ARORA S L *Phys. Rev. Lett.* **24** 359 (1970)
- 20 CHISTAKOV I G, SCHABISCHEV L S, JARENOV R I and GUSAKOVA L A *Mol. Cryst. Liquid Cryst.* **7** 279 (1969)

DISCUSSION

Gray: When preparing samples of *p*-alkoxybenzoic acids for optical microscopy and determination of transition temperatures there is clear evidence for some decomposition or chemical change. The samples rapidly fill with small bubbles and transition temperatures steadily fall on repeated heating/cooling cycles. This would be caused by (a) decarboxylation giving an anyl alkyl ether—a *dipolar* species, or (b) anhydride formation which would give water plus a dipolar species similar to part of your proposed polymer. I wonder whether you have any evidence to show that such possibilities are not important in your observations? In your anisotropy of conductivity experiments you are heating the materials for 6–7 hours at high temperatures, and we observe formation of bubbles during microscopy experiments of only a few minutes' duration. The importance or otherwise of such chemical changes could be proved by physical studies of samples after carrying out your experiments, *e.g.* mass spectrometry would detect anhydride.

Finally it is perhaps worth noting that anhydride formation is a reversible process and may account for some of the differences you observe on heating and cooling cycles. Also decarboxylation is a possible surface catalysed reaction which may vary in its importance with experimental conditions.

Carr: There is evidence that the results are affected by decomposition of the sample, but we have found *p*-nonyloxy-benzoic acid to be a reasonably stable material compared to other liquid crystals with a comparable-temperature range. After using a sample 15 or more hours it can be reheated

from the solid and results comparable to those shown in figures 4 and 5 can be obtained. The second set of measurements will be affected, but the time dependence and a dip below isotropic-nematic transition will be present. Preliminary measurements have indicated that a time dependent mechanism was not effective in the smectic C phase which implies that a reversible chemical process is unlikely but this needs to be checked further. However, the possibility of a reversible chemical process should be considered to explain some of the observations while passing through the isotropic-nematic transition. All these measurements will be checked further.

Schnur : Have the equilibrium constants been determined for the formation of the dimer in the isotropic phase? What do you think the effect of solutes — structure maker and structure breaker — would be on the polymorphism of these materials?

Carr : Benzoic acid and some other similar materials have been investigated. I do not remember who investigated benzoic acid, but the conclusion was that the concentration of the monomer would be too small to appreciably affect results comparable to those presented here. Studies involving the addition of solutes need to be carried out.

Chandrasekhar : Has the real part of the electric susceptibility been studied? In particular, I would like to know if the mean dielectric constant shows an increase at the transition?

Carr : We have not made any measurements of this as yet.

de Vries : Am I correct in understanding that all the results you presented were for *p*-nonyloxybenzoic acid?

Carr : A slight dip in the conductivity anisotropy vs. temperature curve just below the nematic-isotropic transition was observed for *p*-heptyloxybenzoic acid, but we have not observed after a few hours of use. We have observed both positive and negative conductivity anisotropy in *p*-octyloxybenzoic acid, but it was not tried to observe a time dependence yet. These two materials will be further investigated. It appears that they will be much more difficult to study than *p*-nonyloxybenzoic acid.

Blinic : Cannot spectroscopy tell you about the dimers, polymer, etc.?

Demus : I want to remark that according to our IR measurements* there is no jump in the dissociation of the dimers of alkoxybenzoic acids.

Billard : Do you propose to study other systems with hydrogen bonding?

Carr : We feel that there is more work that needs to be done on the *p*-*n*-alkoxybenzoic acids before investigating other similar systems.

* Kolbe A and Demus D *Z. Naturforsch.* 23 1237 (1968)

Soft mode dynamics in nematic liquid crystals

R BLINC, S LUGOMER and B ŽEKS

Institute "J. Stefan", University of Ljubljana, Ljubljana, Yugoslavia

Abstract. The dynamic properties of the molecular model proposed by Maier-Saupe for nematic liquid crystals are investigated. A rotationally invariant form of the Hamiltonian predicts the existence of two different diffusive optic soft modes in the nematic phase in addition to a doubly degenerate acoustic "magnon" mode which is the Goldstone mode of the isotropic-nematic transition.

1. Introduction

Maier and Saupe¹ have proposed a simple microscopic model for nematic liquid crystals. Whereas the static properties of this model were studied in great detail, the dynamic properties do not seem to have been investigated at all. It is the purpose of this paper to elucidate the dynamics of the Maier-Saupe (MS) model with particular emphasis on the existence of soft modes the condensation of which should result in an isotropic-nematic phase transition. The problem of the existence of the symmetry recovering Goldstone modes the frequency of which should vanish in the long wavelength limit in the low symmetry phase will be discussed. It will be shown that these modes which are a necessary consequence of the breaking of a continuous symmetry group at the isotropic-nematic phase transition are not predicted by the usual form of the MS Hamiltonian as this does not contain the full symmetry of the high temperature phase. A rotationally invariant form of the MS Hamiltonian, on the other hand, does predict the existence of the Goldstone modes.

The present work is thus complementary to the macroscopic approach to liquid crystal dynamics²⁻⁵ as well as to the approach⁶ which is the extension of the microscopic theory of collective modes in classical liquids.

2. The Hamiltonian

Taking into account dispersion forces between anisotropic molecules and averaging over their centre-of-mass positions, Maier and Saupe¹ derived the following Hamiltonian:

$$\mathcal{H} = - \sum_{i,j} A_{ij} \left(\frac{3}{2} \cos^2 \theta_{ij} - \frac{1}{2} \right) \quad (1)$$

where θ_{ij} is the angle between the long axes of the molecules i and j . A_{ij} is a constant which measures the strength of the interaction.

To minimize the free energy associated with the above orientational interaction the molecules prefer – below a certain temperature – a parallel orientation of the long axes of the molecules. It is this orientational long range ordering which characterizes the onset of the nematic phase.

The above Hamiltonian (1) is usually replaced by a separable interaction

$$\begin{aligned} \mathcal{H}_{MS} &= - \sum_{i,j} A_{ij} \left(\frac{3}{2} \cos^2 \theta_i - \frac{1}{2} \right) \left(\frac{3}{2} \cos^2 \theta_j - \frac{1}{2} \right) \\ &= - \sum_{i,j} A_{ij} \eta_i \eta_j \end{aligned} \quad (2)$$

where θ_i is the angle between the long axis of the i^{th} molecule and the preferred direction in space, i.e., the nematic axis, and where

$$\eta_i = \left(\frac{3}{2} \cos^2 \theta_i - \frac{1}{2} \right) = \left(\frac{3}{2} n_{z,i}^2 - \frac{1}{2} \right) \quad (3)$$

Here we specified the orientation of a given molecule in space by the unit vector \mathbf{n}_i :

$$\mathbf{n}_i = (\sin \theta_i \cos \varphi_i, \sin \theta_i \sin \varphi_i, \cos \theta_i) \quad (4)$$

It should be noted that the Hamiltonian (2) does not contain the full symmetry of the isotropic phase. With the help of the unit vectors \mathbf{n}_i and \mathbf{n}_j which specify the orientations of the two molecules, expression (1) can be written as

$$\mathcal{H} = - \frac{3}{2} \sum_{i,j} A_{ij} (\mathbf{n}_i \cdot \mathbf{n}_j)^2 + \frac{1}{2} \sum_{i,j} A_{ij} \quad (5)$$

which can be contrasted with the usually used form of the Maier-Saupe Hamiltonian as given by expression (2):

$$\mathcal{H}_{MS} = - \sum_{i,j} A_{ij} \left(\frac{3}{2} n_{z,i}^2 - \frac{1}{2} \right) \left(\frac{3}{2} n_{z,j}^2 - \frac{1}{2} \right)$$

Whereas the difference between these two forms is not significant in the static case, it is important when dynamic properties are investigated.

Since we are not taking into account the relative motion of the centers of gravity of the molecules, the second term in expression (5) is a constant and can be left out. In the mean field approximation (MFA) we can rewrite expression (5) as:

$$\begin{aligned} \mathcal{H}_1^{\text{MFA}} = & -\frac{3}{2} \cdot 2 \sum_j A_{ij} [\langle n_{jx}^2 \rangle n_{ix}^2 + \langle n_{jy}^2 \rangle n_{iy}^2 \\ & + \langle n_{jz}^2 \rangle n_{iz}^2 + 2 \langle n_{jz} n_{jy} \rangle n_{ix} n_{iy} + 2 \langle n_{jx} n_{jz} \rangle n_{iy} n_{iz} \\ & + 2 \langle n_{jy} n_{jx} \rangle n_{iz} n_{ix}] \end{aligned} \quad (6)$$

Rotationally invariant Maier-Saupe Hamiltonian

In the homogeneous case, where $\langle n_{jx}^2 \rangle = \langle n_x^2 \rangle$ etc., we can rewrite the MFA Hamiltonian (eq. 6) as

$$\begin{aligned} \mathcal{H}^{\text{MFA}} = & -\frac{3}{2} V_0 [\langle n_x^2 \rangle n_x^2 + \langle n_y^2 \rangle n_y^2 + \langle n_z^2 \rangle n_z^2 \\ & + 2 \langle n_x n_y \rangle n_x n_y + 2 \langle n_x n_z \rangle n_x n_z + 2 \langle n_y n_z \rangle n_y n_z] \end{aligned} \quad (7)$$

where

$$V_0 = 2 \sum_{j \neq i} A_{ij}$$

The self-consistent equations are now

$$\langle n_\alpha n_\beta \rangle = \frac{\int n_\alpha n_\beta \exp(-\beta \mathcal{H}^{\text{MFA}}) \cdot d\Omega}{\int \exp(-\beta \mathcal{H}^{\text{MFA}}) d\Omega}, \quad \alpha, \beta = x, y, z \quad (8)$$

The integration goes over the whole solid angle and is performed with the help of expression (6).

In the high temperature isotropic phase we find:

$$\langle n_x^2 \rangle = \langle n_y^2 \rangle = \langle n_z^2 \rangle = \frac{1}{3} \quad (9a)$$

$$\langle n_x n_y \rangle = \langle n_x n_z \rangle = \langle n_y n_z \rangle = 0 \quad (9b)$$

This solution, which exists at all temperatures, corresponds to $\langle \eta \rangle = 0$.

In order to investigate the low temperature solution, let us assume that the molecules order along the z axis, and that there is no preferential ordering in the xy plane. In such a case we have

$$\langle n_x n_y \rangle = \langle n_x n_z \rangle = \langle n_y n_z \rangle = 0 \quad (10a)$$

$$\langle n_x^2 \rangle = \langle n_y^2 \rangle = \frac{1}{2} (1 - \langle n_z^2 \rangle) \quad (10b)$$

It should be noticed that this assumption breaks the symmetry of the high temperature phase. From expression (3) and (4) we see that

$$\langle n_z^2 \rangle = \frac{1}{3} (2 \langle \eta \rangle + 1) \quad (11a)$$

$$\langle n_x^2 \rangle = \langle n_y^2 \rangle = \frac{1}{2} (1 - \langle \eta \rangle) \quad (11b)$$

When we insert expressions (10a – 11b) into eq. (7), it reduces to

$$\mathcal{H}^{\text{MFA}} = -V_0 \langle \eta \rangle \eta$$

thus demonstrating that in the homogeneous static case there is no difference between the usual and the rotationally invariant form of the MS Hamiltonian.

Dynamic properties

We shall assume that the collective normal modes in liquid crystals are so strongly overdamped that the real part of the mode frequency may be neglected in comparison with the imaginary one and the system can be treated in a relaxational approximation.

Let us now investigate the dynamic properties of the Hamiltonian

$$\mathcal{H} = -\frac{3}{2} \sum_{i,j} A_{ij} (\mathbf{n}_i \cdot \mathbf{n}_j)^2 \quad (12)$$

The relaxational equations of motion for the deviations from the MFA solutions are

$$\frac{d}{dt} \langle n_{i\alpha} n_{i\beta} \rangle_t = -\frac{1}{T_1} \left[\langle n_{i\alpha} n_{i\beta} \rangle_t - \overline{\langle n_{i\alpha} n_{i\beta} \rangle_t} \right] \quad (13)$$

where $\alpha, \beta = x, y, z$ and

$$\overline{\langle n_{i\alpha} n_{i\beta} \rangle_t} = \frac{\int \exp(-\beta \mathcal{H}_i^{\text{MFA}}) n_{i\alpha} n_{i\beta} d\Omega}{\int \exp(-\beta \mathcal{H}_i^{\text{MFA}}) d\Omega} \quad (14)$$

$\mathcal{H}_i^{\text{MFA}}$ is given by expression (6), and $\langle n_{i\alpha} n_{i\beta} \rangle_t$ by

$$\langle n_{i\alpha} n_{i\beta} \rangle_t = \langle n_{i\alpha} n_{i\beta} \rangle + \delta \langle n_{i\alpha} n_{i\beta} \rangle e^{-t/\tau} \quad (15)$$

Introducing collective coordinates by the Fourier transform

$$\delta \langle n_{\alpha} n_{\beta} \rangle_{\mathbf{q}} = \sum_i \delta \langle n_{i\alpha} n_{i\beta} \rangle e^{i\mathbf{q} \cdot \mathbf{R}_i} \quad (16)$$

and using expression (15) we find:

$$\begin{aligned} \frac{T_1}{\tau} \cdot \delta \langle u_\alpha u_\beta \rangle_{\mathbf{q}} &= \delta \langle n_\alpha n_\beta \rangle_{\mathbf{q}} - \frac{3}{2} \beta V_{\mathbf{q}} [\langle n_\alpha n_\beta n_x^2 \rangle \delta \langle n_x^2 \rangle_{\mathbf{q}} \\ &+ \langle n_\alpha n_\beta n_y^2 \rangle \delta \langle n_y^2 \rangle_{\mathbf{q}} + \langle n_\alpha n_\beta n_z^2 \rangle \delta \langle n_z^2 \rangle_{\mathbf{q}} + n_\alpha n_\beta n_x n_y \delta \langle n_x n_y \rangle_{\mathbf{q}} + \\ &+ 2 \langle n_\alpha n_\beta n_x n_z \rangle \delta \langle n_x n_z \rangle_{\mathbf{q}} + 2 \langle n_\alpha n_\beta n_y n_z \rangle \delta \langle n_y n_z \rangle_{\mathbf{q}} + \\ &+ \frac{3}{2} \beta V_{\mathbf{q}} \langle n_\alpha n_\beta \rangle [\langle n_x^2 \rangle \delta \langle n_x^2 \rangle_{\mathbf{q}} + \langle n_y^2 \rangle \delta \langle n_y^2 \rangle_{\mathbf{q}} + \langle n_z^2 \rangle \delta \langle n_z^2 \rangle_{\mathbf{q}}] \end{aligned} \quad (17)$$

where $V_{\mathbf{q}}$ is given by

$$V_{\mathbf{q}} = 2 \sum_j A_{1j} e^{i\mathbf{q} \cdot (\mathbf{R}_1 - \mathbf{R}_j)}$$

We thus have a system of six linear equations for the fluctuation eigenvectors $\delta \langle n_\alpha n_\beta \rangle_{\mathbf{q}}$ ($\alpha, \beta = x, y, z$). The eigenvectors must satisfy the relation

$$\delta \langle n_x^2 \rangle + \delta \langle n_y^2 \rangle + \delta \langle n_z^2 \rangle = 0 \quad (18)$$

so that only five of these equations are independent. This corresponds to the fact that the nematic order parameter is as pointed out by de Gennes⁷ – a symmetric second rank tensor of zero trace which has five independent components.

The nature of the solution for τ depends on the averages

$$\langle n_x^4 \rangle = \langle n_y^4 \rangle = \frac{3}{8} \langle \sin^4 \theta \rangle = \frac{3}{8} - \frac{3}{4} \langle \cos^2 \theta \rangle + \frac{3}{8} \langle \cos^4 \theta \rangle \quad (19a)$$

$$\langle n_z^4 \rangle = \langle \cos^4 \theta \rangle \quad (19b)$$

$$\langle n_x^2 n_z^2 \rangle = \langle n_y^2 n_z^2 \rangle = \frac{1}{2} \langle \sin^2 \theta \cos^2 \theta \rangle = \frac{1}{2} \langle \cos^2 \theta \rangle - \frac{1}{2} \langle \cos^4 \theta \rangle \quad (19c)$$

$$\langle n_x^2 n_y^2 \rangle = \frac{1}{8} \langle \sin^4 \theta \rangle = \frac{1}{8} - \frac{1}{4} \langle \cos^2 \theta \rangle + \frac{1}{8} \langle \cos^4 \theta \rangle \quad (19d)$$

In the isotropic phase, $T > T_c$, one easily finds that

$$\langle n_x^4 \rangle = \langle n_y^4 \rangle = \langle n_z^4 \rangle = \frac{1}{8} \quad (20a)$$

$$\langle n_x^2 n_y^2 \rangle = \langle n_y^2 n_z^2 \rangle = \langle n_x^2 n_z^2 \rangle = \frac{1}{16} \quad (20b)$$

and all five possible fluctuations relax with the same wave vector dependent relaxation time:

$$T_1/\tau(\mathbf{q}) = (1 - \beta V_{\mathbf{q}}/5) \quad (21)$$

This result is easy to understand. The ellipsoid, which can be ascribed to the equilibrium value of the order parameter tensor, reduces to a sphere for $T > T_c$. Above T_c all orientations of the order parameter tensor are thus equivalent and therefore all possible deformations relax with the same relaxation time. Expression (21) predicts a critical slowing down

of $\tau(\mathbf{q})$ as $\beta V_{\mathbf{q}}/5 \rightarrow 1$. Depending on the value of \mathbf{q} for which $V_{\mathbf{q}}$ is a maximum we find — after the diffusive soft mode has condensed out — a homogeneous nematic ($\mathbf{q} = 0$) or a spiral cholesteric ($\mathbf{q} \neq 0$) low temperature phase.

In the following we shall be concerned with the nematic solution.

If one assumes that $V_{\mathbf{q}}$ is isotropic

$$V_{\mathbf{q}} \approx V_0 - aq^2 \quad (22)$$

we see that

$$T_1/\tau(\mathbf{q}) = 1 - (T_0/T) + \beta aq^2/5, \quad \beta = 1/(kT) \quad (23a)$$

The above diffusive soft mode has thus an optic character ($1/\tau \neq 0$ for $\mathbf{q} = 0$) except at the stability limit T_0 where

$$T_1/\tau(\mathbf{q}) = \beta aq^2/5 \quad (23b)$$

The degeneracy of the soft mode is lifted in the nematic phase. We find two different diffusive optic soft modes:

$$(i) \quad T_1/\tau(\mathbf{q}) = 1 - 3\beta V_{\mathbf{q}} \langle n_x^2 n_y^2 \rangle \quad (24a)$$

with the eigenvectors

$$\delta \langle n_x n_y \rangle_{\mathbf{q}} \neq 0 \text{ or } \delta \langle n_y^2 \rangle_{\mathbf{q}} - \delta \langle n_x^2 \rangle_{\mathbf{q}} \neq 0 \quad (24b)$$

and

$$(ii) \quad T_1/\tau(\mathbf{q}) = 1 + \frac{9}{2} \beta V_{\mathbf{q}} (\langle n_x^2 n_z^2 \rangle - \langle n_x^2 \rangle \langle n_z^2 \rangle) \quad (25a)$$

with the eigenvectors

$$\delta \langle n_x^2 \rangle_{\mathbf{q}} + \delta \langle n_y^2 \rangle_{\mathbf{q}} = -\delta \langle n_z^2 \rangle_{\mathbf{q}} \quad (25b)$$

in addition to a doubly degenerate diffusive acoustic mode

$$(iii) \quad (T_1/\tau(\mathbf{q}) = 1 - 3\beta V(\mathbf{q}) \langle n_x^2 n_z^2 \rangle = (V_0 - V_{\mathbf{q}})/V_0) \quad (26a)$$

with the eigenvectors

$$\delta \langle n_x n_z \rangle_{\mathbf{q}} \neq 0, \quad \delta \langle n_y n_z \rangle_{\mathbf{q}} \neq 0 \quad (26b)$$

The fifth mode, which would represent a rotation of the nematic order parameter ellipsoid around the z -axis, is not a real normal mode of the system in view of our assumption of the isotropy in the xy plane. If, however, our order parameter tensor would be biaxial — i.e., a general ellipsoid and not axially symmetric one — the fifth mode would be present too.

The nature of the four nematic order fluctuation modes is illustrated in figure 1. The first mode (i) represents a change in the magnitude of the two smaller principal axes of the order parameter ellipsoid with the

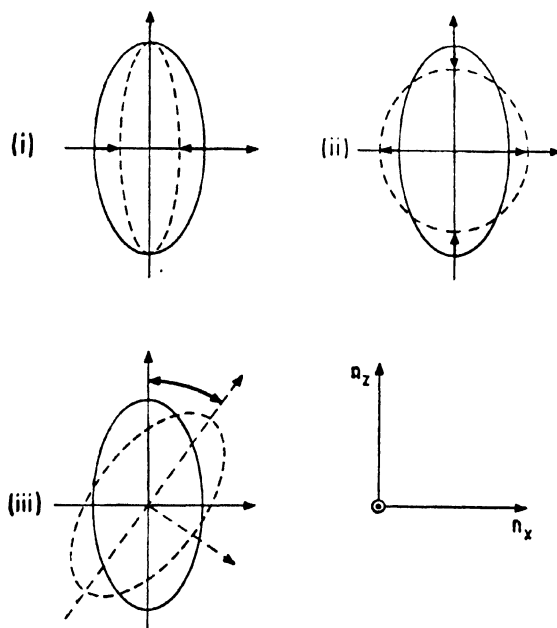


Figure 1 Illustration of the normal mode motion for the four nematic order parameter modes as obtained from the rotationally invariant form of the Maier-Saupe Hamiltonian. The doubly degenerate second sound mode (iii) is the Goldstone mode of the transition.

largest (z) axis remaining constant. The increase in the magnitude of the x axis is compensated by a decrease in the magnitude of y axis and *vice versa*. It can be called a "biaxial" nematic soft mode, since it tends to destroy the "uniaxial" nematic symmetry. The second mode (ii) represents a decrease in the magnitude of the z axis which is compensated by an increase in the x and y principal axes and *vice versa*. It is a "uniaxial" nematic soft mode. Whereas the above two modes thus represent a change in the magnitude of the local anisotropy, the doubly degenerate third mode (iii) represents a rotation of the local anisotropy out of the z direction. The rotational ellipsoid rotates in the xy or the yz plane. It is this last mode which is the Goldstone mode⁸ of the isotropic-nematic transition.

In the transition from the isotropic liquid to the nematic phase the continuous rotational symmetry decreases⁹ from O_3 to $T_3 \times O_3$ (isotropic liquid $\rightarrow T_3 \times D_{2\infty}^x$ (nematic phase)

$$O_3 \rightarrow D_{2\infty}^x \times D_{2\infty}^y \times D_{2\infty}^z \quad (27)$$

The Goldstone mode tries to recover the symmetry which is broken in the low temperature phase. Its frequency vanishes in the long wavelength limit ($1/\tau \rightarrow 0$, $q \rightarrow 0$) and the motion corresponds to the continuous group $D_{2\infty}^x \times D_{2\infty}^y$ which is broken at T_c .

The temperature dependence of the relaxation times τ^{-1} of these three modes is shown in figure 2 for $q = 0$. The frequencies $1/\tau$ of the modes (i) and (ii) vanish at the stability limit of the nematic phase.

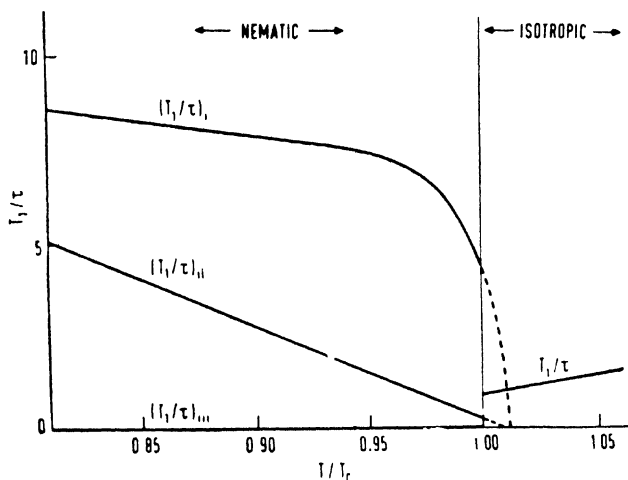


Figure 2 Temperature dependence of the four nematic order parameter fluctuation modes for $q = 0$.

References

- 1 MAIER W and SAUPE A *Z. Naturforsch.* 13A 564 (1958); 14A 882 (1959); 15A 287 (1960)
- 2 McMILLAN W L *Phys. Rev.* A4 1238 (1971); A6 936 (1972)
- 3 KOBAYASHI K J *Phys. Soc. Jap.* 29 101 (1970)
- 4 ORSAY LIQUID CRYSTAL GROUP *J. Chem. Phys.* 51 816 (1969)
- 5 BROCHARD F J *Phys. (Paris)* 34 411 (1973)
- 6 KOBAYASHI K K, FRANKLIN W M and MOROI D S *Phys. Lett.* 42A 449 (1973)
- 7 DE GENNES P G *Mol. Cryst. Liquid Cryst.* 7 325 (1969)
- 8 See, for instance, BROUT R *Phase transitions* (W A Benjamin Inc., New York) (1965)
- 9 BROWN G H, DOANE, J W and NEFF V D *Critical Reviews on Solid State Sciences* 303 (Sept. 1970)

Some new types of electrohydrodynamic flow patterns in nematic liquid crystals

P P KARAT and N V MADHUSUDANA

Raman Research Institute, Bangalore 560006, India

Abstract. Electrohydrodynamic flow patterns in a homeotropically aligned nematic liquid crystal have been studied employing a geometry in which the observation direction is along the optic axis of the undistorted sample and the electric field direction perpendicular to it. A possible mechanism for the observed pattern, which is consistent with the Carr-Helfrich model, is discussed.

Interesting new observations are also described of dc and ac field induced distortions of nematic droplets suspended in the isotropic phase at the nematic-isotropic transition temperature.

Introduction

There have been a large number of studies of the Williams domains using the so-called 'sandwich' geometry. In this geometry, a nematic liquid crystal of negative dielectric anisotropy is homogeneously aligned between two transparent electrodes. If a dc or low frequency ac field is applied there appears, above a certain threshold voltage, a regular pattern of striations *perpendicular* to the undistorted director. The mechanism of this process is well established: a small bend distortion in the medium produces a space charge in that region because of the conductivity anisotropy. The action of the applied electric field on the space charge leads to the stable hydrodynamic flow pattern which at higher voltages gives way to turbulence^{1, 2}.

Flow patterns in a homeotropically aligned sample

Recently, we³, made some observations using a different geometry: the specimen was homeotropically aligned between two glass plates, and the electric field was applied perpendicular to the undistorted director between two copper or aluminium foils which served as spacers (figure 1a). Observations were made perpendicular to the glass plates (along the X-direction) and above a certain dc or low frequency voltage, regular patterns were found (figure 2). Similar observations have been independently reported by Chang⁴.

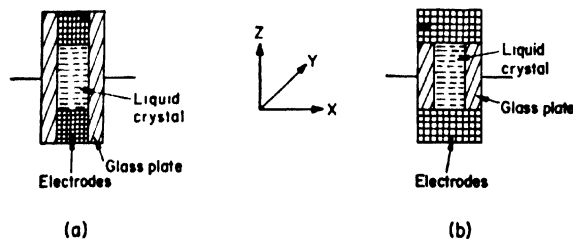


Figure 1 The geometry of the experimental set up for observing the electrohydrodynamic distortion patterns in a homeotropically aligned sample. The electric field is non-uniform in (a) and uniform in (b). Observations are made in the X-direction and the cross section of the sample is $\sim 170 \mu \times 40 \mu$.

The earliest observation in this geometry was in fact made by Fredericksz and Zolina⁵. However, at that time the exact explanation of the electrohydrodynamic phenomenon was not known.

The electric field in the above set up (figure 1a) is evidently non-uniform because of the fringing of the field at the edges of the electrodes. In order to eliminate any possible effects due to this, we repeated the experiment with a uniform field. The end faces of two non-magnetic steel blocks were polished and small glass pieces cut from microscope cover slips were placed in between, such that a narrow channel was available for containing the liquid crystal (figure 1b). As the thin edges of the cover slip ($\sim 170 \mu$) could not be treated with lecithin to get a homeotropic alignment, the specimen was subjected to a strong magnetic field. Observations were made along the magnetic field by means of specially constructed microscope which could be slipped into the hole in the Zeeman pole piece of the electromagnet. The sample size was comparable to the one used in the earlier experiments, the X, Y and Z dimensions being approximately 40μ , 1 cm and 170μ respectively. All the observations were made on *n-p*-methoxybenzylidene-*p*-butylaniline (MBBA). A dc or low frequency ac electric field was applied between the steel blocks. When the magnetic field was high, it was observed that the specimen did not exhibit the regular pattern that was observed with a non-uniform electric field. However, dust particles could be seen to move up and down in between the electrodes almost in a straight line, *i.e.*, there was a motion in the plane containing the direction of observation and the electric field direction (the XZ plane), in agreement with the Carr-Helfrich model. Moreover, a few vertical 'walls' could be seen in the field of view. They were rather similar to the walls seen in figure 2b and were clearly visible when the analyser (with no polariser) was vertical (Z-axis) but not so when the analyser was perpendicular to the electric field direction.

We can now think about a possible interpretation of the observed pattern. In the usual sandwich configuration, the distance between the

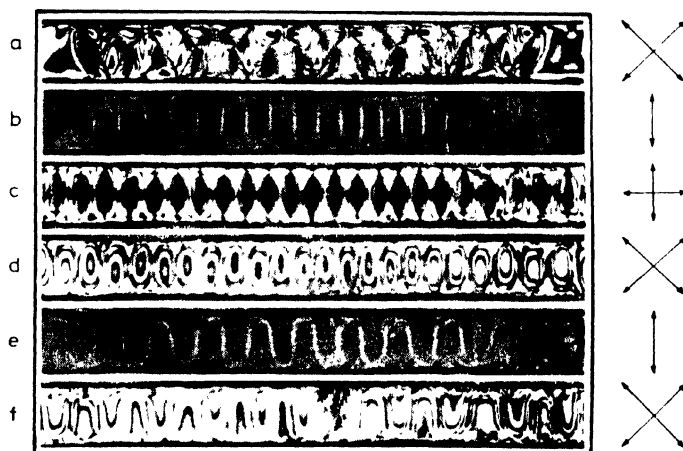


Figure 2 Electrohydrodynamic patterns in MBBA, magnification $\times 120$. The arrows on the right hand side indicate the settings of the nicols (a) dc, 35V, (b), (c) & (d) 20 cps, 32V, (e) & (f) 100 cps, 45V

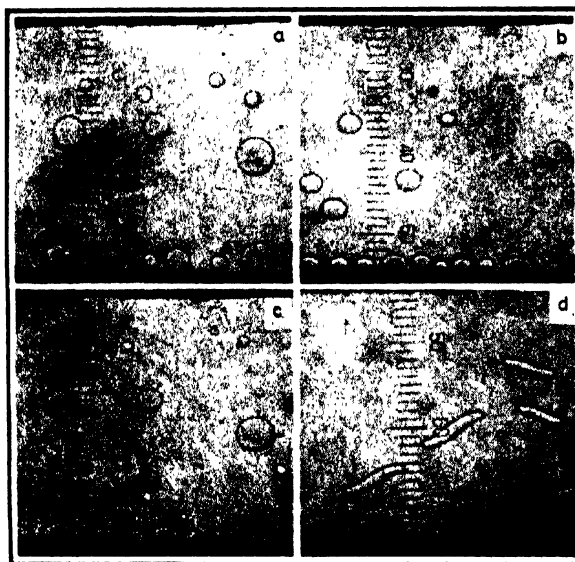


Figure 4 Electrohydrodynamic distortions of nematic droplets suspended in the isotropic phase at the transition temperature (a) undistorted droplets under zero field; (b) 200 cps, 100 V; (c) 500 cps, 100 V and (d) 50 cps, 200 V.

electrodes is a small fraction of the length available perpendicular to the field (X direction) and it is well known that the repeat distance in the cellular flow pattern is determined by the distance between the electrodes. Therefore, several cells are formed with a periodicity along the X axis, the neighbouring striations corresponding to cellular motion of opposite sense so that the total angular momentum is zero. However, in the present configuration the distance between the electrodes is $\sim 4\text{--}5$ times the space available in the lateral (X) direction. Hence it is not possible to have more than one cell to be formed at any given value of the Y coordinate. Hence it is likely that, in order to conserve angular momentum, neighbouring regions of the liquid crystal along the Y-direction assume opposite senses of rotation. In other words, whereas in the usual sandwich geometry, neighbouring domains with opposite senses of the vortices meet as shown in figure 3a, due to the physical restrictions imposed by the present configuration they meet as shown in figure 3b. This can explain the patterns shown in figure 2 under various combinations of the polarizer and analyser orientations. Further, as was noted in our earlier

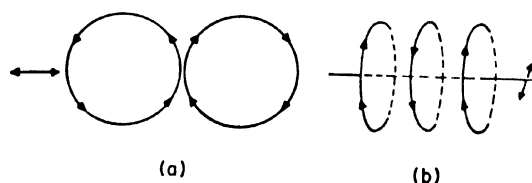


Figure 3 The sense of vortex motion in adjacent domains (a) in the sandwich geometry and (b) in the proposed model for the geometry shown in figure 1.

publication³, in the setting corresponding to figure 2c, dark bands could be seen to sweep across the domains from one wall to the other and back, the bands in adjacent domains moving in opposite directions. In the polariser and analyser setting of figure 2d, corresponding changes could be seen in the walls between the domains. We have undertaken further experiments to test this model.

Observations in homogeneously aligned samples

When the specimen prepared as described in the previous section is turned through 90° , about the Z-axis we get a homogeneously aligned sample, the magnetic field now acting parallel to the Y-direction (figure 1). Again the field induced electrohydrodynamic flow resulted in a set of domains when viewed along the X-axis. According to the Carr-Helfrich model the cellular motion is in a plane perpendicular to the direction of observation (*i.e.*, in the YZ plane) and the walls between the domains could be clearly seen at all settings of the analyser.

Electrohydrodynamic distortions of nematic droplets

Another interesting type of distortion was found during the studies described above. If the temperature of the sample is maintained at the nematic-isotropic transition point T_* , nematic droplets can be seen suspended in the field of view (figure 4a). If a dc or a low frequency ac electric field is applied between the electrodes, beyond a threshold voltage, the droplets get deformed and become elliptically-shaped with the major axis of the ellipse normal to the electric field direction (figure 4b, c). (The photographs of the droplets were taken with a flash light as there was considerable motion in the field of view.) The voltage necessary to deform the droplets increases with increasing frequency of the ac field and at very high frequencies, no deformation can be observed. As the voltage at the lower frequencies is increased, further deformation takes place and the droplets assume the form shown in figure 4d. Air bubbles or dust particles could be seen to have vortex motion inside the droplets, indicating an electrohydrodynamic origin of these deformations.

Acknowledgements

We are deeply indebted to Professor S Chandrasekhar for many useful discussions.

References

- 1 CARR E F *Mol. Cryst. Liquid Cryst.* **7** 253 (1969)
- 2 HELFRICH W J. *Chem. Phys.* **51** 4092 (1969)
- 3 MADHUSUDANA N V, KARAT P P and CHANDRASEKHAR S *Curr. Sci.* **42** 147 (1973)
- 4 CHANG R *Mol. Cryst. Liquid Cryst.* **20** 267 (1973)
- 5 FREEDERICKSZ N and ZOLINA V *Trans. Faraday Soc.* **29** 919 (1933)

DISCUSSION

Brown: Some years ago, we observed distortions of droplets similar to the ones shown here. We have mentioned this in a report to the Air Force.

Anomalous alignment and domain formation in nematic liquid crystal : ethoxyphenylazophenyl hexanoate

M N AVADHANLU and C R K MURTY

Department of Physics, Andhra University Post-Graduate Centre,
Guntur 5

Abstract. The effect of electric field on the molecular alignment in the liquid crystal ethoxyphenylazophenyl hexanoate is investigated using dielectric constant measurements at 1 MHz. The long axes of the molecules are found to align parallel to the electric field at very low audio frequencies and change to a perpendicular direction above 1 kHz. The threshold voltage for anomalous alignment is obtained as a function of the frequency of the externally applied electric field. This is correlated with the behaviour of the domain formation. The threshold voltages are found to be the same in both the cases.

Introduction

Since the first experiments of Jezewski¹ and Kast², the effect of the external electric fields on a nematic sample remained controversial³. The subsequent discovery of domains by Williams⁴ and Kapustin⁵ in nematic samples under the action of a d.c. or low a.f. electric fields contributed to this confusion. Carr⁶⁻⁸ tried to solve the problem by making use of dielectric loss measurements at microwave frequencies on the nematics p-azoxyanisole (PAA) and anisalamino-phenylacetate (AAPA) in the presence of external electric fields. Based on the observations made by Svedberg⁹ and himself⁸ regarding the conductivity of PAA and AAPA, Carr concluded that the anisotropic character of conductivity is the cause of their unusual behaviour in the presence of electric fields. According to Carr's model⁸ the torque exerted by the electric field on the space charge accumulated at the boundaries of the misaligned regions due to conductivity anisotropy in the sample competes with the torque on charges appearing in the same region due to anisotropic dielectric polarization. The interactions may balance each other, in which case no anomalous alignment will be observed, or conductivity anisotropy may predominate producing vortical flows which are seen as Williams-Kapustin domains. Helfrich¹⁰ used this model and derived an expression for d.c. threshold voltage that gives rise to Williams - Kapustin domains, while Dubois - Violette *et al.*¹¹ extended Helfrich's theory to cover time dependent fields.

The work of Carr⁸ and others^{12, 13} shows that the effect of electric fields can be categorized into two regimes according to the frequency of

the applied field. (1) The low frequency region where anomalous alignment of the director takes place and is attributed to the dominant role played by conductivity anisotropy. Hence it is called the conduction regime. (2) Relatively high frequency region where normal alignment of the director occurs due to dielectric anisotropy and the space charge fails to follow the reversals of electric field. This is called the dielectric regime. The two regimes are separated by a well-defined frequency called the cutoff frequency (f_c). The Orsay Group¹³, Parker *et al.*¹⁴ and Grueler *et al.*¹⁵ demonstrated the close relation between the electric and optical behaviour of nematics under the influence of electric fields.

Subsequently McLemore and Carr¹⁶ have shown that a highly pure sample does not exhibit Williams-Kapustin domains proving that ionic conduction is a necessary factor for the anomalous alignment. Finally Carr and his co-workers^{8, 16-18} showed that anomalous alignment of four different kinds can be distinguished in nematic samples depending on the relative signs and magnitudes of the dielectric and conductivity anisotropies.

The present work deals with a detailed investigation of the electric field effects on the nematic liquid crystal-ethoxyphenylazophenyl hexanoate (EPAP-Hex) using dielectric measurements at radio frequencies for the first time. This compound has negative dielectric anisotropy and positive conductivity anisotropy. Hence this is expected to exhibit that class of anomalous effect which is shown by PAA and AAPA.

2. Experimental

The commercial EPAP-Hex sample obtained from Eastman Kodak Co. (USA) was repeatedly recrystallized from petroleum ether till a pure sample exhibiting the liquid crystal phase between 75° - 126°C was obtained. The dielectric constant was determined using a Franklin oscillator-wavemeter combination¹⁹ operating at 1 MHz. The dielectric cell was formed by two metal coated glass plates supplied by Corning Co. (USA). The glass plates were separated by a 0.9 mm diameter copper wire which makes electrical contact with one of the metal surfaces only and serves as the earth lead, while another piece of copper wire of the same diameter makes contact with the second surface and acts as the 'live' terminal. The assembly was held in position by two thick brass plates screwed at the four corners. The capacity of the cell was found to be 19 pf. The cell was housed in a box type electrical furnace to maintain the sample at the required temperature in the liquid crystal phase. The brass plates and the walls of the furnace have windows to facilitate simultaneous visual observations on the formation of domains in the sample. External electric field was applied through suitable electrical connections. In this sort of arrangement external electric field can be applied only parallel to the measuring r.f. field, while magnetic field may be applied parallel or perpendicular to the r.f. field by rotating the cell

through 90° between the pole pieces of the magnets. The resistivity of the sample was measured using a Radart A.C. Millivoltmeter (type 343) in conjunction with a Philips A.F. generator (type GM 2308).

3. Results and discussion

3.1 Electric field dependence of the dielectric constant ϵ

For a negative dielectric anisotropic liquid crystal, external electric field parallel to r.f. measuring field is expected to turn the director, i.e., the long axes of molecules, perpendicular to the electric field direction E such that the measured dielectric constant is higher. But the application of 25 Hz electric field parallel to the r.f. field causes a decrease in the dielectric constant which is anomalous. The decrease in dielectric constant is dependent on both the strength and frequency of the applied electric field. The behaviour of ϵ as a function of E , the electric field strength at different frequencies is shown in figure 1. At each frequency, the dielectric constant has a steady value till the electric field crosses a threshold voltage and afterwards it falls abruptly. The variation of dielectric constant at 960 Hz is interesting. In this case the dielectric constant, instead of keeping steady, increases with the electric field strength upto

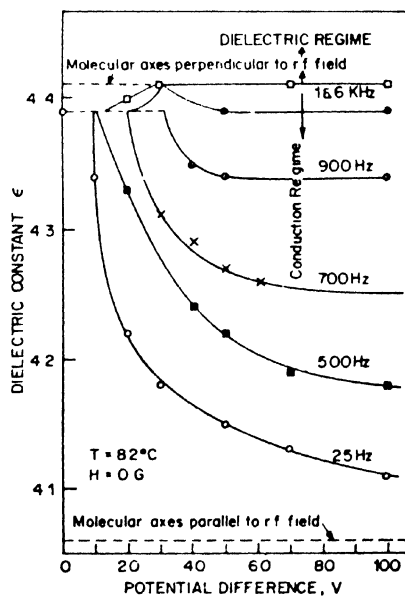


Figure 1 Dielectric constant ϵ at 1 MHz as a function of external voltage V for EPAP Hex at 82°C when magnetic field is not present, the individual curves showing the variation of ϵ at different frequencies of the external electric field

the threshold, and above it, it decreases. The initial increase in ϵ indicates the tendency of the director to prefer a perpendicular orientation with respect to E as expected on dielectric considerations but above the threshold the conductivity anisotropy appears to play a dominant role. The conductivities measured at 200 Hz which is sufficiently high to avoid polarization effects at the electrode surfaces are $\sigma_{\parallel} (= \frac{1}{\rho_{\parallel}}) \approx 1.8 \times 10^{-9}$ mho/cm and $\sigma_{\perp} (= \frac{1}{\rho_{\perp}}) \approx 1.4 \times 10^{-9}$ mho/cm and the conductivity anisotropy is $\Delta \sigma \approx 0.4 \times 10^{-9}$ mho/cm. Thus the sample shows positive conductivity anisotropy, $\frac{\sigma_{\parallel}}{\sigma_{\perp}} \approx 1.3$ which competes with negative dielectric anisotropy. In its behaviour, this is similar to PAA and AAPA.

Simultaneous visual observation of the sample was made through the windows provided in the cell walls. The threshold voltage for the anomalous alignment was found to be in close agreement with the voltage to form the domains in the sample.

3.2 Frequency dependence of alignment of the director

The variation of the dielectric constant, ϵ , as a function of the frequency of the applied dielectric field of strength 1.1 kV/cm is shown in figure 2. As the frequency is increased, the anomalous variation in ϵ decreases. This implies that the nematic director gradually tends to prefer a direction

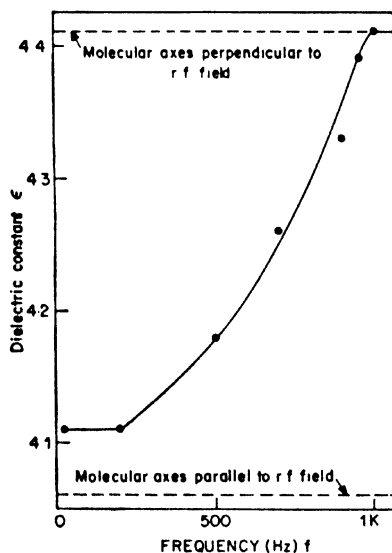


Figure 2 Dielectric constant ϵ at 1 MHz as a function of the frequency 'f' of the external electric field for EPAP Hex at 82°C. Applied field strength 1.1 kV cm⁻¹.

perpendicular to E in an attempt to approach the usual behaviour. The normal alignment is achieved at 970 Hz, and ϵ shows saturation. It may be thought that with an electric field above 970 Hz frequency a complete perpendicular alignment of long axes of the molecules has been attained and the corresponding ϵ value is regarded to represent this situation as shown by the upper dotted line in figure 2. However, the degree of alignment of long axes parallel to the electric field, achieved by low frequency electric fields, is found to be less in comparison with an external magnetic field. The parallel alignment of long axes of molecules caused by a magnetic field of strength 1500 G acting parallel to the r.f. field is shown by the lower dotted line in figure 2.

3.3 Frequency dependence of ϵ in the presence of a magnetic field

The effect of electric field of different frequencies on molecular alignment in the presence of parallel and perpendicular magnetic fields has also been studied. The effect of a 400 G magnetic field acting parallel to the r.f. field is shown in figure 3.

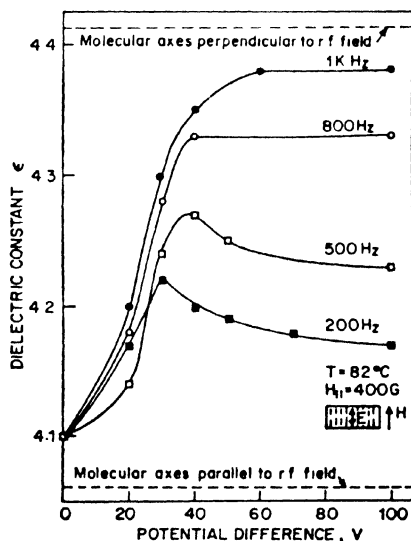


Figure 3 Dielectric constant ϵ at 1 MHz as a function of the external voltage of different frequencies in the presence of a 400 G magnetic field acting parallel to the electric field in EPAP Hex at 82° C.

The changes in the molecular alignment in the presence of a perpendicular magnetic field resemble those without a magnetic field (figure 1). The threshold voltage are higher in this case. The ϵ is nearly constant with increasing E upto a threshold value and then it decreases.

In the case of a parallel magnetic field, the dielectric constant increases with the increasing electric field strength upto a threshold voltage characteristic of each frequency. The increase in ϵ below the threshold voltage suggests that the director is turned away from the magnetic field due to the negative dielectric anisotropy of the material.

In the case of low frequencies, at the threshold voltage the conducting impurities come into operation and anomalous behaviour is exhibited by ϵ , while at 800 Hz and above, ϵ reaches a steady value, indicating that changes due to conductivity anisotropy cease to operate.

In both cases of parallel and perpendicular magnetic fields, there is a definite identifiable threshold voltage, above which only, the anomalous alignment is observed.

3.4 Alignment in the presence of a 500 Hz electric field

The degree of alignment obtained by a 500 Hz electric field at various magnetic field strengths both in a parallel and a perpendicular configuration has been studied. Figure 4 shows the results for the case of parallel magnetic field configuration.

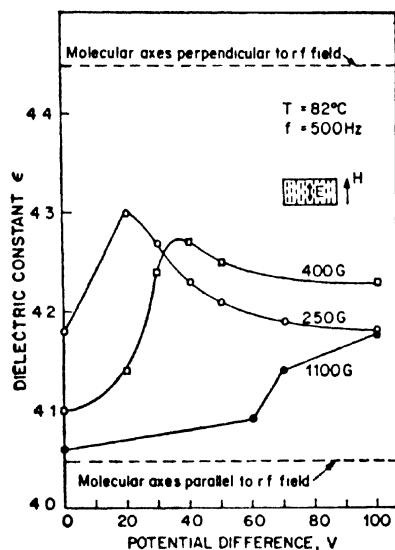


Figure 4 Dielectric constant ϵ at 1 MHz versus external voltage V of frequency 500 Hz in the presence of parallel magnetic field of strengths 250 G, 400 G and 1100 G in EPAP Hex at 82°C.

With 500 Hz electric field, which falls in the conduction regime ($500 \text{ Hz} < f_c$), the director prefers a parallel orientation with respect to the electric field. For low magnetic fields acting parallel to the r.f. field,

the external electric field below the threshold causes perpendicular alignment of the director which can be associated with negative dielectric anisotropy. At the high magnetic field strength of 1100 G anomalous alignment is not observed. This may be due to the fact that the threshold voltage for inducing anomalous alignment varies with magnetic field strength and the voltages used in the present case are not sufficient to cause an anomalous alignment. This is supported by the non-formation of domains. Further the increase in ϵ is less rapid as the strength of magnetic field is changed to high values implying the increasing stabilization achieved by the magnetic fields and the reduced influence of E .

The dielectric behaviour of the sample under the influence of a perpendicular magnetic field resembles the results shown in figure 1.

3.5 Frequency dependence of the threshold voltage V_{th}

The threshold voltage V_{th} for the anomalous alignment is frequency dependent and its dependence in the case of EPAP Hex is shown in figure 5. The nature of variation of V_{th} below the cutoff frequency is found to satisfy the Dubois-Violette *et al.* theory¹¹. According to this theory, the frequency dependence of the threshold voltage in the conducting regime is given by

$$V_{th}^2 = V_H^2 \{ 1 + (\zeta^2 - 1) (f/f_c)^2 \} / \{ 1 - (f/f_c)^2 \} \quad (1)$$

where $V_H = V_0 / (\zeta^2 - 1)^{1/2}$ is the d.c. Helfrich voltage, the d.c. threshold voltage for forming domains, and f_c is the cutoff frequency given by $f_c = (\zeta^2 - 1)^{1/2} / 2\pi\tau$, where τ is the space charge relaxation time given by $\tau^{-1} = 4\pi\sigma_{||} / \epsilon_{||}$. ζ^2 is the Carr-Helfrich-Orsay parameter characteristic of the material and is defined by

$$\zeta^2 = (1 - \frac{\epsilon_{||}}{\epsilon_a} \frac{1}{1 + \eta_0/\gamma_1}) (1 - \frac{\sigma_{||}}{\sigma_{||}} \cdot \frac{\epsilon_{||}}{\epsilon_{\perp}})$$

$\epsilon_a = \epsilon_{||} - \epsilon_{\perp}$ is the dielectric anisotropy;

$\eta_0 = (\eta_1 + \eta_2 - \gamma_1)/2$ where η_1 and η_2 are the Miesowicz viscosity coefficients and γ_1 is the twist viscosity.

Originally Dubois-Violette *et al.* have designated $\Theta = -\epsilon_a (\zeta^2 - 1)$ as the Carr-Helfrich parameter but it has become a common practice to call ζ^2 as the Carr-Helfrich-Orsay parameter^{14, 20}.

The parameter ζ^2 involves many unknowns and cannot be calculated. Instead, the value of ζ^2 ($= 3.5$) is first obtained using the experimental data at 500 Hz and $f_c = 970$ Hz and $V_H = 10$ V as obtained from figure 5. This value is close to 3.2 obtained for MBBA by the Orsay group¹¹. Using the value of $\zeta^2 = 3.5$ in equation (1), V_{th} at other frequencies are calculated and are shown below.

f Hz	V_{th} Calculated Volts	V_{th} expt. Volts
200	10.7	11
500	15.0	15
800	28.9	30
900	47.5	50
950	89.6	90

The calculated threshold voltages are in fair agreement with the experimentally obtained values, and the value 3.5 for ζ^2 may be regarded as reasonable.

In figure 5, the dependence of V_{th} on frequency in the presence of external magnetic fields is also shown which reveals that the influence of a parallel magnetic field is different from that of a perpendicular magnetic field.

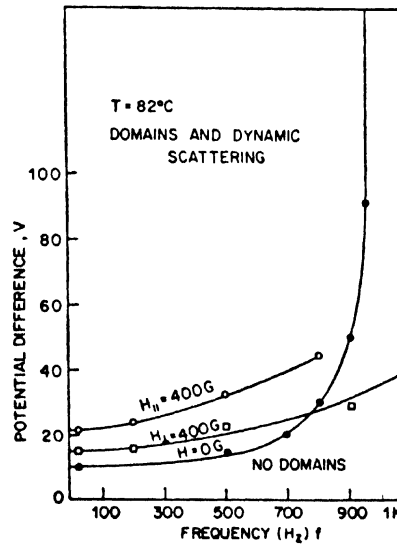


Figure 5 The variation of threshold voltage for the formation of domains with the frequency ' f ' of the external electric field for no-magnetic field case and for parallel and perpendicular magnetic fields of strength 400 G in EPAP Hex at 82°C.

These experiments have not been extended to higher frequencies, into the dielectric regime, to observe the 'fast turn-off mode'¹⁴ as the voltages available with the present experimental system are low.

These results show that the effect of a perpendicular magnetic field is different from that of a parallel magnetic field on the anomalous alignment of the director in the presence of an external electric field. In the absence of a magnetic field, the torque due to conductivity anisotropy has to overcome the torque due to dielectric anisotropy only. When a magnetic field, greater than the critical value as given by Freedericksz-Zolina condition²¹, is introduced perpendicular to E , the director is stabilized into a direction that is hard for the flow of carriers. The conductivity anisotropy has to contest with an additional torque, that due to diamagnetic anisotropy. So stronger electric fields are needed to create the instability in the sample. This means that the nature of variation in ϵ is essentially the same as in the no-field case except for the shift of V_{th} to higher values. When the magnetic field is changed to a parallel configuration, the director aligns into this direction (see inset in figures 3 and 4). This is the easy direction for the carriers and so there will be negligible torque due to conduction anisotropy at lower electric field strengths. But these fields are enough to tip the director and cause an initial increase in ϵ . As the electric field strength is increased, the director is turned away from E and H . This creates misaligned regions in a sample which was originally stabilized by H . Space charge builds up and conductivity anisotropy steps in to restore the director into a direction easy for the carriers and this produces the instability. In the case of strong magnetic fields, the director is highly stabilized along H and the dielectric torque cannot cause the change in its alignment that is needed to produce anisotropic carrier pile-up and that leads to the eventual instability. This view is supported by the only small increase in ϵ when high magnetic fields are applied. It may be that only a few molecules have changed their direction, instead of groups of molecules. Observations similar to the above were made by Twitchel and Carr⁶ and Carr⁸. Helfrich¹⁰ has obtained expressions and has shown that d.c. threshold voltage for anomalous alignment will be greater for parallel magnetic field than for perpendicular field.

These results thus demonstrate that r.f. dielectric constant can be used as an effective probe to elicit information about the nature of the alignment of the director in the presence of external electric and magnetic fields.

Acknowledgements

The authors are grateful to Prof. E. F. Carr for his kind interest and encouragement. One of the authors (MNA) gratefully acknowledges the financial support given by CSIR and NSF.

References

- 1 JEZEWSKI M Z. *Phys.* **51** 159 (1928)
- 2 KAST W Z. *Phys.* **71** 39 (1931)
- 3 GRAY G W *Molecular structure and the properties of liquid crystals*, Academic Press Inc., London (1962)
- 4 WILLIAMS R J. *Chem. Phys.* **39** 384 (1963)
- 5 KAPUSTIN A P and LARIONOVA L S *Kristallografiya*. **9** 297 (1964) (*Sov. Phys. - Cryst.* **9** 235 (1964))
- 6 TWITCHELL R P and CARR E F J. *Chem. Phys.* **46** 2765 (1967)
- 7 CARR E F *Adv. Chem. Ser.* **63** 76 (1967)
- 8 CARR E F *Mol. Cryst. Liquid Cryst.* **7** 253 (1969)
- 9 SVEDBERG T *Ann. Phys.* **44** 1121 (1914)
- 10 HELFRICH W J. *Chem. Phys.* **51** 4092 (1969)
- 11 DUBOIS-VIOLETTE E, DE GENNES P G and PARODI O J. *Phys.* **32** 305 (1971)
- 12 HILMEIER G H, ZANONI L A and BARTON L A *Proc. IEEE* **56** 1161 (1968)
- 13 ORSAY LIQUID CRYSTAL GROUP *Phys. Rev. Lett.* **25** 1642 (1970)
- 14 PARKER J H and CARR E F J. *Chem. Phys.* **55** 1846 (1971)
- 15 GRUELER H and MIER G *Mol. Cryst. Liquid Cryst.* **12** 289 (1971)
- 16 MCLEMORE D P and CARR E F J. *Chem. Phys.* **57** 3245 (1972)
- 17 FLINT W T and CARR E F *Mol. Cryst. Liquid Cryst.* **22** 1 (1973)
- 18 CHOU L S and CARR E F *Phys. Rev. A*. **7** 1639 (1973)
- 19 LE FLVRE R J W, ROSS I G and SMYTHE B M J. *Chem. Soc* 277 (1950)
- 20 MEYER HOFER D and ALAN SUSSMAN *Appl. Phys. Lett.* **20** 337 (1972)
- 21 FREDERICKSZ V and ZOLINA V *Trans. Faraday Soc.* **29** 919 (1933)

Relaxation study of the electric field induced hydrodynamic turbulence in nematic liquid crystals by Raman scattering†

S PAN and C H WANG*

Department of Chemistry, University of Utah, Salt Lake City,
Utah 84112 USA

†Supported by the Office of Naval Research

*Alfred P Sloan Research Fellow

Abstract. Using Raman scattering, we have measured the relaxation time of the electric field induced hydrodynamic turbulence in the bulk of several nematic liquid crystal samples as a function of temperature. The temperature dependent behavior of the liquid crystals of azo-compounds is found to be rather different from that of azoxy compounds. In both the azo and the azoxy compounds the relaxation time can all be fit to the Arrhenius type of activation process. While in the azo compounds the magnitude of the activation energy is found to correlate with the length of the molecule, in the azoxy compounds this correlation does not apply.

1. Introduction

Optical properties of liquid crystals in the nematic phase are sensitive to an applied electric field. For example, when an electric field is applied to thin layers of a nematic material sandwiched between a pair of conducting glass plates, two important electro-optical phenomena occur. At low voltage (but still greater than a certain threshold voltage), the thin liquid crystal layer first develops stationary domain structure, known as William's domain¹. At high voltage, the stationary domain structure gives way to turbulence and the nematic liquid crystal strongly scatters light. The strong light scattering due to the onset of turbulence is referred to as dynamic scattering². It is these effects, domain formation and dynamic scattering, when an external field is applied to liquid crystal films that make liquid crystals important materials for many optical display devices.

The electrohydrodynamic instability that gives rise to dynamic scattering has been the subject of several experimental and theoretical investigations. For thin liquid crystal films of a few μm (micrometer) thickness, the nature of the electrohydrodynamic instability depends on the frequency, field strength of the applied electric field, as well as on the initial degree of alignment³, the thickness of the sample³, and the surface state of the electrodes⁴. Moreover, it depends also on the sign of the dielectric anisotropy of the molecules⁴, impurity levels⁵⁻⁷ and temperature.

In this paper, we wish to report the study of the relaxation of the electrohydrodynamic instability of several liquid crystal bulk samples. Since bulk samples were used, the effects of surface and initial degree of alignment are not important in influencing the turbulence. It should be emphasized that the optical properties of a bulk sample are often quite different from that of a thin film sample.

Our study utilizes the laser Raman scattering technique. The experimental details are described in section 2. The materials that we have studied in this work include some typical azo and azoxy compounds. The azoxy compounds are *p*-azoxyanisole (PAA), 4,4'-Bis (hexyloxy) azoxybenzene (HAB). The azo compounds are *p*-(*p*-ethoxyphenyl-azo) phenyl undecylenate (PPU), *p*-(*p*-ethoxyphenyl-azo) phenyl valerate (PPV) and *p*-(*p*-ethoxyphenyl-azo) phenyl heptanoate (PPH).

2. Experimental

The schematic diagram of the experimental setup is shown in figure 1. A CW He-Ne laser with a power of about 80mW was used to excite the Raman spectra of the liquid crystalline samples. Except for HAB, all samples used in the experiment have been zone refined continuously for about ten days. However, both purified and unpurified HAB samples were used in the experiment. All of these compounds have strong Raman bands in the 1100–1500 cm^{-1} region. Except for the HAB sample, the Raman spectra of all the compounds have been found to agree with those reported in literature^{8–10}. The strong peak at 1141 cm^{-1} reported in ref. 9 was found to be absent in our spectra of both purified and unpurified HAB samples. It is likely that this peak is an undiscriminated He-Ne laser fluorescent line which was mistakenly taken as a Raman peak.

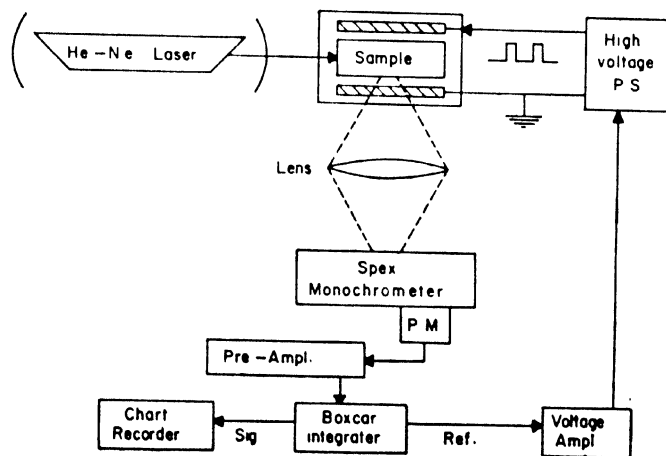


Figure 1 Block diagram of the experimental setup.

To study the electric field effect, we placed the sample between two flat stainless steel electrodes (separated by 2 mm) which are situated in a 1 cm \times 1 cm \times 4 cm rectangular pyrex glass cell. The linearly polarized laser light was made to propagate in a direction perpendicular to the applied electric field. The scattered light was collected in a direction normal to both the incident laser beam and the applied electric field.

The variation of sample temperature was achieved by placing the electrode-containing glass cell in a large aluminium heating block, whose temperature was changed by controlling the current of a heating tape wrapped around the block. The sample temperature was measured by a chromel-alumel thermocouple which was in direct contact with the sample. The sample temperature was accurate to $\sim 1^\circ\text{C}$.

The Raman spectra of the sample with and without the presence of a dc field were taken by simply scanning the monochromator, and the photomultiplier output was processed by a PAR boxcar integrator operating in the continuous gate mode.

In the presence of turbulence due to the application of an electric field, the intensity of all Raman bands are found to decrease drastically, but without any shift in the peak positions. As a result, it is possible to use the Raman intensity to monitor the relaxation behaviour of the electrohydrodynamic turbulence.

The relaxation times (to be defined later) of the electrohydrodynamic turbulence of the various liquid crystals in the nematic phase were measured by scanning the spectrometer to a position corresponding to a certain Raman spectral peak. The change in the spectral peak intensity when the electric field was suddenly turned off was monitored by a FW-130 photomultiplier followed by a boxcar integrator.

The electric field was applied to the electrodes by a power supply which is capable of delivering continuously and variably from 0 to 25 kV dc voltage. The dc voltage was square-wave modulated with a rise time of 2×10^{-4} sec. by applying an external square wave potential provided by the boxcar going through an amplifier.

The boxcar integrator has been used to perform two primary functions: (1) detecting the signal only when the electric field is on; (2) slowly sweeping the interval between the turning off time of the applied pulse and the gate opening time. The time dependent behaviour of the relaxation of the electric field induced turbulence can then be recorded on a strip chart recorder. The pre-amplifier is used mainly for impedance matching between the photomultiplier and the boxcar integrator. The turbulence can be avoided if the applied pulse electric field has very narrow width, thus the electric field effect on the Raman spectra other than the turbulence effect can be separated out (No effect was observed).

3. Results and discussion

The results of the relaxation time measurements are shown in figure 2 as a function of temperature for the samples mentioned above. The applied electric field in our experiment ranges from 3 kV/cm to 12 kV/cm. Within this range the change in relaxation time is negligible within the experimental error. If we refer to the difference between Raman intensities with the field on and off as ΔI , the relaxation time is then defined as the time required for the intensity difference to reach $1/e$ of the ΔI value after the field is suddenly turned off.

According to the scattering geometry used in this experiment, the decrease in Raman intensity due to the onset of turbulence is a measurement of all the light scattered both in the directions parallel and perpendicular to the applied electric field. The relaxation time measured from the scattered light polarized along the external field direction is found to be identical to that perpendicular to the field direction. This indicates that

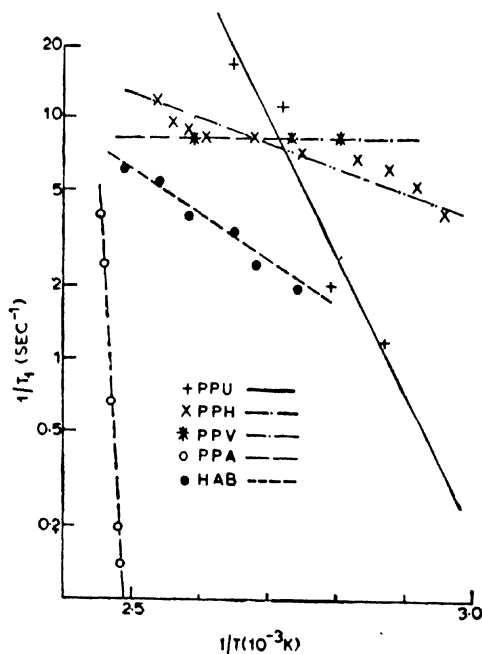


Figure 2 The electrodynamic turbulence relaxation rate ($\frac{1}{T_1}$) for various nematic liquid crystals as functions of the reciprocal of temperature (K) on semi-logarithm plots. The straight lines are the fit to the function, $\frac{1}{T_1} \propto \exp(-E/RT)$; where the values for E are: (1) PPU = 25.5 kcal/mole (2) PPH = 5 kcal/mole (3) PPV = 0 (4) PAA = 255 kcal/mole (5) HAB = 13.5 kcal/mole.

the dynamic scattering is independent of the electric field direction, and there is no molecular alignment induced in the bulk sample by the electric field when turbulence occurs.

Nematic liquid crystals may be regarded as fluids with either positive or negative dielectric anisotropy. For those exhibiting positive dielectric anisotropy (this applies to molecules having large dipole moment in the direction of the long molecular axis), the alignment will be with the molecules' long axes (more accurately the director) parallel to the field under the influence of a DC or AC potential. This has in fact been confirmed.

Field effects on nematic substances having negative dielectric anisotropy are more complicated. Although one intuitively expects that if an externally applied electric field is indeed the prevailing alignment force liquid crystals with negative dielectric anisotropy should align in a direction perpendicular to the external field. However, materials with negative dielectric anisotropy have often been found to align more parallel than perpendicular to the field at low frequency AC or in DC fields because of positive conductivity anisotropy.

In the work on the azo compounds which display positive dielectric anisotropy, Gruler and Meier⁴ have reported that these compounds display domain hydrodynamic flow above the threshold field of about 700 V/cm, but the hydrodynamic flow vanishes at fields greater than 2 kV/cm, due to the fact that at higher fields the domains change into inversion walls. We have found, however, that in the three azo compounds (PPU, PPH and PPV), the phenomena of hydrodynamic flow persists upto a very high field ($> 10^5$ V/cm) in their nematic phases. We have not measured the dielectric anisotropy of PPU, PPH and PPV, but according to the work reported by Avadhanlu and Murthy at this conference¹¹, PPU, PPH and PPV are found to be dielectrically negative. It is therefore of interest to examine further whether the difference in the electrohydrodynamic instabilities between the two types of azo compounds are due to their difference in the dielectric anisotropy.

As shown in figure 2, the relaxation time displays very different temperature dependence for the three azo compounds. For PPV, the relaxation time is practically independent of temperature throughout the nematic range, whereas for PPU, it is strongly temperature dependent. PPH gives results which are intermediate in nature to those of PPU and PPV. From thin film studies, Koelmans *et al.*³ have shown that the turbulence relaxation time should have a temperature dependence similar to shear viscosity.

If the observed temperature dependence of the relaxation rates (T_1^{-1}) given in figure 2 is fit to the Arrhenius relation, PPV then corresponds to a very low activation energy ($E_a \approx 0$), PPH to $E_a = 4.96 \pm 0.5$ kcal/

mole and PPU to $E_a = 25.5 \pm 0.5$ kcal/mole. One notes that the molecular length of PPU is greater than PPH which is in turn greater than PPV. Therefore, on the basis of length considerations, the temperature behavior of the relaxation time seems to correlate with the length of the three molecules.

However, the correlation breaks down in the azoxy liquid crystals. As one sees in figure 2 the relaxation time of PAA is extremely temperature dependent. If one correlates the temperature dependence of the relaxation time according to the Arrhenius expression, one obtains E_a for PAA equal to 255 kcal/mole. In HAB $E_a = 13.5$ kcal/mole was obtained. Since HAB has a considerably greater molecular dimension than PAA, on the basis of the length consideration one would expect that the relaxation time in PAA will be less temperature dependent than in HAB. But only the opposite result was found experimentally. The picture of molecular aggregates consisting of several molecules acting collectively must be invoked in order to account for the enormous activation energy and the large temperature dependence in electrohydrodynamic relaxation time. At the present, no theory is available to account for the observed temperature dependence.

References

- 1 WILLIAMS R J J. *Chem. Phys.* **39** 384 (1963)
- 2 HEILMFIER G, ZONONI L and BARTON L *Proc. IEEE* **56** 1162 (1968)
- 3 KOELMANS H and VAN BOXTEL A M *Phys. Lett.* **32A** 32 (1970);
KOELMANS H and VAN BOXTEL A M *Mol. Cryst. Liquid Cryst.* **12** 185 (1971)
- 4 GRULER H and MEILR G *Mol. Cryst. Liquid Cryst.* **12** 289 (1971)
- 5 CARR E F *Mol. Cryst. Liquid Cryst.* **7** 253 (1969)
- 6 Orsay Liquid Crystal Group *Mol. Cryst. Liquid Cryst.* **12** 251 (1971)
- 7 HELFRICH W J J. *Chem. Phys.* **51** 4092 (1969)
- 8 BULKIN B J and PROCHASKA R T J. *Chem. Phys.* **54** 635 (1971)
- 9 AMER N M and SHEN Y R J. *Chem. Phys.* **56** 2654 (1972)
- 10 WANG C H and LEU A L J. *Amer. Chem. Soc.* **94** 8605 (1972)
- 11 AVADHANLU and MURTHY (this conference)

Thermal instability in a nematic layer

VARAGUR S V RAJAN† and JULES J C PICOT

† *Present Address* : Box 88, Pinawa, Manitoba, Canada, R0E 1L0

Department of Chemical Engineering, University of New Brunswick,
Fredericton, N.B., E3B 5A3, Canada.

Abstract. The natural convection phenomenon in a nematic liquid crystal is examined from the continuum theory point of view as well as by considering the liquid crystal as an isotropic viscoelastic Maxwellian fluid. From the existing theory on the onset of thermal convective instability (" oscillatory instability or overstability " as distinguished from " stationary neutral instability or Bénard convection " for purely viscous, isotropic liquids), it appears that both theories predict a greatly reduced critical or threshold Rayleigh number for the onset of convection. This is because of the destabilizing effect of elastic stress relaxation in the viscoelastic model whereas it is due to the anisotropic viscoelastic and thermal properties in the continuum theory. The presence of rigid boundaries having a stabilizing effect is taken into account in the viscoelastic theory. These ideas are discussed as possible explanations for the unusual boundary effect on the thermal conduction in nematic liquid crystals.

Introduction

Thermal convection in purely viscous fluids heated from below is well understood. Convective flow is caused by the buoyancy forces generated by density gradients in the fluid subjected to a temperature gradient field. This classical Bénard problem is analyzed in great detail in the literature¹ for different types of boundary conditions. Recent analyses^{2,5} seem to indicate that the anisotropic viscoelastic behaviour of nematic liquid crystals along with their anisotropic thermal conductivities offer the possibility of very low critical Rayleigh number for the onset of natural convection in comparison with that for ordinary viscous liquids. These analyses have been made for planar² and homeotropic⁵ samples of nematic MBBA* using the principles of continuum theory⁴. When heated from below², for a planar sample,

$$\Delta T_c \simeq \left(\frac{\mu k_{\parallel} \bar{k}^4 d}{\rho^2 C_g \bar{\alpha}} \right) / \left[1 - \frac{k_{\perp} \alpha_{\parallel}}{\rho C K_{33}} \right] \quad (1)$$

* (*p*-methoxybenzylidene-*p*-*n*-butylaniline)

where

$\Delta T_c = (T_{\text{bottom}} - T_{\text{top}})$ = threshold temperature difference between the two rigid boundaries, μ = viscosity $= (\alpha_3 + \alpha_4 - \alpha_2)/2$; $\alpha_2 < 0$, α_i 's = Leslie viscosity coefficients⁴, K_{33} = bend elastic constant, ρ = density, C = heat capacity, $\bar{\alpha}$ = volumetric expansion coefficient, \bar{k} = wave number of convective oscillation¹ ($\sim \pi/d$), d = sample thickness, $k_{||}$ = thermal conductivity along the nematic axis, k_a = anisotropy $= (k_{||} - k_{\perp}) > 0$ for MBBA.

It is clear from the preceding equation that ΔT_c decreases with increasing d and also with increasing k_a . The sample is thermally unstable at very low ΔT as the degree of anisotropy increases. Using this idea, a qualitative explanation of the thermal conductivity data for MBBA (from anti-light Corporation) and PAA (*p*-azoxyanisole from K & K Laboratories) shown in figures 1 and 2 has been given elsewhere⁷. These data were obtained in a confined thermal conductivity cell heated from above. As discussed in that paper, convective flow can occur even in viscous liquids heated from above in a confined cell with non-uniform boundary temperature distribution. In both MBBA and PAA samples, the data seem to indicate parallel orientation at the surfaces. Also, the degree of anisotropy for PAA is very much less compared to that of MBBA. There is also a possibility of a negative anisotropy for PAA as opposed to the positive anisotropy for MBBA. The sign of anisotropy for PAA is still unresolved in view of the conflicting conclusions of different workers. The presence of impurities may have more influence on the properties of PAA which could be a possible explanation of the above conflict. It is not the object of this paper to repeat this discussion as a complete literature review on heat transport in nematic liquid crystals is available⁶.

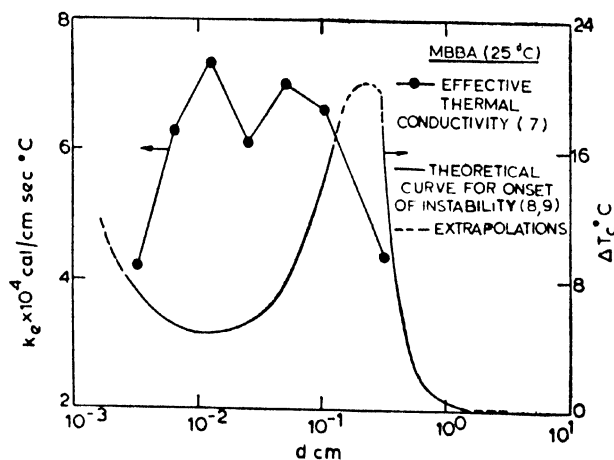


Figure 1 Thermal conductivity data and critical temperature difference calculation for MBBA.

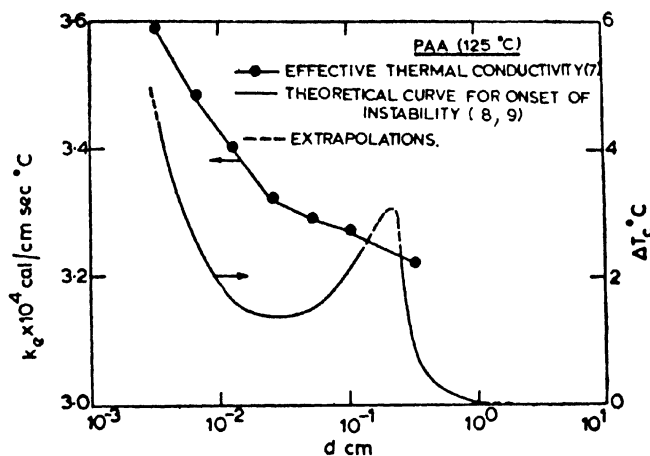


Figure 2 Thermal conductivity data and critical temperature difference calculation for PAA.

In this paper, an alternate possible explanation of the data of figures 1 and 2 will be given on the basis of the theory of heat convection in viscoelastic materials.

Theory

The classical Bénard problem has been recently extended to study the onset of thermal instability in a horizontal layer of viscoelastic fluid, heated from below^{8,9}. The case of a Maxwellian viscoelastic fluid (a special case of the general Oldroyd fluid³) will be considered for this discussion. The analysis is very similar to the one for viscous fluids¹. Approximate solutions for different conditions are available^{8,9} for the case of a viscoelastic fluid layer bounded by two parallel, horizontal infinite planes, heated from below. We will not go into the mathematical details but use only the major conclusions.

The viscoelastic behaviour of nematics is well known. Past experiments with such materials show that they relax in the presence of a reorienting shear or any other type of field. An orientational relaxation time λ attributed to the rotational Brownian diffusivity D_r is of the order of 2 seconds $\lambda \simeq 1/6 D_r$ as reported for PAA (Ref. 13 of 6). Since the shear stress is a function of the molecular orientation⁴, it is assumed as a linear approximation that the stress relaxation time in the Maxwellian model is of the order of λ . The constitutive equation for a Maxwellian fluid is

$$[1 + \lambda (\dot{\gamma} + V_k \cdot \nabla_k)] \tau_{ij} = \mu (V_{i,j} + V_{j,i}) \quad (2)$$

where

τ_{ij} = stress tensor, V_i = velocity vector, μ = viscosity, t = time,
 λ = stress relaxation time $\equiv 0$ for Newtonian fluids.

The onset of thermal instability in such a viscoelastic layer heated from below, as indicated by the mathematical analysis is referred to as 'overstability or oscillatory instability' to differentiate from the ordinary Bénard roll convection or 'neutral stationary instability'. The solutions have been given^{8,9} for the critical Rayleigh number for the onset of convection as follows :

$$Ra_c = \text{function} (Fo, Pr) \quad (3)$$

where

$$Ra_c = \frac{\bar{\alpha}}{k_o} \frac{Cg^2 \Delta T_c d^3}{\mu} = \text{critical Rayleigh number,}$$

$$Pr = \frac{C\mu}{k_o} = \text{Prandtl number,}$$

$$Fo = \frac{\lambda k_o}{\rho C d^2} = \text{Fourier number,}$$

$$k_o = \text{isotropic thermal conductivity} \\ = (k_{||} + 2k_{\perp}) / 3 \text{ for nematics}$$

The solutions^{8,9} as per equation 3, indicate that the presence of elasticity (relaxation time λ) destabilizes the fluid layer thereby considerably lowering Ra_c as compared to that for purely viscous fluids ($\lambda \equiv 0$). The presence of rigid boundaries on the other hand have a stabilizing influence over the fluid layer. Thus, the magnitude of Ra_c is decided by the thickness over d of the fluid layer also.

Table 1 gives the theoretical solution^{8,9} for Ra_c for different parameters. In order to evaluate the ΔT_c for each d , the properties used for the two nematics are tabulated in table 2. The value of k_o is used assuming random bulk orientation of nematic swarms in the free state - i.e., free from the orienting influence of boundaries and fields. This is reasonable in moderately thick samples (in the range of d studied) if we ignore the thin oriented layer near the boundaries and consider the sample to be macroscopically isotropic. It is clear that there is a substantial reduction in Ra_c as λ increases and as d decreases. The case of purely viscous fluids ($Fo = 0$) corresponds to either as $d \rightarrow \infty$ or as $\lambda \rightarrow 0$. In the present case, λ is assumed to be the same for both nematics and also to be independent of d . From the results of table 1, ΔT_c at each d can be calculated for each nematic. The theoretical curve of ΔT_c vs d is shown in figures 1 and 2 for MBBA and PAA respectively. For large gaps, the material tends to behave as an isotropic viscous fluid - i.e., $Ra_c = 1700$ ¹

Table 1 Critical Rayleigh Number Calculations^{8,9}

Pr/Fo	0 ¹	0.1	1	10	100
1	1700	872.2	51.2	4.64	0.459
10	1700	230.0	7.5	—	—
10 ²	1700	128.5	2.2	0.073	0.0049
10 ³	1700	108.0	1.29	—	—
10 ⁴	1700	102.6	1.08	0.0127	0.0002

Table 2 Physical Properties⁷

	MBBA (25° C)	PAA (125° C)
k_0 cal/cm sec °C	4×10^{-4}	3×10^{-4}
C cal/g °C	0.5	0.5
ρ g/cm ³	1.0	1.0
μ g/cm sec	0.4	0.03
$\bar{\alpha}$ (°C) ⁻¹	10^{-3}	10^{-3}

and is independent of d . Thus, a minimum and maximum in the threshold ΔT_c is observed with $\Delta T_c \rightarrow \infty$ as $d \rightarrow 0$ and $\Delta T_c \rightarrow 0$ as $d \rightarrow \infty$. The dotted lines in the figures show the extrapolations and the limits.

In the present data on thermal conductivity, the measurements were made in a confined cell heated from above⁶. As mentioned before⁷, convection can occur in such a cell because of the non-uniform temperature distribution over the surfaces. Since convection is possible, it can occur at very low ΔT_c for the present case of Maxwellian viscoelastic behaviour. As discussed earlier, the anisotropy of the nematics tends to reduce the ΔT_c further. This theory then predicts that the present data may involve convection especially in the region of gaps where ΔT_c shows a minimum. A quantitative comparison is not attempted now because the theoretical solution is limited to the case of isotropic materials heated from below. However, qualitatively, it is concluded that because of convection, one would expect a maximum in the effective conductivity data. This does appear in the experimental data for MBBA samples. The scatter in the region of the maximum is due to the convective flow instability in the material.

The behaviour of the experimental results for PAA is different in that there is a monotonous decrease in the k_e with increasing d . A possible reason for this is due to the degree of anisotropy k_a of PAA being very much less (perhaps of different sign also!) compared to that of MBBA⁷. Thus, if anisotropy is incorporated in the present viscoelastic theory, the effective ΔT_c for MBBA would be far less compared to that of PAA. Since the ΔT used in the measurements for both were of the same order,

convection would be more dominant in MBBA. Thus, it appears that the data for PAA is practically free from convection. A slight discontinuity is however observed in the data of PAA (figure 2) where ΔT_c is a minimum. The decrease in k_e with increasing d was explained as an interfacial effect earlier⁶. The same would be valid now for the convection. For small d , the data appear to be free from convection with conduction being dominant - i.e., $k_e \rightarrow k_{\perp}$ as $d \rightarrow 0$ and similarly for large gaps $k_e \rightarrow k_o$ as $d \rightarrow \infty$ provided $Ra \ll 1700$ to avoid Bénard convection. Even though the k_e values are extrapolated values for zero heat flux, there could still be a convective component for intermediate gaps.

For both MBBA and PAA a minimum k_e is not observed perhaps because d was not sufficiently large. It might not be possible to avoid Bénard convection when d is very large.

Concluding remarks

A possible qualitative explanation of the boundary effect on thermal conduction in nematics on the basis of the theory of thermal instability in viscoelastic materials has been given. A quantitative explanation is possible by improving upon this theory for anisotropic materials like nematic liquid crystals and also by using more accurate properties. The actual ΔT_c may be far less compared to the calculated value since the relaxation time λ may be very large. Recent observations on convection flow cell generation⁵ seem to support this. The direct influence of the boundaries and temperature gradients on the orientation of the molecules below the threshold of instability is also important. There is some amount of approximation in the solution of the theoretical equations. It is not obvious at this stage how the confined cell with heating from above could be theoretically analyzed taking all the above factors into account.

References

- 1 CHANDRASEKHAR S *Hydrodynamic and Hydromagnetic Stability*, Oxford University Press, Chapter II (1961)
- 2 DUBOIS-VIOLETTE E C.R. *Acad. Sci. Paris* 273B 923 (1971)
- 3 FREDRICKSON A G *Principles and Applications of Rheology*, Prentice Hall, Chapter 6 (1964)
- 4 LESLIE F M *Arch. Ratl. Mech. Anal.* 28 265 (1968)
- 5 PIERANSKI P *et. al.*, *Phys. Rev. Lett.* 30 736 (1973)
- 6 RAJAN V S V and PICOT J J C *Mol. Cryst. Liquid Cryst.* 20 55 (1973)
- 7 RAJAN V S V and PICOT J J C *Mat. Res. Bulletin* 9 311 (1974)
- 8 TAKASHIMA M J. *Phys. Soc. Japan* 33 511 (1972)
- 9 VEST C M and ARPACI V S *J. Fluid Mech.* 36 613 (1969)

The theory of reflexion and transmission by plane parallel cholesteric films

RAJARAM NITYANANDA* and U D KINI**

* Materials Research Division, National Aeronautical Laboratory,
Bangalore 560017

** Raman Research Institute, Bangalore 560006, India

Abstract. The theory of propagation in an infinite cholesteric medium is applied here to the problem of a sample bounded by plane parallel surfaces normal to the optic axis. For each circular polarization at normal incidence, the reflected and transmitted waves are found to consist of both circular polarizations. Thus, four coefficients of reflexion and transmission are needed to describe the problem fully. These have been calculated in a closed analytical form, which has the correct behaviour in various limiting cases. Numerical computations are used to investigate the effect of finite sample thickness in modifying the rotation and circular dichroism predicted from the infinite medium theory. This is of importance in interpreting the results of experiments.

Introduction

The theory of the propagation of light along the axis of a cholesteric liquid crystal was first given by de Vries¹ using the Oseen² model for the dielectric tensor, subject to certain approximations. (For a discussion of these approximations, see, Nityananda³, hereafter referred to as I). Recently, an exact solution of this problem was given by Kats⁴ and by Nityananda³. We now use that solution to calculate the reflection and transmission coefficients of a plane parallel cholesteric film. These were approximately calculated by de Vries. The novel feature of our calculation is the presence of both circular polarisations in the reflected and transmitted beams, even if only one circular polarisation is incident. Thus we define 'diagonal' and 'off diagonal' coefficients r_{++} and r_{-+} where, by convention, the second suffix gives the sense of rotation of the electric vector of the incident wave, and the first the sense of the reflected (or transmitted) wave. For example, t_{+-} is the amplitude of the (+) circular component of the transmitted light for the unit incident amplitude of (-) light. The convention is the same as in I, with (+) denoting rotation in the clockwise sense in the xy -plane. This would be called a right circular wave if it travelled along $+z$, but left circular if the wave vector were, along $-z$. For a transparent dielectric at normal incidence, (+) is reflected as (+) and (-) as (-). A right handed cholesteric liquid

crystal, studied at a wavelength near the reflection band, reflects (+) as predominantly (-). In his calculation of the reflection and transmission coefficients, de Vries¹ assumed that the medium on either side of the cholesteric film had a refractive index equal to the average for the cholesteric. Further, the birefringence δn was treated as a small quantity—an approximation which is certainly valid in practice. Under these conditions, the transmitted wave has the same circular polarisation as the incident wave and one circular wave is reflected, completely reversed in sense. This agrees with experimental observations, which approach the conditions assumed since the liquid crystal is enclosed by glass slides. The work of Chandrasekhar and Prasad⁵ based on the dynamical theory led to similar results.

The emphasis in the present paper is on removing the restrictions in earlier treatments. Thus, the birefringence could be large (as is sometimes attained by dissolving optically active molecules in a nematic to form a cholesteric) and the wavelength far from, or close to the Bragg reflection. The refractive index of the surrounding medium can be arbitrary. This additional generality has not led to qualitatively new results, however. Indeed, Chandrasekhar *et al.*⁸ have shown that the dynamical theory leads to close quantitative agreement with the exact solution presented here in practical cases. The coefficients like r_{++} which were neglected in earlier treatments would describe Fresnel reflection for an isotropic dielectric, and would be of the order of the refractive index difference between the cholesteric and the glass slide. A coefficient like t_{-+} would vanish for an isotropic dielectric—the formulae given below show it to be of order δn (this is the local birefringence of the cholesteric). When we come to intensities these estimates are naturally squared, so that neglecting them has not caused serious error in the earlier work.

2. Calculation of the reflection and transmission coefficients

The sample, of thickness T , is assumed to occupy the region between the planes $z = 0$ and $z = T$, with its helical axis parallel to z , *i.e.*, normal to the plane of the sample. This is called the plane texture and is a commonly used experimental geometry. The incident wave is taken to be a general superposition of (+) and (-) circular polarisations, with complex amplitudes E_{+i} and E_{-i} . (We use the suffix 'i' for incident, 'r' for reflected, and 't' for transmitted light.) Its wavevector is $(0, 0, K)$ where $K = \omega/c$ if the region $z < 0$ is free space.

The reflected wave has wave vector $(0, 0, -K)$ and is a superposition of both circular components with amplitudes E_{+r} and E_{-r} . In the region $z > T$, we have a transmitted wave with wave vector $(0, 0, K)$ and circular components $E_{\pm t}$. In what follows we use the notation of I in which the two circular components are written together in the form of a

row or column vector (1×2 or 2×1 matrix). Thus, the incident wave is written as

$$[E_{+1} e^{iK_1 z}, E_{-1} e^{iK_1 z}].$$

The reflected and transmitted waves are written similarly (figure 1).

We now have to match these waves outside the cholesteric to a suitable solution of Maxwell's equations within. This solution is given in the work of Kats⁴ and in that of Nityananda⁵. From general considerations we see that there must be four independent solutions for propagation along the axis because we have two coupled second order differential equations (essentially the wave equation $\nabla \times (\nabla \times \mathbf{E}) = -\frac{1}{c^2} \hat{\epsilon} \frac{\partial^2 \mathbf{E}}{\partial t^2}$ in component form) for E_x and E_y or E_+ and E_- . For example, in an isotropic dielectric, these four solutions could just be two linearly polarised waves along $+z$ and two more along $-z$. For the cholesteric, the four independent solutions are

$$U_{r+} = [e^{iK_1 z}, d e^{i(K_1 - 2Q)z}]$$

$$U_{b+} = [d e^{-i(K_1 - 2Q)z}, e^{-iK_1 z}]$$

$$U_{r-} = [f e^{i(K_1 + 2Q)z}, e^{iK_1 z}]$$

$$U_{b-} = [e^{-iK_1 z}, f e^{-i(K_1 + 2Q)z}]$$

We choose a linear combination of these four solutions with coefficients $t_{r\pm}, t_{b\pm}$ to describe the electric field in the medium*. We have four boundary conditions to fulfil at each interface; one for each cartesian or circular component of the electric and magnetic fields. The magnetic field can be expressed in terms of the electric field using Maxwell's equations. Because the fields have no dependence on x and y , and no z components, these reduce to

$$\frac{i\omega}{c} B_x = i(-k_y E_y)$$

$$\frac{i\omega}{c} B_y = i(k_x E_x)$$

In terms of the circular components $E_{\pm} = \frac{E_x \pm iE_y}{\sqrt{2}}$ we get $(\omega/c) B_{\pm} = \pm ik_x E_{\pm}$. The factor of $\pm i$ means that the magnetic field is at right

* The expressions for K_1 , K_2 , d and f are given in Appendix I along with the reason for the notation.

Table 1. Boundary conditions for the electric field

At $z = 0$:

$$E_{+1} + E_{+r} = t_{t+} + f t_{t-} + t_{b+} + d t_{b-} \quad (1)$$

$$E_{-1} + E_{-r} = d t_{t+} + t_{t-} + f t_{b+} + t_{b-} \quad (2)$$

At $z = T$:

$$\begin{aligned} E_{+1} \exp(iKT) &= t_{t+} \exp(iK_1T) + f t_{t-} \exp[i(K_2 + 2q)T] \\ &+ t_{b+} \exp(-iK_2T) + d t_{b-} \exp[-i(K_1 - 2q)T] \end{aligned} \quad (3)$$

$$\begin{aligned} E_{-1} \exp(iKT) &= d t_{t+} \exp[i(K_1 - 2q)T] + t_{t-} \exp(iK_2T) \\ &+ f t_{b+} \exp[-i(K_2 + 2q)T] + t_{b-} \exp(-iK_1T) \end{aligned} \quad (4)$$

Boundary conditions for the magnetic field

At $z = 0$:

$$K(E_{+1} - E_{+r}) = K_1 t_{t+} + f(K_2 + q)t_{t-} - K_2 t_{b+} - (K_1 - 2q)dt_{b-} \quad (1')$$

$$K(E_{-1} - E_{-r}) = d(K_1 - 2q)t_{t+} + K_2 t_{t-} - f(K_2 + 2q)t_{b+} - K_1 t_{b-} \quad (2')$$

At $z = T$:

$$\begin{aligned} KE_{+1} \exp(iKT) &= K_1 t_{t+} \exp(iK_1T) + f(K_2 + 2q)t_{t-} \exp[i(K_2 + 2q)T] \\ &- K_2 t_{b+} \exp(-iK_2T) - (K_1 - 2q)dt_{b-} \exp[-i(K_1 - 2q)T] \end{aligned} \quad (3')$$

$$\begin{aligned} KE_{-1} \exp(iKT) &= d(K_1 - 2q)t_{t+} \exp[i(K_1 - 2q)T] + K_2 t_{t-} \exp(iK_2T) \\ &- f(K_2 + 2q)t_{b+} \exp[-i(K_2 + 2q)T] - K_1 t_{b-} \exp(-iK_1T) \end{aligned} \quad (4')$$

Eliminating $t_{t\pm}$ and $t_{b\pm}$ as indicated, we obtain expressions for the reflexion and transmission coefficients, which are given in table 2. It is convenient to define various intermediate quantities A , B , X and Y with suffixes from 1 to 4, D and Δ . This is solely to shorten the expressions for r and t . The next section gives the results of numerical calculations based on these formulae.

Table 2

$$A_1 = \frac{1}{2} \left(1 + \frac{K_1}{K} \right), \quad A_2 = \frac{f}{2} \left(1 + \frac{K_2 + 2q}{K} \right), \quad A_3 = \frac{1}{2} \left(1 - \frac{K_2}{K} \right),$$

$$A_4 = \frac{d}{2} \left[1 - \frac{(K_1 - 2q)}{K} \right]$$

$$B_1 = \frac{1}{2} \left(1 - \frac{K_1}{K} \right), \quad B_2 = \frac{f}{2} \left[- \frac{K_2 + 2q}{K} \right], \quad B_3 = \frac{1}{2} \left[1 + \frac{K_2}{K} \right],$$

$$B_4 = \frac{d}{2} \left[1 + \frac{(K_1 - 2q)}{K} \right]$$

$$X_1 = (K_1^2 - K^2) - d^2 (K_1 - 2q + K) (K_1 - 2q - K)$$

$$X_2 = [f(K + K_1) (K_2 + 2q - K) - d(K + K_1 - 2q) (K_2 - K)] \\ \exp[-i(K_1 - 2q - K_2)T]$$

$$X_3 = [d(K_1 - 2q - K) (K + K_2) - f(K + K_2 + 2q) (K_1 - K)] \\ \exp[i(K_1 - 2q - K_2)T]$$

$$X_4 = (K_2^2 - K^2) - f^2 (K_2 + 2q + K) (K_2 + 2q - K)$$

$$D = \exp[-i(K_1 + K_2)T] [(K + K_1) (K + K_2) \\ - df(K + K_2 + 2q) (K + K_1 - 2q)]$$

$$\Delta = (A_1 D + A_3 X_1 + A_4 X_3) (B_3 D + B_2 X_2 + B_1 X_4) \\ - (A_2 D + A_3 X_2 + A_4 X_4) (B_4 D + B_2 X_1 + B_1 X_3)$$

$$Y_1 = D(B_3 D + B_2 X_2 + B_1 X_4), \quad Y_2 = -D(A_2 D + A_3 X_2 + A_4 X_4)$$

$$Y_3 = -D(A_2 D + A_3 X_2 + A_4 X_4), \quad Y_4 = D(A_1 D + A_3 X_1 + A_4 X_3)$$

$$r_{++} = \frac{B_1 Y_1 + B_2 Y_3}{\Delta} + \frac{1}{D\Delta} [B_3 (X_1 Y_1 + X_2 Y_3) + B_4 (X_3 Y_1 + X_4 Y_3)]$$

$$r_{+-} = \frac{B_1 Y_2 + B_2 Y_4}{\Delta} + \frac{1}{D\Delta} [B_3 (X_1 Y_2 + X_2 Y_4) + B_4 (X_3 Y_2 + X_4 Y_4)]$$

$$r_{-+} = \frac{A_4 Y_1 + A_3 Y_3}{\Delta} + \frac{1}{D\Delta} [A_2 (X_1 Y_1 + X_2 Y_3) + A_1 (X_3 Y_1 + X_4 Y_3)]$$

$$r_{--} = \frac{A_4 Y_2 + A_3 Y_4}{\Delta} + \frac{1}{D\Delta} [A_2 (X_1 Y_2 + X_2 Y_4) + A_1 (X_3 Y_2 + X_4 Y_4)]$$

$$\begin{aligned} t_{++} = & \frac{Y_1}{\Delta} \exp [i (K_1 - K) T] + \frac{Y_3}{\Delta} f \exp [i (K_2 + 2q - K) T] \\ & + \frac{1}{D\Delta} [(X_1 Y_1 + X_2 Y_3) \exp \{-i (K_2 + K) T\} \\ & + d (X_3 Y_1 + X_4 Y_3) \exp \{-i (K_1 - 2q + K) T\}] \end{aligned}$$

$$\begin{aligned} t_{+-} = & \frac{[Y_2 \exp \{i (K_1 - K) T\} + Y_4 f \exp \{i (K_2 + 2q - K) T\}]}{\Delta} \\ & + \frac{1}{D\Delta} [(X_1 Y_2 + X_2 Y_4) \exp \{-i (K_2 + K) T\} + d (X_3 Y_2 + X_4 Y_4) \\ & \exp \{-i (K_1 - 2q + K) T\}] \end{aligned}$$

$$\begin{aligned} t_{-+} = & \frac{1}{\Delta} [d Y_1 \exp \{i (K_1 - 2q - K) T\} + Y_3 \exp \{i (K_2 - K) T\}] \\ & + \frac{1}{D\Delta} [f (X_1 Y_1 + X_2 Y_3) \exp \{-i (K_2 + 2q + K) T\} \\ & + (X_3 Y_1 + X_4 Y_4) \exp \{-i (K_1 + K) T\}] \end{aligned}$$

$$\begin{aligned} t_{--} = & \frac{1}{\Delta} [d Y_2 \exp \{i (K_1 - 2q - K) T\} + Y_4 \exp \{i (K_2 - K) T\}] \\ & + \frac{1}{D\Delta} [f (X_1 Y_2 + X_2 Y_4) \exp \{-i (K_2 + 2q + K) T\} \\ & + (X_3 Y_2 + X_4 Y_4) \exp \{-i (K_1 + K) T\}] \end{aligned}$$

The experimental quantities usually studied are optical rotation and circular dichroism. The latter is usually defined by

$$D = \frac{\sqrt{I_+} - \sqrt{I_-}}{\sqrt{I_+} + \sqrt{I_-}}$$

where I_+ and I_- are the intensities of the transmitted beam for equal incident intensities of the two circular polarisations. The above definition contains the implicit provision that (+) light is transmitted

only as $(+)$ and $(-)$ light as $(-)$. Correspondingly, the experimenter does not usually analyse the transmitted light into its circular components before making intensity measurements. We have seen in the previous section that the transmitted light contains both circular polarisations. To conform to the experimental situation, we take the total intensity of these two components as I_+ or I_- in plotting the theoretical curves. Likewise, when computing optical rotation, bearing in mind that the transmitted light is in general elliptic, the major axis of the ellipse is chosen as the direction of the emergent polarisation. In all the numerical examples, the pitch P has been set equal to 0.3571μ and the birefringence $\delta n = 0.07$, the mean refractive index is 1.435 , so that the two principal refractive indices are 1.4 and 1.47 . The thickness T is variable and is indicated in each figure. The reflection band is centered at $\lambda = \bar{n}P = 0.5125 \mu$ and has a width $P\delta n \sim 0.05 \mu$.

Figure 2 shows the reflection coefficient $|r_+|^2$. This measures reflection with change in sense of the circular polarisation, which is the characteristic property of the cholesteric liquid crystal. This is for a sample of thickness 6μ , and shows the oscillations characteristic of finite samples studied by Chandrasekhar and Prasad⁵ and by Dreher, Meier and Saupe⁶. The spacing of these oscillations agree approximately with what would be calculated for a plane parallel film of isotropic dielectric with the same mean refractive index and thickness, but their amplitude is of course greatly enhanced near the reflection band.

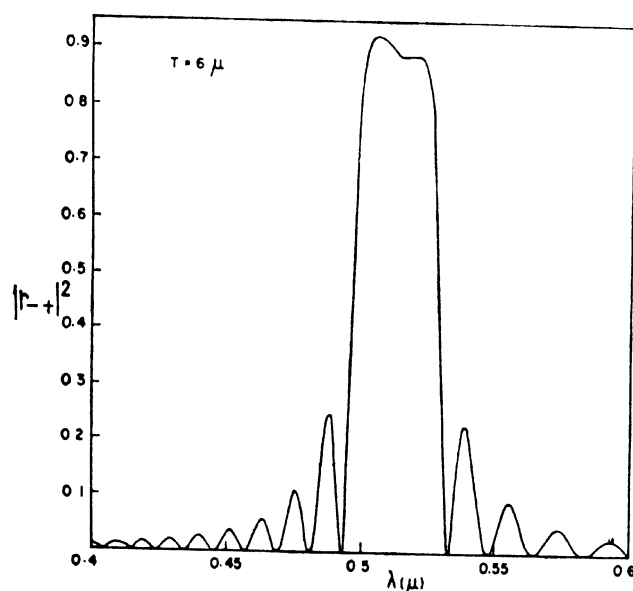


Figure 2 Intensity of reflection with change in sense of circular polarisation as a function of wavelength λ computed from the formula in table 2. The sample thickness is 6μ .

Figure 3 shows the transmitted intensity T and circular dichroism D as functions of wavelength for $4\ \mu$ (figure 3a) and $6\ \mu$ (figure 3b) samples. T is plotted for each circular polarisation separately, as indicated by the symbols (+) and (−) on the respective curves. As expected, the (+) circular component which is Bragg reflected shows a strong dip in transmission at the same wavelength. The circular dichroism shows a strong negative peak there, since $I_- > I_+$. The effect of increasing the sample thickness is seen by comparing figures 3a and 3b. The suppression of the R component in the transmitted beam is more complete, the negative peak in D stronger, and the oscillations more closely spaced. Further we see an approach to the case of an infinite medium which has a flat reflection maximum. The transmission curve approaches a shape with a flat minimum

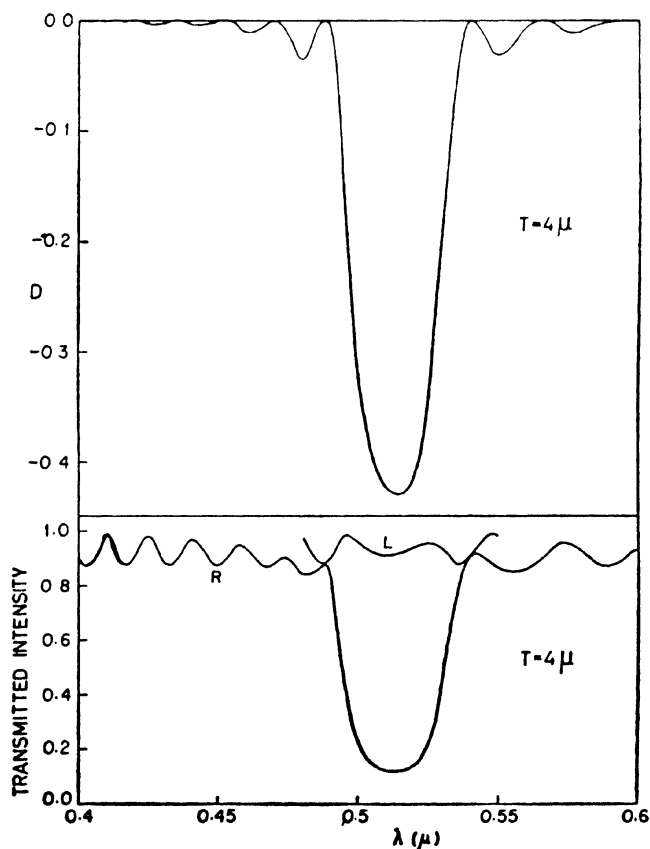


Figure 3a Transmitted intensity T and circular dichroism D computed as functions of wavelength λ . Sample thickness $4\ \mu$.

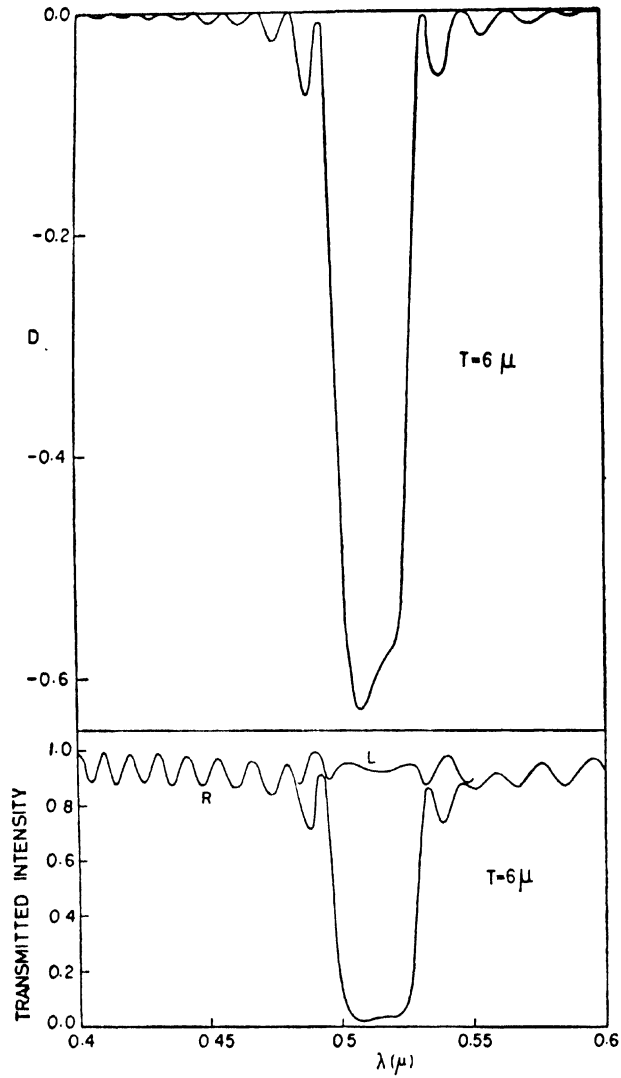


Figure 3 b Transmitted intensity T and circular dichroism D computed as functions of wavelength λ . Sample thickness 6μ .

close to zero. The extinction length of the attenuated normal wave at the centre of the reflection band is $\simeq (P/2\pi) \frac{\bar{n}}{\delta n} \sim 1.4 \mu$ in our example, increasing to ∞ at the edges of the reflection band. Therefore, the infinite medium behaviour first occurs at the centre and then spreads outwards.

It is noteworthy that the circular dichroism does not change sign away from the reflection band for a non-absorbing sample. It tends to zero as the values of T for (+) and (−) circular polarisations tend to equality. The behaviour of absorbing samples is different and the following paper discusses it.

Finally figures 4a and 4b show optical rotation as a function of wavelength near the reflection band for thickness $1\ \mu$ and $3\ \mu$ respectively. The dispersion qualitatively resembles that for infinite samples³. However,

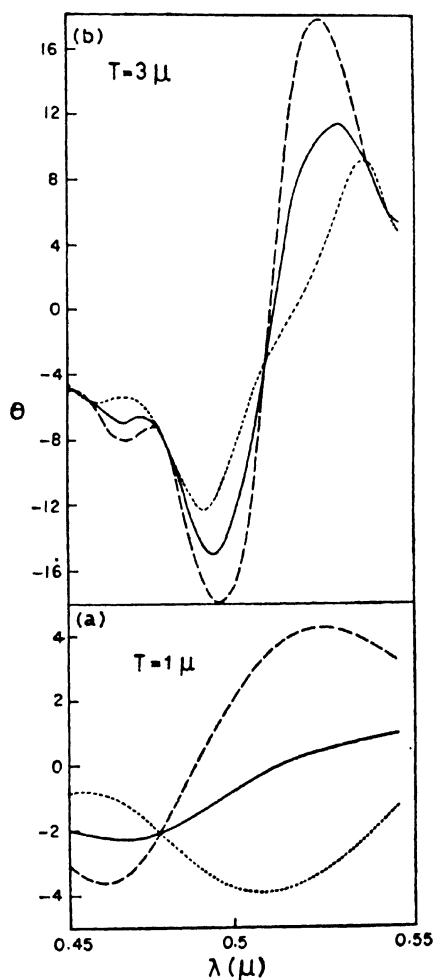


Figure 4 Optical rotation vs λ . The dotted curve is for incident linear polarisation along y , the dashed curve for x . Sample thickness (a) $1\ \mu$ (b) $3\ \mu$.

the curve for $T = 1 \mu$ (which is about 3 times the pitch) reveals that the rotation angle depends on the azimuth of the incident light. The dashed curve shows the rotation for incident linear polarisation along x and the dotted one for y . The director of the cholesteric is taken along x at the plane $z = 0$. The solid line shows the average. Even this average is not proportional to thickness—if it were the solid curves would differ only in scale. Chandrasekhar and Prasad⁵ noted the thickness dependence and studied it experimentally. Ranganath (private communication) has noted the azimuth dependence of the rotation for mixtures of right and left handed cholesterics when the pitch is much larger than the wavelength of light. This azimuth dependence is considerably reduced if the medium on either side of the cholesteric matches its average refractive index.

The behaviour of the rotatory dispersion can be correlated to that of the circular dichroism *via* the Kramers Kronig dispersion relation. As the thickness is reduced the band of circular dichroism widens and is rounded off, so that we expect the maximum and minimum of the rotation to be reduced in strength and shifted outwards. The oscillations in the circular dichroism are reflected in those of rotation*.

Summary

An exact analytical solution of the problem of reflection and transmission at normal incidence by a cholesteric film has been given. This differs from earlier treatments in including off diagonal transmission and reflection coefficients. Numerical calculations show these to be small, and confirm the results of earlier work^{1, 5, 6} on finite specimens.

Appendix I

In the infinite medium theory developed in I the normal waves were given by superpositions of two circular waves of opposite sense, with wave vectors differing by $2q$, for example

$$[e^{iK_1 z}, d e^{i(K_1 - 2q)z}].$$

The term with coefficient unity is called the dominant component. There are two reasons for this—firstly, that the coefficients d and f never exceed 1 (in absolute magnitude) near the reflection band, and secondly, that they vanish in the limiting case of an isotropic dielectric ($\delta n \rightarrow 0$). In the same limiting case, K_1 reduces to $K_n = \frac{2\pi n}{\lambda}$. The suffixes b and f

* Such a correlation can only be qualitative—to our knowledge no quantitative formulation of the dispersion relation has been given for a non-uniform medium like cholesteric. While one can study the analytic properties of K_1 and K_2 , we have seen that these do not directly give rotation and circular dichroism for finite samples.

used in the text refer to 'backward' and 'forward'. The normal wave written above reduces to a circular wave propagating along $+z$ as $d \rightarrow 0$, and would hence be called 'forward'. The formulae for K_1 , K_2 , d and f are given below. ω = frequency of incident light, c = velocity of light in vacuum, ϵ_a and ϵ_b are the principal dielectric constants,

$$\epsilon = \frac{\epsilon_a + \epsilon_b}{2}, \quad \beta = \frac{\epsilon_a - \epsilon_b}{2}, \quad P = \text{Pitch}, \quad q = \frac{2\pi}{P}, \quad K = \frac{\omega}{c}, \quad K_m = \frac{\omega}{c} \sqrt{\epsilon}$$

$$K_1 = q [K_m^2 + q^2 - (4K_m^2 q^2 + \beta^2 K^4)^{1/2}]^{1/2}$$

$$K_2 = -q + [K_m^2 + q^2 + (4K_m^2 q^2 + \beta^2 K^4)^{1/2}]^{1/2}$$

$$d = \frac{K_1^2 - K_m^2}{\beta K^2}, \quad f = \frac{K_2^2 - K_m^2}{\beta K^2}.$$

References

- 1 DE VRIES H *Acta Crystallogr.* **4** 219 (1951)
- 2 OSEEN C W *Trans. Faraday Soc.* **29** 833 (1933)
- 3 RAJARAM NITYANANDA *Mol. Cryst. Liquid Cryst.* **21** 315 (1973)
- 4 KATS E I *Zh. Eksp. Teor. Fiz.* **59** 1854 (1970); *Sov. Phys-JETP* **32** 1004 (1971)
- 5 CHANDRASEKHAR S and SHASHIDHARA PRASAD J *Mol. Cryst. Liquid Cryst.* **14** 115 (1971)
- 6 DREHER R, MEIER G and SAUPE A *Mol. Cryst. Liquid Cryst.* **13** 17 (1971)
- 7 MAUGUIN M C *Bull. Soc. Franc. Miner. Cryst.* **34** 71 (1911)
- 8 CHANDRASEKHAR S, RANGANATH G S and SURESH K A this Conference

Anomalous transmission (Borrmann effect) in absorbing cholesteric liquid crystals

RAJARAM NITYANANDA*, U D KINI**,
S CHANDRASEKHAR** and K A SURESH**

* Materials Science Division, National Aeronautical Laboratory,
Bangalore 560017

** Raman Research Institute, Bangalore 560006

Abstract. The celebrated Borrmann effect is an anomalous increase in transmitted x-ray intensity when a crystal is set for Bragg reflexion. In this paper, it is shown that a similar effect occurs in absorbing cholesteric liquid crystals in the vicinity of the reflexion band. However, in contrast to the x-ray case, the polarization of the wave field and the linear dichroism of the molecules play an essential part.

Numerical computations are presented, based on the general theory of reflexion and transmission by oriented cholesteric films. They illustrate the role of dichroism and sample thickness in determining the magnitude of the effect.

The existence of the effect is established by experimental studies on cholesteryl nonanoate mixed with small quantities of *p*-azoxyanisole or *n*-*p*-methoxybenzylidene-*p*-phenylazoaniline. When the reflexion band is adjusted to overlap with the strongly dichroic band of the solute molecules, the transmission spectrum exhibits the features predicted by theory.

Introduction

The optical properties of a cholesteric liquid crystal are well described by the model of Oseen¹. Locally the molecular axes are, on the average, aligned parallel to a fixed direction as in a nematic, so that this is a principal axis of the local dielectric ellipsoid. As we move along the *z* axis, this direction of preferred alignment (the director) rotates in the *x*-*y* plane, sweeping out an angle *qz* in a distance *z*. The pitch *p* is defined as the distance along *z* in which the director rotates through 2π ; thus $p = 2\pi/q$. The components of the dielectric tensor are periodic functions of position. Many of the features of wave propagation in periodic structures which were first studied in the context of x-ray diffraction by crystals can be observed in cholesterics in the optical range of wavelengths since their periodicity is of this order. The selective

reflexion of one circular polarisation in a band of frequencies, the extinction of that wave within the medium and the anomalous dispersion of the optical rotatory power in this frequency region are well known experimental facts which have been discussed theoretically by de Vries² and Chandrasekhar and Srinivasa Rao³; the latter authors have emphasized the analogy with the dynamical theory of x-ray diffraction.

This paper concerns another striking phenomenon which can occur in an absorbing periodic medium – the Borrmann effect^{4, 5}. First discovered for x-rays incident on highly perfect crystals, this effect consists of an (intuitively) unexpected increase in the transmitted intensity near the Bragg reflexion setting, which is precisely where a decrease in transmission is expected. Hence the name “anomalous transmission”. This is a consequence of the standing wave nature of the disturbance within the medium when the incident frequency is in the reflection band, as will be explained in detail in section 1, which also presents the features special to the cholesteric medium. Section 2 describes calculations based on the theory of reflexion and transmission by plane parallel cholesteric films which has been described in the previous paper⁶. These show the feasibility of observing the effect under suitable conditions. Section 3 presents the results of preliminary experiments on the transmission of light of both circular polarisations by films of cholesteryl nonanoate to which a small amount (< 5%) of dichroic molecule such as *p*-azoxyanisole (PAA) or *n-p*-methoxybenzylidene-*p*-phenylazoaniline (MBPAA) had been added. The curves giving circular dichroism as well as transmitted intensity as a function of wavelength near the reflexion band indeed show the predicted features.

1. Nature of the waves in the cholesteric medium and a qualitative discussion of the Borrmann effect

An exact solution of the normal incidence problem is given in the papers by Kats⁷ and Nityananda⁸. The medium is described by a dielectric tensor with principal values ϵ_a and ϵ_b and principal axes rotating through an angle of 2π in the *x-y* plane per pitch *p* traversed along *z*. The solution of Maxwell's equations under these conditions is given by a combination of two circular waves with opposite sense and wave vectors differing by $2q$. Naturally, there are two such solutions for a given direction of propagation, which would reduce to a pure left circular wave and a pure right circular wave in the limit $\epsilon_a - \epsilon_b \rightarrow 0$. We call these the left and right dominant solutions. In the range of wavelengths near the reflexion band which is of interest here, the amplitude of the dominant component is never less than that of the other component, justifying the name. Further, one of the two solutions (the right dominant for a right handed cholesteric) becomes strongly mixed, near the reflection band. That is, if we write it as a superposition of a right circular wave $\exp(iK_1 z)$ and a left circular wave $d \exp[i(K_1 - 2q)z]$ then the coefficient *d* becomes of the order of 1

for wavelengths near the reflexion band (figure 1 *a*). If we fix the value of z , thereby studying the electric field at one point in the medium, the two circular components add to give an elliptic vibration. The direction of the major axis of this ellipse is the direction in which the two circular waves add (figure 1 *b*). When the coefficient d has an absolute value of 1, the resultant vibration is linearly polarised. As we change z , the relative phase of the two circular components changes by $2qz$. The resultant elliptic vibration therefore changes in azimuth by qz , but has the same ellipticity. Indeed, in a co-ordinate system rotating at the same rate as the director, we have a fixed elliptic vibration as was pointed out by de Vries². This is important for what follows. Away from the reflexion band, the coefficient d is small and we have almost a circular vibration. On the long wavelength side of the reflection band, we obtain an ellipse with major axis along the direction of greater principal dielectric constant

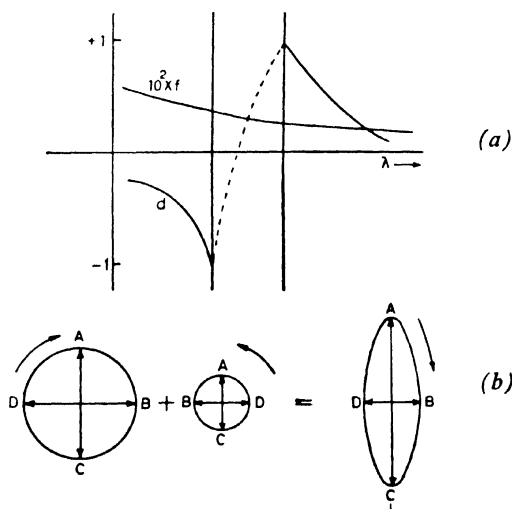


Figure 1 (a) The coefficients d and f which determine the mixed character of the normal waves as functions of wavelength. The dotted part of the curve for d is meant to indicate that $|d|$ remains 1 within the reflection band, while the phase varies from 180° to 0° : that is, d moves along the semicircle of unit radius in the upper half of the complex plane, varying from -1 to +1 as the wavelength increases from one edge of the reflection band to the other.

- (b) Combination of two opposite circular waves to give an elliptic vibration with the same sense as the stronger circular wave and azimuth along the direction in which the electric vectors of the two circular waves are parallel. A B C and D represent four successive states of the vibration separated by 90° in phase or a quarter of a period in time.

say ϵ_a . Since the electric vector is now sampling a direction with greater polarisability, it is natural that the effective refractive index for the wave is greater. On the short wavelength side of the reflexion band, the major axis of the ellipse is directed along the axis with lower principal dielectric constant ϵ_b . We expect that the effective refractive index would now be less than the average for the medium. The dispersion curve (wave vector K as a function of frequency ω) plotted in figure 2, confirms this physical picture. Within the reflexion band the wave is linearly polarised with the azimuth rotating at the same rate as the director and making a fixed angle to it. As we decrease the wavelength, going through the reflexion band,

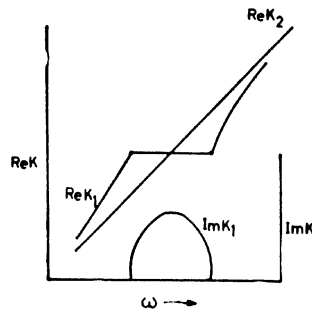


Figure 2 The dispersion relation (wave vector K as a function of frequency ω) for the two normal waves. K_2 is real, while K_1 has an imaginary part which is separately shown.

this angle changes from 0 to 90° as the phase of the complex number d varies from 0 to 180° (figure 1). The second normal wave is only weakly mixed. If we write it as a superposition of a left circular wave $\exp(iK_2 z)$ and a right circular wave $f \exp[i(K_2 + 2q)z]$, then f remains small and shows no remarkable variation near the Bragg reflexion (figure 1a). For qualitative purposes, we can think of this wave as a pure left circular wave which sees only the average medium and has a refractive index \bar{n} , and a simple linear dispersion relation (figure 2) $\omega = (c/\bar{n})k$. We call this the 'indifferent' normal wave. The polarisation behaviour of the normal waves is summarised in figure 3.

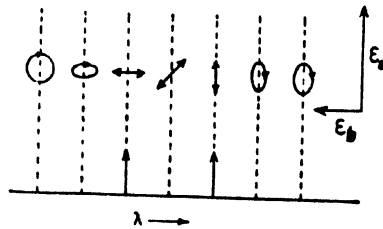


Figure 3 Polarisation of the normal wave as a function of wavelength.

The above description is valid for a non-absorbing cholesteric medium. However, we can assess the effects of dichroism (that is, a different imaginary part for ϵ_a and ϵ_b) by assuming that the polarisation behaviour of the normal waves remains qualitatively unchanged. Taking the imaginary part of ϵ_a to be greater (that is, the more polarisable axis is also the axis of greater absorption) - we see immediately that the attenuation of the first normal wave will be greater than the average on the long wavelength side of the reflexion band since it will be sampling more of the ϵ_a axis, and it will be less than the average on the short wavelength side of the reflexion band. Hence right circular incident light, which couples to this normal wave, should undergo more absorption on the long wavelength side of the band and less on the short wavelength side.

This effect is over and above the extinction of the right circular wave which occurs even in the absence of absorption. Qualitatively, we expect enhanced transmission of the right circular wave on the short wavelength side. This is the Borrmann effect. The reduced absorption in this case is a consequence of the polarisation being at right angles to the highly absorbing axis. For x-rays in crystals the reduced absorption follows from the amplitude of the electric field being small at the absorbing sites (figure 4). Both these are due to the standing wave nature of



Figure 4 A qualitative picture of the Borrmann effect in x-rays. The nodes of the standing wave coincide with the atomic positions giving minimum absorption.

the disturbance in the medium, and both depend on the relative phase of the primary and Bragg reflected waves (the position of the modes in the x-ray case, the polarisation of the linear vibration in the liquid crystal). Since these phases vary continuously (by 180°) as we pass through the Bragg reflection band, the optimum conditions for the Borrmann effect are fulfilled at only one wavelength—in our example at one edge of the reflexion band.

2. Numerical calculations on absorbing cholesterics

Using the formulae of the previous paper⁶ the transmission coefficients of a plane parallel cholesteric slab were calculated as functions of wavelength near the Bragg reflexion for each circular polarisation incident on it. To correspond to the experimental practice, the total transmitted intensity was calculated as the sum of that in the two polarisations, although, predominantly, only the incident circular polarisation is present. The results are also presented in the form of circular dichroism D as a function of wave length, where

$$D = \frac{\sqrt{I_+} - \sqrt{I_-}}{\sqrt{I_+} + \sqrt{I_-}}$$

I_+ and I_- are the transmitted intensities for the + and - circular polarisations. These curves should be compared with the corresponding curves for a non-absorbing cholesteric presented in the previous paper⁶. The pitch p and principal refractive indices n_b and n_a have been chosen to be 3571 Å; 1.4 and 1.47 respectively as for the non-absorbing case. The dichroism Δk has been given the values 0.006, 0.03 and 0.06 successively. Here it is assumed that n_b remains real ($n_b = 1.4$) and $n_a = 1.47 + i \Delta k$. The dichroism has the same sign as the birefringence, *i.e.*, the more absorbing axis of the molecule is taken to be the same as the more polarisable axis.

A plot of the reflection coefficient as a function of wavelength is given for $\Delta k = 0.006$ in figure 5. When compared to the non-absorbing case, it shows asymmetry. This is analogous to the asymmetry of the reflexion as a function of angle which Prins⁹ calculated for x-rays incident on an absorbing perfect crystal. The reflection coefficient is higher on the short wavelength side and falls off towards longer wavelengths.

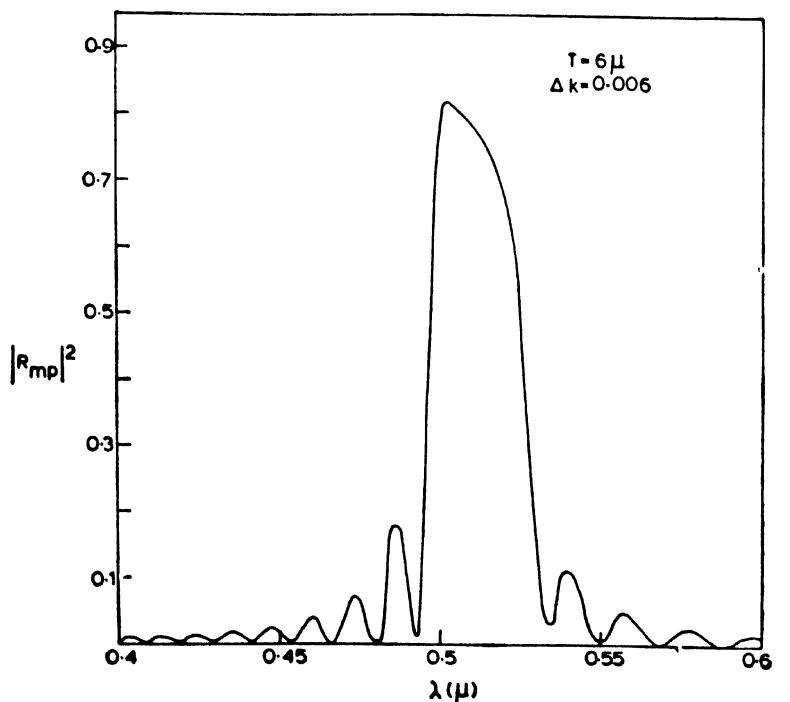


Figure 5 Intensity of reflexion with change in the sense of circular polarisation for an absorbing cholesteric. Thickness $T = 5.6 \mu$; dichroism $\Delta k = 0.006$.

Figure 6 *a* shows the transmitted intensity for the two circular polarisations, and figure 6 *b* the circular dichroism for $\Delta k = 0.006$. The curves

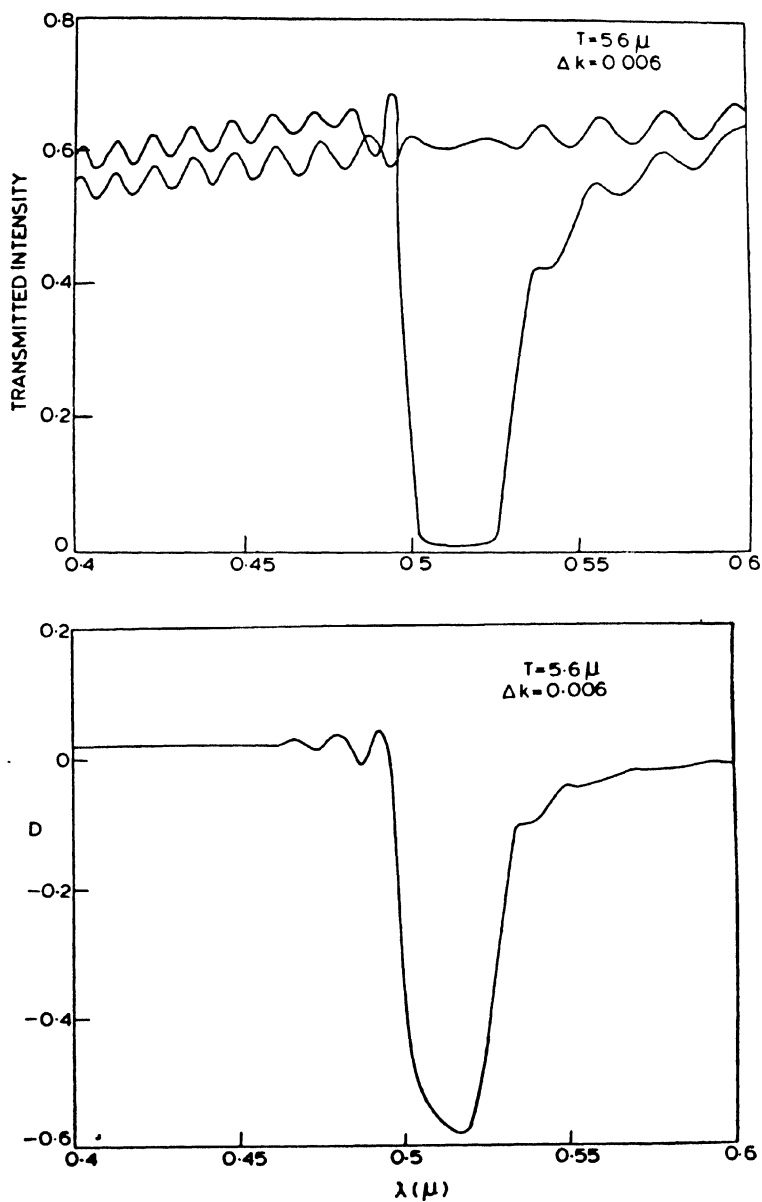


Figure 6 (a) Transmitted intensity, and (b) circular dichroism as function of wavelength.
 $T = 5.6 \mu$, $\Delta k = 0.006$.

are noticeably asymmetric, and the circular dichroism has changed sign on the short wavelength side so that the right circular polarisation which is cut down in the Bragg reflexion is actually enhanced on this side. By itself this does not constitute the Borrmann effect since there is a circular dichroism at short wavelengths which can be predicted from the Mauguin¹⁰ formula for rotation by making Δn complex and it has the right sign. However, this is expected to fall off with increase in wavelength; while

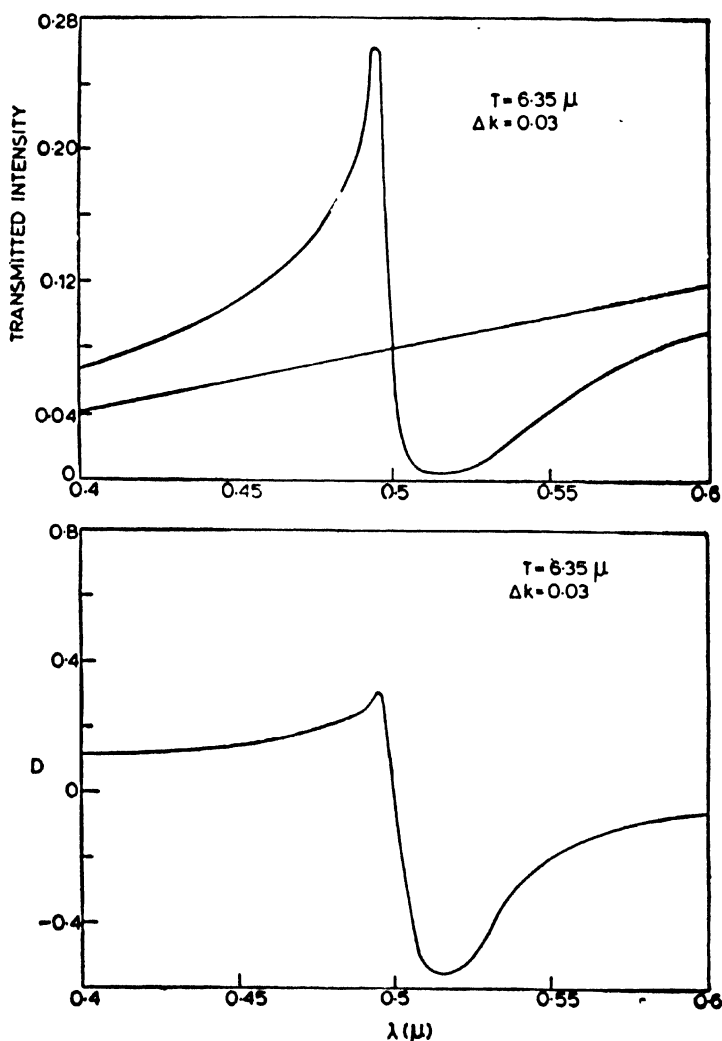


Figure 7 (a) Transmitted intensity, (b) Circular dichroism
 $T = 6.35 \mu$, $\Delta k = 0.03$.

the arguments of section 1 suggest that the transmission of right circular light should show a well defined maximum near the short wavelength edge of the reflexion band. This is brought out clearly in figures 7 *a* and 7 *b* which show the transmission coefficients and D for $\Delta k = 0.03$. This is even clearer in figures 8 *a* and 8 *b* which are for $\Delta k = 0.06$. We also note

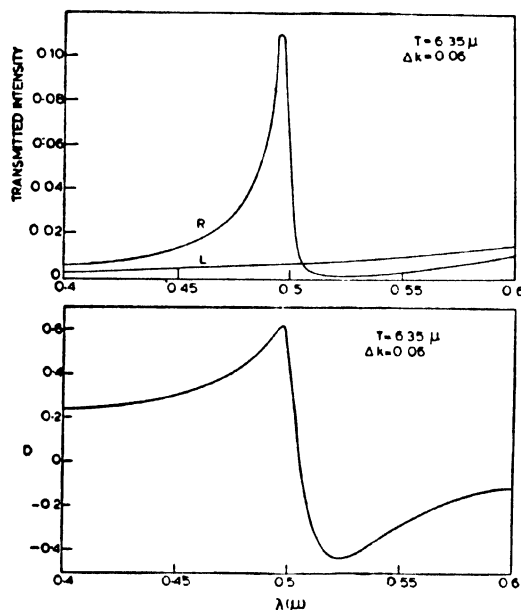


Figure 8 (a) Transmitted intensity, (b) Circular dichroism
 $T = 6.35 \mu$, $\Delta k = 0.06$.

the opposite effects on the long wavelength side, viz., the transmission of right circular light remains low for at least 500 \AA beyond 5140 \AA (which was the centre of reflexion band in the non-absorbing case). This is to be expected from the qualitative arguments of section 1—in this wavelength region the major axis of the ellipse is along the more absorbing axis of the molecules (figure 3).

The broadening and asymmetry of the circular dichroism curve has implications for optical rotation as well. We expect the zero crossing of the optical rotation to shift to longer wavelengths. This effect can be seen in figures 9 *a*, *b* and *c* which show the calculated optical rotation as a function of wavelength for $\Delta k = 0.006$, 0.015 and 0.03 .

3. Experiments

The experiments were carried out on thin samples of cholesteryl nonanoate with small percentages of PAA or MBPAA added. The former gives a

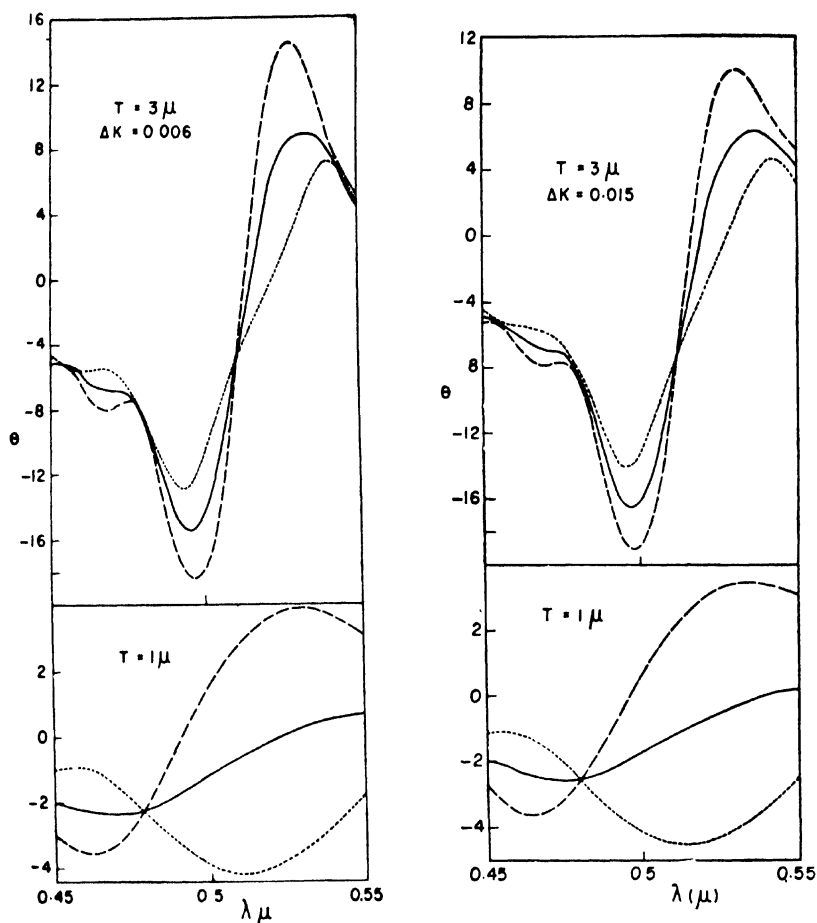


Figure 9 Optical rotation for incident linear polarisation along the director (dashed curve) and perpendicular to it (dotted curve). (a) $\Delta k = 0.006$, (b) $\Delta k = 0.015$.

band of linear dichroism (Δk) at about 3500 Å and the latter at about 3800 Å. They were well oriented in the plane texture and the wavelength of the Bragg reflexion could be controlled by using the temperature dependence of the pitch. The basic technique was to photograph the spectrum of a continuum source (tungsten lamp) through a circular polariser and the given sample. This is done for each circular polarisation separately and the transmitted intensity as a function of wavelength inferred from a microdensitometer trace of the developed photographic plate. Several exposures of the tungsten lamp source without any liquid crystal sample interposed were taken for calibration purposes. The

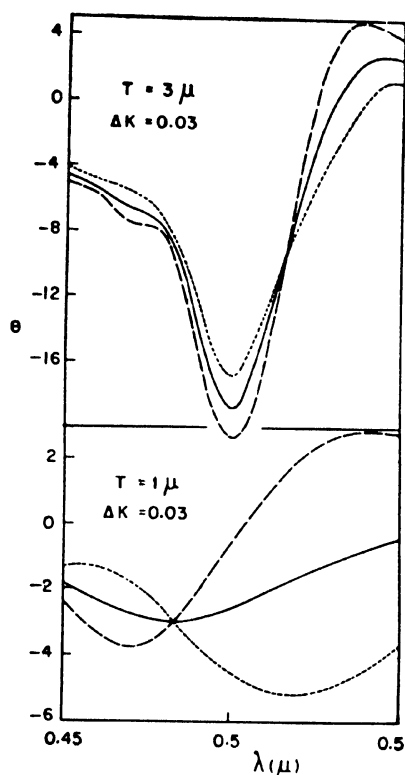


Figure 9c Optical rotation for incident linear polarisation along the director (dashed curve) and perpendicular to it (dotted curve). $\Delta k = 0.03$.

intensity obtained from these calibration curves is in arbitrary but fixed units. It is proportional to the transmission coefficient of the sample at that wavelength. The circular dichroism, which requires only the ratio of the transmission coefficients for the two circular polarisations, is independent of this undetermined factor of proportionality.

The raw microdensitometer traces for non-absorbing sample are shown in figure 10a. The two traces do not cross, showing that the circular dichroism does not change sign. Figure 10b shows the two traces for 2.45% PAA (by weight) in cholesteryl nonanoate. For this composition, we roughly estimate the maximum Δk to be 0.03. The Bragg reflection is at about 3550 Å, as is seen by the dip in the transmission for right circular light. At shorter wavelengths, the transmission has actually risen above that for left circular light. Figure 10c shows the transmission coefficients (in arbitrary units) and figure 10d the circular dichroism for the same sample. Figure 11 shows the results of a similar experiment on 4.25% MBPAA the Bragg reflection being at about 4020 Å.

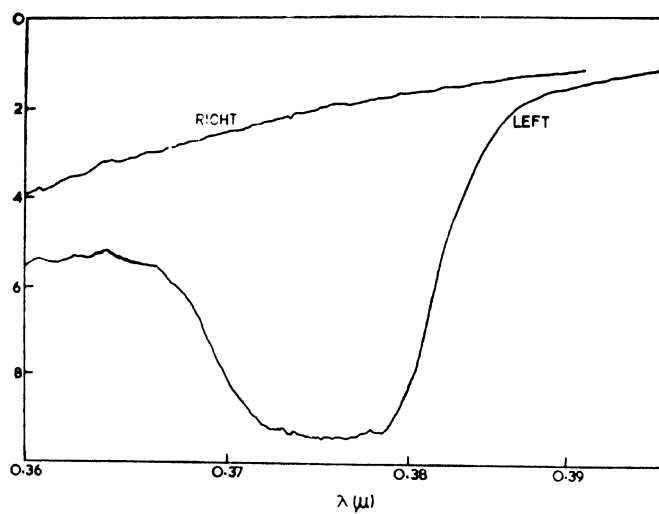
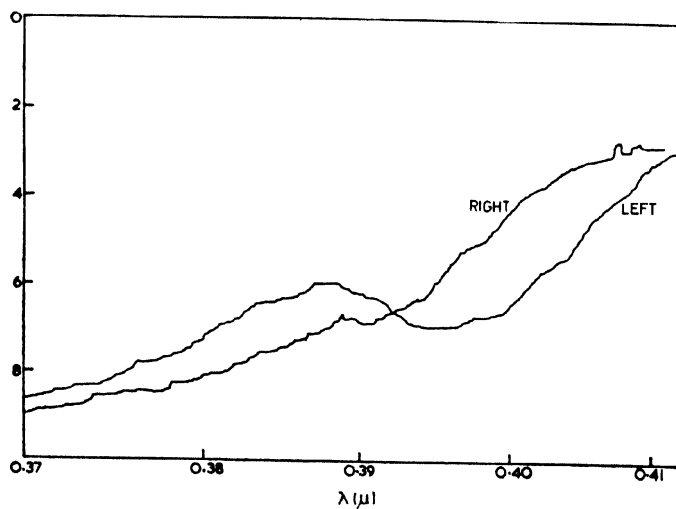
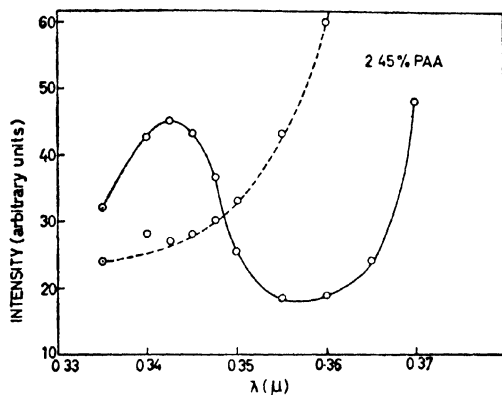


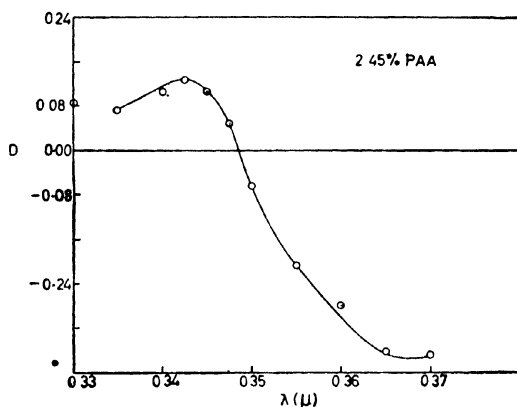
Figure 10 (a) Raw microdensitometer traces for a non-absorbing sample showing qualitatively the behaviour of the transmitted intensity as a function of wavelength for the two circular polarisations.



(b) Microdensitometer traces for the two circular polarisations.



(c) Transmitted intensity for the two circular polarisations (arbitrary units). The dashed line is for right circular polarisation and the solid line for left circular.



(d) Circular dichroism.
Sample : 2.45% PAA in
cholesteryl nonanoate
 $T = 6.35 \mu$.

In interpreting the experimental dichroism curves one must recall that the linear dichroism Δk is a function of wavelength¹¹ showing a maximum and falling off on either side. Since the experimental dichroism curves depend critically on the relative position of the reflexion band and the band of dichroism, we do not expect the resemblance to the theoretical curves of section 2, computed for constant Δk , to be very close. However, the curves do show the maximum at shorter wavelengths which falls off at longer wavelengths, characteristic of the Borrmann effect.

Conclusions

The cholesteric liquid crystal having a periodicity of the same order as the wavelength of light, shows optical effects analogous to those studied in x-ray diffraction. The Borrmann effect has been observed in such a system for the first time, and shows the features expected from theory.

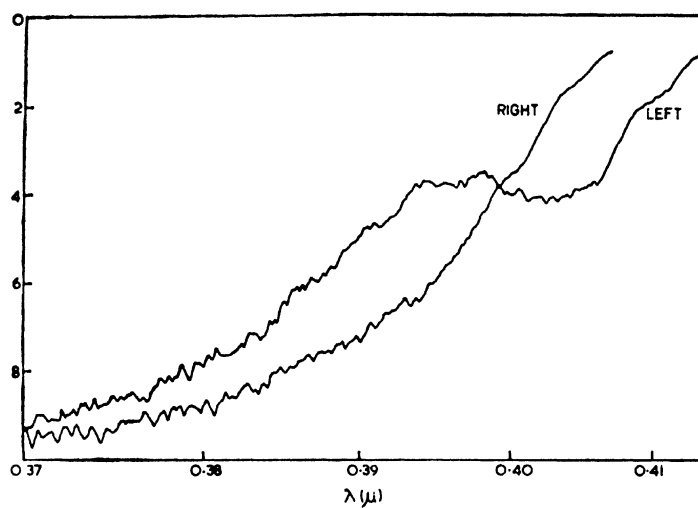
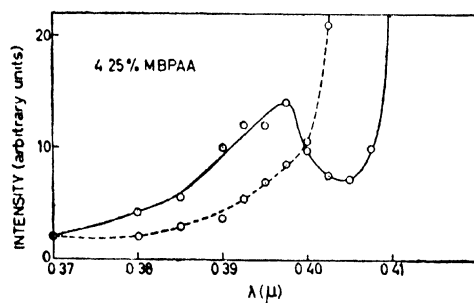
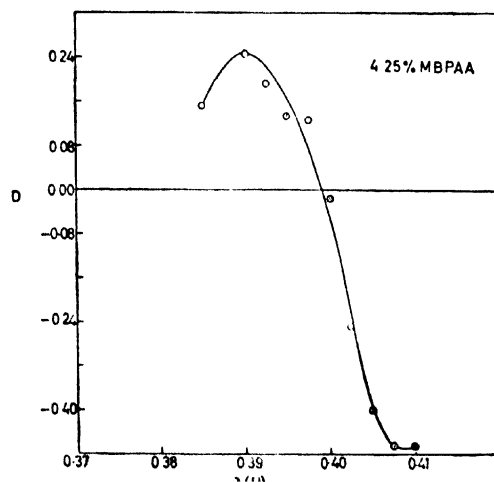


Figure 11 (a) Microdensitometer traces.



(b) Transmitted intensity in arbitrary units. The dashed line is for right circular polarisation and the solid line for left circular.



(c) Circular dichroism.
Sample : 4.25% MBPAA
in cholesteryl nonanoate
 $T = 6.35 \mu$.

Acknowledgements

We would like to thank Dr S. R. Rajagopalan and Dr K. R. Sivaraman for suggestions and help with regard to intensity measurements.

References

1. OSEEN C W *Trans. Faraday Soc.* **29** 833 (1933)
2. DE VRIES H *Acta Crystallogr.* **4** 219 (1951)
3. CHANDRASEKHAR S and SRINIVASA RAO K N *Acta Crystallogr. A* **24** 445 (1968).
4. BORRMANN G Z. *Phys.* **42** 157 (1941)
5. EWALD P P *Rev. Mod. Phys.* **37** 46 (1965)
6. RAJARAM NITYANANDA and KINI U D (this Conference)
7. KATS E I *Zh. Eksperim. Teor. Fiz.* **59** (1854) 1970, *Sov. Phys. - JETP* **32** 1004 (1971)
8. RAJARAM NITYANANDA *Mol. Cryst. Liquid Cryst.* **21** 315 (1973)
9. PRINS A . *Phys.* **63** 477 (1930)
10. MAUGUIN M C *Bull. Soc. Franc. Miner Crist.* **34** 71 (1971)
11. MAIER W and SAUPE A *Z. Phys. Chem. (NF)* **9** 327 (1956)

DISCUSSION

Darbari : How did you measure the thickness of the sample ?

Nityananda : The thicknesses quoted are the nominal thicknesses of the spacers which may be accurate to about 3 or 5%. In the present experiments it is assumed that the sample thickness is the same as that of the spacers.

Billard : In transparent materials if the refractive index is purely imaginary we do not have attenuated waves but only an evanescent oscillation. In a plate you have the optical tunnel effect.

Nityananda : I agree - the extinction of the normal wave in the Bragg reflection is analogous to the attenuation of the evanescent wave in the rarer medium.

Rustichelli : Do you think that, in analogy to x-ray or neutron anomalous transmission, the light anomalous transmission could be used to get information on defects in cholesteric liquid crystals ?

Nityananda : It is possible, however, in liquid crystals conventional optical observation also reveals the disclinations, etc.

Rustichelli : The dynamical theory of x-ray or neutron diffraction foresees an angular amplification of the order of $10^4 - 10^5$ for the diffracted beam

inside a perfect crystal in a plane geometry. Do you think that such an effect will exist also for light in cholesteric liquid crystals with possibilities of useful applications?

Nityananda : I am not familiar with angular amplification, but there is a full analogy with the x-ray dynamical theory, which Ranganath* will be talking about, and we should investigate this.

* Chandrasekhar S, Ranganath G. S. and Suresh K. A., this Conference.

Dynamical theory of reflexion from cholesteric liquid crystals

S CHANDRASEKHAR, G S RANGANATH and
K A SURESH

Raman Research Institute, Bangalore 560006, India

Abstract. The analogy between the optical phenomena exhibited by cholesterics and the diffraction of x rays from perfect crystals is emphasized and some of its consequences are discussed. Difference equations similar to those formulated by Darwin in his dynamical theory lead to simple analytical expressions for the reflexion coefficient, rotatory power and circular dichroism which are shown to be in good agreement with the results of the rigorous electromagnetic treatment. An extension of the theory to absorbing systems at once yields the relevant formulae for the Borrmann effect in cholesterics. It is pointed out that this simple approach should be sufficient for most practical calculations.

Introduction

The reflexion of light from cholesteric liquid crystals at normal incidence can be treated as analogous to the diffraction of x-rays from perfect crystals¹. As the dynamical theory of x-ray diffraction and its applications are now understood quite thoroughly this approach may prove to be useful in elucidating the optical behaviour of cholesterics and in looking for new optical analogues of certain well established x-ray effects. An example of a new phenomenon reported recently is the Borrmann effect in cholesterics².

The aim of this paper is to review the results of the dynamical theory of reflexion from cholesterics and to compare them with the predictions of the rigorous electromagnetic treatment³⁻⁵. It is shown that calculations based on the dynamical theory are sufficiently accurate for most practical purposes.

Kinematical theory of reflexion

We regard the cholesteric structure as a pile of very thin birefringent (quasi-nematic) layers with the principal axes of the successive layers turned through a small angle β . Such a system can, in general, be replaced by a rotator and a retardation plate for light propagating normal to the layers⁶. However, for wavelengths comparable to the pitch P of the helical structure and for sample thicknesses which are not too small (say $> 10 P$) the system can be treated to a very good approximation as a

pure rotator. Under such circumstances, the normal waves may be assumed to be circularly polarized, *i.e.*, right and left circular light travel without change of form, but at slightly different velocities. The refractive indices for the two components are respectively¹

$$\begin{aligned}\mu_R &= \mu - \frac{(\Delta\mu)^2 P}{8\lambda} \\ \mu_L &= \mu + \frac{(\Delta\mu)^2 P}{8\lambda}\end{aligned}$$

and the rotatory power in radians per unit thickness

$$\rho = - \frac{\pi (\Delta\mu)^2 P}{4\lambda^2} \quad (1)$$

where $\Delta\mu = (\mu_1 - \mu_2)$ is the layer birefringence, $\mu = \frac{1}{2}(\mu_1 + \mu_2)$.

When the wavelength of the light in the medium is equal to the pitch, reflexion of one of the circular components takes place and, contrary to usual experience, the reflected wave has the same sense of circular polarization as that of the incident wave. This will be clear from the following simple argument. We shall suppose that the principal axes of the first layer are along OX, OY of a cartesian coordinate system and that the structure is right-handed, *i.e.*, β is positive. Let right circular light given by $D_0 = \begin{bmatrix} 1 \\ i \end{bmatrix}$ referred to OX, OY be incident along OZ. To calculate the reflexion coefficient at the boundary between the $(v+1)$ th and $(v+2)$ th layers, we resolve the incident light vector along the principal axes of the $(v+1)$ th layer which are inclined at an angle $(v+1)\beta$ with respect to OX, OY. The resolved components are

$$\begin{bmatrix} \xi \\ \eta \end{bmatrix} = \begin{bmatrix} 1 \\ i \end{bmatrix} \exp[i\{(v+1)\beta - \varphi_{v+1}\}],$$

where $\varphi_{v+1} = 2\pi\mu_R(v+1)p/\lambda$, p being the thickness of each layer. At the boundary, the ξ vibration emerges from a medium of refractive index μ_1 and the η vibration from a medium of refractive index μ_2 . If ξ' and η' refer to the principal axes of the $(v+2)$ th layer, then the reflected components are⁷

$$\begin{aligned}\begin{bmatrix} \xi' \\ \eta' \end{bmatrix} &= - \frac{\beta \Delta\mu}{2\mu} \begin{bmatrix} i \\ 1 \end{bmatrix} \exp[i\{(v+1)\beta - \varphi_{v+1}\}] \\ &= - iq \begin{bmatrix} 1 \\ -i \end{bmatrix} \exp[i\{(v+1)\beta - \varphi_{v+1}\}],\end{aligned}$$

where $|q| = \beta \Delta\mu / 2\mu$. We make the approximation here that $\sin\beta \approx \beta$, since β is assumed to be very small ($\sim 10^{-2}$ radian). On reflexion a very slight ellipticity is introduced in the transmitted beam, but

we shall neglect this in the present discussion. Transforming back to OX, OY, the reflected wave on reaching the surface of the liquid crystal will be

$$\begin{bmatrix} X \\ Y \end{bmatrix} = -iq \begin{bmatrix} 1 \\ -j \end{bmatrix} \exp [i \{ (2v+3)\beta - 2\varphi_{v+1} \}],$$

which represents a *right circular* vibration travelling in the negative direction of OZ. Clearly the phase difference between this wave and that reflected at the boundary between the first and second layers is $[2(v\beta - \varphi_v)]$. When $\lambda = \mu_n P$, we have $2\pi\mu_n P/\lambda = \beta$ and $\varphi_v = v\beta$ (since $np = P$ and $n\beta = 2\pi$, where n is the number of layers per turn of the helix). Hence the phase factor $\exp [2i(v\beta - \varphi_v)]$ becomes unity irrespective of the value of v , and there results a strong interference maximum. On the other hand, for a left-handed structure, β is negative and $(v\beta - \varphi_v)$ does not vanish when $\lambda = \mu_n P$. Therefore the waves from the different layers will not be in phase and the vibration will be transmitted practically unchanged.

Using the kinematical approximation the reflexion coefficient per turn of the helix is then

$$-iQ = -inq = -i\pi \Delta \mu/\mu. \quad (2)$$

Dynamical theory of reflexion

The complete solution of the problem has to take into account the effect of multiple reflexions. This can be done by setting up different equations closely similar to those used by Darwin⁸ in his dynamical theory of x-ray diffraction. For the purposes of this theory, let us regard the liquid crystal as consisting of a set of parallel planes spaced P apart. Each plane therefore replaces the n birefringent layers per turn of the helix of pitch P . We ascribe a reflexion coefficient $-iQ$ per plane for right circular light at normal incidence. Assuming the kinematical approximation for the n layers, Q is given by (2).

Let T_r and S_r be the complex amplitudes of the primary and reflected waves at a point just above the r th plane, the topmost plane being designated by the serial number zero. Neglecting absorption, the difference equation may be written as

$$S_r = -iQT_r + \exp(-i\varphi) S_{r-1} \quad (3)$$

$$T_{r+1} = \exp(-i\varphi) T_r - iQ \exp(-2i\varphi) S_{r+1}, \quad (4)$$

where $\varphi = 2\pi\mu_n P/\lambda$. The reflexion coefficient is here taken to be the same, on both sides of the plane. Replacing r by $(r-1)$ in (3) and (4), substituting and simplifying, we obtain

$$T_{i+1} + T_{i-1} = yT_i \quad (5)$$

$$S_{i+1} + S_{i-1} = yS_i \quad (6)$$

where

$$y = \exp(i\varphi) + \exp(-i\varphi) + Q^2 \exp(-i\varphi). \quad (7)$$

Suppose that the film consists of m planes. Putting $S_m = 0$, we have from (6)

$$S_{m-2} = yS_{m-1},$$

$$S_{m-3} = yS_{m-2} - S_{m-1} = (y^2 - 1)S_{m-1},$$

$$S_{m-4} = (y^3 - 2y)S_{m-1}, \text{ etc.,}$$

and

$$\begin{aligned} S_0 &= [y^{m-1} - \frac{(m-2)}{1!} y^{m-3} + \frac{(m-4)(m-3)}{2!} y^{m-5} - \dots] S_{m-1} \\ &= f_m(y) S_{m-1} \text{ (say)} \end{aligned} \quad (8)$$

Similarly, from (4), (5) and (7)

$$T_{m-1} = \exp(i\varphi) T_m$$

$$T_{m-2} = [y \exp(i\varphi) - 1] T_m$$

$$T_{m-3} = [(y^2 - 1) \exp(i\varphi) - y] T_m, \text{ etc.,}$$

and

$$T_0 = [f_m(y) \exp(i\varphi) - f_{m-1}(y)] T_m \quad (9)$$

Since from (3),

$$S_{m-1} = -iQT_{m-1} = -iQ \exp(i\varphi) T_m,$$

the ratio of the reflected to the incident amplitude is

$$\frac{S_0}{T_0} = - \frac{iQ f_m(y) \exp(i\varphi)}{f_m(y) \exp(i\varphi) - f_{m-1}(y)} \quad (10)$$

Let us assume a relation in the form $T_{i+1} = xT_i$, so that x satisfies

$$x + \frac{1}{x} = y = \exp(i\varphi) + \exp(-i\varphi) + Q^2 \exp(-i\varphi).$$

We have seen that the reflexion condition is $\mu_R P = \lambda_0$ or $\varphi_0 = 2\pi$. Accordingly we may write

$$\varphi = 2\pi \lambda_0 / \lambda = \varphi_0 + \epsilon,$$

where $\epsilon = -2\pi(\lambda - \lambda_0) / \lambda,$

which is a small quantity in the neighbourhood of the reflexion. Therefore,

$$x + \frac{1}{x} = \exp(i\epsilon) + \exp(-i\epsilon) + Q^2 \exp(-i\epsilon) \quad (11)$$

This suggests that in the neighbourhood of the reflexion we may put

$$x = \exp(-\xi) \exp(-i\phi_0) = \exp(-\xi) \quad (12)$$

where ξ is small and may be complex. From (11) and (12),

$$\xi = \pm (Q^2 - \epsilon^2)^{1/2}.$$

When

$$y = \exp(\xi) + \exp(-\xi) = 2 \cosh \xi,$$

the series in (8) is given by

$$f_m(y) = \frac{\sinh m\xi}{\sinh \xi}. \quad (13)$$

substituting in (10) and simplifying

$$\frac{S_0}{T_0} \approx \frac{-iQ \exp(i\epsilon)}{i\epsilon + \xi \coth m\xi}, \quad (14)$$

or

$$R = \left| \frac{S_0}{T_0} \right|^2 = \frac{Q^2}{\epsilon^2 + \xi^2 \coth^2 m\xi}. \quad (15)$$

From (9) and (13)

$$\begin{aligned} \frac{T_m}{T_0} &= \left[\exp(i\epsilon) \frac{\sinh m\xi}{\sinh \xi} - \frac{\sinh(m-1)\xi}{\sinh \xi} \right]^{-1} \\ &\approx \frac{\xi \operatorname{cosech} m\xi}{i\epsilon + \xi \coth m\xi} \end{aligned} \quad (16)$$

Thus

$$\left| \frac{T_m}{T_0} \right|^2 + \left| \frac{S_0}{T_0} \right|^2 = 1.$$

For a thick specimen, $m = \infty$,

$$\frac{S_0}{T_0} = -\frac{Q}{\epsilon + i\xi} \quad (17)$$

when $-Q < \epsilon < Q$, ξ is real

$$R = \left| \frac{S_0}{T_0} \right|^2 = 1.$$

The reflexion is total within this range. The spectral width of total reflexion $\Delta\lambda = Q\lambda/\pi \approx Q\lambda_0/\pi$. Using (2) $\Delta\lambda = P\Delta\mu$, in agreement with the de Vries theory³.

Illustrative curves of R as a function of wavelength are shown in figure 1. The parameters chosen for the calculation are $\mu = 1.5$, $\Delta\mu = 0.07$, $P = 3330 \text{ \AA}$. The thick specimen gives the well-known flat topped curve of the dynamical theory, while the thin film gives a principal maximum accompanied by subsidiary fringes, which have been observed experimentally^{9,10}. The figure also shows the values computed from the exact theory of Nityananda^{5,11}. In the latter computations, the external isotropic medium (external to the cholesteric specimen) is assumed to have a refractive index of 1.5, so that the contribution of the ordinary Fresnel reflexion coefficient at the cholesteric/isotropic interface is eliminated.

Anomalous rotatory dispersion

If reflexions are neglected, the optical rotation per thickness P of the liquid crystal is $\frac{1}{2}(\varphi_R - \varphi_L)$ and the rotatory power is given by (1). Near the region of reflexion, the right circular component suffers anomalous phase retardation and, under certain circumstances, attenuation as it travels through the medium. Left circular light on the other hand exhibits normal behaviour throughout and as a consequence the rotatory dispersion is anomalous around the reflecting region.

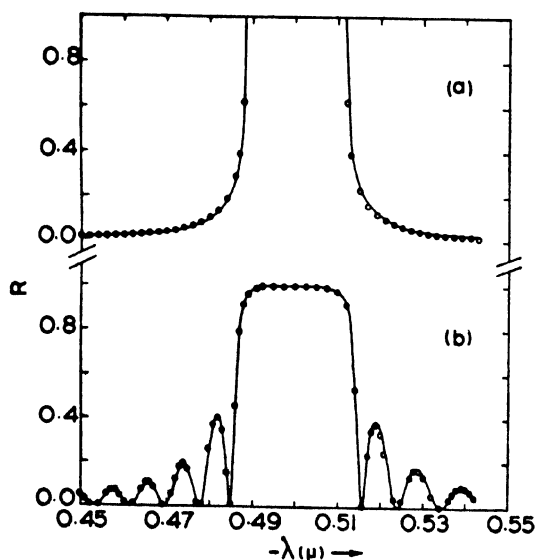


Figure 1 Reflexion coefficient R versus wavelength λ in the non-absorbing case: (a) semi-infinite medium, (b) film of thickness $25P$. Curves are derived from the dynamical theory; circles represent values computed from the exact theory^{5,11}.

Thick specimen

According (12),

$$T_{r+1} = x T_r,$$

where

$$x = \exp(-\xi) \exp(-i\varphi_0)$$

$$\xi = \pm (Q^2 - \epsilon^2)^{1/2}$$

$$\varphi_0 = \varphi_R - \epsilon = 2\pi.$$

Inside the totally reflecting range, ξ is real and therefore the medium becomes highly circularly dichroic. If very thin films are employed, the emergent light is elliptically polarized. It is readily seen that the ellipticity χ produced per thickness P is given by

$$\tan \chi = \frac{1 - \exp(-\xi)}{1 + \exp(-\xi)} = \tanh \xi/2,$$

or

$$\chi \approx \xi/2.$$

The azimuth of major axis of the ellipse after passing through a thickness P is

$$\alpha = \frac{1}{2} (\varphi_0 - \varphi_L) = \frac{\pi P}{\lambda} (\mu_R - \mu_L) + \frac{\pi (\lambda - \lambda_0)}{\lambda} = -\frac{n\gamma^2}{2\beta} + \frac{\pi (\lambda - \lambda_0)}{\lambda}.$$

Here $\gamma = \pi p (\Delta\mu)/\lambda$. Therefore the rotatory power

$$\rho = -\frac{\pi (\Delta\mu)^2 P}{4\lambda^2} + \frac{\pi (\lambda - \lambda_0)}{P\lambda}, \quad (18)$$

which is valid within the range $\lambda_0 - Q/2\pi < \lambda < \lambda_0 + Q/2\pi$.

Outside the totally reflecting range $\xi = i(\epsilon^2 - Q^2)^{1/2}$ and may be positive or negative depending on whether ϵ is positive or negative. Therefore,

$$\begin{aligned} \alpha &= \frac{1}{2} [(\epsilon^2 - Q^2)^{1/2} + \varphi_0 - \varphi_L] \\ &= -\frac{n\gamma^2}{2\beta} - \frac{\epsilon}{2} \left[1 - \left(1 - \frac{Q^2}{\epsilon^2} \right)^{1/2} \right] \end{aligned}$$

Hence the rotatory power

$$\rho = -\frac{\pi (\Delta\mu)^2 P}{4\lambda^2} + \frac{\pi (\lambda - \lambda_0)}{P\lambda} \left[1 - \left(1 - \frac{Q^2}{\epsilon^2} \right)^{1/2} \right] \quad (19)$$

Thin film

For a thin film the phase of the right circular wave can be evaluated from (16) :

$$\frac{T_m}{T_0} = A \exp [-im(\varphi_0 + \phi)]$$

$$\text{where } \tan m\phi = \frac{\epsilon}{\xi \coth m\xi}$$

The optical rotation for thickness P is

$$\frac{1}{2}(\varphi_0 + \phi - \varphi_L) = \frac{1}{2}[(\varphi_R - \varphi_L) + (\phi - \epsilon)]$$

and the rotatory power

$$\rho = -\frac{\pi(\Delta\mu)^2 P}{4\lambda^2} + \frac{(\phi - \epsilon)}{2P}$$

Figures 2 and 3 show some typical calculations based on the above equations. It will be seen that the reflexion, circular dichroism and rotatory power predicted by this theory agree very closely with those of the electromagnetic treatment⁵.

Absorbing systems : The Borrmann effect

Suppose now that the birefringent layers are also linearly dichroic. Let us assume that the principal axes of linear birefringence and linear

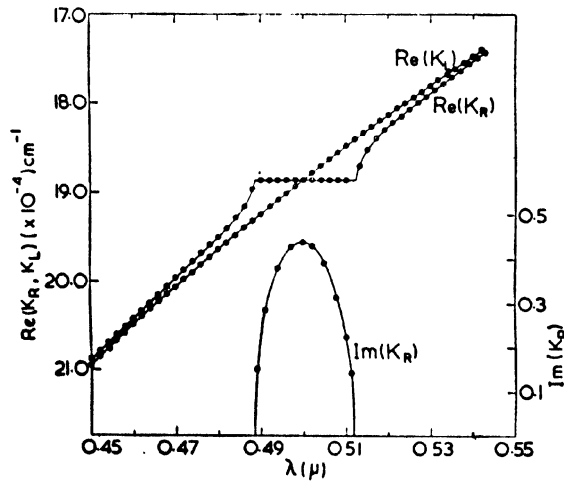


Figure 2 The wave vectors K_R and K_L of the normal waves as functions of λ in a semi-infinite non-absorbing medium. Curves are derived from the dynamical theory ; circles represent values computed from the exact theory⁵.

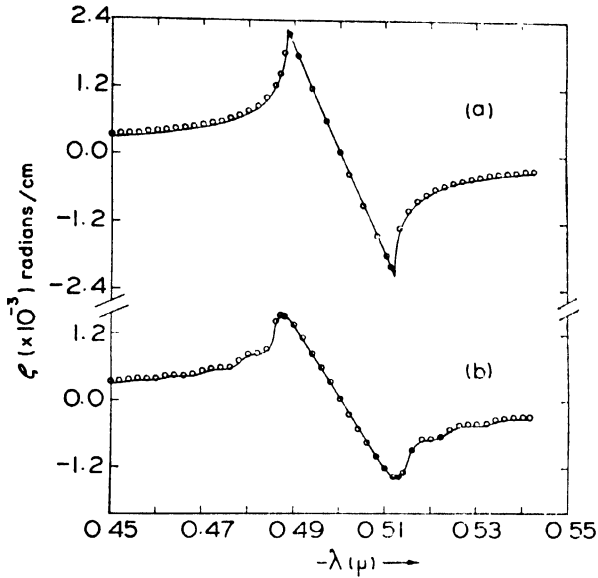


Figure 3 Rotatory power ρ versus λ in the non-absorbing case: (a) semi-infinite medium, (b) film of thickness $25P$. Curves are derived from the dynamical theory; circles represent values computed from the exact theory^{5,11}.

dichroism are the same. If $\hat{\mu}_1$ and $\hat{\mu}_2$ be the principal complex refractive indices of each layer, then the reflexion coefficient \hat{Q} and the phase retardation $\hat{\varphi}$ per pitch also become complex:

$$\begin{aligned}\hat{Q} &= \pi \frac{\Delta \hat{\mu}}{\hat{\mu}} \\ \hat{\varphi}_R &= \frac{2\pi}{\lambda} \hat{\mu}_R P = \frac{2\pi}{\lambda} \hat{\mu} P - \frac{\pi (\Delta \hat{\mu})^2 P^2}{4\lambda^2} \\ \hat{\varphi}_L &= \frac{2\pi}{\lambda} \hat{\mu}_L P = -\frac{2\pi}{\lambda} \hat{\mu} P + \frac{\pi (\Delta \hat{\mu})^2 P^2}{4\lambda^2}\end{aligned}$$

Here

$$\begin{aligned}\Delta \hat{\mu} &= \hat{\mu}_1 - \hat{\mu}_2 & \hat{\mu}_1 &= \mu_1 - ik_1 \\ \hat{\mu} &= \frac{1}{2} (\hat{\mu}_1 + \hat{\mu}_2) & \hat{\mu}_2 &= \mu_2 - ik_2\end{aligned}$$

k_1 and k_2 are the principal absorption coefficients.

All the equations obtained for non-absorbing media are still valid for absorbing systems except that \hat{Q} , $\hat{\varphi}_R$ and $\hat{\varphi}_L$ replace Q , φ_R and φ_L respectively. For example, for the thick specimen, the reflexion coefficient R for the right circular wave, the optical rotatory power $\hat{\rho}$ (which is now complex), the wave vectors \hat{K}_R and \hat{K}_L are given by

$$R = \left| \frac{\hat{Q}}{\hat{\epsilon} \pm (\hat{\epsilon}^2 - \hat{\xi})^{1/2}} \right|^2$$

$$\hat{\rho} = -\frac{\pi (\hat{\Delta}\mu)^2 P}{4\lambda^2} + \frac{\pi (\lambda - \hat{\mu}_R P)}{P\lambda} \left[1 - \left(1 - \frac{\hat{Q}^2}{\hat{\epsilon}^2} \right)^{1/2} \right]$$

$$\hat{K}_R = \frac{2\pi + \hat{\xi}}{P} \quad \hat{K}_L = \frac{(2\pi\mu_L)}{\lambda} \quad (21)$$

Here

$$\hat{\epsilon} = -\frac{2\pi}{\lambda} (\hat{\mu}_R P - \lambda)$$

$$\hat{\xi} = \pm (\hat{Q}^2 - \hat{\epsilon}^2)$$

Figure 4 shows the dependence R , ρ (the real part of $\hat{\rho}$), and the imaginary parts of \hat{K}_R and \hat{K}_L on wavelength. Here $k = \frac{1}{2} (k_1 + k_2) = 0.02$

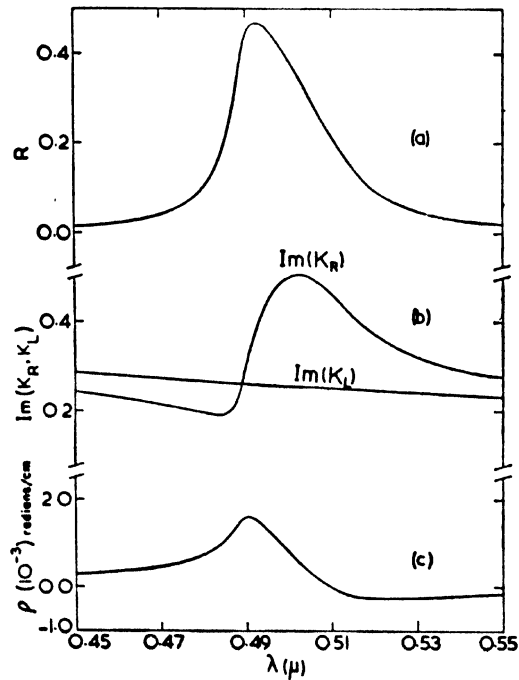


Figure 4 (a) Reflexion coefficient R , (b) imaginary parts of \hat{K}_R and \hat{K}_L , (c) rotary power ρ , plotted as functions of λ for an absorbing semi-infinite medium.

and $\Delta k = (k_1 - k_2) = 0.028$. The interesting result is obtained that on the shorter wavelength side $\text{Im}(K_R)$ is less than $\text{Im}(\hat{K}_L)$, i.e., the right circular wave is less attenuated than the left circular wave, whilst on the longer wavelength side the opposite is true. To observe this effect thin films have to be used.

The transmission coefficients T_R and T_L for the right and left circular waves through an absorbing cholesteric film of thickness mP are given by

$$T_R = \left| \frac{\hat{\xi} \operatorname{cosech} m \hat{\xi}}{\hat{1}\epsilon + \hat{\xi} \coth m \hat{\xi}} \right|^2$$

$$T_L = |\exp(-m\hat{\varphi}_L)|^2 \quad (22)$$

The theoretical dependence of T_R and T_L on wavelength are shown in figure 5, for both the non-absorbing and the absorbing cases for a film thickness of 25 P. The structure being right-handed the right circular component is reflected, and hence in the non-absorbing film ($k = \Delta k = 0$), T_R is always less than T_L . On the other hand, in the absorbing case, T_R shows an enhanced value on the short wavelength side of the reflexion band, which is the analogue of the Borrmann effect. It can be shown that T_L will exhibit an anomalous increase for a left-handed structure (i.e., negative β) and also that the peak transmission will occur on the long wavelength side of the reflexion if Δk is negative. These results are found to be in good quantitative agreement with the rigorous treatment of the phenomenon by Nityananda *et al*².

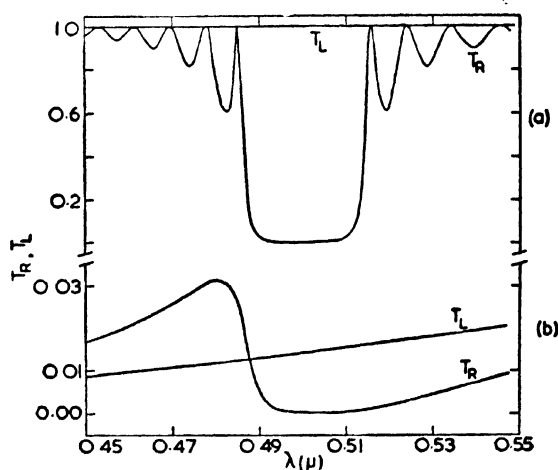


Figure 5 Transmission coefficients T_R and T_L for right and left circular waves for a film of thickness 25P (a) non-absorbing, (b) absorbing. The enhanced transmission for the right circular component in (b) is the analogue of the Borrmann effect.

Concluding remarks

We have shown that the dynamical model yields results in conformity with the more detailed electromagnetic theories. However, the simple treatment presented here has certain limitations. Firstly, it is developed for small ϵ and therefore does not hold good far away from the reflexion band. Secondly, it is strictly valid only for integral values of the pitch and thirdly, it fails when the film thickness is very small (or when the extinction length is of the order of a pitch) as the assumption that the normal waves are circularly polarized is then no longer justified. These limitations can be removed by including the effect of multiple reflexions within the n layers per turn of the helix, which has been neglected in this discussion. The simple difference equations then become matrix difference equations and the resulting solutions can be shown to be fully equivalent to those of the rigorous treatment⁵. However, the calculations presented in previous sections indicate that this more elaborate formulation of the theory is probably not necessary for most practical problems.

Acknowledgements

We are grateful to R Nityananda and U D Kini for providing the numerical results computed from the exact theory.

References

- 1 CHANDRASEKHAR S and SRINIVASA RAO K N *Acta. Crystallogr.* **A24** 445 (1968)
- 2 NITYANANDA R, KINI U D, CHANDRASEKHAR S and SURESH K A, this Conference
- 3 DE VRIES H *Acta Crystallogr.* **4** 219 (1951)
- 4 KATS E I *Sov. Phys.-JETP* **32** 1004 (1971)
- 5 NITYANANDA R *Mol. Cryst. Liquid Cryst.* **21** 315 (1973)
- 6 CHANDRASEKHAR S, RANGANATH G S, KINI U D and SURESH K A *Mol. Cryst. Liquid Cryst.* **24** 201 (1973)
- 7 CHANDRASEKHAR S and RANGANATH G S *Mol. Cryst. Liquid Cryst.* **25** 195 (1974)
- 8 DARWIN C G *Phil. Mag.* **27** 315, 675 (1914); **43** 800 (1922)
- 9 DREIER R, MEIER G and SAUPE A *Mol. Cryst. Liquid Cryst.* **13** 17 (1971)
- 10 CHANDRASEKHAR S and SHASHIDHARA PRASAD J *Mol. Cryst. Liquid Cryst.* **14** 115 (1971)
- 11 NITYANANDA R and KINI U D, this Conference

Circular dichroism in absorbing mixtures of right- and left-handed cholesterics

G S RANGANATH, K A SURESH,
S R RAJAGOPALAN* and U D KINI

Raman Research Institute, Bangalore 560006 India

*National Aeronautical Laboratory, Bangalore 560017, India

Abstract. A rigorous theory of the optical properties of absorbing mixtures of left and right handed cholesteric liquid crystals has been developed. Detailed expressions and illustrative calculations of the dependence of circular dichroism on pitch and sample thickness are presented. Experimental studies have been carried out on a 1.64:1 (by weight) mixture of cholesteryl myristate in which was dissolved 1.48% (by weight) of linearly dichroic β -carotene. The variation of circular dichroism with pitch exhibits anomalous behaviour, the sign of the dichroism being opposite below and above the nematic temperature. The peak value of the circular dichroism (per unit thickness) decreases as the sample thickness increases from 4 to 12.7 μ . These features are in qualitative agreement with the predictions of the theory.

Introduction

Mixtures of right-handed and left-handed cholesteric liquid crystals adopt the helical structure of a cholesteric whose pitch is sensitive to composition and temperature¹⁻³. At a particular composition the pitch approaches infinity and the mixture assumes a nematic structure. For any given composition the rotary power changes sign at a particular temperature – the temperature at which the structure changes handedness. A rigorous theory of the optical properties of such non-absorbing compensated cholesteric was developed recently by Chandrasekhar *et al*⁴. The theoretical dependence of rotatory power on pitch and on sample thickness are in agreement with the experimental variation of the rotatory power with temperature for different sample thicknesses^{3,4}.

Recently Sackmann and Voss⁵ demonstrated experimentally that when linearly dichroic molecules are dissolved in a cholesteric liquid crystal, the medium exhibits circular dichroism in the region of the absorption band of the dye molecule. A theory of the optical properties of such absorbing cholesterics⁶ lead to some interesting conclusions regarding absorbing compensated systems. In this paper we present the theory together with the experimental studies carried out on 1.64 : 1 (by weight) mixture of cholesteryl chloride and cholesteryl myristate (CM)

in which was dissolved 1.48% (by weight) of β -carotene. We find that the theory can account for the experimentally observed features.

Theory

We look upon the cholesteric structure as a helical stack of very thin birefringent layers. Each layer is supposed to have uniaxial symmetry with the principal axes of the successive layers turned through a small angle β . This angle β is taken to be positive for a right handed structure and negative for a left-handed one. We can use the Jones calculus to work out the optical properties of such a medium for light travelling along the helical axis⁷. We are throughout interested in the regime in which the pitch P of the helix is much greater than the wavelength λ of light.

Let 2γ be the phase retardation per layer, *i.e.*,

$$\gamma = \left(\frac{\pi}{\lambda} \right) (\Delta\mu) p$$

where p is the layer thickness and $\Delta\mu$ the layer birefringence. Let k_1 and k_2 be the principal absorption coefficients of the layer. Then the Jones matrix of any layer with reference to its principal axes is

$$G_{\bullet} = \begin{bmatrix} e^{-\gamma} & 0 \\ 0 & e^{i\gamma} \end{bmatrix} \times \begin{bmatrix} e^{-k_1 p} & 0 \\ 0 & e^{ik_2 p} \end{bmatrix} = e^{-\alpha} \begin{bmatrix} e^{-i\hat{\gamma}} & 0 \\ 0 & e^{i\hat{\gamma}} \end{bmatrix}$$

where $\alpha = \frac{k_1 + k_2}{2} p$ and $\hat{\gamma} = \gamma - i \left(\frac{k_1 - k_2}{2} \right) p = \gamma - i\delta$ (say).

(The convention here is that the phase factor at any point z is given by $\exp [-i (2\pi \mu z / \lambda)]$.)

Let the principal axes of the first layer be inclined at an angle β with respect to this OX and OY. Then the Jones matrix of the n^{th} layer with respect to this coordinate system is

$$G_n = S^n G_{\bullet} S^{-n}$$

where

$$S^n = \begin{bmatrix} \cos n\beta & -\sin n\beta \\ \sin n\beta & \cos n\beta \end{bmatrix}$$

and S^n is the inverse of S^{-n} (*i.e.*, $S^n S^{-n} = E$ the unit matrix). For n layers the net Jones matrix is given by

$$\begin{aligned} J_n &= G_n \cdot G_{n-1} \cdot G_{n-2} \dots G_2 \cdot G_1 \\ &= S^n G_{\bullet} S^{-n} S^{-(n-1)} G_{\bullet} S^{-(n-1)} \dots S G_{\bullet} S^{-1} \end{aligned}$$

But $S^m S^n = S^{m+n}$

Hence

$$J_n = S_n (G_o S^{-1})^n \quad (3)$$

If λ_1 and λ_2 are the eigenvalues of $(G_o S^{-1})$ then we can show that (Appendix A)

$$(G_o S^{-1})^n = \frac{\lambda_1^n - \lambda_2^n}{\lambda_1 - \lambda_2} (G_o S^{-1}) - \lambda_1 \lambda_2 \frac{\lambda_1^{n-1} - \lambda_2^{n-1}}{\lambda_1 - \lambda_2} E$$

where λ_1 and λ_2 are given by

$$\lambda_1 = e^{-\alpha} e^{i\hat{\theta}} \text{ and } \lambda_2 = e^{-\alpha} e^{-i\hat{\theta}}$$

with $\cos \hat{\theta} = \cos \hat{\gamma} \cos \beta$

Therefore

$$\begin{aligned} (G_o S^{-1})^n &= e^{-n\alpha} \frac{\sin n\hat{\theta}}{\sin \hat{\theta}} (G_o S^{-1}) - e^{-(n+1)\alpha} \frac{\sin (n-1)\hat{\theta}}{\sin \hat{\theta}} E \\ &\approx e^{-n\alpha} \left[\frac{\sin n\hat{\theta}}{\sin \hat{\theta}} (G_o S^{-1}) - \frac{\sin (n-1)\hat{\theta}}{\sin \hat{\theta}} E \right] \end{aligned} \quad (4)$$

as n is very large compared to unity.

Using (3) and (4) we can completely work out the net Jones matrix J_n in terms of β , γ , k_1 , k_2 and n .

The matrix J_n can be uniquely resolved into a rotator, a retarder, a circularly dichroic plate and a linearly dichroic plate. The unique matrix resolution is given by (Appendix B)

$$J_n = e^{-\chi} \Psi R \Sigma \Phi K \Sigma \Psi^{-1} \quad (5)$$

where

$$\Psi = \begin{bmatrix} \cos \psi & -\sin \psi \\ \sin \psi & \cos \psi \end{bmatrix}$$

$$R = \begin{bmatrix} \cos \rho & -\sin \rho \\ \sin \rho & \cos \rho \end{bmatrix}$$

$$\Sigma = \begin{bmatrix} \cosh \sigma/2 & -\sinh \sigma/2 \\ \sinh \sigma/2 & \cosh \sigma/2 \end{bmatrix}$$

$$\Phi = \begin{bmatrix} e^{-i\varphi} & 0 \\ 0 & e^{-i\varphi} \end{bmatrix} K = \begin{bmatrix} e^{-k} & 0 \\ 0 & e^k \end{bmatrix}$$

where ρ is the rotation, σ the circular dichroism, 2φ the linear phase retardation, $2k$ the linear dichroism and χ the attenuation coefficient. From (3), (4) and (5) we get

$$\begin{aligned}\rho - i\sigma &= n(\beta - \hat{\theta}') \\ \varphi - ik &= \cos^{-1} \left[\frac{\sec^2 n\hat{\theta}'}{\sec^2 n\hat{\theta}} \right]^{\frac{1}{2}} \\ \psi &= \frac{1}{2} [(n+1)\beta - \rho] \\ \chi &= n\alpha\end{aligned}\tag{6}$$

with

$$\hat{\theta}' = \frac{1}{n} \tan^{-1} \left[\frac{\tan \beta}{\tan \hat{\theta}} \tan n\hat{\theta} \right]$$

We shall consider two cases of special interest.

(a) β is very large :

In this case

$$\varphi = k = \psi = 0$$

$$\text{and } \hat{\rho} = \rho - i\sigma \approx -\frac{n\gamma^2}{2\beta}$$

Hence

$$\begin{aligned}\rho &= -\frac{n(\gamma^2 - \delta^2)}{2\beta} \\ \sigma &= -\frac{n\gamma\delta}{\beta}\end{aligned}$$

Therefore the linear dichroism of the layers not only results in circular dichroism but also makes a contribution to optical rotation which is opposite in sign to that due to linear birefringence. However this contribution is usually very small.

(b) β is very small :

In this case we find

$$J_n \approx e^{-\alpha n} \begin{bmatrix} \cos n\beta & -\sin n\beta \\ \sin n\beta & \cos n\beta \end{bmatrix} \begin{bmatrix} e^{-i\gamma n} & 0 \\ 0 & e^{i\gamma n} \end{bmatrix}$$

From this we conclude that at any point in the medium we have two linear vibrations polarized along the local principal axes of the layer.

As we move along the axis of the helix in the direction of light propagation we find that these two vibrations rotate with the principal axes. The phase retardations and amplitude reductions undergone by these two vibrations are the same as in an untwisted nematic. This is the property which is made use of in the so-called twisted nematic devices.

However at intermediate values of β we have to use the complete expressions (6). The parameter σ exhibits a marked dependence on pitch and on sample thickness⁶. Since in actual practice σ is not usually measured directly, we shall present the theoretical results in a manner that enables direct comparison with experiment. The procedure generally consists of measuring the transmitted intensities I_r and I_l for right and left circular light (of equal intensity) incident on the medium and then evaluating the parameter D_0 given by :

$$D_0 = \frac{I_r - I_l}{I_r + I_l + 2(I_r I_l)^{1/2}} \quad (8)$$

To calculate D_0 theoretically we use the following relations (which describe the nature of the emergent light when a right or a left circularly polarized beam is incident on the specimen) :

$$\begin{bmatrix} A_1 \\ A_2 \end{bmatrix} = \frac{1}{(2)^{1/2}} J_n \begin{bmatrix} 1 \\ +i \end{bmatrix} \text{ for right circular light}$$

$$\begin{bmatrix} B_1 \\ B_2 \end{bmatrix} = \frac{1}{(2)^{1/2}} J_n \begin{bmatrix} 1 \\ -i \end{bmatrix} \text{ for left circular light}$$

Then

$$I_r = |A_1|^2 + |A_2|^2$$

$$I_l = |B_1|^2 + |B_2|^2$$

In figure 1 we give the theoretical variation of the dichroic power D (*i.e.*, D_0/t , t being the sample thickness) with inverse pitch/temperature. The theoretical values are calculated for a 1.75:1 CM mixture of 6μ thickness containing dye molecules. The dependence of pitch on temperature was taken from Sackman *et al*². The layer birefringence $\Delta\mu$ at 20°C and 50°C were estimated by fitting the observed rotatory power³ with the de Vries equation⁷. $\Delta\mu$ at intermediate temperatures were obtained by linear interpolation. This is a valid procedure as at these temperatures the de Vries equation holds good. The linear dichroism was taken to be 0.10×10^{-3} at $\beta = 3 \times 10^{-3}$ on the lower temperature side of the nematic point. Further we assumed that the layer birefringence and the layer dichroism decrease at the same rate with increase of temperature. We find that D exhibits anomalous behaviour, the sign of the dichroism being opposite above and below the nematic point. The curve exhibits

some weak oscillations as the pitch/temperature is varied. The theory also leads to an interesting dependence of the dichroic power D on sample thickness. In table 1 we have given the negative peak value of D for various sample thicknesses.

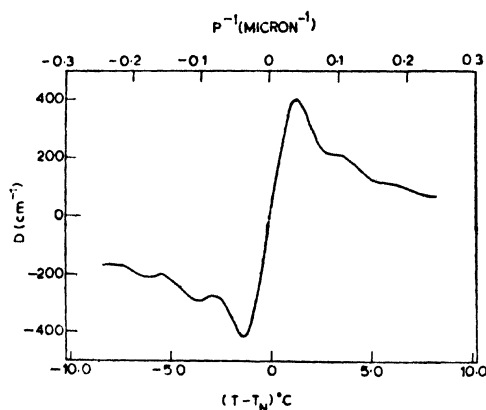


Figure 1 Theoretical dependence of dichroic power on temperature and inverse pitch

It will be seen that as the sample thickness is increased, D increases initially, reaches a maximum and decreases thereafter. In this respect the medium behaves quite differently from normal optically active substances in which the dichroic power is independent of thickness.

Measurements on cholesteryl chloride and cholesteryl myristate mixture

We have measured the dichroic power of a CM mixture (of composition 1.64:1 by weight) as a function of temperature for samples of various thicknesses. The CM mixture was mixed with 1.48% by weight of β -carotene and the combination was heated to 64°C at which temperature a homogeneous melt was formed. As the melt was cooled it adopted a cholesteric structure. The pitch of the cholesteric structure continuously increases with decrease of temperature reaching an infinite value around 51°C. When the system is cooled further it changes its handedness and the pitch gradually decreases. Above 51°C the specimen is right-handed and below this temperature it is left-handed. The dye β -carotene has an absorption band around 4800 Å with strong linear dichroism⁸ ($k_{\parallel} \approx 2.5 k_{\perp}$). Plane texture films of the mixture were prepared between two glass slides whose surfaces were optically flat. Samples of thickness 12.7 and 6.4 μ were obtained using Dupont mylar spacers of thickness 0.50 and 0.25 mils respectively. Mica spacers were used for samples of thickness 4, 8 and 9.5 μ (the uniformity in the thickness of the spacer was tested

Table 1

Sample thickness (in microns)	Negative peak value of D
2	299.8
3	382.5
4	430.2
5	441.3
7	366.5
9	348.6
11	341.0
13	305.9
15	298.5
17	272.8
19	253.6

with a dial gauge, model M1/100B Carl Zeiss Jena). The sample temperature was controlled by inserting the specimen in a suitably constructed heater. The temperature could be read upto $\pm 0.1^\circ \text{C}$ on a previously calibrated thermocouple.

A tungsten filament lamp run on a stabilized power supply was used as the source. The light beam was mechanically chopped at 321 c/s. Using the Meke Pederson reflection grating monochromator (model MP 108) experiments were carried out at 5000 Å. The intensity was sensed by a photomultiplier (model M10 FQS 29 Carl Zeiss Jena) and measured by means of a lock-in amplifier. The error in the intensity measurement was less than 2%.

In figure 2 is shown the experimental dependence of the dichroic power D on temperature for various sample thicknesses. We observe, firstly, that for any given thickness of the sample the temperature variation of power D follows the theoretically predicted behaviour (figure 1). The weak oscillations on the theoretical curve were not detected, presumably because of slight variations in the sample thickness. Secondly, we note that the peak dichroic power (per unit sample thickness) decreases as the sample thickness is increased from 4 to 12.7 μ , which again is in qualitative agreement with the theory.

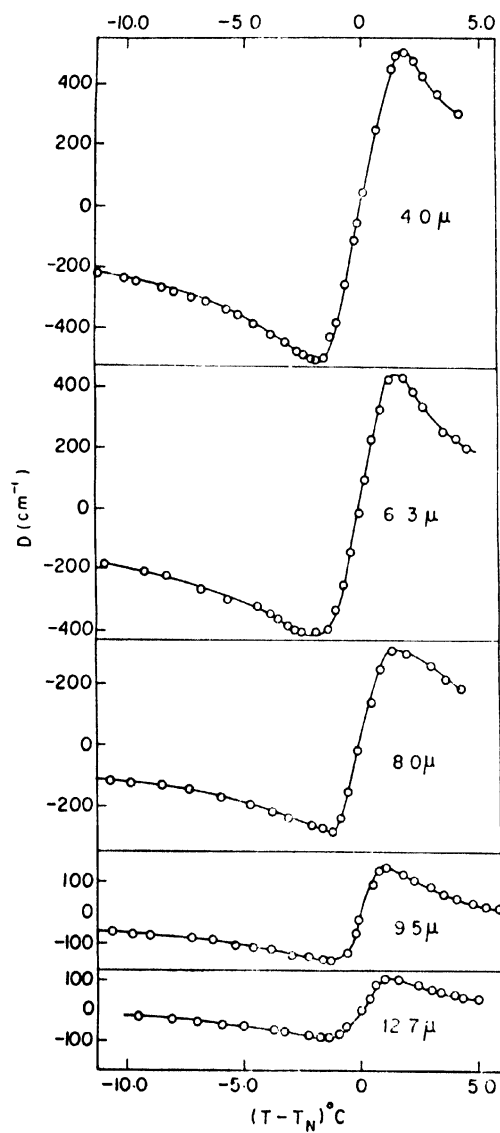


Figure 2 Experimental values of dichroic power versus temperature for different thicknesses of the sample in a 1.64:1 by weight mixture of cholesteryl chloride and cholesteryl myristate containing 1.48% by weight of β -carotene.

Acknowledgements

Our thanks are due to Professor S Chandrasekhar and Professor S Ramaseshan for their helpful suggestions and support throughout this work.

References

- 1 FRIEDEL G *Ann. Phys.* **18** 273 (1922)
- 2 SACKMANN E, MEIBOOM S, SNYDER L C, MEIXNER A E and DIETZ R E *J. Am. Chem. Soc.* **90** 3567 (1968)
- 3 BASSELER H, LARANGE T M and LABIS M M *J. Chem. Phys.* **51** 3213 (1969)
- 4 CHANDRASEKHAR S, RANGANATH G S, KINI U D and SURISH K A *Mol. Cryst. Liquid. Cryst.* **24** 201 (1973)
- 5 SACKMANN E and VOSS L *Chem. Phys. Lett.* **14** 528 (1972)
- 6 RANGANATH G S, CHANDRASEKHAR S, KINI U D, SURISH K A and RAMASLHAN S, *Chem. Phys. Lett.* **19** 556 (1973)
- 7 CHANDRASEKHAR S and SRINIVASA RAO K N *Acta Crystallogr.* **A24** 445 (1968)
- 8 SACKMANN E *J. Am. Chem. Soc.* **90** 3569 (1968)

Appendix A

Let

$$M = (G_0 S^{-1}) = e^{-\alpha} \begin{bmatrix} e^{-i\gamma} \cos \beta & e^{-i\gamma} \sin \beta \\ -e^{i\gamma} \sin \beta & e^{i\gamma} \cos \beta \end{bmatrix} = \begin{bmatrix} a_1 & a_2 \\ a_3 & a_4 \end{bmatrix} \text{ say}$$

Then the eigen values of M are given by

$$M - \lambda E = 0$$

Hence

$$\lambda_1, \lambda_2 = \frac{a_1 + a_4}{2} \pm \left[\left(\frac{a_1 - a_4}{2} \right)^2 - \Delta \right]^{\frac{1}{2}}$$

with $\Delta = a_1 a_4 - a_2 a_3$.

If we select a matrix T such that

$$T = \begin{bmatrix} -a_2 & -a_2 \\ a_1 - \lambda_1 & a_1 - \lambda_2 \end{bmatrix}$$

then

$$T^{-1} M T = \begin{bmatrix} \lambda_1 & 0 \\ 0 & \lambda_2 \end{bmatrix}$$

Hence

$$M = T \lambda T^{-1}$$

$$M^n = T \lambda^n T^{-1}$$

which can be simplified to give

$$M^n = \frac{\lambda_1^n - \lambda_2^n}{\lambda_1 - \lambda_2} M - \lambda_1 \lambda_2 \frac{\lambda_1^{n-1} - \lambda_2^{n-1}}{\lambda_1 - \lambda_2} E$$

Also $a_1 + a_4 = 2e^{-\alpha} \cos \beta \cos \hat{\gamma}$; $\Delta = e^{-2\alpha}$

Hence $\lambda_1 = e^{-\alpha} e^{i\hat{\theta}}$; $\lambda_2 = e^{-\alpha} e^{-i\hat{\theta}}$; $\hat{\theta} = \cos^{-1} (\cos \beta \cos \hat{\gamma})$

Appendix B

Equation (5) can be rewritten as

$$J_n = e^{-\chi} \begin{bmatrix} \cos \hat{\psi} & -\sin \hat{\psi} \\ \sin \hat{\psi} & \cos \hat{\psi} \end{bmatrix} \begin{bmatrix} \cos \hat{\rho} & -\sin \hat{\rho} \\ \sin \hat{\rho} & \cos \hat{\rho} \end{bmatrix} \begin{bmatrix} e^{-i\hat{\varphi}} & 0 \\ 0 & e^{i\hat{\varphi}} \end{bmatrix} \\ \times \begin{bmatrix} \cos \hat{\psi} & \sin \hat{\psi} \\ -\sin \hat{\psi} & \cos \hat{\psi} \end{bmatrix}$$

where $\hat{\psi} = \rho + i\sigma/2$

$$\hat{\rho} = \rho - i\sigma$$

$$\hat{\varphi} = \varphi - ik$$

Using (3), (4) and the above expression we get

$$\begin{aligned} & \left[\cos \varphi \cos \hat{\rho} \pm i \sin \varphi \cos (\hat{\psi} + \rho) \right] \\ &= \cos n\beta \cos \hat{n\theta} + \frac{\tan \beta}{\tan \hat{\theta}} \sin n\beta \sin \hat{n\theta} \pm i \frac{\sin n\hat{\theta}}{\sin \hat{\theta}} \sin \hat{\gamma} \cos (n+1)\beta \\ & \left[\pm \cos \varphi \sin \hat{\rho} + i \sin \varphi \sin (\hat{\psi} + \rho) \right] \\ &= \pm \frac{\tan \beta}{\tan \hat{\theta}} \cos n\beta \sin \hat{n\theta} \mp \sin n\beta \cos \hat{n\theta} + i \frac{\sin n\hat{\theta}}{\sin \hat{\theta}} \sin \hat{\gamma} \sin (n+1)\beta \end{aligned}$$

These equations can be solved to get

$$\tan \hat{\rho} = \frac{\tan n\beta - \frac{\tan \beta}{\tan \hat{\theta}} \tan n\hat{\theta}}{1 + \frac{\tan \beta}{\tan \hat{\theta}} \tan n\beta \tan n\hat{\theta}}$$

$$\cos^2 \hat{\varphi} = (1 + \frac{\tan^2 \beta}{\tan^2 \hat{\theta}} \tan^2 n\hat{\theta}) / (1 + \tan^2 n\hat{\theta})$$

$$2\hat{\psi} + \rho = (n+1)\beta$$

which can be simplified to yield equations (6).

Selective Reflection of light in cholesteryl esters

D DEMUS and G WARTENBERG

Sektion Chemie der Martin-Luther-Universität, 402 Halle,
German Democratic Republic

Abstract. We have measured the temperature dependence of the selective reflection of circularly polarized light in the two homologous series cholesteryl-*n*-alkanoates and cholesteryl-*n*-alkylcarbonates. From the refractive indices of these substances it was possible to calculate the pitch of the structural helix. Some connections with the molecular structure are derived. The results are compared with theoretical considerations found in the literature.

Introduction

The interest in the physical properties of cholesteric liquid crystals has been greatly stimulated by the possibilities which the cholesterics offer for their practical use in thermography and electro-optics. The most important property for these purposes is the selective reflection of circularly polarized light. Little is known about the connection between molecular structure and reflection properties. Therefore we have undertaken measurements on the temperature dependence of the selective reflection from various cholesteryl esters. The pitch of these structures has been calculated using the following equations.

The wavelength λ_{\max} of the selective reflection is connected with the pitch of the structure by

$$\lambda_{\max} = \bar{n} \cdot p \quad (1)$$

$$\bar{n} = \frac{n_x + n_y}{2} \quad (2)$$

n_x and n_y are the indices of one quasi nematic plane of the cholesteric structure. By experiment n_x and n_y are not directly accessible. But Dreher, Meier and Saupe¹ have suggested the possibility of calculating these values by measuring the ordinary and extraordinary indices n_o , n_e respectively of the cholesteric structure:

$$\sin^2 \gamma_1 = \frac{n_x^2}{N^2} \quad (3)$$

$$\sin^2 \gamma_2 = \frac{n_x^2 + n_y^2}{2 N^2} \quad (4)$$

N = index of the prism used for refraction measurement, γ_1, γ_2 = angles of total reflection of the ordinary and extraordinary beam respectively of the cholesteric liquid.

With good approximation we may write

$$\bar{n} = n_o \quad (5)$$

There are differences only in the fourth decimal place, as we have found using the refraction data of Pelzl and Sackmann^{2, 3}.

For the calculation of the pitch with eq. (1) we needed refraction data for different wavelengths, which were not available in the literature. Therefore we have used the simplified dispersion formula (6) of Bottcher and Graber⁴ for the calculation of the required values, on the basis of the dispersion measurements of Pelzl *et al.*^{2, 3}.

$$\bar{n}^2 = 1 + \frac{C \Lambda_o^2 \cdot \Lambda^2}{c^2 (\Lambda^2 - \Lambda_o^2)} \quad (6)$$

where C, Λ_o = constants, Λ = wavelength of light, c = velocity of light.

C is dependent on temperature and on the substance, and ranges from 925 to $970 \cdot 10^{28} \text{ sec}^{-1}$, while $\Lambda_o = 107 \text{ nm}$ is constant for all substances investigated and at all temperatures.

With the supposition of an anharmonic torsional oscillation between neighbouring planes of the cholesteric liquid, Keating⁵ has derived an equation for the temperature dependence of λ_{\max} :

$$\lambda_{\max} = \frac{4 \pi \bar{n} a J \alpha^2}{A' k T} \left(1 + \frac{\beta}{T - T_o} \right)^2 \quad (7)$$

a = thickness of a single layer in the cholesteric structure

J = moment of inertia of the molecules.

k = Boltzmann constant

T = temperature (K), T_o = temperature of the cholesteric/smectic transition

A', α, β = constants.

The term in parentheses in eq. (7) considers the pretransition effects near the cholesteric/smectic transition. Beyond this region this term rapidly vanishes. With good approximation we can use a simplified equation:

$$\lambda_{\max} = \frac{A}{T} \left(1 + \frac{B}{T - T_o} \right)^2 \quad (8)$$

For substances which have no smectic phase the constant B may be neglected and we get:

$$\lambda_{\max} = A/T \quad (9)$$

Here A and B are parameters which have to be adjusted to the experimental results of each substance.

Experimental

We have measured the regions of selective reflection with a Beckman DK - 2A spectrophotometer by drawing the transmission curves for each temperature. The substance was held as a thin film between two quartz plates. Standard spacer plates of 10 to 20 μm provided a constant thickness of the film. This combination of quartz plates was put in a small oven which allowed the temperature to be maintained to a constancy of $\pm 0.05^\circ$. We have measured the temperature by a thermocouple directly between the quartz plates.

For the purpose of obtaining good spectra it is necessary to use well oriented films in the cholesteric plane texture. This texture is produced with some certainty by cleaning the quartz plates with acetone, chromosulfuric acid, water and ethanol and rubbing the plates in one direction with a patch of wool. For some substances we obtained a spontaneous orientation, while for other preparations it was necessary to shift the plates relative to one another.

The substances were prepared by standard methods, described for instance in the cited literature^{2,3}. The transition temperatures of the substances studied are given in tables 1-3.

We use the following abbreviations:

crystalline solid	=	K
cholesteric	=	CH
smectics A, C	=	S _A , S _C
temperature	=	t ($^\circ\text{C}$)

Results and discussion

Cholesteryl Alkanoates

Figure 1 shows the results obtained for cholesteryl propionate. We have measured both with increasing and decreasing temperatures. To prove the reproducibility, each cycle was repeated several times. All measured points fit well into the curve. Cholesterylpropionate shows only a weak temperature dependence of λ_{max} . This temperature dependence is well described by equation (9) (see figure 1). Only in the region about 2°C below the clearing point do we find a deviation, presumably caused by pretransition effects. It should be remarked, that measurements in this region are very difficult. Most substances have a strong tendency to change the plane texture into a focal conic texture which does not reflect circularly polarized light.

Curves of the type of figure 1 have been obtained also for cholesteryl butyrate, valerate and capronate.

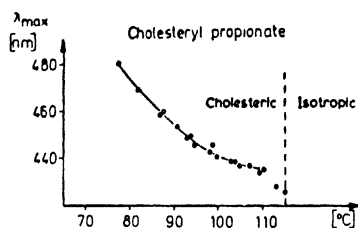
Figure 1 Cholesteryl propionate, λ_{\max} versus t

Table 1. Transition temperatures

Cholesteryl esters

	K	S _A	CH	I
propionate	. 100.6	—	—	. 115.2 .
butyrate	. 97.4	—	—	. 112.4 .
valerianate	. 91.0	—	—	. 97.3 .
capronate	. 98	—	—	. 99 .
heptanoate	. 106.8	—	—	. 93.8 .
octanoate	. 103.8	—	—	. 94.5 .
nonanoate	. 80.2	(. 74.1)	. 90.7 .	
decanoate	. 82.6	(. 75.5)	. 91.5 .	
undecanoate	. 85.0	(. 80.1)	. 90.4 .	
dodecanoate	. 92.4	(. 80.2	. 88.9)	. .
tetradecanoate	. 70.7	. 78.6	. 84.4 .	
hexadecanoate	. 76.6	(. 74.1)	. 82.5 .	
ethyl carbonate	. 83.0	—	—	. 103.5 .
propyl carbonate	. 96.9	—	—	. 99.0 .
butyl carbonate	. 78.0	—	—	. 92.1 .
amyl carbonate	. 106.2	—	—	. * — .
hexyl carbonate	. 108.0	—	—	. * — .
heptyl carbonate	. 79.2	—	—	(. 77.0) .
octyl carbonate	. 53.0	(. 44.5)	. 75.6 .	
nonyl carbonate	. 79.5	(. 45.0	. 77.9)	. .
decyl carbonate	. 76.5	(. 47.2	. 74.0)	. .
undecyl carbonate	. 61.6	(. 51.2)	. 73.0 .	

* Cholesteric phase visible only for a short time at decreasing temperature; measurement of transition temperature was not possible.

Table 2. Cholesteryl esters

	t (°C)	\bar{n}	λ_{\max} [nm]	p [nm]
propionate	78.0	1.507	476.5	316.2
	90.0	1.507	452.0	300.0
	100.0	1.504	443.0	294.5
	110.0	1.499	433.0	289.0
butyrate	90.0	1.507	430.0	285.0
	95.0	1.508	417.0	276.5
	100.0	1.506	405.0	269.0
	105.0	1.505	396.5	263.4
	109.0	1.504	391.0	260.0
valerate	90.0	1.508	406.0	269.0
	92.7	1.508	398.0	264.0
	95.0	1.510	392.0	259.6
	96.2	1.507	390.0	258.8
capronoate	80.0	1.514	400.0	264.0
	85.0	1.513	391.0	258.0
	95.0	1.513	375.0	248.0
	97.0	1.509	372.5	247.0
nonanoate	76.0	1.513	394.0	260.0
	78.2	1.514	383.0	253.0
	85.6	1.514	360.5	238.0
	90.0	1.513	349.0	231.0
decanoate	83.0	1.514	361.5	239.0
	85.0	1.516	354.0	233.5
	87.0	1.516	348.0	230.0
	90.0	1.516	340.5	225.0
undecanoate	80.7	1.519	352.5	232.0
	82.0	1.520	343.0	226.0
	86.5	1.522	324.5	213.0
	88.0	1.522	322.0	211.5
dodecanoate	82.0	1.515	322.0	212.5
	82.0	1.510	337.0	223.1
	85.0	1.516	314.0	207.0
	85.0	1.513	323.0	213.5
	89.0	1.517	308.5	203.4

	t (°C)	n	λ_{\max} [nm]	p [nm]
tetradecanoate	79.0	1.511	334.0	221.0
	79.0	1.508	349.0	231.4
	80.0	1.514	322.0	213.0
	80.0	1.510	337.0	223.0
	83.0	1.514	313.0	206.7
	83.0	1.517	302.5	199.4
hexadecanoate	77.0	1.512	335.0	221.5
	79.0	1.520	316.0	208.0
	81.0	1.522	302.0	198.4
	81.0	1.510	338.0	223.8
<i>Alkyl carbonate</i>				
ethyl carbonate	40.5	1.532	400.0	261.0
	50.0	1.531	390.0	255.0
	80.0	1.524	359.0	235.5
	90.0	1.528	355.0	232.3
propyl carbonate	63.0	1.521	405.0	266.3
	69.0	1.521	388.0	255.1
	80.0	1.518	379.0	249.7
	93.0	1.512	368.0	243.4
butyl carbonate	62.0	1.518	408.0	268.8
	66.0	1.518	404.0	266.0
	79.0	1.513	388.0	256.0
	91.0	1.509	375.0	248.5
heptyl carbonate	65.0	1.509	433.0	286.9
	71.0	1.508	418.5	277.0
	77.0	1.505	404.5	268.8
octyl carbonate	44.0	1.501	735.0	489.7
	46.0	1.501	520.0	344.6
	52.0	1.515	430.0	283.8
	63.0	1.512	416.0	275.0
	72.5	1.508	414.0	274.5
nonyl carbonate	56.0	1.520	380.0	250.0
	60.0	1.521	366.0	244.6
	65.0	1.519	363.5	239.3
	70.5	1.517	358.0	236.0
undecyl carbonate	50.2	1.498	657.0	438.6
	54.0	1.525	355.0	232.8
	61.0	1.527	336.0	220.0
	65.5	1.525	331.5	217.4
	71.3	1.521	329.5	216.6

Table 3

	A	B	λ_{red}	p_{red}
propionate	406 ²	—	430	288
butyrate	386 ²	—	394	259.5
valerianate	380 ²	—	388	257
capronate	373.8 ²	—	375	247.5
nonanoate	357.2 ²	0.072	354	235
decanoate	340.7 ²	0.433	343	223.5
undecanoate	338.2 ²	0.0477	323	212.5
dodecanoate	333.2 ²	0.0354	312, 318	207
tetradecanoate	327 ²	0.020	310	206
	324.1 ²	0.118		214
hexadecanoate	318.3 ²	0.205	309	205
	303.8 ²	0.949		

Cholesteryl alkyl carbonates

ethyl carbonate	360.3 ²	—	350	230
propyl carbonate	367.3 ²	—	364	241
butyl carbonate	370.5 ²	—	377.5	249
heptyl carbonate	378.5 ²	—	409	270
octyl carbonate	372.7 ²	0.108	414	274
nonyl carbonate	347.9 ²	0.049	360	234.5
undecyl carbonate	334.1 ²	0.127	330	216.5

A, B = constants of eq. (8)

λ_{red} , p_{red} = values of λ , p at 3° below the clearing point.

Because of the lack of sufficient supercooling, measurements were not possible for cholesteryl heptanoate and octanoate.

Figure 2 shows the results obtained for cholesteryl nonanoate. This substance has, besides the cholesteric phase, an additional smectic A-phase at lower temperatures. The points for increasing and decreasing temperature fit well into the same curve. The temperature dependence is more pronounced as in the case of cholesteryl propionate and increases with diminishing temperature. It is very strong in the region immediately above the transition S_A/CH . The curve in figure 2 has been calculated according to the theory of Keating and reproduces the experimental results, but not in all temperature regions.

Curves of the type of figure 2 have been obtained for cholesteryl nonanoate, decanoate and undecanoate. All these substances possess a smectic A-modification. In the pretransition regions of the S_A/CH -transitions we found the enhanced temperature dependency of λ_{max} .

Figure 3 gives the third type of experimental results found in the long chain cholesteryl alkanoates. The measurements for cholesteryl tetradecanoate fit into two curves, one for increasing, another for decreasing temperature. Both curves are reproducible, although the exact measurement in the narrow existence range of the cholesteric phase is somewhat difficult because of possible texture changes. These two curves are nearly parallel to each other. The curves correspond to calculations according to the theory of Keating. We have used two sets of constants for this calculation. The strong temperature dependence of this curve indicates clearly pretransitional effects near the S_A/CH transition.

The occurrence of the two nearly parallel curves is not very easy to explain. We have found this phenomenon also for cholesteryl dodecanoate and hexadecanoate. From the measurements of Gruler⁶ it is known that the elastic constants K_{11} and K_{33} increase with increasing alkyl chain in a homologous series. Assuming this is also the case for K_{22} , an enhanced value of K_{22} could explain the hysteresis in the λ_{max} -curves. The system at decreasing temperature may be assumed as a relaxed system and should yield higher values of λ_{max} . For increasing temperature lower values should be expected, as we have found indeed for the tetradecanoate. It is to be remarked that in the graphical plot of λ_{max} versus chain length of the homologous series (figure 13) the values measured for decreasing temperature fit better into the curve. We assume that these values are nearer to equilibrium values than those measured for rising temperature.

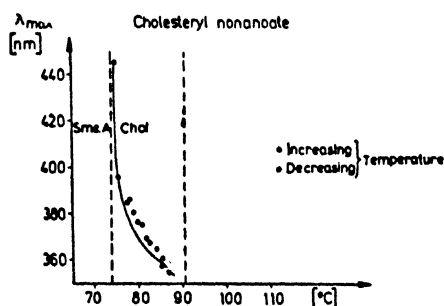


Figure 2 Cholesteryl nonanoate, λ_{max} versus t .

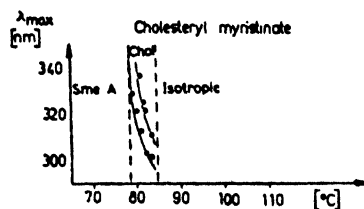


Figure 3 Cholesteryl myristinate, λ_{max} versus t .

Using eq. (1) we have calculated the pitch of the cholesteryl esters with the aid of the indices of refraction measured by Pelzl and Sackmann^{2,3}. Since the indices are not available for all desired wavelengths we have calculated with the simplified dispersion formula (6) of Böttcher⁴ the required indices using the results of Pelzl and Sackmann.

Figures 4-6 show for the already mentioned 3 cholesteryl alkanoates the graphic plot of the pitch *versus* temperatures. The curves show the same peculiarities as the λ_{\max} -plots, namely weak temperature dependence for the propionate, strong temperature dependence for the esters with additional smectic modifications and the double curve for tetradecanoate.

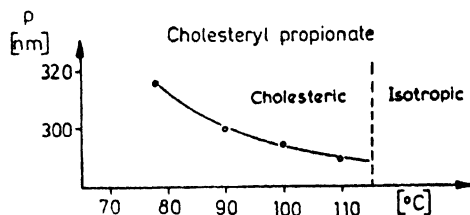


Figure 4 Cholesteryl propionate, p versus t .

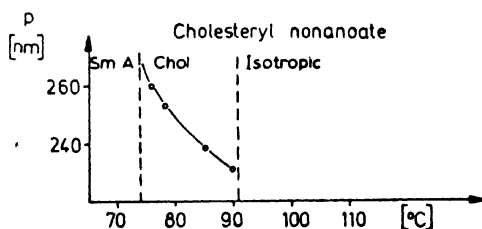


Figure 5 Cholesteryl nonanoate, p versus t .

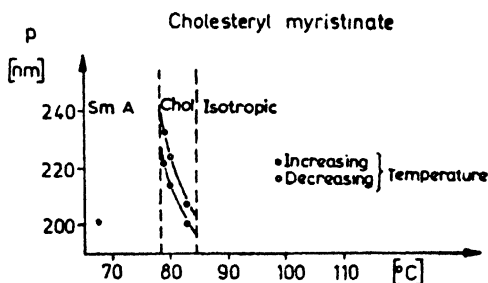


Figure 6 Cholesteryl myristinate, p versus t .

Cholesteryl alkyl carbonates

Figure 7 shows the temperature of λ_{\max} for cholesteryl ethylcarbonates. Since the substance supercools well, the measurements could be extended to temperatures far below the melting point. Measurements with the temperature increasing and decreasing yielded values which fit into a single curve. This curve has been calculated with eq. (9) (curve in figure 7). The agreement with the experiment is good. The temperature dependence is relatively weak.

Curves of this kind have been found also for cholesteryl propylcarbonate, butylcarbonate and heptylcarbonate. Cholesteryl pentylcarbonate and hexylcarbonate could not be supercooled sufficiently.

In analogy with the results for the cholesteryl alkanates with additional smectic phases, cholesteryl octylcarbonate also yielded a curve with a region of very strong temperature dependence of λ_{\max} (figure 8). The calculation (curve in figure 8) does not reproduce the experimental results in all parts. Dependent on the choice of the adjustable parameters for the Keating equation (8) certain parts of the experiments were well reproduced while other parts were not. But we were not able to find parameters which were valid for the whole region.

We have obtained curves of the type of figure 8 also for cholesteryl nonylcarbonate and undecylcarbonate, both substances having additional smectic A-phases.

It is to be remarked that the reflection spectra of the octyl, nonyl and undecylcarbonate stretch over a wide part of the visible spectrum. Therefore these substances are very suitable for the practical use in the thermography with cholesteric liquid crystals.

Cholesteryldecylcarbonate could not be supercooled enough as to allow measurements.

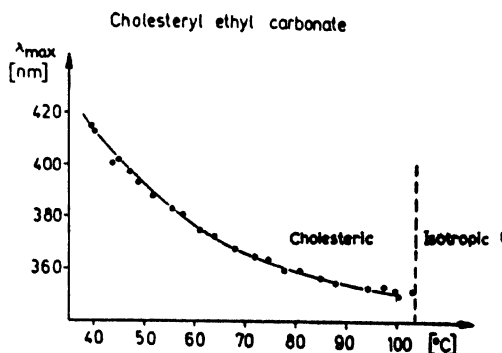


Figure 7 Cholesteryl ethyl carbonate, λ_{\max} versus t .

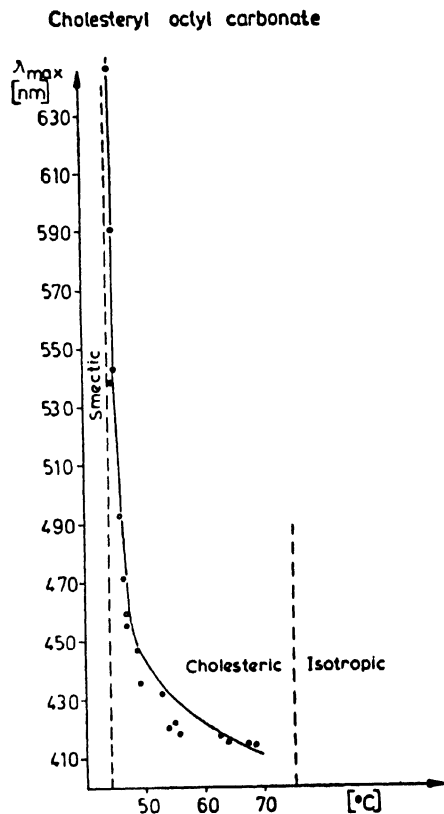


Figure 8 Cholesteryl octyl carbonate λ_{\max} versus t .

Figures 9 and 10 show the graphic plot of the pitch *versus* temperature for cholesteryl ethylcarbonate and octylcarbonate. These curves show the same principal peculiarities as the plots of λ_{\max} *versus* temperature.

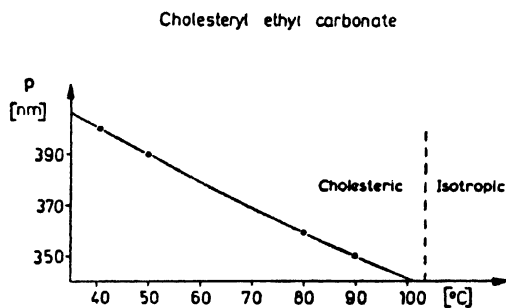


Figure 9 Cholesteryl ethyl carbonate, p versus t .

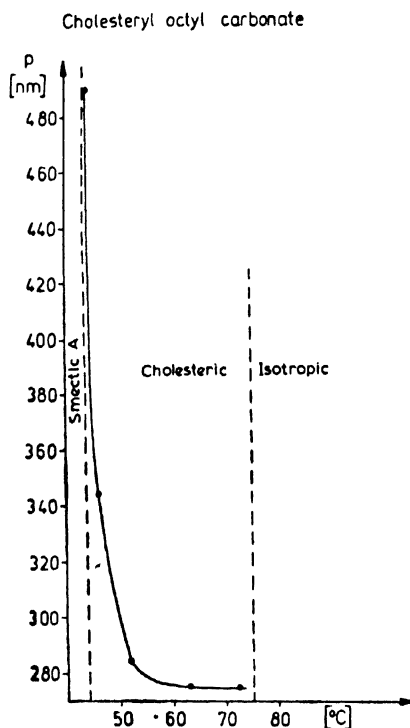
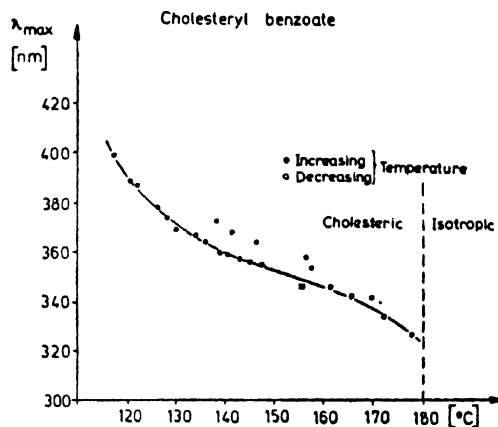


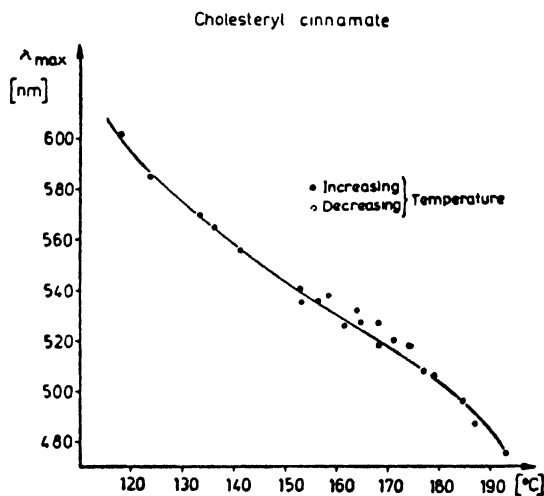
Figure 10 Cholesteryl octyl carbonate, p versus t .

Cholesteryl esters of aromatic acids

Figure 11 shows the results of the measurement of λ_{\max} for cholesteryl benzoate. The investigation was very difficult because of the fact that the substance does not maintain a well-oriented film for a long time and that it decomposes especially at higher temperatures. Therefore the deviations of the points from a smooth curve are greater than for the previously mentioned substances. The temperature dependence is high at lower temperatures, small in the middle regions and again begins to grow at 15° below the clearing point. This type of curve cannot be calculated with the Keating equation, because the unusual part in the region near the clearing point is not to be expected according to the Keating theory. Therefore we have given up the calculation.

Figure 11 Cholesteryl benzoate, λ_{\max} versus t .

Cholesteryl cinnamate yields a curve (figure 12) which is very similar to that of the benzoate. Also the cinnamate tends to decompose at elevated temperatures and the reproducibility of the experimental results is not very good. This compound gives a remarkably wide spectral range of the selective reflection at different temperatures. We have not calculated the curve with the Keating theory. Since there are no measurements of refractive indices for cholesteryl benzoate and cinnamate, the pitch could not be calculated.

Figure 12 Cholesteryl cinnamate, λ_{\max} versus t .

Discussion

Ferguson⁷ has measured λ_{\max} for cholesteryl nonanoate and decanoate. The temperature dependence is somewhat less than in our measurements, possibly indicating differences in the purity.

Kassubeck and Meier⁸ have calculated with eq. (1) the temperature dependence of the pitch for cholesteryl propionate, valerate and nonanoate, starting from λ_0 values and $\bar{n} = \frac{n_o + n_e}{2}$. There are systematic deviations from our values, but the agreement becomes good if for the calculation the right values of \bar{n} (see eqs. 2 and 5) are used.

For all cholesteryl alkanates and alkylcarbonates which possess only a cholesteric but not a smectic phase the Keating equation (9) is valid. All cholesteryl esters which have an additional smectic phase show remarkable pretransition effects in the cholesteric state. They give constants B from 0.02 to 0.9 (table 3).

The experimental λ_{\max} values for most of the esters can be reproduced by the Keating equation (8), but not in the whole temperature region. The pretransition effects are described rather well.

The rising values of p and λ_{\max} in the region near a CH/S_A transition may be regarded as a consequence of the increase in the elastic constant K_{22} .

Alben⁹ and de Gennes¹⁵ have concluded from theoretical considerations that the constant K_{22} should have such a pretransition effect. Till now measurements of K_{22} in a pretransition region are not known to us. But it is to be considered as a remarkable hint that Gruler⁶ and also Cheung and Meyer¹⁰ have found a considerable increase in the constants K_{11} and K_{33} near N/S transitions. Near the transition CH/S or N/S also anomalies in the heat capacity^{11,12} and electrical conductivity¹³ are known. All these effects may be considered as a consequence of the existence of a "smectic short range order" in the nematic liquid, as Arnold¹¹ has pointed out. De Vries¹⁴ later has referred to these as "cybotactic groups".

Figures 13 and 14 show λ_{\max} and p , reduced to a temperature 3° below the clearing points versus chain length of the homologous series cholesteryl alkanates and alkylcarbonates. In the former the values decrease with increasing chain length, possibly with a slight alternation. For the alkylcarbonates we found an increase till $n = 8$ and a decrease for $n = 9$ and 11. We have no explanation for this behaviour.

It should be mentioned that Baessler and Labes¹⁶, Adams, Haas and Wysocki¹⁷ and recently Ko, Tuecher and Labes¹⁸ reported

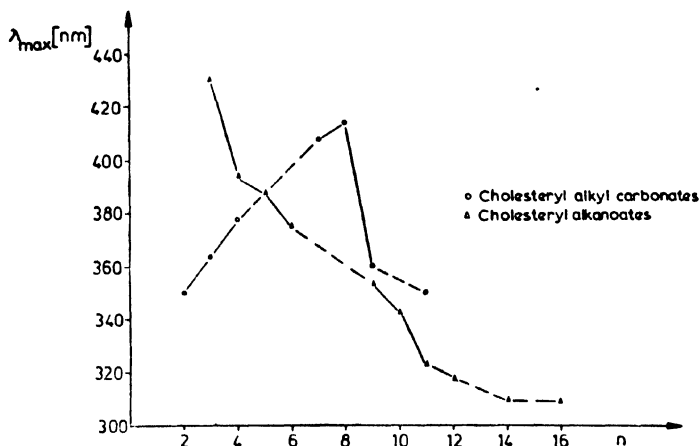


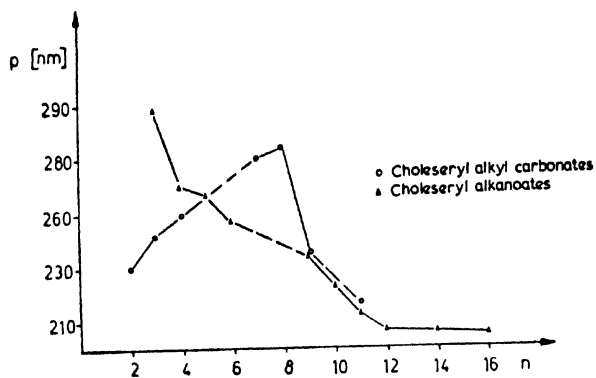
Figure 13 Cholesteryl esters, λ_{\max} versus n .

reciprocal λ_{\max} and p for cholesteryl alkanates. They obtained their values not from the pure substances, but by adding the cholesteryl esters to compensated cholesteric mixtures and measuring the optical properties. The slope of their curve $\frac{1}{\lambda_{\max}}$ versus chain length shows qualitative agreement with our corresponding plot. Because of the very different methods in determining the values quantitative agreement is not to be expected. Ko, Teucher and Labes¹⁸ extended the investigations also to cholesteryl alkylcarbonates. While the curve of the alkanates has an increasing trend, the curve of the alkylcarbonates approaches saturation even for low n . A comparison with our results offers no possibility for discussing the reason of the differences.

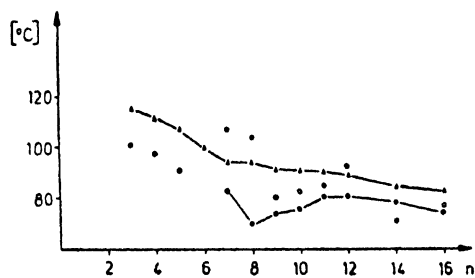
According to theoretical considerations of Goossens¹⁹ the twisted structure of the cholesteric liquids is a consequence of the quadrupole-quadrupole part of the dispersion interaction energy between asymmetric molecules. Because of the complicated structure of the molecules of the cholesteryl esters the influence of increasing alkyl chain on these special intermolecular forces is hardly to be predicted.

Our experimental results indicate a strong temperature dependence of the spectral region of selective reflection of circular polarised light at the cholesteryl esters near the transition CH/S. For the practical use of cholesteric liquids in thermography often a high temperature sensitivity is needed. Our results offer the possibility to obtain by systematic experiments with selected substances, mixtures with the necessary properties. We have developed a number of thermographic mixtures suitable for small

temperature intervals between 15 and 40°C. All these mixtures have an additional smectic phase at temperatures just below the practical useful region.



Cholesteryl alkanates



Cholesteryl alkyl carbonates

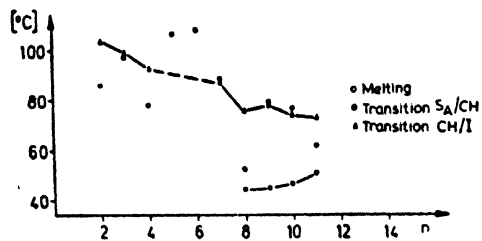


Figure 14 Cholesteryl esters, p versus n .

Acknowledgement

We are indebted to Doz. Dr habil. R Rautschke who kindly supported us in the measurements.

References

- 1 DREHER R, MEIER G and SAUPE A *Mol. Cryst. Liquid Cryst.* **13** 17 (1971)
- 2 PELZL G and SACKMANN H *Z. Phys. Chem.* **254** 354 (1974) see also PELZL G *Dissertation Halle* (1968)
- 3 PELZL G and RETTIG R to be published; see also RETTIG R *Diplomarbeit Halle* (1972)
- 4 BÖTTCHER B and GARBER G *Mol. Cryst. Liquid Cryst.* **14** 1 (1971)
- 5 KEATING P N *Mol. Cryst. Liquid Cryst.* **8** 315 (1969)
- 6 GRÜLER H Z. *Naturforsch.* **28a** 474 (1973)
- 7 FERGASON J L, GOLDBERG N N and NADALIN R J *Mol. Cryst.* **1** 309 (1966)
- 8 KASSUBEK P and MEIER G *Mol. Cryst. Liquid Cryst.* **8** 305 (1969)
- 9 ALBEN R *Mol. Cryst. Liquid Cryst.* **20** 231 (1973)
- 10 CHEUNG L and MEYER R B *Phys. Lett.* **A43** 261 (1973)
- 11 ARNOLD H Z. *Phys. Chem.* **226** 146 (1964); *Z. Chem.* **4** 211 (1964)
- 12 ARNOLD H and ROEDIGER P *Z. Phys. Chem.* **231** 407 (1966); **239** 283 (1968)
- 13 RONDELEZ F *Solid State Commun.* **11** 1675 (1972)
- 14 DE VRIES A *Mol. Cryst. Liquid Cryst.* **10** 31 (1970); **10** 219 (1970)
- 15 DE GENNES P G *Mol. Cryst. Liquid Cryst.* **21** 49 (1973)
- 16 BAESSLER H and LABES M M *J. Chem. Phys.* **52** 631 (1970)
- 17 ADAMS J E, HAAS W and WYSOCKI J J in *Liquid Crystals and Ordered Fluids*, edited by J F JOHNSON and R S PORTER, Plenum Press, New York - London 463 (1970)
- 18 KO K, TEUCHER I and LABES M M *Mol. Cryst. Liquid Cryst.* **22** 203 (1973)
- 19 GOOSSENS W J A *Phys. Lett.* **A31** 413 (1970)

DISCUSSION

de Gennes : There are now measurements of K_{22} , some of them reported here*, which are convenient for this type of calculations wherein the critical behaviour of the 2 phases is shown. Also, there are measurements on similar cholesteryl derivatives. They have seen pre-critical anomalies very similar to what you have described and they have attempted to analyze this in terms of a critical exponent. They find a critical exponent of about 0.6 or so. What is not completely clear to me from what you said is whether you can also describe them in terms of a power law, *i.e.*, in powers of $T - T_c$.

Demus : We have used the Keating equation in a simplified form, where the A and B are adjustable parameters. We have not tried to evaluate the exponent. May be this is also useful.

Brown : In what kind of atmosphere was the experiment carried out? There could be a difference between air and vacuum.

Demus : We did it in normal atmosphere.

* N. V. Madhusudana, P. P. Karat and S. Chandrasekhar - This Conference; G. Durand - This Conference.

Recent developments concerning biphenyl mesogens and structurally related compounds

G W GRAY, K J HARRISON and J A NASH

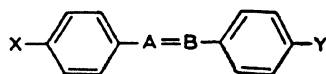
Abstract. The 4'-*n*-alkyl-4-cyanobiphenyls are low melting compounds which are colourless, chemically stable and photochemically stable; some are nematic at room temperature. Suitable mixtures of these materials with 4'-*n*-alkoxy-4-cyanobiphenyls give nematogenic materials melting at 0° C or below and forming stable nematic mesophases of positive dielectric anisotropy which persist until over 60° C. Agreement between observed and predicted transition temperatures for calculated eutectic compositions is good. Methods for further widening the nematic ranges are discussed.

An optically active biphenyl compound of positive dielectric anisotropy has been prepared and incorporated in such mixtures to obtain stable, room temperature cholesterics. These may be used for cholesteric-nematic phase change displays or to obtain twisted nematic displays free from areas of reversed twist.

Higher homologues of the 4'-*n*-alkyl- and 4'-*n*-alkoxy-4-cyanobiphenyls are smectic in some cases at room temperature. Such biphenyl mesogens therefore provide room temperature mesophases of the smectic, nematic and cholesteric types and are valuable for a variety of experimental and technological purposes. Preliminary studies of the smectic mesophases exhibited by these compounds are described.

1. Introduction

Considerable interest has been aroused by our recent reports^{1,2} of a new family of low melting, stable, colourless mesogens derived from biphenyl. These compounds were developed as a result of considering the reasons for the colour and/or chemical/photochemical instability associated with most existing mesogens, with the general structure below, that are used to produce room temperature liquid crystals. These problems are to a large



extent connected with the central A-B linkage [-N-N-; -N=N(O)-; -CH=N-; -CH=C(Cl)-], between the *p*-phenylene rings, which

extends conjugation in the molecules and provides a site for chemical/photochemical attack. We eliminated the problems associated with the A-B linkage by studying 4,4'-disubstituted biphenyls. To counteract the decrease in mesophase-isotropic liquid transition temperature associated with simplifying the structure in this way, the cyano-group was selected as one of the terminal substituents. This also ensured that the materials had a high positive dielectric anisotropy making them suitable for display devices of the type (twisted nematic and phase change) in which we were chiefly interested. To obtain reasonably low melting points, the other terminal substituent was chosen as alkyl or alkoxy.

2. Results and discussion

Table 1 summarises results for the various transition temperatures and the enthalpies of fusion of the most stable crystal forms of some 4'-*n*-alkyl- and 4'-*n*-alkoxy-4-cyanobiphenyls.

Several points of importance may be noted about these results.

(1) Five of the compounds exhibit dimorphism of the solid state. In all cases except that for $X = n\text{-C}_5\text{H}_{11}\text{O}$, the lower melting solid slowly reverts to the higher melting solid on standing. For the *n*-pentyloxy compound, the two solids are apparently unconnected in this way and the situation is summarised as shown in figure 1.

C_3 appears to form C_2 on cooling, quite slowly. On rapid cooling to less than 10°C , C_3 persists for long periods and only if heated does it revert to C_2 by an exothermic transition. C_3 is therefore a monotropic solid, and C_2 and C_1 do not interconvert directly.

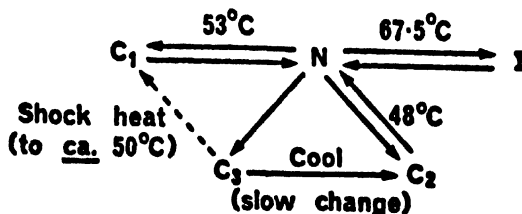
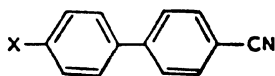


Figure 1 Transitions observed for 4-cyano-4'-*n*-pentyloxybiphenyl. On cooling, the nematic melt may form one, two or all of the solids, C_1 , C_2 and C_3 . If C_2 and C_3 form separately in the preparation and give a junction, C_2 rapidly changes to C_3 . If only C_3 forms, it slowly gives C_2 on standing, unless the temperature is below ca. 10°C when C_3 persists for long periods. If C_3 is then heated to ca. 17°C it changes to C_2 (an exotherm on D.T.A.). However, shock heating of C_3 to temperatures of ca. 50°C apparently gives C_1 which then melts at 53°C .

Table 1. Transition temperatures and enthalpies of melting for the compounds

X	C-S, N or I		S-N	N-I*
	Temp. (°C) §	ΔH (kcal. mol. ⁻¹)†	Temp. (C°)	Temp. (°C)
<i>n</i> -C ₄ H ₉	46.5	5.5	—	(16.5)‡
<i>n</i> -C ₅ H ₁₁	22.5	4.1	—	35
<i>n</i> -C ₆ H ₁₃	13.5	5.8	—	27
<i>n</i> -C ₇ H ₁₅	[15] 28.5	6.2	—	42
<i>n</i> -C ₈ H ₁₇	21	5.3	32.5	40
<i>n</i> -C ₉ H ₁₉	[29.5] 40.5	8.0	44.5	47.5
<i>n</i> -C ₃ H ₇ O	71.5	4.6	—	(64)
<i>n</i> -C ₄ H ₉ O	78	5.6	—	(75.5)
<i>n</i> -C ₅ H ₁₁ O	[48] 53	6.9	—	67.5
<i>n</i> -C ₆ H ₁₃ O	[44] 58	7.1	—	76.5
<i>n</i> -C ₇ H ₁₅ O	[47.5] 53.5	6.9	—	75
<i>n</i> -C ₈ H ₁₇ O	54.5	5.9	67	80

• C = crystal; N = nematic; S = smectic; I = amorphous liquid

* Enthalpies for the N-I transitions were typically in the range 0.1–0.3 kcal. mol⁻¹.

§ Temperatures in square brackets relate to the m.p.s. (C–S or N) for metastable solids so far identified. For the compound with X = C₄H₉O, the metastable solid apparently exists independently and does not revert even on long standing to the higher melting form.

† Enthalpy values relate to the higher melting stable solids where dimorphism occurs.

‡ Temperatures in round brackets are for monotropic N-I transitions.

(2) Of the two types of compound, the *n*-alkyl compounds have the lower N-I temperatures and the lower melting points. Two of these compounds (X = *n*-C₅H₁₁ and *n*-C₆H₁₃) are stable nematic liquids under normal room temperature conditions. The nematic liquids, like that formed by the *n*-heptyl compound, also exist for very long periods in the 'supercooled state at temperatures well below the melting points of the crystals.

(3) The *n*-octyl compound exists as a stable smectic liquid under normal room temperature conditions, and also supercools for long periods well below 21° C.

(4) All the compounds and their mesophases are colourless.

The following observations were first made for 4-cyano-4'-*n*-pentylbiphenyl, but were found to be typical for the compounds in table 1.

(a) Thin films of the nematic liquid, with the upper surface completely exposed to the laboratory atmosphere showed a decrease in the N-I temperature of less than 1° C after 1 week.

(b) Display cells were made from glass with a conductive coating and filled with the nematic liquid. The filling holes were sealed *crudely* with "araldite" or "Torr-seal" (epoxy resins). The cells were heated at 40° C for 1 week in an autoclave in an atmosphere saturated with water vapour. The N-I temperatures fell by less than 1° C. Similar treatment of cells filled with MBBA or cyano-substituted Schiff's bases gave liquids which were *isotropic* at room temperature.

(c) Exposure of the nematic liquid to UV radiation from a mercury vapour lamp for 4 hours caused no change in appearance of the film or any decrease in the N-I temperature.

(d) The low frequency dielectric constants for the nematic liquid at 25° C were $\epsilon_{\parallel} = 17$ and $\epsilon_{\perp} = 6$, a positive dielectric anisotropy, $\epsilon_a = +11$.

(e) The resistivity of the nematic liquid was typically $10^{10} - 10^{11} \Omega \text{ cm}$. at 100 Hz and for oriented samples $\rho_{\perp}/\rho_{\parallel}$ was 1.42.

(f) Controlled alignments of the nematic liquid with the director parallel to the glass or other surface were readily obtained.

In these materials we therefore have nematogens which are free from colour and from the chemical/photochemical instabilities which so adversely affect Schiff's bases, α -chlorostilbenes, etc., and have the necessary physical and electrical properties for use in twisted nematic display cells.

Thus, a 12 μm thick layer of the nematic phase of 4-cyano-4'-*n*-pentylbiphenyl has a low threshold of 1.1 V_{rms} (50 Hz). On AC application, using a 10 kHz signal, a 12 μm thick layer has a delay of 20 msec. and a rise time of 10 msec. at 10 V_{rms} . The decay is of the order 250 msec. although on visual assessment this is about 100 msec. Twisted nematic cells have so far survived continuing life tests of over 2,000 hr while being switched at 1 second intervals with bursts of sine wave AC.

Mixtures of 4'-n-alkyl- and 4'-n-alkoxy-4-cyanobiphenyls

The only adverse features of the pure mesogens listed in table 1 are the short nematic ranges of the low melting 4'-n-alkyl compounds and the comparatively high melting points of the 4'-n-alkoxy compounds.

These problems were overcome by using binary, ternary etc. mixtures of the compounds in table 1. Microscopic observations of the interface edges of thin films of various pairs of compounds from table 1 established that eutectics of lower melting points than the pure compounds were formed. Some trial compositions were prepared to test this conclusion. For example, a binary mixture of the compounds with $X=n-C_5H_{11}O$ (55 mol. %) and $X=n-C_7H_{15}O$ (45 mol. %) gave C-N, 21° C and N-I, 70.5° C. The nematic melt crystallised only slowly at 4° C.

To maximise on the melting point depression obtained for any given mixture, eutectic compositions had to be established. To avoid the lengthy procedure of preparing a large number of mixtures, ideal behaviour of such mixtures was assumed and the Schroder-van Laar equation used³. The equation is

$$\log_e X_A = \frac{\Delta H_A}{R} \left(\frac{1}{T_A} - \frac{1}{T} \right)$$

where X_A is the mol. fraction of component A for which the enthalpy of fusion is ΔH_A . T_A is the melting point of the stable crystal form of component A and T is the melting point of the mixture. For an N component mixture, N such equations exist. These can be solved simultaneously to give X_i and T for the eutectic mixture. A simple procedure involves³ calculations that can be done speedily on a Hewlett Packard 9820 calculator. A value of T is chosen and the mol. fractions ($X_A, X_B, X_C, \dots, X_N$) are evaluated. When the sum

$$\sum_{i=A}^N X_i = 1$$

the value of T is the eutectic temperature and the mol. fractions define the eutectic mixture. Successive approximations allow the eutectic temperatures to be found very quickly. Estimates of the N-I temperatures of eutectics are readily obtained from a linear extrapolation of individual N-I values weighted by the eutectic mol. fraction.

Agreement between predicted and observed transition temperatures for eutectic compositions was good, although the measured C-N temperatures were usually a little lower (2-5° C) than the calculated values. Two typical examples⁴ are given under mixtures 1 and 2 in table 2, the predicted compositions and temperatures being calculated using the relevant temperatures and enthalpies in table 1. Mixtures such as these

can be cooled to -55°C without crystallisation; solidification is usually achieved only by seeding the nematic liquid with one of the components

Table 2. Predicted eutectic mixtures of 4'-substituted 4-cyanobiphenyls and observed nematic ranges ($^{\circ}\text{C}$)

Mixture	Composition X (mol.%)	Predicted		Observed	
		C-N	N-I	C-N	N-I
1	4'-n-C ₅ H ₁₁ 59	3°	37.5°	-2°	37.5°
	4'-n-C ₇ H ₁₅ 41				
	4'-n-C ₇ H ₁₅ 36				
	4'-n-C ₃ H ₇ O 18				
2	4'-n-C ₅ H ₁₁ O 15	0	61	0	60.5
	4'-n-C ₇ H ₁₅ O 12				
	4'-n-C ₈ H ₁₇ O 19				

at low temperatures (-20 to -30°C). Such mixtures can therefore be stored as nematic liquids for long periods in a deep freeze. Mixtures such as 2 which incorporate one or more smectogens have not been found to form smectic phases even at -55°C .

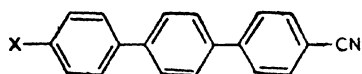
The nematic phases of such mixtures have electrical properties closely similar to those of 4-cyano-4'-n-pentylbiphenyl and the other mesogens listed in table 1. They share the same chemical/photochemical stability and therefore provide excellent wide range nematic mixtures for twisted nematic displays^{2, 4}.

Mixtures of 4'-n-alkyl- and 4'-n-alkoxy-4-cyanobiphenyls with other nematogens

The possibility of further widening the nematic ranges of mixtures of the biphenyl mesogens was investigated by incorporating solutes with higher N-I temperatures.

Unsaturated analogues of the 4'-n-alkyl-4-cyanobiphenyls will have higher N-I temperatures. A sample of 4-cyano-4'-(pent-1'-enyl)biphenyl (C-N, 92.4°C ; N-I, 125.5°C) was prepared, but the compound has a tendency to polymerise in sunlight. Its incorporation in the biphenyl nematic liquid mixtures would consequently detract from their stability and such unsaturated additives are considered unsatisfactory.

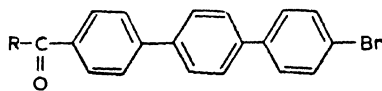
We turned instead to 4'-n-alkyl-4-cyano-*p*-terphenyls since they have very high N-I temperatures and share the chemical/photochemical stability of the biphenyl analogues. This investigation is still in progress but three examples of such substituted *p*-terphenyls are given in table 3. It is noted that the ketonic precursors (see Section 3) of these materials are also mesogens, and their transition temperatures are given in table 4.

Table 3. Transition temperatures and enthalpies* of melting for the compounds

X	C ₂ -C ₁ Temp. (°C)	C ₁ -N Temp. (°C)	C ₁ -N ΔH (kcal. mol. ⁻¹)*	N-I Temp. (°C)
<i>n</i> -C ₃ H ₇	179	182.2	4.8	257.5
<i>n</i> -C ₅ H ₁₁	110	130	4.1	239
<i>n</i> -C ₇ H ₁₅ †	*	134	ca. 4.8	221.8

* The enthalpies of melting are total enthalpies including those for C₂-C₁ transitions. In the case of the *n*-C₇H₁₅ compound, an extremely complex set of polymorphic changes occurs. There are several crystal forms with different melting points, and the sample is never obtained entirely in the form of the most stable solid, C₁. The enthalpy quoted is worked out from the total area under all the melting and crystal-crystal peaks.

† The *n*-C₇H₁₅ compound exhibits a smectic phase which is monotropic with respect to some of the solids, including the most stable crystal, m.p. 134° C, and enantiotropic with respect to others. The S-N transition is 125.5° C. Fuller details about the compound await more detailed investigations.

Table 4. Transition temperatures for the compounds

R	C-S _E or N Temp. (°C)	S _R -S _B Temp. (°C)	S _B -N Temp. (°C)	N-I Temp. (°C)
C ₂ H ₅	223	-	-	282.5
<i>n</i> -C ₄ H ₉	204.5	-	-	248.5
<i>n</i> -C ₆ H ₁₃ *	178	204	212	239

* The types of smectic phase have been assigned solely on the basis of microscopic examination.

To exemplify the effect of adding such *p*-terphenyl compounds (table 3) to the biphenyl mesogens (table 1), some mixtures containing just one *p*-terphenyl compound (4-cyano-4''-*n*-pentyl-*p*-terphenyl) are given in table 5. Eutectic mixture 1 illustrates the effect on 4-cyano-4'-*n*-pentyl-biphenyl of adding 13.3 mol. % of the terphenyl compound. The C-N temperature of the pure biphenyl compound is decreased by about 8-9° C and the N-I temperature is increased by about 30° C. The N-I temperature for mixtures of biphenyls and *p*-terphenyls are typically a little spread (up to about 3° C); the N-I transition line does not change rectilinearly with composition, but has a slight convexity upwards. Mixture 1 crystallises only with difficulty at -30° C.

Table 5. Predicted eutectic mixtures of 4'-substituted 4-cyanobiphenyls and 4''-substituted 4-cyano-*p*-terphenyls and observed nematic ranges (°C)

Mixture	Composition X (mol. %)		Predicted		Observed	
			C-N	N-I	C-N	N-I
1	4'- <i>n</i> -C ₅ H ₁₁	86.7	17	64	13-14	66-69
	4''- <i>n</i> -C ₅ H ₁₁	13.3				
2	4'- <i>n</i> -C ₅ H ₁₁	52.6	0.4	63.3	0	62.5-65.5
	4'- <i>n</i> -C ₇ H ₁₅	35.4				
	4''- <i>n</i> -C ₅ H ₁₁	12				
	4'- <i>n</i> -C ₃ H ₇ O	23.1				
3	4'- <i>n</i> -C ₅ H ₁₁ O	22.9	9	91	5*	91-92
	4'- <i>n</i> -C ₇ H ₁₅ O	18.8				
	4'- <i>n</i> -C ₈ H ₁₇ O	23.9				
	4''- <i>n</i> -C ₅ H ₁₁	11.3				

* The mixture forms a glass at -20° C and crystallisation has so far not been achieved. The glass has become a fully mobile nematic liquid by 5° C.

Mixture 2 in table 5 shows that, by using 12 mol. % of the terphenyl compound, a simple ternary mixture can be produced that has the same C-N temperature but a wider nematic range than the more complex quinary mixture 2 containing only biphenyl mesogens (see table 2).

Mixture 3 (table 5) shows that, using more complex eutectic mixtures, high N-I temperatures (approaching 100° C) can be realised, in this particular case by incorporating only 11.3 mol. % of the terphenyl compound. This mixture makes available a mobile nematic liquid over a temperature range of approx. 86° C from 5° C.

Segregation on storage does not occur with any of the above mixtures of biphenyls, but with mixtures containing *p*-terphenyls it is important that eutectic compositions are prepared accurately or segregation of any excess of the *p*-terphenyl compounds may occur.

Cholesteric liquid crystals containing 4'-substituted 4-cyanobiphenyls

If 10% by weight of cholesteryl chloride or nonanoate is incorporated in 4-cyano-4'-*n*-pentylbiphenyl or one of the mixtures referred to above, room temperature cholesterics are produced. These have high ϵ_a values and perform well in cholesteric-nematic phase change devices^{2, 4}. Use of a cholesteric additive is also a good means of ensuring that twisted nematic films are free from areas of reverse twist⁵.

Such derivatives of cholesterol are however less chemically/photochemically stable than the biphenyl nematogens and their use as solutes introduces a source of decomposition.

Ideally, a chemically/photochemically stable, optically active compound exhibiting a cholesteric phase is needed. To achieve the desired stability, we prepared pure optically active 4-cyano-4'-(2"-methylbutyloxy) biphenyl (compound I). This melts at 53.5°C, but does not exhibit a mesophase. This was not unexpected, as the chain branching in the alkyl group will greatly lower⁶ the mesophase-isotropic liquid transition temperature relative to that of the *n*-butyloxy compound. However, the compound consists of elongated molecules and so it should have a latent tendency to form a mesophase, *i.e.*, there should be a latent I-Ch temperature which can never be achieved because crystallisation of the melt always occurs first on cooling. Reasonably high concentrations of compound I should therefore be tolerable by host nematic liquids without destroying the cholesteric properties. Indeed, an estimate of the latent I-Ch temperature was obtained by extrapolating the line through the transition temperatures for mixtures of various compositions of compound I in either 4-cyano-4'-*n*-pentylbiphenyl (PCB) or a binary mixture of biphenyl mesogens (figure 2). The low slopes of the lines indicate the latent tendency of compound I to give a cholesteric phase, and the intercepts of these lines on the temperature axis on extrapolation to 100% of the optically active biphenyl gives values of 6° and 12°C for the latent I-Ch temperature.

To illustrate the use of this material ($\Delta H = 3.5 \text{ kcal. mol.}^{-1}$), we quote one reasonably low melting (C-Ch, 11.5°C) and fairly wide range eutectic cholesteric mixture (Ch-I, 53°C) prepared from compound I (40 mol. %) and the *n*-pentyl (21 mol. %), *n*-heptyl (17 mol. %) and *n*-octyl (22 mol. %) ethers of 4-cyano-4'-hydroxybiphenyl. Crystallisation does not occur on shock cooling to -55°C and only slow crystallisation can be induced by seeding at -20°C. The cholesteric liquid crystal has a pitch of 4.0 μm . and a 50 μm . layer gave completion of the phase change at 27 V_{rms} ($5.4 \times 10^5 \text{ Vm.}^{-1}$)⁷.

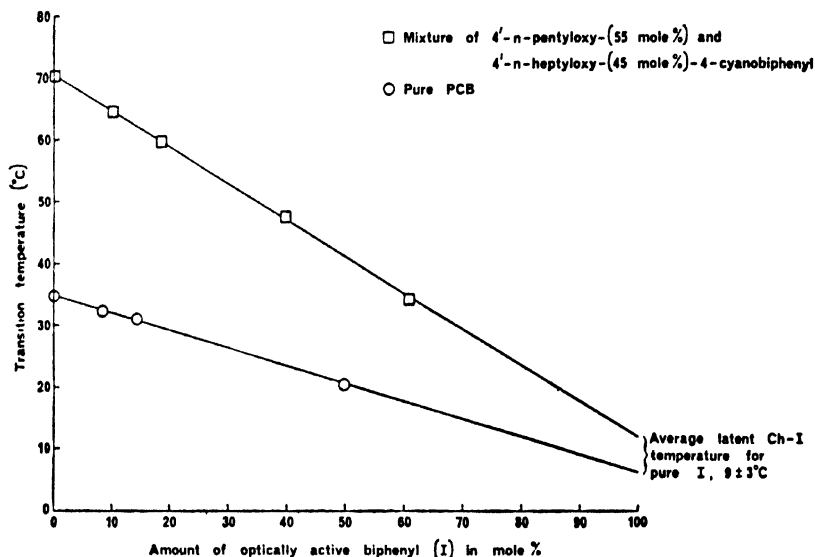


Figure 2 Plot of mesophase-isotropic liquid transition temperatures for (a) a mixture of two biphenyl nematogens (\square), (b) pure 4-cyano-4'-n-pentylbiphenyl-PCB (O) against the amount (mol. %) of dissolved, optically active 4-cyano-4'-(2"-methylbutyloxy) biphenyl (I)

The optically active compound I is therefore a valuable means of producing stable cholesterics with highly positive ϵ_a values for use in cholesteric-nematic displays which have several advantages over dynamic scattering displays. Furthermore, as little as 1% of the optically active compound I induces a pitch of the required order (approx. $100 \mu\text{m}^2$) to avoid areas of reverse twist in twisted nematic cells prepared using mixtures of biphenyl nematogens. In both these uses, the chemical/photochemical stability of the host nematic is preserved.

The smectic phase of the 4'-n-alkyl- and 4'-n-alkoxy-4-cyanobiphenyls

Three of the higher members of the two series of biphenyl mesogens in table 1 exhibit smectic phases, the *n*-octyl compound giving a stable smectic liquid crystal at room temperature. Still higher members of the series, particularly the *n*-alkyl series, are low melting smectogens which give no nematic phases. For example, a non-eutectic mixture, C-S, 57.0 and S-I, 89.1°C , is formed from the C_{12} , C_{14} , C_{16} and C_{18} ethers.

The smectic phase exhibited by these compounds has not been characterised and is probably novel in type². The enthalpy for the S-N change is very small—of the same order or less than that for the N-I transitions. The smectic phase has a strong tendency to be completely homeotropic,

and so no texture for it can be described. The interference figure is therefore readily obtained and is positive uniaxial. Standard compounds exhibiting classified smectic phases of the various kinds in the temperature region in which the biphenyl mesogens exhibit their smectic phase are not common. However, some miscibility studies have been made despite differences in the transition temperatures for the pairs of compounds. The smectic phase of the biphenyl mesogens seemed immiscible with S_A , S_B and S_C phases and did not apparently belong to any of these classes. The phase is homeotropic, but not isotropic, and so is not S_D .

To check that the smectic is not S_A or S_B , preliminary x-ray studies were carried out by Dr. J. Lydon⁹ of Leeds University, using for convenience the room temperature smectic phase of the *n*-octyl compound. The x-ray diffraction pattern is different from that of any other thermotropic smectic phase yet reported. It shows a sharp inner ring corresponding to a spacing of approx. 30 Å and two diffuse outer rings in the 4-4.5 Å region. The layer thickness does not therefore correspond to the molecular length which is approx. 22 Å. It is suggested that each smectic layer consists of two sheets of the elongated molecules which lie with their long axes normal to the layer planes, but with the *n*-alkyl chains completely overlapping in the centre of the layer. Both surfaces of a given smectic layer would therefore consist of the terminal cyano-groups associated with the two sheets of overlapping molecules. The two diffuse rings may relate to features of the molecular packing in two different directions in the planes of the layers. Further studies of this smectic phase are now being made (J. Lydon, unpublished work), but on the evidence presently available the smectic phase does not conform with de Vries's classification of hitherto known smectic phases, based on their x-ray diffraction patterns¹⁰. The smectic phase seems therefore to be of a new type.

It is emphasised however that only one compound, *i.e.*, the *n*-octyl derivative, has as yet been examined by x-ray methods. We have not yet had time to carry out miscibility studies on the C_{12} , C_{14} , C_{16} and C_{18} ethers of which the quaternary mixture does give a fan-texture similar to S_A or S_B . At the present moment, therefore, we cannot be certain whether

(a) the higher homologues of the *n*-alkoxy compounds do give the new smectic phase, or

(b) the new smectic phase, which is obviously structurally similar to a S_A or S_B , gives a texture similar to these phases when the alkyl chain of the alkoxy group is sufficiently long.

A decision between these possibilities awaits further experimental study:

3. Experimental

Preparation of materials

*4-Bromo-*p*-terphenyl* was prepared by the method of Cade and Pilbeam¹¹. Yields were inferior to that (48.5%) reported by these authors and ranged from 25–45%. Contamination of the crude product with *p*-terphenyl and 4,4'-dibromo-*p*-terphenyl differed in its relative extent from one run to another, and variable losses were involved in obtaining pure monobromo-compound (*M*, 309) which had m.p. 227–8° C (lit. m.p. 220–2° C).

*4-Bromo-4''-propionyl-*p*-terphenyl*. 4-Bromo-*p*-terphenyl (16 g., 0.052 mol.) was dissolved in pure, dry nitrobenzene (450 ml.) and lightly crushed anhydrous aluminium trichloride (8 g., 0.06 mol.) was added. Propionyl chloride (6 g., 0.065 mol.) dissolved in nitrobenzene (50 ml.) was added to the stirred mixture at 0–5° C over a period of 20 min. The mixture was left to stand overnight at room temperature, after which it was poured onto a mixture of ice, water and concentrated hydrochloric acid and stirred for 30 min. The organic layer, diluted with chloroform, was separated, washed with water and steam distilled to remove solvents. The solid residue was extracted into chloroform; the dried extract was evaporated to dryness and the residue crystallised twice from ethylene glycol monomethyl ether, in the first case using decolourising carbon. Colourless crystals (11.5 g., 61%) of the ketone (Found: C, 68.8; H, 4.4; Br, 22.3%; *M* 365, C₂₁H₁₇BrO requires C, 69.0; H, 4.65; Br, 21.9%; *M* 365) were obtained (single spot on t.l.c.). A further crystallisation did not alter the m.p. of 223° C (see also table 4).

By the same method, we prepared and purified (1) 4-bromo-4''-n-pentanoyl-*p*-terphenyl (single spot on t.l.c.) in a yield of 63% (Found: C, 70.0; H, 5.4; Br, 20.0%; *M* 393. C₂₃H₂₁BrO requires C, 70.2; H, 5.35; N, 20.3%; *M* 393), m.p. 204.5° C (see also table 4) and (2) 4-bromo-4''-n-heptanoyl-*p*-terphenyl (single spot on t.l.c.) in a yield of 74% (Found: C, 71.2; H, 6.0; Br, 18.7%; *M*, 421. C₂₅H₂₃BrO requires C, 71.3; H, 5.9; Br, 19.0% *M*, 421) m.p. 178° C (see also table 4).

*4-Bromo-4''-n-propyl-*p*-terphenyl*. Potassium hydroxide (5.6 g., 0.1 mol.) 98% hydrazine hydrate (8 ml.), diethylene glycol (500 ml.) and water (2 ml.) were stirred until the potassium hydroxide had dissolved. 4-Bromo-4''-propionyl-*p*-terphenyl (12.2 g., 0.033 mol.) was added slowly at a temperature of 130° C. A vigorous reaction occurred and the heating rate was reduced. After completion of the addition, the mixture was heated at 130–150° C for 2 hr. While distilling off volatile matter, the temperature was raised to 180° C and held there for 4 hr. On cooling, solid separated from the mixture. This was dissolved in chloroform, water added and the organic layer separated. The chloroform solution was washed thoroughly with water, dried and evaporated to dryness. The residue was sublimed at a bath temperature of 210° C at 0.2 mm. and the sublimate crystallised from toluene.

The colourless crystals (8.2 g., 68%) (single spot on t.l.c.) had m.p. 249.5° C. unaffected by further crystallisation (Found: C, 71.5; H, 5.3; Br, 22.4%; *M*, 351. $C_{21}H_{19}Br$ requires C, 71.8; H, 5.45; Br, 22.75%; *M* 351).

Using the same method, we prepared and purified (1) 4-bromo-4'-*n*-pentyl-*p*-terphenyl (single spot on t.l.c.) in a yield of 67% (Found: C, 72.4; H, 5.9; Br, 21.0%; *M*, 379. $C_{23}H_{23}Br$ requires C, 72.8; H, 6.1; Br, 21.1%; *M*, 379), m.p. 251° C and (2) 4-bromo-4'-*n*-heptyl-*p*-terphenyl (single spot on t.l.c.) in a yield of 60% (Found: C, 73.5; H, 6.4; Br, 19.4%; *M*, 407. $C_{25}H_{27}Br$ requires C, 73.7; H, 6.6; Br, 19.7%; *M*, 407), m.p. 225° C.

4-Cyano-4'-*n*-propyl-*p*-terphenyl. A mixture of 4-bromo-4'-*n*-propyl-*p*-terphenyl (7 g., 0.02 mol.), dried cuprous cyanide (5.75 g., 0.03 mol.) and anhydrous dimethylformamide (90 ml.) was heated for 12 hr under reflux. The cooled reaction mixture was poured into a solution of hydrated ferric chloride (7.3 g.) in water (75 ml.) containing concentrated hydrochloric acid (1.5 ml.) and the mixture heated and stirred at 60–70° C for 20 min. Organic material was extracted into chloroform and the extract washed with 5*N*-hydrochloric acid, water, 10% aqueous sodium hydroxide and water in that order. The dried extract was freed from solvent by evaporation and the residue purified by column chromatography on silicic acid using chloroform to elute the column. The cyano-compound (single spot on t.l.c.) was finally sublimed at a bath temperature of 200–210° C at a pressure of 0.3 mm. The colourless product (2.4 g., 40%) had m.p. 182.2° C (see also table 3) (Found: C, 88.6; H, 6.5; N, 4.6%; *M*, 297. $C_{22}H_{19}N$ requires C, 88.8; H, 6.45; N, 4.7%; *M*, 297).

By the same procedure we obtained colourless samples of (1) 4-cyano-4'-*n*-pentyl-*p*-terphenyl (single spot on t.l.c.), m.p. 130° C (see also table 3) in a yield of 43% (Found: C, 88.5; H, 7.2; N, 4.3%; *M*, 325. $C_{24}H_{23}N$ requires C, 88.6; H, 7.1; N, 4.3%; *M*, 325) and (2) 4-cyano-4'-*n*-heptyl-*p*-terphenyl (single spot on t.l.c.), m.p. 134° C (see also table 3) in a yield of 45% (Found: C, 88.2; H, 7.5; N, 3.9%; *M*, 353. $C_{26}H_{27}N$ requires C, 88.4; H, 7.6; N, 4.0%; *M*, 353).

(–) 4-Cyano-4'-(2'-methylbutyloxy)biphenyl. (a) To a solution of toluene-*p*-sulphonyl chloride (18 g., 0.094 mol.) in dry pyridine (75 ml.) at –5° C, commercial (–) 2-methylbutan-1-ol (7.5 g., 0.085 mol.) was added in one portion. The solution was maintained below 0° C and stirred for 2 hr. Water (15 ml.) was added in portions of 1, 1, 1, 2, 5 and 5 ml. at 5 min. intervals, the temperature being maintained below 5° C. The solution was diluted with water (75 ml.), shaken with chloroform and the extract washed successively with water 2*N*-sulphuric acid, water, 15% aqueous sodium bicarbonate and water, and finally dried. The chloroform was removed and the residue distilled. (–) 2-Methylbutyl toluene-*p*-sulphonate (31.5 g., 76.5%) was collected as a colourless oil, b.p. 149° C at 0.5 mm.

(b) To 4-cyano-4'-hydroxybiphenyl² (1.95 g., 0.1 mol.), a solution of sodium (0.23 g., 0.1 g. atom) in dry ethanol (30 ml.) was added and the

mixture stirred until a solution was obtained. The ethanol was distilled off under reduced pressure, dry dimethylformamide (55 ml.) and the tosylate (1.93 g., 0.11 mol.) were added and the reaction mixture was heated and stirred at 110–130° C for 7 hr. After leaving to stand overnight, the mixture was poured into water (100 ml.) and the organic matter extracted into ether. The extract was washed successively with water, 15% aqueous sodium bicarbonate and water, and then dried. After removing the solvent, the residue was purified by column chromatography on silicic acid using chloroform for elution. The product was crystallised from ethanol and finally distilled (b.p. 130–135° C at 0.3 m.m.). The yield of colourless solid, m.p. 53.5° C, was 0.64 g. (24%) (Found: C, 81.7; H, 7.6; N, 5.0%; *M*, 265. $C_{18}H_{19}NO$ requires C 81.7; H, 7.6; N, 5.0%; *M*, 265). The product gave a single spot on t.l.c. on silicic acid using chloroform as solvent ($R_F = 0.4$), and the specific rotation of a chloroform solution $[\alpha]_D^{20} = +10^\circ$. The purity of the product was 99.6% as measured by g.l.c.

4-Bromo-4'-(pent-1"-enyl)biphenyl. (a) 4-Bromo-4'-*n*-pentanoylbiphenyl² (1.6 g.) dissolved in dry ether (50 ml.) was added (30 min.) with stirring to lithium aluminium hydride (1 g.) in ether (50 ml.). Stirring was continued for 30 min. and the mixture was then heated under reflux (15 min.). Excess of reducing agent was destroyed (ethyl acetate) and a solution of ammonium chloride added. The ether layer was separated, washed with ammonium chloride solution and with water and then dried. Removal of the ether gave a solid (single spot on t.l.c.) which was crystallised from a mixture of toluene and petroleum ether b.p. 40–60° C). The colourless alcohol (1.1 g., 68%), m.p. 107° C had *M*, 319 ($C_{17}H_{19}BrO$ requires *M*, 319).

(b) The above alcohol (1 g.) was dissolved in 99% formic acid (50 ml.) and heated under reflux for 20 min. The mixture was poured into water (150 ml.) and the product extracted into ether. The extract was washed with water and dried. Removal of the ether and crystallisation of the residue gave the colourless olefin, 0.8 g. (85%), m.p. 165° C. Mass spectrometry gave the required value of *M*, 301, but revealed traces of dimer and trimer. The tendency to polymerise was demonstrated by t.l.c. which revealed a succession of spots of lower R_F values which appeared after exposure of the monomer to sunlight and gradually intensified with length of exposure of the monomer to sunlight.

4-Cyano-4'-(pent-1"-enyl)biphenyl. 4-Bromo-4'-(pent-1"-enyl)biphenyl (15 g.) was converted into the cyano-compound by heating with cuprous cyanide according to the procedure given above for 4-cyano-4'-*n*-propyl-*p*-terphenyl. Exposure of the reaction mixture and product to light was kept to a minimum. The product from column chromatography was crystallised twice from petroleum ether (b.p. 60–80° C). The colourless crystals, m.p. 92.5° C (also N-I, 125.5° C) were obtained in a yield of 44% (Found: C, 87.2; H, 7.0; N, 5.6%; *M*, 247. $C_{18}H_{17}N$ requires C, 87.4; H, 6.8; N, 5.7%; *M*, 247). The product gave a single spot

on t.l.c. and was less rapidly polymerised by the action of light than the bromo-precursor.

Physical measurements

Optical microscopy was carried out using a Nikon L-Ke polarising microscope (Projectina Co. Ltd., Skelmorlie, Ayrshire, Scotland) fitted with a Mettler FP 52 hot stage and programmed temperature controller (Mettler Instruments AG, CH-8606 Greifensee - Zurich, Switzerland) by means of which transition temperatures were measured. Observations and measurements at low temperatures were made using a polarising microscope and cold stage (C. Reichert, Optische Werke AG, Wien, Austria).

All mesogens were examined by D.T.A. using a low temperature thermal analyser (Stanton Redcroft Limited, Copper Mill Lane, London) to check on the number of transitions and the temperatures of transition obtained by optical microscopy.

Enthalpies of transition were measured using a Du Pont thermal analyser fitted with a D.S.C. cell [Du Pont Co. (U.K.) Limited, Hitchin, Herts.].

Molecular weights were measured by mass spectrometry (M.S. 902) and elemental analyses were carried out by Weiler and Strauss, 10, Carlton Road, Oxford. Gas liquid chromatography was done using a glass column (1.5 m long and 2 mm internal diameter) packed with 3% OV225 on Gas Chrom. Q (100-120 mesh) at 230°C using a nitrogen gas flow of 12 ml./min.

Acknowledgement

This work was carried out under contract to the Ministry of Defence.

References

- 1 GRAY G W, HARRISON K J and NASH J A, *Electron. Lett.* 9 130 (1973)
- 2 GRAY G W, HARRISON K J, NASH J A, CONSTANT J, HULME D S, KIRTON J and RAYNES E P, *Proceedings of the Symposium on Ordered Fluids and Liquid Crystals*, 166th National A.C.S. Meeting, Chicago, August 1973 (edited by R. S. Porter and J F Johnson) p. 617 (1974)
- 3 HARRISON K J, HULME D S and RAYNES E P, *Chem. Commun.* 98 (1974)
- 4 ASHFORD A, CONSTANT J, KIRTON J and RAYNES E P, *Electron. Lett.* 9 118 (1973)
- 5 RAYNES E P, *Electron. Lett.* 9 101 (1973)
- 6 GRAY G W and HARRISON K J, *Symposium of the Faraday Soc.* 5 54 (1971)
- 7 GRAY G W, HARRISON K J, NASH J A and RAYNES E P, *Electron. Lett.* 9 616 (1974)
- 8 RAYNES E P, to be published
- 9 LYDON J, unpublished results, but see *Nature* 252 221 (1974)
- 10 DE VRIES A, *Proceedings of the Fourth International Liquid Crystal Conference, Kent, Ohio, August 1972*
- 11 CADE J A and PILBEAM A, *J. Chem. Soc.* 114 (1964)

DISCUSSION

Demus : Are nitro-compounds less stable than cyano-compounds, especially in DC field?

Gray : We did prepare the nitro analogues of several of the cyano compounds reported in my paper. The compounds are yellow, and the phases are either monotropic or of a narrow enantiotropic range. We did not therefore pursue these materials further and have not examined the stabilities of the mesophases of the nitro compounds in DC fields.

Surendranath : Have you any comments on the effects of substituents in 2,2' and 3,3' positions in the alkyl cyanobiphenyl system? Have any studies been made on the effect of lateral substituents in the terphenyl system?

Gray : From our earlier studies of the effects of lateral substituents on biphenyl mesogens carried out many years ago, we know that introduction of such substituents into the cyanobiphenyls under discussion would give very low N-I temperatures. The compounds would therefore be either *strongly* monotropic nematic or non-mesomorphic. The introduction of lateral substituents into the cyano-*p*-terphenyl mesogens is a much more interesting subject for study.

de Vries : Was the x-ray diffraction pattern with the low diffuse outer rings obtained with monochromatic radiation or with filtered radiation? In my own work I have always worked with filtered radiation. In that case one always obtains an additional diffuse ring corresponding to about 9 Å spacing. This ring is caused by the white radiation. Because of the presence of this ring we would not be able to notice the second diffuse outer ring mentioned by you. Thus it could well be present in all S phases.

Gray : The x-ray diffraction diagram was obtained using monochromatic radiation.

Demus : We have found that nitro and cyano compounds tend to homeotropy. Have you the same experience?

Gray : The 4-cyano-4'-*n*-alkyl- and -4'-*n*-alkoxybiphenyls behave very well with regard to surface alignment. On *clean* surfaces, homeotropic alignment is easily achieved, but on rubbed surfaces, alignment parallel to the surfaces is readily given as required for twisted nematic displays.

New series of thermotropic liquid crystals with low temperature smectic A phase

J CANCEILL, C GROS, J BILLARD* and J JACQUES

Laboratoire de Chimie organique des Hormones

Abstract. Series of derivatives of fluorene and 9, 10-dihydrophenanthrene with diverse alkyl, alkoxy or acyl groups have been synthesised. Many members have a lateral methyl group on a chain. Most of compounds exhibit one or several liquid crystalline phases. The temperatures of transitions are given. The contribution of the emplacement of the lateral methyl group on the liquid crystallinity is studied. The nature of some mesophases is determined by isomorphy. The best compound having a smectic A phase at low temperatures has a melting point at 21 °C. Many mixtures with a smectic A phase at lower temperatures are possible. With these compounds one can have focal conic and homeotropic textures without difficulty. The compounds described, either pure or in mixtures, are uncoloured and stable in air.

1. Introduction

Many different series of stable and colourless compounds showing a stable nematic phase at room temperature, suitable for applications, are currently available. Some applications (information and storage displays¹, monochromators for x-rays of large wavelength, etc.) require a smectic A phase satisfying the same conditions. The availability of such phases simplifies many physical measurements and makes easier the fundamental study of this modification of condensed matter. Except the 4,4'-diheptylazoxybenzene² which is coloured yellow, most of the substances showing a low temperature smectic A phase do not have sufficient chemical stability. Hence most of the series studied so far do not seem favourable.

Gray and Ibbotson³ obtained smectic phase with fluorene derivatives (figure 1): four esters of 7-alkoxyfluorene-2-carboxylic acids and four 2-acetyl-7-alkoxy fluorenes. These results led us to study more completely the disubstituted fluorenes and, by extension, the 9, 10-dihydrophenanthrenes disubstituted in 2 and 7 (figure 1).

* Physique de la Matière condensée, Collège de France, Paris and Université des Sciences et Techniques de Lille, France.

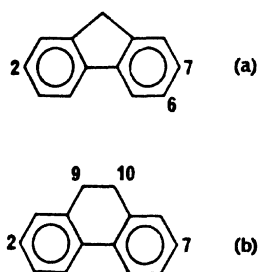


Figure 1 Structural formulae of the hydrocarbons : (a) fluorene ; (b) dihydro-9, 10-phenanthrene.

2. Methods of preparation

The general method of preparation is shown schematically in figure 2. It works just as well for the derivatives of fluorene as for those of the 9, 10-dihydrophenanthrene. Firstly, it consists in condensing the acid

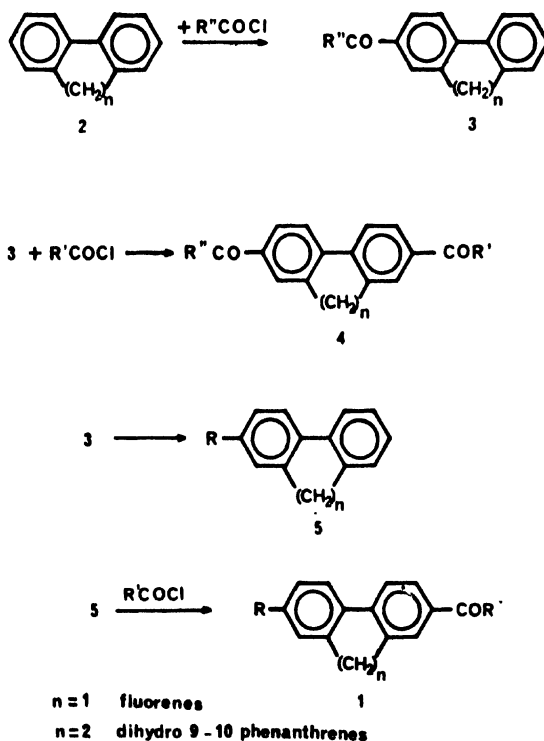


Figure 2 General method for the preparation of the fluorenes and disubstituted 9, 10-dihydrophenanthrenes.

chloride (the Friedel-Crafts reaction) on the suitable hydrocarbon 2 to obtain the ketones of type 3, which when submitted under similar conditions to the same acid chloride or to a different one give way to the diketones 4. By reduction using the Kishner-Wolff, or the Clemmensen method or any other method of hydrogenation, the ketones of type 3 give rise to the alkylated compounds 5, which by the Friedel-Crafts reaction with suitable acid chlorides easily lead to the product 1. Except where specifically stated in the text all these compounds are colourless.

3. Mesophases

The transitions of the prepared compounds have been studied with a differential scanning calorimeter (Perkin-Elmer DSC 2). The textures of the phases have been observed between cover slips with a polarizing microscope (Leitz Panphot) equipped with a heating and cooling stage (Mettler, F P5). Using the contact method⁴ some of these phases have been identified by isomorphy⁵ with mesophases of reference compounds of the Halle School⁶. Among these ninety five mesomorphogenic compounds studied until 1968, eighty one have a smectic A phase (S_A) sixteen a smectic B phase (S_B), thirty four a smectic C (S_C), and fifty one a nematic phase (N).

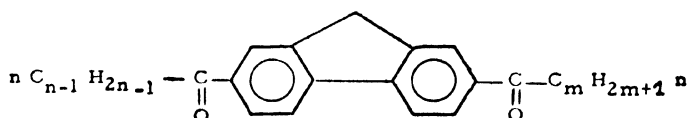
A. Disubstituted fluorenes

(a) 2, 7-DISUBSTITUTED FLUORENES WITH NORMAL ALKYL CHAINS

(1) 2, 7-di-n. acylfluorenes

The compounds of this series are mentioned in table 1. None of these compounds has a stable smectic A phase below 100° C. If the molecule is

Table 1 Transition temperatures of the 2-7-di-n. acylfluorenes :



$$^n C_{n-1} H_{2n-1} - \text{C}(=\text{O}) - \text{fluorene} - \text{C}(=\text{O}) - C_m H_{2m+1}^n$$

n-1	m	S	S_A	L
4	4	—	—	155
4	8	—	101	154.5
4	11	—	100.5	151
6	6	141.5	149.5	159.5
6	11	—	105	155.5
11	11	—	133	148.5
15	15	133.5	—	139

In this table, as also in the following ones, the temperatures are indicated in Celsius degrees for the transition between a lower temperature stable phase and the phase indicated at the top of the column. The data written here are those of second heating if they are different from those obtained at the first heating.

symmetric and the alkyl chains long enough, the smectic A phase is replaced by a phase which seems to be smectic B.

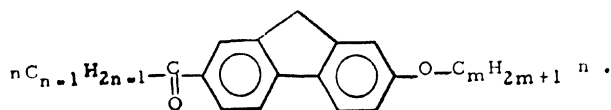
(2) 2-*n*-acyl-7-*n*. alkoxyfluorenes

These compounds are listed in table 2. The smectic A phase of the compound $n = 4$, $m = 8$ has a very anisotropic viscosity and is very homeotropic, it forms Grandjean terraces easily. The crystals appearing by cooling of the smectic A phase are like needles and are bent : their direction of lengthening is at every point perpendicular to the lengthening direction of focal conics from which they are formed. It is a case of pseudomorphosis of the smectic A phase resembling those noticed by Friedel⁷. The transition enthalpies are :

$$C \rightleftharpoons S_A : 6.20 \text{ kcal/mole}$$

$$S_A \rightleftharpoons L : 2.35 \text{ kcal/mole}$$

Table 2 Transition temperatures of the 2-*n*. acyl-7-*n*. alkoxy fluorenes :

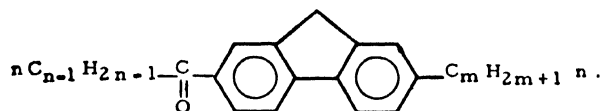


$n-1$	m	S_A	L
4	8	114	152
6	3	106	152
6	8	117	149
6	14	105.5	133
7	1	106 *	108 *
8	1	98 *	108.5 *
9	1	100 *	110 *
10	1	97.5 *	109 *
11	8	109	138

* From Ref. (3)

(3) 2-*n*. acyl-7-*n*. alkylfluorenes

The six compounds of this type which have been prepared are listed in table 3. On cooling the S_A phase of the compound $n - 1 = 4$, $m = 9$ there appears a monotropic crystal modification which is in equilibrium with S_A supercooled at 94.5°C . The compound $n - 1 = 6$, $m = 5$ shows two crystal - crystal transitions at 72.5 and 76°C . The kinetic of this last transition is

Table 3 Transition temperatures of the 2-n. acyl-7-n. alkyl fluorenes :

n-1	m	S _B ?	S _A	L
4	9	—	101.5	111.5
6	5	(92)	93	125
8	5	—	79.5	121
8	9	—	108.5	115.5
11	5	—	99	114.5
11	9	—	101	112.5

The temperature in paranthesis indicates a monotropic transition.

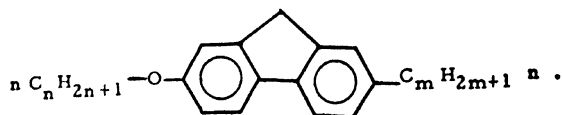
very slow and by heating, at 1°C/min, the middle crystalline phase becomes, at 90°C, a monotropic smectic B phase. The S_A phase of the compound n-1=11, m=5 stays in supercooled state until 65°C where it gives rise to a monotropic crystalline modification. This last one, heated, gives a monotropic smectic A phase at 91°C which leads to the stable crystalline phase at 91.5°C by an exothermic transformation. During the crystallisation of n-1=8, m=5 and n-1=11, m=5 compounds, the preparations cracks: the specific volumes of the crystalline phases are smaller than those of S_A mesophases. The S_A supercooled phase of n-1=11, m=9 is, at 94°C, in equilibrium with a second monotropic crystalline modification.

(4) 2-n. alkoxy-7-n. alkylfluorenes

The five compounds of this kind which have been prepared are listed in table 4. The n=8, m=5 compound presents a crystal-crystal transition at 73°C. The crystals obtained by cooling of the S_A phase have the same properties as those of the n=4, m=8 compound of table 2.

(b) 2, 7-DISUBSTITUTED FLUORENES WITH BRANCHED ALKYL CHAINS

Gray and Harrison⁸ have shown that a lateral methyl group on an alkyl chain could increase the smectic thermal stabilities in esters of the 4-benzylideneamino-cinnamic acids. We have prepared some racemic mixtures of fluorenes with branched chains hoping to obtain in certain cases mesomorphic compounds which are optically active or diastereo-isomeric.

Table 4 Transition temperatures of the 2-n. alkoxy-7-n. alkyl fluorenes :

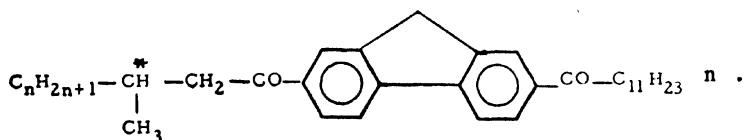
n	m	S _A	L
3	7	—	104.5
8	5	93.5	102
8	7	94.5	97.5
8	12	83	93
14	7	82.5	90

(1) 2-(3-methylacyl)-7-n. dodecanoylfluorenes

Two racemic mixtures have been prepared (table 5). The smectic phases stable at a low temperature have not been identified yet.

(2) 2-(2-methylnonanoyl)-7-n. pentylfluorene

This racemic mixture does not show a mesophase. It melts at 62° C and the supercooled liquid is in equilibrium with a second monotropic crystalline modification at 45.5° C.

Table 5 Transition temperatures of the 2-(3-methyl-acyl)-7-dodecanoyl-fluorenes (racemic mixtures) :

n	?	S _C ?	S _A	L
3	—	78	92.5	102
6	78.5	82	94.5	98.5

(3) 2-(2-methylacyl)-7-n. alkoxyfluorenes

Among the four racemic mixtures prepared (table 6) only one possesses a S_A phase. It is stable at nearly surrounding temperature.

(4) 2-*n*-heptanoyl-7-(2-methyl-*n*-undecyloxy)-fluorene

The racemic mixture melts at 95°C. A monotropic S_A mesophase is in equilibrium with the supercooled liquid at 91.5°C.

Table 6 Transition temperatures of the 2-(2-methyl-acyl)-7-*n*-alkoxyfluorenes (racemic mixtures):

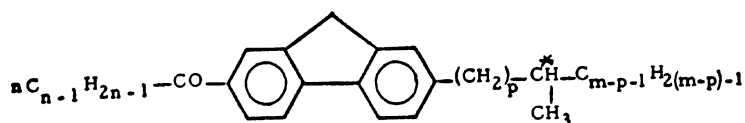
$$\text{C}_{n-2}\text{H}_{2n-3}-\overset{*}{\underset{\text{CH}_3}{\text{CH}}}-\text{CO}-\text{fluorene}-\text{O}-\text{C}_m\text{H}_{2m+1}$$

<i>n</i> -2	<i>m</i>	S _A	L
4	3	—	91
4	8	34.5	36.5
9	3	—	69
9	8	—	55

(5) 2-*n*-acyl-7-(methylalkyl)-fluorenes

Among the prepared compounds (table 7) some of them possess a stable S_A phase. The *n* - 1 = 4, *m* = 9, *p* = 1 compound has a second crystalline monotropic modification in equilibrium with its monotropic S_A mesophase at 40°C. The specific volumes of crystalline stable phases of the compounds *n* - 1 = 4, *m* = 9, *p* = 1; *n* - 1 = 8, *m* = 5, *p* = 3 and *n* - 1 = 8, *m* = 6, *p* = 2 are smaller than those of their mesophases. The S_A phases of the compounds *n* - 1 = 4, *m* = 6, *p* = 2 and *n* - 1 = 8, *m* = 9, *p* = 2 present quite perfect homeotropy between cover slips. The crystals obtained from a homeotropic area give, by melting, a homeotropic area whatever be the extinction angle. The compound *n* - 1 = 5, *m* = 5, *p* = 3 presents a crystal - crystal transition at 81.5°C and the compound *n* - 1 = 8, *m* = 5, *p* = 3 at 74°C. The compound *n* - 1 = 11, *m* = 6, *p* = 2 presents another transition under 66°C. The compound *n* - 1 = 11, *m* = 9, *p* = 0 has a second crystalline monotropic phase in equilibrium with the supercooled liquid at 60.5°C. The compound *n* - 1 = 9, *m* = 9, *p* = 0 has a monotropic mesophase in equilibrium with S_A supercooled at 60.5°C.

The farther from the nucleus fluorene is the side methyl group greater is the temperature range of the mesophases S_A of these compounds.

Table 7 Transition temperatures of the 2-n. acyl-7-(methyl alkyl)-fluorenes (racemic mixtures) :

n-l	m	p	S _A	L
2	6	2	107	108.5
2	9	2	(93)	98.5
4	6	2	61	97.5
4	9	0	—	42
4	9	1	(61)	71.5
4	9	2	51	84
4	11	1	(57.5)	61
5	5	3	99	102
6	5	3	88	105
8	5	3	80.5	100.5
8	6	2	63.5	89
8	9	0	—	62
8	9	2	61.5	78.5
11	6	2	66	85.5
11	9	0	—	71
11	9	1	(75.5)	78
11	9	2	67.5	76.5
11	11	1	—	76

(6) 2-(2-methylhexyl)-7-octyloxyfluorene

This racemic mixture melts at 59.5°C and has a monotropic S_A mesophase in equilibrium with the supercooled liquid at 56°C.

(c) VARIOUS FLUORENES

With a view to exploring for new materials, three fluorenes not belonging to the preceding series have been synthesised.

(1) *2-n. heptanoyl-6-n. pentylfluorene*

This 2, 6-substituted fluorene (figure 1) does not possess any mesophase ; it melts at 87°C. The homologue 2, 7-disubstituted (table 3) possesses a stable S_A phase between 93 and 125°C. The 2, 6-derivatives seem to be less favourable than the 2, 7-derivatives.

(2) *2-n. pentonoyl-7-n. dodecanoyl-9-fluorenone*

This compound, yellow colored, is S_A between 149 and 183.5°C.

(3) *2-n. dodecanoyl-7-n. octyloxy-9-fluorenone*

This compound, yellow colored, is S_A between 95 and 131°C.

B. 2, 7-disubstituted 9, 10-dihydrophenanthrenes

To our knowledge, the preparation and the description of the properties of some of these compounds have never been studied by chemists interested in mesomorphic properties.

(a) 9, 10-DIHYDROPHENANTHRENES DISUBSTITUTED WITH NORMAL ALKYL CHAINS

(1) *2, 7-di-n. heptanoyl-9, 10-dihydrophenanthrene*

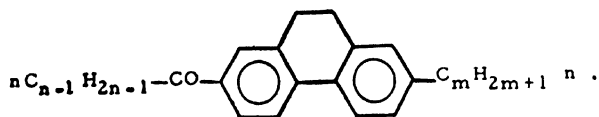
This compound melts at 58°C and possesses a smectic A monotropic phase in equilibrium with the supercooled liquid at 35°C.

(2) *2-n. acyl-7-n. alkyl-9, 10-dihydrophenanthrenes*

Most of these compounds (table 8) possess smectic A phases stable at low temperatures. The S_A and N phases of the compounds $n - 1 = 2$, $m = 8$ and $n - 1 = 4$, $m = 7$ show perfect homeotropy.

(3) *2-n. pentyl-7-n. heptyl-9, 10-dihydrophenanthrene*

This compound melts around 22°C and does not possess mesophase, which is the reason why we have mainly explored compounds with an acyl group.

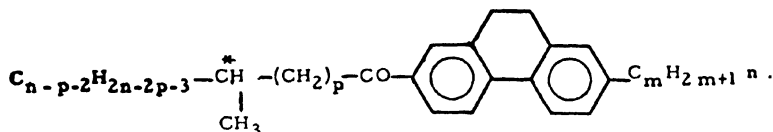
Table 8 Transition temperatures of the 2-*n*. acyl-7-*n*. alkyl-9, 10-dihydro-phenanthrenes :

<i>n</i> -1	<i>m</i>	<i>S</i> _A	<i>N</i>	<i>L</i>
2	8	—	31.5	39
2	9	—	45	47.5
3	6	—	—	32.5
3	8	—	(20)	36.5
4	5	—	(34)	40
4	6	(30)	(32)	41
4	7	(30)	(36)	(39)
4	8	22.5	31.5	33
4	9	34	36.5	38
5	5	29.5	—	38.5
5	6	34	—	42
5	7	39	—	42.5
5	8	33	—	48
5	9	40	—	46
6	5	30	—	49
6	6	28	—	51
6	7	40	—	55
6	8	35.5	—	56
7	5	(51.5)	—	57.5
7	6	(49)	—	50
8	5	54	—	57
8	6	56.5	—	61.5

(b) 2, 7-DISUBSTITUTED 9, 10-DIHYDROPHENANTHRENES WITH A BRANCHED CHAIN

(1) 2-(methylacyl)-7-*n*. alkyl-9, 10-dihydrophenanthrenes

The three racemic mixtures prepared are listed in table.9. Only one homolog, the methyl of which is very far from the nucleus, has a stable *S*_A mesophase.

Table 9 Transition temperatures of the 2-(methyl-acyl)-7-n. alkyl-9, 10-dihydrophenanthrenes (racemic mixtures):

n-p-2	p	m	S _A	L
2	2	5	—	21
6	1	7	—	33.5
2	5	8	46	50

(2) 2-n. acyl-7-(methylalkyl)-9, 10-dihydrophenanthrenes

This series, which has the most interesting compounds, is listed in table 10. Two of these compounds are smectic between 21 and 37° C. The compound $n-1=8$, $m=9$, $p=2$ has a perfect homeotropy between two cover slides treated with hexadecyl ammonium bromide^{9,10} and shows focal conics between untreated slides; the molar enthalpies of its transitions are 4.0 and 1.12 kcal/mole ($\pm 5\%$).

(c) VARIOUS 2, 7-DISUBSTITUTED 9, 10-DIHYDROPHENANTHRENES

(1) 2-cyano-7-n. alkyl-9, 10-dihydrophenanthrenes

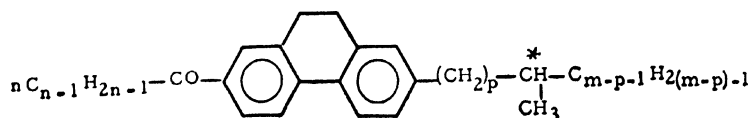
Neither of the two compounds prepared exhibits a mesophase (hexyl $T_f = 67^\circ\text{C}$, 3-methylnonyl $T_f = 52^\circ\text{C}$).

(2) 7-(3-methylnonyl)-9, 10-dihydrophenanthrene-2-carboxylic acid

This compound has a stable nematic phase between 160 and 169° C.

C. 2, 7-di-n. heptanoylphenanthrene

This compound has a stable mesophase S_A between 146.5° C and 166° C. The similar dihydro-9, 10 [Section 3 B. (a) (1)] melts at a lower temperature but does not possess a stable mesophase.

Table 10 Transition temperatures of the 2-n. acyl-7-(methyl-alkyl)-9,10-dihydrophenanthrenes (racemic mixtures) :

n-1	m	p	S _A	L
4	6	3	(19.5)	33
4	9	6	26.5	30
5	5	3	(34)	60
5	6	2	(28)	37
5	6	3	(28)	48.5
5	9	6	21	37
6	5	3	(42)	43.5
6	9	2	29	33
6	9	6	33	50
7	9	2	(26)	39
7	9	3	(35)	48
8	5	3	—	61
8	6	2	39	42
8	6	3	(44.5)	57
8	9	2	21	37.5
8	9	3	23.5	35.5
8	9	6	54	59
9	9	2	30	37
9	9	6	50.5	59
10	9	2	33	39
10	9	6	50.5	59
11	5	3	—	61
11	6	3	(47)	58
11	9	2	(35)	36
11	9	6	31	62
15	9	6	46	60

4. Identification of mesophases by isomorphy

The smectic B phase of the 2, 7-di-n. hexadecanoylfluorene (table 1) is identified by its total miscibility with the one of the ethyl 4-(4'-propoxy-benzylideneamino) cinnamate¹¹ : figure 3. This same reference compound was used to identify the smectic A phase of the 2, 7-di-n. heptanoylfluorene (table 1) : figure 4.

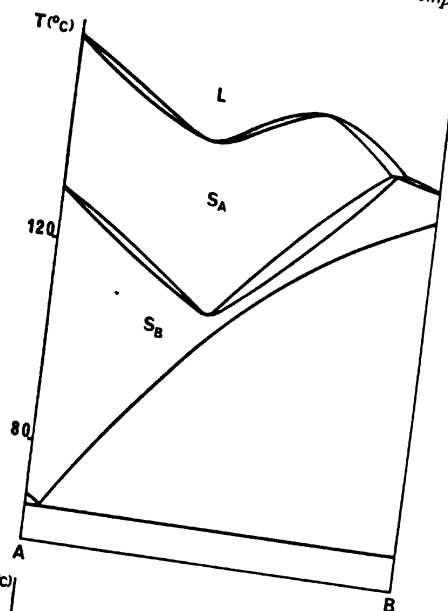


Figure 3
Isobaric phase diagram of the mixtures of ethyl 4-(4'-n-propoxybenzylideneamino) cinnamate (A) and of di-2-7-n. hexadecanoylfluorene(B).

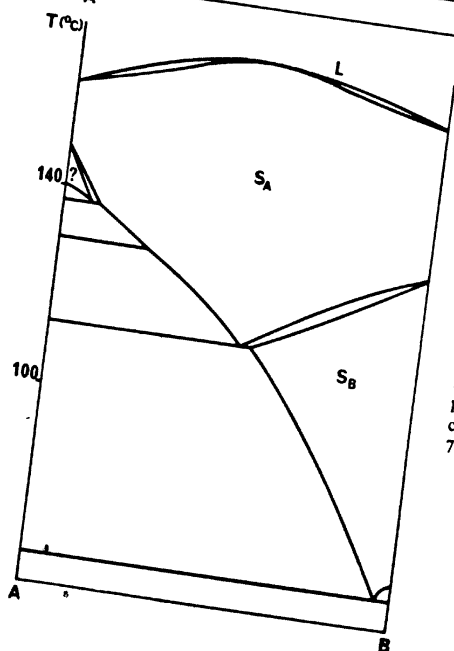


Figure 4
Isobaric phase diagram of the mixtures of ethyl 4-(4'-n-propoxybenzylideneamino) cinnamate (B) and of di-2-7-n. heptanoylfluorene (A).

To identify the smectic A phase of the 2-(3-methylhexanoyl)-7-dodecanoylfluorene (table 5) we have used intermediary components. We have used the 4-acetyl-(4'-butoxybenzylidene) aniline*, whose smectic A and nematic phases are isomorphic¹³ with those of ethyl 4-(4'-ethoxybenzylideneamino) cinnamate¹²: figure 5. We have used the 4-chloro-(4'-n. pentoxybenzylidene) aniline and the 4-chloro-(4'-n. butoxybenzylidene) aniline, the two smectic phases of which are isomorphic¹³. One of these phases is isomorphic with the smectic A phase of 4-acetyl-(4'-n. butoxybenzylidene) aniline and the other one is isomorphic¹³ with the smectic B phase of the ethyl 4-(4'-methylbenzylideneamino) cinnamate¹⁴. An isomorphy (figure 6) proves that the 2-(3-methylhexanoyl)-7-dodecanoyl fluorene has a smectic A phase. The smectic phase of the di-n. dodecanoyl-2, 7-fluorene (table 1) is identified by isomorphy with the smectic A phase of the 4-chloro-(4'-n. hexyloxybenzylidene) aniline (figure 7), which is itself isomorphic with the smectic A phase of the 4-chloro-(4'-n. pentyloxybenzylidene) aniline¹³. The smectic phase of the 2-n. nonanoyl-7-(4-methylpentyl) fluorene (table 7) is isomorphic with the smectic A phase of the ethyl 4-(4'-methylbenzylideneamino) cinnamate¹⁴: figure 8.

To identify the smectic A phase of the 2-n. nonanoyl-7-(3-methylnonyl)-9, 10-dihydrophenanthrene (table 10) we have used its isomorphy with the smectic phase of the 4-pentylphenol-4-n. octyloxybenzoate (figure 9) which is itself isomorphic of the one of the 4-cyano-4'-octyloxybiphenyl¹³; this last one is identified by isomorphy with the smectic A phase of the 2-n. nonanoyl-7-(4-methylpentyl) fluorene (see above)¹³.

5. Discussion

It has been remarked¹⁵ that the more rigid is the central part of the mesomorphogenic molecules, greater is the reduction of transition temperatures. The central parts of the fluorenes and of 9, 10-dihydrophenanthrenes are rigid and really some homologs of these series have low transformation temperatures. Generally the transition temperatures of the 9, 10-dihydrophenanthrenes are lower than those of the fluorenes: table 1 and Section III B. (a) (1): Tables 3 and 8. This can be correlated with the non-parallelism of the two aromatic rings in the 9, 10-dihydrophenanthrene. The effects of a side methyl group branched on an alkyl chain have been observed in the case of the esters of arylidenaminocinnamic acids⁸. A side methyl group generally lowers the transition temperatures (Tables 3 and 7, 8 and 9, 8 and 10.) When the chain lengths are the same the S_A mesophases are generally more stable if the side methyl group is farther from the nucleus: tables 7 and 10. This effect chiefly results from the increasing of the clearing temperature. The 2-n. acyl-7-n. alkyl-9, 10-dihydrophenanthrenes (table 8) give nematic phases at low temperatures.

* Prepared by Mr. Liebert of the Laboratoire associé au C.N.R.S. de Physique du Solide de l'Université de Paris Sud.

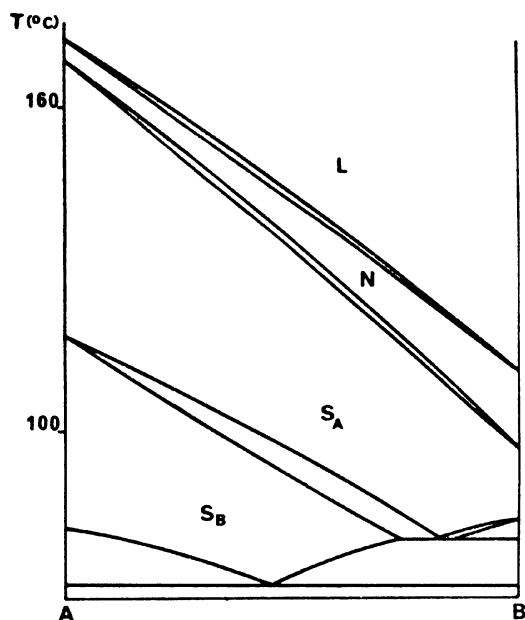


Figure 5

Isobaric phase diagram of the mixtures of 4-acetyl-(4'-butoxybenzylidene)-aniline (B) and of ethyl 4-(4'-ethoxybenzylideneamino) cinnamate (A).

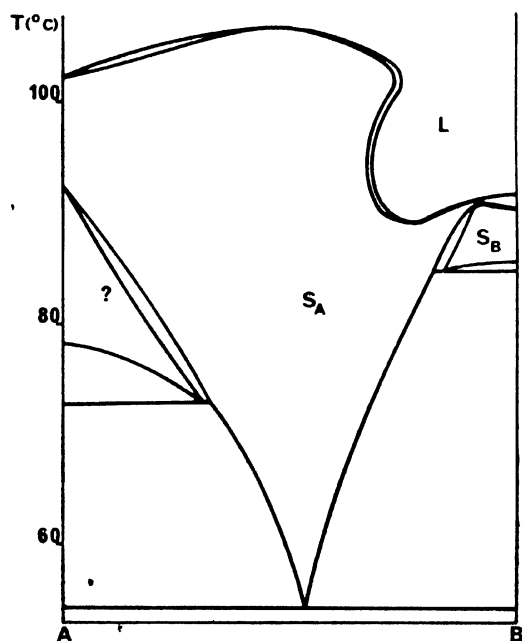
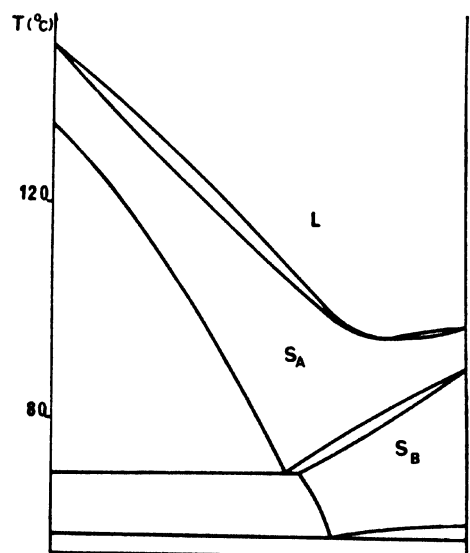
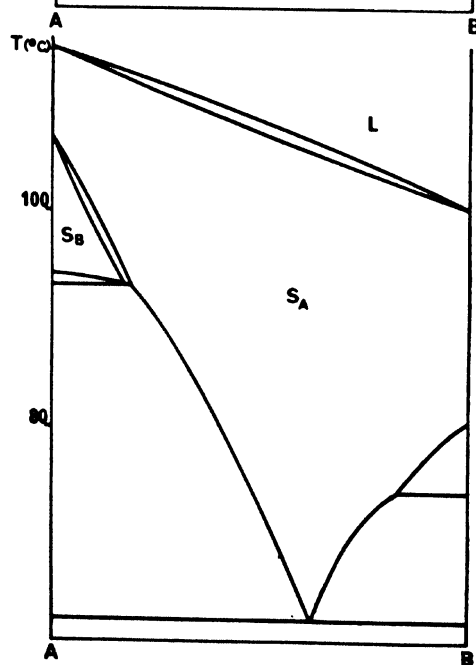


Figure 6

Isobaric phase diagram of the mixtures of 4-chloro-(4'-n-butoxybenzylidene)-aniline (B) and of 2-(3-methylhexanoyl)-7-n. dodecanoylfluorene (A).

**Figure 7**

Isobaric phase diagram of the mixtures of 4-chloro-(4'-n. hexyloxybenzylidene)-aniline (B) and of di-2-7-n. dodecanylfuorene (A).

**Figure 8**

Isobaric phase diagram of the mixtures of 2-n. nonanoyl-7-(4-methylpentyl)-fluorene(B) and of ethyl 4-(4'-methylbenzylideneamino) cinnamate (A).

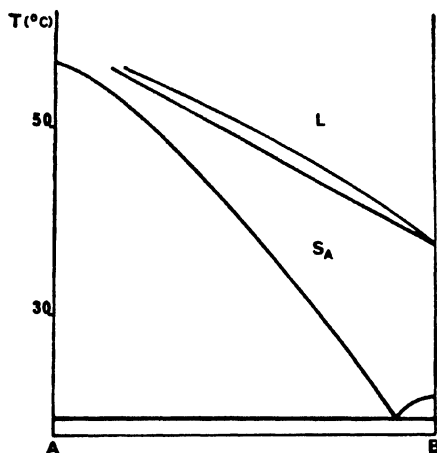


Figure 9 Isobaric phase diagram of the mixtures of 2-n. nonanoyl-7-(3-methylnonyl)-9, 10-dihydrophenanthrene (B) and of 4-n. pentyphenol-4-octyloxybenzoate (A).

6. Conclusion

Numerous fluorene and 9, 10-dihydrophenanthrene derivatives have smectic and nematic phases. A and B smectic phases have been identified. Colourless mixtures which are chemically stable and which are smectic A at room temperature are now available.

Acknowledgements

This work is supported by the Centre national de la Recherche scientifique and the Délégation générale à la Recherche scientifique et technique. We also thank Mr B Soulestin for his technical assistance.

References

- 1 KAHN F J *Appl. Phys. Lett.* **22** 111 (1973)
- 2 VAN DER VEEN J, DE JEU W H, WANNINKHOF M W M and TIENHOVEN C A M *J. Phys. Chem.* to be published
- 3 GRAY G W and IBBOTSON A *J. Chem. Soc.* 3228 (1957)
- 4 KOFLER L and KOFLER A *Thermo-Mikro Methoden* (Verlag Chemie, Weinheim) (1954)
- 5 BILLARD J *Bull. Soc. Fr. Minéral. Cristallogr.* **95** 206 (1972)
- 6 SACKMANN H and DEMUS D *Mol. Cryst. Liquid Cryst.* **21** 239 (1973)
- 7 FRIEDEL G *Ann. Phys. (Paris)* **18** 312 (1922)
- 8 GRAY G W and HARRISON K J *Mol. Cryst. Liquid Cryst.* **13** 37 (1971)
- 9 HALLER I *J. Chem. Phys.* **57** 1400 (1972)

- 10 PROUST J E, TER MINASSIAN L and GUYON E *Solid State Commun.* **11** 1227 (1972)
- 11 ARNOLD H Dissertation, Halle (1959)
- 12 DEMUS D and SACKMANN H *Z. Phys. Chem.* **238** 215 (1968)
- 13 DUBOIS J C and BILLARD J J. *Phys. (Paris)* to appear
- 14 SACKMANN H and DEMUS D *Z. Phys. Chem.* **222** 143 (1963)
- 15 VAN DER VEEN J and GROBBEN A H *Mol. Cryst. Liquid Cryst.* **15** 239 (1971)

DISCUSSION

Gray: Chemical reactions on fluorene compounds are often more complex than those on biphenyls, presumably because of the occurrence of side reactions which make products harder to purify. This could reflect a chemical instability of the fluorene ring system. However, you state that your interesting new fluorene mesogens are chemically stable. Have you any comment on this observation, and have you checked whether your materials are photochemically stable?

Billard: We have just exposed a sample of dihydrophenanthrene derivative to air and daylight for a period of six months. No change of the clearing point was observed.

Schnur: As you may know the 9-10-dihydrophenanthrenes have been used in dye lasers. Can you comment on the stability of your compounds in intense monochromatic blue near ultraviolet light.

Billard: I have not done any experiments in this field. My answer is the same as for the preceding question.

Influence of molecular structure on mixed mesomorphism in some binary systems

J S DAVE and K L VASANTH*

Chemistry Department, M. S. University of Baroda, Baroda 390002, India

Abstract. Some binary systems formed by non-liquid crystalline Schiff base components with *p*-*n*-butoxybenzoic acid and *p*-acetoxybenzal-*p*-phenetidine as liquid crystalline components are studied with a view to finding the effect of structure on mixed mesomorphism. In the case of systems with *p*-*n*-butoxybenzoic acid, although qualitatively there appears to be no change in the mode of mixed liquid crystal formation, no quantitative derivation has been possible as in the case of systems with *p*-acetoxybenzal-*p*-phenetidine, a liquid crystalline Schiff base.

Binary systems comprising liquid crystalline *p*-*n*-butoxybenzoic acid and non-liquid crystalline substituted benzoic acids are also investigated. Group slope values could be deduced from the slope of transition lines of these systems. The magnitudes of group slope values in this case are low but the order of efficiency of the end groups obtained agrees with the one obtained by Dave *et al.* In the case of binary systems, *p*-acetoxybenzal-*p*-phenetidine with *p*-methoxybenzoic acid or *p*-ethoxybenzoic acid the transition curves exhibit a tendency towards concavity.

1. Introduction

Mixed mesomorphism in binary mixtures in which one or both components are liquid crystal are known¹⁻⁹. In general, binary systems exhibiting mixed mesomorphism can be of three types: (1) where both the components are mesomorphic, (2) where only one component is mesomorphic, and (3) where both the components are non-mesomorphic. Here we describe mixed mesomorphism of the second type in which the mesomorphic component is a nematic liquid crystal. A nematic mesophase consists of long rod shaped molecules having relatively high translational freedom but only a restricted rotational freedom. A non-mesomorphic substance dissolved in such a nematic liquid will find itself in an anisotropic environment and may affect the mesomorphic characteristics of the nematic liquid crystal in an interesting manner. The extent of the disturbance caused will depend on the structural features of the added non-mesomorphic component.

* *Present Address*: Chemistry Department, P.S.G. College of Technology, Coimbatore 641004, India.

p-n-Butoxybenzoic acid is a nematic liquid crystal. Binary systems with *p-n*-butoxybenzoic acid as the mesomorphic component and Schiff bases and substituted benzoic acids as the non-mesomorphic component have been investigated. With a view to studying the effect of molecular structure on mixed liquid crystal formation, the binary mixtures of the same non-liquid crystalline compounds are studied in which *p-n*-butoxybenzoic acid is replaced by another nematic liquid crystalline component viz. *p*-acetoxybenzal-*p*-phenetidine, a Schiff base compound.

2. Materials and methods

The Schiff base compounds were prepared by refluxing equimolar quantities of the corresponding aldehydes and anilines in alcohol till the condensation was complete. The products were isolated and crystallized several times from suitable solvents like alcohol, benzene, etc. till the compounds gave sharp melting points.

p-Ethoxybenzoic acid and *p-n*-butoxybenzoic acid were prepared by boiling under reflux for nearly 2-3 hours 1 mole of *p*-hydroxybenzoic acid dissolved in 2 mole of alcoholic potassium hydroxide with 1.1 mole of the appropriate alkyl iodide. Under these conditions little or no esterification took place. The free acid liberated by the addition of conc. hydrochloric acid was crystallized from glacial acetic acid to obtain fine crystals. *p*-Ethoxybenzoic acid was obtained as white prism-like crystals, m.p. 197°C^{10} and *p-n*-butoxybenzoic acid was obtained as white shining prism-like crystals, m.p. $147^{\circ}\text{--}160^{\circ}\text{C}^{11}$.

2.1 Purification of Materials

The non-mesomorphic substituted benzoic acids studied were of pure quality obtained from B. D. H. and were purified by repeated crystallization from suitable solvents till sharp melting points were obtained.

2.2 Method of Investigation

The binary systems were investigated by the optical method of Dave and Dewar⁴. Precise measurements were, however, made with the Leitz Ortholux Polarizing microscope equipped with a Leitz heating stage.

Two series of binary systems were investigated. In the first series (A) the liquid crystalline component is *p-n*-butoxybenzoic acid and in the second series (B) the liquid crystalline component is *p*-acetoxybenzal-*p*-phenetidine. The non-liquid crystalline components common for both the series are listed in table 1, along with the respective slopes of the transition lines.

3. Results and discussion

The solid-mesomorphic and mesomorphic-isotropic transition temperatures for the binary systems of the series (A) read from the phase diagrams

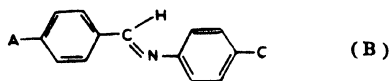
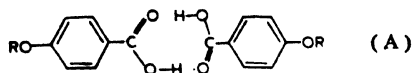


Table 1 Slopes of the transition lines for binary systems of series (A) and (B)

System No.	Non-liquid crystalline component	Slope of the transition line ($^{\circ}\text{C}/\text{mole}\% \times 10$)	
		Series (A)	Series (B)
1.	<i>p</i> -Nitrobenzal- <i>p</i> -phenetidine	5.0	1.5
2.	<i>p</i> -Anisal- <i>p</i> -anisidine	11.0	4.0
3.	<i>p</i> -Chlorobenzal- <i>p</i> -phenetidine	9.0	8.3
4.	<i>p</i> -Dimethylaminobenzal- <i>p</i> -phenetidine	13.0	6.5
5.	<i>p</i> -Anisal- <i>p</i> -chloroaniline	11.0	9.0
6.	<i>p</i> -Methoxybenzoic acid	2.0	concavity
7.	<i>p</i> -Ethoxybenzoic acid	—	concavity

are recorded in tables 2 and 3. The eutectic temperatures and the melting points of the pure components which are experimental values are given in table 2. Similar data for the series (B) except for system No. 6 and 7 have been published elsewhere⁶.

In the binary systems where the non-liquid crystalline solute molecules and the liquid crystalline solvent molecules are basically similar in shape, size and structure and also possess polar groups, mixed liquid crystal formation is greatly facilitated. Mixed liquid crystal formation takes place over a wider area and the slopes of the transition curves will be low as compared with the binary systems of dissimilar molecules⁴⁻⁶; the slope of the transition line is a measure of the tendency of the non-liquid crystalline substance towards mixed liquid crystal formation.

The molecules of *p*-*n*-butoxybenzoic acid form dimers and as can be seen below, compared with the Schiff bases they possess a more linear structure. The molecules of Schiff bases although they have essentially a linear structure, because of the central azomethine group, they will have

Table 2 Solid-mesomorphic temperatures for the binary systems of series (A). The eutectic temperatures and the m.p. of pure components are experimental values. The other temperatures were read from the phase diagrams.

System No.*	Mole % <i>p</i> - <i>n</i> -Butoxybenzoic acid										Eutectic	
	0	10	20	30	40	50	60	70	80	90	100	Mole% Temp. °C
1	123.5	121.0	118.5	116.0	113.2	110.6	108.0	112.0	121.5	133.0	147.0	64.8 107.0
2	148.0	143.2	138.2	133.5	128.6	124.0	125.0	131.0	133.0	136.2	147.0	54.9 121.5
3	123.0	119.0	115.0	111.2	107.2	105.8	110.5	115.8	122.0	130.8	147.0	47.0 104.5
4	148.0	143.2	138.5	133.5	128.2	122.8	124.5	131.4	137.0	142.2	147.0	54.5 120.0
5	92.0	90.2	88.5	100.5	110.6	119.0	124.6	127.2	128.0	134.0	147.0	19.6 88.0
6	184.0	176.6	168.5	160.5	152.0	143.0	132.5	119.8	124.5	134.0	147.0	71.5 117.5
7	196.0	191.0	185.0	177.0	164.5	149.0	138.5	130.5	129.8	132.0	147.0	75.5 126.5

* Serial numbers refer to the compounds given in table 1.

Table 3 Nematic liquid-isotropic liquid transition temperatures for binary systems of series (A). The values are read from the phase diagrams.

System No.	Mole % <i>p</i> - <i>n</i> -Butoxybenzoic acid										Triple point	
	30	40	50	60	70	75	80	85	90	95	100	Mole % Temp. °C
1	(114.6)	125.0	133.0	139.6	145.5	148.0	150.0	153.0	155.5	157.5	160.0	30.6 115.5
2	—	—	—	—	(127.2)	(131.8)	138.0	143.5	149.0	155.0	160.0	74.5 132.2
3	—	109.6	118.0	126.2	134.5	138.5	143.0	147.0	151.5	155.5	160.0	38.0 108.0
4	—	—	—	—	(125.0)	(130.2)	(136.0)	141.2	147.0	153.4	160.0	82.5 138.5
5	—	—	—	(117.5)	128.0	133.0	138.5	144.0	149.2	154.5	160.0	69.5 127.0
6	(154.5)	154.5	154.6	155.0	155.6	156.0	156.5	157.2	158.0	159.0	160.0	37.0 154.5
7	(166.0)	165.0	164.0	163.0	162.2	161.8	161.5	161.0	160.5	160.2	160.0	39.5 165.0

Values in parenthesis indicate monotropy.

Table 4 Solid-mesomorphic temperatures for the binary systems of substituted benzoic acids. The eutectic temperatures and the m.p. of pure components are experimental values. The other temperatures were read from the phase diagrams.

System No.*	Mole % <i>p</i> - <i>n</i> -Butoxybenzoic acid										Eutectic	
	0	10	20	30	40	50	60	70	80	90	100	Mole % Temp. °C
1	241.0	233.0	224.0	214.0	201.8	186.0	170.5	157.5	146.0	137.5	147.0	89.5 137.0
2	236.0	227.5	219.0	210.0	200.0	189.0	175.5	158.2	137.0	138.0	147.0	82.0 131.5
3	177.0	170.5	162.0	151.5	140.0	127.0	113.5	119.5	129.0	138.0	147.0	61.2 111.5
4	251.0	244.5	236.5	227.0	217.0	204.0	191.0	174.0	150.0	137.5	147.0	86.0 134.0
5	269.0	260.0	250.0	241.6	232.0	221.8	209.0	193.5	170.0	137.0	147.0	89.5 136.0
6	213.0	207.5	202.0	195.5	188.5	180.0	170.0	157.5	143.5	139.0	147.0	84.5 136.0

* Serial numbers refer to the compounds given in table 6.

Table 5 Nematic liquid-isotropic liquid transition temperatures for the binary systems of substituted benzoic acids. The values are read from the phase diagrams.

System No.	Mole % <i>p</i> - <i>n</i> -Butoxybenzoic acid										Triple point	
	30	40	50	60	70	75	80	85	90	95	100	Mole % Temp. °C
1	—	—	(181.0)	174.0	168.0	166.0	163.5	162.0	161.0	160.0	160.0	55.5 177.0
2	—	—	—	—	—	153.5	154.2	155.5	157.0	158.2	160.0	62.5 153.0
3	—	(139.0)	142.5	146.0	149.5	151.5	153.0	155.0	157.0	158.5	160.0	40.5 139.2
4	—	—	—	—	—	(153.5)	154.5	155.2	156.5	158.0	160.0	79.0 154.0
5	—	—	—	—	—	—	(153.0)	154.2	156.0	157.5	160.0	85.0 154.0
6	—	—	—	—	—	—	(134.0)	139.5	145.2	152.0	160.0	83.5 138.0

Values in parenthesis indicate monotropy.

some difficulty in close packing and consequent alignment with the molecules of *p-n*-butoxybenzoic acid dimers; as a result steep transition lines may be expected.

This is so in the binary systems comprising *p-n*-butoxybenzoic acid and non-mesomorphic Schiff bases in spite of the polar groups present in the latter. It is evident from the results in table 1, that the slopes of the transition lines in these binary systems differ markedly from those obtained from the study of the mixtures of the Schiff bases individually with *p*-acetoxybenzal-*p*-phenetidine, a liquid crystalline Schiff base, the two molecules being isomorphous.

An attempt to derive group slope values in the same way as in the case of binary mixtures of non-mesomorphic Schiff bases with *p*-acetoxybenzal-*p*-phenetidine and *p*-azoxyanisole separately was without any success. No quantitative derivation is possible and the order of group efficiency obtained in the cases of mixtures of non-liquid crystalline Schiff bases with liquid crystalline Schiff base, *p*-acetoxybenzal-*p*-phenetidine and with *p*-azoxyanisole⁴⁻⁶, could not be obtained in this study as the solute molecules are not similar to the molecules of the liquid crystalline component, *p-n*-butoxybenzoic acid. It should, however, be said that qualitatively there appears to be no basic difference in the nature of mixed liquid crystal formation in both the series (A) and (B).

With a view to having further evidence on mixed liquid crystal formation in mixtures of isomorphous substances, some binary systems comprising liquid crystalline *p-n*-butoxybenzoic acid and non-liquid crystalline substituted benzoic acids have been studied. The solid-mesomorphic and mesomorphic-isotropic liquid transition temperatures for these binary systems are recorded in tables 4 and 5 respectively. Both the components of the binary systems form dimers and possess identical linear structure. In such cases it should be expected that the effect of the end groups would be specific and additive giving rise to a fairly quantitative derivation. The group slope values derived from the slopes of the transition lines given in table 6 are arranged in the order of their efficiency towards mixed liquid crystal formation as under:

End Groups:	NO ₂	>	OC ₂ H ₅	>	OCH ₃	>	Cl	=	CH ₃	>	Br	>	I	>	OH
Group slopes:	—		—		1.0		1.6		1.6		1.8		2.3		7.2

The magnitudes of these group slope values are low compared with those obtained by Dave *et al.* The magnitudes of group slope values for NO₂ and OC₂H₅ groups cannot be derived in the usual manner as the transition lines show an upward trend. However, the order of efficiency of the end groups towards mixed liquid crystal formation agrees with the one obtained by Dave *et al.*⁴⁻⁶.

The difference in the magnitudes of the group slope values can be ascribed to the fact that in the case of benzoic acid mixtures, the two

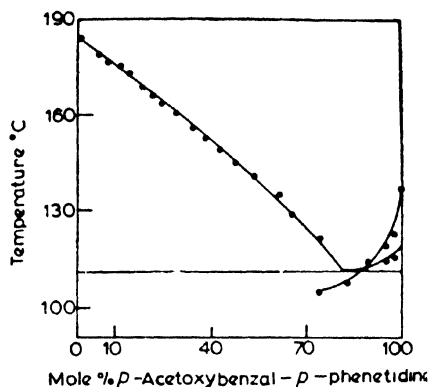


Figure 1

Mixed liquid crystal formation in the system *p*-acetoxybenzal-*p*-phenetidine : *p*-methoxybenzoic acid.

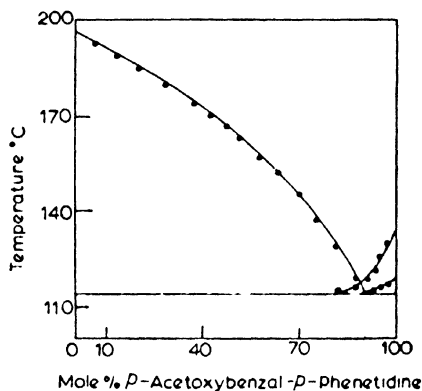


Figure 2

Mixed liquid crystal formation in the system *p*-acetoxybenzal-*p*-phenetidine : *p*-ethoxybenzoic acid.

components are comparatively linear which will contribute to the greater degree of packing between the molecules compared with the mixtures of Schiff bases and also the mixtures of Schiff bases with *p*-azoxyanisole⁴⁻⁶. Since the molecules of Schiff base compounds and *p*-azoxyanisole are not as linear as the benzoic acid molecules, it can be expected that the packing will not be as compact as in the case of benzoic acid molecules.

The study of the binary systems *p*-acetoxybenzal-*p*-phenetidine : *p*-methoxybenzoic acid and *p*-acetoxybenzal-*p*-phenetidine : *p*-ethoxybenzoic acid support the view that generally there will be a difficulty in packing of the molecules together if these are not similar. The transition curves of these systems (figures 1 and 2) exhibit a tendency towards concavity which fairly resembles the rounded minimum obtained in the system of *p*-azoxyanisole : *p*-methoxycinnamic acid of de Kock¹.

It can be said that although the magnitudes of group slope values may differ the general order of efficiency of the end groups would remain the same, provided the components of the binary systems are similar, and that the concavity in the transition curves indicates the dissimilarity of the structure of the solute and solvent molecules and hence their difficulty in packing together.

Table 6 Slopes of the transition lines for the binary systems—*p*-*n*-Butoxybenzoic acid mixed with various components:

System No.	Non-liquid crystalline component	Slopes of the transition line (°C/mole% × 10)
1	<i>p</i> -Nitrobenzoic acid	—
1a	<i>p</i> -Ethoxybenzoic acid (System No. 7, Tables 2 and 3)	—
1b	<i>p</i> -Methoxybenzoic acid (System No. 6, Tables 2 and 3)	2.0
2	<i>p</i> -Chlorobenzoic acid	3.3
3	<i>p</i> -Toluic acid	3.2
4	<i>p</i> -Bromobenzoic acid	3.6
5	<i>p</i> -Iodobenzoic acid	4.6
6	<i>p</i> -Hydroxybenzoic acid	14.5

Acknowledgement

The authors are thankful to Prof. Suresh Sethna for his keen interest in the work.

References

- 1 de KOCK A C Z. *Phys. Chem. (Leipzig)* **48** 129 (1904)
- 2 BOGOJAWLENSKY A and WINOGRADOW N Z. *Phys. Chem. (Leipzig)* **60** 433 (1907); **64** 229 (1908)
- 3 WALTER R. *Chem. Ber.* **58B** 2303 (1925)
- 4 DAVE J S and DEWAR M J S *J. Chem. Soc.* 4616 (1954); 4305 (1955)
- 5 DAVE J S and LOHAR J M *Proc. Nat. Acad. Sci. India* **29A** (Part I) 35 (1960); **29A** (Part III) 260 (1960); **32A** (Part II) 105 (1962); *Indian J. Chem.* **4** 386 (1966); *J. Chem. Soc.* 1473 (1967)
- 6 DAVE J S, PATEL P R and VASANTH K L *Mol. Cryst.* **2** 125 (1966); *Indian J. Chem.* **4** 505 (1966); **7** 498 (1969); *Mol. Cryst. Liquid Cryst.* **8** 69 (1969); *J. Indian Chem. Soc.* **47** 815 (1970)

- 7 GIBSON H W and POCHAN J M Paper presented at the Fourth International Liquid Crystal Conference, Kent State University, Kent, Ohio, 1972 ; Abstract No. 160.
- 8 CHISTYAKOV I G and GUSAKOVA L A *Kristallografiya* **14** 153 (1969)
- 9 LAWRENCE A S C *Liquid crystals and ordered fluids* (Plenum Press, New York) p. 289 (1970)
- 10 BENNETT G M and JONES B J. *Chem. Soc.* 420 (1939)
- 11 GRAY G W and JONES B J. *Chem. Soc.* 4179 (1953)

DISCUSSION

Demus : In binary systems in nearly ideal cases the clearing points are connected by a straight line. Therefore the efficiency of order concerning the slope of this curve should be the same as it determines the clearing point of the second compound (also if this clearing point is monotropic). Have you compared this efficiency of order of the groups with the values given in Gray's book ?

Vasanth : Yes, the order of the groups is broadly similar.

Sarma : What are the mixing ratios of the two components ?

Vasanth : The mixing ratio of the two components varied from 0 to 100%.

Mesomorphic behaviour of cholesteryl esters

V. Cholesteryl 6-*n*-alkoxy-2-naphthoates

J S DAVE and GEORGE KURIAN

Chemistry Department, M. S. University of Baroda, Baroda 390002, India.

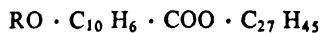
Abstract. A homologous series of thirteen esters of cholesterol was synthesised by reacting 6-*n*-alkoxy-2-naphthoyl chlorides with cholesterol. All the esters are enantiotropic cholesteric with large phase length. The smectic phase commences at the pentyloxy derivative. The higher members exhibit both smectic and cholesteric mesophases. The cholesteric - isotropic transition points lie on two falling curves, one for odd and the other for even numbers of carbon atoms in the alkoxy chain. The smectic-cholesteric transition points lie on a smooth curve which rises to a maximum and then falls off. The thermal stabilities of the present series are compared with those of other related homologous series.

1. Introduction

The unique structure of the cholesteric liquid crystals gives rise to a number of optical properties not exhibited by the nematic and smectic liquid crystals; it is because of such properties that these compounds find very many applications. Not much work has been done till recently on the synthesis of aryl esters of cholesterol. Dave *et al.* studied the liquid crystalline behaviour of homologous series of *p-n*-alkoxybenzoates¹ *trans-p-n*-alkoxycinnamates², *p-n*-alkoxybenzylidene-*p'*-aminobenzoates³ and 4-*n*-alkoxy-1-naphthoates of cholesterol⁴. They have also reported the mesomorphic behaviour of a number of 4-*n*-alkoxy-1-naphthylidene Schiff base compounds⁵⁻⁷. Wiegand studied the influence of the position of substituents in dianisal-diamino naphthalenes on mesomorphism⁸. In another study Gray and Jones observed that 6-*n*-alkoxy-2-naphthoic acids are mesomorphic whereas the 7-*n*-alkoxy-2-naphthoic acids and 4- and 5-*n*-alkoxy-1-naphthoic acids are non-mesomorphic⁹. These studies show that there exists a relationship between the position of the substituent in a naphthalene moiety and the tendency of the molecules to exhibit mesomorphism. Here we present the mesomorphic behaviour of 6-*n*-alkoxy-2-naphthoates of cholesterol.

2. Results and discussion

A homologous series of thirteen esters of cholesterol was synthesized by reacting 6-*n*-alkoxy-2-naphthoyl chlorides with cholesterol. The melting points and transition temperatures are compiled in table 1.

Table 1 Cholesteryl-6-*n*-alkoxy-2-naphthoates

Compound	R	Transition temperature (°C)		
		C - S	C - Ch	Ch - I
			or S - Ch	
1	CH ₃	—	183.0	302.5
2	C ₂ H ₅	—	198.0	310.0
3	C ₃ H ₇	—	184.0	287.5
4	C ₄ H ₉	—	193.0	290.5
5	C ₅ H ₁₁	174.0	179.5	278.0
6	C ₆ H ₁₃	158.0	196.0	278.0
7	C ₇ H ₁₅	149.5	211.5	266.5
8	C ₈ H ₁₇	151.0	224.5	268.0
9	C ₉ H ₁₉	153.0	226.0	264.5
10	C ₁₀ H ₂₁	140.5	230.5	258.0
11	C ₁₂ H ₂₅	142.0	230.0	248.0
12	C ₁₆ H ₃₃	117.0	216.5	229.0
13	C ₁₈ H ₃₇	110.0	208.0	221.0

All these esters are enantiotropic cholesteric. The smectic phase commences at the pentyloxy derivative. Even the last member of the series shows both smectic and cholesteric mesophases. All the compounds give plane cholesteric texture. At the juncture of the smectic-cholesteric transition a colour change is observed both while heating and cooling. In the last two members the focal conic smectic texture turns to a homeotropic texture on heating. When the cholesteric-isotropic transition points are plotted against the number of carbon atoms in the alkoxy chain they show the odd-even effect, as exhibited by other mesomorphic homologous series. The smectic-cholesteric transition points lie on a smooth curve which rises to a maximum at decyloxy derivative and then falls off (figure 1).

In the corresponding 4-*n*-alkoxy-1-naphthoates of cholesterol¹⁴ the methoxy and octyloxy to octadecyloxy derivatives are enantiotropic cholesteric, the rest being monotropic cholesteric; the smectic phase appears at the dodecyloxy derivative as a monotropic phase and persists as such upto the octadecyloxy derivative, the last member investigated. These two series are structurally similar, the only difference being the substitution in the naphthalene nucleus.

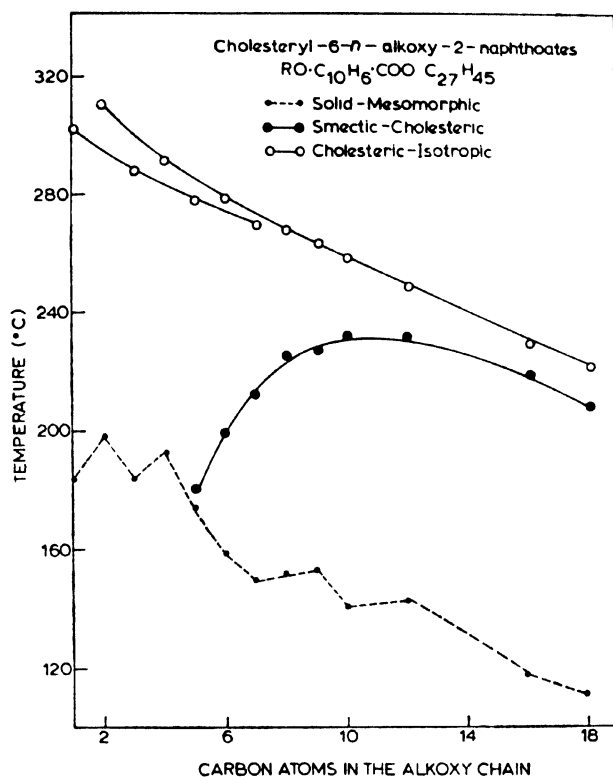
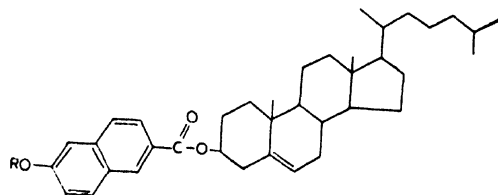


Figure 1 Transition temperature as a function of the number of carbon atoms in the alkyl chain.

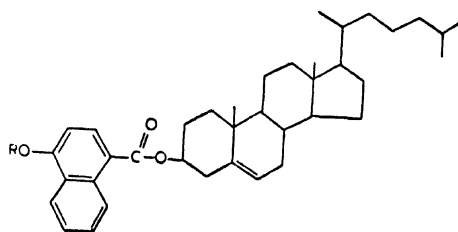
The thermal stabilities of the present series (A) are compared with those of the following series:

- (1) 4-*n*-alkoxy-1-naphthoates of cholesterol⁴ — (B)
- (2) *trans-p-n*-alkoxycinnamates of cholesterol² — (C)
- (3) *p-n*-alkoxybenzoates of cholesterol¹ — (D)

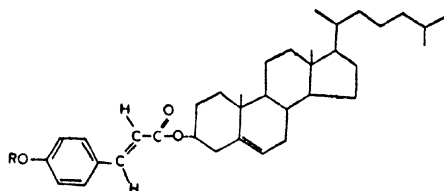
The average thermal stabilities and the comparative geometry of these series are given in table 2.



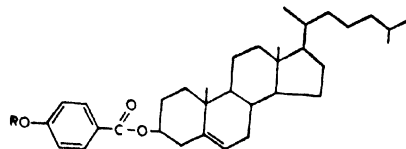
A



B



C



D

Table 2 Average transition temperature (°C)

	A	B	C	D
Cholesteric-Isotropic (C ₁ -C ₁₈)	269.0	159.8	251.8	224.0
Smectic-Cholesteric (C _{12,16,18})	218.2	98.5	176.6	170.3
Commencement of the smectic phase	C ₃	C ₁₂	C ₁₀	C ₇

The mesophases of series (A) are thermally more stable than those of series (D). Compared to series (D) the former is more polarized and a little longer; even though the breadth of the molecules of series (A) may be increased a little, this will be compensated by the increase in length. Thus the thermal stabilities of both the mesophases are increased almost to the same extent.

The mesophases of series (C) are thermally less stable than those of series (A), the decrease in thermal stability being more pronounced in the smectic phase than in the cholesteric phase. The cholesteric thermal stability of series (A) is higher by 17°C compared to the smectic one which is higher by 41°C. Gray has reported that 6-*n*-alkoxy-2-naphthoic acids and *trans-p-n*-alkoxycinnamic acids are similar in shape and size⁹. The molecules of 6-*n*-alkoxy-2-naphthoates of cholesterol should therefore be similar in shape and size to those of *trans-p-n*-alkoxycinnamates of cholesterol, and therefore the effect should be similar on the two mesophases. But series (A) contains one more aromatic ring compared to the ethylenic bond in series (C), *trans-p-n*-alkoxycinnamates of cholesterol. This makes the molecule of series (A) more polarizable and consequently more mesomorphic. However the effect is, as noted above, more pronounced on the smectic thermal stability compared to the cholesteric one. The reason may be that the ethylenic bond in *trans-p-n*-alkoxycinnamates of cholesterol makes the close packing of the molecules more difficult and thus the lateral attractions will be reduced more, which in turn will reduce the thermal stability of the smectic phase.

Structurally series (A) and (B) are similar but in thermal stabilities they differ the most. The two series differ in the position of the substituents in the naphthalene nucleus, the carboxy and alkoxy groups being

at 2- and 6-positions in series (A) whereas they are at 1- and 4-positions in series (B). The 2, 6 substitution in the naphthalene nucleus makes the molecule linear whereas 1, 4 substitution makes the molecule a little broad. The changes in the chemical constitution of a mesomorphic compound can radically alter the mesomorphic properties of the compound. The increase in the intermolecular separation due to the size of a substituent will decrease the mesomorphic thermal stabilities, the smectic mesophase often being affected more. But here, in the case of series (B), the thermal stabilities of both the phases are almost equally affected. This is because molecules of series (A) are a little longer and the substitution at the 2, 6 positions in the naphthalene nucleus brings about the separation of the dipolar parts of the molecule, which makes the molecules of series (A) more polarizable. This will almost compensate the little breadth increasing effect in the molecules of series (B) and both cholesteric and smectic thermal stabilities of series (A) are increased almost equally.

The smectic mesophase commences rather early, *i.e.*, at the pentyl ether in series (A). This is much earlier than in all other known cholesteryl ester series. It is rather difficult to predict the exact commencement of the smectic mesophase in a mesomorphic homologous series, but the survey of different homologous series reveals that the increase in the breadth delays the commencement of the smectic phase. The earlier commencement of the smectic phase in the present series than in series (B), (C) and (D) is to be expected. Series (B) is broader than series (A) and so the commencement of smectic phase should naturally be delayed and it is at the twelfth member. Series (C) is almost equal in length and breadth to series (A) but the polarizability of series (C) is much less than that of series (A). This delays the commencement of the smectic phase in series (C) which is at the tenth member. Series (D) is short in length and less polarizable than series (A), which would decrease thermal stabilities and also delay the commencement of the smectic phase. But series (A) is a little broader than series (D) and so the commencement of smectic phase in series (D) is not delayed to a great extent; it commences at the seventh member.

3. Experimental

3.1 Transition temperatures

Preliminary measurements were made by the optical method of Dave and Dewar¹⁰. The precise measurements were however made by Leitz Ortholux Polarizing Microscope equipped with a Leitz heating stage. The temperature of the sample was raised gradually and within the critical region of the transition temperature to be noted the heating was regulated at 2°C per minute.

3.2 Preparation of compounds

6-Acetyl-2-methoxy naphthalene was prepared by the method of Robinson and Rydon¹¹.

Different 6-*n*-alkoxy-2-naphthoic acids were prepared according to the method of Gray and Jones¹², from 6-acetyl-2-methoxy naphthalene. The melting points and transition temperatures agree with the reported ones.

6-*n*-Alkoxy-2-naphthoyl chlorides were prepared by treating the corresponding alkoxy naphthoic acids with excess of thionyl chloride and a drop of pyridine and heating on a water bath till the evolution of the hydrogen chloride gas ceases. Excess thionyl chloride was distilled off under reduced pressure using a water pump.

6-*n*-Alkoxy-2-naphthoates of cholesterol: Equimolecular proportions of cholesterol (0.005 mol) and the acid chloride were dissolved in dimethylaniline (10 ml) and heated at 150°C in a round bottom flask in an oil bath for about two hours. The mass was then added to crushed ice. The precipitate was then washed with dilute H₂SO₄ followed by water. The crude product was dried and crystallized from chloroform-alcohol mixture (1 : 1) to fine white needles. The transition temperatures are given in table 1 and the analytical data recorded in table 3.

Table 3 Cholesteryl-6-*n*-alkoxy-2-naphthoates

Compound	Molecular Formula	% Required		% Found	
		C	H	C	H
1	C ₃₉ H ₅₄ O ₃	82.06	9.54	82.35	9.37
2	C ₄₀ H ₅₆ O ₃	82.14	9.65	82.04	9.26
3	C ₄₁ H ₅₈ O ₃	82.24	9.76	82.08	9.40
4	C ₄₂ H ₆₀ O ₃	82.28	9.86	82.21	9.39
5	C ₄₃ H ₆₂ O ₃	82.35	9.96	82.31	9.88
6	C ₄₄ H ₆₄ O ₃	82.43	10.07	82.13	9.92
7	C ₄₅ H ₆₆ O ₃	82.51	10.16	82.22	10.00
8	C ₄₆ H ₆₈ O ₃	82.58	10.25	82.54	10.21
9	C ₄₇ H ₇₀ O ₃	82.62	10.33	82.49	9.86
10	C ₄₈ H ₇₂ O ₃	82.70	10.41	82.71	10.13
11	C ₅₀ H ₇₆ O ₃	82.80	10.57	82.79	10.32
12	C ₅₄ H ₈₄ O ₃	82.96	10.84	82.94	10.36
13	C ₅₆ H ₈₈ O ₃	83.12	10.96	83.20	10.57

Acknowledgements

The authors are thankful to the Gujarat State Industrial Research Committee, Ahmedabad, for providing a Research Grant to one of us (G.K.). The authors are also thankful to Prof. Suresh Sethna for his keen interest in the work.

References

- 1 DAVE J S and VORA R A *Liquid crystals and ordered fluids* (Plenum Press, New York) p. 477 (1970)
- 2 DAVE J S and VORA R A *Mol. Cryst. Liquid Cryst.* **14** 319 (1971)
- 3 DAVE J S and KURIAN G Fourth International Liquid Crystal Conference, Kent State University, Kent, Ohio, 1972, *Mol. Cryst. Liquid Cryst.* **24** 347 (1973)
- 4 DAVE J S and VORA R A Unpublished work
- 5 DAVE J S, KURIAN G, PRAJAPATI A P and VORA R A *Mol. Cryst. Liquid Cryst.* **14** 307 (1971)
- 6 DAVE J S, KURIAN G, PRAJAPATI A P and VORA R A *Curr. Sci.* **41** 415 (1972)
- 7 DAVE J S, KURIAN G, PRAJAPATI A P and VORA R A *Indian J. Chem.* **10** 754 (1972)
- 8 WIEGAND C Z. *Naturforsch.* **9b** 516 (1954)
- 9 GRAY G W and JONES B *J. Chem. Soc.* 683 (1954)
- 10 DAVE J S and DEWAR M J S *J. Chem. Soc.* 4616 (1954)
- 11 ROBINSON R and RYDON H N *J. Chem. Soc.* 1394 (1939)
- 12 GRAY G W and JONES *J. Chem. Soc.* 678 (1954)

**Mesomorphic behaviour of schiff base compounds - IV :
N,N'-Di(4-*n*-alkoxy-1-naphthylidene)*p*-azoanilines and
N(4-*n*-alkoxy-1-naphthylidene)-4'-aminoazobenzenes**

J S DAVE, and A P PRAJAPATI

Chemistry Department, M.S. University, Baroda 390002, India.

Abstract. Two mesomorphic homologous series containing a naphthalene nucleus and an azo group have been prepared by condensing different 4-*n*-alkoxy-1-naphthaldehydes with *p*-azoaniline and 4-aminoazobenzene and their mesomorphic behaviour studied.

In series I, N,N'-di(4-*n*-alkoxy-1-naphthylidene)*p*-azoanilines, all the members exhibit enantiotropic nematic mesomorphism. The smectic phase commences from the dodecyl derivative as a monotropic phase; tetra-, hexa- and octadecyl derivatives are enantiotropic smectic and nematic. In series II, N(4-*n*-alkoxy-1-naphthylidene)-4'-aminoazobenzenes, the first three members are non-mesomorphic. Butyl to heptyl, hexadecyl and octadecyl derivatives are monotropic nematic; the others are enantiotropic nematic. Tetradecyl to octadecyl derivatives exhibit a smectic phase which is monotropic in nature.

The plots of transition temperatures against the number of carbon atoms in the alkyl chain in series I behave in a normal manner whereas those in series II show an ascending tendency. The thermal stabilities and the commencements of the smectic phases of the two series are compared with those of other related series.

1. Introduction

Mesomorphic properties of some homologous series of Schiff bases containing a naphthalene nucleus are known. Wiegand prepared and studied liquid crystalline properties of 1:4, 2:6 and 1:5 anisilidene amino-naphthalenes¹. Dave *et al.* reported the mesomorphic behaviour of homologous series obtained by condensing 4-*n*-alkoxy-1-naphthaldehydes with benzidine², *p*-phenylenediamine³ and *p*-aminobenzoic acid⁴. Arora and Ferguson studied a benzylidene Schiff base series containing an azo group⁵. It was thought that the introduction of an azo group in naphthylidene Schiff base series would be interesting and therefore the series N, N'-di(4-*n*-alkoxy-1-naphthylidene)*p*-azoanilines and N(4-*n*-alkoxy-1-naphthylidene)-4'-aminoazobenzenes were synthesised and their mesomorphic behaviour studied.

2. Results and discussion

Series I

A homologous series of fourteen Schiff bases was prepared by condensing 4-*n*-alkoxy-1-naphthaldehyde with *p*-azoaniline. The melting points and transition temperatures are compiled in table 1.

Table 1 N, N'-di(4-*n*-Alkoxy-1-naphthylidene)*p*-azoanilines RO · C₁₀H₆ · CH : N · C₆H₄ · N : N · C₆H₄ · N : CH · C₁₀H₆ · OR

Compound	R	Temperatures of transition (°C)		
		C-S	C-N or S-N	N-I
1	CH ₃	—	278.5	310.0
2	C ₂ H ₅	—	291.0	320.0
3	C ₃ H ₇	—	241.0	311.5
4	C ₄ H ₉	—	243.0	315.5
5	C ₅ H ₁₁	—	228.5	301.0
6	C ₆ H ₁₃	—	227.5	297.0
7	C ₇ H ₁₅	—	217.5	277.0
8	C ₈ H ₁₇	—	207.5	269.5
9	C ₉ H ₁₉	—	190.5	255.0
10	C ₁₀ H ₂₁	—	183.5	246.0
11	C ₁₂ H ₂₅	(164.5)	172.0	227.5
12	C ₁₄ H ₂₉	162.5	175.0	213.0
13	C ₁₆ H ₃₃	154.0	178.5	201.5
14	C ₁₈ H ₃₇	144.5	178.0	191.5

Value in parenthesis indicates monotropy.

All the members in this series exhibit enantiotropic nematic mesomorphism. The smectic phase commences at the dodecyl derivative as a monotropic phase. Tetra-, hexa- and octadecyl derivatives are enantiotropic smectic and nematic. When the transition points are plotted against the number of carbon atoms in the alkyl chain (figure 1), the nematic-isotropic transition points lie on two falling curves which exhibit the odd-even effect, the even members occupying the upper curve as usual. The smectic-nematic curve rises smoothly to a maximum through the hexadecyl derivative and then levels off. It does not merge with the nematic-isotropic curve. In the corresponding benzidine series the last two members, the hexadecyl and octadecyl derivatives, are purely smectic. The two series differ in the central group. The benzidine series has a biphenyl central group whereas the present series contains an azobenzene

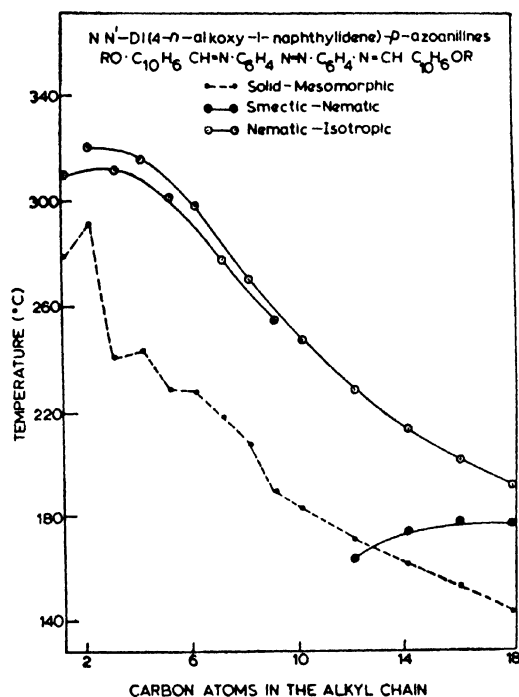
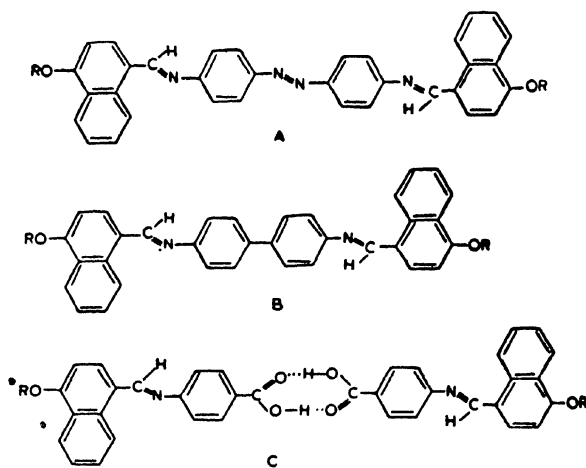


Figure 1 Transition temperatures as a function of numbers of carbon atoms in the alkyl chain.



central group. The absence of a pure smectic phase in the last members of the present azoaniline series can be due to the presence of the azo group which probably makes the present series less linear than the corresponding benzidine series.

Table 2 summarizes the average thermal stabilities and the commencement of the smectic phase of the following series: N, N'-di (4-*n*-alkoxy-1-naphthylidene) *p*-azoanilines (A), N, N'-di (4-*n*-alkoxy-1-naphthylidene) benzidines (B)² and 4-*n*-alkoxy-1-naphthylidene-*p*-amino-benzoic acids (C)⁴.

Table 2 Average thermal stabilities (°C)

			A	B	C
Nematic	—	Isotropic	280.0	269.0	26.0
C ₄	—	C ₁₀			
Smectic-Nematic or Isotropic			178.0	194.5	175.0
C ₁₆	—	C ₁₈			
Commencement of smectic phase			C ₁₂	C ₉	C ₁₂

Series (A) and (B) provide an interesting comparison. As discussed above the molecules of the two series differ in only one respect; the series (A) contains an additional azo group in the centre of the molecule. This group will make the molecule of series (A) more polarizable but at the same time less linear than that of series (B). It is, therefore, not surprising that the nematic thermal stability of series (A) is increased by 11° C due to the higher polarizability and increased length of the molecule. The reduction in the smectic thermal stability of series (A) by about 16.5° C can be attributed to the increased breadth of the molecule due to the presence of the azo group.

Compared to series (C) (dimer) both the thermal stabilities of the present series are higher. The nematic thermal stability is increased by 64.0° C whereas the smectic thermal stability is increased by only 3.0° C. It can be seen from the geometry of the molecules that the two series are almost of the same length but the series (C) contains a central dimerised carboxyl group whereas series (A) has a central -N=N- group. The azo (-N=N-) group makes a fully conjugated system, whereas the hydrogen bond in the acid dimer in series (C) will not transmit the effect of conjugation in the two dimer units and thus the series (A) will be more polarizable than series (C). Thus both the thermal stabilities in the series (A) should be increased, but the increase in smectic thermal

stability is much less compared to the increase in nematic thermal stability. This may be attributed to the presence of $-N=N-$ group in series (A) which makes its molecules thick and broad due to reduced linearity and the breadth has a more pronounced effect on the smectic phase.

The smectic mesophase in the present series commences at the dodecyl derivative only. In series (B) it makes its appearance at nonyl derivative. This delay in the appearance of the smectic phase is expected as the series (A) is less linear and thick compared to series (B). The increased breadth not only reduces the smectic thermal stability but also delays the commencement of the smectic phase. The smectic phase appears at the twelfth member for both the series (A) and (C). The smectic thermal stabilities of the two series are almost the same and it should not be surprising that the commencement of the smectic phase in two series should coincide.

Series II

Series II consists of a homologous series of Schiff base compounds obtained by condensing 4-*n*-alkoxy-1-naphthaldehydes with 4-aminoazobenzene. The melting points and transition temperatures of these compounds are compiled in table 3.

Table 3 N(4-*n*-alkoxy-1-naphthylidene)4'-aminoazobenzenes
 $RO \cdot C_{10}H_6 \cdot CH : N \cdot C_6H_4 \cdot N : N \cdot C_6H_5$

Compound	R	Temperatures of transition(°C)		
		C-S	C-N or S-N	N-I
15	CH ₃	—	* (47.5)	132.5
16	C ₂ H ₅	—	* (97.0)	145.5
17	C ₃ H ₇	—	* (78.0)	123.0
18	C ₄ H ₉	—	(103.0)	125.5
19	C ₅ H ₁₁	—	(91.5)	107.5
20	C ₆ H ₁₃	—	(105.0)	117.0
21	C ₇ H ₁₅	—	(99.0)	104.0
22	C ₈ H ₁₇	—	97.5	103.5
23	C ₉ H ₁₉	—	86.0	100.0
24	C ₁₀ H ₂₁	—	89.5	102.0
25	C ₁₂ H ₂₅	—	91.5	100.5
26	C ₁₄ H ₂₉	(53.5)	94.5	98.0
27	C ₁₆ H ₃₃	(67.5)	(95.5)	97.0
28	C ₁₈ H ₃₇	(73.5)	(92.0)	95.0

Values in parenthesis indicate monotropy.

*Values obtained by extrapolation of the curves.

In this series the first three members are non-mesomorphic. Butyl to heptyl derivatives are monotropic nematic ; Octyl to tetradecyl derivatives are enantiotropic nematic and the last two members investigated, hexadecyl and octadecyl derivatives are monotropic nematic. The tetradecyl to octadecyl derivatives exhibit a monotropic smectic phase.

The plots of nematic-isotropic transitions against the number of carbon atoms in the alkyl chain show a marked odd-even effect (figure 2). It is interesting to note that this curve shows an ascending tendency in the beginning as the alkyl chain is increased and then it falls off slightly towards the end of the series. The nematic-isotropic curves are extrapolated and the obscure transition temperature values are obtained for methyl to propyl derivatives. These values lie well below the crystallization points of these compounds and that is probably the reason why these members are non-mesomorphic.

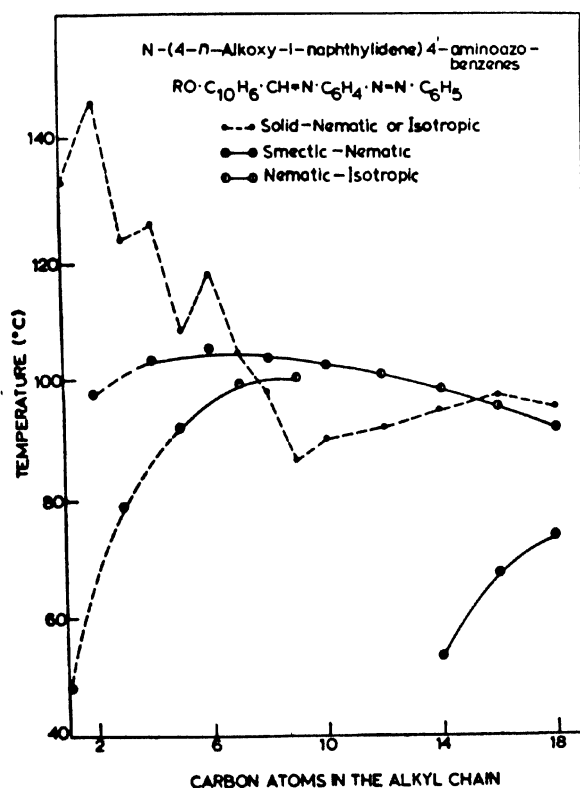


Figure 2 Transition temperatures as a function of number of carbon atoms in the alkyl chain.

The ascending tendency of the nematic-isotropic transition curve of this series may be attributed to two reasons:

1. These molecules are short and broad. The reduction in the length to breadth ratio makes the close packing of the molecules comparatively difficult and as the alkyl chain is lengthened the increased polarizability makes the mesophase thermally more stable thus giving rise to an ascending tendency of the mesomorphic-isotropic curve. After it reaches a maximum value further increase in the alkyl chain reduces the end to end cohesions and the curve levels up or shows a falling tendency⁶.

2. As the alkyl group is attached to one end of the molecule only, it is imbalanced⁷. Thus the thermal stability of the mesophase is low.

This type of nematic-isotropic curve is also observed in the series 4-*n*-alkoxy-1-naphthylidene-*p*-phenitidines⁸. Here also the molecules are short and broad and at the same time imbalanced due to the difference in the end chains.

It should be mentioned here that Weygand has reported such a behaviour in the series N(*p*-*i*-alkoxybenzylidene)-1'-aminonaphthalene-4'-azobenzenes⁹.

Table 4 summarizes the average thermal stabilities of the following series: 4-*n*-alkoxy-1-naphthylidene-*p*-aminoazobenzenes (D), *p*-*n*-alkoxybenzylidene-*p*-aminoazobenzenes (E) and 4-*n*-alkoxy-1-naphthylidene-*p*-azoanilines (A).

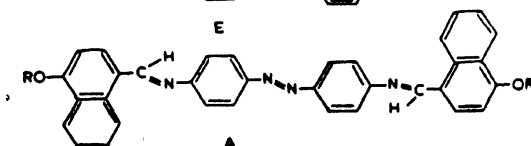
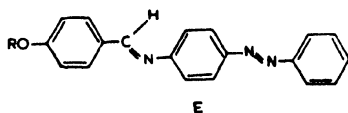
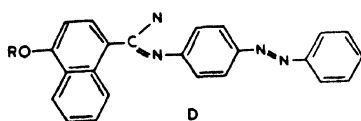


Table 4 Average thermal stabilities

			D	E	A
Nematic	—	Isotropic	100.5	170.0	280.0
C ₄	—	C ₁₀			
Smectic-Nematic or Isotropic			70.5	151.0	178.0
C ₁₆	—	C ₁₈			
Commencement of smectic phase			C ₁₄	C ₄	C ₁₂

Both the nematic and smectic thermal stabilities of series (D) are less than those of series (E). This is expected as the two series have the same structure except for the naphthalene nucleus in the molecules of series (D) in place of benzylidene part of the molecules in series (E). The naphthalene nucleus increases the breadth of the molecule, thus reducing both the thermal stabilities.

Compared to series (A), the series (D) is short and less polarizable and naturally the thermal stabilities of series (D) will be less than those of series (A). Actually the nematic thermal stability is affected more than the smectic one. The second naphthalene nucleus in series (A) increases the breadth of the molecules and thus the average smectic thermal stability of series (A) is not increased to the same extent as the nematic thermal stability, the breadth having a more pronounced effect on the smectic phase.

The smectic phase appears very late in the series (D) at the tetradecyl derivative compared to the butyl derivative in the case of series (E). The naphthalene nucleus makes the close packing of the molecules more difficult and reduces the lateral attractions to a considerable extent, thus delaying the commencement of the smectic phase. In series (A) the smectic phase commences at the twelfth member. Series (A) is much longer and more polarizable than series (D), but the molecules of series (A) because of the two naphthalene units, will be a little broader than those of series (D) and therefore, the commencement of the smectic phase in series (A) is a little delayed upto the dodecyl derivative.

3. Experimental

Determination of transition temperatures

Preliminary measurements were made by the optical method of Dave and Dewar¹⁰. The precise measurements were, however, made by the Leitz Ortholux Polarizing microscope equipped with a heating stage. The

temperature in the neighbourhood of the transitions to be noted, was raised at the rate of two degrees per minute and the temperatures for various transitions were recorded by standard thermometers.

Preparation of compounds

4-*n*-alkoxy-1-naphthaldehydes were prepared as reported earlier².

p-azoaniline

(a) *p*-azonitrobenzene from *p*-nitroaniline¹¹. 5 g of *p*-nitroaniline were dissolved in 12.5 ml of concentrated sulphuric acid and diluted to 55 ml with water and 20 g of potassium persulphate were added to it in small portions at 60–70° C. After one hour the brown precipitates were obtained which were collected by filtration. They contained some *p*-dinitrobenzene. This was removed by steam distillation. The residue was recrystallized from glacial acetic acid and then from toluene to orange needles, m.p. 216° C; yield 50%.

(b) *p*-azoaniline from *p*-azonitrobenzene¹²: A mixture of 10 g of *p*-azonitrobenzene, 100 g of crystalline sodium sulphide, 100 ml of water and 300 ml of alcohol was refluxed for half an hour. The precipitated mass was filtered hot. It was recrystallized from ethyl alcohol to orange needles, m.p. 246° C; yield 40%.

Schiff bases

N,N'-di(4-*n*-alkoxy-1-naphthylidene)*p*-azoaniline Schiff base compounds were prepared by refluxing 4-*n*-alkoxy-1-naphthaldehydes (2.0 mol) with *p*-azoaniline (1.0 mol) in ethyl alcohol for about one hour and recrystallizing the product several times from nitrobenzene or chloroform into fine needles or plates, which gave sharp melting points and transition temperatures. The analytical data are summarized in table 5. Yield was about 70%.

Table 5 N,N'-di(4-*n*-alkoxy-1-naphthylidene)*p*-azoanilines

Compound	Molecular formula	% Required N	% Found N
1	C ₃₆ H ₂₈ O ₂ N ₄	10.22	10.00
2	C ₃₈ H ₃₂ O ₂ N ₄	9.72	9.69
3	C ₄₀ H ₃₆ O ₂ N ₄	9.27	9.26
4	C ₄₂ H ₄₀ O ₂ N ₄	8.86	8.90
5	C ₄₄ H ₄₄ O ₂ N ₄	8.49	8.22
6	C ₄₆ H ₄₈ O ₂ N ₄	8.14	8.03
7	C ₄₈ H ₅₂ O ₂ N ₄	7.82	7.56

Compound	Molecular formula	% Required N	% Found N
8	C ₅₀ H ₅₆ O ₂ N ₄	7.53	7.20
9	C ₅₂ H ₆₀ O ₂ N ₄	7.25	7.00
10	C ₅₄ H ₆₄ O ₂ N ₄	7.00	6.82
11	C ₅₈ H ₇₂ O ₂ N ₄	6.54	6.45
12	C ₆₂ H ₈₀ O ₂ N ₄	6.14	6.12
13	C ₆₆ H ₈₈ O ₂ N ₄	5.79	5.56
14	C ₇₀ H ₉₆ O ₂ N ₄	5.47	5.23

N(4-*n*-alkoxy-1-naphthylidene)4'-aminoazobenzenes were prepared by refluxing equimolecular amounts of 4-*n*-alkoxy-1-naphthaldehydes and 4-aminoazobenzene in ethyl alcohol for about one hour. The product was crystallized from acetone into fine needles or plates which gave sharp melting points and transition temperatures. The analytical data are summarized in table 6. Yield was about 75%.

Table 6 N(4-*n*-alkoxy-1-naphthylidene)4'-aminoazobenzenes

15	C ₂₄ H ₁₉ ON ₃	11.50	11.59
16	C ₂₅ H ₂₁ ON ₃	11.09	10.69
17	C ₂₆ H ₂₃ ON ₃	10.69	10.76
18	C ₂₇ H ₂₅ ON ₃	10.31	10.47
19	C ₂₈ H ₂₇ ON ₃	9.97	9.93
20	C ₂₉ H ₂₉ ON ₃	9.65	9.32
21	C ₃₀ H ₃₁ ON ₃	9.35	9.04
22	C ₃₁ H ₃₃ ON ₃	9.07	9.14
23	C ₃₂ H ₃₅ ON ₃	8.80	9.10
24	C ₃₃ H ₃₇ ON ₃	8.55	8.49
25	C ₃₅ H ₄₁ ON ₃	8.09	7.95
26	C ₃₇ H ₄₅ ON ₃	7.68	7.99
27	C ₃₉ H ₄₉ ON ₃	7.30	7.27
28	C ₄₁ H ₅₃ ON ₃	6.97	6.61

Acknowledgement

The authors are thankful to Prof. Suresh Sethna for his keen interest in the work.

References

- 1 WIEGAND C Z *Naturforsch* 9b 516 (1954)
- 2 DAVE J S, KURIAN G, PRAJAPATHI A P and VORA R A *Mol. Cryst. Liquid Cryst.* 14 307 (1971)
- 3 DAVE J S, KURIAN G, PRAJAPATHI A P and VORA R A *Curr. Sci.* 41 415 (1972)
- 4 DAVE J S, KURIAN G, PRAJAPATHI A P and VORA R A *Indian J. Chem.* 10 754 (1972)
- 5 ARORA S L and FERGASON J L *Simp. Faraday Soc. No. 5 Liquid Crystals* p. 97 (1971)
- 6 GRAY G W *Molecular structure and the properties of liquid crystals* (Academic Press, New York) p 230 (1962)
- 7 DIETRICH H J and STEIGER E L *Mol. Cryst. Liquid Cryst.* 16 263 (1972)
- 8 DAVE J S, KURIAN G and PRAJAPATHI A P (Unpublished work)
- 9 WIEGAND G *Hand-und Jahrbuch der chem. Physik.* 2 Chap. C (Akad. Verl. Leipzig) (1941) *Chem. Abstr.* 37 1078 (1943)
- 10 DAVE J S and DEWAR M J S *J. Chem. Soc.* 4616 (1954)
- 11 COOK A H and JONES D G *J. Chem. Soc.* 1314 (1939)
- 12 ASHLEY J N, BARBER H J, EWINS A J, NEWBERY G and SELF A D H *J. Chem. Soc.* 112 (1942)

DISCUSSION

Demus: Have you established the type of smectic mesophases.

Prajapati: No

Gray: In your compounds, it is of course very reasonable to assume that the pairs of 1, 4-disubstituted naphthalene nuclei adopt a *trans*-arrangement. My question is whether you have any physical evidence to back up this assumption?

Prajapati: No. No physical measurements have been made. It is only on the basis of our experimental results.

Mesomorphic behaviour of substituted phenylbenzoates - I : *p* (*p'*-*n*-alkoxybenzyloxy) toluenes

J S DAVE and R A VORA

Chemistry Department, M.S. University of Baroda,
Baroda 390002, India.

Abstract. A homologous series of mesomorphic esters was prepared by reacting *p*-cresol with *p*-*n*-alkoxybenzoyl chlorides. The first five members are non-mesomorphic. Hexyl, heptyl, octyl, dodecyl and tetradecyl derivatives are monotropic nematic whereas nonyl and decyl derivatives are enantiotropic nematic. The smectic mesophase appears at the nonyl derivative as a monotropic phase and remains monotropic throughout in succeeding homologues. Hexadecyl and octadecyl derivatives are non-mesomorphic. The plot of the transition temperatures versus the number of carbon atoms in the alkyl chain shows the usual odd-even effect and exhibits a tendency for rising nematic-isotropic transitions in ascending series. The nematic-isotropic transition curve rises to a maximum at the dodecyl derivative and then levels off. The smectic-nematic transition curve rises smoothly and does not merge with the nematic-isotropic curve. The thermal stabilities of the present series are compared with those of the other related homologous series, the present series being less mesomorphic than the other related homologous series.

1. Introduction

Recently low melting nematic liquid crystalline compounds are finding wide and varied applications. Much of recent synthesis research has therefore been directed towards preparing low temperature nematic liquid crystals. Rosenberg and Champa¹, Patel², Fishel and Patel³ and Dietrich and Steiger⁴ have reported low melting mesomorphic compounds. Majority of these are Schiff base compounds. Steinstrasser⁵ has reported some phenyl mono- and bis- benzoates exhibiting low temperature mesomorphism. With a view to exploring the possibility of getting simple and stable low temperature compounds the present series has been prepared and its mesomorphic properties studied.

2. Results and discussion

The melting points and transition temperatures of the compounds synthesized by reacting *p*-cresol with different *p*-*n*-alkoxybenzoyl chlorides are reported in table 1.

Table 1 *p*(*p*'-*n*-alkoxybenzoyloxy)toluenes
 $\text{RO} \cdot \text{C}_6\text{H}_4 \cdot \text{COO} \cdot \text{C}_6\text{H}_4 \cdot \text{CH}_3$

Compound	R	Transition temperatures (°C)		
		Smectic	Nematic	Isotropic
1	CH ₃	—	[23.0]*	67.0
2	C ₂ H ₅	—	[35.0]*	105.0
3	C ₃ H ₇	—	[34.0]*	99.0
4	C ₄ H ₉	—	[44.0]*	79.0
5	C ₅ H ₁₁	—	[43.5]*	70.0
6	C ₆ H ₁₃	—	(51.5)	64.0
7	C ₇ H ₁₅	—	(51.5)	57.5
8	C ₈ H ₁₇	—	(57.5)	59.5
9	C ₉ H ₁₉	(44.0)	52.0	58.0
10	C ₁₀ H ₂₁	(51.0)	56.0	60.5
11	C ₁₂ H ₂₅	(57.0)	(61.5)	64.0
12	C ₁₄ H ₂₉	(59.0)	(61.0)	70.0
13	C ₁₆ H ₃₃	[56.5]*	[59.0]*	72.0
14	C ₁₈ H ₃₇	[53.5]*	[56.0]*	76.5

Values in the parenthesis indicate monotropy.

* Values obtained by extrapolation.

The first five members of the series are non-mesomorphic. Mesomorphism appears at the hexyl derivative. Hexyl, heptyl, octyl, dodecyl and tetradecyl derivatives are monotropic nematic whereas nonyl and decyl derivatives are enantiotropic nematic. The smectic mesophase appears at the nonyl derivative as a monotropic phase and remains monotropic throughout in succeeding homologues. Hexadecyl and octadecyl derivatives are non-mesomorphic. The plot of transition temperatures versus the number of carbon atoms in the alkyl chain (figure 1) shows the odd-even effect for the nematic-isotropic transition.

The trend of the nematic-isotropic transition temperature curve shows a rising tendency as the series is ascended. It rises to the maximum at the dodecyl derivative and then levels off. Generally in a normal

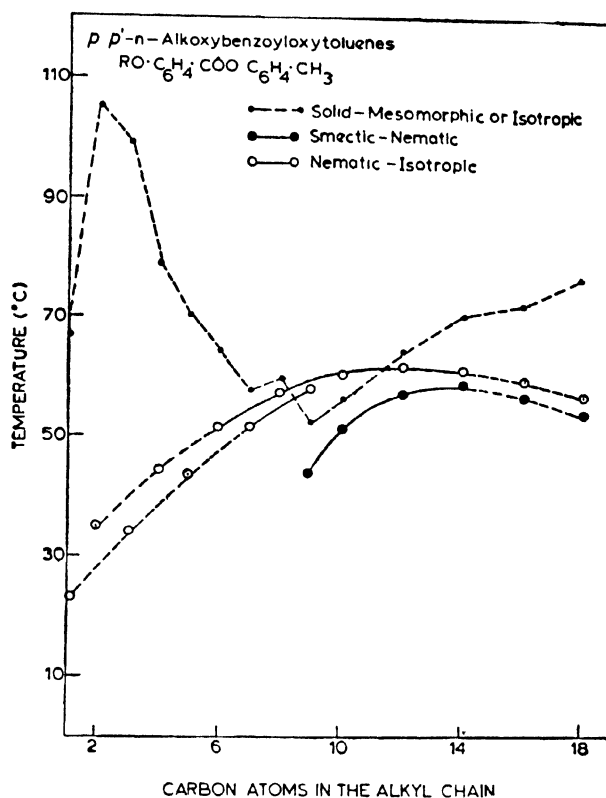


Figure 1 Transition temperatures as functions of the number of carbon atoms in the alkyl chain.

homologous series the nematic-isotropic transition temperature curve falls smoothly with increase in the alkyl chain length. An ascending nematic-isotropic transition temperature tendency is observed in some homologous series^{2,4,6-9}. Gray⁶ has explained this type of behaviour observed in the substituted biphenyl Schiff bases by attributing this phenomenon to a decrease in the ratio of lateral to terminal interactions due to steric hindrance, because of the broadening of the molecules.

Dietrich and Steiger⁴ attributed this phenomenon in the series *N*(*p*-*n*-alkoxybenzylidene)-*p*'-*n*-alkylanilines to their low intermolecular forces. This is indicated by their low transition points and expected because of the absence of strong permanent dipoles and shortness of the alkyl chains. The present series is similar to the series *N*(*p*'-*n*-alkoxybenzylidene) *p*'-*n*-alkylanilines; the difference is in the middle group and in the end alkyl chain. The intermolecular forces in the present series

would be reduced a little more and naturally the ascending tendency of the nematic-isotropic transition temperatures should be expected.

The levelling off in the nematic-isotropic transition temperature curve in the present series may be due to the weakening of the terminal attractions, which begin to play their part in determining the temperature of the nematic-isotropic transition as the series is ascended.

Smectic-nematic and nematic-isotropic transition temperature curves are extrapolated and the obscure transition temperatures are obtained for these members. These extrapolated values lie well below the crystallization points of these compounds and that is probably the reason why these members are non-mesomorphic.

Table 2 summarizes the average thermal stabilities and comparative geometry of the present series (A), and these are compared with those of *p*(*p*'-*n*-alkoxybenzoyloxy) acetophenones (B)¹⁰ and *n*(*p*'-*n*-alkoxybenzylidene)*p*'-*n*-butylanilines (C)².

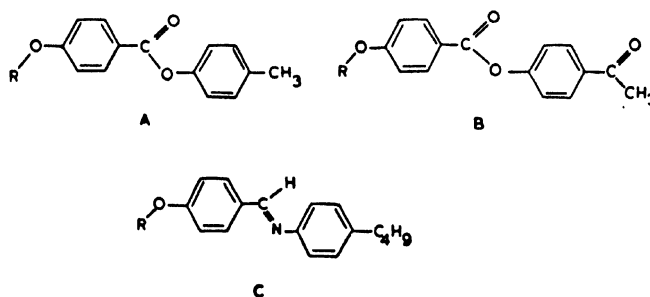


Table 2 Average transition temperature (°C)

	A	B	C
Nematic-Isotropic (C ₆ -C ₇)	51.5	90.25	77.0
Smectic-Nematic (C ₉ -C ₁₄)	52.8	99.5	84.7
Commencement of the smectic phase	Nonyl derivative	Pentyl derivative	Butyl derivative

The thermal stabilities of series (A) are lower than those of series (B) and (C). The difference in series (A) and (B) is in the end group, molecules of series (B) having a -COCH₃ end group with a permanent dipole moment. The molecules of series (B) would be more

polarizable than those of series (A) resulting in the higher thermal stabilities in the mesophases of series (B).

In the case of series (C), the main difference is in the middle group; series (A) has the --COO-- middle group whereas series (C) possesses --CH=N-- middle group. The oxygen atom of the central carbonyl group will be bumping into the non-bonded sides of the adjacent hydrogens of the aromatic ring thereby causing considerable strain on the molecule. This will cause some twist around the C-O bond and force the benzene ring with the ester linkage out of the plane of the molecule; this will reduce the coplanarity of the molecule and increase the thickness¹¹. Thus both the thermal stabilities of series (A) are less than those of series (C).

The smectic mesophase commences early in series (B) and (C) and the smectic-nematic curves join the nematic-isotropic curves in both the series at octyl derivative, whereas in series (A) the smectic mesophase commences at the nonyl derivative and the extrapolated smectic-nematic and nematic-isotropic curves do not merge. Series (B) has a dipolar --COCH_3 group at one end whereas the series (A) has only an alkyl group at that end. This may be the reason for the late commencement of the smectic phase in series (A). The main difference between series (A) and (C) is in the middle group. As discussed before the molecules of series (A) will be less coplanar than the molecules of series (C). This may be the reason for the late commencement of smectic phase in series (A).

3. Materials and methods

Melting points and transition temperatures were determined by the optical method of Dave and Dewar¹². The precise measurements were, however, made by the Leitz Ortholux Polarizing microscope equipped with a heating stage.

Preparation of compounds

1. *p*-*n*-Alkoxybenzoic acids and *p*-*n*-alkoxybenzoyl chlorides were prepared as described by Dave and Vora¹³.

2. Equimolecular quantities of *p*-*n*-alkoxybenzoyl chlorides and *p*-cresol are taken in a round bottom flask heated on a water-bath for thirty minutes and then on a sand-bath just to boiling. The mass is poured in ice-cold water. The solid separated is filtered, washed with dilute sodium hydroxide solution followed by water and dried. The esters are crystallized from alcohol into white plates or needles till constant melting points and transition temperatures are obtained. These are reported in table 1. The analytical data are recorded in table 3.

Table 3. *p* (*p'*-*n*-alkoxybenzoyloxy) toluenes.

Compound	Molecular formula	% Found		% Required	
		C	H	C	H
1	C ₁₅ H ₁₄ O ₃	74.52	5.54	74.38	5.78
2	C ₁₆ H ₁₆ O ₃	74.52	5.92	75.00	6.25
3	C ₁₇ H ₁₈ O ₃	75.86	6.68	75.55	6.66
4	C ₁₈ H ₂₀ O ₃	75.75	6.82	76.05	7.04
5	C ₁₉ H ₂₂ O ₃	76.25	7.10	76.51	7.38
6	C ₂₀ H ₂₄ O ₃	76.88	7.43	76.91	7.69
7	C ₂₁ H ₂₆ O ₃	77.41	7.72	77.30	7.92
8	C ₂₂ H ₂₈ O ₃	77.76	7.90	77.64	8.23
9	C ₂₃ H ₃₀ O ₃	78.03	8.21	77.96	8.47
10	C ₂₄ H ₃₂ O ₃	78.11	8.53	78.26	8.69
11	C ₂₆ H ₃₆ O ₃	78.30	8.67	78.78	9.09
12	C ₂₈ H ₄₀ O ₃	79.49	9.02	79.24	9.43
13	C ₃₀ H ₄₄ O ₃	79.58	9.37	79.64	9.73
14	C ₃₂ H ₄₈ O ₃	79.73	9.63	80.00	10.00

Acknowledgement

The authors are thankful to Prof. Suresh Sethna for his keen interest in the work.

References

- 1 ROSENBERG H N and CHAMPA R A *Mol. Cryst. Liquid Cryst.* 11 191 (1970)
- 2 PATEL P R *J Indian Chem. Soc.* 50 514 (1973)
- 3 FISHEL D L and PATEL P R *Mol. Cryst. Liquid Cryst.* 17 139 (1972)
- 4 DIETRICH H J and STEIGER E L *Mol. Cryst. Liquid Cryst.* 16 263 (1972)
- 5 STEINSTRASSER R paper presented at the Fourth International Liquid Crystal Conference, Kent State University, Kent, Ohio, 1972, Abstr. No. 119
- 6 GRAY G W *Molecular structure and properties of liquid crystals* (Academic Press, London) 1962 p. 235
- 7 WEYGAND C *Hand- und Jahrbuch der Chem. Physik.*, Vol. 2, chap. C (Akad. Verl. Leipzig) 1941; *Chem. Abstr.* 37 1078 (1943)

- 8 HALLER I and COX R J in *Liquid crystals and Ordered fluids* (Plenum Press, New York) 1970 p. 393
- 9 CASTELLANO J A and MCCAFFREY M T in *Liquid crystals and Ordered fluids* (Plenum Press, New York) 1970, p. 293
- 10 DAVE J S and KURIAN G Presented at the Fifth International Liquid Crystal Conference, Stockholm, Sweden, 1974
- 11 ARORA S L FERGASON J L and TAYLOR T R *J. Org. Chem.* 35 4055 (1970)
- 12 DAVE J S and DEWAR M J S *J. Chem. Soc.* 4616 (1954)
- 13 DAVE J S and VORA R A in *Liquid crystals and ordered fluids* (Plenum Press, New York) 1970 p. 477

Influence of liquid crystalline solvents in chemical reactions *

WILLIAM E BACON

Liquid Crystal Institute, Kent State University, Kent, Ohio 44242 USA

Abstract. The influence of the liquid crystalline state on chemical reactions is reviewed. Polymerization of mesomorphic molecules is briefly discussed. A review of the reactions of non-mesomorphic molecules dissolved in liquid crystalline solvents includes a comparison of first and second-order rearrangements, pyrolysis and polymerizations in thermotropic liquid crystalline and isotropic solvents. Also a comparative study of the kinetics of hydrolysis in lyotropic liquid crystalline and isotropic phases is reviewed.

Introduction

The initial investigation of chemical reactions in nematic liquid crystalline solvents was reported by Svedberg some fifty years ago¹, and only within the past ten years has there been a renewed interest in this field. The influence of the liquid crystalline state upon chemical reactions is studied by utilizing mesomorphic reactant molecules directly or by dissolving non-mesomorphic reactants in mesomorphic solvents. Some examples to illustrate the former are: polymerization of the liquid crystalline monomers as cholesteryl acrylate², *p*-alkoxybenzylidene-*p*-aminostyrenes³, and *p*-substituted phenyl acrylates⁴. Examples of the latter are: rearrangement reactions in nematic solvents⁵, polymerization of *p*-methacryloxybenzoic acid dissolved in mesomorphic *p*-alkoxybenzoic acid solvents⁶ and the polymerization of phenylacetylene in nematic and cholesteric solvents⁷.

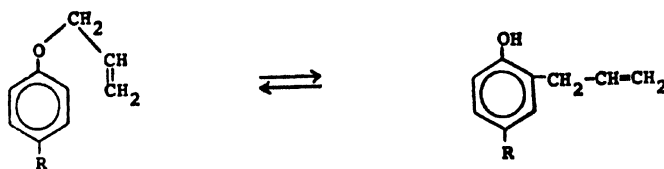
The polymerization of *p*-methacryloxybenzoic acid in the smectogenic solvent, *p*-cetyloxybenzoic acid, or the nematic solvent, *p*-heptyloxybenzoic acid was done with free radical initiators and compared with the isotropic solution in dimethylformamide as a reference system^{6, 8}. The overall rate constant for the polymerization reaction in the smectic or nematic solvent was found to be higher than in dimethylformamide and the average molecular weight was higher in the smectic phase. The organization of the monomer molecules within a mesomorphic solvent appears to have a considerable influence on the kinetics of polymerization and the molecular weight distribution⁶.

Claisen rearrangements in liquid crystalline solvent

Although the work cited demonstrates the influence of the liquid crystalline media in bimolecular reactions, a study of a similar influence in

* Presented by Professor Glenn H Brown

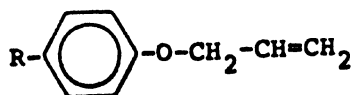
intramolecular reactions was undertaken by determining the kinetics of the Claisen rearrangement and the thermodynamic quantities by which this influence can be described⁵. The Claisen rearrangement in the nematic solvent, di (*p*-methoxyphenyl) *trans* cyclohexane-1, 4-dicarboxylate, was evaluated by measuring the rate of rearrangement of a series of *para*-substituted allyl phenyl ethers in two different solvent systems, *i.e.*, a nematic and an isotropic solvent. The Claisen rearrangement is shown in the following equation



where R is $-\text{CH}_3$, $-\text{Cl}$, $-\text{CN}$ and $-\text{NO}_2$

The rate constants for the rearrangements at three temperatures, calculated from the first order rate equation, are recorded in table 1.

Table 1 Rate constants for claisen rearrangement in nematic solvent



Temp. $\pm 0.05^\circ$	R	$k \times 10^6 \text{ sec}^{-1}$	Temp. $\pm 0.05^\circ$	R	$k \times 10^6 \text{ sec}^{-1}$
160	$-\text{CH}_3$	4.17 ± 0.02	160	$-\text{CN}$	1.38 ± 0.01
185		32.8 ± 0.60	185		12.1 ± 0.18
200		95.3 ± 3.5	200		40.9 ± 3.0
160	$-\text{Cl}$	3.41 ± 0.05	160	$-\text{NO}_2$	1.23 ± 0.02
185		26.9 ± 0.40	185		10.3 ± 0.25
200		83.6 ± 1.2	200		42.7 ± 1.2

The energy of activation, E_a , was obtained from the Arrhenius plot for each substituted allyl phenyl ether and such a plot for the rearrangement of allyl *p*-cyanophenyl ether is shown in figure 1.

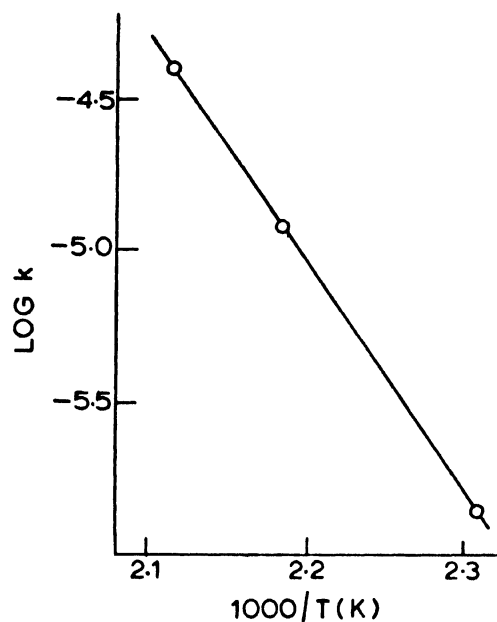
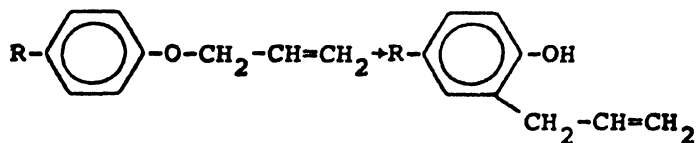


Figure 1 Arrhenius Plot for the rearrangement of allyl *p*-cyano-phenyl ether in nematic solvent.

The activation parameters for the rearrangement of a series of *p*-substituted allyl phenyl ethers using the nematic solvent are given in table 2, and the activation energies are reliable to 1 kcal/mole and the entropies of activation to one entropy unit.

Table 2 Activation parameters in nematic solvent



R	E_a †	ΔH^\ddagger §	Log A §	ΔS^\ddagger *
CH ₃	31.9	29.8	10.7	-10.2
Cl	32.6	30.5	10.9	- 9.3
CN	34.7	32.6	11.6	- 6.1
NO ₂	35.8	33.7	12.0	- 4.1

† kcal/mole

§ Calculated at 185°

* cal/deg/mole

The reaction rates and activation parameters for the Claisen rearrangement found in the nematic phase of the solvent are compared with two different solvents in the isotropic phase: (a) di (*p*-methoxyphenyl) *trans* cyclohexane-1, 4-dicarboxylate at 220° and 230°; (b) diphenyl ether at 160°, 185° and 200°. The Arrhenius plot (figure 2) of the data for the rearrangement of allyl *p*-cyanophenyl ether in the solvent, di (*p*-methoxyphenyl) *trans* cyclohexane-1, 4-dicarboxylate at five different temperatures, three in the nematic range and two in the isotropic range of the solvent shows no discontinuity and indicates that the influence of the temperature on the rate of reaction is the same regardless of the structure of the solvent.

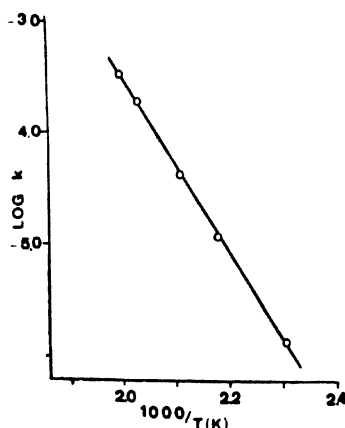


Figure 2 Arrhenius plot for the rearrangement of allyl *p*-cyano-phenyl ether in the nematic and isotropic phase of the liquid crystalline solvent.

A similar plot for allyl *p*-nitrophenyl ether also describes a straight line. The influence of the structural aspect of the nematic solvent upon these rearrangements is also apparent from a comparison of the activation parameters (table 3) with the isotropic solvent, diphenyl ether.

Table 3 Comparison of activation parameters

Nematic Solvent

R	E_a	ΔH^*	ΔS^*
-CH ₃	31.9 kcal/mole	29.8 kcal/mole	- 10.2 cal/deg/mole
-Cl	32.6	30.5	- 9.3
-CN	34.7	32.6	- 6.1

Isotropic Solvent †

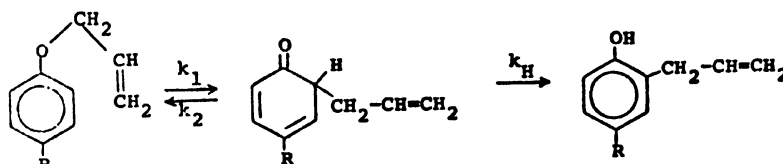
R	E_a	ΔH^*	ΔS^*
-CH ₃	31.9 kcal/mole	29.8 kcal/mole	- 10.7 cal/deg/mole
-Cl	33.2	31.1	- 8.6
-CN	34.3	32.2	- 7.7

* Calculated at 185°

† Diphenyl ether

The similarity of the reaction order and the activation parameters in the nematic and isotropic solvents indicates similar rate-determining steps for the reaction in both types of solvent.

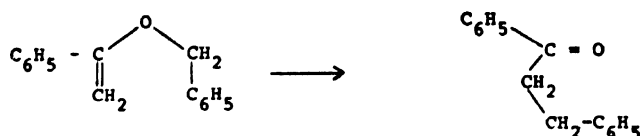
The reported first-order rate constants for the Claisen rearrangements in isotropic solvents are recognized to be composites of the rate constants of the individual steps:



In isotropic solvents the rate determining step is k_1 , since the enolization step, k_H is very rapid. The intramolecular nature of this reaction which proceeds through a cyclic intermediate is well documented in isotropic solvents and the similarity of activation parameters and the order of the reactions in nematic solvents indicates a similar mechanism. The problem of measuring the influence of the nematic solvent upon the Claisen rearrangement is limited to the rate-determining step, that is, the formation of the cyclic intermediate state. Therefore, the similar influence of the nematic and isotropic solvents in this reaction is expected because of the unimolecular nature of the reaction. The influence of isotropic solvents on reactions is more pronounced in higher order reactions and therefore we undertook a study of a second-order isomerization reaction.

The rearrangement of α -benzylstyrene in nematic solvent

The isomerization of α -benzylstyrene⁹ shown in the following equation is a second-order reaction reported to undergo a free radical chain mechanism¹⁰.



Solutions of the reactant in nematic or isotropic solvent are homogeneous single phases that readily isomerize in the absence or presence of benzoyl peroxide. The product, β -phenylpropiophenone was isolated (80–5%) from the thermal isomerization of α -benzyloxystyrene dissolved in either the nematic or isotropic solvent indicating that the major product is similar in both solvents. The change in concentration of the alkoxytyrene was monitored by the change in absorption of the carbonyl group at 5.85μ for β -phenyl propiophenone and is described by the following equation:

$$d[A]/dt = -k[A]^2$$

The integrated form is

$$(1/A) - (1/A_0) = kt$$

where A_0 is the initial concentration of the ether and A is the concentration after time, t . The second-order rate constants for the reaction in nematic and isotropic solvents are shown in table 4, and are about four times larger in the nematic solvent than in the diphenyl ether.

Table 4 Rate constants for isomerization of α -benzyloxystyrene

Temp.	$k \times 10^5$ liters mol ⁻¹ sec ⁻¹	
	Nematic Solvent *	Diphenyl ether
169 \pm .05	11.6 \pm 0.5	3.60 \pm 0.2
179 \pm .05	24.6 \pm 0.5	6.10 \pm 0.2
189 \pm .04	49.7 \pm 0.7	11.0 \pm 0.4

* Di (*p*-methoxyphenyl) *trans* cyclohexane-1,4-dicarboxylate

The Arrhenius plots are shown in figure 3. The greater slope of line B for the nematic solvent clearly indicates that the rate constants increase faster in the nematic than in the isotropic solvent. This is an interesting observation, that is, the rate of the reaction and the energy of activation in the nematic solvent are higher than in the diphenyl ether.

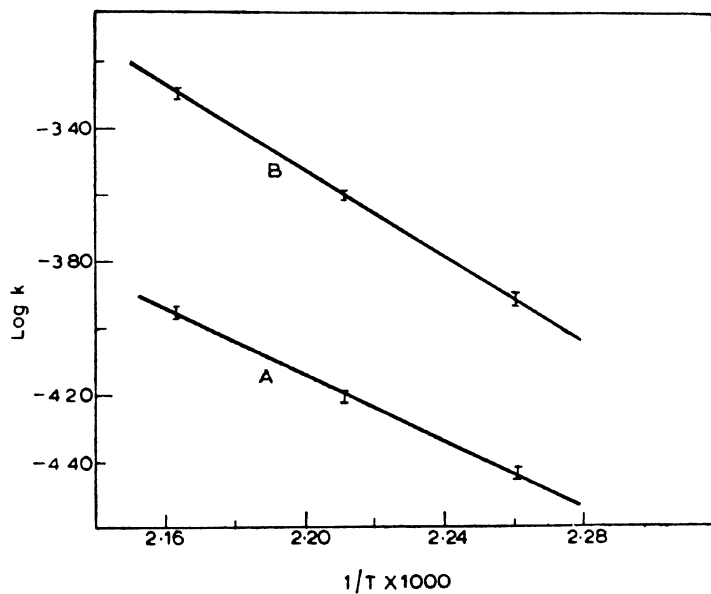


Figure 3 Arrhenius plot for α -benzyloxystyrene isomerization.

The activation parameters for this reaction in the nematic and isotropic solvents are collected in table 5, and they are reliable to 1 kcal/mole with the entropy of activation within one entropy unit.

Table 5 Activation parameters for α -benzyloxystyrene

Solvent	E_a	ΔH^\ddagger	ΔG^\ddagger	ΔS^\ddagger *
Nematic*	29.0	27.2	34.3	-15.9
Diphenyl Ether	22.0	20.2	35.5	-34.0

* Di (*p*-methoxyphenyl) *trans* cyclohexane-1,4-dicarboxylate

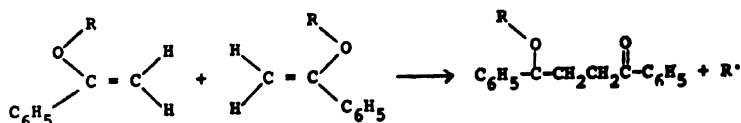
† kcal/mol. *

calculated at 180°

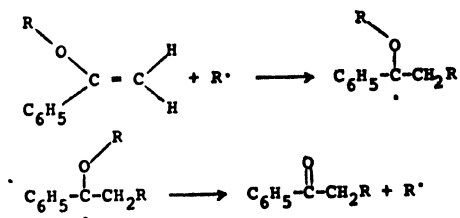
* kcal/deg/mol

Our findings for the isomerization of α -benzyloxystyrene in nematic and isotropic solvents are in accord with previous work. We assume the mechanism for this reaction is the same as reported in the following mechanism¹⁰.

Initiation:



Propagation:



Termination:



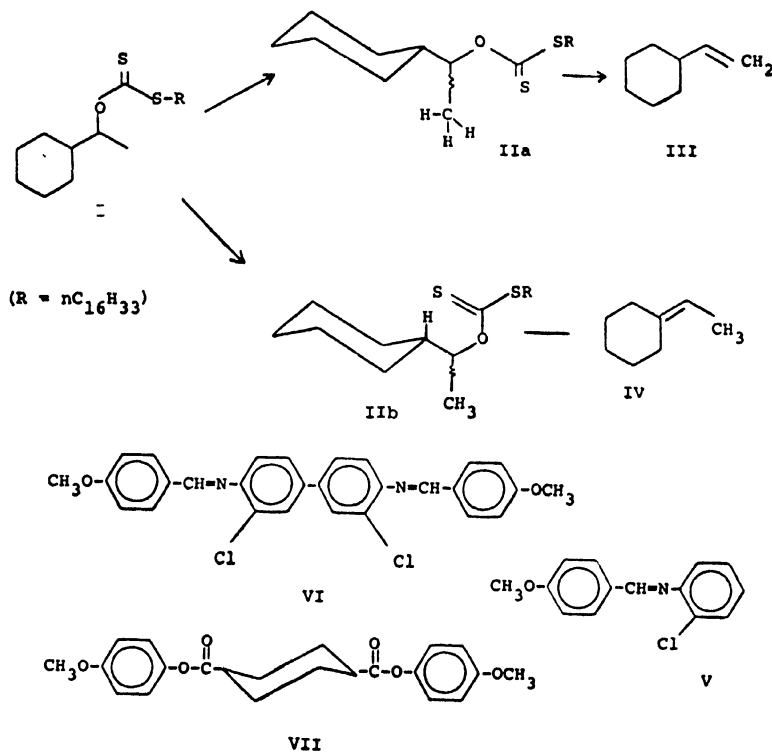
The rate-determination step is the initiation reaction in this mechanism.

A comparison of activation parameters in table 5, with the rate constants in table 4 for the reaction in the two different solvents shows a higher energy of activation and rate constant for the reaction in the nematic solvent. The hindered rotation of the solute molecules in the nematic solvent leads to a loss of entropy when they combine. The entropy of activation is therefore greater and the rate likewise greater for the reaction in the nematic solvent. The effect of the greater ΔH for the reaction in the nematic solvent is clearly counterbalanced by an increase in ΔS since the ΔG values do not differ significantly between the two solvents. Perhaps the oriented α -benzyloxystyrene molecules dissolved in the nematic solvent facilitates interaction with the neighbouring reactant molecules thus promoting the initiation step for the reaction.

Xanthate pyrolysis in nematic solvents

The influence of liquid crystalline solvents in directing the course of a pyrolysis reaction was recently reported¹¹. The pyrolysis of a substituted xanthate in liquid crystalline solvents gave a yield of olefins twice as large as that obtained for the reaction in isotropic solvents. The pyrolysis of xanthate, I, for which there are two such transition states, II a, and II b, leads to mixtures containing vinylcyclohexane, III, and ethylenecyclohexane, IV. The liquid crystalline solvents were, VI, VII, and the

isotropic solvents used for comparison were decalin and the anil V :



The total yield of olefins as a function of time is shown in figure 4 to be about twice as much in the liquid crystalline solvents as in the isotropic solvents. Data to determine whether the nematic liquid crystalline phase influences the distribution of olefins in the product mixture were not available.

The author feels that this effect is due to the ordered nematic phase and not to any particular effects of functional groups within the solvents used¹¹. The isotropic solvent (V), and the nematic solvent (VI), which have essentially the same functionality gave different results. In addition, the non-polar isotropic solvent, decalin gave results similar to the more polar isotropic solvent (V), while the nematic solvent (VII), an ester, behaves like the nematic solvent (VI) a basic amine. Although the details of the effect are yet to be clarified, the implication for synthetic chemistry is clear.

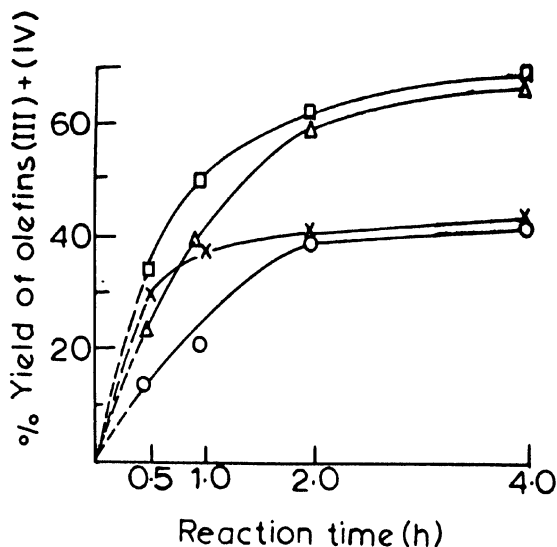


Figure 4 Pyrolysis of xanthate (I), in various solvents. Reactions at $160 \pm 0.2^\circ$. Concentration of (I) = 4%. Points shown are the average of two runs. X: solvent (V), non-liquid crystalline; Δ : solvent (VI), liquid crystalline; \square : solvent (VII), liquid crystalline; \circ : decalin, non-liquid crystalline. Yields are calculated from g.c. traces using a cyclohexene standard. Sensitivity factor = sample/standard = 0.85.

Hydrolysis reactions in lyotropic liquid crystalline phases

Systems of surfactants, alcohol and water are reported to contain liquid crystalline phases in addition to the isotropic solutions¹². Recently, a study of the change in the rate of hydrolysis of *p*-nitrophenyl laurate as a measure of the influence of the liquid crystalline phases upon a chemical reaction was reported¹³. The lyotropic liquid crystalline solvent selected in this work is water-hexadecyltrimethylammonium bromide-hexanol because the phase equilibria and the structure of the different phases have been studied by different methods^{14,15}.

The rates of hydrolysis were determined in the liquid and liquid crystalline phases for a series with a constant alcohol-hexadecyltrimethylammonium bromide ratio as a function of the water concentration. Reaction rates were determined in liquid crystalline phases: the lamellar "neat" phase N, the "middle" phase M, and in the liquid phase L in the system shown in figure 5. The pseudo-first-order reaction rate constants were determined from the slope of the extinction of the phenolate ion as a function of time. Since the water content varied considerably within each phase, second-order "rate constants" were calculated by division of the molar concentration of water. The rate constants in the liquid isotropic phase L are shown as a function of the water content in figure 6. No difference

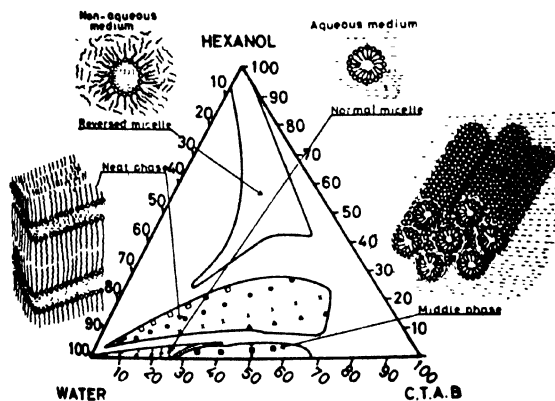


Figure 5 Regions and structure for the phases of the system water-cetyltrimethylammonium bromide-hexanol.

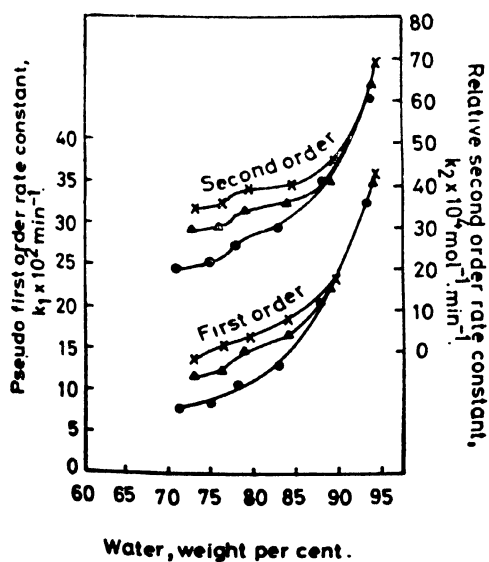


Figure 6 Reaction rates in the aqueous isotropic liquid phase L. The hexanol-CTAB ratio (w/w) were \times 0.01 (X), \times 0.08 (Δ), and \times 0.13 (\bullet).

in the rate constant was found when the alcohol-hexadecyltrimethylammonium bromide ratio was varied at water content in excess of 90% by weight. A distinct decrease in reaction rate was observed with less water and increasing the relative alcohol content. The apparent second-order rate constants are also shown in figure 6.

Figure 7 shows the rate constants as a function of water per cent for the reaction in the liquid crystalline phase N. Note the pronounced increase in the rate constants when the percentage of water is increased from 45 to 70 per cent. The second order rate constants are approximately unchanged at water contents above or below this range. The reaction rate increases by a factor of three when the ratio of hexanol-hexadecyltrimethylammonium bromide was increased from 0.2 to 0.7 (w/w). In general, the rates were higher in the liquid crystalline phase than in the isotropic liquid solution L at the corresponding water content.

The liquid crystalline phase M is extremely viscous and because of experimental difficulties only a few determinations of the reaction rates are reported in figure 8. Note an increase of the reaction rate when the water concentration is increased which is similar to the results obtained for the lamellar phase N. Although the rates are generally lower the second-order rate constants in the lamellar phase N are higher compared to the results obtained in the isotropic liquid region L.

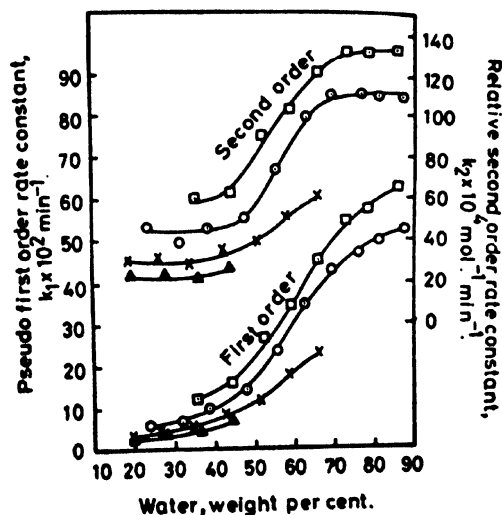


Figure 7 Reaction rates in the liquid crystalline neat phase N. The hexanol-CTAB ratio (w/w) were 0.77 (\square), 0.55 (\circ), 0.34 (\bullet), and 0.23 (Δ).

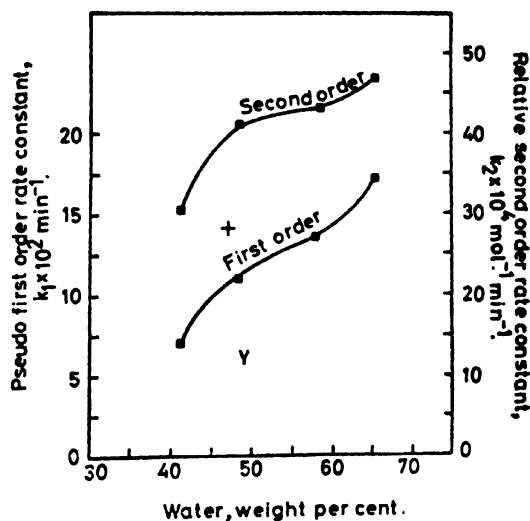


Figure 8 Reaction rates in the liquid crystalline middle phase M. The hexanol-CTAB ratios (w/w) were 0.02 (γ), 0.06 (\blacksquare) and 0.10 (+).

This investigation gave evidence of a catalytic effect of cationic substances associated in liquid crystalline phases¹³. A great deal of work on the enhancement of the reaction rates at the critical micelle concentration of hexadecyltrimethylammonium bromide is reported¹⁶. At concentrations in excess of the critical micelle concentrations in the system water-hexanol-hexadecyltrimethylammonium bromide shows the micelle structure changes with the concentration of the CTAB. An examination of the reaction rates obtained in this investigation in the light of the information on micellar structures shows a pronounced dependence of the reaction rate on variation in micellar structure. The increase in the reaction rate constants when the system changes from liquid isotropic phase to the middle phase indicates the presence of a structural change influencing the hydrolyses reaction.

Polymerization of phenylacetylene in nematic, cholesteric and isotropic solvents

The thermal polymerization of phenylacetylene in nematic, cholesteric and isotropic solvents was recently reported⁷. Phenylacetylene was selected as the monomer because it readily oligomerizes to give cyclic and linear products as well as high polymers. The dissolution of this linear molecule in liquid crystalline media tends to orient the long axes of the solute and solvent parallel to one another thereby influencing the kinetics of the

reaction. The rate constants for this reaction in the three solvent systems were determined by following the change in concentration of the phenylacetylene as a function of time with a Perkin-Elmer 337 equipped with Ordinate Scale Expansion. The peak intensity at 3280 cm^{-1} due to C-H stretching in phenylacetylene was found to be proportional to the concentration of the monomer. The change in concentration as a function of time for the thermal polymerization in nematic, cholesteric and isotropic solvents follows the second-order rate equation:

$$d(A)/dt = -k(A)^2$$

The rate constant, k is obtained from the slope of the line in the plot $(1/A) - (1/A_0)$ versus time. The rate constants for the polymerization reaction in the three solvent systems are shown in table 6 and it is apparent the rate is faster in liquid crystalline solvents than in the isotropic solvent, *p*-xylene. Although the details of the influence of the liquid crystalline solvent in accelerating the rate of polymerization are unclear, the comparison of the rate constants in the mesomorphic and isotropic phases of the same solvent will determine if the ordered structure exerts a catalytic effect.

Table 6 Rate constants for the thermal polymerization of phenylacetylene at 150° .

Solvent	$k \times 10^6\text{ l. mol.}^{-1}\text{ sec.}^{-1}$
Nematic ^a	87.2
Cholesteric ^b	44.9
Isotropic ^c	2.4

^a di (*p*-methoxyphenyl) *trans* cyclohexane-1,4-dicarboxylate

^b Prepared by the addition of 4.4 mol. % of cholestanyl *p*-methylbenzoate to the nematic.

^c *p*-xylene

Further analysis of the cyclic products from the oligomerization of phenylacetylene as well as isolation of the linear polymers will indicate which of the three types of addition of phenylacetylene to itself is produced in the various solvents.

In summary, the evidence indicates the liquid crystalline solvents exert an influence on chemical reactions and this interesting role is currently unfolding. Whether it parallels the influence of the micellar media or the crystalline state awaits development.

References

- 1 SVEDBERG T *Kolloid Z.* **18** 54 (1916)
- 2 TOTH W J and TOBOLSKY A V *J. Polym. Sci. B* **8** 289 (1970)
- 3 PALEOS C M, LARONGE T M and LABES M M *Chem. Commun.* 115 (1968)
- 4 STRZELFCKI L and LIEBERT L *Bull. Soc. Chim. Fr.* **2** Pt. 2, 597 (1973)
- 5 BACON W E and BROWN G H *Liquid Crystals* 3, Part II, p. 584 (Gordon and Breach, Science Publishers, Inc., New York) 1972
- 6 AMERIK Y B, KONSTANTINOV I I, KRENTZEL B A and MALACHAEV E M *Vysokomol. Soedin; Ser. A* **9** (12) 2591 (1967)
- 7 BACON W E *Amer. Chem. Soc. Northeast Regional Meeting, Rochester, New York, October 14-17 (1973)*
- 8 BLUMSTEIN A, KITAGAWA N and BLUMSTEIN R *Mol. Cryst. Liquid Cryst.* **12** 215 (1971)
- 9 BACON W E, SANG J and BROWN G H *Fourth International Liquid Crystal Conference, August 21-25 (1972)*
- 10 WIBERG W E, KINTNER R R and MOTELL E L *J. Amer. Chem. Soc.* **85** 450 (1963)
- 11 BARRETT W E and WON SOHN J *Chem. Soc. Sec. D* 1002 (1971)
- 12 HYDE A J, LANGEBRIDGE D M and LAWRENCE A S C *Discuss. Faraday Soc.* **18** 239 (1954)
- 13 AHMAD S I and FRIBERG S J *Amer. Chem. Soc.* **94** 5196 (1972)
- 14 EKWALL P, MANDELL L and FONTELL K J *Colloid Interface Sci.* **29** 639 (1969)
- 15 EKWALL P, MANDELL L and SOLYOM P J *Colloid Interface Sci.* **35** 519 (1971)
- 16 CORDES E H and DUNLAP R B *Accounts Chem. Res.* **2** 329 (1969)

NMR Spectra of molecules oriented in a lyotropic mesophase Part I: The spectra of pyridazine, pyrimidine and pyrazine†

C L KHETRAPAL*, A C KUNWAR* and A V PATANKAR**

*Raman Research Institute, Bangalore 560006, India

**Bhabha Atomic Research Centre, Bombay 400085, India

Abstract. A lyotropic mesophase formed by a 14 : 1 : 1 : 20 mixture (by weight) of sodium dodecyl sulphate, sodium sulphate, decanol and heavy water is used to study the PMR spectra of pyridazine, pyrimidine and pyrazine. Since the ordering of the molecules is much lower in this case compared to that in a thermotropic mesophase, analysis of the spectra was considerably simplified. Some of the dipolar couplings could be guessed fairly accurately even from the first order analysis. The geometry information and the order parameters are derived in each case. Ratios of interproton distances thus determined are compared with those obtained from the studies in the thermotropic mesophase. For pyrimidine and pyrazine they are found to agree. However, in pyridazine a deviation of about 5% in one of the distance ratios is observed. This may be attributed to a hydrogen bonded complex formed between pyridazine and water in the lyotropic phase. In pyridazine, the S -value along the C_2 axis of symmetry is found positive and that perpendicular to the plane of the ring negative as in thermotropics. The order parameter in the ring plane along an axis perpendicular to the symmetry axis has the largest positive value. In pyrimidine, the S -value of the axis perpendicular to the plane of the ring is negative and its magnitude decreases with the increase of temperature such that at 45°C it is nearly zero. The order parameter of the symmetry axis has the largest positive value.

For pyrazine it was possible to determine the signs of the order parameters in this phase by assuming the signs of the indirect spin-spin couplings. This was not possible in thermotropic liquid crystal solvents. The S -value of an axis perpendicular to the ring plane was found positive as for most of the aromatics in a lyotropic mesophase.

1. Introduction

The use of a lyotropic mesophase formed by a mixture of C_8 or C_{10} alkyl sodium sulphate, the corresponding alcohol, sodium sulphate and water (or heavy water) in approximate ratios of 8 : 1 : 1 : 10 has earlier been suggested as the orienting medium in NMR experiments¹⁻³. Studies in a lyotropic phase aimed at the elucidation of molecular structure are relatively rare

†An extension of the work submitted to the Third Symposium on Ordered Fluids and Liquid Crystals held in Chicago in August 1973

compared to those in a thermotropic mesophase. This is probably due to the fact that the orientation processes in the former are much slower and are rather critically dependent on the concentration and the purity of the ingredients. On the other hand such a phase complements a thermotropic mesophase in that some of the substances which are not soluble in the latter may dissolve in the former. Further, such a phase permits the spinning of the sample without destroying the orientation in commonly available magnetic fields where the direction of the field and the axis of the sample spinning are perpendicular to each other. This results in relatively sharp lines (with widths $\approx 1-2$ Hz). Another feature of such a phase is the relatively low molecular order of the dissolved species which sometimes (1) simplifies the spectra such that it may be possible to estimate the NMR parameters from the first order analysis to a reasonable accuracy, and (2) makes it possible to derive the information which is lost as a result of the dominating nature of the dipolar couplings. Studies on such a phase coupled with those in a thermotropic mesophase may permit the determination of the components of the chemical shift tensor in systems with C_{2v} -symmetry.

In the present paper, we report the results obtained from the PMR spectra of the title compounds dissolved in a phase (referred to as II hereafter) formed by a 14 : 1 : 1 : 20 mixture (by weight) of sodium dodecyl sulphate, decanol, sodium sulphate and deuterium oxide. The phase proposed earlier¹⁻³ (referred to as I hereafter) differs from II in having sodium decyl sulphate instead of sodium dodecyl sulphate in addition to somewhat different relative proportions of the ingredients.

2. Experimental

About 2% (by weight) of the solute was added to the phase and the mixture was centrifuged for about half an hour. The solutions thus prepared were transferred to the 5 mm NMR sample tubes and kept for spinning in the magnetic field for several hours (≈ 7) before the spectra were finally recorded on a Varian A-60 NMR spectrometer. The line-width varied from 1-2 Hz. The sweep time and the sweep width used were 5000s and 500 Hz respectively. Spectra of pyrimidine and pyrazine were recorded at 45 °C whereas pyridazine was studied at 35 °C. In addition, pyrimidine was also studied at 35 °C for comparison of the various results.

The statistical error in the measurements of line positions was 0.2 Hz.

3. Results and discussion

3.1. Analysis of the spectra

Spectra of pyridazine, pyrimidine and pyrazine are shown in figures 1-3 respectively. Since the spectrum of pyrazine is symmetrical about the centre, only the upper-field half of the spectrum is shown in figure 3.

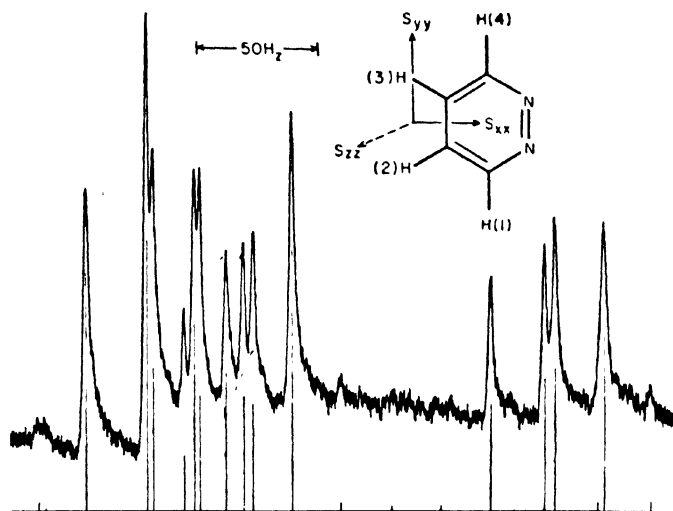


Figure 1 Observed and calculated PMR spectra of pyridazine oriented in the lyotropic phase (II). Spectrometer: A 60. Concentration: 2% (by weight). Temperature: 35° C.

In pyridazine and pyrimidine, since the chemical shifts between the various protons are relatively large compared to the direct dipolar couplings, it was possible to assign some of the groups of lines to particular protons and hence some of the parameters could be guessed fairly accurately from the first order analysis, e.g., for pyridazine (figure 1), the highest field quartet forms about half of the spectrum due to protons 2 and 3 and for pyrimidine (figure 2), the doublet of quartets at the highest field arises due to proton 3.

In pyrazine (figure 3), the spectrum consists of a symmetrical doublet of sextets⁴. In each sextet four lines are independent of the isotropic spin-spin couplings and are in the intensity ratio of 1:1:1:2. The remaining two lines with a total relative intensity of 3 are split up by the isotropic couplings in an approximate intensity ratio of 1:2; they usually overlap^{5,6} in the spectra in thermotropic liquid crystals. On the other hand the separation between these two lines provides approximately $\frac{3}{2} (J_{23} + J_{13})$. The sign of this quantity relative to that of the direct couplings can be derived from the analysis. Information on the molecular orientation can thus be obtained.

The final analysis was carried out with the help of the LAOCOONOR programme⁷ which also contains the definitions of the coupling constants and the chemical shifts ($\nu_i - \nu_j$). In the analysis, the chemical shifts and

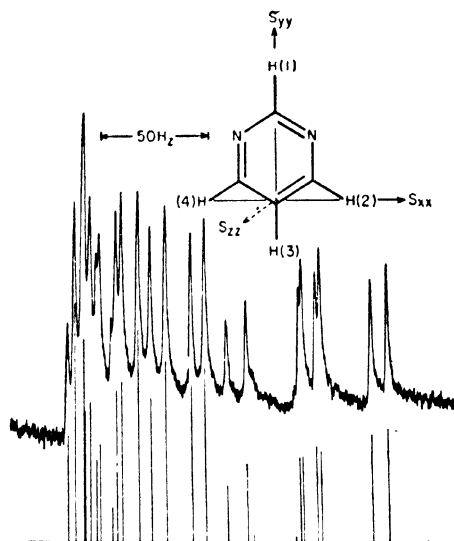


Figure 2 Observed and calculated PMR spectra of pyrimidine oriented in the lyotropic mesophase (II). Spectrometer: A 60. Concentration: 2% (by weight). Temperature: 45°C.

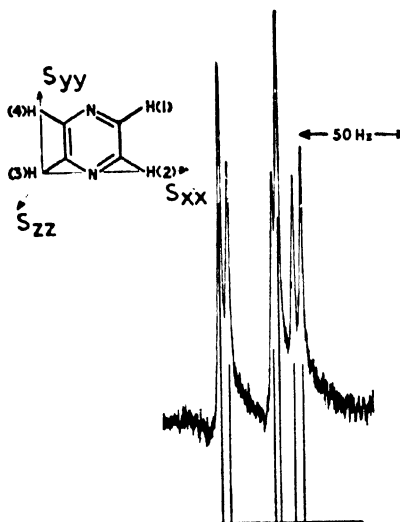


Figure 3 Observed and calculated PMR spectra of pyrazine oriented in the lyotropic mesophase (II). Only upper-field half of the symmetrical spectrum is shown. The highest field line is 174.6 Hz from the spectral centre. Spectrometer: A 60. Concentration: 2% (by weight). Temperature: 45°C.

the direct dipolar coupling constants were iterated upon and the values of the indirect couplings used were taken from the literature on the spectra in the isotropic media^{8,9}. The calculations were carried out on a CDC-3600 computer. The root mean square error between the observed and the calculated line positions was 0.24 Hz, 0.26 Hz and 0.08 Hz for pyridazine, pyrimidine and pyrazine respectively. The maximum error of any line position from its experimental value was found to be 0.46 Hz for pyridazine, 0.50 Hz for pyrimidine and 0.08 Hz for pyrazine. Values of the parameters thus obtained are given in table 1.

The signs of the direct dipolar couplings were found as given in table 1 on the valid assumption that the signs of the major indirect spin-spin couplings in these cases are positive.

By carrying out iterations on the indirect coupling constants in addition to the direct ones and the chemical shifts, it was found that the direct couplings and the chemical shifts do not change beyond their experimental errors given in table 1. It was also found that (1) in pyridazine, $J_{12} = 5.31$ Hz, $J_{13} = 1.79$ Hz and the other couplings could not be determined with any reasonable precision, (2) in pyrimidine, it was not possible to obtain any of the indirect couplings accurately, and (3) in pyrazine, it was possible only to estimate the value of $(J_{13} + J_{14})$ as 1.6 ± 0.2 Hz. This sum is expected to have a positive sign by analogy with substituted benzenes and hence the signs of the direct couplings are as given in table 1. This information could not be derived from the spectrum of pyrazine in a thermotropic mesophase because of the overlap of the lines which are dependent upon the indirect spin-spin coupling constants⁴.

3.2. Molecular geometry

The relations between the direct dipolar couplings and the ratios of the interproton distances reported in the literature^{4,11} were used to obtain the geometry information reported in table 2. The values within parentheses are those obtained from the study in the thermotropic mesophase. The errors of the distance ratios given in table 2 correspond to those derived by changing the dipolar couplings by the amount of their deviations (table 1) such that maximum deviations in these ratios from their mean values were obtained.

Table 2 indicates that the agreement between the distance ratios obtained in the lyotropic and the thermotropic mesophases is satisfactory for pyrimidine and pyrazine. However, there are significant deviations between the values for pyridazine. We have also made an investigation on pyridazine dissolved in the lyotropic mesophase (I)¹. We find $r_{12}/r_{23} = 0.951$, $r_{13}/r_{23} = 1.673$ and $r_{14}/r_{23} = 1.894$ in agreement with the values obtained in the lyotropic mesophase (II). An investigation on pyridazine dissolved in 4-ethoxybenzylidene-4-*n*-butylaniline was also made. The distance ratios obtained in this phase are in agreement with those

Table 1 Spectral parameters in pyridazine, pyrimidine and pyrazine oriented in lyotropic mesophase (II). Numbering of protons refers to figures 1, 2 and 3.

Pyridazine		Pyrimidine		Pyrazine	
Parameter	Value (Hz)	Parameter	Value (Hz)	Parameter	Value (Hz)
D_{12} (= D_{34})	-16.49 ± 0.09	D_{12} (= D_{14})	-3.44 ± 0.05	D_{12} (= D_{34})	103.72 ± 0.03
D_{13} (= D_{24})	-7.41 ± 0.11	D_{13}	-4.70 ± 0.05	D_{13} (= D_{24})	-1.28 ± 0.03
D_{14}	-6.39 ± 0.05	D_{23} (= D_{34})	13.96 ± 0.04	D_{14} (= D_{23})	-11.35 ± 0.03
D_{23}	-44.38 ± 0.07	D_{24}	6.53 ± 0.05		
$\nu_2 - \nu_1$	88.58 ± 0.10	$\nu_1 - \nu_2$	-23.53 ± 0.17		
		$\nu_3 - \nu_2$	75.65 ± 0.08		

Table 2 Distance ratios for pyridazine, pyrimidine and pyrazine as determined from the present investigations. The numbering refers to the figures 1, 2 and 3.

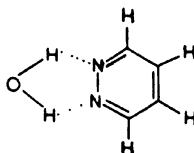
Distance ratio	Pyridazine τ	Pyrimidine τ	Pyrazine
r_{12}/r_{23}	0.943 ± 0.014 (0.988 ± 0.010) φ	$1.611 \pm 0.018 \mu$ (1.62 ± 0.01) $*$	0.607 ± 0.002 (0.602 ± 0.008) \dagger
r_{13}/r_{23}	1.673 ± 0.010 (1.693 ± 0.007) φ	$1.898 \pm 0.017 \mu$ (1.90 ± 0.02) $*$	1.170
r_{14}/r_{23}	1.908 ± 0.006 (1.890 ± 0.004) φ	1.611	1.000
r_{24}/r_{23}	1.673	$1.697 \pm 0.004 \mu$ (1.706 ± 0.004)	1.170

φ ref. 10; $*$ ref. 11; \dagger ref. 4. Values obtained from thermotropic mesophase.

τ Values of the distance ratios obtained from the phase (I) are: $r_{12}/r_{23} = 0.951$; $r_{13}/r_{23} = 1.673$; for pyridazine and 1.611 and 1.896 respectively for pyrimidine.

μ Values at 45°C ; those at 35°C are 1.629, 1.915 and 1.701 respectively. The two agree with each other within experimental error.

obtained earlier in the thermotropic mesophase¹⁰. Thus the distance ratio r_{12}/r_{23} in the lyotropic mesophase is about 5% shorter than in the thermotropic phase. It may arise from a specific molecular interaction of pyridazine with either the thermotropic or the lyotropic mesophase with the result that the structure determined in that phase does not truly represent that of the pyridazine molecule. Earlier, from spectroscopic studies^{12,13}, a hydrogen bonded interaction of the type



involving the non-bonding electrons of nitrogen has been postulated between pyridazine and water. These studies, therefore, provide a method to study some of the weak molecular interactions specially where the atoms directly involved in the interaction cannot be used as the probes.

For pyrimidine, exactly the same distance ratios in the two lyotropic phases were obtained (table 2) even though the molecular orientations are quite different.

3.3. Molecular Order

The lyotropic mesophase orients differently in the magnetic field compared to the thermotropic one in that it permits spinning of the sample about its axis in a direction perpendicular to the magnetic field without destruction of the orientation. For comparing the S -values under similar conditions of concentration and temperature, measurements in pyrimidine were carried out at two different temperatures, namely 45°C and 35°C. The results are summarized in table 3.

Table 3 shows that the magnitude of the S -values is in general larger in the phase (I) than in (II). The S_{xx} value is more negative in pyridazine than in pyrimidine at the same temperature (35°C). At higher temperature ($\approx 45^\circ\text{C}$), the S_{xx} value in pyrimidine becomes almost zero. At 45°C the S_{xx} value in pyrazine is positive. In pyridazine and pyrimidine, the largest S -values are found along the largest molecular axes. This behaviour is similar to what is observed for these molecules in thermotropic liquid crystals^{10,11}. It should be pointed out that in pyridazine the values of the order parameters reported in table 3 might have been modified due to the formation of the hydrogen bonded complex discussed in

Table 3 S -values in Pyridazine, Pyrimidine and Pyrazine in the lyotropic mesophase (II) at the same concentrations. * The indexing of the S -values refers to the coordinate systems in figures 1, 2 and 3.

S -value	Pyridazine *	Pyrimidine †		Pyrazine ‡
	35° C	35° C	45° C	45° C
S_{xx}	0.00059 ± 0.00014 (0.0005) φ	-0.00516 ± 0.00005	-0.00425 ± 0.00004 (-0.00651) φ	0.00738 ± 0.00002
S_{yy}	0.00564 ± 0.00001 (0.0079) φ	0.00537 ± 0.00009	0.00428 ± 0.00007 (0.00526) φ	-0.01509 ± 0.00011
S_{zz}	-0.00623 (-0.0084) φ	-0.00021	-0.00003 (0.00125) φ	0.00771

φ Values in the phase (I)

* $r_{22} = 2.481 \text{ \AA}$ (assumed); † $r_{11} = 4.274 \text{ \AA}$ (assumed); ‡ $r_{33} = 4.274 \text{ \AA}$ (assumed) $1 \text{ \AA} = 10^{-10} \text{ m}$.

section 3.2 and they need not correspond to the true values for the uncomplexed molecule. For pyrazine, the signs of the order parameters could not be obtained in thermotropics⁴ and hence no such comparison could be made.

Recently, we came across the following papers by Long *et al* :

(A) *Mol. Cryst. Liquid Cryst.* **21**, 299 (1973) and **32**, 137 (1973)

(B) *Proc. Am. Chem. Soc. meeting* edited by J F Johnson and R S Porter (Plenum Press) p. 147 (1974)

Results on pyrazine, pyrimidine and pyridazine in the lyotropic phase (I) are reported in paper (A) and in the paper (B), those in a new lyotropic phase formed by potassium laurate, decanol, potassium chloride and D₂O are given.

Our results agree with those given in papers (A) and (B) for pyrazine ; however, deviations outside the reported experimental errors are noticeable within references (A) and (B).

For pyrimidine in phase (I), the results are not consistent within the two references in (A). Besides in paper (A), the authors iterate upon J_{24} also and derive a value equal to 5.3 ± 0.4 Hz at 311 K and 7.6 Hz at 305 K for it. This is actually consistent with our finding that this J-value cannot be determined to any reasonable precision from such measurements. Our results on the molecular geometry of pyrimidine in phase (I) are nearly in agreement with those reported in reference (B).

In pyridazine, our results in the phase (II) do not agree with those given in references (A). However, the distance ratios determined in phase (I) from the present measurements and those derived from the data reported by Long *et al* (A) at 309 K are not in too bad an agreement. In pyridazine again, Long *et al* find that J_{12} varies from 5.0 ± 0.2 Hz at 305 K to 6.4 ± 0.6 Hz at 314 K which is too large a variation. Such a procedure in fact increases uncertainties in the determination of D -values.

References

- 1 LAWSON K D and FLAUTT T J *J. Amer. Chem. Soc.* **89** 5489 (1967)
- 2 BLACK P J, LAWSON K D and FLAUTT T J *Mol. Cryst. Liquid Cryst.* **7** 201 (1969)
- 3 BLACK P J, LAWSON K D and FLAUTT T J *J. Chem. Phys.* **50** 542 (1969)
- 4 DIEHL P and KHETRAPAL C L *NMR-Basic principles and progress*, P DIEHL, E FLUCK and R KOSFELD (Springer-Verlag, Berlin) **1** 47 (1969)
- 5 BULTHUIS J, GERRITSEN J, HILBERS C W and MACLEAN C *Recl. Trav. Chim.* **87** 417 (1968)
- 6 YANNONI C S, CEASAR G P and DAILEY B P *J. Amer. Chem. Soc.* **89** 2833 (1967)
- 7 DIEHL P, KHETRAPAL C L and KELLERHALS H P *Mol. Phys.* **15** 333 (1968)
- 8 GIL V M S *Mol. Phys.* **9** 443 (1965)
- 9 GRONOWITZ S, NORRMAN B, GESTBLOM B, MATTHIASSEN B and HOFFMAN R A *Ark. Kemi* **22** 65 (1964)

- 10 BURNELL E E and DeLANGE C A *Mol. Phys.* **16** 95 (1969)
- 11 KHETRAPAL C L, PATANKAR A V and DIEHL P *Org. Mag. Res.* **2** 405 (1970)
- 12 MOHR S C, WILK W D and BARROW G M *J. Amer. Chem. Soc.* **87** 3048 (1965)
- 13 LINNELL R H *J. Chem. Phys.* **34** 698 (1961)

DISCUSSION

Dhingra : In pyridazine-water complex, how do you rule out the possibility of a 1 : 2 complex ?

Khetrpal : Firstly, as I stated earlier, our results cannot predict whether it is 1 : 1 complex or 1 : 2 complex or whether at all the hydrogen bonds are formed. The differences in the structural parameters observed in the lyotropic and the thermotropic phases are indicative of the fact that there are solvent-solute interactions either in the thermotropic or in the lyotropic phase. A survey of the literature on pyridazine-water systems leads us to believe the formation of the complexes of the type mentioned. Secondly, in the case of a 1 : 2 type of complex, I would have expected deviations in the structural parameters for all the compounds studied.

PMR studies on N-methyl formamide oriented in a liquid crystalline nematic phase†

C L KHETRAPAL*, A C KUNWAR* and
K R K EASWARAN**

*Raman Research Institute, Bangalore 560006, India

**Molecular Biophysics Unit, Indian Institute of Science,
Bangalore 560012, India

Abstract. The PMR spectrum of N-methyl formamide dissolved in the nematic phase of 4-methoxybenzylidene-4-amino- α -methyl cinnamic acid-*n*-propyl ester is reported. The four interproton dipolar couplings are derived. Using reasonable values for the bond lengths and the bond angles, it is found that the results are consistent with the molecule having a plane of symmetry containing the fragment H.CO.NH.C. Assuming the H-CO-N fragment to be rigidly planar, this plane of symmetry may 'effectively' arise also from two rapidly interconverting conformations in which the remaining two bonds meeting at the nitrogen atom are bent either below or above this plane; the angles of bend are less than 10° .

Information on the mode of rotation of the methyl group about the N-C bond is derived.

The results establish that N-methyl formamide contains predominantly the '*trans*' species (NH and the C=O groups in the *trans* position). In addition, some weak lines, which arise from the '*cis*' species (NH and the C=O group in the *cis* position) present to a much smaller extent are detected.

1. Introduction

During recent years, there has been considerable interest in theoretical calculations related to the conformation of peptides and proteins¹⁻⁶. In most of these studies a completely planar peptide unit has been used, whereas, in some cases, it has been pointed out that the peptide unit is non-planar^{6,7}. In view of the importance of such studies, it is essential to establish experimentally whether the peptide unit is planar or not; NMR studies in a nematic solvent provide an easy method for this purpose⁸. *Since monosubstituted amides are the simplest structures which contain the peptide bond, it is convenient to investigate them first in order to obtain information on more complicated systems. In the present

†Communication No. 41 from the molecular Biophysics Unit.

paper, which is the first in the series, results obtained from the PMR study of N-methyl formamide (figure 1) dissolved in a nematic solvent are reported.

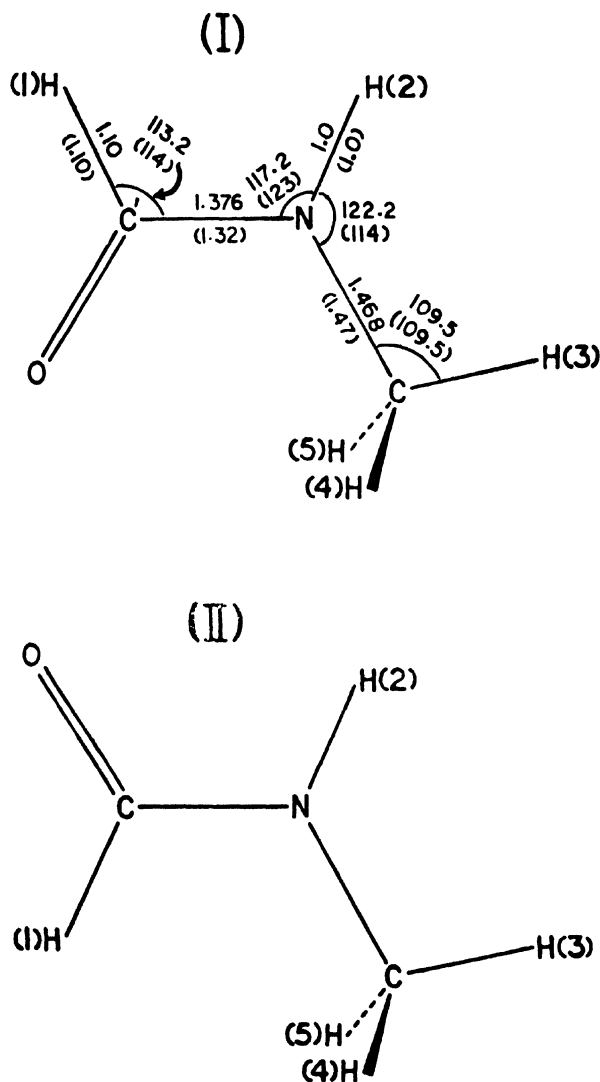


Figure 1 Structure of N-methyl formamide. Structure I is referred to as the 'trans structure' and structure II as the 'cis structure'. The bond lengths are given in units of 10^{-10} m and the bond angles in degrees. The two different structural data given are discussed in the text.

The PMR spectrum of N-methyl formamide has been studied earlier in the isotropic phase⁹⁻¹¹. It has been found that both the 'trans' (structure I) and the 'cis' (structure II) species are present at room temperature. The presence of both the rotational isomers indicates a relatively high barrier to internal rotation. An estimated value of 20-28 Kcal./mole for the barrier to internal rotation¹² supports this point of view. One of the isomers is found to be present to the extent of about 92% and the other about 8%. Further, from studies of a large number of substituted amides including ¹⁵N enriched compounds and the effects of solvents like benzene on the methyl proton resonances in N-methyl formamide, it has been shown that it is the 'trans' configuration (structure I) which is present predominantly ($\approx 92\%$). NMR spectra of molecules dissolved in a liquid crystalline nematic phase which contain information about the molecular geometries provide direct knowledge of whether the 'cis' or the 'trans' species is more abundant. Such results are also reported in the present paper.

In the isotropic phase spectrum, the resonance of the N-H proton has been found to be considerably broadened due to the quadrupolar relaxation of ¹⁴N nuclei. Analyses of the single and the double resonance PMR spectra of ¹⁵N substituted N-methyl formamide^{10, 11} provide the signs and the magnitudes of the inter-proton indirect spin-spin coupling constants. They have been used in the analysis of the spectrum in the nematic phase described in the paper.

2. Experimental

A 16.7 mole per cent solution of commercially available N-methyl formamide was prepared in 4-methoxybenzylidene-4-amino- α -methyl cinnamic acid *n*-propyl ester (a). The spectrum (figure 2) of the solution was recorded at probe temperature ($\approx 30^\circ\text{C}$) on a varian HA-100 spectrometer in the field sweep mode without 'lock'.

The average line-width was 7 Hz. Several spectra were recorded and the mean line positions were measured. The statistical error in the measurement of line positions was found to be 1.0 Hz with no line deviating by more than 2.0 Hz from the mean value.

3. Results and discussion

3.1. Analysis of the spectrum

Analysis of the spectrum was carried out with the help of the LAOCOONOR¹³ programme adapted to the IBM-360/44 computer. During the analysis, the direct dipolar couplings between nuclei *i* and *j* (D_{ij} 's as defined in the LAOCOONOR programme) and the chemical shifts ($\nu_i - \nu_j$)

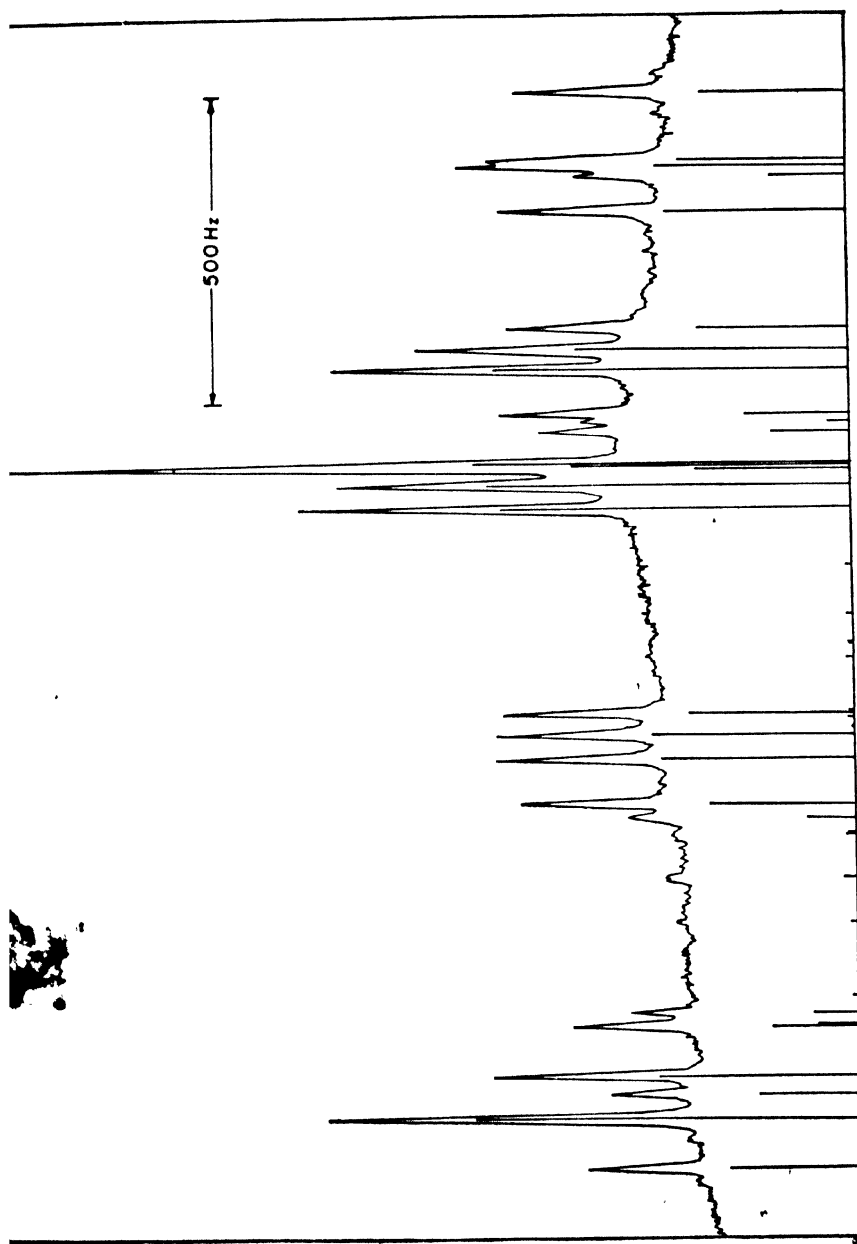


Figure 2 Observed and calculated PMR spectra of N-methyl formamide dissolved in the nematic phase of (a). Solute concentration ≈ 16.7 mole per cent; Probe temperature $\approx 30^\circ\text{C}$; Spectrometer frequency $\approx 100\text{ MHz}$. The calculated spectrum corresponds to the observed spectrum which do not appear in the

were iterated upon. Values of the isotropic couplings were taken from the literature¹¹ and were not iterated upon. An r.m.s. error of 0.7 Hz was obtained between the observed and the calculated line positions with no line deviating by more than 3.0 Hz even when the overlapping lines were included in the analysis. The calculated spectrum is shown below the observed one in figure 2. Values of the parameters obtained are given in table 1. A comparison of the observed and the calculated spectra in figure 2 shows that some of the weak lines in the observed spectrum do not appear in the calculated one. They may arise from the 'cis' species present in much lower abundance. This portion of the spectrum has now been studied by accumulating sufficient number of spectra with the help of a suitable 'time averaging' computer; the results will be published elsewhere²².

Table 1. Spectral parameters for *N*-methyl formamide dissolved in the nematic phase of (a). Numbering of protons refers to that given in structure (I).

Nuclear pair (i, j)	Coupling constants (Hz)		(ν _i - ν _j) Hz
	Indirect (J _{ij})	Direct dipolar (D _{ij})	
(1, 2)	1.9	-376.96 ± 0.8	123.3 ± 3.4
(1, 3)	-0.8	- 44.39 ± 0.6	533.1 ± 3.4
(1, 4), (1, 5)			
(2, 3)	4.9	- 36.35 ± 0.7	
(2, 4), (2, 5)			
(3, 4)	does not	163.20 ± 0.2	
(3, 5), (4, 5)	affect		

Errors of the parameters given in the table 1 were determined as described in the literature¹³.

3.2. Conformational information

The proton spectrum of one conformation of *N*-methyl formamide provides four interproton direct dipolar coupling constants. If the molecule does not possess a plane of symmetry, the four inter-proton dipolar couplings do not even provide the order matrix which has 5 independent elements.

In order to obtain any structural information in such a case, it is essential either to study the isotopically enriched (^{13}C and ^{15}N) species or to accumulate sufficient number of spectra with the help of a suitable computer for obtaining the direct couplings with nuclei which are present in low natural abundance. If on the other hand the molecule possesses a plane of symmetry, only three direct couplings are needed to describe the molecular order. If, therefore, a reasonable geometry for the molecule is used to compute iteratively the three elements of the order matrix¹⁶ (the S -values) from the four direct dipolar coupling constants, an acceptable fit (*i.e.*, within experimental errors of the dipolar coupling constants) between the observed and the 'best fit' computed dipolar coupling constants indicates that either $\text{H}\cdot\text{CO}\cdot\text{NH}\cdot\text{C}-$ lie on one plane, or a rapid inversion about the nitrogen atom introduces an 'effective' plane of symmetry as discussed below.

To the best of our knowledge, the structural data on N -methyl formamide does not seem to have been reported. However, the microwave data on formamide are available^{14, 15}. Of these, the more recent data¹⁵ together with the HCH bond angle equal to 109.5° and $\text{C}'\text{-H}$ and the N-C bond lengths equal to 1.10 \AA and 1.468 \AA respectively given in structure I (hereafter referred to as data I) have been used in the present calculations. A survey of the literature revealed that the data I differ from those conventionally used for the structure of the peptide unit⁶. These data (referred to as data II hereafter) given within parentheses in structure I were also used for the calculations in order to derive more reliable conclusions. Such a procedure gives an estimate of the errors arising out of the uncertainties in the structural data used.

In the present work, we discuss the possibility of the molecule possessing a plane of symmetry. We consider the following two cases:

Case 1. A rigid planar conformation for the fragment $\text{H}\cdot\text{CO}\cdot\text{HN}\cdot\text{C}$;
and

Case 2. Two energetically equivalent rapidly inter-converting non-planar conformations.

Case 1 - A rigid planar conformation: In this case, the coupling constants D_{13} and D_{23} are influenced by the mode of rotation of the methyl group about the N-C bond as in the toluenes^{17, 20} and the π -methylcyclopentadienyl manganese tricarbonyl complex¹⁸. The equations relating the dipolar couplings, D_{13} and D_{23} , with the molecular geometry and the S -values are similar to those reported earlier^{18, 19} and were introduced into the 'SHAPE' programme¹⁷ for the 'best fit' calculations, together with the equations for D_{12} and D_{34} ¹⁹. The 'best fit' calculations for the S -values were thus made using the fixed geometry (data I and data II). The following possibilities about the mode of rotation of the methyl group were considered:

(a) A hindered rotation in a '3-fold' potential such that one of the C-H bonds of the methyl group lies in the plane containing C', H (1), O and N. In this case, both the possibilities, *i.e.*, (1) when the methyl C-H bond in the plane is pointing away from the N-H proton (referred to as 'staggered' hereafter) or (2) it is towards the N-H proton (referred to as 'eclipsed' hereafter) were considered.

(b) A hindered rotation in a '6-fold' potential such that one C-H bond of the methyl group is in the plane of symmetry as described above. This is equivalent to having both the 'eclipsed' and the 'staggered' configurations with equal probability.

(c) A free rotation of the methyl group.

In all these calculations the methyl group itself was considered rigid and influences of all types of molecular vibrations on the dipolar couplings were neglected. Further, in the calculations, the trans-configuration of *N*-methyl formamide was assumed. Values of the 'best fit' parameters obtained using the 'SHAPE' programme are given in table 2. Errors of the *S*-values were estimated to be 0.0003 in each case using the errors of the observed *D*-values given in table 1. The 'r.m.s. error' given in table 2 is the 'weighted root mean square error' between the observed and the 'best fit' calculated *D*-values using the modified 'SHAPE' programme, where all the coupling constants were given equal weights.

It was found that there is no significant difference between the '6-fold' and the 'free rotation' cases and hence they are included in the same column in table 2.

Table 2 shows that the coupling constant D_{13} is the one which is most significantly influenced by the mode of rotation of the methyl group, for both the data sets used. It is also seen from the table that the magnitude of this coupling constant is larger than the observed value (table 1) for the 'eclipsed' and smaller for the 'staggered'. It is, therefore, logical to expect the values for the '6-fold' or 'free rotation' cases (which contain both the '3-fold' cases considered) to be closer to those observed. It is actually found to be so as seen from table 2. The r.m.s. error of about 0.2 Hz for the '6-fold' or the 'free rotation' cases using 'data I' seems to support the assumption of the plane of symmetry in the molecules. Table 2 also shows that the data are strongly dependent upon the mode of rotation of the methyl group and the geometrical data used. The r.m.s. errors of 1.09, 1.41 and 2.05 Hz obtained for the 'eclipsed' and the 'staggered' cases using 'data I' and 'staggered' case using 'data II' are certainly outside the experimental errors. Although the r.m.s. errors of 0.65 and 0.75 Hz obtained for 'data II' are of about the same order of magnitude as the experimental errors of the observed coupling constants (table 1), the deviations in D_{13} are much larger and are outside the experimental errors. Consequently, in order to obtain a more direct and

Table 2. 'Best-fit' parameters obtained with the help of the modified 'SHAPE' programme for N-methyl formamide oriented in the nematic phase of (a). Numbering of the protons refers to that given in structure I. The data are for the rigid planar conformation described in 'case I' in the text.

Parameter	Using 'data I' given in structure I			Using 'data II' given within parentheses in structure I			
	'eclipsed'	'staggered'	'6-fold' or 'free rotation'	'eclipsed'	'staggered'	'6-fold' or 'free rotation'	
D_{12}	-376.90 Hz	-377.01 Hz	-376.97 Hz	-376.92 Hz	-377.03 Hz	-376.99 Hz	
$D_{13} = D_{14} = D_{15}$	-46.42 Hz	-41.75 Hz	-44.00 Hz	-45.63 Hz	-40.50 Hz	-42.96 Hz	
$D_{23} = D_{24} = D_{25}$	-36.91 Hz	-35.67 Hz	-36.25 Hz	-36.60 Hz	-35.62 Hz	-36.08 Hz	
$D_{34} = D_{35} = D_{45}$	162.63 Hz	163.90 Hz	163.31 Hz	162.88 Hz	164.15 Hz	163.53 Hz	
S_{xx}^*	.0153	.0154	.0153	.0153	.0154	.0154	
S_{yy}^*	.0177	.0283	.0229	.0188	.0334	.0258	
S_{zz}^*	-.0330	-.0437	-.0382	-.0341	-.0488	-.0412	
$-S_{xy}^*$.0214	.0134	.0175	.0224	.0128	.0178	
r.m.s. error	1.09 Hz	1.41 Hz	0.21 Hz	0.65 Hz	2.04 Hz	0.75 Hz	

* Refers to the Cartesian coordinate system where the x and y axes lie in the plane of the symmetry with x-axis as the N-C axis. The S-values are calculated using a distance between the methyl protons equal to 1.78×10^{-10} m.

reliable information on the ($\text{C}-\text{N}-\text{C}^{\text{H}}$) fragment, more reliable geometrical data on *N*-methyl formamide should be available and the isotopically enriched ^{13}C and ^{15}N species should be studied. In the latter case besides, getting more direct coupling constants (which make it possible to obtain some of the geometrical data), it would be possible to derive the results independent of the mode of rotation of the methyl group. Work on these lines is in progress.

The above calculations for the 'free rotation' case were also made assuming the 'cis' configuration (structure II) (obtained by a 180° rotation of the $\text{H}(1)\text{C}'\text{O}$ plane about $\text{C}'-\text{N}$ bond) of the molecule. It was found that the r.m.s. error between the observed and the 'best-fit' calculated D -values is 49.03 Hz for 'data I' and 54.72 Hz for 'data II'. The results, therefore, directly establish that the 'trans' species are predominant in *N*-methyl formamide and the calculated spectrum corresponds to these.

Case 2—Two energetically equivalent rapidly interconverting non-planar conformations: A conformation of this type, where the molecular reorientation is slower than the rate of inter-conversion, also needs three S -values to describe the molecular order. Let us consider the two bent conformations with the $\text{N}-\text{H}$ and $\text{N}-\text{C}$ bonds which bend on the same side of the effective plane of symmetry and make an angle $\pm \theta$ with it; the positive sign applies to one conformation and the negative to the other. In such a case, three S -values and the angle θ are to be determined from the four dipolar coupling constants. One, therefore, normally expects a 'perfect fit' between the observed and the 'best fit' calculated dipolar coupling constants. It was actually found to be so for the various modes of rotation of the methyl group discussed in case 1 except for the 'eclipsed' case, for which the minimum r.m.s. error between the observed and the calculated dipolar couplings was obtained for the 'planar' structure (*i.e.*, for $\theta = 0$). The programme 'SHAPE' was suitably modified and adapted to IBM 360/44 computer to carry out these calculations. The resulting S -values and the angles (θ 's) are given in table 3 for the various possibilities considered except for the 'eclipsed' case for which the values given in table 2 are valid. In this case also, no significant differences were observed for the 'free rotation' and the '6-fold' cases and hence the data for these are given in the same column in table 3.

Table 3 shows that, for the two rapidly inter-converting bent conformations of *N*-methyl formamide, the NMR results are in conformity provided (θ) is less than 10° . The value of θ in fact varies from 3 to 10° depending upon the assumed structural data and the mode of rotation of the methyl group. An error of about 5° is estimated for the value of θ given in table 2.

Table 3. 'Best fit' parameters for N-methyl formamide considering two rapidly inter-converting configurations as described in 'case 2' in the text.

Parameter	Using 'data I' given in structure I		Using 'data II' given within parentheses in structure I	
	'staggered'	'6-fold' or 'free rotation'	'staggered'	'6-fold' or 'free rotation'
S_{xx}^a	.0166	.0155	.0173	.0160
S_{yy}^a	.0265	.0225	.0304	.0245
S_{zz}^a	-.0431	-.0380	-.0477	-.0405
S_{xz}^a	.0147	.0177	.0145	.0185
θ (in degrees)	8.3	3.2	10.2	6.2

^aRefers to the Cartesian coordinate system where the axes x and y lie in the 'effective' plane of symmetry (containing atoms C', H(1), O, N). The x-axis is along the axis of rotation of the methyl group in a 'rigid-planar' configuration as in case 1. The S-values are calculated using the scaling distance of 1.78×10^{-10} m between the protons of the methyl group.

As pointed out earlier, for the 'eclipsed' form, an acceptable fit between the observed and the calculated dipolar couplings is obtained neither for the rigidly 'planar conformation' nor for the two 'rapidly inter-converting bent conformations' when reasonable bond lengths and bond angles are used. These results indicate that the 'eclipsed' form alone may not be present in N-methyl formamide if the bond length and the bond angle data used are correct.

As mentioned earlier, more definite and reliable information on the conformation of N-methyl formamide is expected to be derived from the isotopically enriched (^{13}C and ^{15}N) species: the work on these lines is in progress.

Acknowledgement

The authors are grateful to Professor G N Ramachandran not only for suggesting the problem but also for his active interest in the stage-wise progress of the work. One of the authors (KRKE) is thankful to

U S Public Health Service for the partial financial support under Grant No. AM 15964. The authors would also like to acknowledge Professor Hirota* and his colleagues for sending their results on formamide to Professor G N Ramachandran, prior to publication.

References

- 1 RAMACHANDRAN G N AND SASISEKHARAN V *Adv. Protein Chem.* **23** 283 (1968)
- 2 SCHERAGA H A *Adv. Phys. Org. Chem.* **6** 103 (1968)
- 3 KEIR L B *Molecular orbital studies of drug action*, (Academic Press, New York) (1971)
- 4 GOVIL G and SARAN A *J. Chem. Soc. (A)* 3624 (1971)
- 5 PULLMAN B *Int. J. Quantum Chem.* **4** 319 (1971)
- 6 RAMACHANDRAN G N, LAKSHMINARAYAN A V and KOLASKAR A S *Biochim. Biophys. Acta* **303** 8 (1973) and the related references therein
- 7 RAMACHANDRAN G N *Biopolymers* **6** 1494 (1968)
- 8 DIEHL P and KHETRAPAL C L *NMR-Basic principles and progress* ed DIEHL P, FLUCK E and KOSFELD R (Springer-Verlag Berlin, Heidelberg, New York) Vol. **1** (1969)
- 9 LAPLANCHE L A and ROGERS M T *J. Amer. Chem. Soc.* **86** 337 (1964)
- 10 RANDALL E W and BALDESCHWIELER J D *J. Mol. Spect.* **8** 365 (1962)
- 11 BOURNAND A J R and RANDALL E W *Mol. Phys.* **8** 567 (1964)
- 12(a) SUZUKI I *Bull. Chem. Soc. Japan* **35** 540 (1962)
- (b) NEUMAN (Jr) R C, JONAS V, ANDERSON K and BARRY R *Biochem. Biophys. Res. Commun.* **44** 1156 (1971)
- 13 DIEHL P, KHETRAPAL C L and KELLERHALS H P *Mol. Phys.* **15** 333 (1968)
- 14 KURLAND R J and WILSON (Jr) E B *J. Chem. Phys.* **27** 585 (1957)
- 15 COSTAIN C C and DOWLING J M *J. Chem. Phys.* **32** 158 (1960).
- 16 SAUPE A *Z. Naturforsch.* **20a** 572 (1965)
- 17 DIEHL P, HENRICH P M and NIEDERBERGER W *Mol. Phys.* **20** 139 (1971) and the references therein.
- 18 KHETRAPAL C L, SAUPE A, KUNWAR A C and KANEKAR C R *Mol. Phys.* **22** 1119 (1971)
- 19 KHETRAPAL C L and SAUPE A *J. Mag. Res.* **9** 275 (1973)
- 20 DIEHL P, HENRICH P M, NIEDERBERGER W, and VOGT J *Mol. Phys.* **21** 377 (1971)
- 21 HIROTA E, SUGISAKI R, NIELSEN C J and SORESENSEN G O *J. Mol. Spect.* **49**, 251 (1974)
- 22 KHETRAPAL C L, KUNWAR A C and RAMAPRASAD S (unpublished)

* Recently, Hirota *et al*²¹ have re-determined the structure of formamide with the help of microwave spectroscopy. These data give a minimum r.m.s. error of 0.09 Hz between the observed and the 'best-fit' calculated *D*-values for a planar structure of the fragment H.CO.NH.C in N-methyl formamide; this 'minimum' is obtained for the 'free-rotation' of the methyl group about the N-C bond and using the HCH bond angle, the C-H and the N-C bond lengths equal to those for data I described in the text.

DISCUSSION

Sharma : Have you verified results for formamide ?

Khetrapal : No. The molecule formamide can be studied for obtaining such an information only if the coupling of at least one of the hetero-nuclei are observed. Such a study can be done either by taking the samples enriched in ^{13}C and/or ^{15}N or by the use of F.T.NMR. In absence of such facilities, this work has not been undertaken. However, Reeves and his group have studied the ^{15}N -enriched formamide dissolved in a lyotropic mesophase and they find a non-planar structure (Mol. Phy. 1973).

NMR spectra of bicyclic compounds oriented in the nematic phase Part III : The spectrum of benzo(b)thiophene

C L KHETRAPAL*, A C KUNWAR* and A SAUPE†

*Raman Research Institute, Bangalore 560006, India

†Liquid Crystal Institute, Kent State University, Kent, Ohio 44242, USA

Abstract. From the PMR spectrum of benzo(b)thiophene dissolved in a nematic solvent, the shape of the proton skeleton of the molecule is determined. The results are consistent with the molecule being planar. No significant distortions in the geometry of the benzene and the thiophene rings are observed. Information on the molecular orientation is derived. It is found that the molecule orients in the nematic phase such that the largest positive S-value is along the longest molecular dimension.

1. Introduction

The compounds possessing the benzo(b)thiophene nucleus (figure 1) have found applications in the dye industry and are known to possess insecticidal properties¹. In spite of these applications, the structure of benzo(b)thiophene molecule does not seem to have been reported. An easy and convenient procedure to obtain information on the molecular geometry is provided by NMR spectroscopy in nematic solvents as discussed earlier for some other bicyclic compounds²⁻⁵. The benzo(b)thiophene molecule has a lower symmetry than the bicyclic compounds studied earlier, which possess two perpendicular planes of symmetry. There are fifteen different inter-proton dipolar coupling constants in benzo(b)thiophene compared to nine in the other bicyclic compounds. They provide directly information on the relative arrangement of protons and indirectly on the planarity of the carbon skeleton, in addition to the molecular order. A study of the spectra due to ¹³C in addition, may provide direct information on the geometry of the carbon skeleton. In the present paper, the results obtained from the PMR spectrum of benzo(b)thiophene without the ¹³C-H satellites are reported. The ¹³C-H satellites are not observed in the natural abundance of ¹³C without sufficient spectral accumulations. It may also be mentioned that the results reported in the present paper do not take into account the 'vibrational effects' on the observed dipolar couplings.

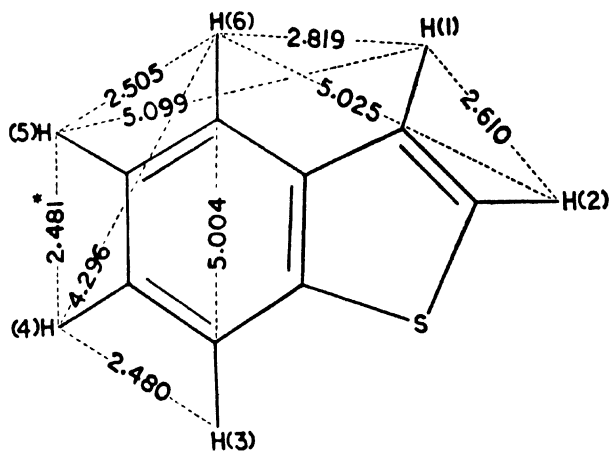


Figure 1 The structure of benzo(b)thiophene. Interproton distances given in the figure are in units of 10^{-10} m.

* The scaling distance $r_{45} = 2.481 \times 10^{-10}$ m (assumed).

2. Experimental

A 12 mole per cent solution of locally available benzo(b)thiophene was prepared in 4-ethoxy-benzylidene-4-*n*-butylaniline(a). The solution (in a 5 mm NMR sample tube) was stored horizontally for a few days before recording the final spectrum (figure 2) at 30°C on a Varian XL-100 spectrometer. The spectrum was recorded in two parts with sweep widths of 2500 Hz and sweep times of 2500 s. The strongest line in one part served as the 'lock-signal' while the other part was being recorded. The total spread was 3830 Hz and the average line width was 6 Hz. The mean statistical error in the measurement of line positions determined by repeated recordings was 1.2 Hz. The maximum deviation of any line position from the mean value was less than 3 Hz.

3. Result and discussion

3.1. *Spectral analysis*: Analysis of the spectrum was carried out iteratively with the help of the LAOCOONOR⁶ programme on a CDC-3600 computer. In the final analysis, only the chemical shifts ($\nu_i - \nu_j$) and the direct dipolar couplings (D_{ij} as defined in the LAOCOONOR programme) were iterated upon; the indirect spin-spin couplings (J_{ij}) were given the same values as those obtained from the spectrum in the isotropic media⁷. Values of the derived parameters are given in table 1 along with those of the indirect coupling constants used. The root mean square error between the experimental and the calculated line positions was 1.1 Hz with a maximum deviation of 2.7 Hz for any line. All the

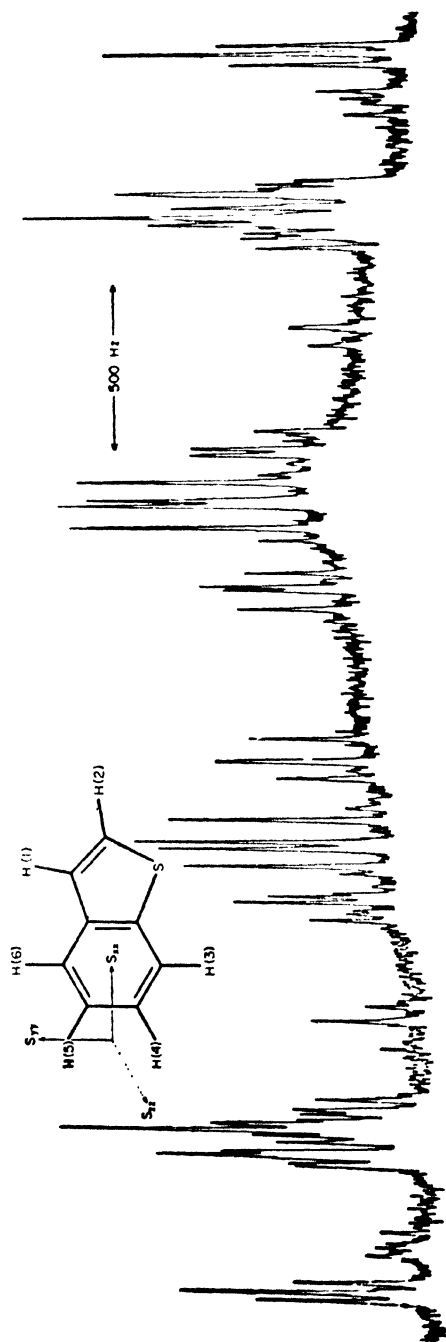


Figure 2 PMR spectrum of benzo(b)thiophene dissolved in the nematic phase of (a). Solute concentration = 12 mole per cent ; Temperature = 30° C; Spectrometer frequency = 100 MHz.

Table 1 Results of spectral analysis for benzo(b)thiophene oriented in the nematic phase of (a). Numbering of protons refers to figure 1.

ij	Coupling constants			Parameter	Value
	J_{ij} (assumed)	D_{ij} (experimental)	D_{ij} (calculated 'best-fit')		
12	5.45	-544.0 ± 0.9	-544.0	$\nu_1 - \nu_6$	24.2 ± 0.9 Hz (48.96)*
13	0.84	-7.8 ± 0.8	-7.4	$\nu_2 - \nu_6$	16.3 ± 0.7 Hz (40.38)*
14	-0.12	-35.9 ± 0.7	-34.3	$\nu_3 - \nu_6$	3.4 ± 1.4 Hz (-6.95)*
15	0.03	-106.4 ± 0.9	-106.4	$\nu_4 - \nu_6$	27.3 ± 1.4 Hz (47.16)*
16	-0.29	-726.9 ± 0.2	-726.9	$\nu_5 - \nu_6$	20.1 ± 0.7 (45.03)*
23	0.03	-55.9 ± 0.4	-55.8	$S_{xx} \uparrow$	0.1324
24	0.50	-40.5 ± 0.5	-42.4	$S_{yy} \uparrow$	-0.0028
25	0.02	-53.2 ± 0.1	-52.7	$S_{xy} \uparrow$	-0.0257
26	0.17	-120.4 ± 0.8	-120.0	r_{12}/r_{45}	1.052 ± 0.01
34	8.13	-926.4 ± 0.1	-926.4	r_{13}/r_{45}	2.055 ± 0.02
35	1.06	-74.8 ± 0.4	-74.9	r_{16}/r_{45}	1.136 ± 0.01
36	0.74	3.5 ± 0.8	3.5	r_{26}/r_{45}	2.025 ± 0.02
45	7.14	22.3 ± 0.6	22.4	r_{34}/r_{45}	1.000 ± 0.01
46	1.21	-14.4 ± 0.8	-15.0	r_{36}/r_{45}	2.017 ± 0.02
56	8.04	-603.4 ± 1.0	-603.4	r_{46}/r_{45}	1.731 ± 0.02
				r_{56}/r_{45}	1.010 ± 0.01

$\uparrow r_{45} = 2.481 \text{ \AA}$ (assumed). $1 \text{ \AA} = 10^{-10} \text{ m}$.

* Values in the isotropic phase⁷.

111 observed lines were assigned for the analysis. Errors of the parameters given in table 1 are the standard deviations obtained from the LAOCOONOR programme. Errors of the parameters were also estimated by changing the observed line positions by ± 1.2 Hz, the accuracy of measurement, in such a way that the position of each line deviated from its calculated value by the maximum possible amount. These values were then used to calculate the spectral parameters iteratively. The errors thus obtained (*i.e.*, the difference between the parameters obtained this way and those obtained using the measured line positions) were found to be smaller than the standard deviations given by the LAOCOONOR programme and hence only the latter are given in table 1. The large errors arise from the fact that relatively large number of parameters are to be determined (15 dipolar couplings and 5 internal chemical shifts) from the experimental line positions. A similar situation has been encountered in the analysis of the spectrum in the isotropic medium⁷.

3.2. Molecular geometry: If one assumes a plane of symmetry in the benzo(b)thiophene molecule, 3 independent parameters are needed to define its orientation and 9 inter-proton distances suffice to describe the geometry of the proton skeleton. There are 15 different dipolar couplings and if one assumes a scaling distance, such a system is over determined by 4 coupling constants as far as the determination of the geometry of the proton skeleton and the molecular order from the inter-proton dipolar couplings is concerned. If self-consistent results are obtained in the iterative calculations which compute the geometry and the degree of order using a 'weighted least square fit' method, the assumption about the plane of symmetry in the molecule is justified. The programme SHAPE⁸ was used for such calculations. All the coupling constants were given equal weights. The direct couplings corresponding to the 'best-fit' parameters are included in table 1. The order parameters and the ratios of the HH distances are also included in the same table.

Table 1 shows that some of the observed, and the 'best-fit' calculated dipolar couplings deviate beyond their experimental errors. A maximum deviation of 1.9 Hz is found for D_{24} . Deviations of similar magnitudes have been observed in some other cases also^{9,10} and are attributed to several effects like the neglect of the influence of molecular vibrations and the solvent effects, in addition to experimental errors. The results can be considered as consistent with the assumption of a plane of symmetry in the molecule. In figure 1, various inter-proton distances determined assuming $r_{45} = 2.481 \times 10^{-10}$ m are given in units of 10^{-10} m.

It is seen from table 1 and figure 1 that the geometry of the phenyl part does not deviate, beyond the experimental error, from the benzene ring geometry, unlike in the other rigid bicyclic molecules where significant deviations have been detected in this part of the molecule^{2, 3, 11}.

The distance r_{12} between the protons of the thiophene ring in this case is found to be 2.61×10^{-10} m under the assumption of $r_{45} = 2.481 \times 10^{-10}$ m. It is very close to the corresponding value (2.64×10^{-10} m) in thiophene¹².

The results, therefore, indicate that there are no significant distortions in the geometry of the benzene and the thiophene rings in benzo (b)thiophene.

3.3. Molecular orientation: For the purpose of obtaining the order parameters, the Cartesian coordinate system was chosen such that the axes X and Y lie in the molecular plane with Y-axis being the line joining protons 4 and 5. The values of the order parameters given in the table obtained using the SHAPE programme were derived by assuming $r_{45} = 2.481 \times 10^{-10}$ m. The largest positive S -value (S_{xx}) along the X-axis is in agreement with the fact that the largest S -value corresponds to the largest molecular dimension. Similar results have been obtained for the other rigid bicyclic molecules studied earlier^{2, 3, 11}.

Acknowledgments

The authors are grateful to Professor M R Padhya of the University Department of Chemical Technology, Bombay for supplying the sample of benzo(b)thiophene. One of the authors (AS) is grateful to the National Science Foundation of USA for the partial support to buy the XL-100 spectrometer under grant No. GP-10481.

References

- 1 CAMPAIGNE E, KNAPP D R, NEISS E S and BOSIN T R *Advances in Drug Research*, Ed HARPER N J and SIMMONDS A B (Academic Press, London & New York) Vol. 5, 1 (1970)
- 2 KHETRAPAL C L and KUNWAR A C *Mol. Cryst. Liquid Cryst.* 15 363 (1972)
- 3 KHETRAPAL C L, SAUPE A and KUNWAR A C *Mol. Cryst. Liquid Cryst.* 17 121 (1972)
- 4 DEREPE J M, DEGELAEN J and VAN MEERSSCHE M *J. Chim Phys.* 67 1875 (1970)
- 5 DEREPE J M, DEGELAEN J and VAN MEERSSCHE M *Org. Magn. Res.* 4 551 (1972)
- 6 DIEHL P, KHETRAPAL C L and KELLERHALS H P *Mol. Phys.* 15 333 (1968)
- 7 BALKAN F and HEFFERMAN M L *Aust. J. Chem.* 25 327 (1972)
- 8 DIEHL P, HENRICH P M and NIEDERBERGER W *Mol. Phys.* 20 139 (1971)
- 9 KHETRAPAL C L, KUNWAR A C and SAUPE A *J. Magn. Res.* 7 18 (1972)
- 10 SEGRE A L and CASTELLANO S *J. Magn. Res.* 7 5 (1972)
- 11 KHETRAPAL C L and PATANKAR A V, *Mol. Cryst. Liquid Cryst.* 15 367 (1971)
- 12 BAK B, CHRISTENSEN D, HANSEN-NYGAARD L and RASTRUP-ANDERSEN J, *J. Mol. Spect.* 7 58 (1961)

DISCUSSION

Sharma : How can you derive r_e -values from the observed D -values?

Khetrapal : For the calculation of the relative equilibrium geometry, one needs to apply the anharmonic and the harmonic vibrational corrections to the observed dipolar couplings. However, since the computation of the anharmonic terms in general is not practical, a suggestion has been made by Lucas to derive the 'average structure' from the direct dipolar couplings by taking into account only the 'harmonic corrections' (Molecular Physics 1971 and 1972).

Thermal studies of benzylideneaniline liquid crystals

MICHIO SORAI, TERUO NAKAMURA and SYŪZŌ SEKI
Department of Chemistry, Faculty of Science, Osaka University,
Toyonaka, Osaka 560, Japan

Abstract. The thermal behavior of a series of anils (*N-p*-alkoxybenzylidene-*p'-n*-alkylanilines) with low temperature mesomorphic ranges has been examined between -185 °C and 100 °C by differential thermal analysis. As a consequence, glassy states of smectic mesophase were established for the first time. Significant differences between the glassy smectic state and the glassy nematic or the glassy isotropic-liquid states have been indicated. Heat capacity measurements have also been made for *N-p*-ethoxybenzylidene-*p'*-butylaniline in the range from 14 to 375 K. An attempt has been made to interpret the mesomorphic transition from nematic to isotropic liquid in terms of critical phenomena.

Introduction

From a thermodynamic point of view the study of liquid crystal is interesting in the sense that a cooperative phase transition can be realized even in a fluid state. Thermodynamic quantities such as heat capacity, enthalpy and entropy certainly provide useful information as to the energetic aspects inherent in a mesophase transition and are indispensable for comprehensive understanding of the relationship between the mesomorphic transition and the molecular dynamics.

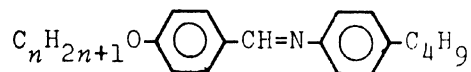
In comparison with abundant studies on liquids by thermal analyses, precise calorimetric investigations have been extremely scarce. This is partly due to the fact that most liquid crystals possess their mesomorphic ranges at rather high temperatures. Recent findings of new compounds with low-temperature mesomorphic ranges such as substituted benzyldeneanilines (Schiff bases)¹⁻⁶, stilbenes⁷, and tolans⁸ provide suitable subjects for precise calorimetric measurements. The heat capacity of MBBA (*N-p*-methoxybenzylidene-*p'*-butylaniline), which is well known as a room-temperature nematic liquid crystal, has been measured by Mayer *et al*⁹ and Shinoda *et al*¹⁰. We have measured the heat capacity of OHMBBA¹¹, which is an *o*-hydroxy analogue of MBBA, and found a glassy state of the nematic phase. As an extension of the previous study we will report in this paper the heat capacity of *N-p*-ethoxybenzylidene-*p'*-butylaniline (EBBA for short). An attempt will be made to interpret

the mesomorphic transition from nematic to isotropic liquid in terms of critical phenomena.

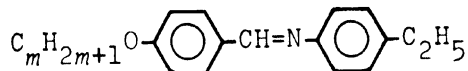
In connection with our recent findings of glassy states in some liquid crystals¹¹⁻¹³, we will present further evidences for the existence of glassy liquid-crystalline states in simple Schiff bases with low temperature mesomorphic ranges. The glassy states were confirmed with differential thermal analysis. As a consequence, glassy smectic states were established for the first time in this study. As will be given below, significant differences were found between the glassy state of the smectic phase and that of the nematic or the isotropic liquid.

Experimental

Materials. We have studied the thermal properties of two series of benzylidencaniline compounds of the form



where $n = 1$ (MBBA), $n = 2$ (EBBA), $n = 4$ (BOBUTA), $n = 5$ (PENTOBUTA), $n = 6$ (HEXOBUTA) and $n = 8$ (OCTOBUTA), and



where $m = 4$ (BOETHA) and $m = 6$ (HEXOETHA). All compounds were prepared by condensation in refluxing ethanol of the respective *p*-*n*-alkoxy-benzaldehydes and the appropriate *p*-*n*-alkylaniline (Tokyo Kasei Kogyo Co., Ltd. and Wako Pure Chemical Industries, Ltd.). Crystalline products were purified by multiple recrystallization from ethanol or *n*-hexane. Elemental analyses were satisfactory for all compounds.

Identification of the mesophases for some compounds was made by using a polarizing microscope (Olympas Model TOS) equipped with a hot-stage. However, characterization of the mesophases for the remaining compounds followed the results by Flannery and Haas³.

Thermal Properties.

The thermal behaviors of all materials were examined between -185°C and 100°C by differential thermal analysis (DTA)¹⁴. The amount of specimen used for DTA was about 500 mg.

Heat capacity of EBBA was measured with an adiabatic calorimeter¹⁵ between 14 and 375 K. The amount of specimen was about 18 g and a platinum resistance thermometer based on IPTS-68 scale was used.

Thermal behavior

Typical results of DTA for the present materials are represented in figures 1-8, respectively. Prior to describing the detailed thermal behavior for particular specimens, we refer to the meaning of various abbreviations and procedures used in common through these figures. A crystalline state is denoted as a symbol "C", while "C₁", "C₂", are used to distinguish different crystalline polymorphs. Smectic, nematic, and isotropic liquid phases are shown by the symbols "S", "N", and "Iso" respectively. When there exist more than two, smectic mesophases, subscripts I, II, and III are adopted according to the previous notations³. In each figure Run 1 shows a heating curve of a crystalline material up to its isotropic liquid at an average rate of 2.5 K min⁻¹. Run 2 in figures 1-7 and run 3 in figure 8 correspond to the cooling curve of the isotropic liquid at a rate greater than -10 K min⁻¹. The final run gives a heating curve at an average rate of 2.5 K min⁻¹ from the lowest temperature to an isotropic liquid. A melting peak and/or a peak due to crystallization in a cooling curve are shaded in order to distinguish them from the other ones. Melting point and glass transition temperature are marked with T_m and T_g , respectively.

MBBA:

Since the first synthesis by Kelker and Scheurle¹, this compound has been known as a room-temperature nematic liquid crystal having a relatively simple molecular structure and also as a sample on which various kinds of investigations have been made. Thermal behavior of this material, however, seems to be very sensitive to the existing impurities. The transition temperature from nematic to isotropic liquid, T_e , so far reported are widely distributed: for example, 41 °C (polarizing microscope)¹, 39.5 °C (DTA)³, 43.85 ± 0.2 °C (heat capacity C_p),⁹ and 46.987 °C (C_p)¹⁰. We examined the effect of impurities upon the transition temperature by use of DTA. The specimen purified by vacuum distillation of a commercial product showed the mesophase transition at $T_e = 37.3$ °C, while further purifications by recrystallization two or three times from ethanol raised the T_e to 43 °C and 44.5 °C, respectively. The endothermic peak due to the mesophase transition became sharper according to the degree of purification. On the other hand, the specimen freshly prepared and purified by recrystallization three times from ethanol exhibited the mesophase transition at 48 °C.

Figure 1 shows the successive runs of DTA. When cooling was not rapid enough, partial crystallization from the supercooled nematic liquid was observed around -30 °C. However, when the cooling was faster than -10 K min⁻¹, almost all the portion of the supercooled nematic phase brought about around -70 °C a glassy state which is thermodynamically a non-equilibrium state. On heating, a typical glass transition phenomenon was observed at -72 °C, followed by an irreversible crystallization. This is

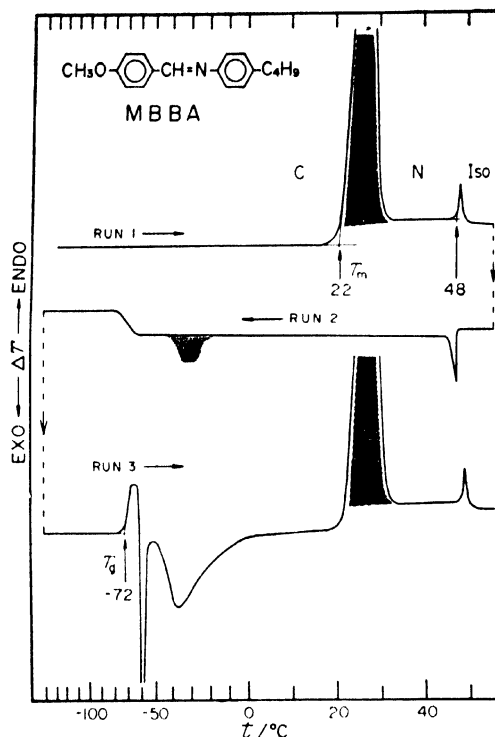


Figure 1 DTA curves of MBBA

the second example in which the glassy state of nematic mesophase has been realized^{11,13}.

EBBA: As shown in figure 2, the nematic state was supercooled to 20 °C, but at this temperature it crystallized into a metastable crystalline form. The cooling rate of -500 K min^{-1} was still not great enough to establish a glassy liquid-crystal. The result of heat-capacity measurements will be given in the next section.

BOBUTA (see figure 3): This compound melted at 14.5 °C and exhibited three mesophases (S_{II} , S_I , and N). On cooling the smectic S_{II} , a new phase was observed regardless of the cooling rate. Although its identification has not been made, it is very likely that this phase belongs to a metastable smectic state rather than a metastable crystal. Run 4 gives a heating curve of this new phase. An endothermic anomaly similar to a glass transition was observed between -115 and -60 °C, and then a phase transition from the metastable-S to the S_{II} occurred at 6 °C. This temperature just corresponds to the value previously reported as T_m^3 . But this is not the normal melting point because the specimen well annealed below 6 °C melted at 14.5 °C.

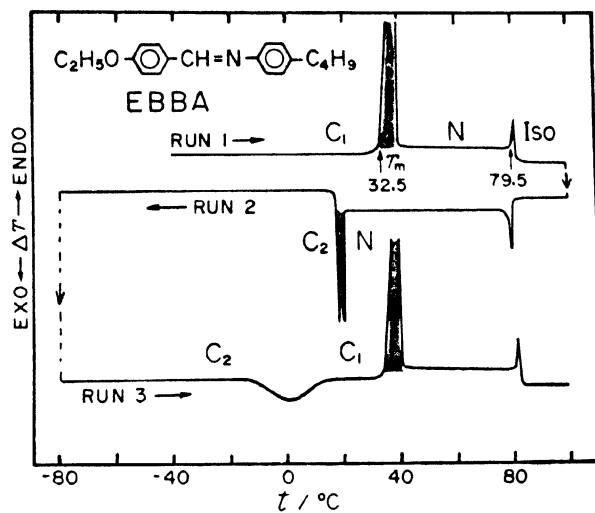


Figure 2 DTA curves of EBBA

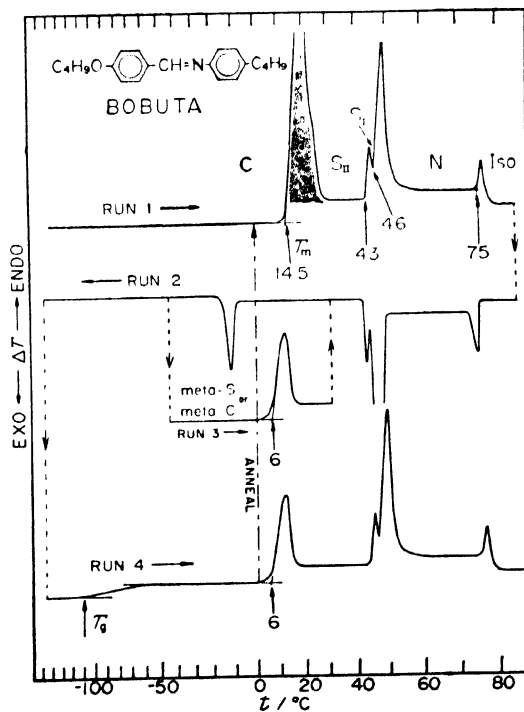


Figure 3 DTA curves of BOBUTA

PENTOBUTA (see figure 4): Unlike the previous result³, the present DTA curve showed merely two mesophases, namely S and N. The smectic phase was easily quenched to give a glassy state. A clear glass transition phenomenon was observed in a heating curve at -92°C .

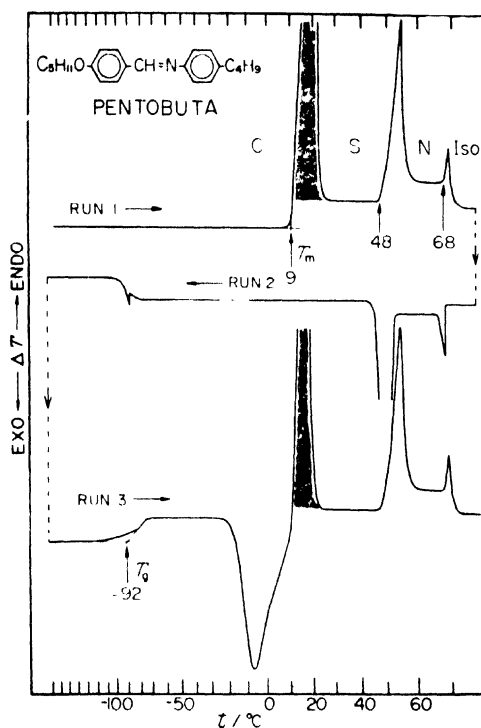


Figure 4 DTA curves of PENTOBUTA

HEXOBUTA (see figure 5): Among the eight materials studied here, HEXOBUTA exhibited polymorphism with as many as four mesophases, *i.e.* S_{III} , S_{II} , S_I , and N. The transition temperatures were approximately the same as those reported by Flannery and Haas³, although they failed to observe the melting point. The mesophase S_{III} was easily supercooled to about -60°C and finally gave rise to a glassy state. The glass transition temperature was determined to be -93°C .

OCTOBUTA (see figure 6): This compound is of particular interest as it represents a rare example of smectic trimorphism without an accompanying nematic phase³. A glassy state of the smectic mesophase S_{III} was

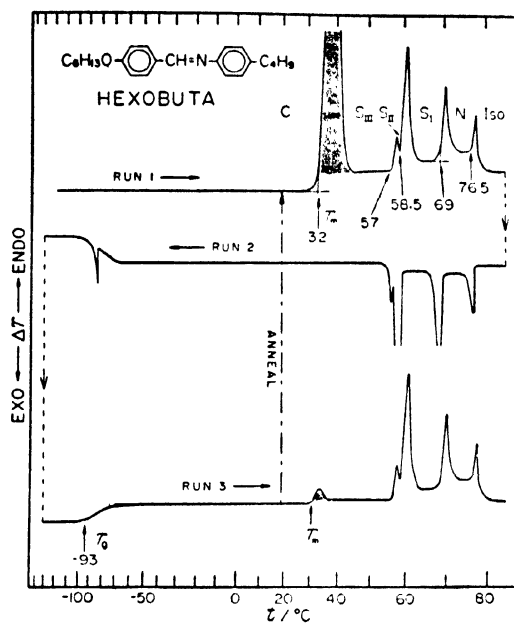


Figure 5
DTA curves of HEXOBUTA

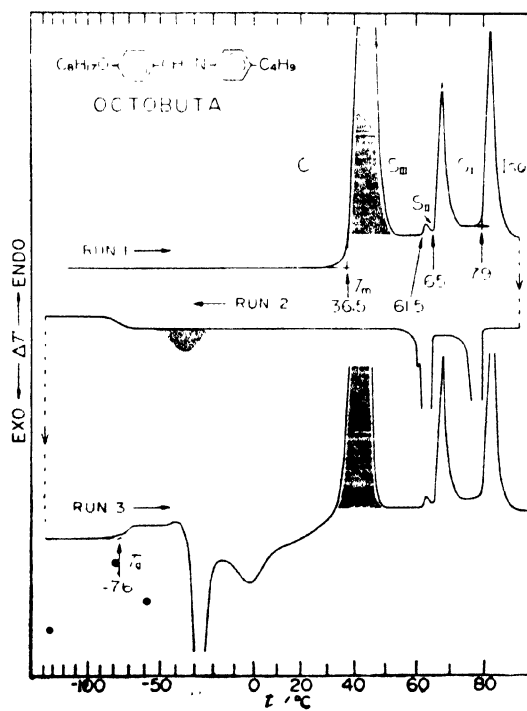


Figure 6
DTA curves of OCTOBUTA

also established for OCTOBUTA ($T_g = -76^\circ\text{C}$). When cooling was not rapid enough, a partial crystallization occurred around -30°C .

BOETHA (see figure 7): Contrary to the previous work³, an extra mesophase S_{11} was found reproducibly in addition to the mesophases of S_1 and N. BOETHA was unique in the series studied, in that the smectic phase S_{11} was easily supercooled to -185°C , but DTA curve showed no glass transition phenomenon. Although there still remains a possibility that the glass transition temperature may lie below -185°C , it seems unlikely that only this compound has such a low T_g compared with other homologous series. Further experiments will be needed to make clear the thermal behavior of BOETHA.

HEXOETHA (see figure 8): Murase⁴ has reported only one mesophase, *i.e.* nematic, but the present results evidently demonstrated the existence

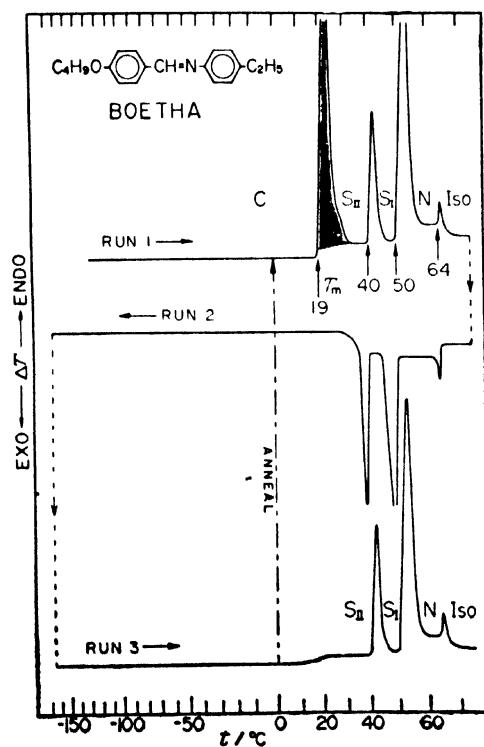


Figure 7 DTA curves of BOETHA

of an additional smectic phase as well as a solid-solid transition at 14 °C. When cooling was faster than -10 K min^{-1} , the smectic phase was supercooled and a glassy smectic state was obtained. In a rapid cooling process, however, a small exothermic peak was observed around -10 °C . This thorn-like peak should not be regarded as a partial crystallization because the peak area did not depend on the cooling rate. On the other hand, the glassy smectic state was transformed into the supercooled smectic phase through a glass transition phenomenon at -89 °C , followed by a crystallization to a metastable crystalline form C_4 around -20 °C . A phase transition from the C_4 to another metastable crystalline form C_3 took place at 25 °C and the latter melted at 35 °C , which was 6 K lower than the normal T_m .

The glass transition temperatures and the mesomorphic transitions for all compounds are summarized in table 1.

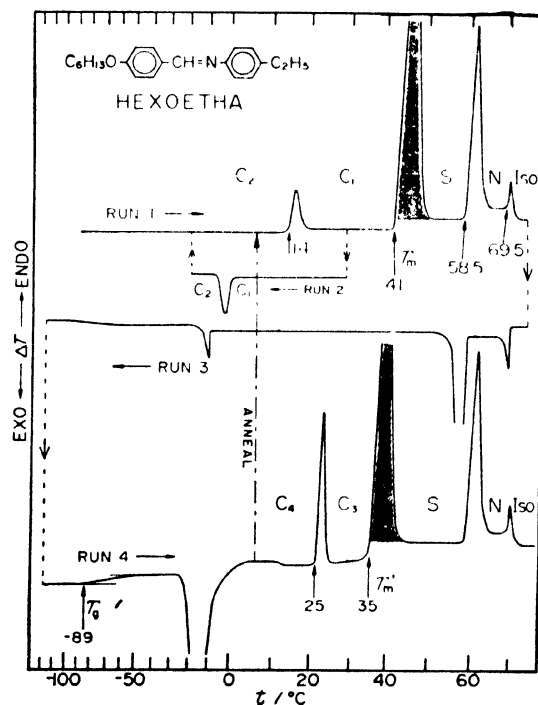


Figure 8 DTA curves of HEXOETHA

Table 1 Substituted Schiff base transition temperatures ^a

Compound	R ₁	R ₂	Glassy Liquid Crystal ?	t _g /°C	Temperature °C of transition				Isotropic Liquid
					S _{III}	S _{II}	S _I	Nematic	
MBBA	CH ₃	C ₄ H ₉	Yes (Nematic)	-72				22 (20) [17]	48 (41) [39.5]
EBBA	C ₂ H ₅	C ₄ H ₉	No					32.5 (36) [37]	79.5 (80) [83]
BOBUTA ^b	C ₄ H ₉	C ₄ H ₉	Probably Yes (Smectic)	-115		14.5 [7]	43 [41]	46 [46]	75 [75]
PENTOBUTA	C ₅ H ₁₁	C ₄ H ₉	Yes (Smectic)	-92		[24]	[52]	48 [54]	68 [71]

Compound •	Temperature °C of transition							Isotropic Liquid	
	R ₁	R ₂	Glassy Liquid Crystals ?	<i>t_f</i> /°C	S _{III}	S _{II}	S _I		Nematic
• HEXOBUTA	C ₆ H ₁₃	C ₄ H ₉	Yes (Smectic)	-93	32 [?]	57 [59.5]	58.5 [60.5]	69 [70]	76.5 [78]
• OCTOBUTA	C ₈ H ₁₇	C ₄ H ₉	Yes (Smectic)	-76	36.5 [39.5]	61.5 [66]	65 [69.5]		79 [83.5]
• BOETHA	C ₄ H ₉	C ₂ H ₅	?		19		40 [39]	50 [48] < 51.5 >	64 [62.5] < 66 >
• HEXOETHA ^c	C ₆ H ₁₃	C ₂ H ₅	Yes (Smectic)	-89			41	58.5 [59 >	69.5 [71.5 >

a : Values in (), [] and < > from references 1, 3 and 4 respectively.

b: Mesophase transition at 6 °C in metastable state.

c : Solid-solid transition at 14 °C.

Heat capacity

The results of heat capacity measurements on EBBA are plotted in figure 9. The concentration of impurities involved in the calorimetric sample was determined to be 0.25 mole % from the melting-point depression. The melting point T_m was 305.62 K, and the enthalpy and the entropy of fusion were 27.09 kJ mol⁻¹ and 88.71 J K⁻¹ mol⁻¹, respectively. The temperature of transition, T_c , from nematic to isotropic liquid was 349.08 K, and the enthalpy and the entropy changes due to this mesomorphic transition were 1.553 kJ mol⁻¹ and 4.524 J K⁻¹ mol⁻¹, respectively.

As was in the case of OHMBBA¹¹, the present mesophase transition was characterized by a considerable pretransition effect. This effect is obviously reflected in a large tail of the heat-capacity curve below T_c . The excess heat capacity arising from this mesomorphic transition, C (excess), was varied with the critical-point exponents α' and α for ϵ ($\equiv |T - T_c| / T_c$), when $T \rightarrow T \pm 0$, by

$$C(\text{excess}) \sim \epsilon^{-\alpha'} \quad \text{for } T < T_c$$

and

$$C(\text{excess}) \sim \epsilon^{-\alpha} \quad \text{for } T > T_c.$$

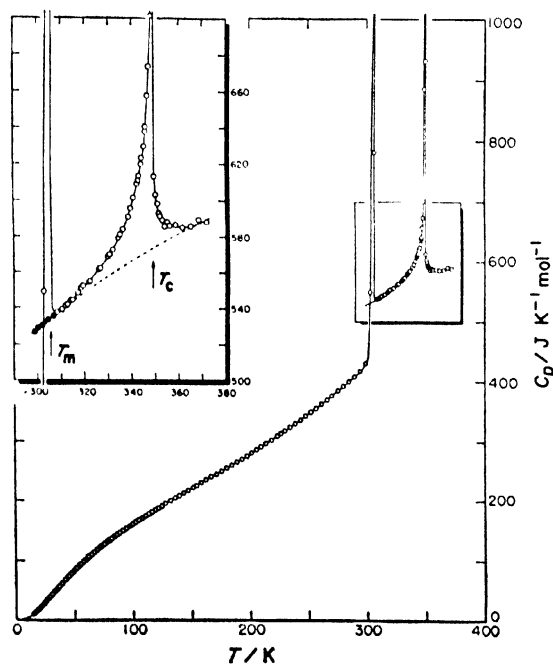


Figure 9 Heat capacity of EBBA

The values of both α' and α were 0.7 in the temperature region $10^{-4} < \epsilon < 10^{-1.5}$. This fact implies that the present mesomorphic transition may be described in terms of a second-order phase transition, though the numerical value of 0.7 seems to be rather large compared with the usual values obtained for typical critical phenomena such as the gas-liquid or the ferromagnetic critical phenomena.

Discussion

The main aim of this work was to examine the existence of glassy state in some liquid crystals with low temperature mesomorphic ranges. In this regard, we could successfully realize the glassy liquid-crystalline states for six materials. In particular, the glassy states of smectic states were established for the first time in the present investigation. We have already reported the new findings of the glassy states for the metastable cholesteric phase in cholesteryl hydrogen phthalate¹² and for the stable nematic phase in OHMBBA^{11,13}. Now that the glassy smectic states were realized in this study, all kinds of glassy states for smectic, nematic, and cholesteric mesophases have been proved to exist.

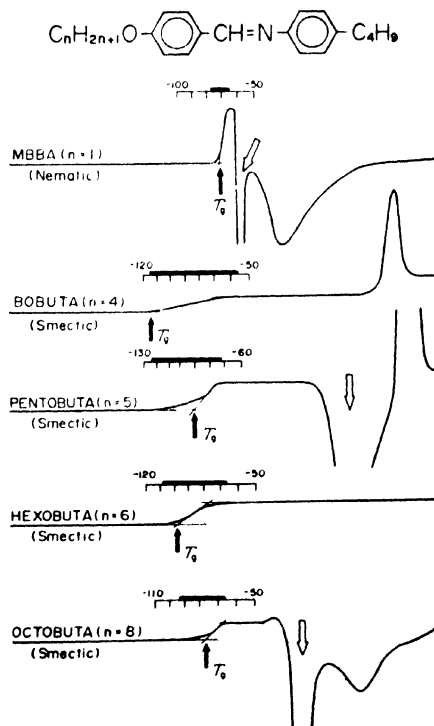


Figure 10 DTA curves around T_g of N-p-alkoxybenzylidene-p'-butylanilines

From a thermodynamic standpoint, a glassy state is, in general, identified by the following three criteria: (i) existence of a glass transition temperature T_g , (ii) enthalpy relaxation phenomena around T_g , and (iii) finite value of a residual entropy at absolute zero. Since we have not measured the low-temperature heat capacity of the present glass-forming materials, only the criteria (i) and (ii) may be applicable to the present systems. One of the most characteristic features concerning the glassy smectic state was that the glass transition effect occurred in a rather wide temperature region compared with those for the glassy nematic and the glassy isotropic liquid states. This situation is illustrated in figures 10 and 11 where four kinds of OHMBBA-homologues¹¹ are also shown for comparison. The glass transition phenomena for the present smectic glasses occurred over a wide interval of 30 ~ 60 K, while those for the glassy nematic and the glassy liquid appeared in a narrow interval of 10 ~ 15 K. This fact implies that in a glassy smectic state the relaxation time of molecular motions cannot be described by a single value.

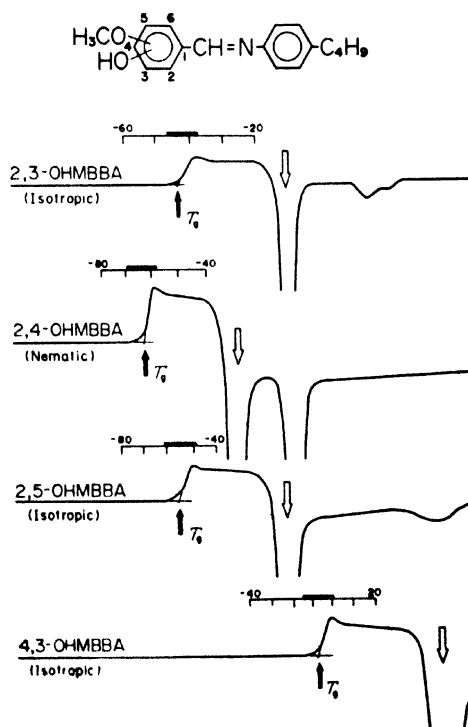


Figure 11 DTA curves around T_g of N-alkoxyhydroxybenzylidene-*p*-butylanilines

It is interesting to note that a smectic state seems to be easily quenched compared with a nematic state, although the short-range molecular order in a crystalline state is believed to be conserved more closely in a smectic phase than in a nematic phase.

Finally, it should be emphasized that the glassy state of pure substances should be distinguished strictly from the supercooled liquid state in the sense that the latter is a metastable equilibrium phase while the former is a non-equilibrium one and not restricted to liquid state of matter. It has been widely recognized that a glassy state may be of quite wide occurrence in condensed matter, and that the concept of glass transition may be understood in terms of a relaxational effect depending on the particular degrees of freedom in a condensed state. In fact, such transitions may be encountered even in crystalline materials having plastic phases^{16,17}, and some crystals with hydrogen-bond networks¹⁸⁻²⁰. Rare examples, in which multiple glass-transition phenomena were found in a single compound, have also been reported²¹.

Molecular crystals with plastic phases consist of spherical molecules and may be looked upon as isotropic crystals with disordered molecular orientation, while liquid crystals, which consist of elongated and rectilinear molecules, are regarded as anisotropic liquids having a tendency towards ordered orientation. Moreover, both the plastic and the liquid-crystalline phases belong to an intermediate state between a typical crystal and an isotropic liquid. In these respects, it will be interesting to compare the glassy state of liquid crystal with that of plastic crystal. Quantitative discussions will be made after precise heat capacity measurements at low temperatures.

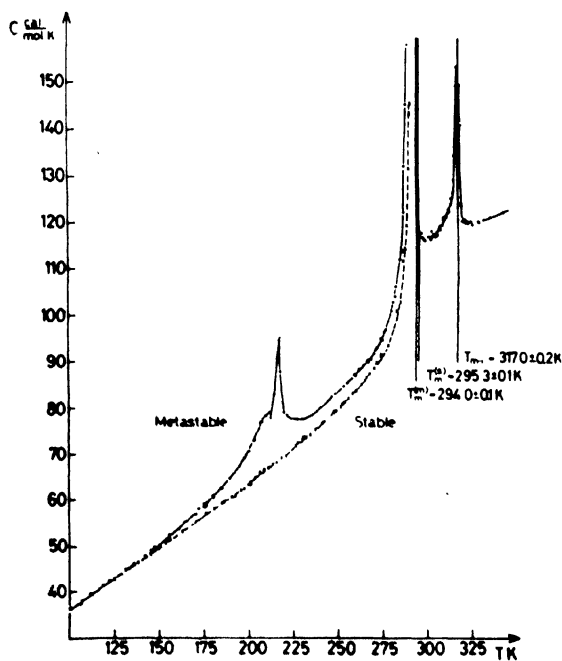
References

- 1 KELKER H and SCHEURLE B *Angew. Chem.* **81** 903 (1969)
- 2 TEUCHER H, PALEOS C M and LABES M M *Mol. Cryst. Liquid Cryst.* **11** 187 (1970)
- 3 FLANNERY J B and HAAS W J *Phys. Chem.* **74** 3611 (1970)
- 4 MURASE K *Bull. Chem. Soc. Japan* **45** 1772 (1972)
- 5 CHAMPA R A *Mol. Cryst. Liquid Cryst.* **16** 175 (1972); **19** 233 (1973)
- 6 DOLPHIN D, MULJIANI Z, CHENG J and MEYER R B *J. Chem. Phys.* **58** 413 (1973)
- 7 YOUNG W R, AVIRAM A and COX R J *Angew. Chem.* **83** 399 (1971)
- 8 MALTHETE J, LECLERCQ M, GABARD J, BILLARD J and JACQUES J *C.R. Acad. Sci. Ser. C* **273** 265 (1971)
- 9 MAYER J, WALUGA T and JANIK J A *Phys. Lett.* **41A** 102 (1972)
- 10 SHINODA T, MAEDA Y and ENOKIDO H The 24th Annual Meeting of the Chemical Society of Japan (1971), Osaka; The 8th Japanese Calorimetry Conference (1972), Okayama
- 11 SORAI M and SEKI S The 4th International Liquid Crystal Conference (1972), Kent State University; *Mol. Cryst. Liquid Cryst.* (in press)
- 12 TSUJI K, SORAI M and SEKI S *Bull. Chem. Soc. Japan* **44** 1452 (1971)
- 13 SORAI M and SEKI S *Bull. Chem. Soc. Japan* **44** 2887 (1971)
- 14 SUGA H, CHIHARA H and SEKI S *Nippon Kagaku Zasshi* **82** 24 (1961)
- 15 SUGA H and SEKI S *Bull. Chem. Soc. Japan* **38** 1000 (1965)

- 16 ADACHI K, SUGA H and SEKI S *Bull. Chem. Soc. Japan*. **41** 1073 (1968); **43** 1916 (1970); **44** 78 (1971); **45** 1960 (1972)
- 17 ADACHI K, SUGA H, SEKI S, KUBOTA S, YAMAGUCHI S, YANO O and WADA Y *Mol. Cryst. Liquid Cryst.* **18** 345 (1972)
- 18 MATSUO T, OGUNI M, SUGA H and SEKI S *Proc. Japan Acad.* **48** 237 (1972)
- 19 HAIDA O, MATSUO T, SUGA H and SEKI S *Proc. Japan Acad.* **48** 489 (1972)
- 20 HAIDA O, SUGA H and SEKI S *Proc. Japan Acad.* **49** 191 (1973)
- 21 HAIDA O, SUGA H and SEKI S *Proc. Japan Acad.* **48** 683 (1972); *Chem. Lett.* **79** (1973)

DISCUSSION

Janik: You interpret your DTA data as an evidence of a glassy state in MBBA. We published three papers on MBBA, which we however interpret as an evidence of two crystalline modifications, a metastable and a stable one. The first paper [*Phys. Lett.* **41A**, 102, (1972)] concerns calorimetric data. Figure 1 presents them. As it may be seen, both solid modifications detected in calorimetry have sharp melting points, which is not supporting your glassy state interpretation.



The second paper [*Acta. Phys. Polon.* (1973) 483] gives the IR evidence of the two modifications. Figure 2 shows the results: (a) corresponds to nematic MBBA, (b) corresponds to the metastable modification of 87 K, (c) the same at 263 K, (d) corresponds to stable modification of 83 K, (e) the same at 263 K.

The third paper (*Mol. Cryst. Liquid Cryst.* to be published) gives the far IR results. Figure in p. 520 shows (top) the FIR spectrum of the stable modification and (bottom) the same of the metastable one. The IR and FIR spectra are characteristic of a crystalline substance.

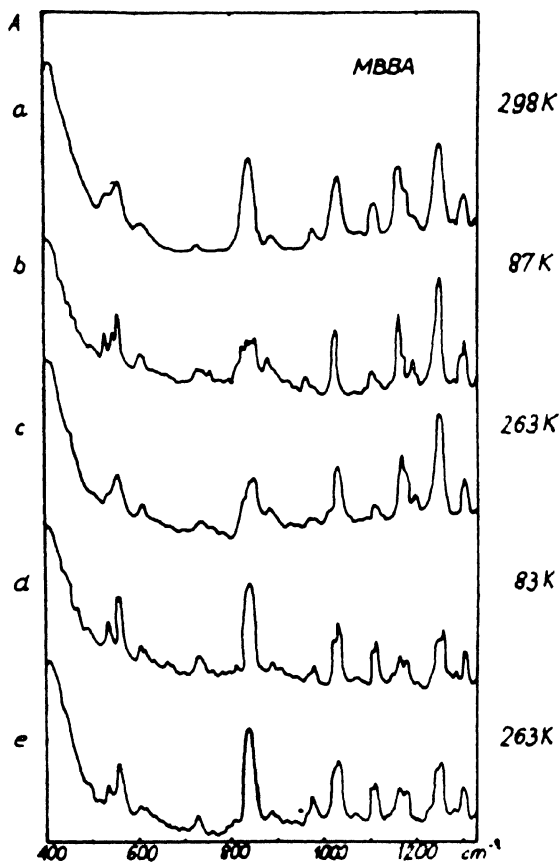
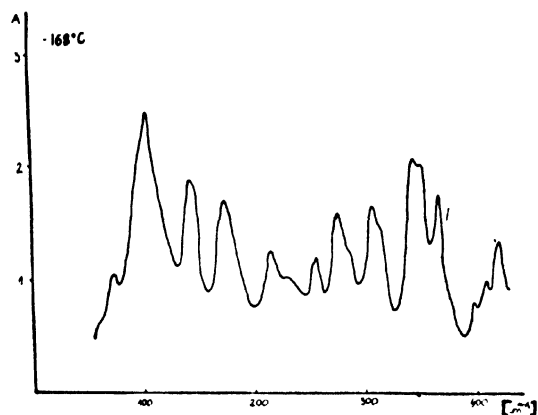
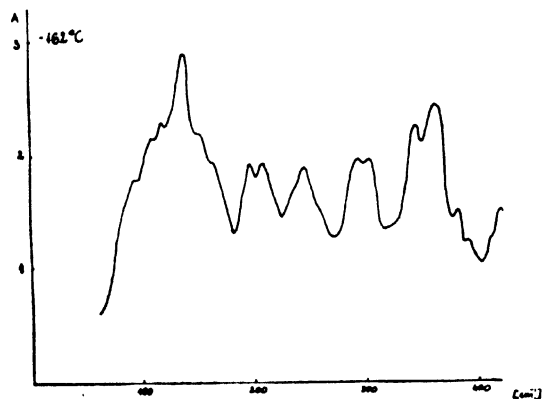


Figure 2



Bulkin: I have the following comment: I do not see that you have presented convincing evidence for a glassy liquid crystal. There is thermodynamic evidence but no optical evidence. It appears to me that your results could be expressed by two solid forms, having different specific heats and a small ΔS of transition between them. As Dr. Janík has shown in his far infrared spectra of the two forms, both have well defined lattice vibrations. If one was a glassy state, it would be expected to have a much broader spectrum in this region.

Sorai: I cannot agree to the first half of your comment. First of all, the concept of glassy state in itself can be identified only from thermodynamic point of view. Although optical and/or structural methods are

useful to obtain auxiliary evidence, they fail to distinguish between the glassy and the supercooled states. In the case of OHMBBA, we have succeeded in finding (i) a glass transition temperature, T_g , (ii) enthalpy relaxation effect around T_g and (iii) existence of residual entropy at zero Kelvin. In the case of MBBA, the first two criteria are fulfilled by differential thermal analysis. Therefore, I have no doubt that the glassy states were established for these two substances. Further evidence is that the present glassy state was realized by super-cooling respective nematic phases *without crystallization*. In this regard, the state obtained here can be regarded as glassy liquid crystal.

Secondly, I should point out that you and Dr. Janik are misunderstanding our experimental result. Dr. Janik *et al* have measured the heat capacities of the stable and the metastable crystalline phases of MBBA obtained *after crystallization*. Accordingly, Dr. Janik's experiments are concerned with two crystalline forms, while ours are the stable crystalline form and the glassy liquid crystal.

The role of liquid crystals in the organization of living systems

E J AMBROSE

Chester Beatty Research Institute, London SW3 6JB, England

Abstract. Recent work has shown that actinomycin filaments are found in a large number of different cell types. In striated muscle they exhibit a 3-dimensional order; this is reduced to a 2-dimensional order in smooth muscle and to tactoid forms resembling nematic liquid crystals in amoebae, slime moulds and mammalian fibroblast and other cells.

Factors controlling the liquid crystalline states of these filaments in biological systems and their biological interaction will be described.

Introduction

Although physical chemists and biologists have long recognized the relevance of phenomena studied in liquid crystals to an understanding of living systems, the experimental investigations have presented great difficulties. Biological systems are multicomponent and contain numerous types of macromolecules, inorganic ions, etc. In addition, any disturbance of the living system for experimental purposes may cause irreversible damage and it is the labile systems which are in fact of most interest from the point of view of liquid crystalline properties. Nevertheless, progress has been made and there is an increasing awareness amongst biologists of the need for such investigations, if the nature of life is eventually to be understood.

One of the first demonstrations of liquid crystalline phenomena in a well characterised biological system was made by Bernal and Fauxkuchen¹ who used x-ray diffraction to investigate solutions of tobacco mosaic virus. Rod-like particles of 152 Å diameter and 3000 Å in length occur which associate in parallel alignment in aqueous solution, giving rise to a characteristic diffraction pattern. The rods themselves are formed by the linear aggregation of the corpuscular virus particles. This system illustrates clearly three of the rather general characteristics of a number of proteins and nucleoproteins which exhibit partially ordered structures resembling nematic liquid crystals:

1. The great length of the particles in comparison with the size of the organic molecules which form liquid crystals.
2. Generation of these rod-like structures by linear aggregation of spherical units sometimes to form helices or superhelices.

3. Parallel alignment of the elongated particles as in nematic liquid crystals, *e.g.*, structures of this type occur in cellular cytoplasm.

The other main field of investigation at the cell level has long been cell membranes. Since the early work on soap solutions, it has been realised that lipid molecules with polar end groups such as soap molecules and phospholipids are capable of stabilizing sheet-like structures of the type found in cellular membranes. Advances in this field have come from work with model systems notably by Luzatti² and by direct investigations of the natural membranes³ particularly by optical microscopy and x-ray diffraction techniques, which do not disturb the structure during observation. Fortunately, fixation of some liquid crystalline solutions leads to the stabilization of certain forms related to the structure in solution. If used with caution, electron microscopy can therefore be of value in the study of liquid crystalline phenomena in cellular systems, particularly when the structural units are of large dimensions.

Partly from such studies it is now generally agreed that the basic structure of cell membranes depends on the stability of the phospholipid bilayer, in which the molecules lie with the polar groups facing the aqueous phase and the paraffin chains lie within the inner lipid layer, and are coated with an outer layer of protein. This model for the plasma membrane was proposed by Danielli³. In this case the structure resembles a smectic liquid crystal.

In so far as cellular secretions and tissue structures are concerned, liquid crystalline properties play an interesting role. Most of these structures are formed from solutions of proteins, glycoproteins or polysaccharides in which order is first established. Increasing concentration within the solution, followed by drying processes in many cases leads to the formation of a gel and later a solid state, in which the arrangement of molecules is closely related to that initially established in the liquid crystal. Cholesteric liquid crystals play an important role in this case as demonstrated, for example, in the work of Robinson⁴ on solutions of synthetic polypeptides and the insect cuticle.

We will now consider in more detail the role of nematic, smectic and cholesteric liquid crystals in particular examples in biology.

Nematic liquid crystals

There are two classes of fibres observed in the cytoplasm of a large proportion of both plant and animal cells. These are the microfilaments and microtubules. Microfilaments are mainly of two diameters, 60 Å and 100 Å. Microtubules are hollow filaments 270 Å in diameter, extremely uniform and of high rigidity.

(a) Microfilaments

60 Å microfilaments are found just beneath plasma membrane in many types of mammalian cells such as fibroblasts, macrophages, etc.⁵. For example, in plate Ia is shown the appearance of a cell in the stereoscan microscope after removing the plasma membrane by etching the surface after ionic bombardment (ion etching)⁶. These sub-surface filaments are seen to be highly oriented in sheets and lie parallel to the surface. In some cases the filaments may be aggregated into cylindrical bundles as shown in plate Ib. The 60 Å microfilaments are almost identical in chemical constitution to the actin filaments found in smooth muscle; a progressive increase in the degree of order existing within these assemblies of filaments can in fact be observed as one passes from the general sub-surface forms present in most tissue cells, as illustrated in plate Ia and Ib, to contractile cells such as smooth muscle (figure 1c) and finally to

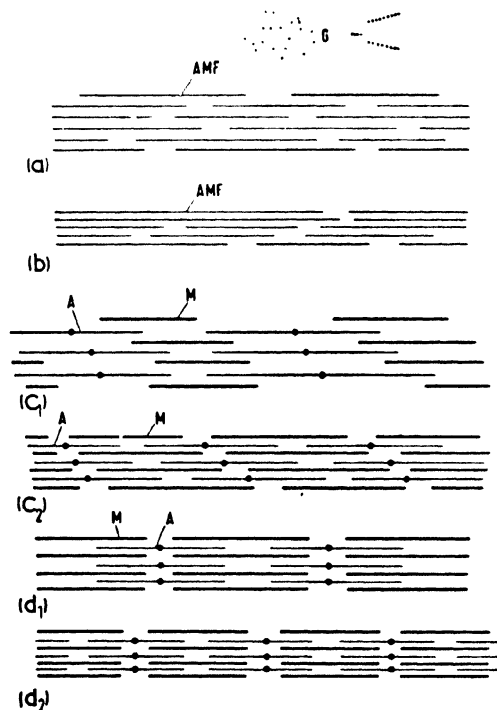


Figure 1 Microfilaments in cells. (a) Sub-surface microfilaments, Lamellar form
 •G. Globular sub-units. (b) Sub-surface microfilaments. Aggregated bundles. c₁ Actin (A) and Myosin (B) filaments in smooth muscle (resting); c₂ The same after contraction; d₁ Actin (A) and Myosin (B) filaments in striated muscle (resting); d₂ The same after contraction.

striated muscle, as shown in figure 1d. The 60 Å actin filaments are in all cases associated in some way with myosin molecules and the actino-myosin complex so formed provides a contractile system able to convert the chemical energy stored in adenosine triphosphate (ATP) into mechanical work. The myosin molecules in striated muscle are organized as shown in figure 1d and are able to slide between the actin filaments during contraction according to Huxley's model for muscular contraction⁷. The arrangement of myosin in smooth muscle is similar, but the three-dimensional order is reduced, fibres being staggered along the fibre axis as shown. Within the sub-surface microfilaments occurring in other cells the location of the myosin molecules has not yet been determined. The less regular arrangement of the filaments in these cell types do not necessarily represent more primitive and undifferentiated cell types. Each system has an important biological role in which the liquid crystalline state plays an important role, *e.g.*, the surfaces of cells are highly dynamic systems in which pseudopodial formation and wave-like movements to provide locomotion, establishment and breaking of intercellular contacts, all fulfil major functions during the development and stabilisation of organisms. The sub-surface structures shown in figure 1a and 1b are able to provide a contractile system capable of generating movements within a liquid crystal, so that the surface is in a state of flux. Orientation and disorientation of filaments occurs together with gel-sol-gel transformations in quick succession. An even more labile situation may exist when the individual filaments disaggregate into their constituent globular units of about 60 Å diameter and then reaggregate. Clearly, the degree of orientation within this system will depend upon filament length, *i.e.*, on the degree of aggregation, and on filament concentration; a third factor that is of importance is the shape of the enveloping plasma membrane. A flat lamellum, as shown in figure 2a will, for example, produce sheets of filaments as shown also in plate 1a, whereas a cylinder as shown in figure 2b will be stabilized to a high degree of linear orientation in the form of a sheath of sub-surface filaments. The spreading fan-like membrane, as seen on the leading edge of many cells, figure 2c, will produce disorientation of microfilaments (plate 1c & 1d). These are known as *network* filaments. Such a system may well be self-perpetuating leading to the maintenance of a highly turbulent and actively moving region of the cell, as is, in fact, to be found in the case of time lapse filming of living cells.

Smooth muscle cells have a very different biological role. They are contractile cells, closely adhering to other cells and tendons. They contract extremely slowly in some cases being called upon to maintain a state of tension for long periods, *e.g.*, for periods of hours or days as in the case of *Mytilus* muscle. The microfilaments exhibit secondary order as shown in figure 1c. This permits a regular contractile mechanism involving the sliding of both actin and myosin molecules relative to each other but with much greater possibilities for maintaining tension due to the staggering of the elements, than can be achieved with smooth muscle

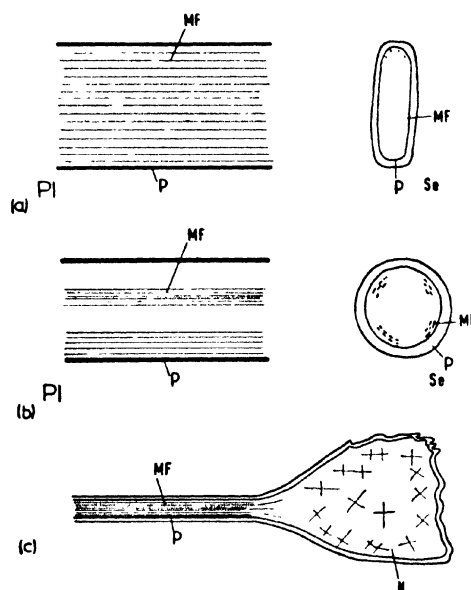


Figure 2 Control of sub-surface microfilaments by the enveloping plasma membrane. (a) lamellar form; (b) cylindrical form; (c) spreading fan-like membrane. P-Plan, Sc-Section, MF-Microfil, N-Network.

and for maintaining tension at different muscle lengths. The three-dimensional smectic liquid crystal of striated muscle, on the other hand, leads to the generation of rapid and highly coordinated contractions, which reach their extreme form in insect flight muscle. In this case sliding occurs between actin and myosin filaments, but not between the actin filaments. Tension increases progressively with contraction.

(b) Microtubules

Microtubules are also formed from globular elements which aggregate in spiral filament form to generate hollow tubes as shown in figure 3a. They are comparatively rigid structures and almost invariably are seen as unbending rods in electron microscope sections. They can truly be called the components of the cellular *cytoskeleton*. Unlike the micro-filaments they are generated and broken down comparatively slowly, generally originating from an aggregation centre such as the centriole, which lies in the cytoplasm near the nuclear membrane. Certain drugs such as *colcemid* and *vinblastine* react specifically on microtubules and cause them to disaggregate without producing other cellular damage. In figure 3c₁ and 3c₂ is shown the effect of colcemid on glial cells. The elongated

form is lost due to breakdown of microtubules after treatment with colcemid. Melanocytes and melanoma cells behave similarly, but cell locomotion is not interrupted, cell surface movements continue, due to

the integrity of the sub-surface microfilaments. An extreme development of cytoplasmic microtubules is shown by *Heliozoa*, organisms much studied by Porter⁸ on the electron microscope. These organisms exhibit numerous spikes (axopods) as shown in figure 3b. These axopods are packed with microtubules, arranged in highly regular crystalline arrays.

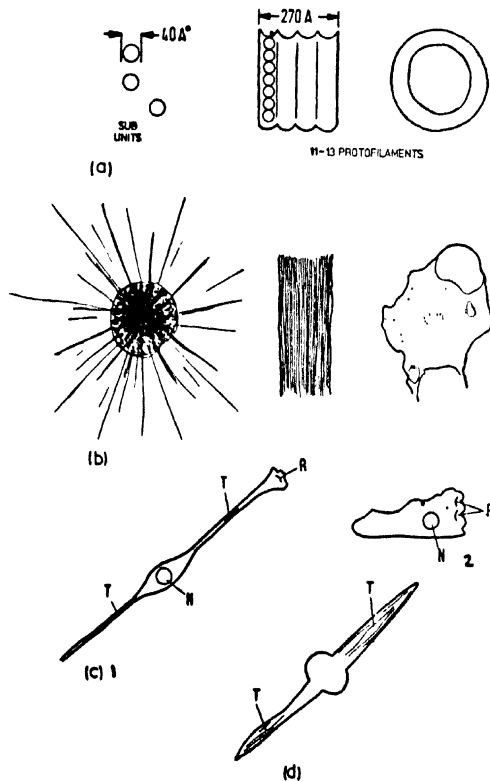
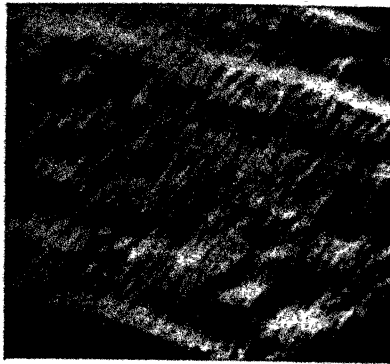


Figure 3 Control of cell shape by microtubules and microfilaments. (a) sub-units and assembly of microtubules; (b) microtubules in axopodia of *Heliozoa*; (c) 1. Shape of glial cell elongated form maintained by microtubules; 2. The same after treatment with colcemid; (d) Effect of cytochalasin B on glial cell.



Stereoscan microscopy of instantly frozen cells

Plate I (a) BHK 21 fibroblast cell spread flat on glass showing highly oriented sub-surface microfilaments after ion etching to remove plasma membrane. x 10,800.

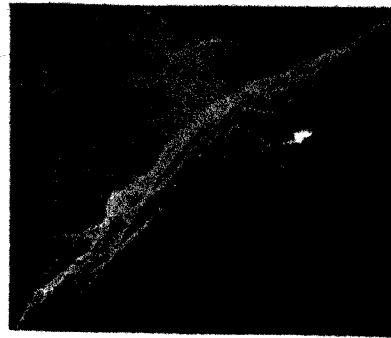


Plate I (b) Human glial cell after ion etching to show bundles ($\sim 500 \text{ \AA}$ diameter) of microfilaments beneath the surface.



Plate I (c) Region of fan-like expansion at the leading edge of glial cell. Showing various catastrophes (cusp and waves).

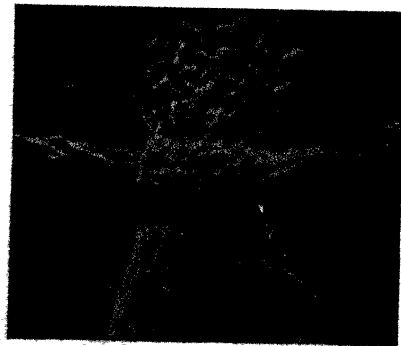


Plate I (d) A fan-like expansion similar to (c) after ion etching. Lower region of cylindrical pseudopodium shows oriented microfilaments. Orientation is not shown in upper region of ruffled membrane activity.



Plate II (a) Microvillae (hair and spikes) formed at the edge of two adjacent fibroblasts.

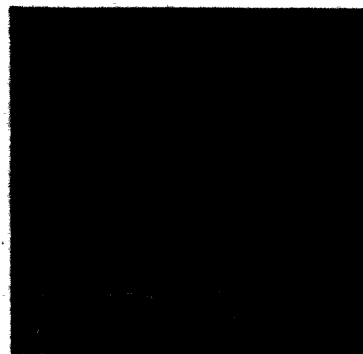


Plate II (b) Appearance of human glial cells with extremely fine pseudopodia.

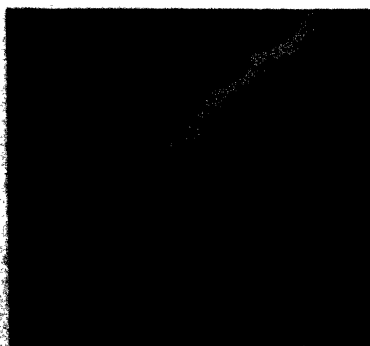


Plate II (c) Appearance of malignant glial cell (Glioblastoma) showing irregular and truncated pseudopodia.



Plate II (d) The same after ion etching show disordered sub-surface structures.

Such structures are also capable of generating internal cytoplasmic movements as has been clearly shown by Porter⁸. In fact, microtubules form the main structure of the spindle during mitosis; the centromeres attached to chromosome fibres carry the chromosomes to the daughter poles along the microtubules. This type of movement within the cytoplasm is quite distinct from the sub-surface movements generated by microfilaments and is comparatively slow. Microfilaments, on the other hand, are sensitive to the drug *cytochalasin B* which reversibly disrupts the organisation of microfilaments without affecting microtubule organisation. Figure 3d illustrates the effect of such treatment with *cytochalasin B* on a glial cell. The highly oriented processes maintained by microtubules are not disturbed by *cytochalasin B*, whereas the growth cone on region of ruffled membranes ceases to function due to disruption of microfilaments; cellular locomotion therefore ceases.

Recent studies of microfilaments and microtubules in cells have led to a much clearer understanding of the molecular basis for cell shape and morphogenesis at the cell level. Cell shape can be studied most conveniently in monolayer tissue culture; e.g., table 1 and in figure 5 are summarized the characteristic shapes of a few of the cell types found in mammalian tissues including man.

These shapes represent *steady states*. They are the shapes to which the cell will revert after a minor disturbance. The stability of all living cells requires a constant supply of energy even for the cells in a steady state. If this energy supply is cut off, the cell will die rapidly. Various ionic and other gradients must be maintained at the cell membrane by pumping mechanisms. In addition to the steady states described above transient disturbances are generated continuously at the surfaces of living mammalian cells. These can take the form of curve-like motions (ruffled membranes) (plate Ic and Id) generation of microvillae (plate IIa), etc. At first sight, an analysis of disturbances of this kind would appear to be extremely difficult. A mathematical theory which is of general application to all disturbances arising from a shock wave has been developed by René Thom and is relevant to all types of physical and biological systems. The theory has been applied to the problem of disturbances at cell surfaces by Ambrose⁹. The general conclusions are summarised in figure 4. Only five general types of disturbance or catastrophe can be generated at cell surfaces; these are the fold, the cusp, the wave and the crest, the hair and the jet (as shown in figure 4). All of these can in fact be observed in stereoscan electron micrographs of cell surfaces and in time lapse films of living cells as shown in plates I and II. The shock waves responsible for the generation of these transient shape changes in cells arise in the main from the sudden local release of energy which generates a shock wave, presumably due to contraction of microfilament assemblies. They persist for a time and the cell surface then reverts to one of the steady states shown in figure 5.

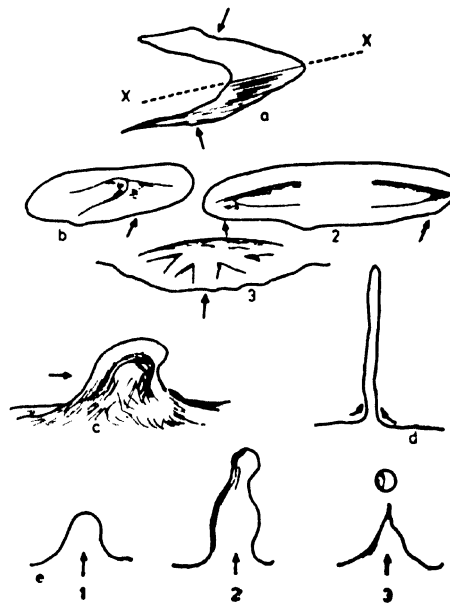


Figure 4 Ordinary catastrophies after René Thom, arrow indicates the direction of propagation of the shock wave which generates the catastrophe. (a) The fold, (b) The cusp - 1. single cusp; 2. two cusps forming a trough; 3. star shaped group due to pressure on a rigid sheet, (c) The crest (of a wave) and the arch, (d) The hair. (e) The jet - 1. early stage; 2. middle stage; 3. late stage.

Table 1

Cell type	Properties of cell surface and microfilaments
Fibroblast (Fan-like lamellar form)	High cell substrate adhesion. Sheet-like microfilaments. Linear groups of microtubules.
Fibroblast (Spindle form)	Cell substrate adhesion mainly at leading edge. Microfilament sheath. Ordered microtubules.
Epithelial cell	Very high cell substrate adhesion. Less ordering of microfilaments. Few microtubules.
Lymphocyte	Highly labile cell surface leading to dancing motion on substrate. Few microtubules.

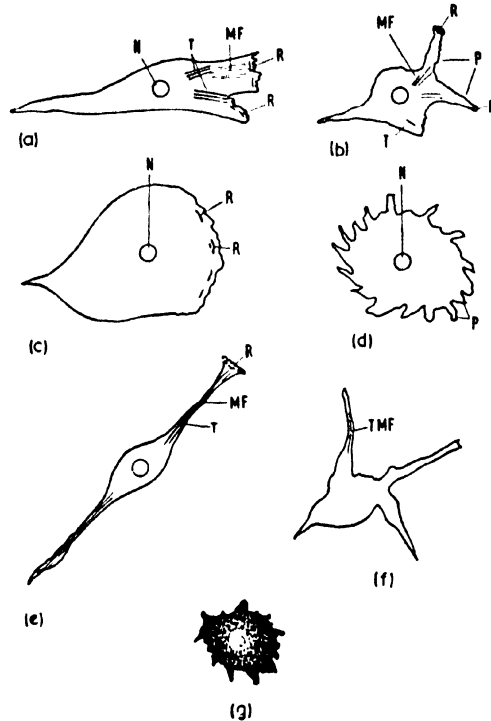


Figure 5 Changes in cell shape in malignant cells. (a) normal fibroblast in culture N - nucleus, T - microtubules, MF - microfilaments, R - ruffled membranes (b) tumour cell derived from fibroblast (sarcoma cell) of organization of microtubules and microfilaments P - polypodial formation, R - ruffled membranes (c) normal epithelial cell in culture N - nucleus, R - ruffled membrane (d) tumour cell derived from epithelium N - nucleus, P - polypodia (e) normal glial cell in culture (connective tissue cell of brain) T - microtubules, MF - microfilaments, R - ruffled membranes (f) malignant glial cell T - MF - disturbed microtubules and microfibrils (g) highly anaplastic and dedifferentiated tumour cell.

(c) *Smectic liquid crystals*

The lipid bilayer formed by phospholipid molecules has long been recognized as forming the basis for the structure of cell membranes⁹. The multilayer type of smectic liquid crystal is well seen in nerve myelin. What has been a puzzle for a great many years has been the problem of explaining how the protein and glycoprotein molecules, which constitute 40-50% of the membrane, can be fitted into the bilayer model. Beautiful freeze-etching work of Benedetti and Emmelot¹⁰ and others has thrown light on this problem and a model recently proposed by Singer and Nicholson¹¹ fits the data extremely well. According to this model there

are integral molecules (I) of globular proteins and glycoproteins which lie within the lipid bilayer as shown in figure 6. Some of these molecules penetrate from outside of the membranes to the inside; they may carry pores for ion transport, etc. Others only partially penetrate the membrane. In addition peripheral proteins (P) lie loosely attached to the outer surface. These are generally glycoproteins, particularly sialomucoproteins. The important point about the Singer and Nicholson model is that it exhibits liquid crystalline properties. The lipid bilayer is a fluid in which the integral proteins are free to move. This has been clearly shown to be the case by de Peters and Raft¹², *e.g.*, in the capping phenomenon in lymphocytes in which surface antigens can be shown by fluorescent labelling methods to migrate under certain conditions to form a cap near the urodele of the lymphocyte. According to present evidence this modified smectic liquid crystal provides an excellent model for cellular membranes, particularly for the plasma membrane.

(d) *Cholesteric liquid crystals*

The main interest in cholesteric liquid crystals in biology centres round the study of cellular secretions. In this case one is generally concerned with reasonably homogeneous material and the interpretation in terms of liquid crystalline behaviour becomes more straightforward. The beautiful work of Robinson⁴ on the cholesteric liquid crystals found in solutions of synthetic polypeptides was extended later to the study of the insect cuticle¹⁵. Observations of beetle chitin in polarised light revealed as cholesteric structure remarkably similar to that seen in the solutions of synthetic polypeptides.

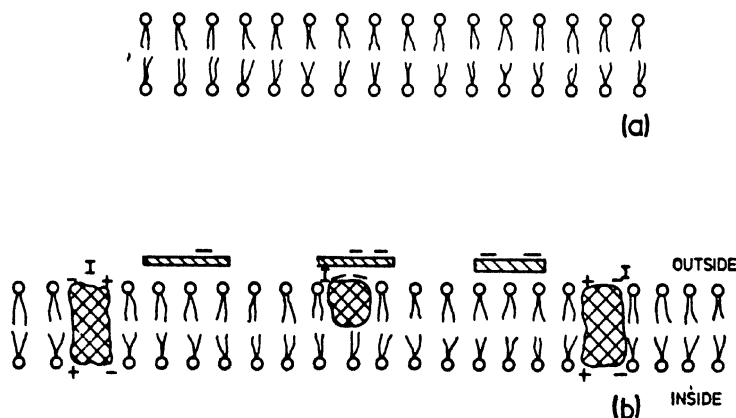


Figure 6 Model for plasma membrane (Singer and Nicholson⁴) (a) phospholipid bilayer (b) integral proteins (I) within the bilayer; outer coat of sialomucoproteins (negatively charged).

Another system which may be of interest but which has not yet been fully investigated from this point of view is the formation of the plant cell wall. In this case cellulose fibres are produced by both longitudinal polymerisation and by lateral aggregation. Unlike a cholesteric liquid crystal the fibres are deposited in layers in which the fibres lie parallel to each other but with a rotation through a large and constant angle with reference to the previous layer.

(c) Liquid crystals in cancer cells

The phenomena described above have proved to a surprising extent to be relevant to an understanding of the characteristics of cancer cells at the molecular level. Cancer is in the main a reversion to a more primitive and less differentiated function than that of the normal tissues from which it is derived. It has been clearly shown by ion etching experiments with human brain tumours and with other cells⁶⁻¹³ that the malignant change is associated with a disturbance of the organisation of sub-surface microfilaments. The decrease in organisation of sub-surface microfilaments in cancer is correlated with a loss of ability to generate the fan-like lamellipodium characteristic of normal cells, and the uniformity of ruffled membrane activity is reduced. The surface of the malignant cell becomes highly irregular in its movements, producing many blebs and spike pseudopodia of non-uniform size (polypodia), unlike the microvillae of constant size in normal cells. These are illustrated in figure 5. Studies of the behaviour of normal cells and malignant cells in their interactions with intact living tissues using a new time lapse filming technique in 3-dimensions¹⁴ have shown that these changes in cell surface movements in malignancy may be important in permitting the tumour cells to achieve a point of anchorage between normal epithelial cells. The uniform ruffled membrane of the non-malignant cells on the other hand causes them to glide on epithelial and other surfaces within achieving permanent anchorage. This anchorage phenomenon plays a major role in the most dangerous aspect of cancer, the invasion and spread of the cells into normal tissues.

Changes in the plasma membrane itself which may be connected with liquid crystalline phenomena have recently come to light. Some of the integral proteins shown in figure 6b carry receptor sites for plant agglutinins and specific cellular antigens. In cancer, these receptors migrate within the plane of the membrane to form clusters. The tumour cells are therefore more readily aggregated by these lectin molecules (wheat germ agglutinin and concanavalin A). The liquid crystalline properties of the lipid bilayer must permit such migrations of protein molecules within the plane of the membrane. The increase in cholesterol content found in tumour cell membranes could possibly play some role in this behaviour.

General conclusions

Molecular biology has led to great advances in our understanding of the genetic code, protein synthesis and cell growth generally. But there are certain important questions which the biologist must ask and which are outside the thinking of the molecular biologist, *e.g.*, what is the function of a given organ in relation to the life of the organism as a whole? How has this organ been designed? These problems have been discussed in an excellent CIBA foundation Symposium on 'Principles of Biomolecular Organisation'¹⁶.

The word 'design' is used in some papers of this CIBA Symposium. We do not need to consider the philosophical implications of this word in this paper but rather the usage of the engineer. We ask the question: 'What is the structure and inter-relation of the parts of a given organ which enable it to function for the benefit of the organism as a whole?' Ultimately such developments in the embryo are under genetic control. But thinking in terms of the biochemistry of the genetic code, synthesis of nucleic acids, proteins, actin microfilaments, phospholipids, polysaccharides, etc., tells us very little. The building units of life are remarkably similar from bacteria to man. This is where the study of liquid crystals becomes important; these studies show that the long range order in the supermolecular structure of liquid crystals can be controlled extremely accurately by simple physico-chemical parameters such as:

1. Concentration of macromolecules
2. Relative proportions of the components
3. The ionic environment, particularly by bivalent cations such as calcium and magnesium.

Part of the genetic code may be involved during development in the regulation of such parameters in *space* and *time* and hence to the eventual control of the development of the highly complex structures found in the organisms of higher organisms. So far this field of investigation has hardly been explored, but it might be a fruitful field for future work.

It is a particular pleasure for me to take part in this Conference in Bangalore, organised so well by Professor Chandrasekhar. My first interest in the study of living cells came from collaboration with Dr A R Gopal Ayengar, who comes from Bangalore and became Director of the Bio-medical Group, Bhabha Atomic Research Centre, Trombay. He is an excellent cytologist whom I met when I was working as a molecular biologist interested in protein structure; we collaborated in London at the Chester Beatty Research Institute to study the liquid crystalline properties of the nucleoprotein of chromosomes in living cells, and were able to show that chromosomes exhibited long range order which could be modified reversibly by changing the ionic environment¹⁷.

Acknowledgement

This work has been supported by grants from the Cancer Campaign for Research and from the Medical Research Council, UK.

References

- 1 BERNAL J D and FANKUCHEN I J. *Gen. Phys.* **25** 147 (1941)
- 2 LUZZATI V 'Biological Membranes' ed. Chapman Academic Press (1968).
- 3 DANIELLI J, Cold Spring Harbor Symp. Quant. Biol. **6** 190 (1938)
- 4 ROBINSON CONMAR, First International Conference on Liquid Crystals, Kent, Ohio, USA (1965); ed BROWN G H, DIENES G J and LABES M M (Gordon and Breach, London)
- 5 WESSELLS N K, SPOONER B S and LUDIENA MARILYN A *Locomotion of tissue cells*, CIBA Symposium; ed ABERCROMBIE M pp. 53-76 (1973)
- 6 AMBROSE E J, BATZDORF U, OSBORN J and STUART P R *Nature* **227** 397 (1970)
- 7 HUXLEY H E and HANSON J *Nature* **173** 973 (1954)
- 8 PORTER K R *Principles of biological organisation*, CIBA Foundation Symp. ed WOLSTENHOLME G E W and O'CONNOR M pp. 308-343 (1966)
- 9 AMBROSE E J *Symposium of Faraday Society* **5** 175 (1971)
- 10 BENEDETTI E L and EMMELOT P J. *Cell. Biol.* **29** 299 (1965)
- 11 SINGER S J and NICOLSON G L *Science N.Y.* **175** 720 (1972)
- 12 DE PETERS S and RAFF M C *Locomotion of tissue cells*, CIBA Symposium, ed ABERCROMBIE M pp. 27 (1973)
- 13 AMBROSE E J, BATZDORF U and EASTY DOROTHY M *Neuropathol. Exp. Neurology* **31** 597 (1972)
- 14 AMBROSE E J and EASTY DOROTHY M *Differentiation* **I** 39-50; **II** 277-284 (1973)
- 15 NEIRLLE A C and CAVENEY S *Biol. Rev.* **44** 531 (1969)
- 16 *Principles of biological organisation*, CIBA Foundation Symp. ed WOLSTENHOLME G E W and O'CONNOR M (1966)
- 17 AMBROSE E J and GOPAL AYENGAR A R *Nature (London)* **169** 652 (1952)

DISCUSSION

Rustichelli: Could you comment on the contribution the neutron and x-ray diffraction can give in the study of microfilaments and liquid crystals involved in biological materials?

Ambrose: It is usual to employ these methods. The x-ray diffraction and electron diffraction studies can be carried out in parallel in the case of muscles, etc. But when we come to cells that I have been talking about the amount is so small that it is extremely difficult. These are really well defined chemical entities and many people have been isolating these materials, so that a great deal could be done on the liquid crystal properties using x-ray diffraction.

Lytotropic liquid crystals and foam stability

H SAITO and S FRIBERG

The Swedish Institute for Surface Chemistry, Stockholm, Sweden

Abstract. The influence of different association conditions of surfactants on the stability of foams was demonstrated by determination of the stability of foams formed from different liquid and liquid crystalline phases in the system water, hexadecyltrimethylammonium bromide (CTAB) and hexanol.

The results showed that the presence of the aqueous phase was necessary for the stability of the foam and that the liquid crystalline phase displayed an influence in enhancing the stability only when combined with the aqueous isotropic phase. The alcoholic phase had a detrimental effect on the stability.

The interpretation of the results led to a simple explanation of the fact that certain substances, *e.g.*, alcohols of medium chain length, may serve both as foam stabilizers and breakers.

1. Introduction

The structure of lyotropic liquid crystals has been investigated in great detail during the two decades following the first suggestions of structural arrangements¹⁻³. Among the important contributions the structure determinations by Luzzati⁴⁻⁶, the lipid mesostructures by Larsson⁷ and the numerous investigations on the liquid crystalline regions in three-component systems by Ekwall^{8,9} especially deserve merit. Some of the structures of lyotropic liquid crystals and of micelles encountered in systems of water, ionic surfactants and amphiphiles such as alcohols are presented in figure 1.

The stability of foams¹⁰ has in general been related to the colloid stability of thin films¹⁰⁻¹³ by which the distance relations of the mutually independent Van der Waals' attraction potential and the electric double layer repulsion potential are the dominant factors^{14, 15}.

In this article we wish to expound the influence of the introduction of a third phase with liquid crystalline structure on the stability of foams. The general importance of the association of water, surfactants and amphiphiles on the stability of emulsions and foams has been suggested several years ago¹⁶⁻¹⁹, but the first reports in which well defined and separated phases were mixed to establish the critical conditions for the stability are comparatively recent²⁰⁻²².

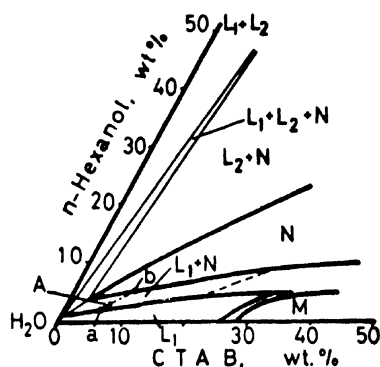


Figure 1 Different phases in the water-rich part of the system, water, cetyltrimethylammonium bromide (CTAB) and hexanol¹⁸. L_1 and L_2 = aqueous and alcohol solution. M and N = liquid crystalline phases.

This article will deal with investigations on the role of the liquid crystal in foam stability and the application of these results to the action of foam-breaking compounds.

2. Foam stability

2.1 Experimental results

The system water, hexanol (C_6OH) and cetyl trimethylammonium bromide (CTAB)²³ was used to prepare an aqueous micellar solution in equilibrium with a lamellar liquid crystalline phase. The three components with a total composition according to A, figure 1, were mixed, stored at 30°C for five days and the two phases (a and b, figure 1) separated by centrifugation at 500 g during 5 hr. at this temperature and mixed in varying proportions according to legends to figures 3 and 4.

Foams from these mixtures were prepared by shaking in 100 ml flasks and thermostated at 30°C. After different times the foam from the upper part was collected by suction into a syringe.

The collected material was transferred to a capillary which was sealed by fusion and thermostated at 30°C for 24 hr. After separation of the two phases by centrifugation the liquid crystalline fraction of the mixture was determined. The results (figure 2) showed a pronounced enrichment in the foam for the mixtures which were initially poor in liquid crystal content. Higher primary contents of liquid crystal gave lower increase in the foam; even counted as *relative* displacement of the liquid (figure 3). The aqueous solution was slightly more dense than the liquid crystalline phase. In order to confirm that this factor had no influence on the relative drainage a liquid and a liquid crystal of reversed density ratio (figure 4) were used. Table 1 demonstrates the enrichment of the liquid crystal.

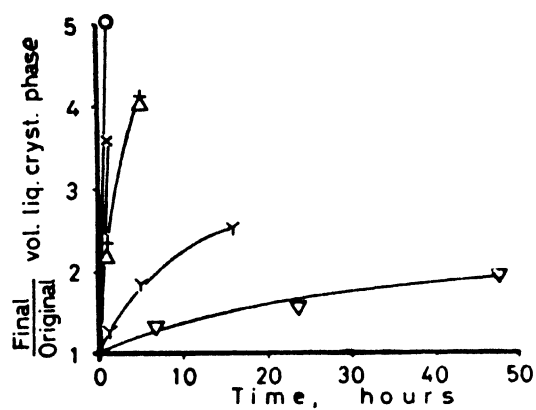


Figure 2 The ratio of final volume of liquid crystalline phase in the foam to the liquid crystal volume in initial mixture versus time of foam storage.

Sign	×	O	+	Δ	Y	▽
Initial volume %	1.6	4.8	7.8	12.1	23.5	36.8

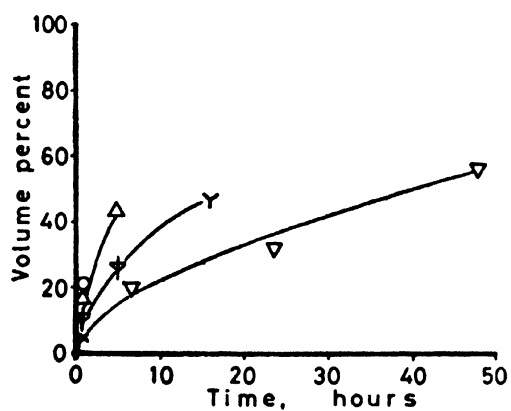


Figure 3 The volume percentage of the initial solution which is replaced with liquid crystalline phase in the foam versus time.

Sign	×	O	+	Δ	Y	▽
Initial volume % l.c. phase	1.6	4.8	7.8	12.1	23.5	36.8

Table 1. The volume percentage of liquid crystalline phase in the non-aqueous foams. Initial compositions of these samples are illustrated in figure 5.

No	Volume % of liquid crystalline phase	
	Initial mixture	Foams after 1 hour
1	43.2	78.6
2	33.1	70.6
3	32.2	67.1

2.2 Discussion

In order to interpret the results it is necessary to observe that no significant increase of liquid crystal could be observed in freshly formed foams; it occurred only in foams which had experienced some drainage. Figure 2 demonstrates the gradual increase of the liquid crystal/liquid ratio with time.

Regarding this information it is evident that the enrichment is due to a slower drainage of the liquid crystal than of the liquid. Knowledge of the location of the liquid crystal within the foam is then essential for the understanding of the liquid crystal enhancement of foam stability²².

Figure 5 shows a thin film, which was drawn from a mixture of a liquid crystal and an isotropic liquid. In figure 5b the light is polarized, in figure 5a not polarized. According to these photos anisotropic material to transmitted light was collected into the Plateau border. Considering this result, it appears reasonable to assume that the liquid crystal is being enriched at the junctions between foam lamella. The liquid crystal phase located at these junctions should drain more slowly than the isotropic liquid and serve as a reservoir at the border of the foam lamella of the highly concentrated surfactants of optimal composition.

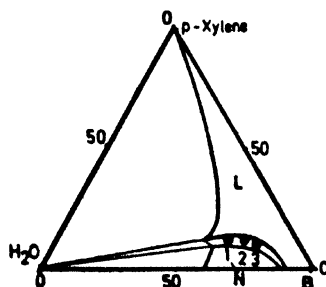


Figure 4 Compositions of mixtures for non-aqueous foams in the system water, *p*-xylene and octylamine: octanoic acid (1:1) denoted by B.

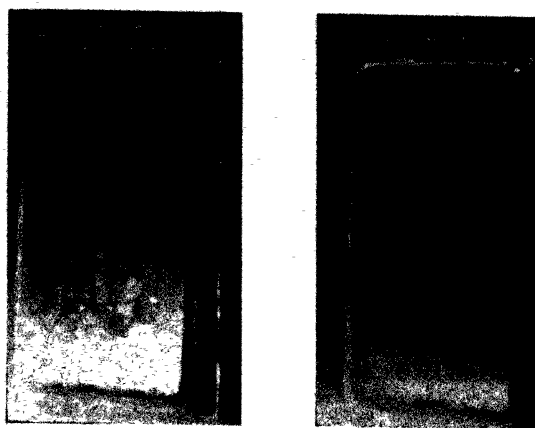


Figure 5 A thin film from a mixture of a liquid crystal and an isotropic liquid (a) Transmitted light not polarized; (b) Transmitted light polarized.

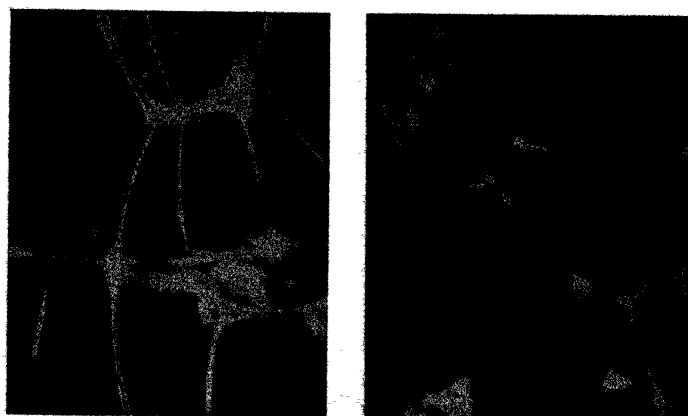


Figure 6 Foams from the mixture of a liquid crystal and an isotropic liquid (a), and from a liquid containing dispersed particles of polyethylene ($\phi = 2-15$) μm (b).

The liquid crystal, being considerably more viscous than the liquid, may also enhance the stability of the foam in a similar manner as solid particles. These accumulate at the junction points of the foam (figure 6) exerting a strong stabilizing effect by reduction of the foam drainage.

3. Foam breaking

It is well known that amphiphilic substances such as alcohols, esters, etc., with a chain length of the magnitude of ten carbon atoms are efficient foam breakers²⁴⁻²⁶.

On the other hand it is also well known that alcohols, e.g., lauryl alcohol, serve excellently as foam stabilizers. The apparent contradiction of these two statements could be resolved by a systematic observation on the dependence of foam stability in the various regions in a system such as water, hexanol (C_6OH) and cetyl trimethylammonium bromide (CTAB). The system (figure 7²³) contains an isotropic solution with normal micelles (L_1), an isotropic solution with inverse micelles (L_2) and two liquid crystalline phases of which one (N) has a lamellar structure.

The foams were prepared by shaking a volume of 5 ml of the mixture in a 15 ml stoppered test tube. The time for the foam height to be reduced to half the height of the glass tube was determined by visual observation.

Figure 8 describes the results schematically. When the mixture only contains two liquids the stability of the foam was small, the time for half-life was of the order of 30 seconds. For those areas, where the lamellar liquid crystalline phase was present in additions to the two liquids the time was increased to a magnitude of 1 hr. Removal of the alcoholic solution phase increased the time further to a few hours. Mixtures of the aqueous liquid isotropic phase and the lamellar liquid crystalline phase gave the most stable foams of all; half-life times of the magnitude 25-50 hr.

The alcoholic solution and its mixtures with the liquid crystalline phase gave extremely unstable foams of half-life times of less than thirty seconds. The area between L_2 and the marked areas in the aqueous corner did not foam.

3.1 Discussion

The results illustrated the influence of the presence of three of the phases in the diagram. Each of the phases had a characteristic effect which may be described in different terms.

The alcoholic phase had a highly detrimental effect on the stability; the pure phase gave extremely unstable foams, which was also the case with combinations with *one* of the other phases.

The aqueous isotropic solution was essential in order to obtain a stable foam. The combination with the alcoholic solution gave unstable foams and constituted an exception; partly explained by the low concentrations of surface active substance being present.

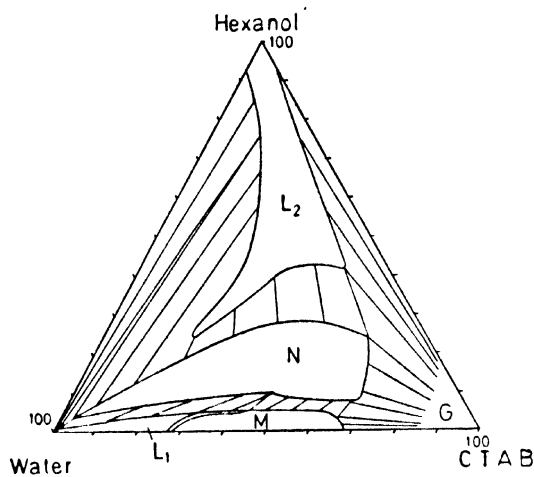


Figure 7 Phase diagram of ternary system water, cetyltrimethylammonium bromide and *n*-hexanol (23). L_1 and L_2 = aqueous and alcohol solution M and N = liquid crystalline phases. G = solid CTAB.

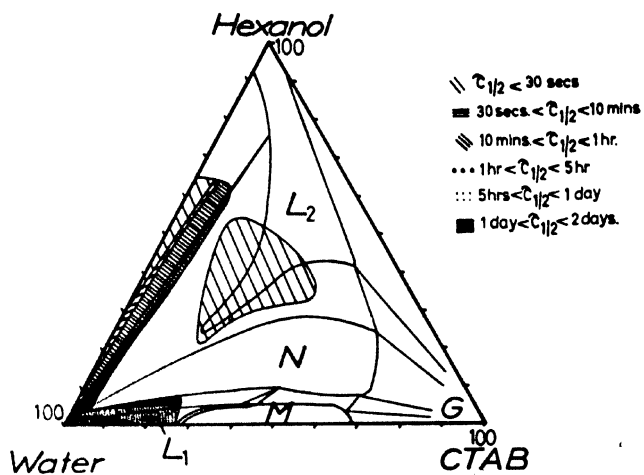


Figure 8 Stability of foams from the ternary system water, cetyltrimethylammonium bromide and *n*-hexanol.

The liquid crystalline phase served as a stabilizer for foams in which the aqueous phase was present. The phase alone in combination with the alcoholic solution was not sufficient to give stability to the foams; neither did the pure liquid crystalline phase. A black film could be drawn from the lamellar phase pointing to foam stability²⁷. The thinning process was however different from the thinning of a liquid film. In the latter, the change from a thick film to the black state takes place gradually. For the liquid crystalline phase the thinning was a stepwise process giving the black film directly. The black film did not change its thickness with time.

A black film from the liquid crystalline phase was obtained only after careful and slow raising of the frame on which the film developed. It appears probable that the attempts to form foams from the liquid crystalline phase failed because the formation of a bubble is too fast a process. The formation of a black film was not possible in the highly perturbed environment of a foaming process.

Summarizing the results an explanation can be formed for the fact that alcohols of medium chain length may serve both as *stabilizers* and *breakers* for foams.

In the first function they are added in such a small amount that the alcohol-surfactant ratio still is less than what corresponds to the liquid crystalline phase in figure 9. The formation of a liquid crystalline phase will enhance the foam stability.

If on the other hand the foam breaker is added dropwise to the foam as the pure alcohol or as the alcoholic solution the foam will break. The reason for this is that the site where the drop touches the foam will be transformed to an alcoholic solution since the *local* alcohol-surfactant ratio will be higher than what corresponds to the liquid crystalline phase (Region A, figure 9). The breaking of the foam will take place at that

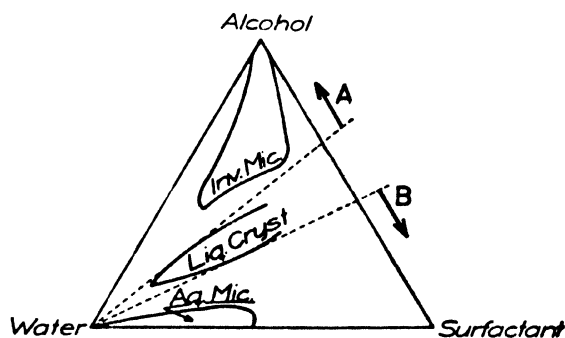


Figure 9 Alcohol/surfactant ratios by which alcohols can act as foam breakers lie above line A; as foam stabilizers lie below line B.

site, surrounding bubbles will break from the perturbation caused by the first and the process will continue until the surfactant-alcohol ratio is sufficiently large corresponding to the region B in figure 9.

This process has been observed experimentally in a foam; the results will be reported elsewhere.

Acknowledgement

The project was supported by Swedish Board for Technical Development. Dr John B Brown kindly revised the language of the text.

References

- 1 STAUFF J *Kolloid-Z* **89** 224 (1939)
- 2 MCBAIN J W and LEE W W *Oil and Soap* **20** 17 (1943)
- 3 DOSCHER T and VOLD R J *Phys. Colloid Chem.* **52** 97 (1948)
- 4 LUZZATI V, MUSTACCHI H and SKOULIOS A E *Nature (London)* **180** 600 (1957)
- 5 LUZZATI V and REISS-HUSSON F *Nature (London)* **210** 1351 (1966)
- 6 LUZZATI V and SPEGT P A *Nature (London)* **215** 701 (1967)
- 7 LARSSON K Z. *Phys. Chem.* **56** 173 (1967)
- 8 EKWALL P, MANDELL L and FONTELL K *Mol. Cryst.* **8** 157 (1969)
- 9 EKWALL P, MANDELL L and FONTELL K *Proc. 5th Int. Congr. Surf.-Act. Subst., Barcelona* 1968 p. 1059
- 10 KITCHENER J A *Rec. Progr. Surf. Sci.* **1** 51 (1964)
- 11 "Thin liquid films and boundary layers" *Spec. Discuss. Faraday Soc.* No. 1 (1970)
- 12 CLUNIE J S, GOODMAN J F and INGRAM B T *Surface Colloid Sci.* **3** 167 (1971)
- 13 SHELUDKO A *Adv. Colloid Interface Sci.* **1** (No 4) (1967)
- 14 VERWEY E J W and OVERBEEK J Th. G *Theory of the stability of lyophobic colloids* (Elsevier, Amsterdam) (1948)
- 15 DERJAGUIN B *Acta Physicochem USSR* **14** 633 (1941)
- 16 SALISBURY R, LERRALLEN E E and CHAWKILL L T *J. Amer. Pharm. Sci.* **43** 117 (1954)
- 17 BURT B W *J. Soc. Cosm. Chem.* **16** 465 (1965)
- 18 LACHAMPT F and VILA R M *Amer. Perfumer Cosmet.* **82** 29 (1967)
- 19 SWARBRICK J J *J. Soc. Cosm. Chem.* **19** 187 (1968)
- 20 FRIBERG S, MANDELL L and LARSSON M *J. Colloid Interface Sci.* **29** 155 (1969)
- 21 FRIBERG S and RYDHAG L *Kolloid-Z. Z. Polym.* **244** 233 (1971)
- 22 FRIBERG S and AHMAD S I *J. Colloid Interface Sci.* **35** 175 (1971)
- 23 EKWALL P, MANDELL L and FONTELL K *J. Colloid Interface Sci.* **29** 639 (1969)
- 24 ROSS S and MCBAIN J W *Ind. Eng. Chem.* **36** 570 (1944)
- 25 ROSS S *Chem. Ind.* **64** 757 (1949)
- 26 KRUGLYAKOV P M and TAUBE P R *Zh. Prikl. Khim. (Leningrad)* **44** 129 (1971)
- 27 SONNTAG H *Kolloid. Zh.* **33** 529 (1971)

Further study on multi-color display devices with twisted nematic liquid crystals

SHUNSUKE KOBAYASHI* and TERUO SHIMOMURA†

Institute of Physical and Chemical Research, Wako, Saitama 351, Japan

* Present address : Department of Electronic Engineering,
Faculty of Technology, Tokyo University of Agriculture and
Technology, Koganei, Tokyo 184, Japan.

† On leave of absence from Kyushu Institute of Design

Abstract. The electro-optical characteristics of twisted nematic cells are described. Studies have been carried out on a 90° twisted cell as well as off 90° twisted cells. The materials used in these experiments were nematics of positive dielectric anisotropy. A device with a 90° twist is shown to allow over twenty different combinations of alphanumerics and background colors by changing the combination of a neutral-color polarizer and colored polarizers which have dichroism. Off 90° twisted nematic devices are shown to reveal a voltage controllable color formation using a pair of neutral color polarizers.

1. Introduction

Several display devices using twisted nematic (TN) structure are described in the literature¹⁻⁶. According to these authors, it is shown that the TN device has advantages in that the operation voltage and power consumption are lower as compared with those of the dynamic scattering (DS) mode⁷, and that the view angle is wider as compared with that of a field effect device using *n*-type materials⁸⁻¹⁰.

In a previous paper the authors showed that two different modes of multi-color formation are available using TN devices¹¹. In the present paper, more detailed descriptions of multi-color formation using TN devices are given.

2. Description of device panels

The twisted nematic devices utilize a thin layer of nematic material with positive dielectric anisotropy; in practice, an example of LC material used in our devices was a room temperature mixture of MBBA, EBBA and BBBA in weight proportions 3 : 2 : 1.

The desired wall orientation was obtained by the method of a combination of surfactant treatment and rubbing; this procedure determines the quality of single crystallinity of the aligned liquid crystals, and consequently the quality of the displayed numbers or symbols.

In the ordinary TN devices, the orientation of molecules at the surface of the electrodes differs by 90° . Besides this, off 90° twisted devices were tried; in these cases, the twist angles were chosen to have an arbitrary value from 0° to 80° .

3. Performance of multi-color display devices with 90° twisted nematics

It is known that the observed threshold voltages of the TN devices are material dependent⁶; the threshold and saturation voltages of the above-mentioned mixture were 2 and 6 volts, respectively.

In figure 1 some examples of multi-color LC indications for electronic digital clocks are shown. All the figures shown in figure 1 are the pictures of the TN-LC panels with a 90° twist operated in a transmission mode using a white light source. The applied voltage was 6V (ac 5 kHz, rms).

All the figures in figure 1 except (A) and (A') are bi-colors. A mono-color indication as shown in figure 1 (A) and (A') is realized by combining a neutral-color polarizer with a dichroic polarizer; the spectral transmission of this combination is shown in figure 2. In a real device as shown in figure 1 (A) and (A') the difference of transmission curves denoted as crossed and parallel corresponds to on-off of the application of the field. In figure 1 (A) and (A') the relative directions of the two polarizers are parallel, and crossed respectively.

As a reference, in figure 3 is shown the spectral transmission of a pair of neutral-color polarizers which have similar characteristics as those of the polarizers used in the indication. Characteristics of the neutral-color polarizers are not ideal since they show a blue color when crossed, and transmission in parallel condition is not sufficient. Ideally, they must show true black and white colors. For real display purposes, improved neutral-color polarizers must be used.

The bi-color indications as shown in figure 1 (B) - (F) and (B') - (F') are realized by combining a neutral-color polarizer with composite-color polarizers which are made from two crossed-dichroic polarizers having different colors. An example of spectral transmission of a combination of a neutral-color polarizer and a composite-color polarizer is shown in figure 4. This combination was used for the bi-color indication shown in figure 1 (C) and (C'); when the direction of the neutral-color polarizer coincides with that of a green polarizer, say, then the indicated color is red at zero field, and is switched to green by the application of the field, and *vice versa*.

In a similar way many different mono-color and bi-color indications are available for display by choosing different color polarizers.

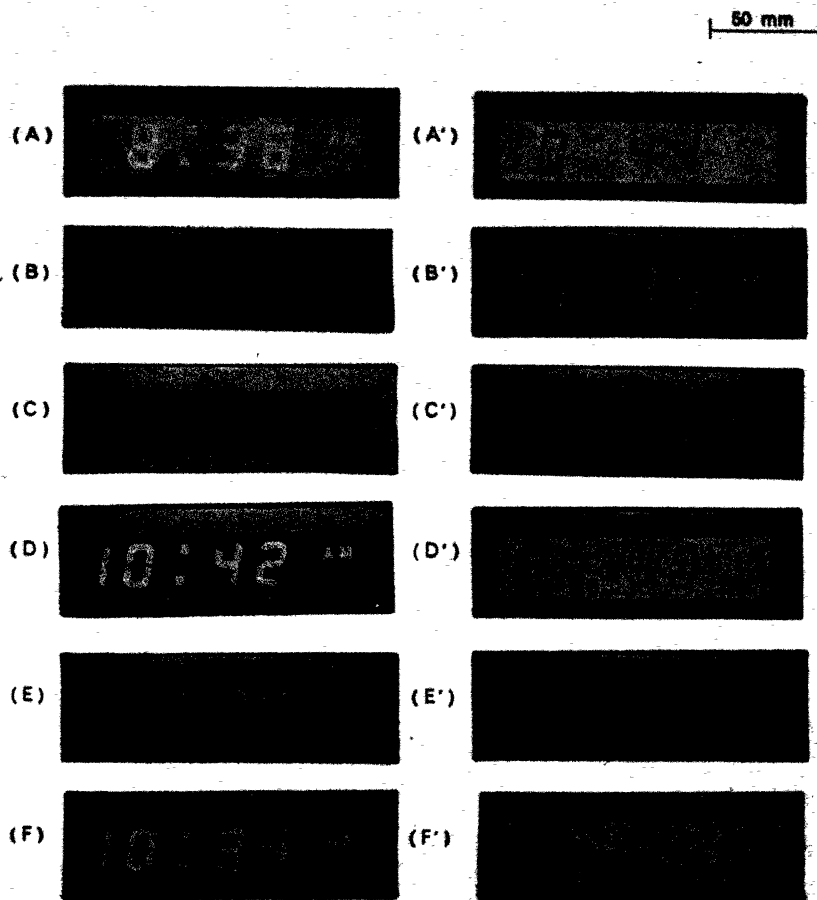


Figure 1 Multi-color indication panels with twisted nematics for clocks. (A), (A') are mono-color and others are bi-colors. These were produced by combining a neutral-color polarizer and dichroic-color polarizers. Light source is ordinary white light. Devices are operated at 6 V (ac rms).

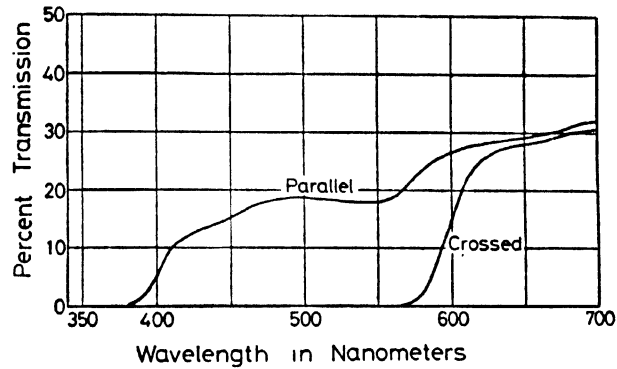


Figure 2 Spectral transmission of a combination of a neutral-color polarizer and mono-color polarizer which has dichroism. Polarizers neutral color - Red.

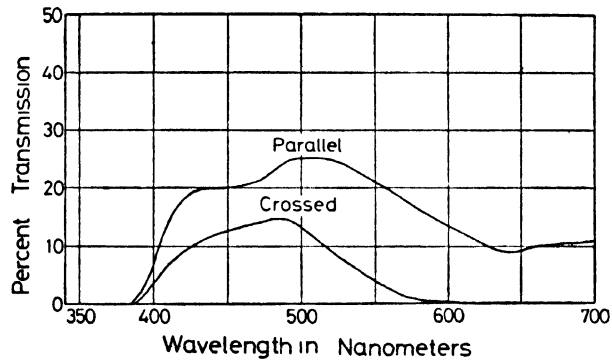


Figure 3 Spectral transmission of a pair of neutral-color polarizers. Polarizers neutral color - Blue.

In a real TN device, the liquid crystal film itself shows faint colors during turn-off time and when it is observed in a direction off-normal to the panel^{6, 11}. This phenomenon may be explained by considering the birefringence of the liquid crystal medium. Therefore real color of a TN panel is a composition of the above-mentioned color of polarizers and that of the LC layer itself.

Other electro-optical characteristics are as follows: the turn-on time and turn-off time of a TN device are 20 ms and 60 ms respectively at room temperature; over 15,000 hours of continuous operation has been proved, the power consumption of a cell was shown to be about $0.5 \mu\text{W}/\text{cm}^2$, and the view angle is 100° or more. These values are compatible with the requirements of the display panels of watches, clocks, calculators and other indicators.

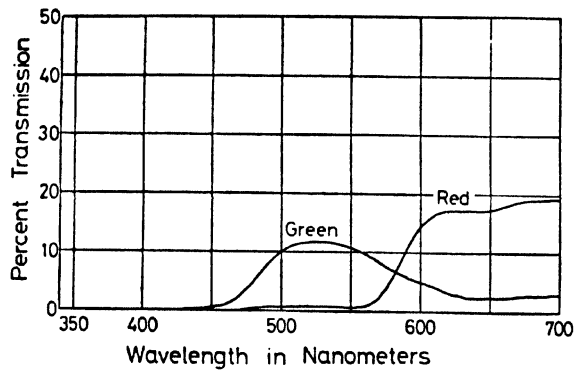


Figure 4 Spectral transmission of a combination of a neutral-color polarizer and a composite-dichroic-color polarizer. This combination is used for the indication shown in figure 1 (C) and (C'). Polarizers, neutral color Red green.

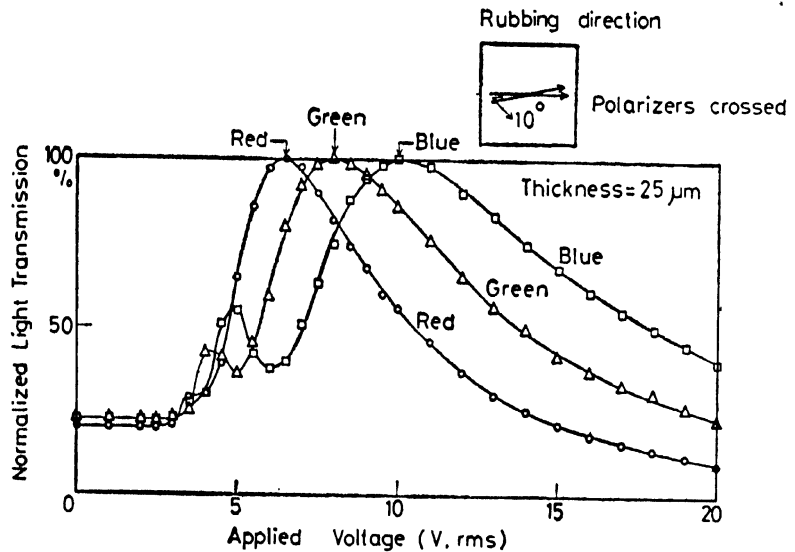


Figure 5 Voltage controllable color formation with a twisted nematic. *p*-type nematic material is twisted by 10° . Operated by an ac 5kHz field.

4. Characteristics of voltage controllable color formation in twisted nematic panels

In figures 5–8 is shown transmission of monochromatic light beam through the off 90° twisted nematic panels *versus* applied voltage (ac 5 kHz, rms). Twist angles are increased systematically from figure 5 to figure 8.

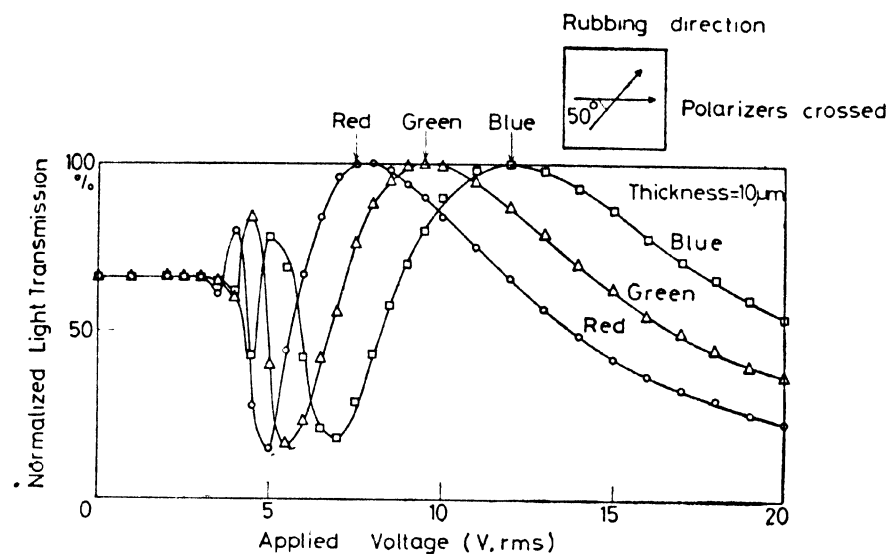


Figure 6 Voltage controllable color formation with a TN cell. Twist angle 50°.

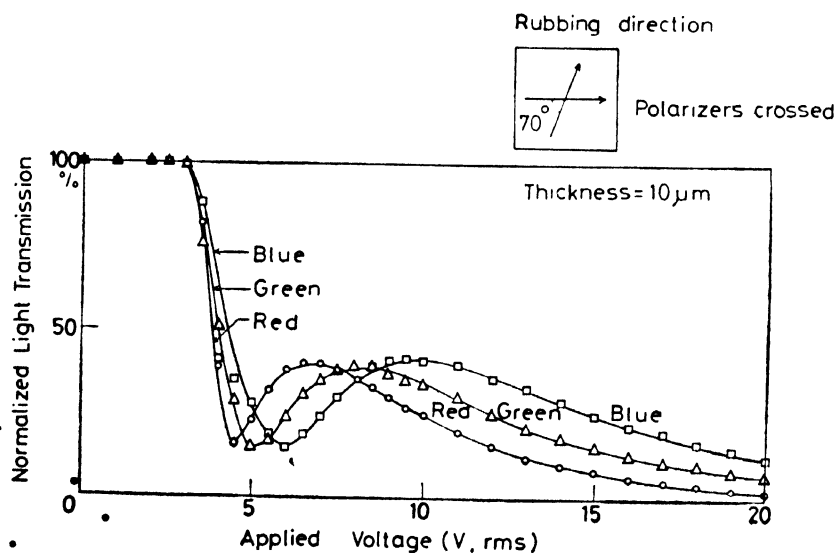


Figure 7 Voltage controllable color formation with a TN cell. Twist angle 70°.

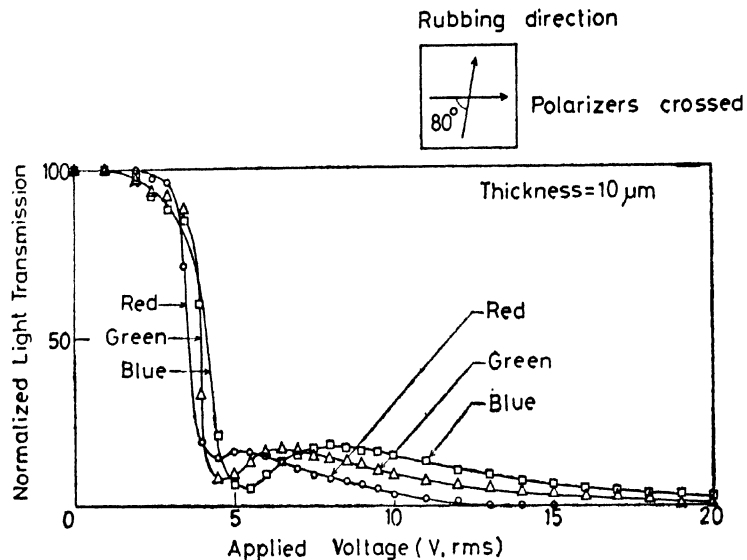


Figure 8 Voltage controllable color formation with a TN cell. Twist angle 80°.

The LC material used in these measurements is a *p*-type material described in section 2. Except in the case of figure 5, the thickness of the cell is 10 μm.

The wavelengths of the three light beams are 650, 534 and 456 nm corresponding to red, green and blue. A pair of crossed-neutral polarizers was used.

By comparing figures 5-8, it is clear that the most distinct voltage controllable color formation is possible by choosing the twist angles to be below 10°. By this way, it is possible to reveal more homogeneous and larger area patterns as compared with the DAP device⁸⁻¹⁰.

The order of the appearance of the colors is red-green-blue in figures 5-8; on the other hand, this appearance is inverted in the case of field effect devices with *n*-type material⁸⁻¹⁰. This difference can be illustrated by considering the difference in the initial conditions of each mode.

According to independent experiments, many maxima and minima in the data of the light transmission vs applied voltage were recognized when the content of *p*-type material was increased.

As the twist angles are increased the transmission below threshold increases and the color formation becomes faint.

The cases for which twist angles are between 80° and 110° are almost equivalent to the ordinary TN device with a 90° twist described in the previous section. In order to get homogeneous and clear pattern indication in a TN device, the present authors sometimes adopted a 80° twist device. The advantage of this is believed to outweigh the disadvantage that a certain small amount of the transmission and color formation is seen even in the saturation region, *i.e.*, above 6 volts in figure 8.

Acknowledgement

The authors express their heartfelt thanks to the staff of Sanritsu Co. for their cooperation in measuring the characteristics of the polarizers.

References

- 1 SCHADT M and HELFRICH W *Appl. Phys. Lett.* **18** 127 (1971)
- 2 JONES D and LU S *SID Int. Symp. Digest of Technical Papers*, p. 100 (1972)
- 3 KMFTZ A R *SID Int. Symp. Digest of Technical Papers*, p. 66 (1973)
- 4 BOLLER A *et al.* *Proc. IEEE* **60** 1002 (1972)
- 5 FERGASON J L *U.S. Pat.* 373186 (May 8, 1973)
- 6 KOBAYASHI S and TAKEUCHI F *SID Int. Symp. Digest of Technical Papers*, p. 40 (1973)
- 7 HEILMEIR G H, ZANONI L A and BARTON L A *Proc. IEEE* **56** 1162 (1968)
- 8 SCHIEKEL M F and FAHRENSCHON K *Appl. Phys. Lett.* **19** 391 (1971); *SID Int. Symp. Digest of Technical Papers*, p. 98 (1972)
- 9 SOREF R A and RAFUSE M J *J. Appl. Phys.* **43** 2029 (1972)
- 10 KAHN F J *Appl. Phys. Lett.* **20** 199 (1972)
- 11 KOBAYASHI S, TAKEUCHI F and SHIMOMURA T presented at *Int. Conf. Solid State Devices*, Aug. 29-31, 1973 Tokyo; supplement of the Japan Society of Applied Physics, **43** 131 (1974)

is larger along the long axis, the material is referred to as positive, and on the other hand, if it is greater at right angles, it is referred to as negative.

The effect of molecular alignment must be overcome before we can distort a liquid crystal with an electric field. The electric field at which this occurs is

$$E = \left(\frac{\pi}{d} \right) \left(\frac{k}{\Delta \epsilon} \right)^{\frac{1}{2}}$$

where d is the distance between electrodes, $\Delta \epsilon$ the dielectric anisotropy and k the elastic constant.

Of practical interest is the fact that for parallel electrodes, the threshold value for the field reduces to an applied voltage, which is expressed as

$$V = \pi \left(\frac{k}{\Delta \epsilon} \right)^{\frac{1}{2}}$$

Thus, variations of the thickness in the layer will not affect the uniformity of the device. If the spacing between two parallel electrodes had to be very closely controlled, this would severely limit the applications of nematic liquid. In this case nature has been fortuitous to allow rather large deviations in the flatness and parallel construction.

The pure field effect in liquid crystals allows modulation of light in a number of ways. If a nematic layer is oriented parallel to the surfaces of a pair of conductive transparent glass plates and when such a cell is placed between linear crossed polarizers such that the aligned direction is at 45° to the polarizer, we will get maximum transmission. If this material is positive, that is, the director tends to align parallel to the applied field, the transmission will be a maximum for zero field and will be reduced by the application of a field.

Test devices of this type have been built which show a variable birefringence and traverse the total range of colors on applying 25 volts (figure 1). For use in this application, the electrical resistivity of the material should be as high as possible. Increase in sensitivity can be made by increasing the dipole moment along the long axis, and decreasing the elastic constant. The same effect can be obtained by using an electrically negative material aligned perpendicular to the electrodes. In this case, there is almost no way predicting the direction which the liquid crystals will bend out the field direction. Therefore linear polarizers do not always give the best results.

By rubbing plates in suitable directions it is possible to produce twisted nematics with any desired angle of twist^{2,4}. The mechanism is simply that the liquid crystal is elastically deformed by the surface constraints such that the director of the nematic material is oriented in a

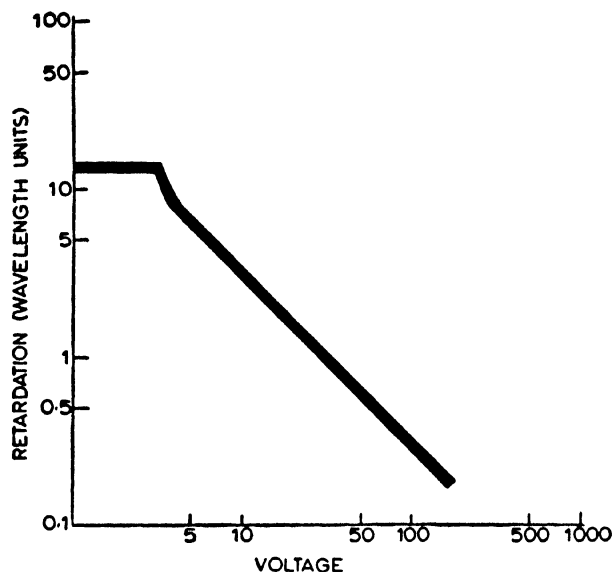


Figure 1 Relative retardation of a parallel oriented liquid crystal film 37 microns thick.

helical manner. By application of a field parallel to the twist axis, the direction of the molecules at the centre of the sample can be made to become parallel to the twist axis. This occurs at a very sharp level and we have a resulting bilevel operation.

If such a device with a 90° twist is placed between parallel polarizers no light will be transmitted at zero voltage and it will be equivalent to two crossed polarizers. When an electric field is applied to the device the structure will untwist at a well defined voltage and allow light transmission. If, however, the same device is placed between crossed-polarizers, then at zero voltage, light is transmitted and the polarizers will effectively act as though they are parallel. However, with the application of a critical voltage, the plane of polarization will no longer be rotated 90° and no light will be transmitted. Thus, we have a device which will act as a shutter for transmitted light. In figure 2, curves show typical transmission as a function of voltage for bilevel display.

Typical twisted nematic LCD

The mechanism involved in the operation of a twisted nematic liquid crystal display⁵ is shown in figure 3. The construction of the cell involves a thin ($6\text{--}10\text{ }\mu\text{m}$) layer of room temperature nematic liquid crystal material with a positive dielectric anisotropy. The uniform alignment

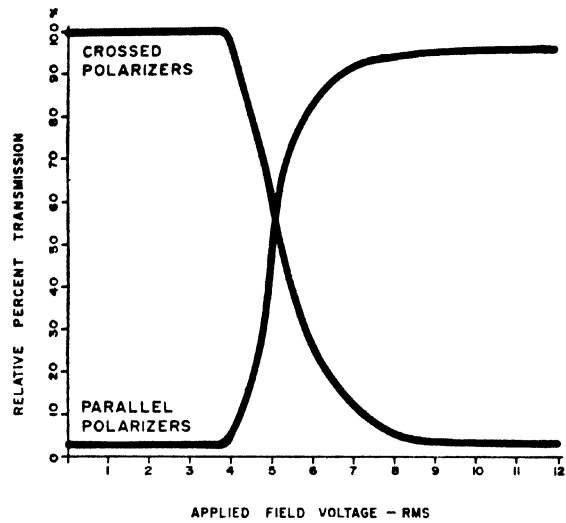


Figure 2 Light transmission of a 12 micron thick bilevel liquid crystal cell as a function of applied voltage.

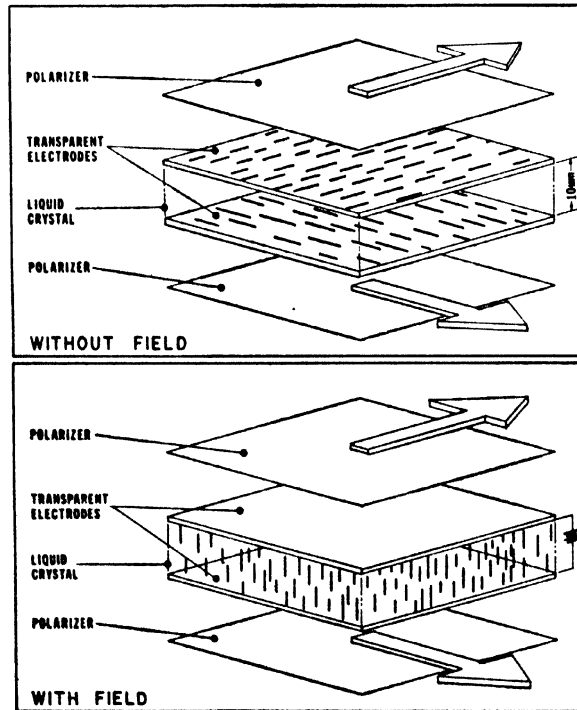


Figure 3 Operational mechanism involved in a twisted nematic field effect cell.

of the liquid crystal on the inner surfaces of the conductive transparent glass plates is achieved by treating the latter with special coatings. By this procedure a uniform alignment of the liquid crystal parallel to the walls is obtained. The display is assembled in such a way that the alignment direction on the front plate is at right angles to that on the back plate. The cell thus obtained has the liquid crystal medium in the form of 90° twist and has the ability of rotating linear polarized light by 90° . Application of dc or ac electric field causes the liquid crystal medium to untwist and become parallel to the field, thus reducing the rotation practically to zero. By having crossed or parallel polarizers on the display, when the electric field is applied, one can either have normally open or closed display.

Speed of response

The speed of response of a field effect liquid crystal display depends on the applied voltage, the viscosity, the thickness and the elasticity of the liquid crystal film. Of these variables the elasticity and the viscosity are material parameters and are the concern of the chemist. These parameters change with the temperature and the direction of alignment of the liquid crystal.

The variable of concern to the circuit designer is the applied voltage and to the display designer it is the thickness of the liquid crystal film. In figure 4 we have shown the response of a liquid crystal to various square wave impulses. The liquid crystal used is a proprietary material FELIX 10. In the case of five volts as applied voltage, we never achieve maximum extinction and have a slow turn on and turn off as would be expected from figure 2. Of major interest in design is the ability to control the turn on time with a steep pulse and a properly chosen wave form which will decrease the turn off time. This assumes however, that the device is not designed for any special application of the user.

In most cases by varying the thickness of the display a considerable range of response times can be obtained. Basically the sacrifice which occurs will be in length of life since the thinner the device the higher the fields impressed across it will be. However, we have seen earlier the voltage for the threshold does not change. The dependence on thickness goes as the square of the electrode spacing and therefore we can get a response time four times faster with a film which is half the thickness. A practical limit at this time precludes liquid crystals thinner than 1 micron from being used for display. However, this allows rise times of 1 millisecond to be attained.

Voltage

- The turn on voltages for all field effect liquid crystals is a function of the relative dielectric anisotropy. This, of course, is a function of the particular liquid crystal material used. Recently some low melting point

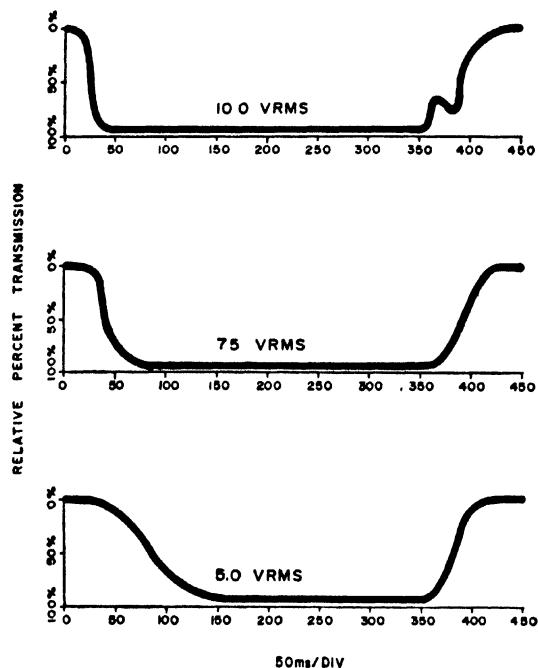


Figure 4 Optical transmission as a function of time for an applied 1 kHz square wave pulse for a period of 350 milliseconds on a bilevel shutter 12 microns thick.

biphenyl compounds of positive anisotropy⁶ have been reported. Measurement of electrical resistivity⁷ on some of these compounds is in the range of 10^7 – 10^8 ohm cm. and it has been further observed⁷ that the resistivity values change erratically, though these changes did not cause any damage to the device performance.

In our laboratory we have found that it is possible to have thresholds as low as 0.7 volt. There is no true theoretical limit for the threshold voltage. However, there are a number of practical limitations. The principal one is the non-availability of organic materials with the appropriate dielectric anisotropy necessary for the low threshold of voltages. From a materials standpoint, we can postulate a range of threshold voltages determined by the properties of materials which go from infinity to an arbitrarily low voltage. From a practical standpoint this may be in the neighbourhood of 0.5 to 0.7 volts. For this type of material it would be easy to operate from $1-\frac{1}{2}$ logic.

Power requirements

One of the most intriguing aspects of the field effects are their low power requirements. In most practical applications it is desirable to

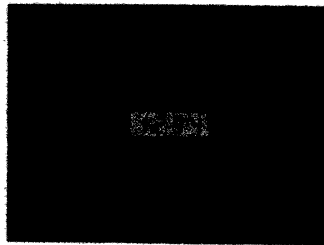


Plate 1(a) Back lighted field effect liquid crystal display. Photograph taken about 5 feet away from the display.



Plate 1(b) Same display as in the left, but with no back light. Photographed in reflected light under normal room illumination.

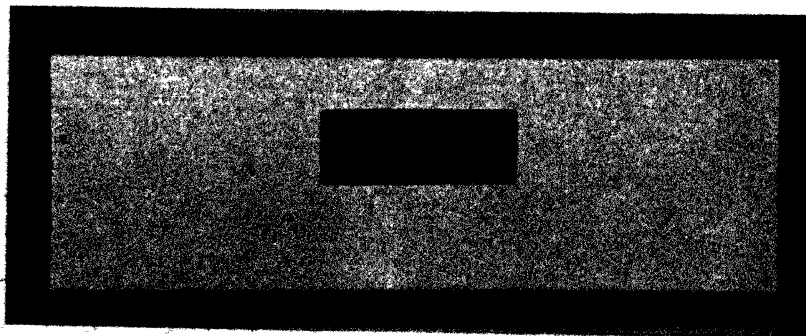


Plate 1(c) Similar display as in top right, but was photographed only 1 foot away.

reduce the material conductivity and therefore the leakage current to a minimum. In the field effect device the interaction with the liquid crystal is a pure field effect and therefore leakage current is undesirable. By going to very high electrical resistivities, a number of factors become apparent. The principal one is that the charging of the capacitor elements is the major contribution of current. Liquid crystal devices have been built using FELIX 10 which have RC time constants of 30 seconds or greater. Our extrapolated values for these materials indicate that we would be able to achieve 10^{16} ohm cm. resistivity and therefore time constants of 30 minutes or longer which would make practical storage devices. Thus, the dielectric storage in the capacitor would allow us to update information only as it changes. The obvious applications of such a device are in any device which requires ultra low power and conservation of logic. In production, displays which have currents as low as 0.5 nanoamps for a 0.4" high digit have been constructed.

Conclusions

The field effect liquid crystal displays are now ready for application. Many of the early problems which have confronted all liquid crystal displays have become considerably less important with a field effect display. Combinations of lower power and lower voltage make it possible to envisage a whole line of new devices based on the interactions of nematic liquid crystals with electric fields.

Liquid crystal displays utilizing field effect technology are commercially available in many different sizes for a variety of purposes. Some photographs of these are shown in Plate 1.

References

- 1 LEHMANN O Z. *Phys. Chem.* **4** 464 (1889)
- 2 ZOCHER H *Trans. Faraday Soc.* **29** 945 (1933)
- 3 FERGASON J L, TAYLOR T R and HARSCH T B *Electro-Technology* January 1970
- 4 MAUGUIN C *Bull. Soc. franc. Miner. Crist.* **34** 71 (1911)
- 5 FERGASON J L U.S. Pat. 3,731,986 (May 8, 1973)
Assigned to International Liquid Xtal Co.
- 6 GRAY G W, et al *Electron Lett.* **9** 130 (1973)
- 7 ASHFORD A, et al *Electron Lett.* **9** 118 (1973)

AUTHOR INDEX

- | | |
|---|------------------------------|
| ACHARD M F, 215 | GASPAROUX H, 215 |
| ARORA S L, 553 | GRAY G W, 381 |
| AMBROSE E J, 523 | GROS C, 397 |
| AVADHANLU M N, 289 | GRUNBAUM, 155 |
| | GULIK-KRZYWICKI T, 115 |
| BACON W E, 455 | |
| BILLARD J, 131, 397 | HARDOUIN F, 215 |
| BLINC R, 277 | HARRISON K J, 381 |
| BROCHARD F, 1 | |
| BULKIN B J, 155 | JACQUES J, 397 |
| | JAHNIG F, 31 |
| CANCEILL J, 397 | JANIK J A, 253 |
| CARR E F, 263 | JANIK J M, 253 |
| CHANDRASEKHAR S, 57, 117, 225, 237,
325, 341 | |
| CHISTYAKOV I G, 79 | KALYANI V, 75 |
| CROXTON C A, 237 | KARAT P P, 225, 285 |
| | KENNELLY T, 155 |
| DAVE J S, 415, 427, 435, 447 | KHETRAPAL C L, 471, 483, 495 |
| DE GENNES P G, 1 | KINI U D, 311, 325, 353 |
| DEMUS D, 189, 363 | KOBAYASHI S, 545 |
| DE VRIES A, 93 | KRISHNASWAMI S, 247 |
| DOMON M, 131 | KUNWAR A C, 471, 483, 495 |
| DURAND G, 23 | KURIAN G, 427 |
| | |
| EASWARAN K R K, 483 | LESLIE F M, 41 |
| | LOK W B, 155 |
| FERGASON J L, 553 | LUGOMER S, 277 |
| FRIBERG S, 537 | LUZZATI V, 115 |

- MADHUSUDANA N V, 57, 225, 285
MATEU L, 115
MORZOTKO D, 189
MURTY C R K, 289
- NAKAMURA T, 503
NASH J A, 381
NITYANANDA R, 311, 325
- OTNES K, 253
- PAN S, 299
PATANKAR A V, 471
PICOT J J C, 305
PRAJAPATI A P, 435
- RAJAGOPALAN S R, 353
RAJAN V S V, 305
RAMASESHAN S, 117
RANCK J L, 115
RANGANATH G S, 341, 353
RATNA B R, 69
RESHAMWALA A S, 117
ROSCIZEWSKI K, 253
- SADASHIVA B K, 69, 117
SADLER D M, 115
SAITO H, 537
SAUPE A, 495
SCHNUR J M, 175
SEKI S, 503
SHASHIDHAR R, 69, 117, 247
SHERIDAN J P, 175
SORAI M, 503
SURENDRANATH V, 117
SURESH K A, 325, 341, 353
- TARDIEU A, 115
- VAINSHTEIN B K, 79
VANI G V, 75
VASANTH K L, 415
VENUGOPALAN S, 167
VIJAYA M S, 69
VORA R A, 447
- WANG C H, 299
WARTENBERG G, 363
WROBEL S, 253
- ZEKS B, 277

SUBJECT INDEX

- Activation parameters in nematic solvents 457
- 2-*n*-acyl-7-*n*-alkyl-9, 10-dihydro-phenanthrenes 406
- 2-*n*-acyl-7-(methyl alkyl)-9, 10-dihydro-phenanthrenes 408
- 2-*n*-acyl 7-(methyl alkyl)-fluorenes 404
- p*-*n*-alkoxybenzoic acids
 - electrical properties 263
- N*-*p*-alkoxybenzylidene-*p'*-*n*-alkyl anilines 503
 - transition temperatures 512
- p* (*p'*-*n*-alkoxybenzoyloxy) toluenes 448
- 4'-*n*-alkoxy-4-cyanobiphenyl 381
 - enthalpies of transition 387
 - transition temperatures 387
- N*-(4-*n*-alkoxy-1-naphthylidene)-4'-amino azobenzene 439
- N*-(4-*n*-alkoxy-1-naphthylidene)-*p*-azo-anilines 436
- 4-*n*-alkoxy-3'-substituted biphenyl
 - carboxylic acids
 - enthalpies of transition 203
 - transition temperatures 203
- p*-*n*-alkyl-*p'*-*n*-alkoxytolans
 - enthalpies of transition 148
 - transition temperatures 148
- 4'-*n*-alkyl-4-cyanobiphenyl 381
 - enthalpies of transition 383
 - transition temperatures 383
- p*-*n*-alkyl *p'*-methoxytolans 150
 - enthalpies of transition 150
 - transition temperatures 150
- p*-anisaldazine
 - surface tension 249
- anomalous alignment 289
- antiferroelectric short range order 57, 69
- Arrhenius law 32, 457
- p*-azoxyanisole (PAA)
 - Cole-Cole diagram 256
 - dielectric relaxation 254
 - far-infrared spectra 158, 167
 - orientational order parameter 91
 - P-T diagram 121
 - Raman scattering 157, 300
 - surface tension 249
 - thermal conductivity 307
 - twist elastic constant 230
 - vibrational spectra 156
- p*-azoxyphenetole (PAP)
 - P-T diagram 122
 - twist elastic constant 230
- Bénard convection 305
- benzo(b)thiophene
 - NMR spectra 495
- Bethe approximation 67
- birefringence
 - electric 57, 69
 - magnetic 57, 69

- 2-5-bis-(4-*n*-alkoxy phenyl)-pyrazines
 - enthalpies of transition 197
 - transition temperatures 197
- 2-5-bis-(4-*n*-alkoxy phenyl)-pyrazines
 - enthalpies of transition 199
 - transition temperatures 199
- bis-(4'-*n*-decyloxy benzal)-2-chloro-1,4-phenylenediamine
 - diamagnetic anisotropy 222
 - magnetic susceptibility 222
- 4-4'-bis(hexyloxy)azoxybenzene
 - Raman scattering 302
- Borrmann effect in cholesterics 325, 348
- Bragg reflexion from cholesterics 325
- calorimetric studies 189
- cancer cells
 - liquid crystals in 533
- β -carotene 358
- Carr-Helfrich model 285
- catastrophies in cell surfaces 530
- cell shapes
 - changes in 531
- C-H stretching vibration 161
- cholesteric liquid crystals
 - absorbing systems 325
 - anomalous transmission (Borrmann effect) 325
 - circular dichroism 317, 329, 347, 353
 - compensated mixtures 353
 - dynamical theory of reflexion 341
 - optical rotation 321, 346
 - pitch and its temperature variation 367, 371
 - refractive indices 367
 - selective reflexion from cholesteryl esters 363
 - theory of reflexion and transmission by thin films 325
 - transition temperatures 366, 428
- cholesteryl-6-*n*-alkoxy-2-naphthoates 428
- cholesteryl alkyl carbonates 378
 - benzoate 375
 - cinnamate 375
 - ethyl carbonate 372
 - myristate 370
 - nonanoate 370
 - octyl carbonate 373
 - propionate 371
- Claisen rearrangement 456
- classification of liquid crystals 93
- Clausius-Clapeyron equation 128
- Cole-Cole diagram 255
- conductivity anisotropy 267
- continuum theory of nematics 42
- critical divergence
 - of elastic constants 16, 225
 - of viscosity coefficients 31
- p*-cyanobenzylidene-*p*'-octyloxyaniline, (CBOOA)
 - bend elastic constant 232
 - diamagnetic anisotropy 218
 - magnetic susceptibility 217
 - Rayleigh scattering 27
 - twist elastic constant 233
- cybotactic nematics
 - ordinary 95
 - skewed 95
- cylindrical Patterson function 83
- Debye-Waller factor 258
- N,N'-di(4-*n*-alkoxy-1-naphthylidene)*p*-azoanilines 436
- di-*n*-alkyl-4,4'-azoxy cinnamates
 - enthalpies of transition 192
 - transition temperatures 192
- di-*n*-alkyl azoxy- α -methyl cinnamates
 - enthalpies of transition 195
 - transition temperatures 195

- di-*n*-alkyl-*p*-terphenyl-4,4'-dicarboxylates
 - enthalpies of transition 202
 - transition temperatures 202
- diamagnetic anisotropy, experimental
 - determination 223
- dichroic polarizers 546
- dichroic power 358
- dielectric properties
 - field dependence 291
 - frequency dependence 293
 - low frequency 72, 266
 - microwave 263
 - negative anisotropy 554
 - positive anisotropy 57, 72, 545, 554
 - relaxation 254
- differential scanning calorimetry 148, 177
- differential thermal analysis 119, 504
- dimers 265
- dipole moment 57, 256
- dispersion relation 328
- displacement function 80
- display devices
 - field effect 553
 - multicolor 546
 - twisted nematic 545, 553
- domain formation 289
- dynamic scattering 299
- elastic energy of smectic A 3, 25
- electric field effects 270, 285, 289, 299
 - field effect displays 545, 553
- electrohydrodynamic flow patterns 285, 299
- electron density map 78
- enthalpies of transition 148, 150, 177, 192, 195, 197, 199, 202, 203, 383, 387
- p*-ethoxybenzoic acid
 - P-T diagram 125
- 4-ethoxybenzylidene-4'-*n*-butylaniline (EBBA)
 - dichroic difference spectra 164
 - heat capacity 514
 - infrared spectrum 162
 - molecular orientation in 496
- p*-(*p*'-ethoxyphenylazo)phenyl heptanoate
 - Raman scattering 302
- p*-(*p*'-ethoxyphenylazo)phenyl hexanoate
 - dielectric constants 291
- p*-(*p*'-ethoxyphenylazo)phenyl undecylenate
 - Raman scattering 302
- p*-(*p*'-ethoxyphenylazo)phenyl valerate
 - Raman scattering 302
- ethyl ether *p*-anisalamino cinnamic acid
 - structure 84
- ethyl-4 (4-ethoxybenzylidene amino)-cinnamate 106
- eutectic mixtures 386
 - optical activity 390
 - photochemical stability 384
- eutectic point 152
- eutectic temperature 385
- Faraday method 215
- far-infrared spectra 155, 167
- field effect displays 545, 553
- flip-angle method 215
- foam stability 537
- Fourier-Bessel transform 83
- Frank-Oseen energy function 43
- Freedericksz transition 225
- friction coefficient 17
- gauche* states 35
- glassy state 503

- heat capacity measurements 514
- 4'-*n*-hexyl-4-cyanobiphenyl 69
 - electric birefringence 70
 - magnetic birefringence 70
- high pressure studies 117
- hydrodynamics 4, 31
- hydrogen bonded interaction 478
- hydrolysis in lyotropics 455, 464
- infrared optical activity 163
- infrared spectra 162
- interaction parameters 58
- intermediate nematics 96
- intermolecular distances 103
- ion etching 525
- isobaric phase diagram 397
- isomerization
 - rate constants for 460
- isomorphy 399, 408
- Jones matrix 354
- kinetics of hydrolysis in lyotropics 455
- Krieger-James approximation 58
- lamellar phase of lipid / water 1
- lattice vibrations
 - of nematogenic crystals 156
- linear dichroism 356
- lipids
 - charged 1
 - chloroplast 2
 - hydrodynamics of lipid/water systems 1
 - mitochondrial 2
 - uncharged 1
- X-ray structural studies 115
- liquid surface 237
- liquid-vapour transition zone 237
- living systems, liquid crystallinity in 523
- low frequency dielectric properties 72, 266
- lyotropic mesophases
 - as solvent in NMR 471
 - foam stability 537
 - hydrodynamics 1
 - living systems 523
 - kinetics of hydrolysis 455
 - X-ray studies 115
- magnetic properties of smectics 215
- Maier-Saupe Hamiltonian 278
- p*-methoxybenzoic acid
 - P-T diagram 125
- n-p*-methoxybenzylidene-*p'*-*n*-butylaniline (MBBA)
 - electric field effects 286
 - neutron scattering measurements 256
 - thermal conductivity 306
 - vibrational spectra 161
- n-p*-methoxybenzylidene *p*-phenylazoaniline
 - crystal structure 75
- p*-methoxycinnamic acid
 - dielectric loss 265
- 2-(2-methylacyl)-7-*n*-alkoxyfluorenes
 - transition temperatures 403
- 2-(3-methylacyl)-7-dodecanoylfluorenes
 - transition temperatures 402
- n*-methyl formamide
 - NMR spectra 483
- microfilaments 525
- microtubules 527
- microwave dielectric properties 263
- Miesowicz viscosity 32
- mixed mesomorphism in binary systems 415
 - nematic-isotropic transition
 - temperatures 419, 421
 - solid-mesomorphic transition
 - temperatures 418, 420
- monomer 265

- nematic order 57
- neutral-color polarizers 546
- neutral stationary instability 308
- neutron quasielastic scattering 256
- p*-nonyloxybenzoic acid
 - conductivity anisotropy 268
 - dielectric loss 264, 266, 271
 - structure 85
- nuclear magnetic resonance 471, 483, 495
- Oblique modes in lipid/water system 9
- p*-octyloxybenzoate *p*'-pentyl benzene
 - diamagnetic anisotropy 219, 220
 - magnetic susceptibility 219
- 4-*n*-octyloxy-4-cyanobiphenyl 391
 - dielectric constants 72
- odd-even effect 428, 436, 448
- Onsager-Parodi relation 32
- optical activity 390
- orientational model potential 240
- orientational order parameter
 - in the vicinity of the surface 240
 - long range 57
 - short range 57, 69
- oscillatory instability 308
- pendant drop method 248
- penetration length 24
- permeation 7, 26
- peritectic point 152
- phase diagrams for mixtures 131
- photo-chemical stability 384
- plasma membrane 532
- Poincaré sphere 227
- polymerization 455
 - rate constants for 468
- pressure induced mesomorphism 117
- pretransition effects 31, 58, 69, 225, 303
- P-T diagram 117
- pyrazine, pyridazine, pyrimidine
 - NMR spectra 471
- Raman spectra 157, 175
- Rayleigh number 308
- reaction rates in lyotropics, 455
- René Thom catastrophes 530
- Rosciszewski theory 254
- rotatory jumps 257
- Schroder-Van Laar equation 385
- second sound 10
- single particle potential 239
- slip modes 11
- Slippage
 - coefficient of 7
- smectic A
 - hydrodynamics 1
 - magnetic properties 215
 - Raman scattering 176
 - Rayleigh scattering 23
 - X-ray studies 84, 98
- smectic B
 - Raman scattering 176
 - X-ray studies 85, 99
- smectic C
 - dielectric studies 272
 - magnetic properties 221
 - Raman scattering 176
 - X-ray studies 85, 98
- smectic D, X-ray studies 87, 99
- smectic E, X-ray studies 87
 - normal 100
 - tilted 100
- smectic F, x-ray studies 99
- smectic G, x-ray studies 100
- smectic H, x-ray studies 100

terephthal-bis-(4-*n*-butylaniline) (TBBA)

DSC traces 177

enthalpies 177

Raman spectrum 175

transition temperatures 177

X-ray studies 102

textures

batonnets 128

focal conic 128

schlieren 128

thermal conductivity 306

thermal stability 431, 442, 450

transition enthalpies, *see* enthalpies

translatory jumps 257

trans states 35

threshold voltage in nematics

285, 289, 545, 553

triple points 117

twist elastic constant 225

twist viscosity 34, 234

twisted nematic cells 384

twisted nematic display devices 545, 553

electro-optical characteristics 547

multicolor 546

voltage controllable color formation
in 548

twisted nematics orientation patterns 41

undulation mode 13, 27

vibrational spectra 155, 167

virtual transitions 134

viscosity coefficients 31

frequency dependence 35

temperature dependence 32

wall quenching effect 24

William's domains 299

X-ray studies

of lamellar phases of lipid/water
systems 115of thermotropic liquid crystals
79, 83, 93, 391

of nematogenic crystal 75

PRAMANA

a journal of physics

Published monthly by the Indian Academy of Sciences, in collaboration with the Indian Physics Association and the Indian National Science Academy.

Editor :

S. RAMASESHAN

National Aeronautical Laboratory, Bangalore

Joint Editor :

B. M. UDGAONKAR

Tata Institute of Fundamental Research,
Bombay.

Annual subscription rates :

(Two volumes of six issues each per year)

Institutions & Libraries \$ 30 or £ 12

Individuals \$ 20 or £ 8

Pramana is not sold as single issues.

Orders may be sent to :

The Indian Academy of Sciences,
Bangalore - 560006, India.

COLLECTED WORKS OF S. PANCHARATNAM

With a foreword by G. W. Series FRS

Pancharatnam worked under Raman in Bangalore and later in Oxford. This collection of his papers include some that were to have been part of a monograph that he was unable to complete before his death. The earlier papers describe interesting and unfamiliar phenomena in the optics of crystals and extensions of the theory of polarized light which Pancharatnam devised to interpret them. The later papers concern optical pumping, exhibiting in particular the properties which arise from the anisotropic, time-dependent susceptibility of the pumped medium. This book should appeal to those engaged in research in optics, atomic physics or quantum electronics

**Oxford University Press,
pp 530, £ 10**

